

AF-IR-840011

FILE COPY

REMOVED  
DATE

1989

**FEL '89  
CONFERENCE DIGEST**

(2)

AD-A219 185

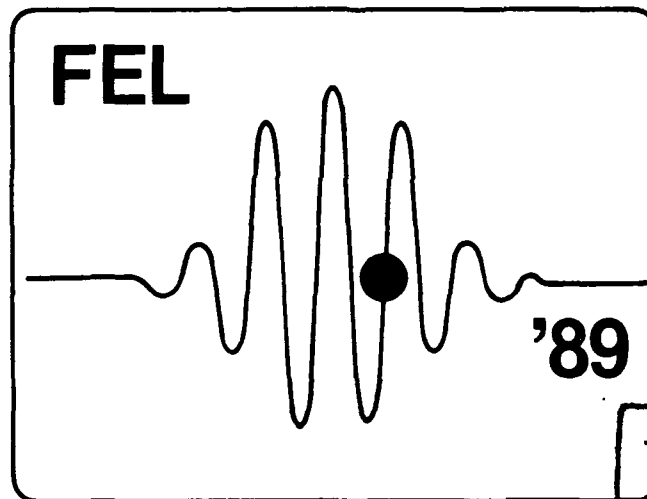
*11th International Conference on*

**FREE ELECTRON  
LASERS**

S

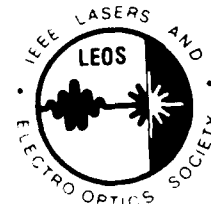
MARCH 6 1990

CD



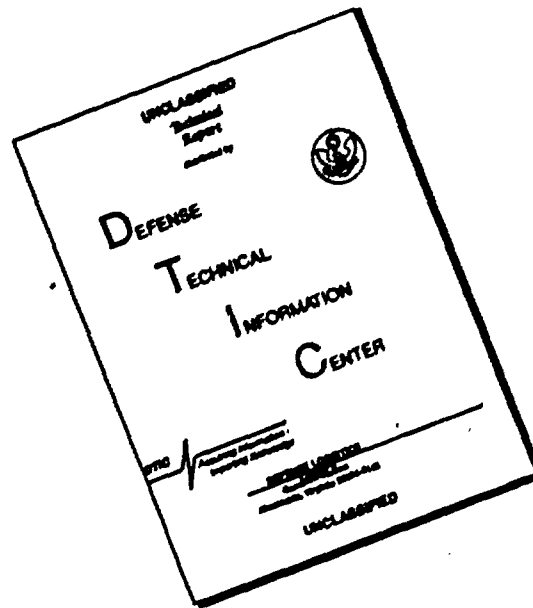
DISTRIBUTION STATEMENT 5  
Approved for Release by NSA  
Date 10-10-2013

August 28 - September 1, 1989  
Ritz Carlton Hotel  
Naples, Florida



90 02 23 028

# DISCLAIMER NOTICE



THIS DOCUMENT IS BEST QUALITY AVAILABLE. THE COPY FURNISHED TO DTIC CONTAINED A SIGNIFICANT NUMBER OF PAGES WHICH DO NOT REPRODUCE LEGIBLY.

# **FEL '89**

## **11th International Conference On Free Electron Lasers Conference Digest August 28 - September 1, 1989**

Ritz Carlton Hotel  
Naples, Florida, USA

**Sponsored by the IEEE Lasers & Electro-Optics Society**

Support Provided by:  
Air Force Office of Scientific Research  
Office Of Naval Research  
TRW



The papers in this book comprise the digest of the meeting mentioned on the cover and title page. They reflect the author's opinions and are published as presented and without change, in the interests of timely dissemination. Their inclusion in this publication does not necessarily constitute endorsement by the editors, the Institute of Electrical and Electronic Engineers, Inc.

Copyright and Reprint Permissions: Abstracting is permitted with credit to the source. Libraries are permitted to photocopy beyond the limits of U.S. copyright law for private use of patrons those articles in this volume that carry a code at the bottom of the first page, provided the per-copy fee indicated in the code is paid through the Copyright Clearance Center, 29 Congress Street, Salem, MA 01970. Instructors are permitted to photocopy isolated articles for noncommercial classroom use without fee. For other copying, reprint or republication permission, write to Director, Publishing Services, IEEE, 345 E. 47th St., New York, NY 10017. All rights reserved. Copyright © 1989 by The Institute of Electrical and Electronics Engineers, Inc.

Accession For	
NTIS	<input checked="" type="checkbox"/>
DTIC	<input type="checkbox"/>
Unannounced	<input type="checkbox"/>
Justification	
By	50.00
Distribution	
Codes	
Dist	/or
A-1 21	

Price: \$50.00 per Gail Walters  
IEEE/LEOS  
TELECON

3/1/90

VG





## **PREFACE**

With this Digest an effort has been made to disseminate in a timely manner most of the scientific information interchanged during the XIth International Free Electron Laser Conference held in Naples, Florida from August 28 through September 1, 1989. The editors take this opportunity to thank all contributors and the LEOS staff for making this effort successful.

Luis R. Elias  
Isidor Kimel

## ***FEL'89 CONFERENCE COMMITTEES***

### **Conference Chair**

Luis Elias, CREOL, University of Central Florida, Orlando, FL

### **Local Organizer**

Isidoro Kimel, CREOL, University of Central Florida, Orlando, FL

### **Conference Program Committee**

Robert E. Behringer, Ballena Systems Corp., Alameda, CA  
Stephen V. Benson, Duke University, Durham, NC  
David A. Deacon, Deacon Research, Palo Alto, CA  
George R. Neil, TRW, Inc., Redondo Beach, CA  
Howard Schlossberg, AFOSR, Washington, DC  
Earl D. Shaw, AT&T Bell Laboratories, Murray Hill, NJ  
Jack M. Slater, Spectra Technology, Inc., Bellevue, WA  
Victor L. Granatstein, University of Maryland, College Park, MD  
Yoshiyuki Kawamura, Institute of Physics & Chemical Research, Saitama, Japan  
Cha-Mei Tang, Plasma Physics Division, Naval Research Lab., Washington, DC  
John E. Walsh, Dartmouth College, Hanover, NH  
Roger W. Warren, Los Alamos National Scientific Lab, Los Alamos, NM  
Rodolpho Bonifacio, Universita Degli Studi Di Milano, Milano, Italy  
Ilario Boscolo, Universita Degli Studi Di Milano, Milano, Italy

### **International Executive Committee**

George Bekefi, M.I.T., Cambridge, MA  
William Colson, Berkeley Research Associates, Berkeley, CA  
K. Mima, Osaka University, Japan  
B. Newnam, Los Alamos National Laboratory, Los Alamos, NM  
Claudio Pellegrini, Brookhaven National Lab., Upton, NY  
Donald Prosnitz, Lawrence Livermore National Laboratory, Livermore, CA  
C.W. Roberson, Office of Naval Research, Arlington, VA  
Andrew Sessler, Lawrence Berkeley Laboratory, Berkeley, CA  
Charles Brau, Vanderbilt University, Nashville, TN  
Avi Gover, Tel Aviv University, Tel Aviv, Israel  
John Madey, Duke University, Durham, NC  
J. Ortega, LURE, Orsay, Cedix, France  
Michael Pode, Daresbury Nuclear Physics Lab., UK  
A. Renieri, E.N.E.A., Rome, Italy  
T. Smith, TRW, Redondo Beach, CA  
Phillip Sprangle, NRL, Washington, DC  
M.J. van der Wiel, FOM-Institute, The Netherlands

# TABLE OF CONTENTS

<b>KEYNOTE ADDRESS, STATUS OF FEL TECHNOLOGY, J. Madey</b>	2
<b>PR1.1 A SYNOPSIS OF RESEARCH AT THE DUKE FEL LABORATORY, S.V. Benson, J.M.J. Madey, and R.I. McCormick.</b>	5
<b>PR1.2 PROGRAM TO GENERATE INTENSE FEL BY INDUCTION LINAC AT ILT/LE OSAKA UNIVERSITY, K. Imasaki, T. Akiba, K. Mima, S. Kuruma, N. Ohigashi, Y. Tsunawaki, S. Nakai, and C. Yamanaka, Y. Kitagawa, K. Sawai, M. Miyamoto, H. Yoshioka, H. Ohtani, T. Matsumoto.</b>	7
<b>PR1.3 THE LISA PROJECT IN FRASCATI INFN LABORATORIES, M. Castellano, A. Ghigo, P. Patteri, F. Tazzioli, F. Ciocci, G. Dattoli, A. Dipace, G.P. Gallerar.o, A. Renieri, E. Sabia, A. Torre, N. Cavallo, F. Cevenini.</b>	9
<b>PR1.4 DELTA, A NEW STORAGE-RING FEL FACILITY AT THE UNIVERSITY OF DORTMUND, D. Nolle, F. Brinker, M. Negrazus, D. Schirmer, K. Wille.</b>	11
<b>TH1.3 ENHANCEMENT OF THE FREE ELECTRON COHERENT HARMONIC GENERATION BY USE OF THE DISPERSIVE FUNCTION ON A STORAGE RING, R. Prazères, J.M. Ortega.</b>	13
<b>TH1.5 ANGULAR STEERING OF THE FEL FAR-FIELD RADIATION BEAM, E. Jerby.</b>	15
<b>RE1.1 ON-AXIS HOLES IN INTERFEROMETER MIRRORS, J. Feinstein, A.H. Ho, R.H. Pantell.</b>	18
<b>RE1.2 MODE CONTROL ON SHORT-PULSE FELS USING A MICHELSON-MIRROR RESONATOR, E.B. Szarmes, S.V. Benson, and J.M.J. Madey.</b>	20
<b>RE1.3 RESONATOR MODES IN HIGH GAIN FREE ELECTRON LASERS, X. Ming, D. A.G. Deacon, J.M.J. Madey.</b>	23
<b>RE1.4 MEASUREMENTS OF UV INDUCED ABSORPTION IN DIELECTRIC COATINGS, D.A.G. Deacon, M.H. Bakshi, M. Cecere, A.M. Fauchet.</b>	25
<b>RE1.5 FAR INFRARED QUASI-OPTICAL RESONATOR FOR CERENKOV FREE ELECTRON LASER, F. Ciocci, G. Dattoli, A. De Angelis, A. Dipace, A. Doria, G.P. Gallerano, M.F. Kimmitt, A. Renieri, E. Sabia, A. Torre and J.E. Walsh.</b>	27
<b>P1.1 THE INDUCTION FEL DESIGN FOR WHITE SANDS MISSILE RANGE, G.R. Neil, J.A. Edighoffer, J.M. Rawls, P. Livingston.</b>	29
<b>P1.2 OPTIMAL BASIS EXPANSION FOR SOLVING TIME DEPENDENT SCHRÖDINGER EQUATION: SIMULATION OF GUIDING AND MULTIMODE MECHANISMS, D. Iracane, J.L. Ferrer.</b>	31
<b>P1.3 THEORY OF HARMONIC RADIATION USING A SINGLE-ELECTRON SOURCE MODEL, M.J. Schmitt and C.J. Elliott.</b>	33
<b>P1.5 A DEMONSTRATION OF LOSS MODULATION AND CAVITY DUMPING IN A FREE-ELECTRON LASER OSCILLATOR, S. V. Benson, J.M.J. Madey, E.B. Szarmes, P. Metty, M. Curtin, A. Bhowmik and J. Brown.</b>	36
<b>P1.8 IS IT NECESSARY TO ASSUME A NEUTRALIZING UNIFORM BACKGROUND WHEN DEVELOPING A THEORY FOR THE FEL IN THE COLLECTIVE REGIME? A. Bourdier, J.M. Buzzi.</b>	39

<b>P1.9 A MODIFIED TWISS PARAMETER OPTICAL TREATMENT FOR SPACE CHARGE DOMINATED ELECTROSTATIC ACCELERATOR FREE ELECTRON LASERS, D.J. Larson.</b>	41
<b>P1.10 THREE-DIMENSIONAL SIMULATION OF FREE-ELECTRON LASER HARMONICS WITH FRED, W.M. Sharp, E.T. Scharlemann, and W.M. Fawley.</b>	43
<b>P1.11 A EXPERIMENTAL STUDY OF A SHIELDED PULSED ELECTROMAGNET WIGGLER CONCEPT, C. Zhou, M. Wang.</b>	45
<b>P1.12 LASING ON THE THIRD HARMONIC, R.W. Warren, L.C. Haynes, D.W. Feldman, W.E. Stein and S.J. Gitomer.</b>	46
<b>P1.13 ELECTRON-BEAM QUALITY DEGRADATION IN A LONG UNDULATOR, H. Takeda and L.E. Thode.</b>	48
<b>P1.14 SIMULATIONS ON INVERSE ACCELERATOR AND HARMONIC GENERATION, K. Mima, K. Ohi, N. Ohigashi, S. Kuruma and S. Nakai.</b>	50
<b>P1.15 STABLE-UNSTABLE RESONATOR FOR FREE-ELECTRON LASERS WITH A STEPPED GRATING FOR SIDEBAND SUPPRESSION, A.H. Paxton, M.J. Schmitt.</b>	52
<b>P1.16 FREQUENCY-TUNABLE, HIGH POWER MICROWAVE EMISSION FROM CYCLOTRON AUTORESONANCE MASER OSCILLATORS DRIVEN BY MICROSECOND, INTENSE ELECTRON BEAMS, R.M. Gilgenbach, J.G. Wang, J. Choi, C.A. Outten, and T. Spencer.</b>	54
<b>P1.17 SPIKE RADIATION FROM THE COLUMBIA FEL, J.W. Dodd and T.C. Marshall.</b>	56
<b>P1.18 INTERPRETATION OF FEL GAIN AND MAGNETIC FIELD ERRORS ON THE SCA/FEL, R. Rohatgi and J.C. Frisch.</b>	58
<b>P1.19 COMPUTER SIMULATIONS OF A 100 GHz CARM OSCILLATOR WITH BRAGG REFLECTORS, T.H. Kho and A.T. Lin.</b>	60
<b>P1.20 PROGRESS REPORT ON BEIJING FEL PROJECT, J. Xie, J. Zhuang, Y. Wang, S. Zhong, R. Ying, C. Mao.</b>	62
<b>P1.21 THE VARIABLE DISPERSION ELECTRON SPECTROMETER AT THE SCA/FEL, R.L. Swent, J.C. Frisch and T.I. Smith.</b>	64
<b>P1.22 COMPARATIVE ANALYSIS OF OPTICAL TRANSITION RADIATION BASED ELECTRON BEAM EMITTANCE MEASUREMENTS FOR THE LOS ALAMOS FREE-ELECTRON LASER, D.W. Rule, R.B. Fiorito, A.H. Lumpkin, R.B. Feldman and B.E. Carlsten.</b>	66
<b>P1.24 DESIGN OF A HIGH FIELD TAPERABLE HELICAL WIGGLER, J. Vetrovec.</b>	68
<b>P1.25 OPTICAL KLYSTRON CONFIGURATION FOR A HIGH GAIN X-RAY FREE ELECTRON LASER, J. C. Gallardo and C. Pellegrini.</b>	70
<b>P1.26 ANALYTICAL TREATMENT OF ELECTRON TRAJECTORY STRAIGHTNER ISSUES IN FREE-ELECTRON LASERS, C.J. Elliott and D.C. Quimby.</b>	73
<b>P1.31 A PROPOSED FEL INJECTOR AT IAE, X. Zhai, W. Zhou, Z. Weng, T. Wu, C. Liu, Y. Lu, X. Shi, T. Yang.</b>	76
<b>P1.32 FULLY AUTOMATIC WIGGLER-FIELD TEST AND CORRECTION, R.B. Feldman and R.W. Warren.</b>	78

<b>P1.33 TIME DEPENDENT MEASUREMENTS ON THE STANFORD SCA/FEL</b> , J.C. Frisch, J.E. Edighoffer.	80
<b>P1.34 STABILITY REQUIREMENTS FOR RF LINAC-DRIVEN FREE-ELECTRON LASERS</b> , W.E. Stein, W.J.D. Johnson, J.F. Power, and T.J. Russell.	82
<b>P1.35 NONCOLLINEAR FEL AND INVERSE FEL SCHEMES</b> , A.A. Varfolomeev, Y.Y. Lachin.	84
<b>P1.36 DEVELOPMENT OF A HYBRID PERMANENT MAGNET UNDULATOR PROTOTYPE FOR FREE ELECTRON LASERS</b> , F. Rosatelli, L. Barbagelata, A. Matrone, G. Ottonello, P. Prati, D. Tommasini, F. Ciocci, A. Renieri, E. Sabia.	86
<b>EX1.1 FREE ELECTRON LASER OSCILLATION ON THE SUPER-ACO STORAGE RING AT ORSAY</b> , M.E. Couprie, C. Bazin, J.M. Ortega, R. Prazères, M. Velghe, Y. Petroff and M. Billardon.	91
<b>EX1.2 A REVIEW OF THE STANFORD MARK III INFRARED FEL PROGRAM</b> , S.V. Benson, W.S. Fann, B.A. Hooper, J.M.J. Madey, E.B. Szarmes, B. Richman, L. Vintro.	93
<b>EX1.4 INITIAL RESULTS FROM THE FREE-ELECTRON LASER MASTER OSCILLATOR/POWER AMPLIFIER EXPERIMENT</b> , A. Bhowmik, M. S. Curtin, and W.A. McMullin, S.V. Benson, J.M.J. Madey, B.A. Richman, and L. Vintro.	96
<b>EX1.5 PALADIN OPERATION WITH A 25-M-LONG WIGGLER</b> , T.J. Orzechowski, J.L. Miller, F.W. Chambers, Y.P. Chong, J. Edighoffer, P. Lee, D. Prosnitz, E.T. Scharlemann, and J.T. Weir.	98
<b>UN1.1 WORKSHOP RESULTS ON SMALL-PERIOD WIGGLER DESIGNS</b> , R.L. Sheffield, J.H. Booske, R.W. Warren, K. Halbach, B. Danly, R.H. Jackson, P. Walstrom, J. Slater, and A. Toor.	100
<b>UN1.2 PULSED-COIL MICROWIGGLERS</b> , R.W. Warren, D.W. Feldman, D. Preston.	104
<b>UN1.3 MICROUNDULATOR FIELDS</b> , I. Kimel, L.R. Elias.	106
<b>UN1.4 IN SEARCH OF A MEANINGFUL FIELD ERROR SPEC FOR WIGGLERS</b> , B. Bobbs, G. Rakowsky, P. Kennedy, R. Cover and D. Slater.	108
<b>UN1.5 WIGGLER ERROR REDUCTION THROUGH SHIM TUNING</b> , S.C. Gottschalk, J.M. Slater, D.C. Quimby, K.E. Robisonson.	110
<b>UN1.6 DISPERSION INTERFERENCE IN THE PULSED WIRE MEASUREMENT METHOD</b> , O. Shahal, B.V. Elkonin, J.S. Sokolowski.	112
<b>PR2.2 STATUS AND RESEARCH OBJECTIVES OF THE DUTCH FREE ELECTRON LASER FOR INFRARED EXPERIMENTS</b> , P.W. van Amersfoort, R.W.B. Best, R. van Buuren, P.F.M. Delmee, B. Faatz, C.A.J. van der Geer, D.A. Jaroszynski, P. Manintveld, W.J. Mastop, B.J.H. Meddens, A.F.G. van der Meer, D. Oepts, J. Pluygers, and M.J. van der Wiel.	114
<b>PR2.3 A MICROWIGGLER FREE-ELECTRON LASER AT THE BROOKHAVEN ACCELERATOR TEST FACILITY</b> , K. Batchelor, I. Ben-Zvi, R. Fernow, J. Gallardo, H. Kirk, C. Pellegrini, A. van Steenbergen, A. Bhowmik.	116
<b>P2.1 NUMERICAL TREATMENT OF ELECTRON TRAJECTORY STRAIGHTENER ISSUES IN FREE-ELECTRON LASERS</b> , D.C. Quimby, C.J. Elliott.	118
<b>P2.3 THE HYBRID UNDULATOR FOR THE NIST-NRL FREE-ELECTRON LASER</b> , R.G. Johnson, D.L. Mohr, M.A. Wilson, S. Penner, F.C. Younger, B. Ng, and K.M. Thomas.	120
<b>P2.4 INEX SIMULATIONS OF THE LOS ALAMOS HIBAF FREE-ELECTRON LASER MOPA EXPERIMENT</b> , J.C. Goldstein, B.E. Carlsen and B.D. McVey.	122

<b>P2.5 BEAM PROFILE AND POSITION DIAGNOSTIC IN THE ADVANCED TEST ACCELERATOR (ATA) PALADIN FEL EXPERIMENT, Y.P. Chong, P. Lee, T.J. Orzechowski, J.L. Miller, J.T. Weir.</b>	124
<b>P2.7 PAPA - A PARTICLE TRACING CODE IN PASCAL, E.H. Haselhoff, and G.J. Ernst.</b>	126
<b>P2.10 HIGHER-POWER FREE-ELECTRON LASERS, S. Johnston.</b>	128
<b>P2.11 STATUS AND DESIGN OF THE NRL IREC MASER EXPERIMENT, A.W. Fliflet, R.B. McCowan, W.M. Manheimer, and P. Sprangle.</b>	130
<b>P2.13 THE INVESTIGATION OF AN OPTICAL KLYSTRON, V.L. Granatstein, B. Levush, M.C. Wang.</b>	132
<b>P2.14 HIGH PERFORMANCE PURE PERMANENT MAGNET UNDULATORS, G. Rakowsky, B. Bobbs, W. McMullin, G. Swoyer, R. Burke.</b>	135
<b>P2.16 OPTICAL RESONATOR FOR THE NIST-NRL FREE ELECTRON LASER, B. C. Johnson, R.G. Johnson, D.L. Mohr, and M.S. Price.</b>	137
<b>P2.17 APPLICATIONS OF HARMONIC GENERATION OF PICOSECOND PULSES FROM A FREE ELECTRON LASER, B.A. Hooper, S.V. Benson, R.C. Straight, and J.M.J. Madey.</b>	139
<b>P2.19 DIRECT SPECTRAL MEASUREMENTS OF THE UCSB FEL, G. Ramian and J. Hu, S.G. Evangelides, T.S. Chu, B.G. Danly, R.J. Temkin, and T.G. Sollner.</b>	142
<b>P2.20 TECHNOLOGICAL REQUIREMENTS FOR A CONTINUOUS WAVE FREE ELECTRON LASER, D.J. Larson.</b>	144
<b>P2.24 A MICRO-FABRICATION COMPATIBLE WIGGLER DESIGN SCALABLE TO SUB-MILLIMETER PERIODS, R.H. Jackson, H. Bluem.</b>	146
<b>P2.25 FEL PERFORMANCE WITH PURE PERMANENT MAGNET UNDULATORS HAVING OPTIMIZED ORDERING, R.A. Cover, B.L. Bobbs, G. Rakowsky, S.P. Mills.</b>	148
<b>P2.26 INITIAL RESULTS OF OPERATING THE ROCKETDYNE UNDULATOR IN A TAPERED CONFIGURATION, M. Curtin, A. Bhowmik, J. Brown, W. McMullin, P. Metty, S. Benson and J.M.J. Madey.</b>	150
<b>P2.27 FUNDAMENTAL MODE AMPLIFIER PERFORMANCE OF THE NRL UBITRON, D.E. Pershing, H. Bluem, H.P. Freund, R.H. Jackson.</b>	152
<b>P2.28 STUDY OF LISA FEL OPERATION WITH PREBUNCHED BEAM, M. Castellano, A. Ghigo, P. Patteri.</b>	154
<b>P2.29 A PROPOSED FIR-IR METAL-GRATING FEL EXPERIMENT, J. Walsh, E. Fisch, E. Marshall, E. Price, M. Kimmitt, G.P. Gallerano, A. Doria, A. Renieri, Y. Xu.</b>	156
<b>P2.30 PROSPECTS FOR A SOFT X-RAY FEL POWERED BY A RELATIVISTIC KLYSTRON-HIGH GRADIENT ACCELERATOR (RK-HGA) H.D. Shay, W.A. Barletta, S.S. Yu, E.T. Scharlemann, R. Schlueter, and G.A. Deis.</b>	158
<b>P2.31 DESIGN OF A HIGH-CURRENT INJECTOR FOR THE NIST-NRL FREE ELECTRON LASER, R.I. Cutler and E.R. Lindstrom, S. Penner.</b>	160
<b>P2.32 TWEL - A HYBRID TWT/FEL INTERACTION, E. Jerby.</b>	162

<b>P2.34 STATUS OF THE AERIFEL SYSTEM</b> , M. Ohkubo, M. Sugimoto, M. Sawamura, K. Mashiko, E. Minehara, M. Takabe, J. Sasabe and Y. Kawarasaki.	165
<b>P2.35 ENERGY MEASUREMENT OF THE ELECTRON BEAM BEYOND THE PALADIN WIGGLER</b> , J. Edighoffer, Y.P. Chong, P. Lee, T.J. Orzechowski, A.C. Paul, T. Smith, and J.T. Weir.	166
<b>EX2.1 THE NIST-NRL FREE-ELECTRON LASER FACILITY</b> , R.G. Johnson, R.L. Ayres, J.B. Broberg, R.I. Cutler, P.H. Debenham, B.C. Johnson, E.R. Lindstrom, D.L. Mohr, J.E. Rose, J.K. Whittaker, N.D. Wilkin, and M.A. Wilson, S. Penner, C.M. Tang, P. Sprangle.	169
<b>EX2.2 SCA/FEL STATUS</b> , J.C. Frisch, R. Rohatgi, H.A. Schwettman, T.I. Smith and R.L. Swent.	173
<b>EX2.3 CYCLOTRON AUTORESONANCE MASER EXPERIMENTS</b> , A. DiRienzo, G. Bekefi, C. Leibovitch, B. Danly.	175
<b>EX2.4 BANDWIDTH NARROWING BY SEED INJECTION OF A FREE-ELECTRON LASER</b> , A. Amir, J. F. Knox-Seith, M. Warden.	177
<b>EX2.5 140 GHZ MICROWAVE EXPERIMENTS IN ELF-II</b> , A.L. Throop, R.A. Jong, D.P. Atkinson, J.C. Clark, B. Felker, S.W. Ferguson, W.E. Nexsen, B.W. Stallard, W.C. Turner, M.A. Makowski.	184
<b>TH2.2 ANALYTICAL STUDY OF MULTIMODE COMPETITION</b> , I. Kimel and L. R. Elias.	186
<b>TH2.4 ANOMALOUS (STIMULATED) REFRACTION INDUCED BY THE FREE-ELECTRON LASER INTERACTION</b> , F. Hartemann and G. Mourier.	188
<b>AC1.2 ACCELERATOR DESIGN AND CALCULATED PERFORMANCE OF THE LOS ALAMOS HIBAF FACILITY</b> , B.E. Carlsten, L.M. Young, M.E. Jones, B. Blind, E.M. Svaton, K.C. D. Chan, and L.E. Thode.	190
<b>AC1.3 A DEVELOPMENT OF A TANDEM ELECTROSTATIC ACCELERATOR QUASI-CW FEL</b> , I. Ben-Zvi, B.V. Elkonin, A. Fruchtmann, J.S. Sokolowski, A. Gover, E. Jerby and H. Kleinman, B. Mandelbaum, A. Rosenberg, J. Shiloh, G. Hazak, O. Shahal.	192
<b>P3.1 MODE STABILITY IN A SHEET-BEAM FREE ELECTRON LASER WITH SIDE-WALLS</b> , T.M. Antonsen, Jr. and E. R. Stanford.	194
<b>P3.2 RESONATOR MODE MATCHING FOR FREE ELECTRON LASER (FEL) OPTICAL GUIDING</b> , K.C. Sun, B.D. McVey, and R.L. Tokar.	196
<b>P3.3 THREE-DIMENSIONAL SIMULATIONS OF SIDEBAND IN A MILLIMETER-WAVE FREE ELECTRON LASER</b> , Z. Yang, S. Tian, Y. Jiang.	198
<b>P3.4 DEVELOPMENTS IN ON-LINE, ELECTRON BEAM EMITTANCE MEASUREMENTS USING OPTICAL TRANSITION RADIATION TECHNIQUES</b> , R.B. Feldman, A. H. Lumpkin, D.W. Rule, R.B. Fiorito.	200
<b>P3.5 OPTICAL DESIGN AND PERFORMANCE OF AN XUV FEL OSCILLATOR</b> , J.C. Goldstein, B.D. McVey, and B.E. Newnam.	202
<b>P3.6 ANHARMONIC BETATRON MOTION IN FREE ELECTRON LASERS</b> , J.J. Barnard.	204

<b>P3.7 STATISTICAL VARIATION OF FEL PERFORMANCE DUE TO WIGGLER FIELD ERRORS</b> , P. Kennedy, B. Bobbs, G. Rakowsky, and R. Cover.	206
<b>P3.8 MINIMIZED EMITTANCE GROWTH WITH ELLIPTICAL BEAM PIPES IN FEL</b> , K.C.D. Chan.	208
<b>P3.9 PULSE COMPRESSION ON THE MARK III FEL USING ENERGY CHIRPING</b> , E.B. Szarmes, S.V. Benson, and J.M.J. Madey.	210
<b>P3.11 SPECIFIC OPTICAL PROPERTIES OF MULTILAYER MIRRORS FOR S.R. FEL EXPERIMENTS</b> , M.F. Velghe, M.E. Couprie, M. Billardon.	215
<b>P3.12 NUMERICAL STUDIES ON MODE COMPETITION IN LONG-PULSE FELS.</b> , R. Hajima, H. Ohashi and S. Kondo.	217
<b>P3.13 CONSEQUENCES OF SHORT ELECTRON BEAM PULSES IN THE FELIX PROJECT</b> , D.A. Jaroszynski, D. Oepts, A.F.G. van der Meer, P.W. van Amersfoort, W.B. Colson.	219
<b>P3.14 PARAMAGNETIC AND DIAMAGNETIC CORRECTIONS TO THE ELECTRON DYNAMICS IN A FREE-ELECTRON LASER WITH GUIDE FIELD</b> , F. Hartemann.	222
<b>P3.15 DESIGN OF A 12 MEV RECIRCULATING BEAM ELECTROSTATIC ACCELERATOR FEL</b> , D.J. Larson and L.R. Elias.	224
<b>P3.16 A COMPARISON OF THEORY AND EXPERIMENT IN AN ALL FEL MASTER OSCILLATOR/POWER AMPLIFIER SYSTEM</b> , S.V. Benson, J.M.J. Madey, B. Richman, L. Vintro, A. Bhowmik, W. McMullin.	226
<b>P3.17 COMPUTER SIMULATION OF CATHODE HEATING BY BACK BOMBARDMENT IN THE MICROWAVE ELECTRON GUN</b> , C.B. McKee and J.M.J. Madey.	230
<b>P3.18 THE ETA-II INDUCTION LINAC AS A HIGH AVERAGE POWER FEL DRIVER</b> , W.E. Nexsen, D.P. Atkinson, D.M. Barrett, Y.C. Chen, J.C. Clark, L.V. Griffith, H.C. Kirbie, M.A. Newton, A.C. Paul, S. Sampayan, A.L. Throop, W.C. Turner.	235
<b>P3.19 FINAL DESIGN AND COLD TESTS FOR A HARMONIC UBITRON AMPLIFIER EXPERIMENT</b> , H. Bluem, R.H. Jackson, D.E. Pershing, J.H. Booske, V.L. Granatstein.	237
<b>P3.20 ONDINE: STUDIES ABOUT A HIGH POWER MICROWAVE, FEL AT C.E.S.T.A.</b> , H. Bottollier-Curtet, J. Bardy, C. Bonnafond, C. Bruno, J. Delvaux, A. Devin, P. Eyl, J. Gardelle, G. Germain, J. Labrousche, J. Launspach, P. Le Taillandier, and G. Pitel.	239
<b>P3.21 INTERACTION BETWEEN A RELATIVISTIC ELECTRON BEAM AND A RELATIVISTICALLY STRONG ELECTROMAGNETIC PUMP WAVE</b> , A. Bourdier, J.M. Buzzi.	241
<b>P3.22 GAS LOADED FEL AT <math>\lambda = 600 \text{ \AA}</math></b> , M. Özcan, R.H. Pantell, J. Feinstein, A. Ho, H.D. Dulman.	243
<b>P3.23 MICROWIGGLER FREE ELECTRON LASER EXPERIMENT</b> , S.C. Chen, G. Bekefi, R. Stoner.	245
<b>P3.25 MICRO-UNDULATOR RESEARCH AT UCSB</b> , K. P. Paulson.	248



<b>P3.26 LELIA: INDUCTION ACCELERATOR STUDIES FOR HIGH PEAK POWER FEL APPLICATION AT THE CENTRE D'ETUDES SCIENTIFIQUES ET TECHNIQUES D'AQUITAINE (C.E.S.T.A),</b> J. Launspach, J.M. Angles, M. Angles, P. Anthouard, J. Bardy, C. Bonnafond, H. Bottollier-Curtet, G. Bouquet, C. Bruno, J. Delvaux, A. Devin, P. Eyharts, P. Eyl, J. Gardelle, G. Germain, J. Labrousche, P. Le Taillandier, Y. Prenveille, W. Stadnikoff, and M. Thevenot.	250
<b>P3.29 STUDIES ABOUT APPLICATION OF FREE ELECTRON LASER TO INERTIAL CONFINEMENT FUSION,</b> K. Imasaki, T. Yamanaka, K. Mima, S. Kuruma, S. Nakai, C. Yamanaka, T. Akiba, K. Ohi.	252
<b>P3.31 COMPACT RF LINAC FREE-ELECTRON LASERS,</b> R.L. Sheffield, R.W. Warren, B.E. Carlsten, and J.C. Goldstein.	254
<b>P3.34 THE IMPACT OF FIELD ERROR REDUCTION TECHNIQUES ON FEL PERFORMANCE,</b> W.P. Marable, E. Esarey and C.M. Tang.	256
<b>P3.36 WAVEGUIDE EFFECTS IN SUPERRADIANT FREE-ELECTRON LASERS,</b> W.M. Sharp and S.S. Yu.	258
<b>EX3.2 HARMONIC GENERATION - STRENGTH AND MODE SHAPE,</b> B.E. Newman, R.W. Warren, D.W. Feldman and W.E. Stein.	261
<b>EX3.3 THE LOS ALAMOS HIGH-BRIGHTNESS ACCELERATOR FEL (HIBAF),</b> W.D. Cornelius, S. Bender, K. Meier, L.E. Thode and J.M. Watson.	263
<b>EX3.4 FIRST DEMONSTRATION OF A FREE-ELECTRON LASER DRIVEN BY ELECTRONS FROM A LASER IRRADIATED PHOTOCATHODE,</b> M. Curtin, G. Bennett and R. Burke, S. Benson, J.M.J. Madey, A. Bhowmik, P. Metty.	265
<b>EX3.5 INEX APPLIED TO THE BOEING AEROSPACE FEL SYSTEM,</b> R.L. Tokar, L.M. Young, B.D. McVey, L.E. Thode, A. H. Lumpkin, K.D. Chan, A.D. Yeremian, D.H. Dowell, A.R. Lowrey, S.C. Bender and R. Justice.	267
<b>TH3.1 CURRENT RESEARCH IN FEL THEORY,</b> E.T. Scharlemann.	269
<b>TH3.2 TRANSVERSE AND PARALLEL BEAM QUALITY IN FREE-ELECTRON LASERS,</b> C.W. Roberson, B. Hafizi.	273
<b>TH3.4 EQUILIBRIUM SELF-FIELD-INDUCED CHAOS IN ELECTRON ORBITS IN FREE ELECTRON LASERS,</b> C. Chen and R.C. Davidson.	276
<b>PR3.1 OBELIX - THE OXFORD FREE ELECTRON LASER PROJECT,</b> W.W.M. Allison, C.A. Brau, C.B. Brooks, G. Doucas, W.A. Gillespie, A.R. Holmes, D.A. Jaroszynski, M.F. Kimmitt, P.F. Martin, J.H. Mulvey, C.R. Pidgeon, M.W. Poole, J.N. Elgin.	278
<b>PR3.2 A NOVEL WIGGLER DESIGN FOR USE IN A HIGH-EFFICIENCY FREE-ELECTRON LASER,</b> J. Feinstein, A.H. Ho, R.H. Pantell.	280
<b>PR3.3 STATUS REPORT ON THE LOW-FREQUENCY PHOTO-INJECTOR AND ON THE INFRARED-FEL EXPERIMENT (ELSA),</b> R. Deica.	282
<b>EX4.1 CONFIRMATION OF SINGLE MODE FEL OPERATION,</b> L.R. Elias, I. Kimel.	285
<b>EX4.2 A REVIEW OF OPTICAL GUIDING EXPERIMENTS DONE WITH THE COLUMBIA FEL,</b> T.C. Marshall, A. Bhattacharjee, S.Y. Cai, S.P. Chang, J.W. Dodd.	287
<b>EX4.3 HARMONIC GENERATION EXPERIMENTS ON THE MARK III FREE ELECTRON LASER,</b> D.J. Bamford and D.A.G. Deacon.	289
<b>EX4.5 RECENT RESULTS OF THE ENEA-FRASCATI UNDULATOR FEL EXPERIMENT,</b> F. Ciocci, G. Dattoli, A. De Angelis, A. Dipace, A. Doria, G.P. Gallorano, L. Giannessi, A. Renieri, E. Sabia, A. Torre, D. Jaroszynski.	291

<b>AP1.1 17.1 GHz FREE-ELECTRON LASER AS A MICROWAVE SOURCE FOR TeV COLLIDERS</b> , R.A. Jong, R.D. Ryne, G.A. Westenskow, S.S. Yu, D.B. Hopkins, A.M. Sessler.	293
<b>AP1.2 CURRENT APPLICATIONS USING THE UCSB FREE-ELECTRON LASER</b> , J. Kaminski.	297
<b>AP1.3 APPLICATIONS OF INFRARED FEL IN PICOSECOND AND NONLINEAR OPTICAL SPECTROSCOPIES</b> , W.S. Fann, S. Benson, J.M.J. Madey, S. Etemad, G.L. Baker, L. Rothberg, M. Roberson and R.A. Austin.	299
<b>AP1.5 HIGH AVERAGE POWER CW FREE ELECTRON LASERS FOR APPLICATION TO PLASMA HEATING: DESIGNS AND EXPERIMENTS</b> , J.H. Booske, V.L. Granatstein, T.M. Antonsen, Jr., S. Bidwell, Y. Carmel, W.W. Destler, P.E. Latham, B. Levush, I.D. Mayergoyz, D.J. Radack, Z.X. Zhang, H.P. Freund.	
<b>PLENARY PAPER VEPP-3 STORAGE RING OPTICAL KLYSTRON: LASING IN VISIBLE AND ULTRAVIOLET REGIONS</b> , G.N. Kulipanou, V.N. Litvinenko, I.V. Pinayev, V.M. Popik, A.N. Skrinsky, A.S. Sokolov and N.A. Vinokurov.	303
<b>POST DEADLINE PAPERS</b>	306
<b>PD.3 NEW FEATURES IN WEAK-FIELD AND STRONG-FIELD FELS</b> , W.B. Colson.	
<b>PD.7 OPERATION OF THE MIT/SRL 1.2 MeV ALL-SOLID-STATE INDUCTION LINAC</b> , D. Goodman, D. Bix, D. Clarke, R. Klinkowstein, R. Shefer, W. Menninger, B. Danly, R. Temkin.	312
	314

**MONDAY, AUGUST 28**

# Keynote Address

## STATUS OF FEL TECHNOLOGY

John Madey  
Duke University  
Durham, NC

- ⇒ The Nature of the FEL Revolution
- ⇒ Present Research Directions
- ⇒ Accomplishments in 1989
- ⇒ How to Proceed in an Indifferent and Chaotic World

### THE NATURE OF THE REVOLUTION:

The FEL is a revolutionary means to convert electrical energy to light offering the potential for:

- ⇒ High Power
- ⇒ High Efficiency
- ⇒ Elimination of the Limits to Wavelength and Tuneability
- ⇒ Precise Control of Pulse Length and Pulse Structure
- ⇒ Diffraction-limited Mode Quality
- ⇒ High Reliability

### PRIOR REVOLUTIONS

⇒ Conversion of Thermal Energy to Mechanical Energy:

- the steam engine
- the internal combustion engine
- the gas turbine engine

⇒ Conversion of Mechanical Energy to Electricity, and the Control Thereof

⇒ Conversion of Electricity to Radio and Microwave Energy, and the Control Thereof

## EFFECTS OF PRIOR DEVELOPMENTS ON CIVILIZATION

### ⇒ Production, Distribution and Services:

- Large Scale Manufacturing
- Modern Agriculture
- Road, Rail, Ocean and Air Transportation
- Central Power Distribution Systems
- Public Education
- Medical Care
- National Defense

### ⇒ Management:

- Long Distance Communications
- Acquisition and Analysis of Data
- Coordination and Control of Production, Distribution, and Services

### ⇒ Research:

- Development of Advanced Materials, Devices, and Systems
- Enhancement of Efficiency of Existing Processes and Reduction of Pollution
- Extension of Life, and the Improvement of the Quality of Life

## POSSIBLE IMPACT OF FELS

### ⇒ Production, Distribution and Services:

- industrial-scale photochemistry
- fabrication of advanced electronic devices
- space power transmission
- ballistic missile defense
- surgical and diagnostic procedures

### ⇒ Research:

- development and characterization of advanced materials and devices
- Enhancement of efficiency of existing thermal and chemical processes
- Biomedical Research and the development of more effective clinical procedures

### ⇒ Management:

- remote acquisition of atmospheric and geochemical data

## GENERAL DIRECTIONS OF PRESENT FEL RESEARCH

- ⇒ Short Wavelength Operation
- ⇒ Long Wavelength Operation
- ⇒ High Efficiency Operation
- ⇒ Technology Integration
- ⇒ Research Applications

### 1989 RESEARCH ACCOMPLISHMENTS

#### Short Wavelength Operation:

- ⇒ Novosibirsk
- ⇒ Orsay

#### Long Wavelength Operation:

- ⇒ UCSB

#### High Efficiency Operation:

- ⇒ Livermore/TRW
- ⇒ Los Alamos/Boeing

#### Technology Integration:

- ⇒ Boeing/Los Alamos
- ⇒ Rocketdyne/Duke

#### Research Applications:

- ⇒ Duke
- ⇒ Stanford
- ⇒ UCSB

### HOW TO PROCEED IN AN INDIFFERENT AND CHAOTIC WORLD

#### Frustrations of a Revolutionary:

- ⇒ ignorance
- ⇒ indifference
- ⇒ opposition

#### Solutions ( from G. Washington, B. Franklin and others ) :

- ⇒ work to help the people who need you
- ⇒ operate from a base which will support a long term effort
- ⇒ emphasize responsiveness

## PR1.1

### A Synopsis Of Research At The Duke FEL Laboratory

S.V. Benson, J.M.J. Madey and R.I. McCormick  
Department of Physics, Duke University, Durham, NC

Existing accelerator technology has the capability to support the operation of a wide range of short wavelength, high peak power FEL light sources.

We have focused at Duke on the exploitation of RF linac and storage ring technology to develop FEL systems for research in device physics, laser technology, and the basic physical and medical sciences.

#### OUTLINE

#### FELs at Duke

- FELs at Duke
  - Other Experimental Opportunities
  - Facilities Development
  - University Contributions
  - Facilities Description
  - Remaining Obstacles
- MKIII FEL
  - 1 GeV Linac and Storage Ring
  - Other FELs

#### University Contributions

#### Other Experimental Opportunities

- Synchrotron Radiation
  - Detector Metrology
  - Radiation Damage Studies
  - Light Isotope Production
- Departmental Enthusiasm
  - Faculty/Trustees Support
  - Staff Assistance
  - \$4.6 million

### Facilities Description

- Feb 88 - Remove 4 MeV Accelerator
- Jul 88 - Preliminary Design
- Nov 88 - Required Demolition
- Jun 89 - Detailed Design
- Aug 89 - Transformer Installation
- Oct 89 - Control Room
- Nov 89 - Electrical Installation
- Jun 90 - Shielding

### Summary

- New Facility Unique
  - Originally Designed for Purpose
  - Tunnel Safer, More Efficient
  - Room for Significant Expansion
- MK III Facility Proceeding More Slowly
- Opportunities for Collaboration with Large and Diverse Community

### Facilities Development (New Lab)

- Jan 88 - Preliminary Estimates
- Apr 88 - Architects Selected
- Aug 88 - Programmatic Design
- Apr 89 - Detailed Design
- May 89 - Bids Requested
- Jun 89 - Bids Received
- Aug 89 - Start Construction
- Feb 90 - Partial Occupancy
- Nov 90 - Completion

### Obstacles

- New Building
  - Weather
  - Regulatory/ Other Guidance
- MK III Facility
  - Shielding
  - Funding



## PR1.2

### Program to Generate Intense FEL by Induction Linac at ILT/ILE Osaka University

K. Imasaki, T. Akiba\*, K. Mima\*, Y. Kitagawa\*, K. Sawai\*, S. Kuruma, M. Miyamoto\*, H. Yoshioka\*, H. Ohtani\*, T. Matsumoto\*, N. Ohigashi\*\*, Y. Tsunawaki\*\*\*, S. Nakai\* and C. Yamanaka

Institute for Laser Technology

\*Institute of Laser Engineering, Osaka University, Suita, Osaka, JAPAN

\*\*Faculty of Engineering, Kansai University, Suita, Osaka, JAPAN

\*\*\*Faculty of Engineering, Osaka Industrial, Daito, Osaka, JAPAN

#### Abstract

Effort has been made to build free electron laser system with high power output. Induction linac whose designed parameter was 9 MeV, 3 kA with 100 ns pulse duration was completed.

Experiments for beam transport and beam injection into wiggler magnet system were studied. Oscillation and amplification experiments on the wavelength of submillimeter are underway.

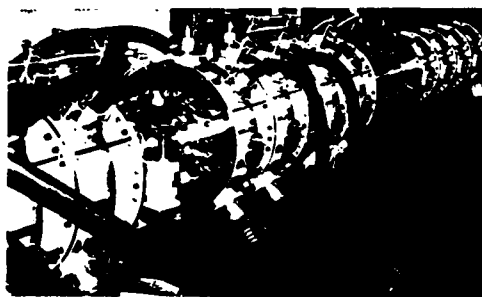
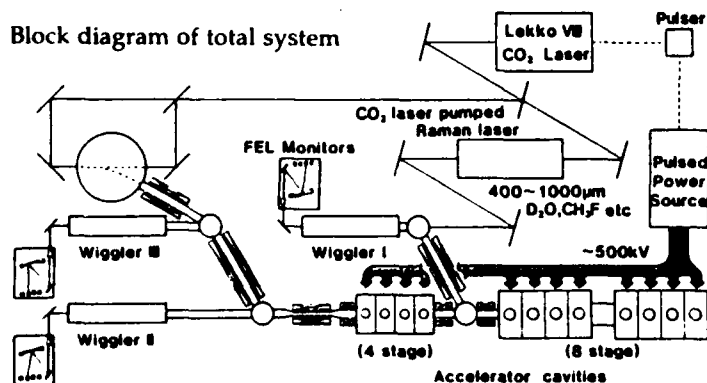
#### PURPOSE OF OUR WORKS FOR FEL

- |           |  |
|-----------|--|
| Date      | <ul style="list-style-type: none"> <li>•to understand high power FEL and related physics</li> <li>•CO<sub>2</sub> laser-E beam interaction (light emission and acceleration)</li> <li>•Inverse tapered wiggler (PI-14) (acceleration)</li> </ul> |
| Near Term | <ul style="list-style-type: none"> <li>•application to higher gradient Acceleration<sup>1)</sup> for a compact high energy accelerator<sup>2)</sup></li> </ul>   |
| Future    | <ul style="list-style-type: none"> <li>•Inertial confinement fusion energy driver for reactor (P3-29)<sup>3)</sup></li> </ul>  |

FEL Facility at ILT/ILE Osaka Univ.

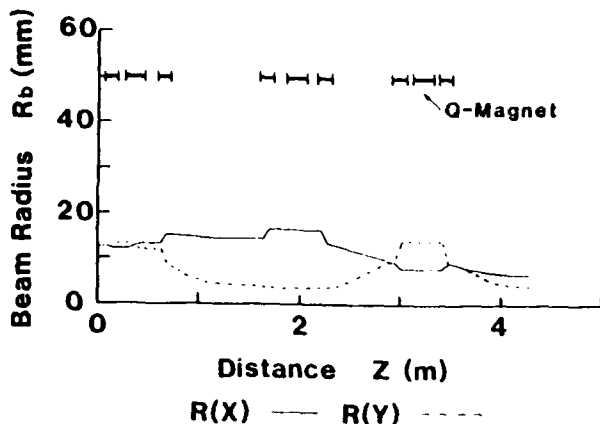
- Induction Linac
  - 12 stage x (500 ~ 750 kV)
  - 5 kA (at e- gun)
  - 100 ns pulse length
  - $\Delta E = \pm 2\%$
- E-Beam Gun
  - brightness ~  $10^4$  A/cm<sup>2</sup>rad<sup>2</sup>
- Beam Transport
  - Solenoid/Hermholtz coil /Triplet Q-Mag./Steering Mag.
  - Beam aperture at entrance of transport section
  - emittance selector
- Wiggler
  - Wiggler I : planer permanent magnet  
 $\lambda_w = 6$  cm  $N = 30$   $K = 0.5 \sim 2$  (Tapered)
  - Wiggler II : Helical pulsed electro-magnet  
 $\lambda_w = 3$  cm  $N = 30$   $K = 0.5 \sim 1$
  - Wiggler III : pulsed electro magnet  
 $\lambda_w = 3$  mm  $N = 100$   $k = 0.1$  (under designing)

Block diagram of total system

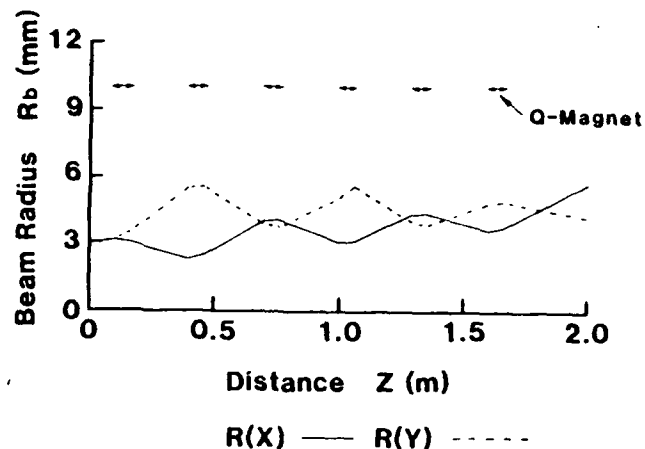


Picture of Accelerator

### Beam Transport to Wiggler



### Beam Transport in Wiggler



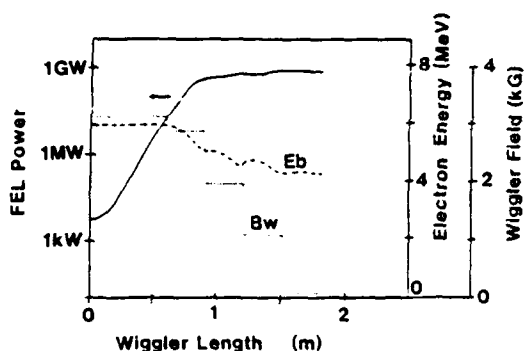
### System I

#### MOPA System

Oscillator: CO<sub>2</sub> laser pumped Raman laser

(Gas: D<sub>2</sub>O, CH<sub>3</sub>F etc.)

~MW output, Multimode)



We may expect

100~1000MW level output

### System II

Oscillator

$$G - \left\{ G_M l_c e^{-f_a l_c} (1 - 2f_R) \right\}^{\frac{\tau_p}{2l_c/c}} > 1$$

$G_M$ : Gain for maximum growing mode

$f_a$ : Attenuation factor of waveguide (0.2)

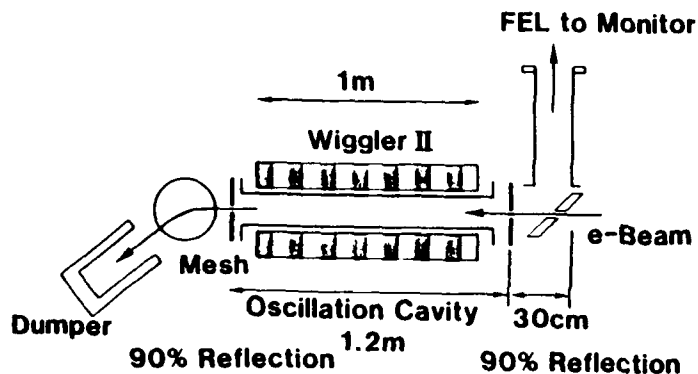
$f_R$ : Mirror loss (10 %)

$\tau_p$ : Pulse length (~ 60 ns)

$l_c$ : Cavity path length (~ 1.2 m)

$C$ : Light velocity

$$\begin{aligned} G &\sim 100 & G_M &\approx 4/\text{m} & f_a &\approx 0.2/\text{m} \\ f_R &= 0.1 & \tau_p &= 60 \text{ ns} \\ l_c &= 1.2 \end{aligned}$$



### References

- 1) A. Sessler, AIP Proceedings 91 (1982) 163  
and D. Prosnitz, IEEE NS 30 (1983) 2754
- 2) K. Imasaki, et al., ILE 8724P (1987)
- 3) K. Imasaki, et al., Rev. Laser Engineering 17  
(1989) 71

# PR1.3

## The LISA Project In FRASCATI INFN Laboratories

M.Castellano, A.Ghigo, P. Patteri, F.Tazzioli

INFN, C.P. 13, 00044 Frascati (Rome), Italy

N.Cavallo, F.Cevenini

INFN-Sezione di Napoli and Univ. di Napoli-Dipart. di Fisica, 80125 Napoli, Italy

F. Ciocci, G. Dattoli, A. Dipace, G.P. Gallerano

A. Renieri, E. Sabia, A. Torre

ENEA-CRE Frascati, 00044 Frascati (Rome), Italy

A test superconducting electron linac accelerator (LISA) is in construction at Frascati INFN National Laboratories.

The design beam energy will be 25 MeV with 5 A peak current, invariant emittance  $\gamma\epsilon_{x,y} = 10^{-5} \pi \text{ m} \cdot \text{rad}$  and energy spread  $\Delta E/E < 2 \cdot 10^{-3}$ .

A FEL will be realized in the IR at  $11 < \lambda < 18 \mu\text{m}$  using a 50 period hybrid undulator of 4.4 cm period. Macropulse averaged power of 500 W and peak power of 1.25 MW are expected.

Operation in the third harmonic at  $4 < \lambda < 6 \mu\text{m}$  and further developments are also presented.

### Main parameters of LISA (Accelerator + FEL)

Energy (MeV)	25
Energy with recirculation (MeV)	49
Bunch length (mm)	2.5
Bunch charge (pC)	40
Peak current (A)	5
Duty cycle	$\leq 10\%$
Average macropulse current (mA)	2
Invariant emittance ( $\pi \text{ m rad}$ )	$10^{-5}$
Energy spread (@25 MeV)	$2 \times 10^{-3}$

Number of undulator periods	50
Undulator wavelength (cm)	4.4
Undulator parameter $K_{rms}$	$0.5 + 1.0$
Radiation wavelength ( $\mu\text{m}$ ) @ 25 MeV	$11 + 18$
Optical cavity length (m)	6
Cavity losses, passive + output (%)	$< 2$

Macropulse duration (ms)	$< 10$
" rep. rate (Hz)	10
" av. power (W)	500
Micropulse duration (ps)	$< 10$
" rep. rate (MHz)	50
" peak power (MW)	1.25

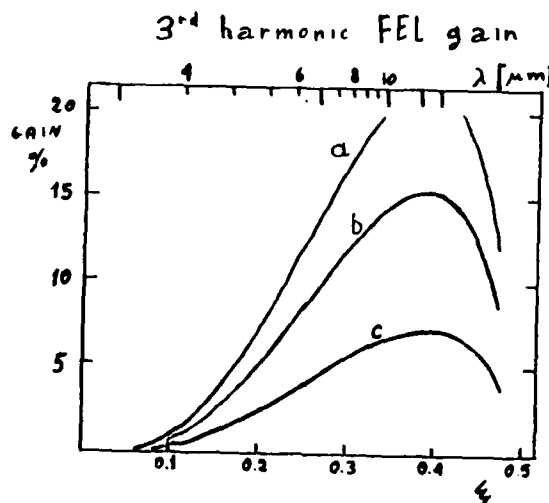
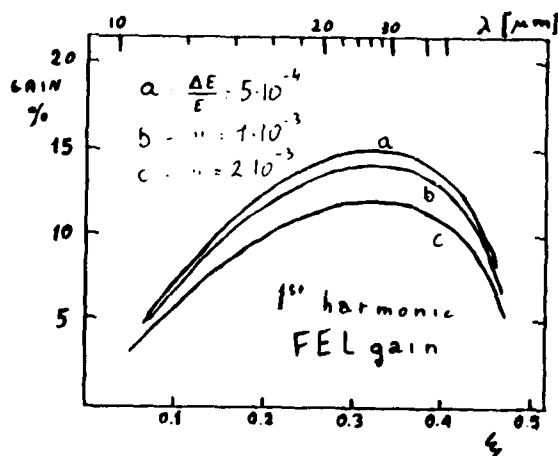
A hybrid undulator to be built by Ansaldo Ricerche in Genoa in collaboration with the ENEA group will be used. A prototype 8 period long has been realized and is under test.

The final choice of the undulator parameters - period and number of poles - will be defined after the completion of the test.

The lower limit to the undulator period is given by the requirement of a gap of 2 cm.

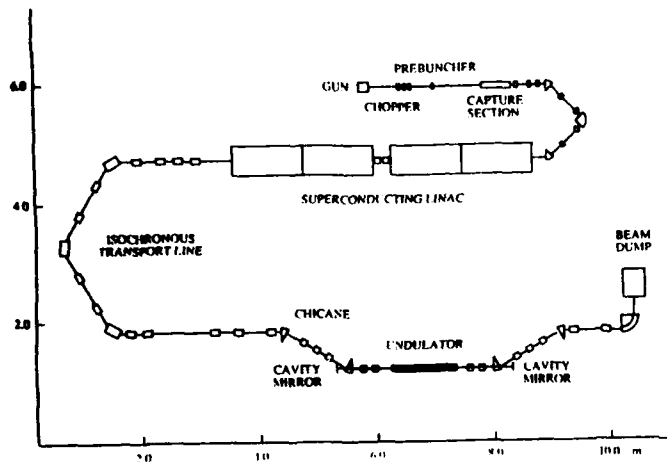
Table 3 - Undulator (tentative parameters)

Hybrid type (NdFeB magnets)	
Numbers of poles	50
Period (mm)	44
Pole width (mm)	60
Gap height (mm)	20
$K_{rms}$	$0.5 + 1.0$



The injection system is composed by

- 100 keV thermionic gun
- chopper (50 MHz plates + 500 cavity)
- prebuncher (2500 MHz cavity)
- 1 MeV preaccelerator and capture section
- isochronous arc at  $\beta = .94$

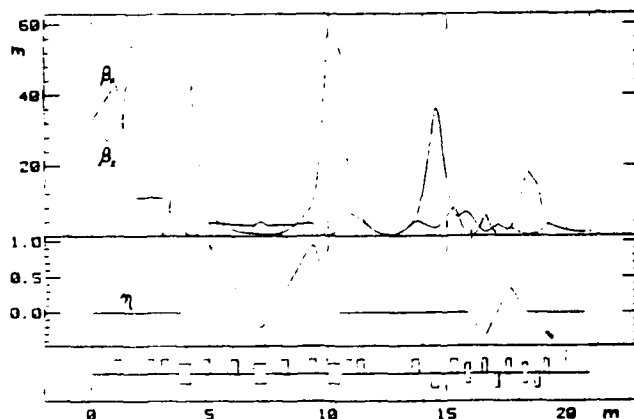


Schematic of the LISA accelerator + FEL layout

The machine lattice is designed to get in the undulator

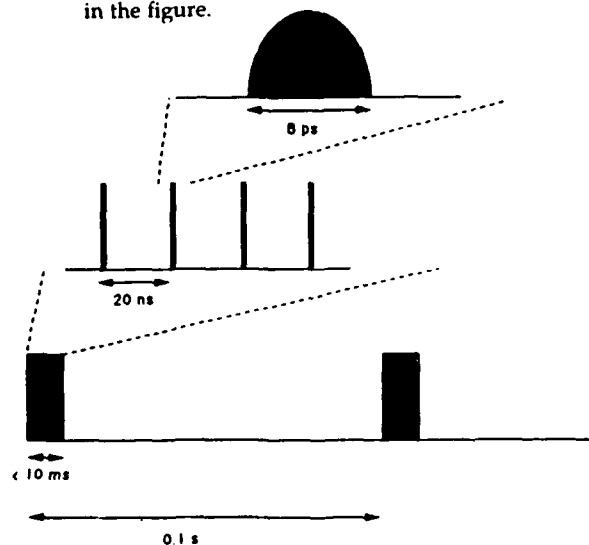
- high peak current  $\rightarrow$  non-dispersive transport
- $e^-$  beam cross section adjustable to match the optical cavity mode
- low sensitivity to beam variation at linac output
- small room taken away at the undulator ends to allow to use a short cavity

but dispersive transport is possible if micropulse length variation is required



The main accelerator is a 500 MHz SC linac which accelerates the beam up to 24 MeV at the nominal field gradient of 5 MeV/m.

The final beam time structure is sketched in the figure.



The duty cycle of the macropulse is restricted to  $\leq 10\%$  for radiation safety reason, not for machine limits.

When effective energy recovery will be operative it will be possible to extend the duty cycle.

## THE CONTROL SYSTEM OF LISA

The control system has been designed to take care both of the accelerator and of the FEL experiment since a close interaction is foreseen for the machine operation, particularly in the energy recovery experiment.

A multilevel structure allows at the same time controlling and testing the machine operation and modelling its performances.

## TIME SCHEDULE

Building activities started in March 89 and are scheduled to be completed by Autumn 89.

All the main accelerator components will be delivered by the end of the same year.

Commissioning of the machine is foreseen to be performed in the first half of 1990.

The undulator is expected to be built within one year from the order; its delivery should closely follow the end of commissioning of the accelerator.

# PR1.4 DELTA, a New Storage-Ring-FEL Facility at the University of Dortmund

F. Brinker, M. Negrazus, D. Nölle, D. Schirmer, K. Wille  
University of Dortmund, FRG

This paper presents the concept of the new FEL facility at the 1.5 GeV electron storage ring DELTA, currently under construction at the University of Dortmund. Furthermore, detailed information about the accelerator itself and the first FEL experiment ( FELICITA I ) are given.

DELTA,  
a New Storage-Ring-FEL Facility at the University of Dortmund

Dirk Nölle et al.

Dortmund ELectron Test Accelerator

an Excellent Driver for FEL Experiments

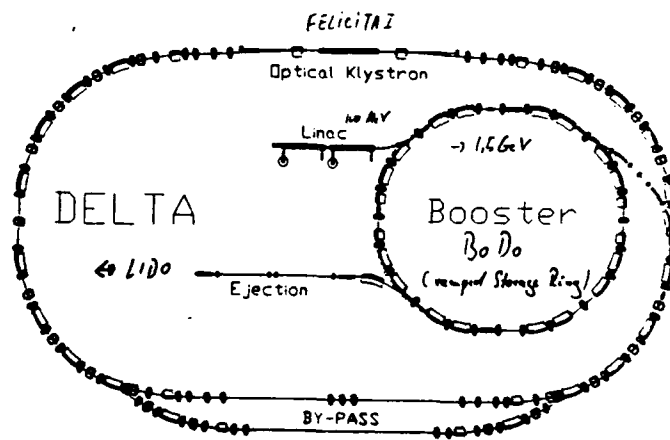
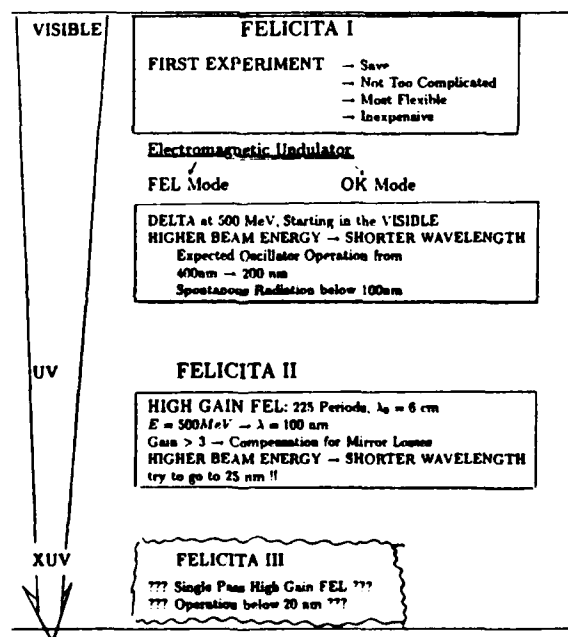
## I. The Storage Ring DELTA

## II. The Concept of the DELTA FEL Facility

## III. The First FEL Experiment FELICITA 1

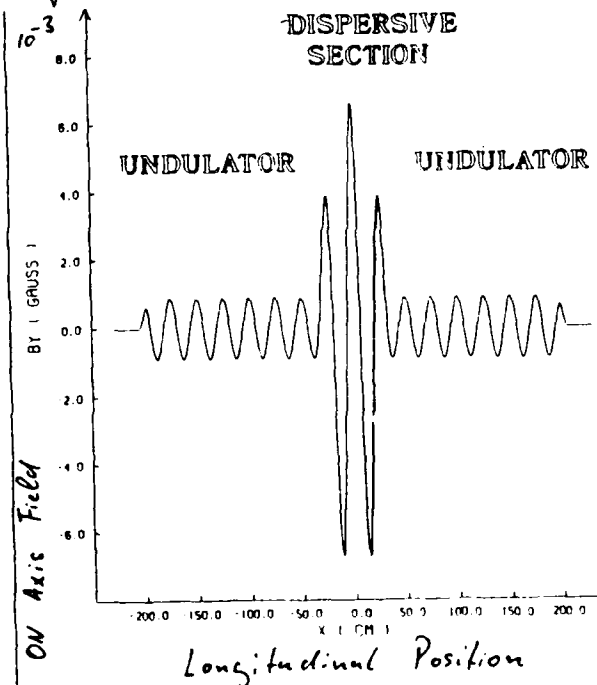
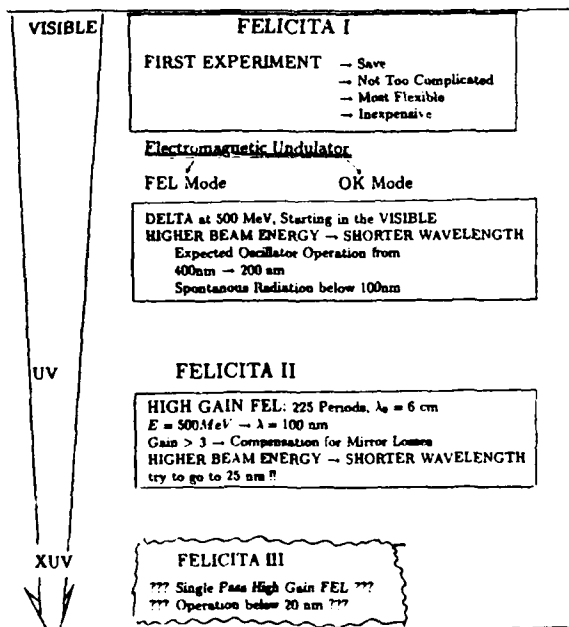
- It is a Test Accelerator.
  - Much Time for Testing, Developing and Experiments
  - Improvement of Accelerator Performance for Special FEL Purpose.
- Two about 20 m Long Straight Sections.
- By-pass Installation Possible
- Low Emittance
- High Peak Current
- Beam Energies from < 500 MeV to 1.5 GeV
- About 20 Highly Motivated Young Physicists

### The Concept of the DELTA FEL Facility

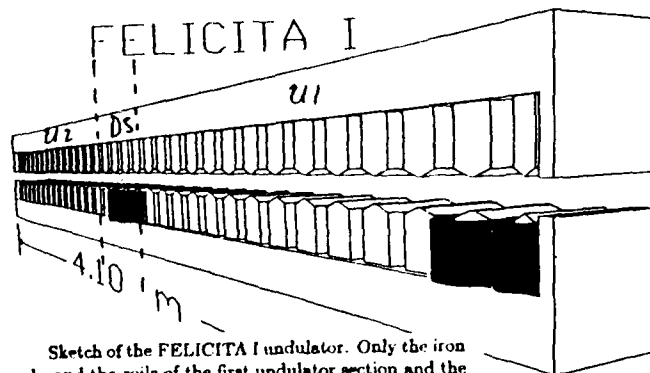


Layout of the DELTA FEL facility. On the top, the setup of the first experiment FELICITA I is sketched. On the bottom the 14 m by-pass, available for FEL devices, is presented.

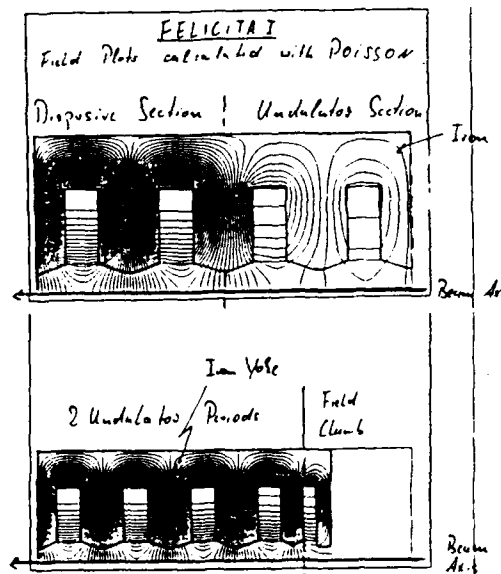
# The Concept of the DELTA FEL Facility



Longitudinal field of the FELICITA I undulator in OK mode. The field calculations, done with POISSON show a nearly cosine dependency of the field in the two undulator sections, and the much stronger field in the dispersive section.



Sketch of the FELICITA I undulator. Only the iron yoke and the coils of the first undulator section and the dispersive section are sketched. As the first and last seven period and the two central periods have different current circuits, it is possible to switch between FEL and OK operation simply by changing the currents in the these circuits. Therefore, it is possible to operate the device as an FEL undulator with 16 equal periods or as an optical klystron with two undulators, of 7 periods each, and a dispersive section made of two periods.



This picture shows two field plots of the FELICITA I undulator. On the top the limit between the dispersive section and an undulator section is shown. Below the the first two periods of an undulator section are presented. In front of the first pole the so called field climb can be seen, minimizing the fringe fields outside the undulator.

## References

- 1: N. Marquardt: Proceedings of the 1989 Particle Accelerator Conference, Chicago 1989, to be publ.
- 2: P. Elleaume: Journ. de Phys. 41 C1, pp. 333, 1983
- 3: J. Le Duff: Nucl. Instr. and Meth. A239, p.83, 1983
- 4: J. Bjorken, S. Mtingawa: Part. Accel., 13, p.115, 1983
- 5: D.T. Attwood et al: AIP Conference Proceedings, No. 118, p.294, 1983
- 6: G. Dattoli, A. Renieri: Nuovo Cim., 59 B, p. 1, 1980
- 7: M.T. Menzel, H.K. Stokes: User's guide for the POISSON / SUPERFISH group of codes, Los Alamos National Laboratory, LA-UR 87-115, 1987
- 8: A. Bizzari et al: ENEA RT/TIB/85/49

# THI.3

## ENHANCEMENT OF THE FREE ELECTRON COHERENT HARMONIC GENERATION BY USE OF THE DISPERSIVE FUNCTION ON A STORAGE RING

R. Prazères, J.M. Ortega.

LURE, CNRS/CEA/MEN, bât. 209d, université de Paris-Sud  
91405 Orsay cedex FRANCE  
(\*) Ecole Supérieure de Physique Chimie  
10 rue Vauquelin 75231 Paris cedex, France.

### Abstract:

An alternative to the Free Electron Laser (FEL) oscillator at short wavelength ( $\lambda < 2000 \text{ \AA}$ ) is the "Coherent Harmonic Generation" (CHG) process with an external laser. However, this coherent emission is rather weak, particularly on high harmonics ( $n \geq 5$ ). This paper shows that the introduction of an "energy dispersive function" on a storage ring increases the CHG by several orders of magnitude.

Enhancement of the Free Electron Coherent Harmonic Generation by use of the dispersive function on a storage ring

LURE.

CNRS / CEA / MEN

Université de Paris-Sud, Orsay

R. Prazères, C. Bazin, M. Bergher, M. Billardon  
M.E. Couprie, P. Guvot-Sionnest, J.M. Ortega  
M. Velehe, Y. Perroff

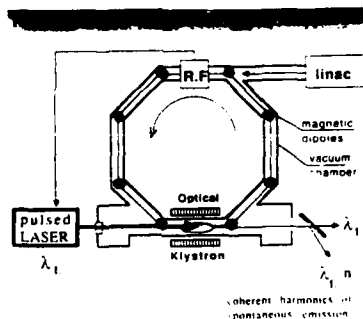
Introduction to CHG process

Influence of the dispersive function  $\eta$

Numerical calculation / Results

Conclusion

An alternative to the Free Electron Laser (FEL) oscillator at short wavelength ( $\lambda < 2000 \text{ \AA}$ ) is the "Coherent Harmonic Generation" (CHG) process with an external laser. However, this coherent emission is rather weak, particularly on high harmonics ( $n \geq 5$ ). This paper shows that the introduction of an "energy dispersive function" on a storage ring increases the CHG by several orders of magnitude.



ACO / 1987 : 3<sup>rd</sup> & 5<sup>th</sup> harmonic of 532nm

Super-ACO : experiment in progress

We define the "spectral ratio" between coherent and incoherent emission for harmonic  $n$  and on axis ( $\theta=0$ ):

$$R_n^{spe}(\lambda\theta) = \frac{I_n^{coh}(\lambda\theta)}{I_n^{incoh}(\lambda\theta)}$$

with laser without laser

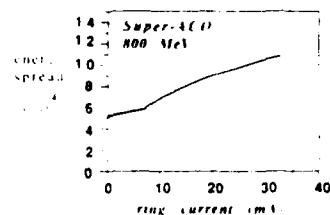
where  $I(\lambda\theta) = \frac{dW}{d\omega d\Omega}$

SPECTRAL RATIO for harmonic "n"

$$R_n^{spe}(\lambda\theta) \approx \frac{1}{3} N_e \frac{J_n^2}{I_n^2} \left( n \cdot [N_e N_d] \Delta\gamma / \gamma \right)$$

with  $I_n^2 = \exp(-16\pi n N_e N_d \sigma_e \sigma_d / \lambda^2)$   
called "modulation rate"

$N_e$  is the number of electrons  
 $J_n$  is the Bessel function of order  $n$   
 $N_d$  is the number of undulator periods  
 $\Delta\gamma$  is the interference order of dispers of the CHG  
 $\sigma_d$  is the maximum energy induced by the laser



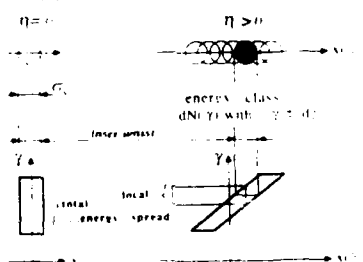
$\sigma_e / \gamma$	$I_1$	$I_2$	$I_3$	$I_4$
1.2	0.2	0.1	1.2	0.4
2.4	1.2	1.2	2.4	1.2
3.6	1.2	1.2	1.2	1.2

CHG decrease strongly for high harmonics

dispersive function

$$\eta = \frac{\Delta\gamma}{\gamma} \quad \eta=0 \text{ in general condition}$$

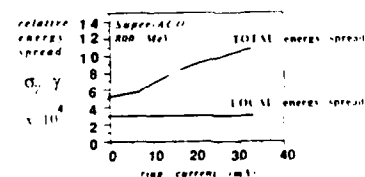
transverse section of the e<sup>-</sup> beam



Each energy class is centered in  $x(x) = \eta(z/z_0)$

The local energy spread for  $x = dx/d\gamma$  is  $\sigma_e \sigma_d / \lambda^2$   
it can be much lower than total energy spread

On the ring Super-ACO we can obtain  $\sigma_e \approx 10^{-4}$  at 800 MeV with  $\sigma_d \approx 400 \text{ \AA}$ .  
Then  
local relative energy spread =  $\frac{\sigma_e \sigma_d}{\lambda^2} \approx 10^{-4}$



\* The use of the function was already proposed by the group of Novosibirsk in 1985, but for the FEL gain

For  $n \neq 0$

1. The "local" energy spread is lowered
2. The horizontal laser waist  $W_L$  can cover a limited section of the e- beam



In the good case where  $W_L/2 < n \sigma_y$

the limited number of e- used for interaction is

$$N_e [W_L/2 n \sigma_y / \gamma] < N_e$$

This gives the new "spectral ratio" ...

For  $n \neq 0$

$$R_n^{spe}(\lambda, \theta) \approx \frac{1}{N_e} \sum_{n=1}^{\infty} A_n \exp(-10 \log n (N+N_d) \sigma_y / \gamma^2)$$

$$J_0^2(\ln 4 n (N+N_d) \Delta \gamma \gamma \cdot \frac{W_L^2}{W_e^2} \frac{W_e}{W_L})$$

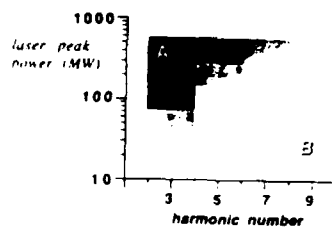
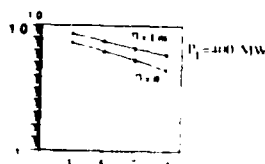
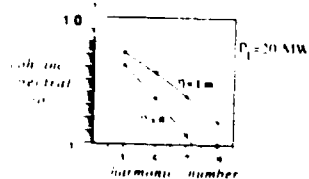
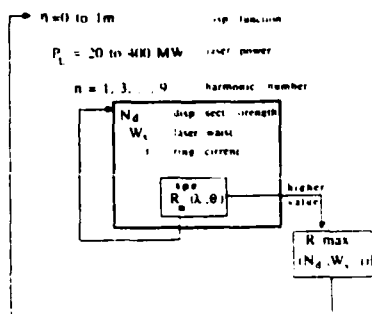
Bessel function: effect of the horizontal laser waist on the max induced energy modulation.  $\Delta \gamma \gamma$  corresponds to a laser waist  $W_L^2$  when  $\mu m$  round beam.

where

$$A = \left( \frac{W_L/2}{n \sigma_y / \gamma} \right)^2 \quad \text{if } W_L/2 < n \sigma_y / \gamma$$

$$A = 1 \quad \text{if } W_L/2 > n \sigma_y / \gamma$$

A numerical calculation has been done for the Super-ACO storage ring of Orsay



horizontal laser waist $W_L$ (mm) chosen by the computer allowing the target spectral ratio	2.6
	2.2
	1.8
	1.4
	1.0
	0.6

1.  $W_L/2 = n \sigma_y / \gamma$  complete overlap between laser beams

2. the transverse section of the laser beam selects only a small part of the e- beam

A mixing of the "energy classes"  $(N, \gamma)$  can be introduced by the horizontal angular spread  $\sigma_{\theta_x}$

The beam size at  $z=0$  position is:

$$\sigma_{\theta_x}^2(z) = \sigma_{\theta_x}^2(0) + z^2 \sigma_{\theta_x}^2$$

replacing it in the Spectral Ratio expression gives:

$$R_n^{spe}(z) = R_n^{spe}(0) \exp(-10 \log n (N+N_d) \sigma_y^2 / \gamma^2) \cdot \exp(-10 \log n \sigma_{\theta_x}^2 z^2)$$

The coh. radiation field is summed along  $z$ :

we find:

$$R_n^{spe}(z) = \frac{1}{\sqrt{2\pi} \sigma_{\theta_x} z} \int_{-\infty}^{\infty} R_n^{spe}(z') \exp(-i k z' z) dz' = (1 + R_n^{spe}(0))$$

With:  $z = 1.5m$ ,  $E_e = 45.8$  and  $(N+N_d) = 100$

we display here the  $\alpha$  coefficient for each harmonic  $n$

n	1	2	3	4
$\alpha$	0.92	0.79	0.64	0.50

This shows that  $\sigma_{\theta_x}$  do not change the order of magnitude of the Spectral Ratio



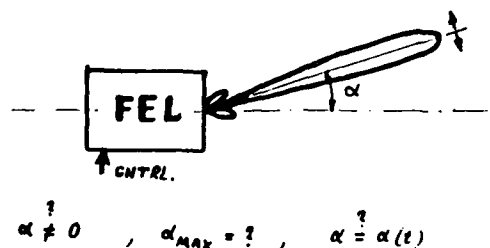
# TH1.5 ANGULAR STEERING OF THE FEL FAR-FIELD RADIATION BEAM

Eli Jerby

Faculty of Engineering, Tel-Aviv University, 69978, ISRAEL \*.

## ABSTRACT

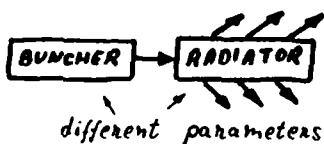
Various concepts for angular steering of the FEL radiation beam in the far-field are presented. These are based on a real-time modification of the FEL synchronism parameters, in both end-fire and broadside schemes. A 2-D model was implemented to analyze the characteristics and limitations of the various beam steering methods. The feasibility of the combined FEL - Phased Array Antenna system is discussed.



## CLASSIFICATION - FEL STEERING METHODS

### LONGITUDINAL: "BROADSIDE" RADIATION

OPTICAL KLYSTRON SCHEMES



### TRANSVERSE: "ENDFIRE" RADIATION

HIGH GAIN FEL

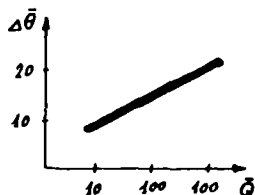
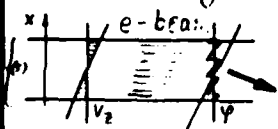


## THE ENDFIRE SCHEMES

- \* High gain FEL
- \* Wide e-beam, with some transverse gradient (in velocity, on density, on  $\beta_w$ , etc.)

ASYMMETRICAL

Example - Velocity shear

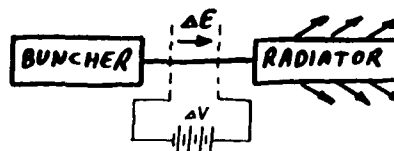


$$\Delta V_z \rightarrow \Delta \theta \rightarrow \Delta \varphi$$

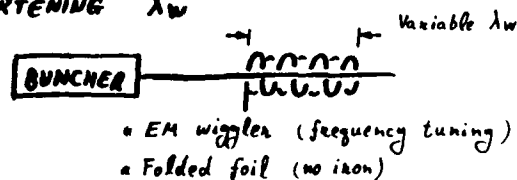
$$\frac{\omega}{V_z(x)} L_w - k_z(x) L_w - k_w L_w \sim 0 \pm \Delta \theta$$

## The Broadside Schemes

### I "BUNCH STRETCHING"



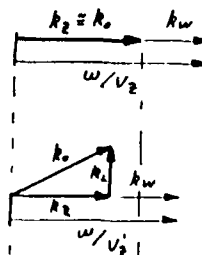
### II SHORTENING $\lambda_w$



## OFF-AXIS SYNCHRONISM DIAGRAMS

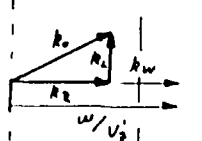
$$\frac{\omega}{V_z} - \langle k_z \rangle - k_w \sim 0$$

### I. ORDINARY FEL :



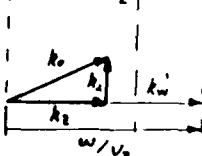
### II. "BUNCH STRETCHING" :

$$V_z > V_z; \omega, k_w = \text{CONST.}$$



### III. SHORTENING $\lambda_w$ :

$$k_w > k_w; \omega, V_z = \text{CONST.}$$



$$k_z = \sqrt{k_0^2 - k_w^2}$$

$$\alpha \sim |k_z|/k_0 - \text{the off-axis angle}$$

\* Present address - Res. Lab. of Electronics, MIT, Cambridge, MA 02139

## THE THEORETICAL MODEL

- 3D MODEL (used here as 2D)
- INCLUDES PREBUNCHING
- ARBITRARY e-BEAM PROFILE (S)

$$\begin{matrix} \vec{E}_{in}(k) \\ \vec{J}_{in}(k) \end{matrix} \rightarrow \boxed{\text{FEL}} \rightarrow \begin{matrix} \vec{E}_{out}(k) \\ \vec{J}_{out}(k) \end{matrix}$$

$$\vec{E}_{out} = \left[ \underline{K} + \underline{D}_1 \right]^{-1} (\vec{E}_{in} + \underline{D}_2 \vec{J}_{in})$$

$\vec{E}_{in}, \vec{E}_{out}$  - FIELD VECTORS, CONSISTS OF SPATIAL FOURIER COEFFICIENTS.

$\underline{K}$  - FREE SPACE PROPAGATION MATRIX.

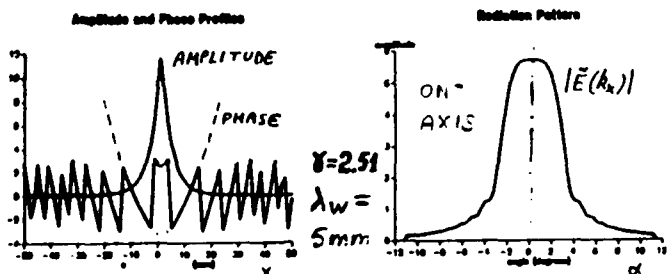
$\underline{D}_1$  - FEL COUPLING MATRIX.

$\underline{D}_2$  - PREBUNCHING MATRIX.

### Example 1: "Broadside" radiation

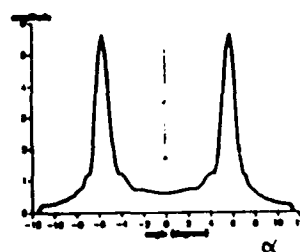
$$\vec{J}_{in} \rightarrow \boxed{\text{RAD.}} \rightarrow \vec{E}_0(k_x) \quad (\text{prebunched FEL})$$

PARAMETERS:  $\lambda = 0.5\text{mm}$ ,  $\lambda_w = 5\text{mm}$ ,  $L_w = 0.3\text{m}$ ,  $\bar{a}_w = 0.3$ ,  $\theta_p = 0.3$



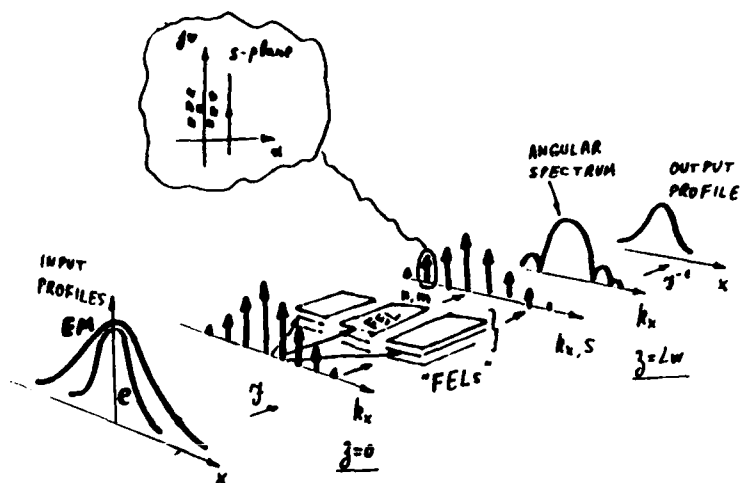
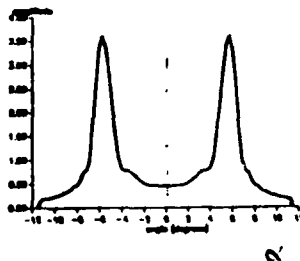
### ① bunch stretching

$$\gamma \rightarrow 2.56$$



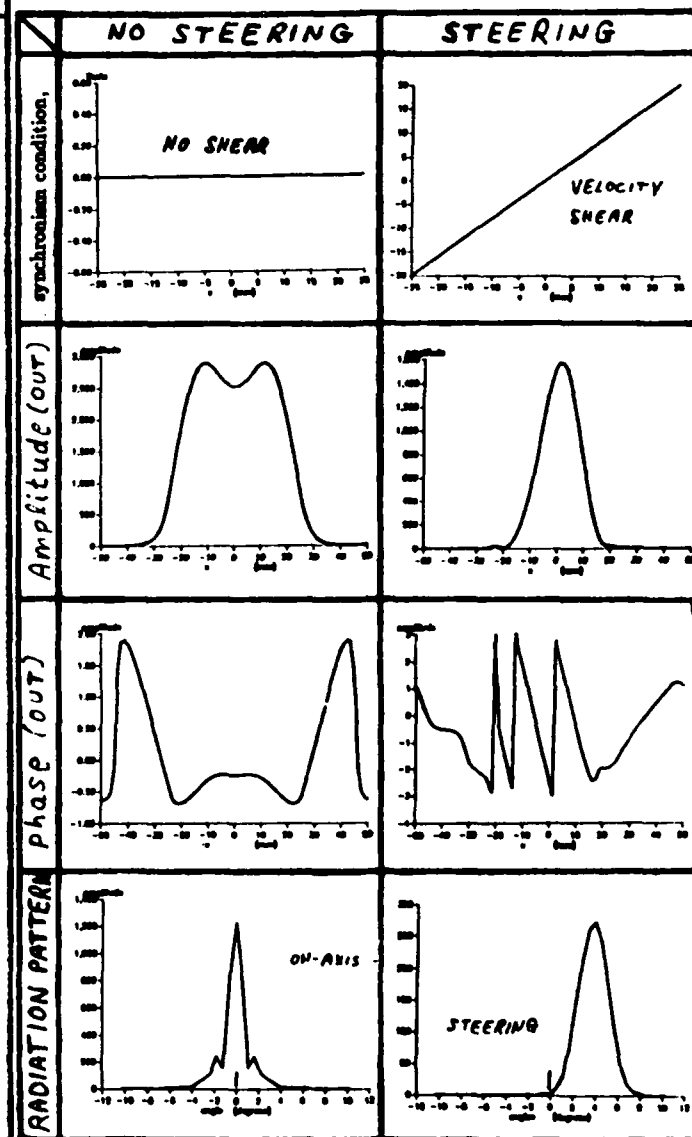
### ② wiggler compression

$$\lambda_w \rightarrow 4\text{mm}$$



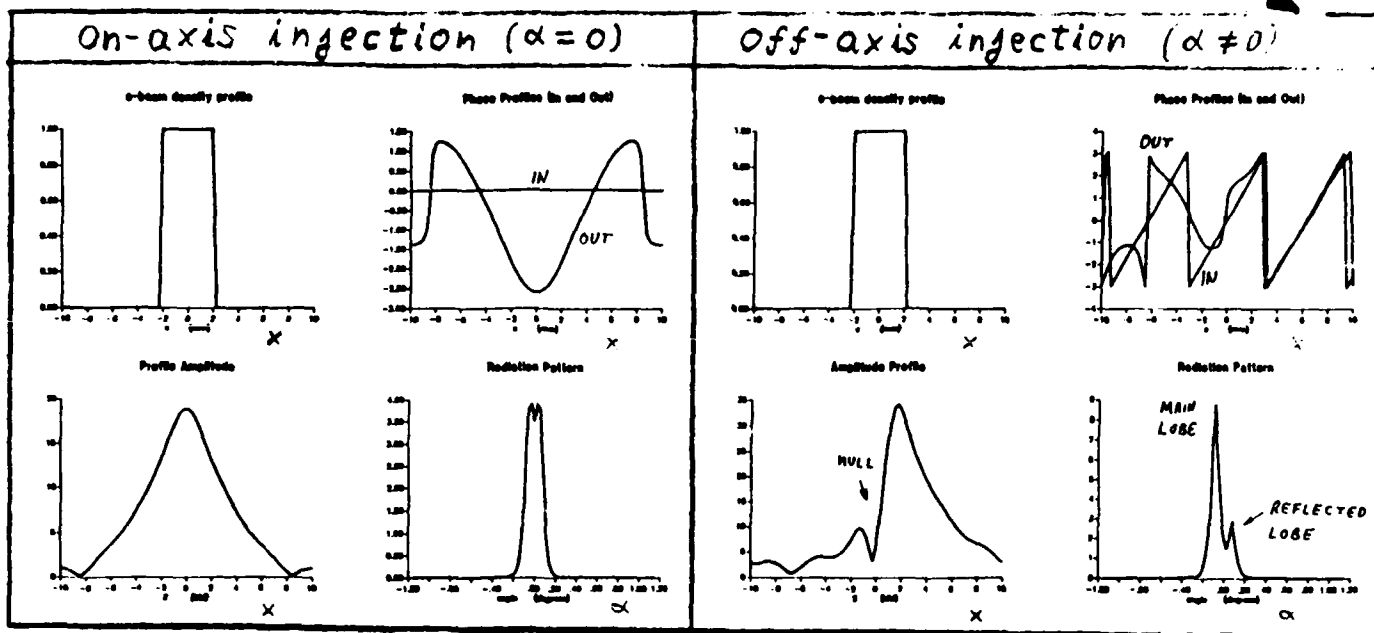
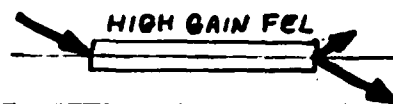
### Example 2: "Endfire" radiation

$\lambda = 1\text{mm}$ ,  $\lambda_w = 2\text{cm}$ ,  $L_w = 4\text{m}$ ,  $\bar{a}_w = 0.6$ ,  $\gamma = 3.8$ ,  $\theta_p = 6$



## Example for off-axis injection

$$\lambda = 10 \mu\text{m}, \lambda_w = 4 \text{ cm}, L_w = 10 \text{ m}, \bar{a}_w = 0.6, \bar{U} = 52, \bar{\theta}_p = 1, \bar{\theta} = 9$$



### LIMITS FOR THE OFF-AXIS ANGLE

(based on simple 1D consideration)

"bunch stretching"  $v_{sc} \rightarrow \alpha_{MAX} = \sqrt{2\lambda/\lambda_w}$

\* conventional FEL -  $\alpha_{MAX} \sim 1/8$  (R) TOO SMALL!

\* miniature wigglers -  $\lambda \sim 0.5 \text{ mm}, \lambda_w \sim 5 \text{ mm}$

$$\alpha_{MAX} \approx \pm 20^\circ \text{ (Reasonable)}$$

Shortening  $\lambda_w$

$$\lambda_w = \lambda_w / 5$$

$$\alpha \approx \sqrt{2(5-1)\lambda/\lambda_w}$$

Narrow e-beam!

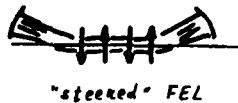
Velocity shear (High-gain FEL)



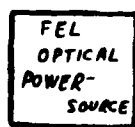
$$\alpha_{MAX} \sim \frac{\lambda \bar{Q}^{1/3}}{2 a_b} \quad \left( \sim 5 \frac{\lambda}{a_b} \right) \Big|_{\bar{Q}=40^3}$$

### APPLICATIONS

(1) Separating e-beam / EM beam paths.

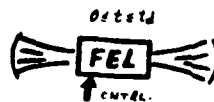


(2) Power divider switch



CONSUMER #1  
CONSUMER #2  
...  
CONSUMER #N

(3) FEL cavity dumping



(5) ??



## On-axis Holes In Interferometer Mirrors

R.H. Pantell, J. Feinstein, A.H. Ho\*  
 Department of Electrical Engineering  
 \*Department of Applied Physics  
 Stanford University  
 Stanford, California U.S.A

Surprisingly low power loss results from the introduction of large holes in resonator mirrors. An analytic solution for the mode pattern in such resonators is obtained using the criterion of maximum laser gain per pass. Such holes permit on-axis electron beam passage and also significantly reduce the peak power density on the mirrors.

### INTERFEROMETER MIRRORS WITH HOLES ON AXIS

R. H. Pantell, A. H. Ho, J. Feinstein  
 Stanford University

#### Advantages:

1. Allows collinear introduction of the electron beam into the cavity. (Shortens cavity, eliminates bending magnets.)
2. Reduces the power density on the mirrors. (Ameliorates the problem of mirror damage.)
3. Increases the small-signal gain.

#### Loss introduced by the hole:

For a cavity length of 5m,  $\lambda = 10\mu\text{m}$ , mirror diameter = 1.55cm, and a hole diameter = 2.6mm, the reflection loss is 0.1% (as compared to a ratio of hole area to optical mode area of 10%).

This work is supported by the U.S. Army Strategic Defense Command in Huntsville and by the National Science Foundation.

#### ANALYSIS:

For a small hole in one mirror, a null in the field at the hole can be obtained with two modes. For a small hole in both mirrors three modes are required.

To compare with the conventional (no hole) interferometer:

- the wiggler and cavity lengths are fixed
- the optical power density on-axis at the edge of the wiggler is one-half the maximum value (as in the conventional confocal resonator)
- the power extracted from the electron beam at saturation is kept constant

A filamentary electron beam is assumed.

### Mirrors With Holes

In cylindrical coordinates with azimuthal symmetry:

$$E = e^{-j\omega t + jkz} \frac{W(z)}{W(z)} e^{-j\omega t} e^{-j\omega z/c} \\ + \sum_p A_p L_p \left( \frac{2r^2}{W} \right) e^{-j(k^2 + 2\omega^2/c^2)z}$$

$L_p(x)$  = Laguerre Polynomials

$$= \frac{e^x}{p!} \frac{d^p}{dx^p} x^p e^{-x}$$

$$L_0 \left( \frac{2r^2}{W} \right) = 1$$

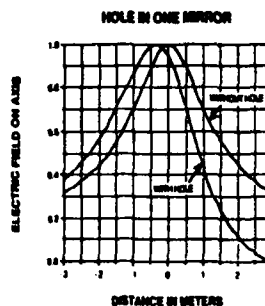
$$L_1 \left( \frac{2r^2}{W} \right) = 1 - 2r^2/W^2$$

$$L_2 \left( \frac{2r^2}{W} \right) = 1 - 4r^2/W^2 + 2r^4/W^4$$

$$W(z) = W_0 \left[ 1 + (z/z_R)^2 \right]^{1/2}$$

$$z_R = \pi W_0^2/\lambda$$

$$R(z) = z \left[ 1 + \left( \frac{z}{z_R} \right)^2 \right]^{-1}$$

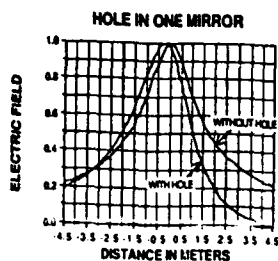


WIGGLER LENGTH = 2m

CAVITY LENGTH = 6m

WITHOUT HOLE:  $Z_T = 1.0m$

WITH HOLE:  $Z_T = 1.5m$

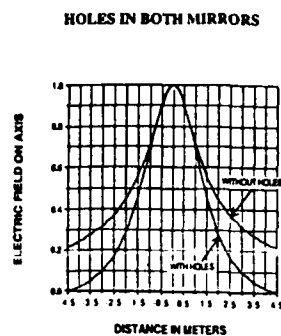


WIGGLER LENGTH = 2m

CAVITY LENGTH = 9m

WITHOUT HOLE,  $Z_T = 1.0m$

WITH HOLE,  $Z_T = 1.5m$



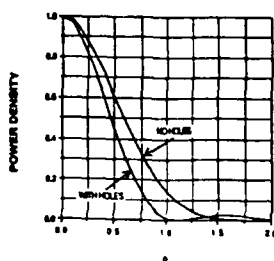
WIGGLER LENGTH = 2m

CAVITY LENGTH = 9m

WITHOUT HOLES,  $Z_T = 1.0m$

WITH HOLES,  $Z_T = 2.0m$

**HOLES IN BOTH MIRRORS**  
POWER DENSITY vs RADIUS AT CENTER OF WIGGLER



$$\rho = r \left( \pi / (\lambda z_T) \right)^{0.5}$$

$z_T$  = Rayleigh length for no-hole case = 1m

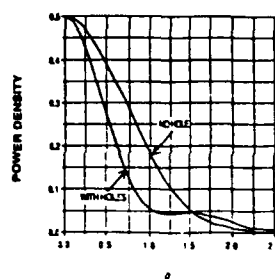
WIGGLER LENGTH = 2m

CAVITY LENGTH = 9m

Optical beam area is reduced by a factor of 3

**HOLES IN BOTH MIRRORS**

POWER DENSITY vs RADIUS AT EDGE OF WIGGLER

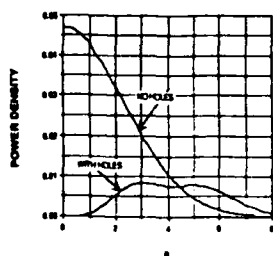


WIGGLER LENGTH = 2m

CAVITY LENGTH = 9m

**HOLES IN BOTH MIRRORS**

POWER DENSITY vs RADIUS AT MIRRORS



WIGGLER LENGTH = 2m

CAVITY LENGTH = 9m

## SUMMARY

With holes in both mirrors, for fixed power extraction at saturation:

- There may be on-line introduction of the electron beam into the cavity.
- The power density on the mirrors is reduced.
- Small-signal gain is increased.
- The added cavity loss is small.

## REI.2

# MODE CONTROL ON SHORT-PULSE FELS USING A MICHELSON-MIRROR RESONATOR

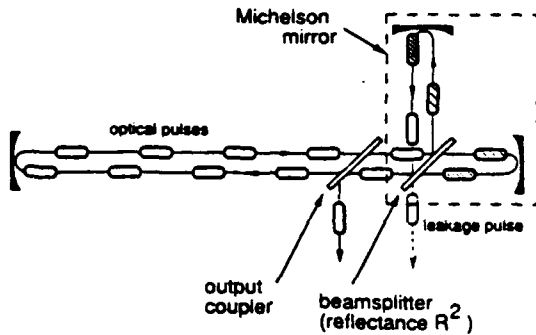
E.B. Szarmes, S.V. Benson, and J.M.J. Madey, Duke University

### OUTLINE of TALK

- 1) Introduction and motivation for using multiple mirror resonators on short-pulse FELs
- 2) Outline of mathematics for analysing mode control
- 3) Computer simulations of Michelson mirror resonators on the Mark III FEL
- 4) Applications to spectroscopy
- 5) Previous experimental effort using the Mark III FEL
- 6) Summary

### Introduction

- Michelson mirror resonator with 1 RF period of delay in the secondary arm
- Pulses build up only if properly phased at beamsplitter
- Phaselocking increases free spectral range of resonator
- Maximum coupling occurs for  $R^2 = 50\%$



### Mathematical Analysis

(N = 4 pulses)

$$E_1(n+1) = e^{\alpha} [E_1(n)^2 + E_4(n-1) r^2 e^{i\phi}]$$

$$E_2(n+1) = e^{\alpha} [E_2(n)^2 + E_1(n) r^2 e^{i\phi}]$$

$$E_3(n+1) = e^{\alpha} [E_3(n)^2 + E_2(n) r^2 e^{i\phi}]$$

$$E_4(n+1) = e^{\alpha} [E_4(n)^2 + E_3(n) r^2 e^{i\phi}]$$

Eigenmode solutions:  $E_i(n+1) = \gamma E_i(n)$   
( $\gamma$  independent of  $i, n$ )

$$\begin{bmatrix} e^{\alpha} r^2 - \gamma & 0 & 0 & \gamma^4 e^{\alpha} r^2 e^{i\phi} \\ e^{\alpha} r^2 e^{i\phi} & e^{\alpha} r^2 - \gamma & 0 & 0 \\ 0 & e^{\alpha} r^2 e^{i\phi} & e^{\alpha} r^2 - \gamma & 0 \\ 0 & 0 & e^{\alpha} r^2 e^{i\phi} & e^{\alpha} r^2 - \gamma \end{bmatrix} [E(n)] = [0]$$

Eigenvalues  $\gamma$  (for  $r^2 = 1/2$  and  $\phi = 0$ ) obtained from

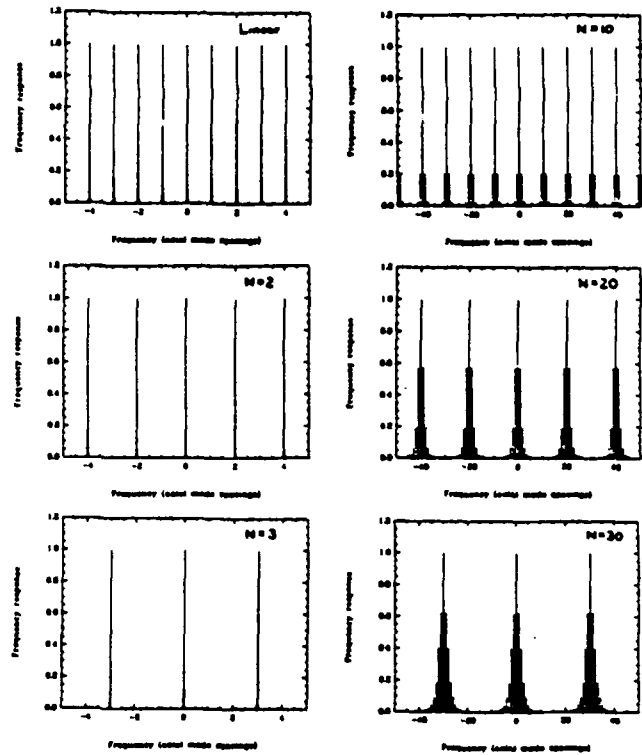
$$\gamma = e^{\alpha} [1/2 + r^2 e^{i\phi} / \gamma^{1/4}] = 1.0000 + j0.0000$$

$$\gamma = e^{\alpha} [1/2 - r^2 e^{i\phi} / \gamma^{1/4}] = -0.0949 \pm j0.3014$$

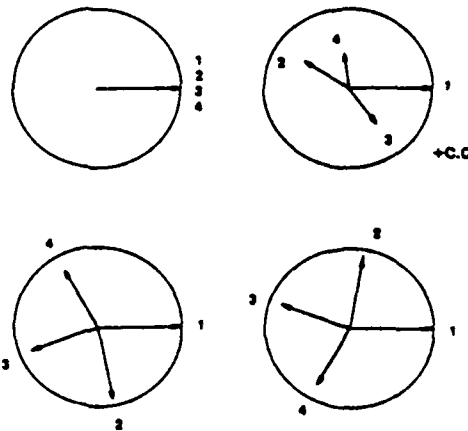
$$\gamma = e^{\alpha} [1/2 + j r^2 e^{i\phi} / \gamma^{1/4}] = 0.5949 + j0.5216$$

$$\gamma = e^{\alpha} [1/2 - j r^2 e^{i\phi} / \gamma^{1/4}] = 0.5949 - j0.5216$$

### Passive CW Frequency Response



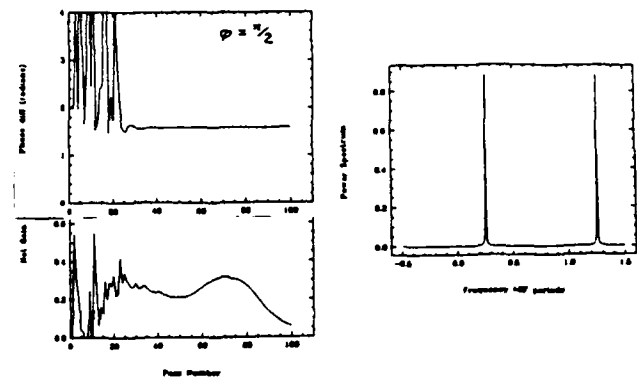
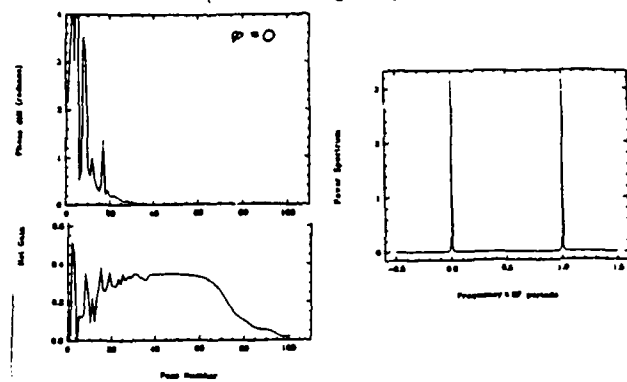
### Corresponding Eigenvectors



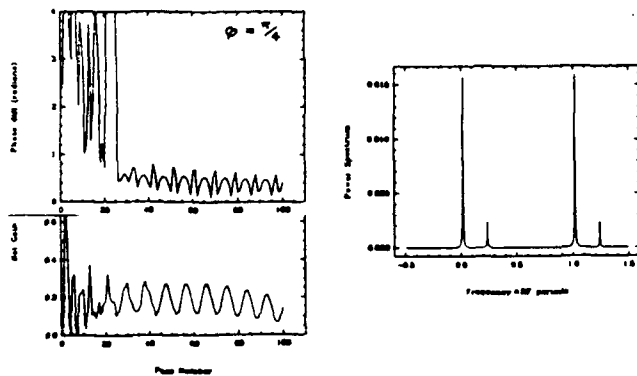
## Numerical simulations

- 1) Build up from noise to saturation using coupled Maxwell-Lorentz equations
- 2) One-dimensional simulation with complex filling factor
- 3) Includes both shot noise and quantum noise
- 4) Investigates dependence on
  - i) number of pulses
  - ii) beamsplitter reflectance
  - iii) Michelson mirror phase offset
  - iv) Michelson mirror detuning
- 5) Parameters appropriate to the Mark III FEL

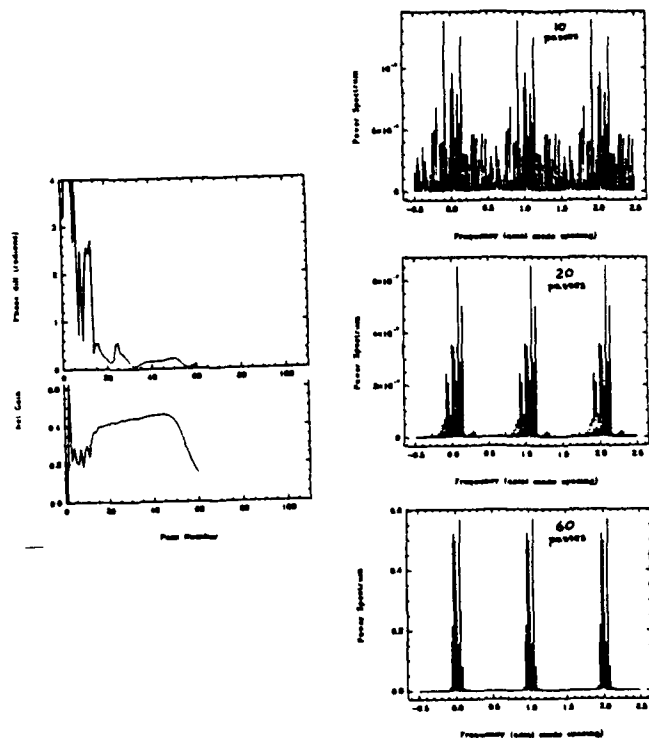
4 pulses - 50% reflectance  
(discrete tuning using  $\phi$ )



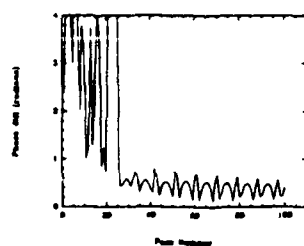
4 pulses - 50% reflectance  
(destructive interference using  $\phi$ )



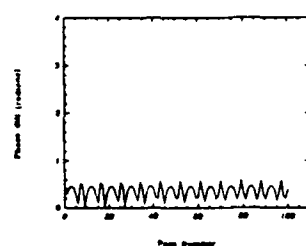
35 pulses - 50% reflectance  
(spectrum evolution)



Simulation

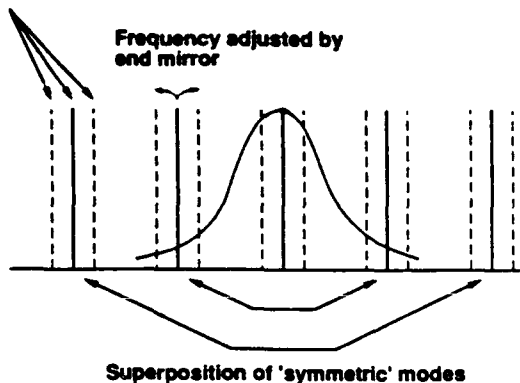


Mode analysis



## Applications to Spectroscopy

Mode selected by  $\sigma$

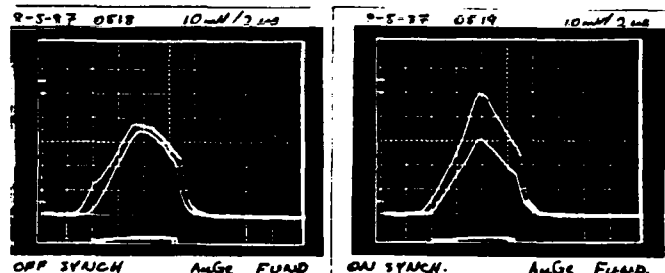


- Combined experiments with

- I) Pulse compression by energy chirping
- II) Loss modulation and cavity dumping

## Experimental Results using the Mark III FEL

- 1) 35 circulating pulses
- 2) 1 RF period of delay in the secondary arm of the interferometer (non-stabilized)
- 2) ZnSe Brewster plate output coupler with one surface serving as the beamsplitter ( $R^2 = 1.4\%$ )
- 3) Outcoupled beam and leakage beam both travel to detector



Detuned Michelson mirror

Synchronous Michelson mirror

Detuning range for Michelson mirror = 8.9 mls

## Summary

- 1) Michelson mirror increases free spectral range of output optical pulse train
- 2) Presented analysis which predicts mode losses and accurately reproduces pulse train evolution
- 3) Can investigate various configurations using complete FEL pulse propagation code
- 4) Resonator has applications in high resolution spectroscopy
- 5) Presented preliminary experimental results using the Mark III FEL



## REI.3

### Resonator Modes in High Gain Free Electron Lasers

Ming Xie, David A. G. Deacon\*, John M. J. Madey\*\*

Lawrence Berkeley Laboratory,  
Berkeley, CA 94720, USA.

\*Deacon Research

900 Welch Road, Palo Alto, CA 94087, USA.

\*\*Department of Physics, Duke University  
Durham, NC 27706, USA.

When the gain in a free electron laser is high enough to produce optical guiding, the resonator mode distorts and loses its forward-backward symmetry. We show that the resonator mode in a high gain FEL can be easily constructed using the mode expansion technique taken separately in the interaction and the free-space regions. We propose design strategies to achieve maximal gain and optimal mode quality, and discuss the stability of the optimized mode.

1. Amplifier region: At high gain, the continuous spectrum of guided modes can be neglected, thus optical field can be expressed as a truncated expansion in a few low order discrete guided modes[1,2,3].

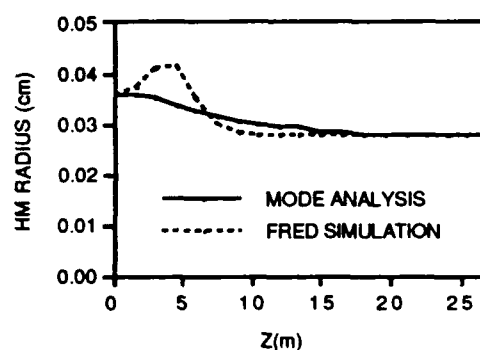
$$E(x,y,z) = \sum_{n=1}^N C_n E_n(x,y) \exp(-i\lambda_n z) \quad (1)$$

For parameters given in table 1 the guided mode expansion (1) is benchmarked with simulation performed with FRED[4] for a high gain amplifier. Five growing and five decaying modes are included in the expansion.

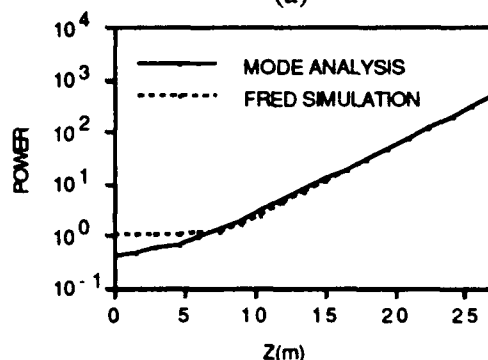
As shown in Figure 1 below one Rayleigh range, the simulation shows a growing mode size due to diffraction, the expansion (1) fails in this region because the continuous modes are neglected. Above about one Rayleigh range, the power in the discrete guided modes grows to a level where diffraction becomes negligible, then two curves converges. About 43% of input power couples into the discrete modes, the remainder goes to the continuous modes. Power grows nearly exponentially after about 15 meter, indicating the dominance of the fundamental mode from there on. The single pass gain is 495 from the mode expansion and 499 from the simulation. At the wiggler exit, radial profiles of the optical intensity from the two approach are indistinguishable, as shown in Figure 2.

2. Free-space regions within cavity: Optical field can be expanded in vacuum modes. The two free parameters in the expansion are determined by maximizing power coupling from the amplified field to a fundamental free-space mode: the Gaussian mode. In our example, 95% of the

power is reached in the fundamental mode, and over 99% of the power in the five low order Gaussian-Laguerre modes.



(a)



(b)

Figure 1. Half-max radius of intensity (a) and power (b) vs. propagation distance along the wiggler.

3. Optimization condition for resonator: The fundamental guided mode has the smoothest phase-front and the highest exponential growth rate, thus to optimize a resonator is to maximize the power in the fundamental guided mode. The

guided modes are not orthogonal, and they have a special property which states: the maximum power coupling to a guided mode is reached if the input field is a complex conjugate of the mode. This means in particular that the input field should have a converging phase-front, opposite to that of the fundamental growing guided modes[2,3,5].

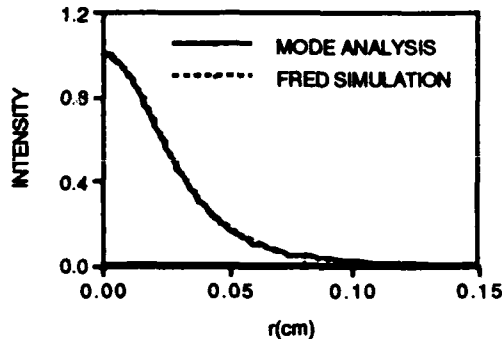


Figure 2. Transverse intensity profile at the wiggler exit. Only two modes are included in the expansion. Since the fundamental guided mode is not but close to a Gaussian, the conjugate input coupling condition can be approximated as requiring the input field to be a complex conjugate of the optimized Gaussian mode at the wiggler exit in free-space expansion. This task can be easily accomplished with spherical cavity mirrors.

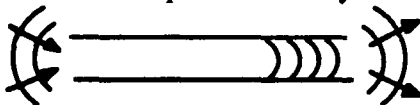


Figure 3. Schematic drawing of an amplifier with a converging input field and a diverging amplified field. Note near the wiggler exit the dominant fundamental guided mode has a diverging phase-front.

4. Transport matrix of a resonator: The optimization condition put two constraints on resonator parameters. If all parameters except two mirror radii are fixed, the two constraints will determine the optimal values for two mirror radii:

$$\begin{aligned} c_1 R_1^2 + c_2 R_1 + c_3 &= 0 \\ d_1 R_1 + d_2 R_2 + d_3 &= 0 \end{aligned} \quad (2)$$

where the coefficients are functions of other resonator geometry parameters and the chosen "free parameters" for the vacuum mode expansion. If the distance from the wiggler exit to the downstream mirror is varied while keeping the full cavity length fixed, Eq.(2) will give two branch of solutions which are shown in Figure 4.

5. Conclusions: Maximal gain and optimal transverse mode quality can be achieved simultaneously by maintaining an input field which optimize the power coupling to the fundamental growing guided mode; a resonator can be made

optimal at high gain when optical guiding occurs and yet stable at low gain when the resonator mode approach the vacuum mode; and finally the downstream mirror can be placed further away from wiggler exit to allow reduction of power loading on cavity mirrors, without sacrificing either gain or mode quality.

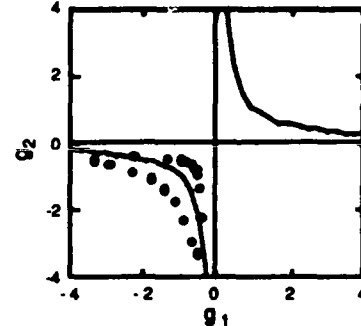


Figure 4. Resonator stability diagram.

Table 1. Parameters for calculation

Electron Lorentz Factor	2000
Electron Beam Current (Amps)	270
Electron Beam RMS Radius (micron)	233
Peak Wiggler Parameter	5.74
Wiggler Length (m)	27
Wiggler Period (cm)	11.4
Optical Wavelength (Å)	2500
Oscillator Cavity Length (m)	54

Input mode to the amplifier is taken as a Gaussian mode focused at the entrance of the wiggler with a minimum spot size of 600 micron and a Rayleigh range of 4.52 meter.

The authors wish to thank John Lasa La for providing FRED simulation data. This work was supported at various time by the Air Force Office of Scientific Research, the Office of Naval Research, the Army Research Office and Department of Energy.

## References

- [1] M. Xie and D.A.G. Deacon, Nucl. Instr. Meth. Phys. Res., A250 (1985) 426.
- [2] M. Xie, D. A. G. Deacon, J. M. J. Madey, Nucl. Instr. Meth. Phys. Res., A272 (1988) 528, and LBL preprint - 26987, to be published in Phys. Rev. A.
- [3] M. Xie, Ph.D. Dissertation, "Theory of Optical Guiding in Free Electron Lasers", Department of Physics, Stanford University, 1988.
- [4] W. M. Fawley, D. Prosnitz, E. T. Scharlemann, Phys. Rev., A30 (1984) 2472.
- [5] G. T. Moore, Nucl. Instr. Meth. Phys. Res., A250 (1985) 381.
- [6] A. E. Siegman, Lasers, University Science Books, 1986.

# RE1.4 Measurements of UV Induced Absorption in Dielectric Coatings

David A.G. Deacon, M.H. Bakshi, M. Cecere, A.M. Fauchet<sup>a)</sup>  
Deacon Research, 900 Welch Road, Suite 203,  
Palo Alto, CA 94304 USA

We discuss the first results obtained from a new testing facility for measuring the induced absorption in dielectric coatings exposed to intense UV radiation. The loss is measured in-situ during exposure, as a function of time for various photon energies, intensities, and background gas pressures.

a) NSLS, BNL, Upton, NY 11973

## MEASUREMENTS OF UV INDUCED ABSORPTION IN DIELECTRIC MIRROR COATINGS

David A.G. Deacon, M.H. Bakshi, M. Cecere

Deacon Research  
900 Welch Rd. Suite 203  
Palo Alto CA 94304  
(415) 326-1226

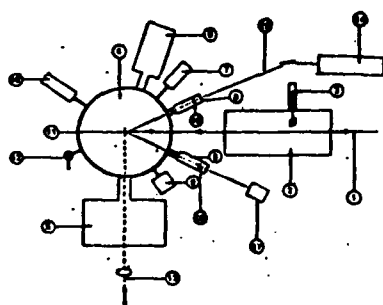
A.M. Fauchet

NSLS, Brookhaven National Lab, Upton NY 11973

Prepared by:  
Douglas I. Baskford

Supported by the SBN NY office,  
managed by CERN.

Presented at the International FEL Conference  
Naples, March, Aug. 28 - Sept. 2, 1989.



Schematic Drawing: UV Photon Induced Loss Measurement Apparatus:

- Figure 1:  
1) UV photon source (w/ trigger)  
2) Photon detector  
3) Sample transfer chamber  
4) X-ray source  
5) Gas pressure gauge  
6) Sample  
7) Laser and rotary feedthrough  
8) Laser focus pin  
9) Chamber  
10) Differential lockout bar  
11) External vacuum chamber  
12) CLAM 100 cryostat  
13) Cryostat pump for the lockout  
14) Standard gas vent  
15) Controlled gas leak valve  
16) In-vacuum laser  
17) Cryo reference station

## PRIMARY EXPERIMENTAL TOOLS

### A) UHV Chamber

$\sim 10^{-10}$  Torr

### B) Multilayer Mirror Samples, Sample Transfer Chamber

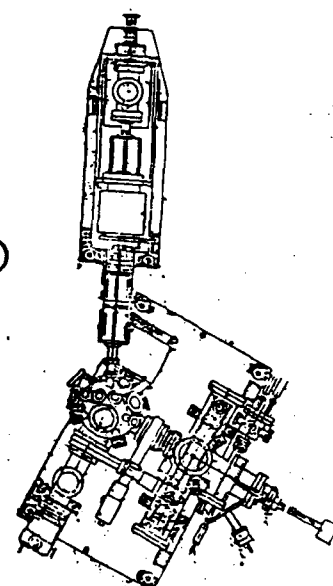
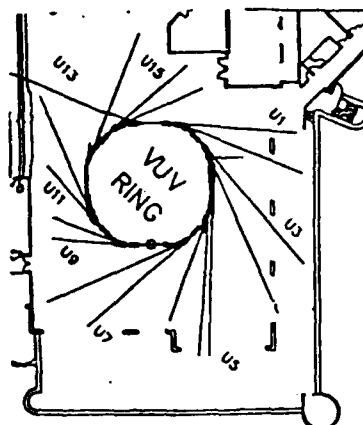
•  $\text{SiO}_2$  /  $(\text{TiO}_2/\text{SiO}_2)_n$  401 nm  
•  $(\text{TiO}_2/\text{SiO}_2)_n$   
•  $\text{SiO}_2$  /  $(\text{TiO}_2/\text{SiO}_2)_n$   
•  $(\text{SiO}_2/\text{SiO}_2)_n$   
• — 332 nm  
• — 432 nm

### C) UV Photons (TOK Undulator, NSLS-UV Ring)

• tunable 6 eV - 37 eV (K=1, energy spread)  
• bandwidth 4% - 15% (synchrotron bandwidth)  
• intensity  $1.2 \text{ w/cm}^2$  (745 MeV, 600 eV)  
8.002 (330 MeV, 100 eV)

### D) In-vacuum Lossmeter

• loss coefficient 1 ppm  
• gas coefficient 3 s (0 exp.)  
• tunable < 100 nm (1 exp.)  
• spot size 300 nm - 150 nm  
600 microns



## EXPERIMENTAL PROGRAM

- 1) Loss - vs. - time
- 2)  $\delta(\text{Loss})$  - vs. - photon energy  
UV intensity  
carbonaceous species  
pressure  
sample temperature  

Continuum Inc  
Sept.-Dec. 79
- 3)  $\delta(\text{Loss})$  - vs. - material  
fabrication
- 4) Suppression techniques for  $\delta(\text{Loss})$

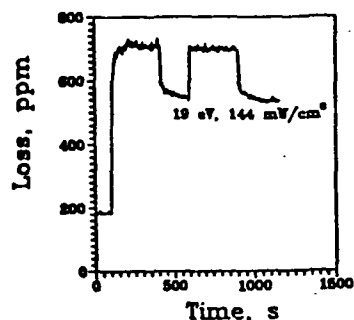


Figure 6: The induced loss obtained at 19 eV photon wavelength is shown for the UV photon parameters as noted in S-TIS sample. The induced loss appears to be exponentially higher at higher photon energy. The "spare time" the graph is generated by computer-aided and opening of the shutter to study the recovery to baseline of UV photon.

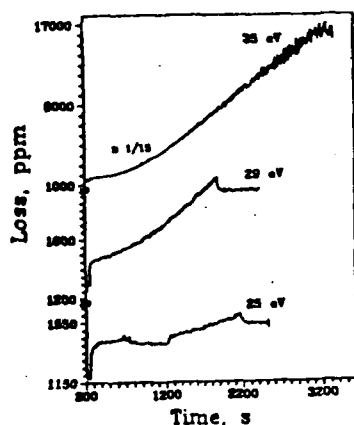


Figure 7: Scattering at S-TIS sample, the figure shows the induced loss following for photon energy between 15 to 25 eV. The exposure was, from bottom to top, 150, 170, and 1800 mW/cm² respectively. The losses begin to become rapidly and consistently in the range.

## SECONDARY EXPERIMENTAL TOOLS

### D) Gas Manifold / Leak Valve / Differential Isolation Line

- Max. P =  $10^{-4}$  Torr
- CO, CO<sub>2</sub>, CH<sub>4</sub>

### E) Residual Gas Analyzer

### F) X-Ray Photoelectron Spectroscopy (XPS)

### G) Ion Sputtering

Fig. 8  
Fig. 9  
Fig. 10  
Fig. 11

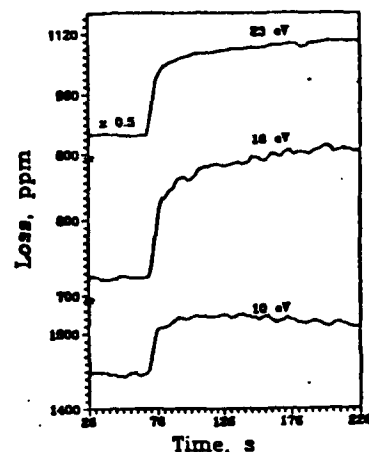


Figure 8: The photon energy dependence of the induced loss is shown for the S-TIS sample at the induced energy. The loss begins with the photon energy at 10 eV, and the opening of the shutter is shown from the top of the loss to the loss. The photon intensity was 10 mW/cm². The loss corresponding to the loss in the middle frame depicts the same rate to show the typical recovery to the loss on closing the shutter following a sample loss.

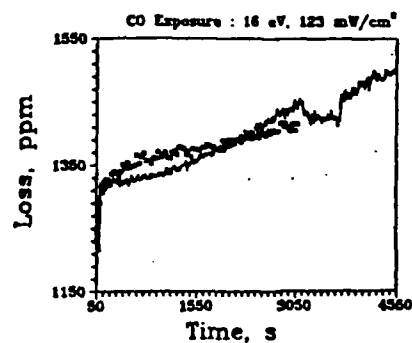


Figure 11: The solid line represents the loss profile when CO gas at  $10^{-4}$  Torr is introduced at the chamber during the exposure to UV photon at 16 eV. The open frame shows the induced loss under exposure to 16 eV photon at about the same intensity with no gas present, for comparison with the gas exposure rate. See text for details.

# REI.5 FAR INFRARED QUASI-OPTICAL RESONATOR FOR Cerenkov FREE ELECTRON LASER

F. Ciocci, G. Dattoli, A. De Angelis, A. Dipace, A. Doria, G.P. Gallerano,

M.F. Kimmitt\*, A. Renieri, E. Sabia, A Torre and J.E. Walsh\*\*

ENEA, Dip. TIB, U.S. Fisica Applicata, P.O.Box 65, 00044 Frascati (Rome), Italy

## ABSTRACT

A Cerenkov free electron laser experiment (C-FEL) employing a 5 MeV microtron electron beam source and providing coherent radiation in the spectral range from 100  $\mu\text{m}$  to 1000  $\mu\text{m}$ , is under way in our laboratories.

Recent tests of a quasi-optical resonator are reported.

\* Permanent address: University of Essex, Colchester (U.K.)

\*\* Permanent address: Dept. Physics and Astronomy, Dartmouth College, Hanover, USA

### REALIZATION OF A FAR INFRARED Cerenkov FREE ELECTRON LASER (1986 -->)

#### • MAIN FEATURES :

- interaction of a relativistic e-beam with a dielectric slab
- tunable laser source in the far infrared (100 - 1000  $\mu\text{m}$ )
- possibility of obtaining high peak power (>1MW)
- compact device ( --> table-top FEL )

#### • e-BEAM PARAMETERS

accelerator	microtron	IN OPERATION
e-beam energy	5 MeV	
e-bunch duration	20 ps	
macropulse duration	3 $\mu\text{s}$	
average current	200 mA	
peak current	4 A	
vert. emittance	64 mm.mrad	
horiz. emittance	18 mm.mrad	
energy spread	0.5 %	

#### • DIELECTRIC SLAB PARAMETERS

material	polyethylene	MANY TESTS PERFORMED
thickness	3 - 30 $\mu\text{m}$	
length	300 mm	
width	25 mm	

### DESIGN OF A LOW ENERGY COMPACT FEL FACILITY

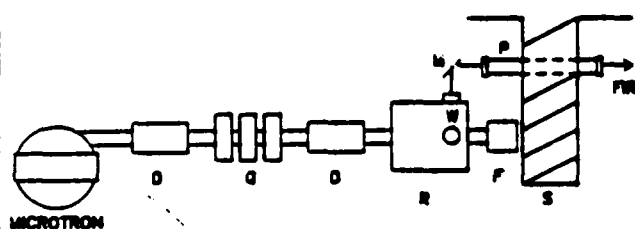
STARTING 1988 THE EXPERIMENTAL LAY-OUT HAS BEEN MODIFIED IN ORDER TO REALIZE A TEST FACILITY FOR COMPACT FEL DEVICES IN THE SUB-MILLIMETER REGION:

- DIELECTRIC LOADED WAVEGUIDE RESONATORS
- METAL GRATINGS
- BARE CAVITIES
- SHORT PERIOD UNDULATORS

#### MAIN FEATURES

- "STRAIGHT LINE" ELECTRON BEAM PROPAGATION
- DESIGN AND REALIZATION OF A RESONATOR CHAMBER WITH INTEGRATED ELECTRON BEAM DIAGNOSTICS, AND CAPABLE OF HOUSING WAVEGUIDE-STRUCTURES UP TO 40 cm LENGTH
- EXTRACTION OF THE LIGHT AT RIGHT ANGLES RESPECT TO THE e-BEAM BY MEANS OF POP-UP "ELECTRON TRANSPARENT" METAL MESHES

### LAY-OUT OF THE EXPERIMENT



D - DEFLECTING COILS  
Q - QUADRUPOLES  
R - RESONATOR CHAMBER  
W - QUARTZ WINDOW  
F - FARADAY CUP

M - PLANE MIRROR  
P - SEALED LIGHT PIPE  
S - CONCRETE SHIELD

### OPTICAL DIAGNOSTICS

WINDOWS : single crystal z-cut quartz

LENSES : TPX ( 10 --> 50 cm focal lengths )

DETECTORS : helium cooled Ge:Ga PC detector  
2x2 mm square  $\lambda_c = 105 \mu\text{m}$   $D^* = 8 \times 10^8 \text{ cm Hz/W}$   
 $R = 3.5 \times 10^{-6} \text{ V/W}$   $\tau = 100 \text{ ns}$

helium cooled Ge:Ga and InSb 5x5 mm square

pyroelectric Moletron P4-32, J3-05 (2.5 V/mJ  $\approx 0.5 \text{ ms}$ )  
Laser Prec. (250 V/mJ  $\tau = 20 \text{ ms}$ )

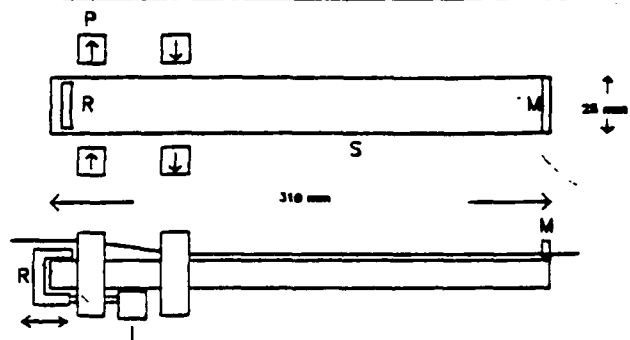
#### WAVELENGTH

ANALYSIS : inductive and capacitive mesh filters  
tungsten wire polarizers (10 --> 300  $\mu\text{m}$ )  
bulk filters (Si, KRS-5, NaCl, Mylar Polyethylene ...)  
far-infrared Fabry-Perot (mesh reflectors)

## MAIN FEATURES OF THE QUASI-OPTICAL RESONATOR

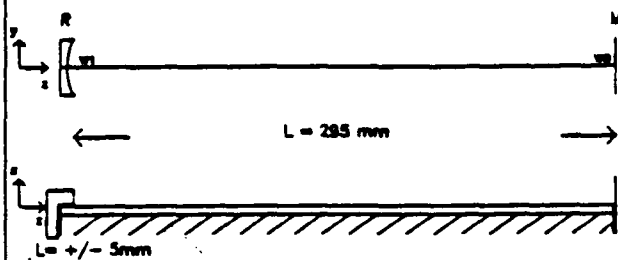
- EASY INJECTION OF THE ELECTRON BEAM ( permanent magnet deflector )  
→ SHORT RESONATOR LENGTH
- HIGH SURFACE QUALITY ( diamond machined copper plates )  
→ BETTER FILM THICKNESS UNIFORMITY
- UNIFORM OUTPUT COUPLING ( wire grating )
- BETTER CONFINEMENT OF THE WAVEGUIDE MODE IN THE HORIZONTAL PLANE
- Q-FACTOR HIGHER AT FIR WAVELENGTHS THAN AT mm WAVELENGTHS
- THE WAVEGUIDE MODES HAVE A SPATIAL DEPENDENCE WHICH CAN BE FACTORIZED IN AN EVANESCENT WAVE TERM IN THE DIRECTION PERPENDICULAR TO THE DIELECTRIC SURFACE, AND A CYLINDRICAL GAUSSIAN-HERMITE TERM IN THE TRANSVERSE DIRECTION PARALLEL TO THE SURFACE

## NEW RESONATOR FOR THE CERENKOV-FEL



- S - diamond machined copper substrate  
R - cylindrical mirror ( 45 cm radius of curvature )  
P - permanent magnet SmCo  
M - wire grid output coupler  
I - inchworm translator for mirror R ( +/- 5 mm travel, 0.1  $\mu$ m res.)

## OPTICAL CHARACTERISTICS



- R : gold coated copper cylindrical mirror 450 mm r.c.  
M : wire grid mirror 500 l/inch R = 98.8 % @  $\lambda = 400 \mu$ m

$$E(x,y) \propto W_0/W(z) \exp[-y^2/W(z)^2] \exp[i\sqrt{2}y/W(z)] \exp(-iqx) \quad q = 2\pi/\lambda y$$

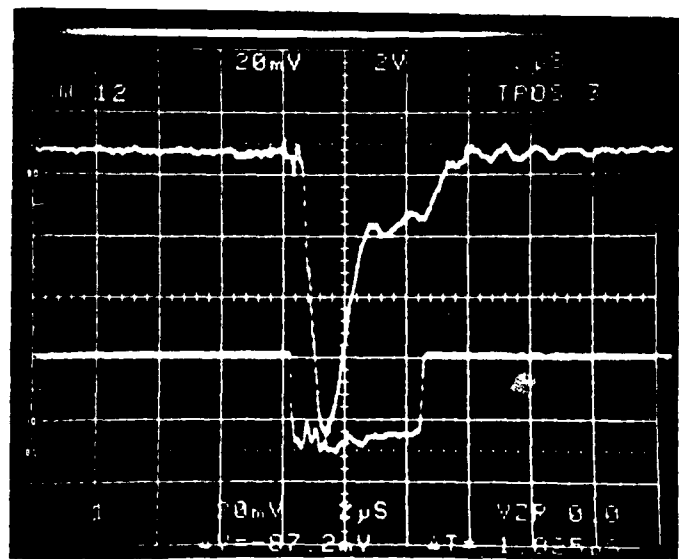
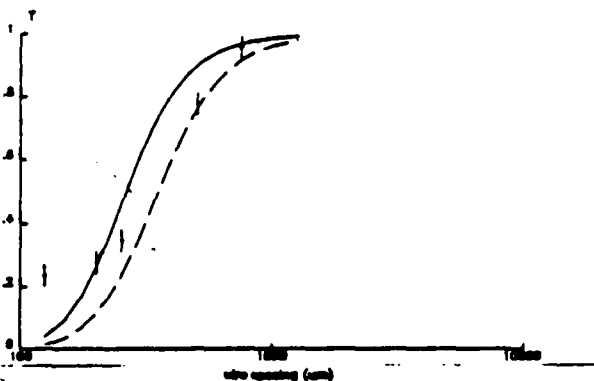
$$W(z) = W_0 \left( 1 + (z/W_0^2)^2 \right)^{1/2} \quad W_0 = 5 \text{ mm}, W_1 = 9 \text{ mm} @ \lambda = 400 \mu\text{m}$$

## PRELIMINARY EXPERIMENTAL RESULTS

- DIFFERENT WAVEGUIDE STRUCTURES HAVE BEEN TESTED BOTH WITH AND WITHOUT DIELECTRIC COATING
- EXCELLENT ELECTRON BEAM INJECTION HAS BEEN ACHIEVED BY MEANS OF THE PERMANENT MAGNET DEFLECTOR. MORE THAN 95% OF THE BEAM CURRENT PASSES ABOVE THE INPUT MIRROR AND IT IS TRANSPORTED THROUGH THE WAVEGUIDE
- A STRONG NON-LINEAR SIGNAL (vs. e-beam current) HAS BEEN OBSERVED, CORRESPONDING TO AN ESTIMATED MACROPULSE OUTPUT POWER 1-10 W, WITH A CLEAR THRESHOLD BEHAVIOUR AT A CURRENT AROUND 60-70 mA
- THE SIGNAL IS QUITE CRITICAL RESPECT TO THE e-BEAM STEERING AND TO THE TUNING OF THE MICROTRON RF DRIVING FREQUENCY
- A SPECTRAL ANALYSIS WITH WIRE GRID FILTERS INDICATED OUTPUT WAVELENGTHS IN THE RANGE 600  $\mu$ m TO 1500  $\mu$ m

## TRANSMISSION OF WIRE POLARIZERS

11  $\mu$ m slab + plate - 6 mm gap  
wire spacing ( $\mu$ m)



## PI.1 The Induction FEL Design for White Sands Missile Range

George R. Neil, J.A. Edighoffer, P. Livingston, TRW Space and Technology Group, J.M. Rawls,  
General Atomics, and I. Smith, Pulse Sciences, Inc.

R1/2104, 1 Space Park  
Redondo Beach CA 90278

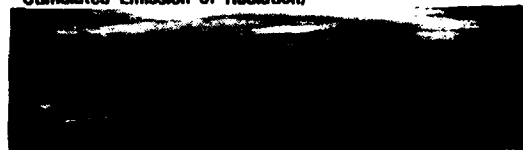
A TRW-led industrial team has designed a high power free electron laser for the White Sands Missile Range to investigate transmission of high average optical power through the atmosphere.



The Ground Based Free Electron Laser Technology Integration Experiment (GBFEL TIE) Program is the first phase of a ground-based Free Electron Laser (FEL) Program managed by the U.S. Army's Strategic Defense Command. It will demonstrate technological feasibility of developing and integrating the Laser and Beam Control Subsystems and demonstrate the ability to efficiently and effectively propagate laser energy through the atmosphere.

Free Electron Lasers (FELs) offer compelling advantages over other laser technologies because they produce a high-quality optical beam with the flexibility to cover a wide range of wavelengths at extremely high powers. The Induction Free Electron Laser (IFEL) also provides pulse format flexibility and is directly scalable to meet Phase II power requirements.

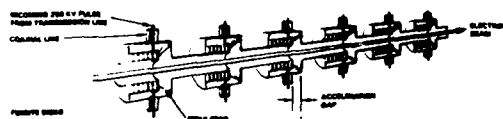
### Lasers (Light Amplification by Stimulated Emission of Radiation)



INDUCTION FREE ELECTRON LASERS (IFELs) use induction accelerators to produce a powerful beam of electrons in a pulse format. High average power is achieved by repetitively pulsing the accelerator. Due to the extremely large electron currents (kilamperes) produced by these machines, very high optical gains ( $10^4$ ) can be achieved in a single pass through the wiggler amplifier without interposing optical elements in the beam path. This preserves the high optical beam quality produced by the long, flat top of the electron pulse.

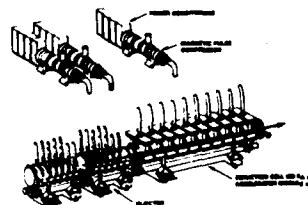


### Induction Linac Operating Principles



Induction cells encircle the electron beam path. Cables feed 250 kV voltage pulses to each accelerator cell gap. The gap voltage is prevented from shorting out on the beamline by high-inductance ferrite disks so that the full accelerating voltage is applied to the beam. As the electrons speed past each acceleration gap, they receive an incremental energy kick, gathering momentum each time. The ferrites then damp out undesirable electromagnetic wake fields produced as the electrons pass. This damping allows extremely high beam currents to be transported.

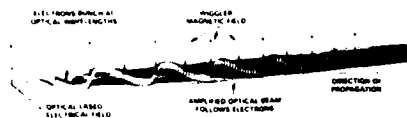
### Induction Linear Accelerator



A pulse of electrons 60 nanoseconds long is produced by thermionic emission (as in TV and radio tubes) from the injector's cathode.

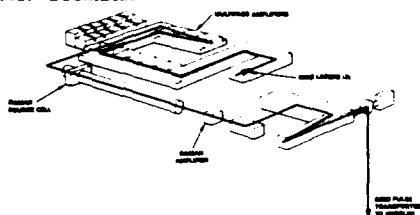
An array of 680 induction cells, grouped 20 per accelerator module, produces electric fields that drive the electrons to approach the speed of light. They exit the 218-meter assembly as a two-millimeter diameter, 1.6-kiloampere beam at 170 MeV. In less than one second, IFELs can be throttled to full power from a low pulse rate, low power drain idle mode used to confirm performance.

## Wiggler Operation



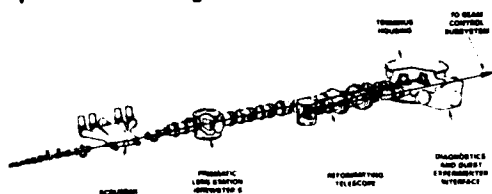
As relativistic electrons are forced to oscillate by the wiggler and interact with the light beam, they bunch into disks separated by the optical wavelength, while providing large exponential gain. After bunching is complete, these disks radiate optical power coherently like antennas. During exponential growth, the optical mode is cleaned up as the central core of the beam rapidly grows more intense and noise drops away in a process called gain guiding. After the bunches form, the electron beam continuously focuses the light beam, guiding it through the tapered region of the wiggler in another process called optical guiding.

## Master Oscillator

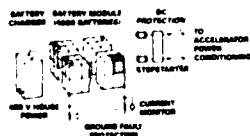


Two highly stable, low power ring lasers produce a photon beam of very narrow bandwidth which is converted to the required pulse shape by a high repetition rate optical chopper. Three slab amplifiers pass the beam back and forth 18 times along a zigzag path. Raman conversion shifts the wavelength close to an atmospheric absorption line. The beam can be switched between wavelengths to change the degree of atmospheric absorption, heating, and thermal blooming. Switching is so fast that atmospheric properties remain constant during the experiment.

## Optical Conditioning

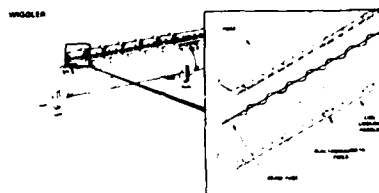


The high quality optical beam containing optical harmonics exits the wiggler and expands by diffraction reducing the power intensity. Three complementary harmonic attenuating techniques (argon, water scrubbers, and prism lens) clean the beam since no single attenuator covers the entire harmonic spectrum. A reforming telescope reshapes the output from a Gaussian to a flat top irradiance distribution. This distribution maximizes Beam Control Subsystem utility and redistributes the thermal load uniformly across the optical surfaces.



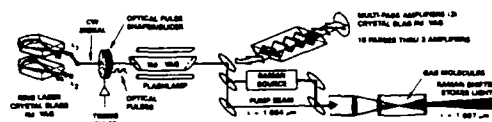
Battery modules provide a highly regulated, reliable prime power source under full control of the TIE operator. Surge demand on the electrical grid is eliminated. Fully protected DC voltage at up to 3.7 kV is provided from each module driving a single accelerator module power train. The sealed batteries use dry electrolytes and require minimal maintenance.

## Wiggler



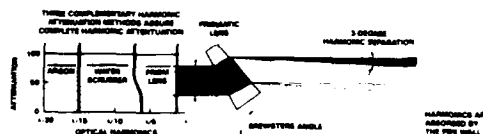
An alternating magnetic field makes the electron beam trajectory wiggle with a period that, in the reference frame of the relativistic electrons, is resonant with, and allows transfer of energy to, the optical beam. Key to efficient wiggler operation is this matching of the magnetic field along the full length of the wiggler as the electron beam energy decreases. The IFEL employs electromagnets that are fairly insensitive to radiation, and their fields can be tapered in real time to match the decrease in electron energy. The magnets are powered using a binomial winding pattern that eliminates steering errors introduced by changes in field strength.

## Master Oscillator Layout



Face pumped, multi-faceted Nd:YAG crystal slabs provide the long beam paths needed to amplify the ring laser pulse. During Raman conversion, the pump beam at 1.064  $\mu\text{m}$  interacts with deuterium molecules to create the required 1.097  $\mu\text{m}$  Raman shifted (Stokes) light for the seed pulse while retaining a linewidth narrower than any atmospheric absorption line.

## Optical Conditioning



Rarified argon filling the vacuum pipe absorbs the hard ultraviolet ionizing radiation. Next, a supersonic steam scrubber strips the beam of its mid-ultraviolet photons. Finally, an uncoated prism refracts the remaining harmonics out of the beam path to be absorbed by an optical beam dump along the pipe wall. This prism is aligned to Brewster's angle (55.4 degrees for fused silica). At this angle, a surface reflects less than 0.2 percent of the incident light. Absolutely no harmonics are transmitted to the Beam Control Subsystem.



## PI.2

### OPTIMAL BASIS EXPANSION FOR SOLVING TIME DEPENDENT SCHRÖDINGER EQUATION : SIMULATION OF GUIDING AND MULTIMODE MECHANISMS

D. IRACANE and J.L. FERRER

Commissariat à l'Energie Atomique, Service PTN, B.P.n°12, 91680 BRUYERES-LE-CHATEL, FRANCE

Free Electron Laser beam propagation can be described by Time Dependent Schrödinger type equations. For strongly time dependent problems, a set of complex static vectors is proposed as a natural basis which enables to solve efficiently a simplified model. Guiding and multimode phenomena are simulated by using this technique.

**PURPOSE OF THE PRESENT WORK:** To provide simulations of a Compton FEL taking into account both bidimensional effects and multimode mechanisms

#### MODELIZATION OF A COMPTON FEL

Singlemode model:

- A KMR model to simulate the longitudinal part of the interaction
- Each longitudinal macro-electron has a constant radial profile  $S(r)$
- Each laser harmonic satisfies a 2D Time Dependent Schrödinger equation

Multimode model:

- The electronic distribution is assumed to be periodique with a periode  $\Lambda_L = N\lambda_L$
- The laser field  $A_L$  is expended as a sum of Fourier modes ( $n < N$ ):  $k_n = (1+n/N)k_L$

Main features:

- Self-consistent filling factor  $R(z) = S(r) \cdot A_L(r, z)$
- The whole system is conservative:  $E(\text{electrons}) + E(\text{laser}) = \text{constant}$
- Guiding effect are qualitatively recovered for a cost comparable to 1D models
- Mode competition and sidebands are simulated from noise to saturation

#### A NEW TECHNIQUE FOR SOLVING TIME DEPENDENT SCHRÖDINGER EQUATION

Equation:  $i\partial_z \varphi = H \cdot \varphi \quad ; \quad \varphi(0) = \varphi_0$

Example :  $H = -\Delta/2k \quad ; \quad \varphi_0 = \exp(-r^2/2\sigma^2)$   
 $\rightarrow \quad \varphi(z) = \exp(-r^2/2\mu^2) \quad ; \quad \mu^2 = \sigma^2 + iz/k$

Problem: for strongly time dependent regimes ( $z/k \gg \sigma^2$ ), techniques using standard basis expansion have poor convergence properties.

Optimal basis: a set of complex static vectors:  $u_n = \exp(in\delta H_B) \cdot u_0$ , where  $u_0$  is a seed vector,  $\delta$  is a time increment,  $H_B$  is an Hamiltonian. Each vector is an instantaneous picture of the propagation of  $u_0$  with  $H_B$ . When  $(u_0, H_B)$  are closed to  $(\varphi_0, H)$ , efficient calculations can be performed. For FEL simulation  $u_0$  is a Gaussian and  $H_B$  is the Laplacian operator.

Main features:

- The Complex Basis  $\{u_n\}$  is characterized by 2 uncorrelated scales, one in  $u_0$  to fit the scale of the initial condition  $\varphi_0$ , one in  $H_B$  to fit the scale of the dynamics  $H$ . In contrast, standard bases are defined as a set of eigenmodes of  $H_B$  and cannot include to scale of the initial condition.
- The Complex vectors  $u_n$  are time independent. So, we avoid spurious non linearities that may appear with time dependent rotating bases.
- The round-trips in a standard cavity are simulated by a matrix multiplication. Moreover, the evaluation of this matrix in the Complex Basis is straightforward.

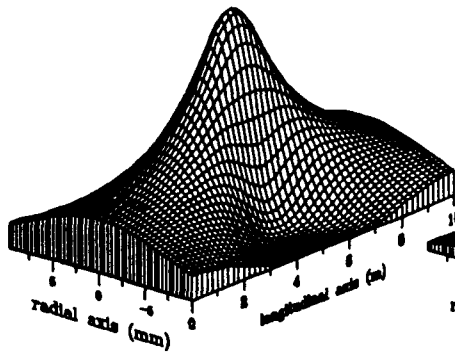


Figure 1

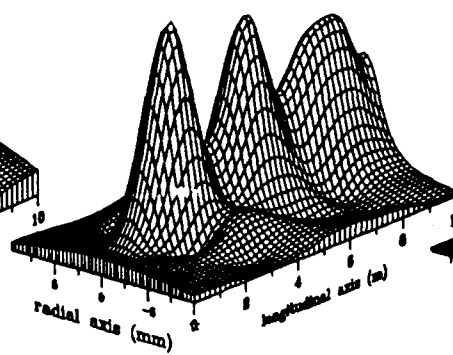


Figure 2

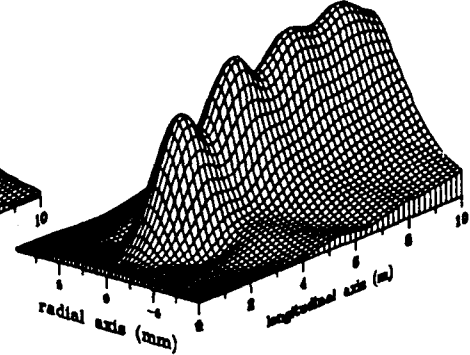


Figure 3

**Illustration of a self-consistent calculation of the gain and the radial profile in an amplifier:**

Fig. 1 - Free propagated laser field in a 10 meter amplifier.

Fig. 2 - Laser propagation in a non tapered wiggler ; the final gain is 4. Note the untrapping of the laser field when the gain decreases.

Fig. 3 - Laser propagation in a tapered wiggler. Gain raises up to 125.

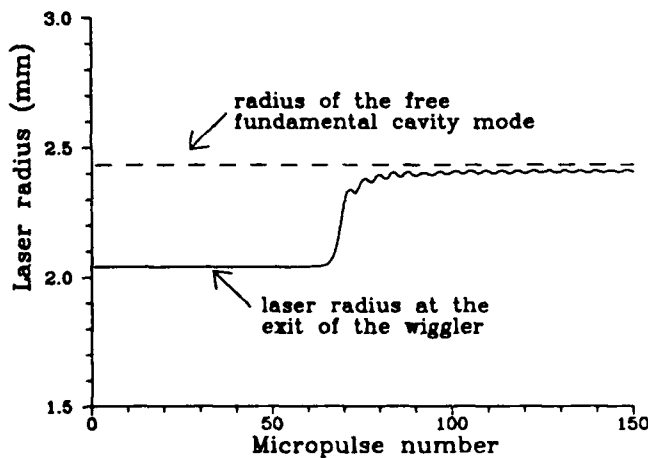


Figure 4

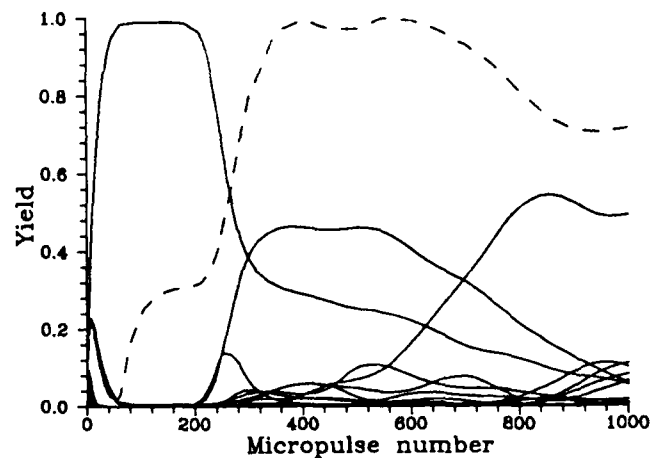


Figure 5

**Illustration of gain guiding and multimode simulation in an oscillator:**

Fig. 4 - Laser mean square radius measured at exit of the wiggler in an oscillator system. Comparison between interacting laser radius and free laser radius shows strong gain guiding and weak diffractive guiding.

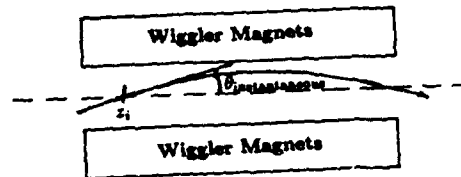
Fig. 5 - Multimode operation: 15 laser modes start from noise at the same level and increase to the saturation. The evolution of the total power  $P$  in a macropulse is given, up to a normalization, by the dashed line. The ratio of the power in a given mode and  $P$  is plotted by a full line. The mode competition leads to a unique mode  $F$  in the 200 first round-trips. Then an expected sideband  $S_1$  raises up. After 600 round-trips a second order sideband appears between  $F$  and  $S_1$ .

M. J. Schmitt and C. J. Elliott  
Los Alamos National Laboratory  
P. O. Box 1663, MS E531  
Los Alamos, New Mexico 87545

The mechanisms that generate harmonic radiation in free electron lasers are explored using a distributed single-electron source model. The model includes the effects of misalignments and transverse gradients of the electron beam and wiggler field. The computed transverse spatial profiles of the harmonics are shown.

• Work performed under the auspices of the U. S. Department of Energy and supported by the U. S. Army Strategic Defense Command

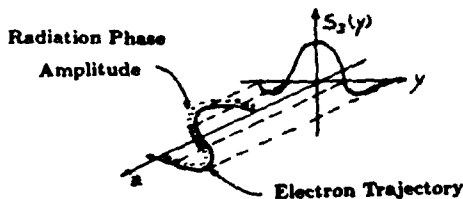
#### Modeling of Misalignments



- Radiation by an electron at the various harmonic frequencies depends on the angle the electron makes with the wiggler axis
- This angle varies as the electron travels through the wiggler due to electron beam misalignment, betatron motion and electron beam focusing
- The instantaneous guiding center angle is calculated for each electron as it travels through the wiggler
- As the angle for each electron changes, the coupling coefficient for each electron for each harmonic is modified via tabulated values

#### IMPETUS FOR AN IMPROVED MODEL

- Electron's radiation phase fluctuates over a wiggler wavelength
- This fluctuation is correlated to specific transverse locations with respect to the electron's guiding center position



- Conventional models average away these fluctuations
- This type of averaging ignores:
  - Even harmonic radiation (which exists for aligned systems)
  - Higher order structure of the harmonic radiation patterns

#### CONCLUSION

The source functions must be modeled explicitly to achieve the correct harmonic radiation pattern

#### Wave Equation Including Discrete Multi-Pole Sources

The wave equation can now be written

$$\left[ 2ifk_z \frac{d}{dz} + \frac{\partial^2}{\partial y^2} \right] E_z = \sum_{l=1,2,3} S_l(y)$$

where the three source terms on the right-hand side are given by:

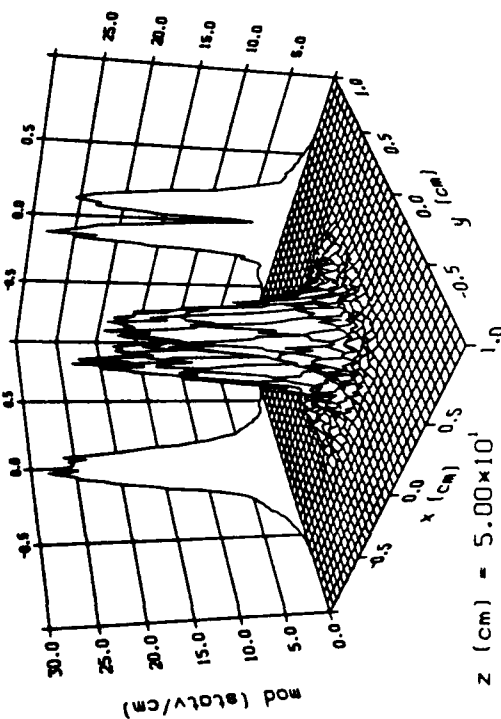
- Mono-pole term
 
$$S_1(y) = \left\langle \frac{14\pi I f k_z a_{w1}}{c} K_1^{(1)}(\xi, \sigma) \delta(y - y_0) \frac{e^{-i/\sigma}}{\gamma} \right\rangle$$
- Di-pole term
 
$$S_2(y) = \left\langle \frac{4\pi I f k_z a_{w1}}{c} K_2^{(2)}(\xi, \sigma) \left[ \delta(y - y_0 - x/2) - \delta(y - y_0 + x/2) \right] \frac{e^{-i/\sigma}}{\gamma} \right\rangle$$
- Tri-pole term
 
$$S_3(y) = - \left\langle \frac{14\pi I f k_z a_{w1}}{c} [K_3^{(1)}(\xi, \sigma) - K_3^{(3)}(\xi, \sigma)] \right. \\ \left. \times \left\{ \delta(y - y_0) - \frac{1}{2} [\delta(y - y_0 - x/2) + \delta(y - y_0 + x/2)] \right\} \frac{e^{-i/\sigma}}{\gamma} \right\rangle$$

where

$$K_l^{(m)}(\xi, \sigma) = (-1)^l \sum_{n=-\infty}^{\infty} J_n(f\xi) [(-1)^m J_{2n+l-m}(\sigma) - J_{2n+l+m}(\sigma)]$$

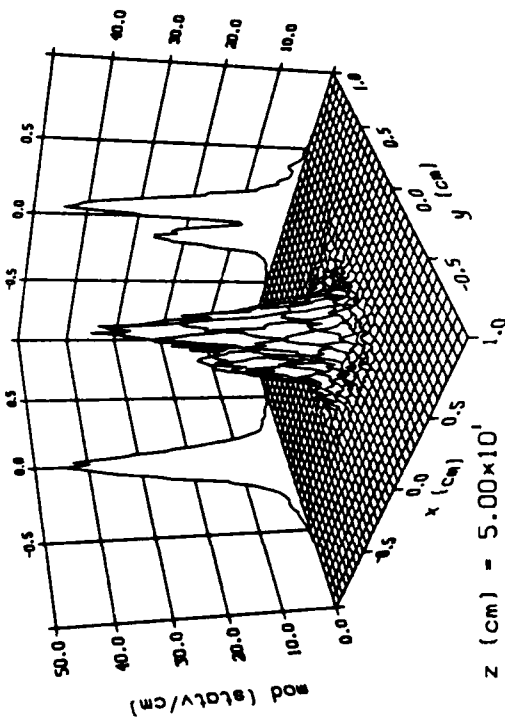
# Los Alamos FEL

Magnitude of the Electric Field without E-beam Tilt  
transverse shape for the  
second harmonic



# Los Alamos FEL

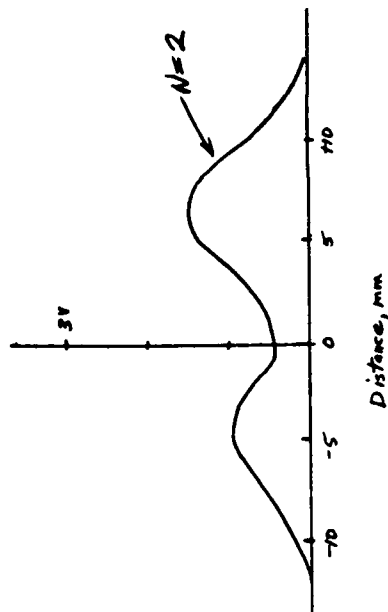
Magnitude of the Electric Field with 2mm E-beam Tilt  
transverse shape for the  
second harmonic



- Los Alamos FEL  
 $\gamma = 40$ ,  $\Delta\gamma/\gamma = 1.2\%$ ,  $I = 400$  Amps,  $\epsilon = 2.1$  mmrad,  $\lambda_w = 2.73$  cm,  $B_w = 3927$  Gauss,  $L_w = 100$  cm,  $\lambda_e = 10.36$   $\mu$ m,  $P_{ave} = .5$  GW,  $z_r = 49.5$  cm,  $G = 16\%$ ,  $\eta = .84\%$

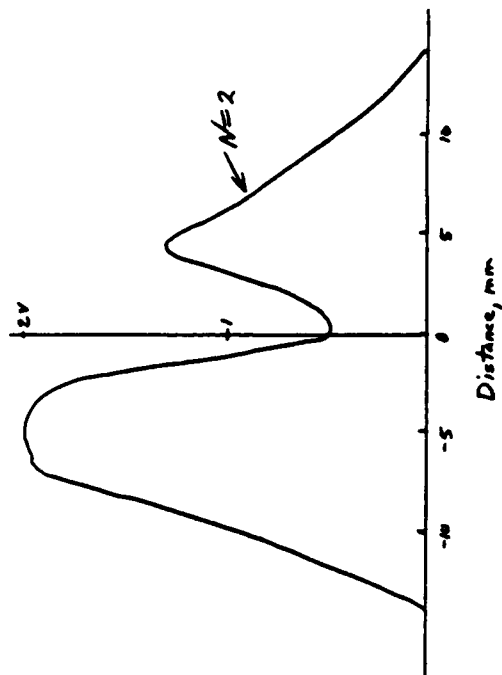
## Los Alamos Fel Oscillator

Experimental Transverse Second Harmonic Intensity Profiles



## Los Alamos Fel Oscillator

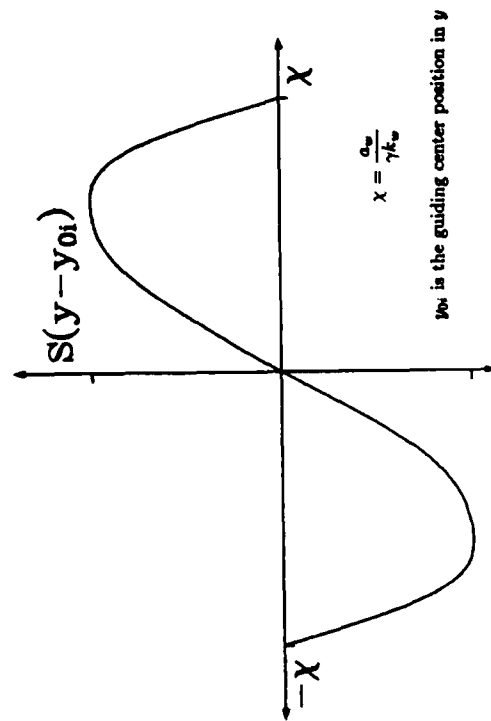
Experimental Transverse Second Harmonic Intensity Profiles  
with Fundamental "Peaking"



### Conventional Modeling Wisdom

- Numerical models assume one discrete source (mono-pole) for each electron located at the electron's guiding center
- The amplitude of this source is equal to the transverse average of the distributed source function (1-D coupling coefficients)
- The single-electron even-harmonic sources can only have non-zero averages caused by angular effects (di-pole coupling neglected)

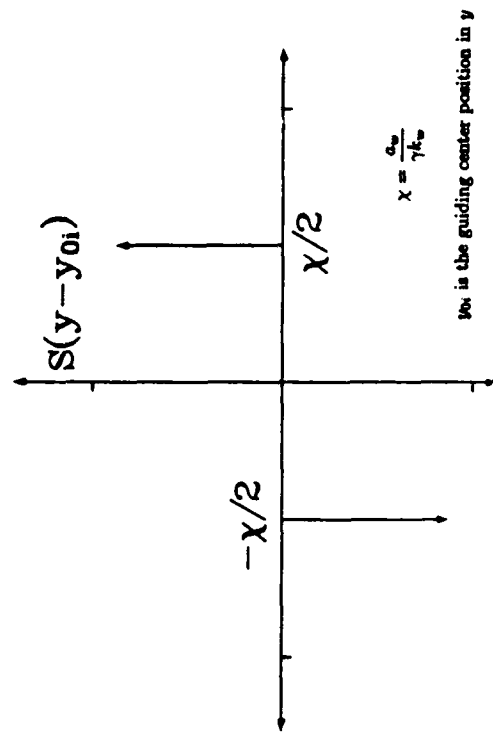
### Analytic Second Harmonic Distributed Single-Electron Source



### Harmonic Modeling with Multi-Poles

- Single-electron theory gives a smoothly varying distributed source function for each electron
- The analytic source function is converted to a discrete ( $\delta$ -function) source function
- The discrete source function is a combination of mono-pole, di-pole and tri-pole terms
- The weights for the various multi-pole terms are obtained by equating the total electron beam source derived from the analytic single-electron source function with that from the discrete single-electron source function
- Higher order multi-poles can be neglected if the transverse density is a smoothly varying function

### Discrete Second Harmonic Distributed Single-Electron Source



## PI.5 A Demonstration of Loss Modulation and Cavity Dumping in a Free-electron Laser Oscillator

Stephen V. Benson, John M. J. Madey and Eric B. Szarmes  
Department of Physics, Duke University  
Durham NC 27706

and

Anup Bhowmik, Jeff Brown, Phillip Metty and Mark Curtin  
Rockwell International, Rocketdyne Division  
6633 Canoga Ave., Canoga Pk. CA 91303

The performance of an intracavity cadmium telluride electro-optic cell in a free-electron laser will be described. The cell, installed in the Stanford Mark III IRFEL, was used to either modulate the optical cavity losses or to dump the stored optical cavity energy or both. The results of the experiments will be presented.

### Abstract

We have installed a cadmium telluride electro-optic cell in the Mark III IRFEL at Stanford and used it both to modulate the cavity losses and to switch out the stored energy in the optical cavity. The cell operates by rotating the polarization of the light in the cavity. This both reduces the gain and increases the losses due to the presence of an intracavity Brewster plate. By rotating the polarization quickly by  $90^\circ$ , it is possible to dump up to half of the intracavity power in a single pass. In order to reduce power levels on the electro-optic cell, we installed a beam expanding telescope to reduce the fluence at the cell by a factor of 10. The cell was driven by either an RF or DC high voltage pulse. The RF pulse was locked to the sixtieth subharmonic of the accelerator frequency which corresponds to the round trip frequency of the optical cavity. Large voltages were required to shut the laser off entirely. The loss modulation was found to be a function of cavity length detuning, as predicted by theory.

### Abstract(cont.)

In order to dump the optical cavity when in DC mode, it was only necessary to apply a pulse to the e-o cell. When the e-o cell was operated in RF mode, the RF was shifted in phase by  $180^\circ$  in order to dump the light. The phase shift was slowed by the high Q of the drive circuit. This caused the cavity dumping to occur over a period of about 5 cavity round trips. Enhancements in the outcoupled power by a factor of ten were seen.

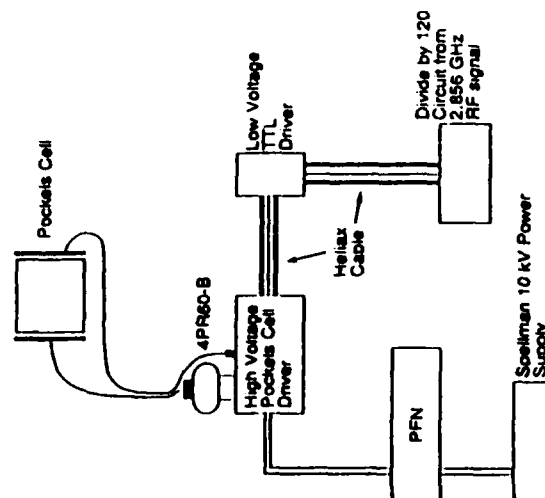
Despite the beam expanding telescope, optical damage of the e-o cell was seen. This eventually shut off the laser when intracavity losses approached 50% per pass.

### Background

The FEL is a laser with extremely high saturation intensity but typically low to intermediate gain. The cavity losses are usually small resulting in output power which is small compared to the saturation power. It would be quite nice if one could dump the intracavity power in order to increase the outcoupled peak power. This has been done in conventional lasers to increase the peak power.

Several problems arise when one attempts to use an electro-optic (e-o) cell in a FEL. The first is that the high intracavity power one is trying to dump causes transient or permanent damage to the e-o cell. The second is that the insertion losses can be rather high, leading to difficulty lasing. One is usually forced to use anti reflection coatings on the e-o cell which reduces the useful bandwidth of the cell. Finally, the voltage of the cell is proportional to the wavelength, which makes long wavelength cavity dumping especially hard to do.

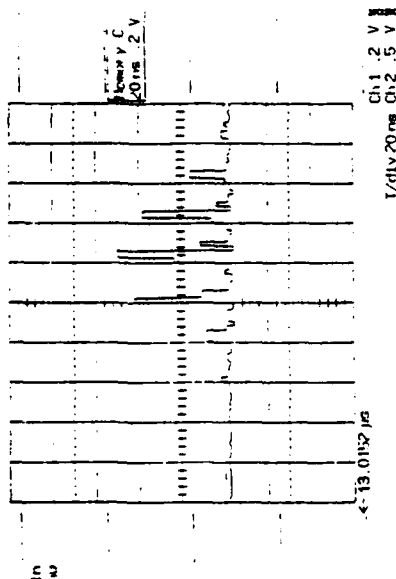
Schematic Circuit for Pockels Cell Driver



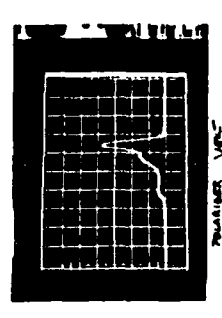


## Cavity dumping

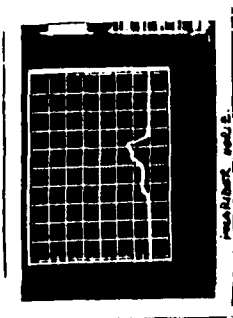
x10 power enhancement after  
3 round trips



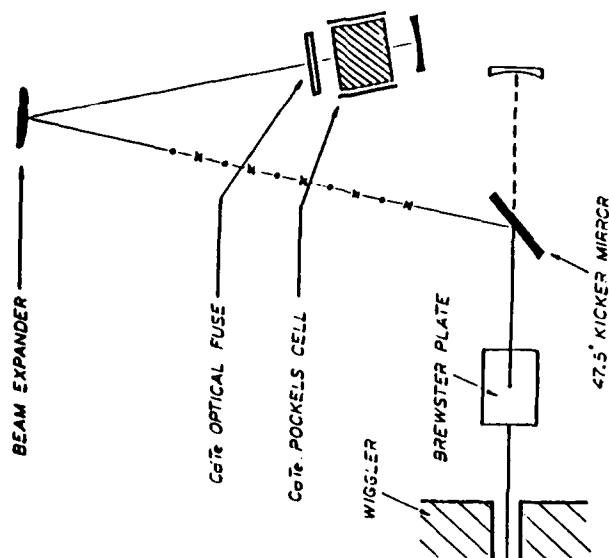
Polarizer Vertical



Polarizer Horizontal

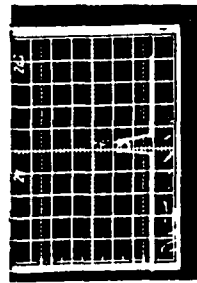
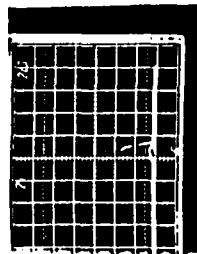


## ELECTRO-OPTIC MODULATOR



## Loss-Modulated Macropulses

## Cavity dumping using tophat pulse (no modulation)

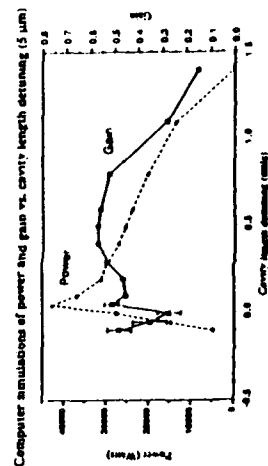


Maximum stable power

Power from shorter cavity

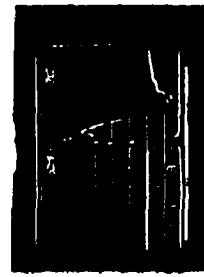
No cavity dumping

E-beam and optical  
macropulses



Optimal cavity dumping

Early 'cavity dumping'  
(i.e. very high losses)



## CONCLUSIONS

- Electro optic cell proved capable of operating at fluences similar to those in a loss-modulated cavity. Transient bleaching was found for higher losses. This occurred at a lower fluence than the permanent damage fluence.
- Initial insertion losses agreed with expectations. Total losses of 16% were measured with 4% losses from the mirrors and Brewster plate. This is in reasonable agreement with the prediction of 11% insertion losses. Insertion losses gradually increased to over 50%. This seems to have been caused by some contaminant which migrated out of the surrounding ceramic.
- Both loss modulation and cavity dumping were seen. Both effects were limited by the speed of the drive electronics. Only 5 or 6 of the 60 possible bunches in the cavity lased, and the cavity was dumped in 5 round trips.
- Electro optic cells appear to be feasible for FELs if the intracavity fluence is kept small and the round trip time is slow enough for electronics to drive the crystal (10 MHz is slow enough). They become less feasible for wavelengths of more than a few microns.



# Pl.8

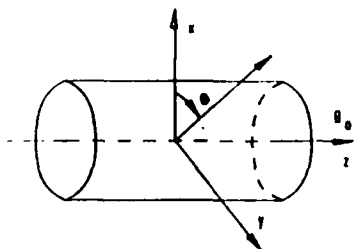
## IS IT NECESSARY TO ASSUME A NEUTRALIZING UNIFORM BACKGROUND WHEN DEVELOPING A THEORY FOR THE FEL IN THE COLLECTIVE REGIME?

A. Bourdier, J.M. Buzzi.

Laboratoire de Physique des Milieux Ionisés, UPR 287 du CNRS  
Ecole Polytechnique, 91128 Palaiseau Cedex (France)

\* Also in Centre d'Etudes de Limeil-Valenton, BP 27,  
94190 Villeneuve-St-Georges Cedex (France)

We start with the Vlasov equation, assuming that there is no neutralizing background in the beam. In our model, the electrons are subjected to an electrostatic field as they propagate along the magnetic field. We obtain a result similar to Bernstein's, plus an additional term which vanishes as  $B_0$  increases.



We consider a nonneutral infinitely long beam propagating along  $\vec{B}_0$ . We work in frames such as  $\langle v_z \rangle = 0$ .

Considering the electron density in the column in constant we find a steady state solution for the Vlasov equation [1,2]. Assuming a rotor equilibrium we find [3]

$$f_0(\vec{r}, \vec{p}) = f_0(H - \Omega_R \mathcal{P}_R, \mathcal{P}_z)$$

$\Omega_R$  is the constant velocity corresponding to the mean azimuthal motion of the column,  $H$ ,  $\mathcal{P}_R$ ,  $\mathcal{P}_z$  are the single-particle constants of the motion (total energy and two canonical momentums). Transforming the Vlasov equation to a frame of reference rotating with angular frequency  $\Omega_R$ , we obtain [4,5]

$$\left( \frac{\partial}{\partial t} + \vec{v} \cdot \nabla \right) f_1 + m(\omega_H + 2\Omega_R) \frac{\vec{B}_0}{|B_0|} \cdot \nabla \frac{\partial}{\partial \vec{p}} f_1(\vec{r}, \vec{p}, t) = -e \vec{E}_1(\vec{r}, t) \cdot \frac{\partial}{\partial \vec{p}} f_0(\vec{p}, \vec{r})$$

when [1-5]

$$\Omega_R \approx \Omega_H = -\frac{\omega_H}{2} \left[ 1 \pm \left( 1 - \frac{2\omega_p^2}{\omega_H^2} \right)^{1/2} \right]$$

$$\omega_H = -\frac{c B_0}{mc}, \quad \omega_p^2 = \frac{4\pi e^2 N_0}{m}$$

In the strong  $B_0$  limit that we consider here, we have

$$\Omega_R \approx -\frac{\omega_p^2}{2\omega_H} = -\frac{c E_0(r)}{r B_0}$$

which corresponds to the  $\vec{E}_0 \wedge \vec{B}_0$  rotation of the column.

In the rotating frame the electric field does not appear and the equilibrium distribution function is spatially uniform.

Following Bernstein [6], we can find again, in the rotating frame, his result for  $f_1$  taking  $\omega_H' = \omega_H + 2\Omega_R$  for the electron cyclotron frequency. We obtain the same result using the trajectory method [7,8,9].

In what follows we work in one of these rotating frames, and we stop using the prime notation.

We consider now that the radial electric field has the following form:

$$\vec{E}_{OT}(\vec{r}, t) = \vec{E}_0(\vec{r}, t) + \delta \vec{E}_0(\vec{r}, t)$$

The electron density is not quite uniform.  $\vec{E}_0(\vec{r}, t)$  is the field due to

the mean density,  $f_0^0$  is supposed to vary slowly with time and space.

Let us look for a condition permitting to assume the electron beam is a plasma.

First we solve the linearized Vlasov Eq. using the general technique of performing Fourier and Laplace transformation. Introducing cylindrical coordinates we obtain

$$e b E_0 \frac{\partial f_1}{\partial p_1} + \omega_B \frac{\partial f_1}{\partial r} = i (\vec{k} \cdot \vec{v} - \omega) f_1 - e f_1' \frac{\partial f_0}{\partial p}$$

we solve this partial differential equation.

$$f_1 = -\frac{1}{\omega_B} e^{-i\theta \sin \varphi} \left\{ \left[ e E_1 + \frac{\partial f_0}{\partial p} \right] (\varphi - \tau) + \frac{e b E_0}{\Psi(\omega_B)} H(\varphi - \tau) \right\} \\ \cdot e^{-i\theta \sin(\varphi - \tau) + i \alpha \tau} \quad \left| \right.$$

$$\text{with } \alpha = (k_{\parallel} v_{\parallel} - \omega)/\omega_B, \quad \beta = \frac{k_{\perp} v_{\perp}}{\omega_B}$$

The wave vector of the electrostatic wave is assumed to be in the (x, z) plane.  $H$  is some bounded function.  $\Psi(\omega_B)$  is some function such as  $\Psi(\omega_B) \rightarrow \infty$  when  $|\omega_B| \rightarrow \infty$ . The expression we have derived for  $f_1$  is the one obtained by Bernstein /6/, plus an additional term which vanished as  $B_0$  increases.

We can find a similar result using the trajectory method /7,9/.

The unperturbed motion of one electron with initial velocity ( $v_0 \cos \varphi, -v_0 \sin \varphi, v_{0\parallel}$ ) and initial position  $\vec{r}_0$  is given by

$f_1$  tends to the expression given by Bernstein /6/ when  $f_0^0 \rightarrow 0$ . As a consequence when this parameter is small enough we can consider we have a plasma.

#### References.

- /1/ R.C. Davidson and R.A. Krall, Phys. Rev. Letters **22**, 813 (1969)
- /2/ R.C. Davidson and R.A. Krall, Phys. Fluids **13**, 1961 (1970)
- /3/ U.L. Degen, Jr. and R.C. Davidson, Phys. Fluids **13**, 2372 (1970)
- /4/ R.C. Davidson, J. Plasma Phys. **6**, 229 (1971)
- /5/ R.C. Davidson, Theory of nonneutral plasmas, Frontiers in Physics, W.A. Benjamin, Inc. (1974)
- /6/ I.D. Bernstein, Phys. Rev. **102**, 10 (1958)
- /7/ L. Mover, Phys. Rev. **116**, 16 (1959)
- /8/ W.D. Jones, H.J. Boucet and J.M. Buzzi, An introduction to the linear theories and methods of electrostatic waves in plasmas, Plenum Press, New-York and London (1985)
- /9/ D. Quemada, Ondes dans les plasmas, Hermann, Paris (1968).

$$\vec{r} = \vec{r}_0 + \frac{1}{\omega_B} \left[ \frac{v_{0\parallel}}{2} \vec{k} \left( 1 - \frac{t}{2} \right) + v_{0\perp} \left( \frac{t \omega_B}{2} \vec{v}_{0\perp} \right) \right]$$

$$\frac{e b E_0}{m \omega_B} = \frac{1}{m} \vec{E}$$

$$\vec{E}(t) = \begin{bmatrix} \cos \omega_B t & \sin \omega_B t \\ -\sin \omega_B t & \cos \omega_B t \end{bmatrix} \vec{E} = \begin{bmatrix} \sin \omega_B t \\ \cos \omega_B t \\ 0 \end{bmatrix}$$

$$\vec{H} = \begin{bmatrix} t & \frac{1}{\omega_B} \left( 1 - \frac{1}{\cos \omega_B t} \right) & 0 \\ -\frac{1}{\omega_B} & t & 0 \\ 0 & 0 & 1 \end{bmatrix}$$

Letting  $t' = t - \theta$ , the solution of the linearized Vlasov Eq. writes /9/

$$f_1 = -\frac{e}{m} \int_0^\infty ds f_1'(\vec{r}', t - s) \cdot \frac{\partial f_0}{\partial \vec{v}}(\vec{v}')$$

We find

$$f_1(\vec{k}, \vec{v}, \omega) = -\frac{e}{m \omega_B} E_1(k, \omega) \cdot \int_0^\infty d\zeta \frac{\partial f_0}{\partial \vec{v}} e^{-i\Phi(\zeta)}$$

with  $\Phi(\zeta) = \alpha \zeta + \beta [\sin(\zeta + \varphi) - \sin \varphi]$

$$= -\frac{e b E_0}{m \omega_B} \frac{\beta}{v_{\perp}} \left( \zeta \sin \zeta + \frac{1}{\omega_B} \cos \zeta + 1 \right)$$

using two different methods we have found that, in the rotating frame,

# PI.9 A MODIFIED TWISS PARAMETER OPTICAL TREATMENT FOR SPACE CHARGE DOMINATED ELECTROSTATIC ACCELERATOR FREE ELECTRON LASERS

D.J. Larson  
Center for Research in Electro Optics and Lasers  
12424 Research Parkway, Orlando, FL 32826

**ABSTRACT** -- The design of electrostatic accelerator Free Electron Lasers requires an optical treatment of the accelerating electron beam that includes the effects of finite emittance, space charge, and acceleration. Use of a canonical transformation allows the problem to be treated in a new coordinate system where the Twiss parameterization of Courant and Snyder may be employed.

$$x'' + K_x x = 0 \quad \text{and} \quad y'' + K_y y = 0$$

Equations 1. For piecewise linear restoring forces the position of a particle evolves as governed by the above differential equations.

$$\alpha_x = -\frac{\pi w_x w_x'}{\epsilon_x}, \quad \beta_x = \frac{\pi w_x^2}{\epsilon_x}, \quad \alpha_y = -\frac{\pi w_y w_y'}{\epsilon_y}, \quad \beta_y = \frac{\pi w_y^2}{\epsilon_y},$$

Equations 2. For a particle beam with an elliptical cross section, with  $w_x$  the dimension of the beam in the  $x$  direction,  $w_x'$  the divergence of the beam in the  $x$  direction,  $w_y$  the dimension of the beam in the  $y$  direction, and  $w_y'$  the divergence of the beam in the  $y$  direction, Courant and Snyder parameterize the beam by the above functions  $\alpha_x$ ,  $\beta_x$ ,  $\alpha_y$ , and  $\beta_y$ .  $\epsilon_x$  and  $\epsilon_y$  are the phase space areas of the beam (the emittances).

$$\gamma_x = \frac{1 + \alpha_x^2}{\beta_x}, \quad \alpha_x' = K_x \beta_x - \gamma_x, \quad \beta_x' = -2\alpha_x, \quad \gamma_y = \frac{1 + \alpha_y^2}{\beta_y}, \quad \alpha_y' = K_y \beta_y - \gamma_y, \quad \beta_y' = -2\alpha_y$$

Equations 3. Courant and Snyder derive the above coupled differential equations relating the functions  $\alpha_x$ ,  $\beta_x$ ,  $\alpha_y$ , and  $\beta_y$ .

$$\frac{dP_x c}{ds} = \frac{qIx}{\pi \epsilon_0 w_x (w_x + w_y) (\beta \gamma)^2 c} \quad \text{and} \quad \frac{dP_y c}{ds} = \frac{qIy}{\pi \epsilon_0 w_y (w_x + w_y) (\beta \gamma)^2 c}$$

Equations 4. Sacherer has shown that the linear contribution of space charge can be included in the analysis via the above equations.

$$P_x = \beta \gamma m_0 c x' \quad \text{and} \quad P_y = \beta \gamma m_0 c y'$$

Equations 5. The momenta may be re-expressed as above.

$$x'' + \frac{(\beta \gamma)'}{(\beta \gamma)} x' - \frac{K_{scx}}{(\beta \gamma)^3} x = 0, \quad \text{and} \quad y'' + \frac{(\beta \gamma)'}{(\beta \gamma)} y' - \frac{K_{scy}}{(\beta \gamma)^3} y = 0.$$

$$K_{scx} = \frac{qI}{\pi \epsilon_0 w_x (w_x + w_y) m_0 c^3} \quad \text{where} \quad \text{and} \quad K_{scy} = \frac{qI}{\pi \epsilon_0 w_y (w_x + w_y) m_0 c^3}$$

Equations 6. Combining Equations 4 and 5 leads to differential equations for the particle trajectories that depend on the first order (acceleration) term.

$$G = -[(m_0 c^2 - q\phi)^2 - (P_x c - qA_x c)^2 - (P_y c - qA_y c)^2 - (m_0 c^2)^2]^{1/2} - qA_s c.$$

Equations 7. The single particle Hamiltonian for particle motion is given above, using distance along the beamline as the independent variable.

$$u = fx, \quad v = fy, \quad P_u = P_x/f, \quad \text{and} \quad P_v = P_y/f.$$

Equations 8. Applying a canonical transformation to the Hamiltonian of Equation 7, using the generating function  $F_2 = fP_u c x + fP_v c y$ , leaves the conjugate coordinates and momenta as given above.

$$G^* = -[(m_0 c^2 - q\phi)^2 - (P_u f c - qA_x c)^2 - (P_v f c - qA_y c)^2 - (m_0 c^2)^2]^{1/2} - qA_s c + P_u c u f' / f + P_v c v f' / f.$$

Equation 9. The transformed Hamiltonian is given above.

$$u'' + K_u u = 0 \quad \text{and} \quad v'' + K_v v = 0$$

$$\text{where} \quad K_u = -\frac{f''}{f} - \frac{K_{scx}}{(\beta\gamma)^3}, \quad \text{and} \quad K_v = -\frac{f''}{f} - \frac{K_{scy}}{(\beta\gamma)^3}$$

$$\text{with} \quad \frac{f''}{f} = -\left[\frac{qE_0}{m_0 c^2}\right]^2 \frac{(\gamma^2 + 2)}{4(\beta\gamma)^4}.$$

Equation 10. By making use of Hamilton's relations on the Hamiltonian of Equation 9, and by specifying  $f = (\beta\gamma)^{1/2}$ , and after tedious algebraic manipulation, the above simple differential equations are obtained. The affect of acceleration is seen in the term containing the accelerating electrostatic field,  $E_0$ , and the space charge affects the particle trajectories through the terms  $K_{scx}$  and  $K_{scy}$ .

$$\alpha_u = -\frac{\pi w_u w_u'}{\epsilon_{nx}} = -\frac{\pi\beta\gamma w_x}{\epsilon_{nx}} \left[ w_x' + \frac{qE_0 w_x}{2\beta^2 \gamma m_0 c^2} \right], \quad \beta_u = \frac{\pi w_u^2}{\epsilon_{nx}} = \frac{\pi\beta\gamma w_x^2}{\epsilon_{nx}}, \quad \gamma_u = \frac{1 + \alpha_u^2}{\beta_u},$$

$$\alpha_v = -\frac{\pi w_v w_v'}{\epsilon_{ny}} = -\frac{\pi\beta\gamma w_y}{\epsilon_{ny}} \left[ w_y' + \frac{qE_0 w_y}{2\beta^2 \gamma m_0 c^2} \right], \quad \beta_v = \frac{\pi w_v^2}{\epsilon_{ny}} = \frac{\pi\beta\gamma w_y^2}{\epsilon_{ny}}, \quad \gamma_v = \frac{1 + \alpha_v^2}{\beta_v}$$

Equations 11. Since the form of Equations 10 is identical to the form of Equations 1, the particle trajectories can be parameterized by the analogous functions  $\alpha_u$ ,  $\beta_u$ ,  $\alpha_v$ , and  $\beta_v$ , related to the beam size and divergence as given above.

$$\alpha_u' = K_u \beta_u - \gamma_u, \quad \beta_u' = -2\alpha_u, \quad \alpha_v' = K_v \beta_v - \gamma_v, \quad \beta_v' = -2\alpha_v$$

Equations 12. The evolution of the modified Twiss parameters is governed by equations identical in form to Equations 3.

Conclusion. The above treatment allows for a determination of the beam envelope evolution including the effects of acceleration, space charge, and emittance. Other linear forces, such as those arising from dipoles, quadrupoles, and undulator magnets, are readily included in the analysis.

# Three-Dimensional Simulation of Free-Electron Laser Harmonics with FRED\*

W. M. Sharp, E. T. Scharlemann, and W. M. Fawley  
Lawrence Livermore National Laboratory  
Livermore, California 94550, USA

FRED3D, a single-mode three-dimensional version of the FEL simulation code FRED, has been modified to follow signal growth at even and odd harmonics of the fundamental frequency. The derivation of the wiggler-averaged particle and field equations is presented, as well as their implementation in FRED3D.

\* Performed jointly under the auspices of the US DOE by LLNL under W-7405-ENG-48 and for the DOD under SDIO/SDC-ATC MIPR No. W31RPD-8-D5005.

## WHAT'S NEEDED TO SIMULATE HARMONICS?

AN ORDERING SCHEME  
ASSUMED FORMS FOR WIGGLER AND SIGNAL FIELDS  
ELECTRON ORBITS IN ASSUMED WIGGLERS  
DERIVATION OF WIGGLER-AVERAGED ELECTRON EQUATIONS  
DERIVATION OF WIGGLER-AVERAGED, FOURIER-TRANSFORMED, DISCRETIZED FIELD EQUATIONS  
VERIFICATION OF ENERGY CONSERVATION  
CONVERSION TO MIXED UNITS USED IN FRED  
IMPLEMENTATION IN FRED

## BASIC EQUATIONS

### ASSUMPTIONS

HIGH ENERGY  $\gamma \gg 1$ ,  $\beta \approx 1$   
LOW BATTING  $\beta_{\perp} \ll 1$ ,  $\beta_{\parallel} \approx 1$   
SMALL SIGNAL AMPLITUDE  $|E| \ll E_0$   
QUANTUM NUMBER  $N \gg 1$   
AXIAL UNIFORMITY  $\rightarrow 1$ -D SIMULATION  
NEGLECTABLE SPACE CHARGE  
ARITHMETIC BEAM PIPE

### ELECTRON EQUATIONS

$$\frac{d\mathbf{p}}{dt} = \frac{e}{c} \mathbf{E} \times \hat{\mathbf{z}} - \frac{e}{c} \mathbf{B} \times \hat{\mathbf{z}} \quad \text{EQUATION}$$

$$\frac{d\mathbf{p}}{dt} = \frac{e}{c} \mathbf{E} \times \hat{\mathbf{z}} - \frac{e}{c} \mathbf{B} \times \hat{\mathbf{z}} - \frac{e}{c} \mathbf{B} \times \hat{\mathbf{z}} \quad \text{EQUATION}$$

$$\frac{d\mathbf{p}}{dt} = \frac{e}{c} \mathbf{E} \times \hat{\mathbf{z}} - \frac{e}{c} \mathbf{B} \times \hat{\mathbf{z}} - \frac{e}{c} \mathbf{B} \times \hat{\mathbf{z}} \quad \text{EQUATION}$$

$$\frac{d\mathbf{p}}{dt} = \frac{e}{c} \mathbf{E} \times \hat{\mathbf{z}} - \frac{e}{c} \mathbf{B} \times \hat{\mathbf{z}} - \frac{e}{c} \mathbf{B} \times \hat{\mathbf{z}} \quad \text{EQUATION}$$

### LORENZ-GAUSS FIELD EQUATION

$$(\nabla_{\perp}^2 + \frac{1}{c^2} \frac{d^2}{dt^2}) \mathbf{E} = -\frac{4\pi e}{c} \mathbf{J}_{\perp}$$

## ORDERING OF TERMS

### BASIC CHOICES

$$\frac{d\mathbf{p}}{dt} = \frac{e}{c} \mathbf{E} \times \hat{\mathbf{z}} - \frac{e}{c} \mathbf{B} \times \hat{\mathbf{z}} \quad \text{EQUATION}$$

### CONSEQUENCES

$$\frac{d\mathbf{p}}{dt} = \frac{e}{c} \mathbf{E} \times \hat{\mathbf{z}} - \frac{e}{c} \mathbf{B} \times \hat{\mathbf{z}} \quad \text{EQUATION}$$

### ESTIMATED SIGNAL AT SATURATION

$$\frac{d\mathbf{p}}{dt} = \frac{e}{c} \mathbf{E} \times \hat{\mathbf{z}} - \frac{e}{c} \mathbf{B} \times \hat{\mathbf{z}} \quad \text{EQUATION}$$

### ELECTRON EQUATIONS

$$\frac{d\mathbf{p}}{dt} = \frac{e}{c} \mathbf{E} \times \hat{\mathbf{z}} - \frac{e}{c} \mathbf{B} \times \hat{\mathbf{z}} \quad \text{EQUATION}$$

### ORDERING CHOICE

$$\frac{d\mathbf{p}}{dt} = \frac{e}{c} \mathbf{E} \times \hat{\mathbf{z}} - \frac{e}{c} \mathbf{B} \times \hat{\mathbf{z}} \quad \text{EQUATION}$$

### SIMPLIFIED ELECTRON EQUATIONS

$$\frac{d\mathbf{p}}{dt} = \frac{e}{c} \mathbf{E} \times \hat{\mathbf{z}} - \frac{e}{c} \mathbf{B} \times \hat{\mathbf{z}} \quad \text{EQUATION}$$

## ASSUMED FIELD FORMS

### WIGGLER FIELDS

$$\mathbf{E}_w = \frac{E_0}{2} \left[ \cos(k_z z) \sin(k_y y) \hat{\mathbf{x}} + \sin(k_z z) \cos(k_y y) \hat{\mathbf{y}} \right]$$

### LINEAR

$$\mathbf{E}_w = \frac{E_0}{2} \left[ \cos(k_z z) \sin(k_y y) \hat{\mathbf{x}} + \sin(k_z z) \cos(k_y y) \hat{\mathbf{y}} \right]$$

### LINEAR WITH PARABOLIC POLES

$$\mathbf{E}_w = \frac{E_0}{2} \left[ \cos(k_z z) \sin(k_y y) \hat{\mathbf{x}} + \sin(k_z z) \cos(k_y y) \hat{\mathbf{y}} \right]$$

### SIGNAL FIELDS

$$\mathbf{E}_s = \frac{E_s}{2} \left[ \cos(k_z z) \sin(k_y y) \hat{\mathbf{x}} + \sin(k_z z) \cos(k_y y) \hat{\mathbf{y}} \right]$$

### WIGGLER

$$\mathbf{E}_w = \frac{E_0}{2} \left[ \cos(k_z z) \sin(k_y y) \hat{\mathbf{x}} + \sin(k_z z) \cos(k_y y) \hat{\mathbf{y}} \right]$$

### LINEAR

$$\mathbf{E}_w = \frac{E_0}{2} \left[ \cos(k_z z) \sin(k_y y) \hat{\mathbf{x}} + \sin(k_z z) \cos(k_y y) \hat{\mathbf{y}} \right]$$

### LINEAR WITH PARABOLIC POLES

$$\mathbf{E}_w = \frac{E_0}{2} \left[ \cos(k_z z) \sin(k_y y) \hat{\mathbf{x}} + \sin(k_z z) \cos(k_y y) \hat{\mathbf{y}} \right]$$

# WIGGLE MOTION

## SOLUTION STRATEGY

WRITE  $x, y, p_z$  AS "SLOW" PART + WIGGLE PART  
 NEGLECT "SLOW" DERIVATIVES IN MOTION EQUATIONS  
 SOLVE FOR WIGGLE PART ORDER BY ORDER  
 SET EQUATIONS FOR SLOW PART BY  
 SUBSTITUTING WIGGLE SOLUTION INTO FULL  
 EQUATIONS AND AVERAGING OVER  $2\pi/\omega_0$

## RESULTS

### HELICAL WIGGLER

$$\begin{aligned}x &= \bar{x} - \frac{1}{k_0} (1 - \frac{1}{2} \frac{v_z^2}{c^2}) \cos(k_0 z) \\y &= \bar{y} - \frac{1}{k_0} (1 - \frac{1}{2} \frac{v_z^2}{c^2}) \sin(k_0 z) \\v_z &= \bar{v}_z \\ \frac{d\bar{x}}{dz} &= -\frac{1}{k_0} \frac{v_z}{c} \sin(k_0 z) \\ \frac{d\bar{y}}{dz} &= -\frac{1}{k_0} \frac{v_z}{c} \cos(k_0 z)\end{aligned}$$

### LINEAR WIGGLER

$$\begin{aligned}x &= \bar{x} - \frac{1}{k_0} (1 - \frac{1}{2} \frac{v_z^2}{c^2}) \cos(k_0 z) + \bar{x}_1 \cos(k_0 z) \\y &= \bar{y} \\v_z &= \bar{v}_z \\ \frac{d\bar{x}}{dz} &= -\frac{1}{k_0} \frac{v_z}{c} \sin(k_0 z) + \bar{x}_1 \sin(k_0 z) \\ \frac{d\bar{y}}{dz} &= 0 \\ \frac{d\bar{v}_z}{dz} &= -\frac{1}{k_0} \frac{v_z}{c} \sin(k_0 z)\end{aligned}$$

# WIGGLE AVERAGING: ELECTRON EQUATIONS

## EXPAND $\bar{p}_z$ ABOUT WIGGLE-AVERAGED POSITION

E.G. FOR HELICAL WIGGLER

$$\begin{aligned}\bar{p}_z &= p_z \{ \cos(k_0 z) + \cos(k_0 z) + \cos(k_0 z) \} \\&= p_z \{ (1 + \frac{1}{2} \frac{v_z^2}{c^2} + \frac{1}{2} \frac{v_z^2}{c^2}) + \cos(k_0 z) + \cos(k_0 z) \} \\&= (1 + \frac{1}{2} \frac{v_z^2}{c^2} + \frac{1}{2} \frac{v_z^2}{c^2}) p_z + \cos(k_0 z) p_z + \cos(k_0 z) p_z\end{aligned}$$

## EXPAND $\bar{x}_1$ ABOUT WIGGLE-AVERAGED POSITION

E.G. FOR HELICAL WIGGLER

$$\bar{x}_1(z) = \bar{x}_1(z_0) - \frac{1}{k_0} \frac{v_z}{c} \sin(k_0 z) + \frac{1}{k_0} \frac{v_z}{c} \sin(k_0 z)$$

## EXPAND $\exp(i k_0 z)$ FOR LINEAR WIGGLER

E.G. FOR SIMPLE LINEAR WIGGLER

$$\begin{aligned}\exp(i k_0 z) &= \exp \{ i k_0 z - i k_0 z \frac{v_z}{c} \sin(k_0 z) \} \\&= \exp \{ i k_0 z - i k_0 z \frac{v_z}{c} \sin(k_0 z) \} \\&= \exp(i k_0 z) \left[ 1 - i k_0 z \frac{v_z}{c} \sin(k_0 z) + \dots \right]\end{aligned}$$

## DISCARD CROSS TERMS SMALLER THAN $O(\epsilon^2)$

AVERAGE  $x, y$  EQUATIONS OVER  $2\pi/\omega_0$

# AVERAGED ELECTRON EQUATIONS

## HELICAL WIGGLER

$$\begin{aligned}\frac{d\bar{x}}{dz} &= \bar{x}_1 - \frac{1}{k_0} \frac{v_z}{c} \sin(k_0 z) + \frac{1}{k_0} \frac{v_z}{c} \sin(k_0 z) \\&= \bar{x}_1 - \frac{1}{k_0} \frac{v_z}{c} \sin(k_0 z) + \frac{1}{k_0} \frac{v_z}{c} \sin(k_0 z) \\&= \bar{x}_1 - \frac{1}{k_0} \frac{v_z}{c} \sin(k_0 z) + \frac{1}{k_0} \frac{v_z}{c} \sin(k_0 z) \\&= \bar{x}_1 - \frac{1}{k_0} \frac{v_z}{c} \sin(k_0 z) + \frac{1}{k_0} \frac{v_z}{c} \sin(k_0 z)\end{aligned}$$

## LINEAR WIGGLER

$$\begin{aligned}\frac{d\bar{x}}{dz} &= \bar{x}_1 - \frac{1}{k_0} \frac{v_z}{c} \sin(k_0 z) + \frac{1}{k_0} \frac{v_z}{c} \sin(k_0 z) \\&= \bar{x}_1 - \frac{1}{k_0} \frac{v_z}{c} \sin(k_0 z) + \frac{1}{k_0} \frac{v_z}{c} \sin(k_0 z) \\&= \bar{x}_1 - \frac{1}{k_0} \frac{v_z}{c} \sin(k_0 z) + \frac{1}{k_0} \frac{v_z}{c} \sin(k_0 z) \\&= \bar{x}_1 - \frac{1}{k_0} \frac{v_z}{c} \sin(k_0 z) + \frac{1}{k_0} \frac{v_z}{c} \sin(k_0 z)\end{aligned}$$

LINEAR WIGGLER WITH PARABOLIC POLES  
 SAME FORM WITH  $\bar{x}_1 \rightarrow \bar{x}_1 + \frac{1}{2} \frac{v_z^2}{c^2}$  AND  $\bar{v}_z \rightarrow \bar{v}_z$   
 IF  $\bar{x}_1 = 0$

# WIGGLE AVERAGING: FIELD EQUATION

## OBTAIN EQUATION FOR $\bar{x}_1$ ALONE

SUBSTITUTE ASSUMED  $\bar{x}_1$  FORM  
 DISCARD  $\bar{x}_1^2/\bar{x}_1$  AND  $\bar{x}_1^2/\bar{x}_1$  TERMS  
 FOR HELICAL WIGGLER  
 LONGER COMPONENTS INTO EQUATION FOR  $\bar{x}_1$   
 MATCH TO  $\exp(i k_0 z)$   
 INTEGRATE IN TIME OVER  $2\pi/\omega_0$   
 FOR LINEAR WIGGLER  
 MATCH LEFT SIDE AS  $\bar{x}_1 = \frac{1}{k_0} \frac{v_z}{c} \sin(k_0 z)$   
 MATCH TO  $\exp(i k_0 z)$   
 INTEGRATE IN TIME OVER  $2\pi/\omega_0$

$$\begin{aligned}\bar{x}_1 &= \frac{1}{k_0} \frac{v_z}{c} \sin(k_0 z) + \frac{1}{k_0} \frac{v_z}{c} \sin(k_0 z) \\&= \frac{1}{k_0} \frac{v_z}{c} \sin(k_0 z) + \frac{1}{k_0} \frac{v_z}{c} \sin(k_0 z) \\&= \frac{1}{k_0} \frac{v_z}{c} \sin(k_0 z) + \frac{1}{k_0} \frac{v_z}{c} \sin(k_0 z)\end{aligned}$$

WRITE  $\bar{x}_1$  IN  $\delta$ -FUNCTION FORM

$$\bar{x}_1 = \frac{1}{k_0} \frac{v_z}{c} \sin(k_0 z) + \frac{1}{k_0} \frac{v_z}{c} \sin(k_0 z)$$

SUBSTITUTE OBTAIN EXPRESSIONS FOR  $\bar{x}_1/\bar{x}_1$  AND  $\bar{v}_z/\bar{v}_z$

EVALUATE (TUNNEL) & INTEGRAL

EXPAND  $\bar{x}_1/\bar{x}_1$  AND  $\bar{v}_z/\bar{v}_z$  ABOUT  $(\bar{x}_1, \bar{v}_z)$

EXPAND  $\exp(i k_0 z)$  IN POWER SERIES

DISCARD TERMS SMALLER THAN  $O(\epsilon^2)$

RETAIN ONLY SLOW VARIATION TERMS

# AVERAGED FIELD EQUATIONS

## GENERAL FORM

$$\bar{x}_1 = \frac{1}{k_0} \frac{v_z}{c} \sin(k_0 z) + \frac{1}{k_0} \frac{v_z}{c} \sin(k_0 z)$$

## SOURCE TERMS

### HELICAL WIGGLER

$$\begin{aligned}\bar{x}_1 &= \frac{1}{k_0} \frac{v_z}{c} \sin(k_0 z) + \frac{1}{k_0} \frac{v_z}{c} \sin(k_0 z) \\&= \frac{1}{k_0} \frac{v_z}{c} \sin(k_0 z) + \frac{1}{k_0} \frac{v_z}{c} \sin(k_0 z) \\&= \frac{1}{k_0} \frac{v_z}{c} \sin(k_0 z) + \frac{1}{k_0} \frac{v_z}{c} \sin(k_0 z)\end{aligned}$$

### LINEAR WIGGLER

$$\begin{aligned}\bar{x}_1 &= \frac{1}{k_0} \frac{v_z}{c} \sin(k_0 z) + \frac{1}{k_0} \frac{v_z}{c} \sin(k_0 z) \\&= \frac{1}{k_0} \frac{v_z}{c} \sin(k_0 z) + \frac{1}{k_0} \frac{v_z}{c} \sin(k_0 z) \\&= \frac{1}{k_0} \frac{v_z}{c} \sin(k_0 z) + \frac{1}{k_0} \frac{v_z}{c} \sin(k_0 z)\end{aligned}$$

### LINEAR WIGGLER WITH PARABOLIC POLES

$$\begin{aligned}\bar{x}_1 &= \frac{1}{k_0} \frac{v_z}{c} \sin(k_0 z) + \frac{1}{k_0} \frac{v_z}{c} \sin(k_0 z) \\&= \frac{1}{k_0} \frac{v_z}{c} \sin(k_0 z) + \frac{1}{k_0} \frac{v_z}{c} \sin(k_0 z) \\&= \frac{1}{k_0} \frac{v_z}{c} \sin(k_0 z) + \frac{1}{k_0} \frac{v_z}{c} \sin(k_0 z)\end{aligned}$$

# CONVERSION TO FRED FORM

## FOURIER TRANSFORM IN $\theta$

$$\bar{x}_1(\theta, z) = \sum_{n=-\infty}^{\infty} \bar{x}_1^{(n)}(z) \exp(in\theta)$$

## REPRESENT $\bar{x}_1$ BY FINITE-SERIES SERIES

$$\begin{aligned}\bar{x}_1(\theta, z) &= \sum_{n=-\infty}^{\infty} \bar{x}_1^{(n)}(z) \exp(in\theta) \\&= \sum_{n=-\infty}^{\infty} \bar{x}_1^{(n)}(z) \exp(in\theta) \\&= \sum_{n=-\infty}^{\infty} \bar{x}_1^{(n)}(z) \exp(in\theta)\end{aligned}$$

## EVALUATE MATRIX OPERATORS FOR 1 AND $\bar{x}_1^2$

### EVALUATE SOURCE VECTORS

$$\begin{aligned}\bar{x}_1 &= \sum_{n=-\infty}^{\infty} \bar{x}_1^{(n)}(z) \exp(in\theta) \\&= \sum_{n=-\infty}^{\infty} \bar{x}_1^{(n)}(z) \exp(in\theta) \\&= \sum_{n=-\infty}^{\infty} \bar{x}_1^{(n)}(z) \exp(in\theta)\end{aligned}$$

## SEPARATE REAL AND IMAGINARY PARTS

# **A EXPERIMENTAL STUDY OF A SHIELDED PULSED ELECTROMAGNET WIGGLER CONCEPT**

C. Zhou, M. Wang.

Southwest Institute of Electronic Engineering, Chengdu, PRC

## **DIGEST:**

In FEL devices, electromagnet wigglers are conventionally used. This wiggler design can be easily fabricated and since it is an electromagnet, the field can be continuously varied over a wide range, thus allowing careful optimization of the FEL design with relative ease. Nevertheless, a significant side leakage flux existing between two adjacent magnets hampers the performance of the magnet. This effect is more serious for short-period electromagnet wiggler.

A new shielded pulsed electromagnet wiggler (SPEW) concept is introduced for reducing the side-leakage flux effect. In this paper, the advantages of SPEW have been investigated with wiggler period  $\lambda_w$  of 12cm, working gap  $2\delta$  of 4.4cm, pulse duration of 2ms and maximum ampere-turns of 12000A.T. It has been found that SPEW has excellent capability of reducing saturation in the core and that the field strength in working gap is up 38%.

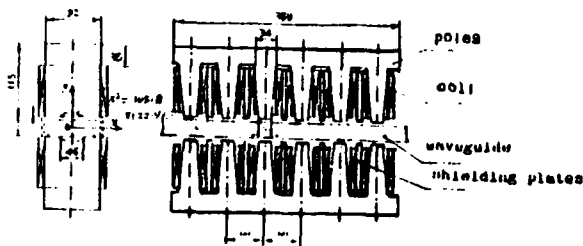


FIG.3 Transverse cut of the SPEW Wiggler Prototype

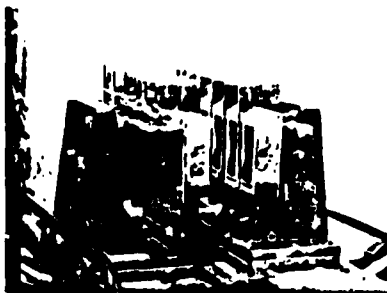


FIG.4 The Photograph shows the SPEW Wiggler Prototype

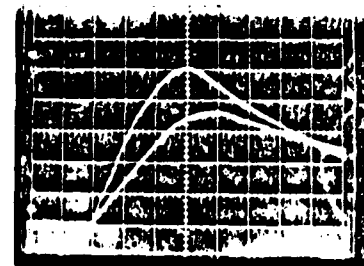


FIG.5 Magnetic field wave form on the wiggler midplane

For both the EM and SPEW

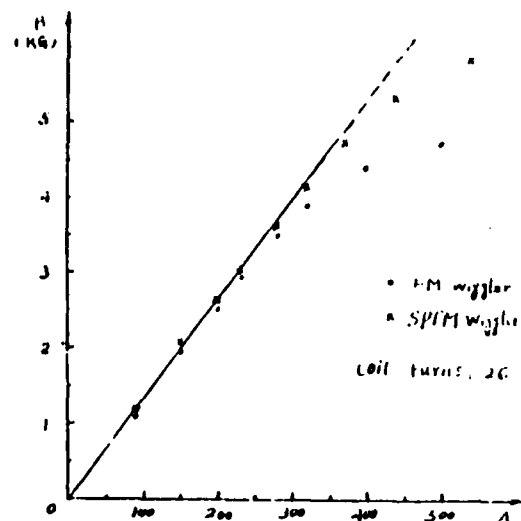


FIG.6 Field measurements at center for both the EM and SPEW

## P1.12

## LASING ON THE THIRD HARMONIC

R. W. Warren, L. C. Haynes, D. W. Feldman, W. E. Stein, and S. J. Gitomer  
 Los Alamos National Laboratory  
 Los Alamos, NM 87545

The Los Alamos Free-Electron Laser has recently lased near  $4\text{ }\mu\text{m}$  on the third harmonic of the fundamental frequency of about  $12\text{ }\mu\text{m}$ . By a choice of intractivity apertures and cavity length, lasing can be forced to occur on both frequencies simultaneously or on either one alone.

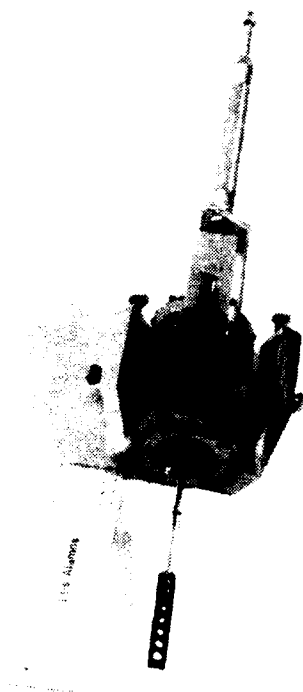
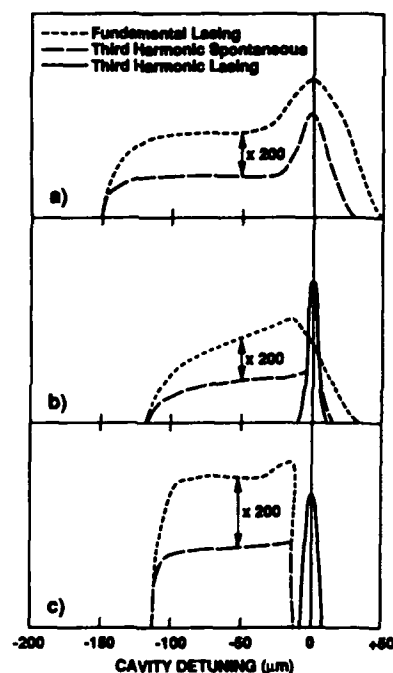


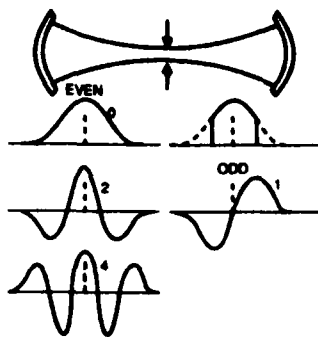
Plate containing apertures of various sizes, inserted near the downstream end of the wiggler.



Detuning curves for lasing on the fundamental, lasing on the third harmonic, and for the third harmonic generated while lasing on the fundamental. Three different apertures were used: a)-none; b)-4.5 mm dia; and c)-3.5 mm dia.



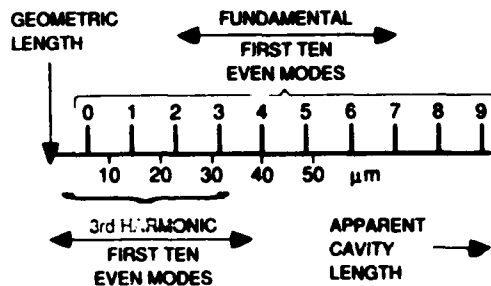
## EFFECT OF APERTURES



Apertures clip the wings of the fundamental mode, introducing high-order transverse modes

Los Alamos

## EFFECTIVE CAVITY LENGTH DEPENDS ON HARMONIC # AND TRANSVERSE MODE #



High-order transverse modes have a group velocity that is slower than the fundamental modes, requiring a shorter cavity length to keep the optical micropulses in step with the electron micropulses.

Los Alamos

TABLE I

Aperture	Dia. (mm)	Calculated loss/pos		Measured loss/pos	
		10.0 μm	2.5 μm	10 μm	2 μm
none		25%	3.9%	15%	6%
#1	4.5	36%	4.0%	29%	4%
2	4.0	50%	5.0%	35%	5%
3	3.5	64%	7.0%	50%	7%
4	2.9	75%	11.0%	75%	NM
5	2.5	86%	23.0%	—	—

Table giving sizes of apertures and the calculated and measured round-trip optical loss for the fundamental and third harmonic.

# PI.13

## Electron-Beam Quality Degradation in a Long Undulator \*

Harunori Takeda and Lester E. Thode

MS-II829, Los Alamos National Laboratory

Los Alamos, New Mexico 87545

Under the influence of space charge or wakefields, the transport of an electron beam through a long undulator can cause a degradation of beam quality. Using the PARMELA code, we simulate a beam pulse that travels through a tapered undulator. The electron beam is focused in both planes using parabolic pole faces in the undulator. The beam emittance and profiles are studied.

### Objects

We consider an electron beam transport  
in a Long Undulator (Untapered & Tapered)

- The Parabolic Pole Faces focus beam in both planes.
- Simulation by PARMELA Code
  - Space Charge
  - Wake Field by bellows
- Comparison with KV Equation (Space Charge)

We study the Effect  
on the Beam emittance & the Beam Size  
by the Space Charge & Wake Field.

- We include the focusing term  
in the K.V. Envelope Equation  
for the Parabolically Pole Faced Undulator.

The KV Envelope equations:

$$\frac{d^2 r_x}{d\tau^2} = -Q_x r_x + \frac{\epsilon^2}{r_x^3} + \frac{2r_y^2}{\gamma^2(r_x + r_y)} \quad (1)$$

$$\frac{d^2 r_y}{d\tau^2} = -Q_y r_y + \frac{\epsilon^2}{r_y^3} + \frac{2r_x^2}{\gamma^2(r_x + r_y)} \quad (2)$$

The Space Charge Effect is proportional to Current  $J$  :

$$r_s^2 \equiv \frac{2eJ}{m_0 \gamma \beta_x c^3}$$

The Undulator Focusing coefficients  $Q_x$  and  $Q_y$  are

$$Q_m \equiv \frac{1}{2} \left( \frac{eB_0}{m_0 c^2 \gamma} \right)^2 \left( \frac{k_m}{k_w} \right)^2 \text{ where } k_x^2 + k_y^2 = k_w^2 \quad (m = x, y)$$

- The Beam Matching Condition  
into the Undulator

The beam ellipse must be erect:  $\alpha_x = \alpha_y = 0$ ,

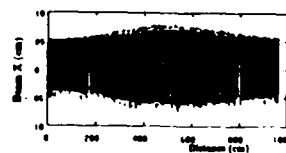
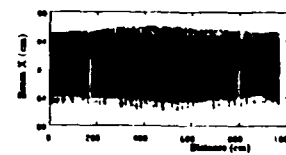
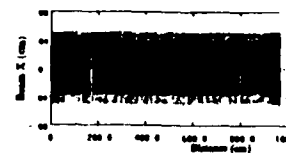
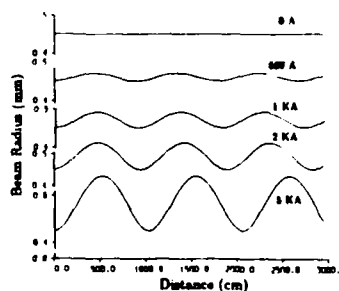
$$\text{and } x_m = \sqrt{\beta_x \epsilon} = \sqrt{\sqrt{2} \epsilon \left( \frac{1}{k_0} \right) \left( \frac{k_m}{k_r} \right)} \quad (3)$$

$$y_m = \sqrt{\beta_y \epsilon} = \sqrt{\sqrt{2} \epsilon \left( \frac{1}{k_0} \right) \left( \frac{k_m}{k_r} \right)} \quad (4)$$

- The Beam Parameters  
used in the Simulation

Beam Energy : 150 MeV, Full  $\delta E/E$  : 0.72%  
Peak Current : 500 A, Emittance :  $7.32 \times 10^{-2} \pi$  mm-mr  
Pulse Length : 21.7 ps

- The K-V Envelopes  
match well with  
the Parmela Calculations.

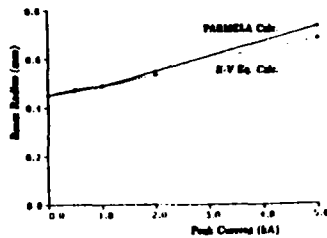


\* Work performed under the auspices of the U.S. Department of Energy and supported by the U.S. Army Strategic Defense Command.

- The Radial Expansion of Beam by the Space Charge

The K-V Equation & Parmela Simulation

- K-V : Uniform, Parmela : Gaussian
- The Beam radius at 4.5 m
- The Current dependence match well.



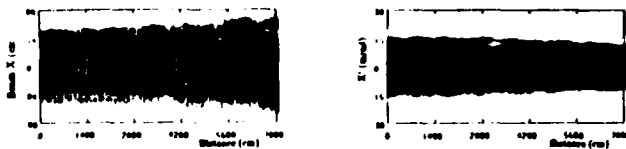
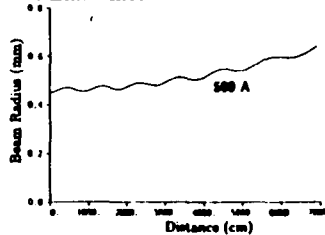
- Tapered 70 m Undulator

- The Matched Beam Expands Beam Waist in the Undulator.

- ◊ With Space Charge (500 A Peak)

The Space Charge Modulates the Matched Envelope.

- The Divergence reduces to maintain a Constant Emittance.



- Conclusion

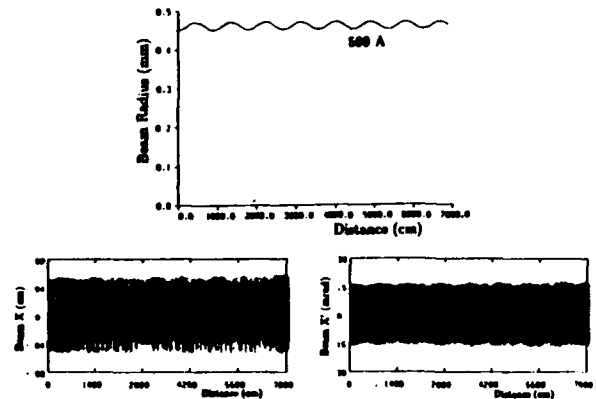
- The emittance ellipse that encloses 90% of particles does not grow with any combination of undulator, space charge and wake field.
- However, the wakefield induced by the beam pipe bellows in the undulator is significant. This doubles the energy spread of the beam that sees the bellows at every 1.2 m.
- The emittance ellipse that encloses 100% of particles (beam halo) grows because of the quiver motion itself, and by the space charge force.
- Comparing the emittance growths including the beam halo, it grows more in the untapered undulator than in the tapered undulator.

- Untapered 70 m Undulator.

- The Matched Beam has Constant beam Waists in the Undulator.

- ◊ With Space Charge (500 A Peak)

- The KV Equation Predicts Envelopes Similar to the Parmela Simulation



- The Emittance Growth in a 100% Ellipse

- The Emittance in a 90 % ellipse has no growth in Tapered, Untapered, Space Charge, Wake field.
- The Wake Field itself has no effect on transverse emittance.
- The wiggle motion in an untapered undulator increase the 100% emittance.

	70m Untapered		70m Tapered	
	x-x'	y-y'	x-x'	y-y'
0A	11%	0%	0%	0%
500 A	23%	15%	17%	13%

- References

1. I. M. Kapchinskij and V. V. Vladimirkij, Proc. Internat. Conf. on High Energy Accelerators. CERN 1959, p. 274
2. E.T. Schaeleman, J. Appl. Phys. P2154, Vol 58, No 6, 15 Sept. 1985

# P1.14

## Simulations on Inverse Accelerator and Harmonic Generation

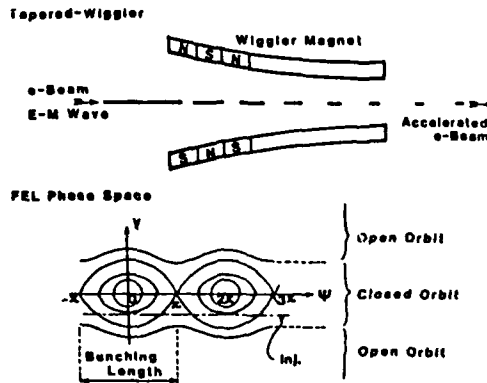
K. Mima, K. Ohia), N. Ohigashia), S. Kurumab), and S. Nakai  
Institute of Laser Engineering, Osaka University, Suita, Osaka, Japan

a) Dept. of Electrical Engineering, Suita, Osaka, Japan

b) Institute for Laser Technology, Suita, Osaka, Japan

### Abstract

The resonant interactions of multi-frequency radiation fields and electron beams in a wiggler have been investigated by the computer simulations. It is found that electrons are accelerated at a high acceleration rate by increasing the wiggler field. The accelerated electron beam is strongly bunched. The bunch size is a fraction of the injected radiation wavelength. The deleterious effects of the spectral spread of the acceleration field are discussed.



(1) Inverse FEL accelerator concept.

### Formulation (1-D)

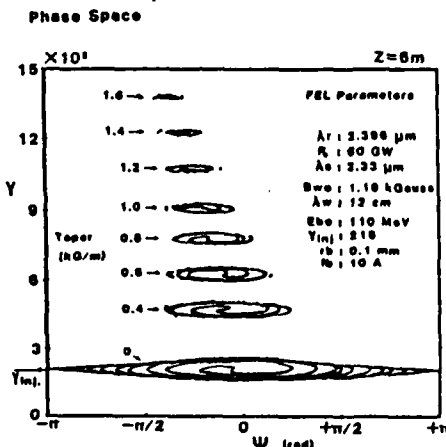
$$\frac{dV_i}{dz} = -\frac{1}{2} \hat{\Omega}_p \frac{\hat{K}_w \hat{A}_w \sin \psi_{w1}}{\hat{A}_i \hat{N}_i}$$

$$\frac{d\psi_{w1}}{dz} = 1 - \hat{K}_w \frac{1 - \beta_{z1}}{\hat{A}_i \hat{N}_i} + \frac{1}{2} \hat{\Omega}_p \hat{\Omega}_w \hat{K}_w \hat{A}_w \frac{\cos \psi_{w1}}{\hat{A}_i \hat{N}_i}$$

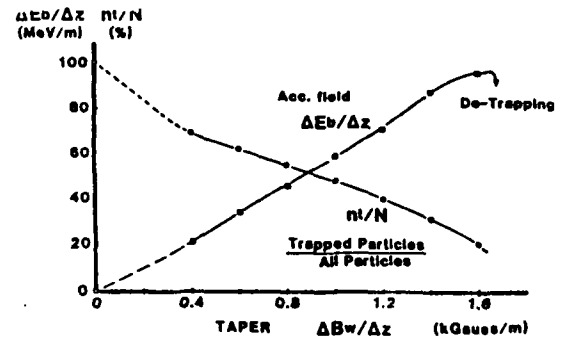
$$\frac{d\hat{A}_w}{dz} = \frac{1}{2} \hat{\Omega}_p \hat{\Omega}_w \hat{K}_w \frac{\sin \psi_{w1}}{\hat{A}_i \hat{N}_i}$$

Where  $\beta_{z1} = \sqrt{1 - \frac{1 + K^2 \cos^2(K_w Z)}{\gamma_1^2}}$

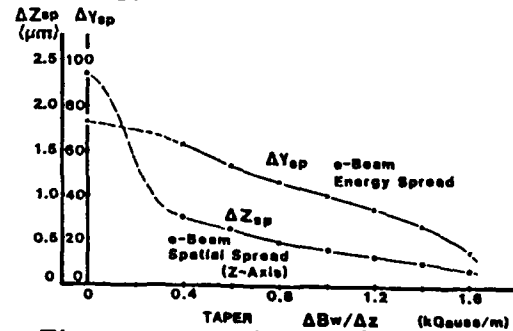
(2) Basic equations for the simulation.



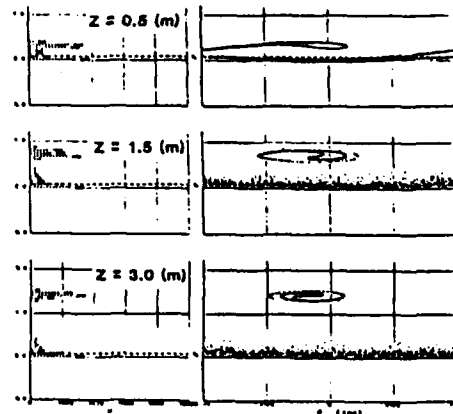
(3) Phase space distributions of accelerated electrons. The phase space area reduces with increasing the acceleration gradient.



(4) Relations of trapped particle fraction and the acceleration rate with the gradient of the wiggler field tapering.

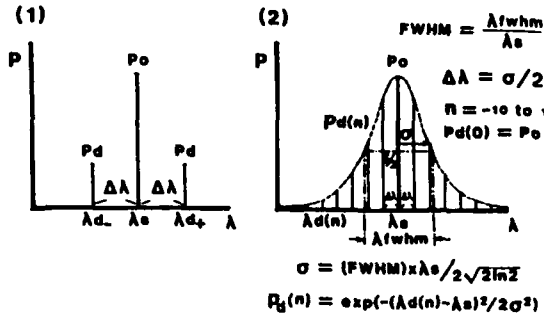


(5) The energy and spatial spread of an electron bunch.

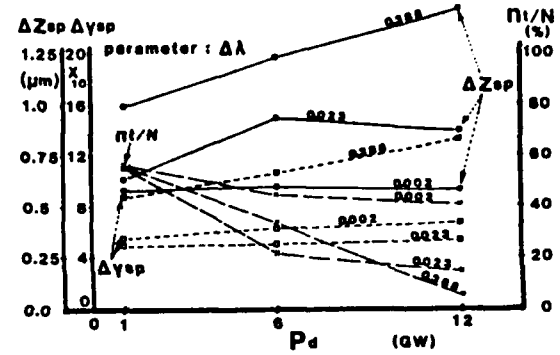


(6) Spatial evolutions of the electron beam phase space distribution.

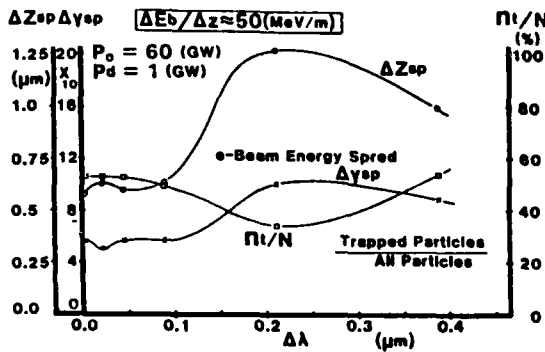
## Simulation



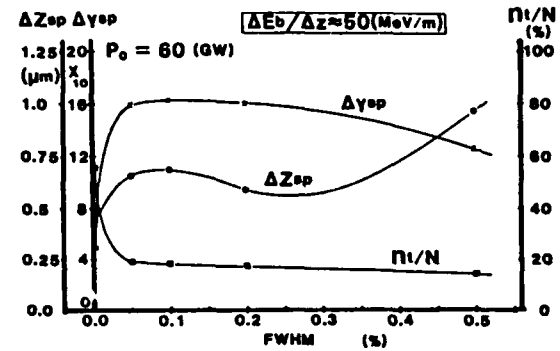
- (7) Effects of sidebands on the electron acceleration. The assumed spectra of the radiation are shown.  
case (1) 2-sidebands  
case (2) gaussian spectrum



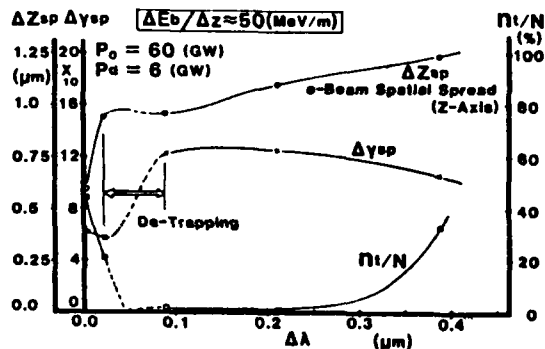
- (10) Sideband power dependences of a bunch spread and the trapped particle fraction.



- (8) The dependences of the phase space spread of an electron bunch, on the sidebands wavelength spread. The sideband intensity is 1/60 with respect to the carrier wave.



- (11) Effects of gaussian spectrum on the bunch length and the trapping fraction.



- (9) The same as Fig.(8) except the sideband intensity is 1/10.

## Summary

- (1) Quite high acceleration rate; 100MeV/m is achieved by the wiggler field tapering with 60 GW of 2.3  $\mu m$  radiation
- (2) The bunch length is reduced by increasing the tapering rate. The bunch width can be less than 0.2  $\mu m$ .
- (3) The side bands heat up the electrons and increase the bunch size significantly.
- (4) The frequency spread of the sideband,  $\Delta\lambda/\lambda$  has to be less than  $1/N_w$

- (12)

# STABLE-UNSTABLE RESONATOR FOR FREE-ELECTRON LASERS WITH A STEPPED GRATING FOR SIDEBAND SUPPRESSION

Alan H. Paxton  
Mission Research Corporation  
1720 Randolph Road, SE  
Albuquerque, NM 87106

Mark J. Schmitt  
Los Alamos National Laboratory E531  
Los Alamos, NM 87545

## ABSTRACT

We propose the stable-unstable ring resonator for use with free-electron lasers. The optical output beam has a rectangular cross section without a central obscuration. A stepped phase grating that disappears at the central frequency is included for sideband suppression. Properties derived using theory and numerical simulation are presented.

### STABLE - UNSTABLE RESONATOR [1,2]

RAY'S WALK OUT OF RESONATOR IN ONE TRANSVERSE DIMENSION  
OUTPUT BEAM IS A FILLED-IN RECTANGLE

RESONATOR OPTIC AXIS IS WELL WITHIN GEOMETRIC MODE

RESONATOR IS STABLE AND HAS GAUSSIAN MODES IN ONE TRANSVERSE DIMENSION

APERTURE LOSSES ARE MINIMIZED BY ORIENTING THE STABLE DIRECTION ACROSS THE WIGGLER GAP

THE BEAM TUBE IS ELLIPTICAL TO AVOID EXCESSIVE CLIPPING OF THE OPTICAL - BEAM SIDELOBES AT THE FOCUS IN THE UNSTABLE DIRECTION

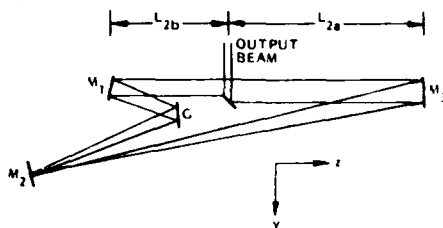
### SUMMARY OF PROPERTIES

PARTIALLY TRANSMITTING MIRROR OR GRATING OUTCOUPLER UNNECESSARY

APERTURE LOSS IN WIGGLER NO WORSE THAN VALUE FOR STABLE RESONATOR

1

### STABLE - UNSTABLE RING RESONATOR: UNSTABLE DIMENSION

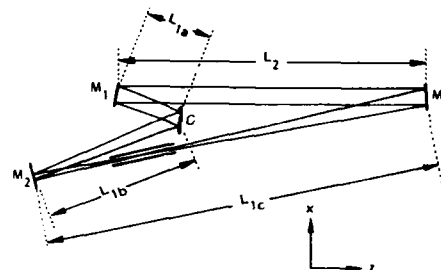


THE FOCAL LENGTHS OF MIRRORS  $M_1$  AND  $M_3$  ARE DIFFERENT FROM VALUES IN STABLE DIMENSION; THIS COULD BE DONE BY SELECTING THE ANGLE OF INCIDENCE TO INDUCE THE REQUIRED ASTIGMATISM

CALCULATED RESULTS BELOW CORRESPOND TO:  $L_{2a} = 750$  cm;  $L_{2b} = 750$  cm; AND THE BEAM WIDTH JUST AFTER THE SCRAPER IS  $h = 1.49$  cm;  $F_1 = F_3 = 3446.8$  cm IN THIS DIMENSION; RESONATOR MAGNIFICATION IS  $M = 1.36$

3

### STABLE - UNSTABLE RING RESONATOR: STABLE DIMENSION



OPTICAL BEAM IS RECTANGULAR IN CROSS SECTION

MIRRORS  $M_1$  AND  $M_3$  ARE CURVED IN THIS DIMENSION WHILE  $M_2$  AND G ARE FLAT

CALCULATED RESULTS BELOW CORRESPOND TO:  $F_1 = F_2 = 3554$  cm IN THIS DIMENSION:  $L_1 = L_{1a} + L_{1b} + L_{1c} = 7100$  cm;  $L_2 = 1500$  cm; BEAM IS ESSENTIALLY COLLIMATED IN REGION WITH LENGTH  $L_2$  AND HAS GAUSSIAN BEAM WIDTH  $w = 1.33$  cm;  $\lambda = 593$  nm WAS USED IN SIMULATION

2

## WHAT ABOUT SIDEBAND SUPPRESSION?

(THE GRATING RHOMB OF THE BOEING BURST MODE RESONATOR PERFORMS THE DUAL FUNCTIONS OF OUTCOUPLING AND SIDEBAND SUPPRESSION [3,4,5,6])

IN OUR STABLE - UNSTABLE RESONATOR, RATHER THAN A GRATING RHOMB, A SINGLE GRATING THAT DISAPPEARS AT THE FUNDAMENTAL FREQUENCY BUT CAUSES PHASE STEPS AT THE SIDEBAND FREQUENCY IS PLACED IN THE EXPANDED PORTION OF THE OPTICAL BEAM

FOCUSING THE BEAM AND PASSING IT THROUGH THE BEAM TUBE ACTS AS A LOW-PASS SPATIAL-FREQUENCY FILTER; THE PHASE STEPS AT THE SIDEBAND FREQUENCY INCREASE THE LOSS OF SIDEBAND RADIATION

4

## STEPPED GRATING

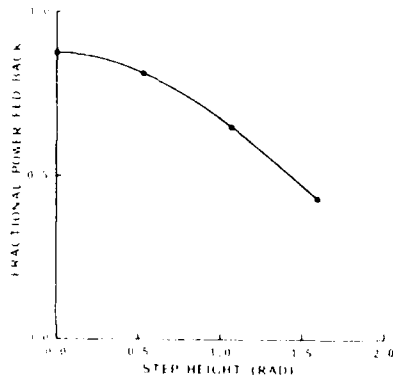


THE STEPS ARE RAISED A DISTANCE  $\Delta z$  ABOVE THE SPHERICAL REFERENCE SURFACE

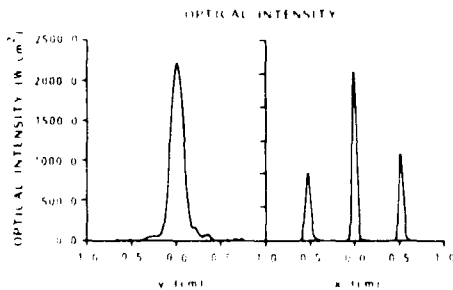
THE STEP HEIGHT IS SELECTED TO SHIFT THE PHASE FRONTS OF LIGHT AT THE CENTER FREQUENCY BY AN INTEGRAL NUMBER OF WAVELENGTHS AND TO CAUSE SIGNIFICANT PHASE SHIFTS AT THE SIDEBAND FREQUENCY

ONLY A FEW PERIODS WILL BE REQUIRED ACROSS THE BEAM WIDTH

CALCULATED RESULTS BELOW CORRESPOND TO A STEPPED GRATING WITH A FLAT REFERENCE SURFACE AT ELEMENT G IN THE DRAWINGS ON PAGES 3 AND 4. A GRATING PERIOD OF  $p = 0.30 w$  WAS USED WITH STEPS ONLY ALONG THE STABLE DIMENSION. THE HALF-WIDTH OF THE BEAM TUBE THROUGH THE WIGGLER WAS  $a = 2.5 w_0$  IN THE STABLE DIRECTION, WHERE  $w_0$  IS THE BEAM WAIST INSIDE THE WIGGLER



FRACTION OF POWER AT SIDEBAND FREQUENCY THAT IS FED BACK. POINTS SHOW CALCULATED BARE-CAVITY RESULTS USING Eqs. 7-9. CURVE DERIVED FROM SIMPLE THEORY IS PLOTTED AS CURVE.



OPTICAL INTENSITY OF SIDEBAND RADIATION AT THE ENTRANCE TO THE WIGGLER. THE EDGES OF AN APERTURE WERE LOCATED AT  $x = \pm 0.2$  cm. THE STEP HEIGHT INDUCED ON THE PHASE OF THE OPTICAL BEAM WAS 1.6 RADIAN.

## DERIVATION OF FRACTIONAL LOSS OF SIDEBAND RADIATION AT BEAM TUBE

ASSUME PHASE FRONTS WITH PERIODIC STEPS OF HEIGHT  $a\lambda_s$  WHERE  $\lambda_s$  IS THE SIDEBAND WAVELENGTH

COMPLEX AMPLITUDE IS

$$F = u(x, y) \left[ \cos \phi + i \sin \phi \sum_{m=1}^{\infty} a_m \sin(mk_s x) \right] e^{i \frac{k_s^2}{2k} z} e^{i(kz - \omega t)} \quad (1)$$

WHERE THE BEAM IS CONVERGING WITH RADIUS  $R$ ,  $\phi = \pi a$ ,  $k_s = \frac{2\pi}{p}$ ,  $K = \frac{2\pi}{\lambda_s}$ ,  $a_m = \frac{1}{m\pi}$  FOR  $m$  ODD,  $a_m = 0$  FOR  $m$  EVEN

COMPONENT AT SPATIAL FREQUENCY  $mk_s$  IS

$$f_m = \frac{1}{2} u(x, y) \sin \phi a_m \left[ e^{i(kz - \omega t)} - e^{i(kz + \omega t)} \right] e^{i \frac{k_s^2}{2k} z} e^{-i \omega t} \quad (2)$$

THE FIRST TERM IN THE BRACKETS GIVES THE WAVE,

$$f_m = \frac{1}{2} u(x, y) \sin \phi a_m e^{i(kz - \omega t)} e^{i \frac{k_s^2}{2k} z} e^{-i \omega t} e^{-i \frac{m^2 k_s^2}{2k} z} \quad (3)$$

WHERE  $x_0 = mk_s R/k$ . THIS IS A TILTED SPHERICAL WAVE WITH ITS FOCUS OFFSET BY  $x_0$  FROM THE FOCUS OF THE ZERO-FREQUENCY COMPONENT

FOR ALMOST ALL THE NONZERO COMPONENTS TO FALL OUTSIDE THE BEAM TUBE AT THE FOCUS,

$$x_0 > a + w_0 \quad (4)$$

WHICH GIVES

$$p < \frac{\pi w}{1 + \frac{a}{w_0}}$$

IF THIS IS SATISFIED, WE CAN ASSUME AN UNABERRATED BEAM INCIDENT ON THE STEPPED GRATING, AND ONLY THE ZERO-SPATIAL-FREQUENCY COMPONENT OF THE SIDEBAND RADIATION MAKES IT THROUGH THE BEAM TUBE.

THE FRACTION OF THE SIDEBAND POWER FED BACK AFTER ONE ROUND TRIP THROUGH THE RESONATOR IS

$$P_f = \eta \cos^2 \phi \quad (5)$$

WHERE  $\eta$  IS THE FRACTIONAL FEEDBACK POWER IF THE GRATING WERE REPLACED BY A FLAT MIRROR

## REFERENCES

1. R.W. JONES, C. CARSON, AND J.F. PERKINS, "NEW LASER RESONATOR WITH UNOSCURED REFLECTIVE OUTCOUPLING AND INTERNAL OPTIC AXIS", AIAA 19TH FLUID DYN., PLASMA DYN., AND LASERS CONF., HONOLULU, HAWAII, JUNE 8-10, 1987.
2. M.J. SCHMITT AND A.H. PAXTON, "FEL'S USING STABLE-UNSTABLE RING RESONATORS" SPIE Vol. 1045, 1989.
3. R.L. TOKAR, B.D. McVEY, AND J.C. GOLDSTEIN, "SIDEBAND SUPPRESSION IN FEL'S USING A GRATING RHOMB", IEEE JQE 24 856, 1988.
4. V.K. VISWANATHAN, P.J. WANTUCK, Q.D. APPERT, D.J. PISTORES, KWOK-ON TONG, "RHOMB GRATINGS FOR SIDEBAND SUPPRESSION", OPTICON '88, SANTA CLARA, OCT 30 - NOV 4, 1988.
5. C.E. KNAPP, V.A. VISWANATHAN, AND Q.D. APPERT, "ANALYSIS OF THE BOEING FEL MIRROR MEASUREMENTS", SPIE Vol. 1047, 1989.
6. J.E. SOLLID, D.W. FELDMAN, AND R.W. WARREN, "SIDEBAND SUPPRESSION FOR FEL'S", PROC 1988 FEL CONF., JERUSALEM, ISRAEL, AUG 29 - SEPT 2, 1988.
7. B.D. McVEY, "THREE-DIMENSIONAL SIMULATION OF FREE ELECTRON LASER PHYSICS", NUCL. INSTRUM. METHODS IN PHYS. RES., A250, 449-455, 1986.

# PI.16

## Frequency-Tunable, High Power Microwave Emission from Cyclotron Autoresonance Maser Oscillators Driven by Microsecond, Intense Electron Beams \*

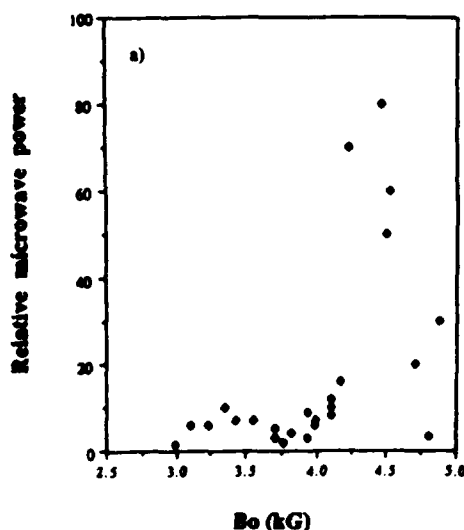
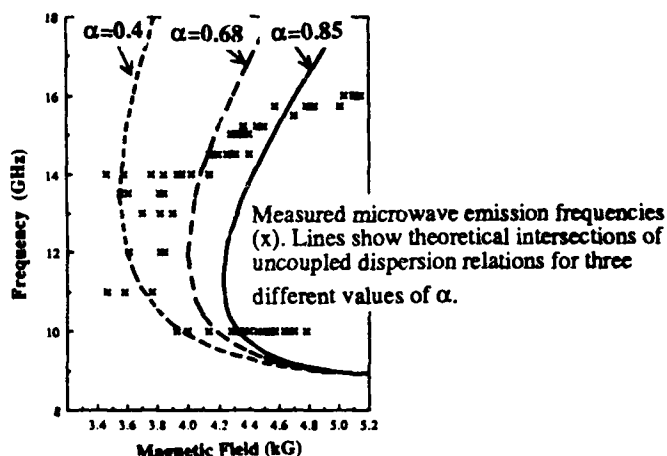
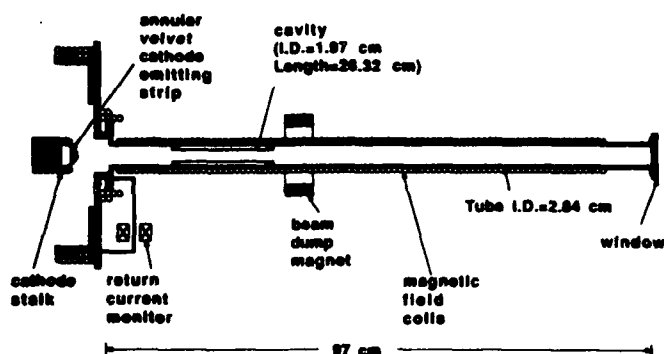
R. M. Gilgenbach, J. G. Wang, J. Choi, C. A. Outten, and T. Spencer,  
Intense Energy Beam Interaction Laboratory,  
Nuclear Engineering Department  
University of Michigan, Ann Arbor, MI 48109-2104

Experiments have been performed in which frequency-tunable (6.6-20 GHz), high power (1-25 MW) microwave radiation has been generated by 2 cyclotron maser oscillators with microwave pulselengths from 0.1  $\mu$ s to 0.8  $\mu$ s. MELBA Maser experiments operated in a unique, long-pulse e-beam parameter range: voltage=0.6-0.8 MV, current=1-15 kA, and pulselength=1-2  $\mu$ s. Mode competition has been observed.

\* Supported by AFOSR, AFWL, and NSF

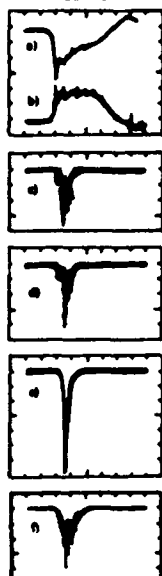
### \* Cyclotron Autoresonance Maser Oscillator

- Febetron generator with peak parameters:  $V=400$  kV,  $I=1$  kA,  $T=0.4$   $\mu$ s
- 500-1000 Amps; TE<sub>11n</sub> modes
- frequency is magnetically tunable:
- \* K-band: 13.5-16.0 GHz @ 3-10 MW in CARM regime
- \* X-band: 10-12 GHz; ~MW due to competing gyrotron modes



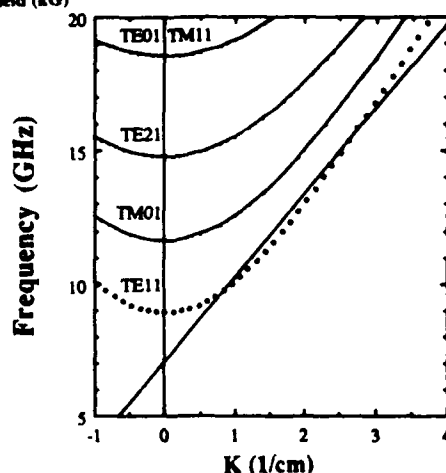
K-band microwave output power as a function of cavity magnetic field. Peak power corresponds to about 10 MW.

100 ns/div



Experimental Data:

- Beam Voltage (160 kV/div)
- Cathode current (0.6 kA/div)
- Microwave signal from 10.0 GHz filter
- K-band microwave signal ( $f > 14.3$  GHz)
- Microwave signal from 15.0 GHz filter
- K-band microwave signal at 4.52 kG



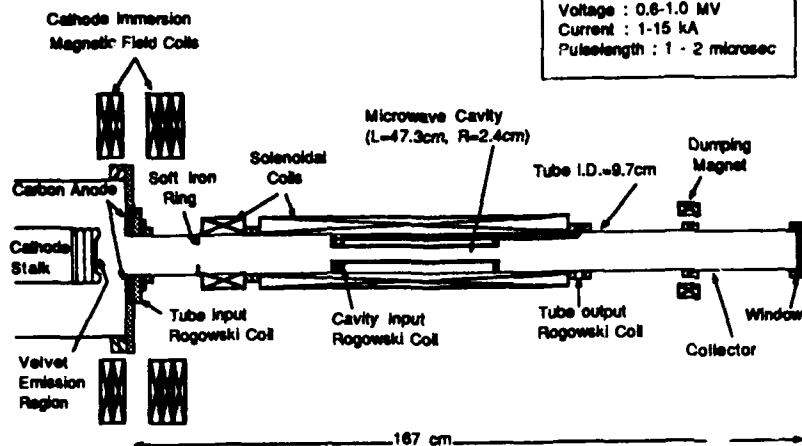
Uncoupled dispersion relations of electron cyclotron wave and cavity-waveguide modes for experiment; parameters are:  $B_0=4.34$  kG,  $V_b=370$  kV, and  $\alpha=0.72$ .



**\* MELBA Microsecond Maser experiments underway with initial parameters:**

- e-beam :  $V=0.6-0.8$  MV,  $I=1-15$  kA  
pulselength=  $1-2 \mu s$
- frequency in X-K-bands (6.6-30 GHz)
- peak power level of 25 MW achieved;  
goal of 100 MW

**The University of Michigan  
MELBA Microsecond Maser**



200 ns/div

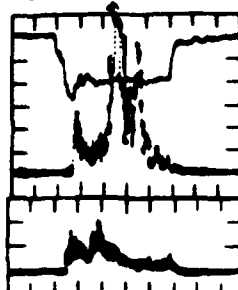


Beam Voltage  
(310 kV/div)

X-band Microwave Power  
(Peak of ~ 25 MW)  
(6.6 GHz < f < 14.1 GHz)

Cavity Input Current  
(1.2 kA/div)

200 ns/div

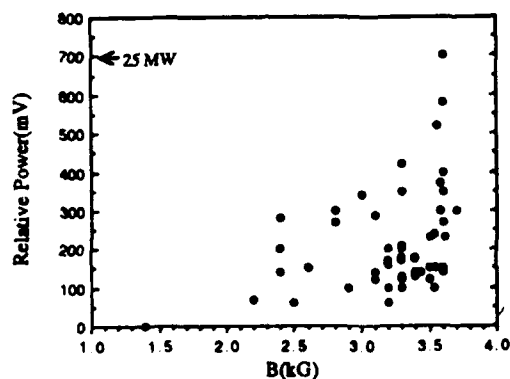


Beam Voltage  
(310 kV/div)

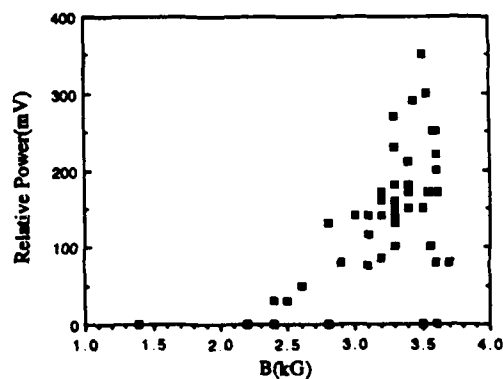
X-band Microwave Power  
(Peak of > 5 MW)  
(6.6 GHz < f < 14.1 GHz)

K-band Microwave Power  
(f > 14.1 GHz)

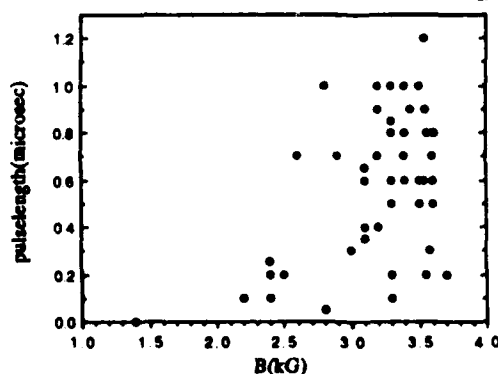
**Peak X-band Microwave Power**



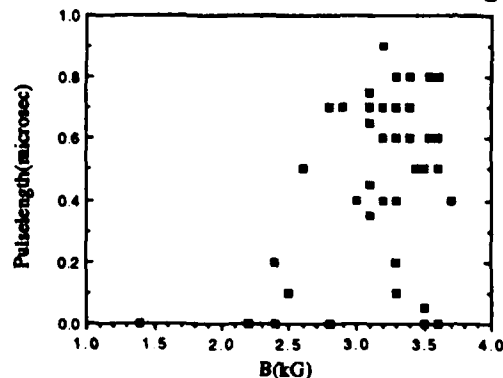
**Peak K-band Microwave Power**



**Total X-band Microwave Pulselength**



**Total K-band Microwave Pulselength**



# PI.17

## Spike Radiation From The Columbia FEL J. W. Dodd and T. C. Marshall Columbia University, Department of Applied Physics New York, New York 10027

We have observed isolated high intensity short duration "spike" pulses of radiation from our 2mm wavelength Raman FEL oscillator. The spiking is related to the emission of strong sidebands, and has been simulated with our 2D waveguide FEL code. We describe a "Young's" experiment from which we determine the spike pulse duration is  $\sim 150$  psec. Research supported by the ONR.

TABLE I

Undulator Period (helical)	1.7cm
Undulator Length	70cm
Electron Beam Energy	800kV
Electron Beam Current Density	$\sim 2\text{kA/cm}^2$
Electron Beam Diameter	4 mm
Electron Beam Pulse Length	150nsec
Waveguide Diameter	18 mm
Wiggler Strength	0.2-0.4
FEL Wavelength	2 mm
Synchrotron Period (typical operation)	$\sim 20\text{cm}$
Power Output	Several MW
Configuration	Oscillator

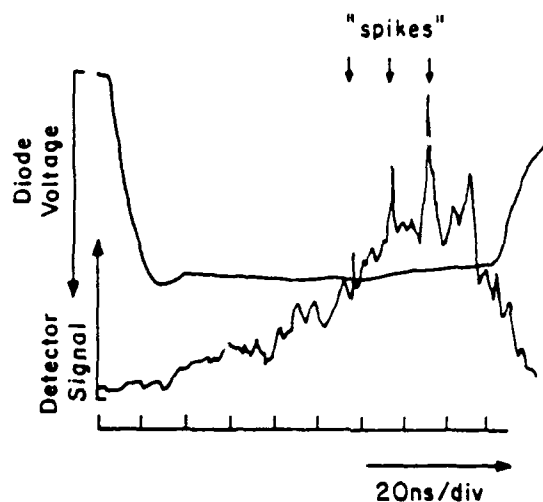


Fig. 1 FEL power, showing three spikes.

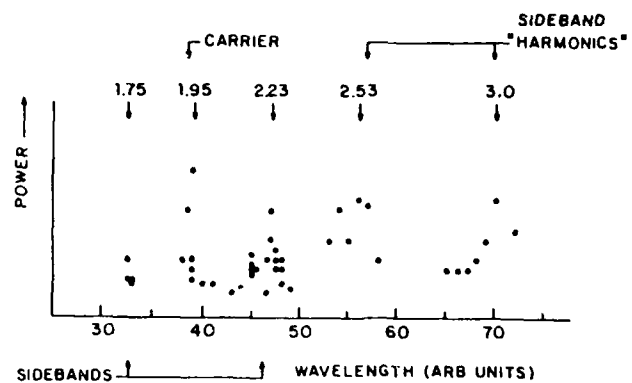


Fig. 2 Experimental sideband spectrum.

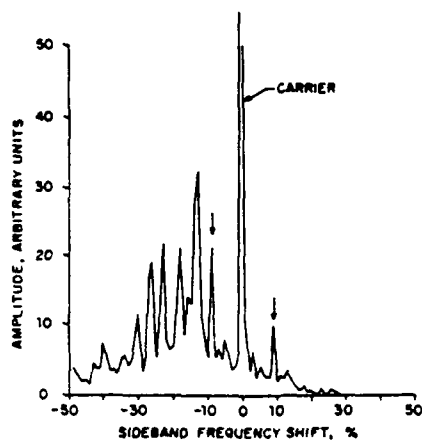


Fig. 3 Computed spectrum.

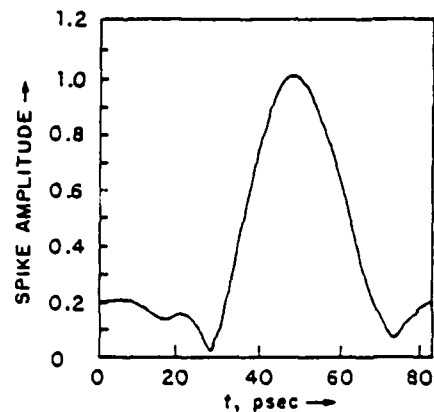


Fig. 4 Computed spike.

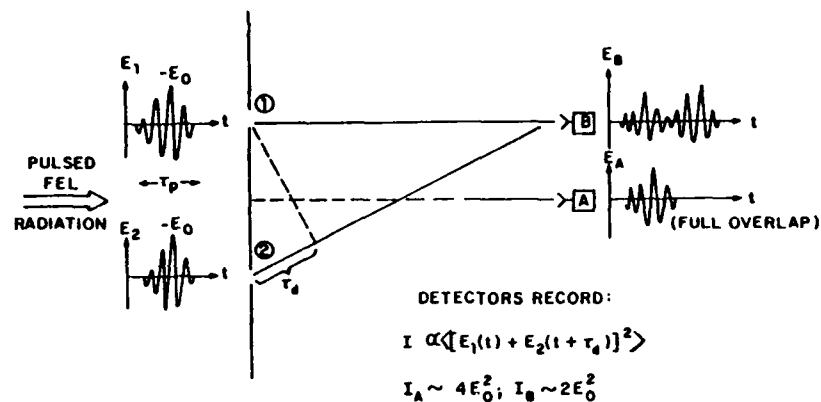


Fig. 5 Young's experiment schematic.

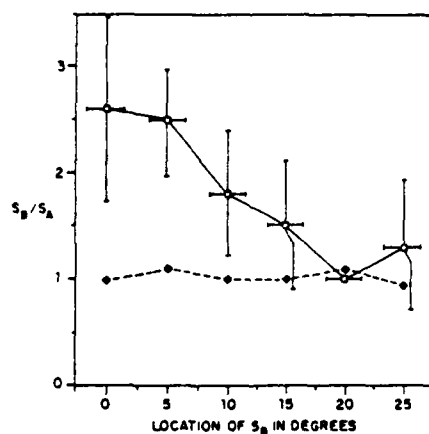


Fig. 6 Young's experiment data:  
circles, spike signal;  
diamonds, average power signal.

# Pl.18 INTERPRETATION OF FEL GAIN AND MAGNETIC FIELD ERRORS ON THE SCA/FEL

R. Rohatgi and J.C. Frisch.

High Energy Physics Laboratory  
Stanford University, Stanford, California 94305-4085

## Abstract

Measurements confirm that, with external steering, wiggler errors (1.2% rms over 120 periods) do not appreciably broaden the spontaneous spectrum. Calculations indicate that larger errors could be tolerated if they did not cause steering errors. Efforts are made to reconcile the observed FEL gain with optical and electron measurements.

## SIMULATION CODE [5]

BFELH - Spontaneous Spectrum

- Single Particle Trajectory 3-D
- Field Errors, Gradients
- Realistic External Steering
- Far-Field Forward Radiated  $\vec{E}$
- Time Steps Uniform to  $\vec{E}$  Observer
- Code Verified up to 7th Harmonic

FGAINA - Small Signal Gain

- Correct Linearized (in  $E$ ) Eqns. [4]
- Follow Several Particles with Different Phase
- Assume Gaussian Mode
- Calculate Evolution of  $E, \phi$
- Code Verified for Ideal Wiggler

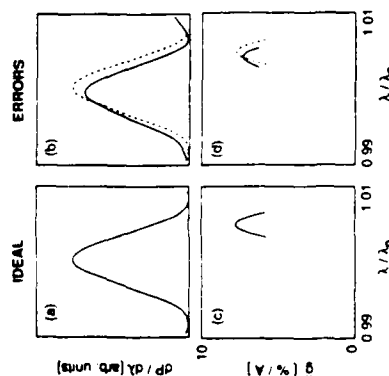
## SCA/FEL PARAMETERS

### ACCELERATOR

- $\gamma = 130$
- $\Delta\gamma/\gamma < 0.1\%$
- $I > 5$  A peak
- 3 ps micropulse
- $> 2$  ms macropulse

### WIGGLER

- $N = 120$  periods
- $\lambda_w = 3.56$  cm
- $K = 0.89$  (peak)
- SmCo
- 8 Sections with external steering
- Field Errors rms: [1], [2]
- 1.2% in Half-Period Field Integral
- 50mV in phase



Computed spontaneous spectrum  $dP/d\lambda$  and gain per Ampere  $g$  versus wavelength for wiggler with zero errors (left) and measured errors (right).  $\lambda_0$  = resonant wavelength.

## GAIN

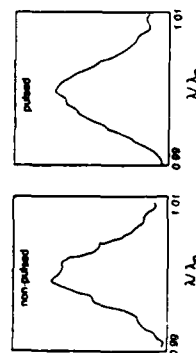
PREDICTION:

7.8 % per Ampere - Ideal Wiggler

7.4 %/A - Using Measured Errors

MEASURED:

0.9 %/A



Measured spontaneous spectrum for (a) non-pulsed beam (b) pulsed beam.

## SPONTANEOUS EMISSION

• 0.84% Consistent with 0.70%

Computed  $\otimes$  0.4% Instrumental Width

• This means our wiggler errors are acceptable.

• 1.0% FWHM with Pulsed Beam Unexplained.

<sup>1</sup> Work supported by ONR N00014-86-K-0118

## EMITTANCE GROWTH!!

- Measured  $7\pi \rightarrow 17\pi$  mm-mr [3]

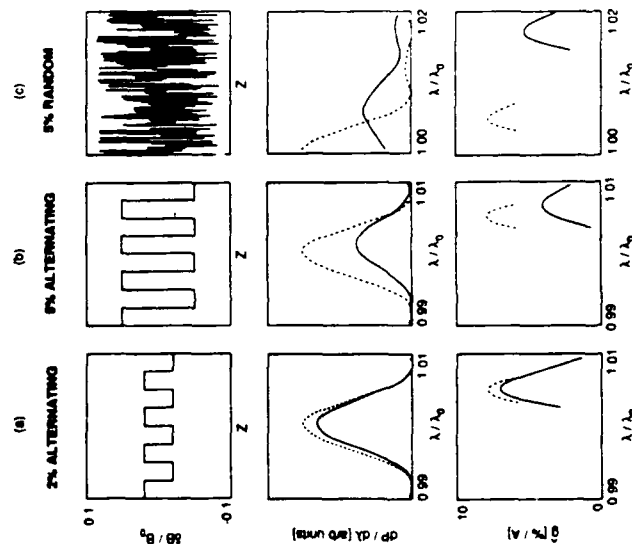
### ANALYSIS:

- Betatron Motion in  $(y, y')$
- Measured Field Errors do not Affect Betatron Motion
- Improperly Matched Ellipse  $\rightarrow$  Betatron Amplitude, Period not same for all Particles
- Ellipse Distortion  $\sim 1\pi$  mm-mr
- Steering Resolution (0.2 mm),  $y$ -offset  $\rightarrow$  Field Gradient
- Ellipse Distortion  $\sim 1\pi$  mm-mr

### \* PLAUSIBLE EXPLANATION for

#### MEASURED GROWTH —

45° QUADRUPOLES JUST UPSTREAM FROM WIGGLER



Field error profile  $B_z$ ,  $(\text{cm})$ , along length of wiggler, spontaneous spectrum  $dN/d\lambda$ , and gain per Ampere  $\beta$  versus wavelength for 3 cases: (a) 15 period sections alternately off by  $\pm 2\%$ , (b) 15 period sections alternately off by  $\pm 5\%$ , (c) 5% rms amplitude errors with internal steering correction. Curves for an ideal wiggler are shown dashed for comparison.

## DISCUSSION

- Spont. Spectrum is Fourier Transform (squares) of  $\vec{E}(t)$  radiated by Single Particle.
- $\vec{E}(t)$  Finite Wave Train 120 periods in Length  $L$
- Overlap with  $\lambda \sim \frac{1}{120}$  sine wave  $\sim 120\lambda$
- $\lambda \sim \frac{1}{120}$  sine waves  $\rightarrow$  zero overlap.
- To affect the Spectrum, require overlap with  $\frac{1}{120}$  sine waves to be comparable to  $\frac{1}{120}$  overlap.
- Ideal wiggler  $\rightarrow$  electrons slip 120 optical wavelengths total
- Error threshold: Field errors generate slip error  $\sim 1$  optical wavelength.

## CONCLUSIONS

- Measured Spontaneous Spectrum in Reasonable agreement with Ideal Spectrum & Simulation
- Field Errors not Responsible for Gain Degradation
- Measured Gain Low by Factor 8 — UNEXPLAINED
- Wiggler does not Degrade Emittance by more than  $\sim 2\pi$  mm-mr
- Our 120 period 1% error Wiggler Requires External Steering to Keep Beam Within Optical Mode
- With external Steering Correction, FEL tolerates Errors up to  $\sim 5\%$ .

## SAMPLE SIMULATIONS

### Pathological:

- Alternate Sections  $\pm 2\%$  Field Strength. Integrated Slip  $0.2\lambda$ . Slight Degradation
- Alternate Sections  $\pm 5\%$   $\rightarrow 50\%$  Gain Degradation.

### Random

- 5% rms with External Steering. 30% Gain Degradation.
- 0.5%, no Steering Correction. Beam Wanders out of Optical Mode.
- 2.5%, no Steering Correction. Spontaneous Spectrum Deteriorates.

## REFERENCES

- O. Shatal & R. Rbhatgi, Proc 8<sup>th</sup> Int'l FEL Conf., to be publ.
- R.W. Warren, NIM A272, 257 (1988).
- R. Svent, private communication.
- B.W.J. McNeil, NIM A259, 240 (1985).
- R. Rbhatgi, HEPL report, to be published.

# PI.19 COMPUTER SIMULATIONS OF A 100 GHz CARM OSCILLATOR WITH BRAGG REFLECTORS

T.H. Kho and A.T. Lin  
UCLA, Dept. of Physics  
Los Angeles, CA 90024

A self-consistent, time-dependent, 3-D particle code has been developed to study the Cyclotron Autoresonance Maser (CARM) interaction in a Bragg resonator. The code has been applied to model a CARM oscillator experiment at the NRL.<sup>1</sup> Tentative simulation results indicate low efficiency for the parameters in the experimental regime, in contrast to theoretical predictions.

## 100 GHz CARM OSCILLATOR EXPERIMENT PARAMETERS

Beam voltage	600 kV
Beam current	200 A
Axial velocity spread	$\Delta v_z/v_z < 3\%$
Magnetic Field	25 kG
Operating mode	TE <sub>61</sub>
$\alpha = v_z/v_z$	0.6

### Resonator parameters:

Mean wall diameter	1.59 cm
--------------------	---------

### Upstream Reflector

Length	3 cm
Ripple depth	0.25 mm
Ripple period	1.68 mm
Reflectivity	99%

### Downstream Reflector

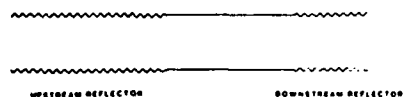
Length	1.5 cm
Ripple depth	0.31 mm
Ripple period	1.68 mm
Reflectivity	90%

Center Section Length	2.6 cm
-----------------------	--------

### Expected performance:

Efficiency	20%
Power	24 MW

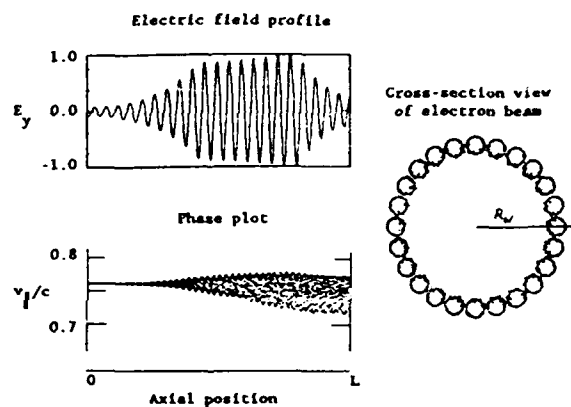
### Schematic of Bragg resonator



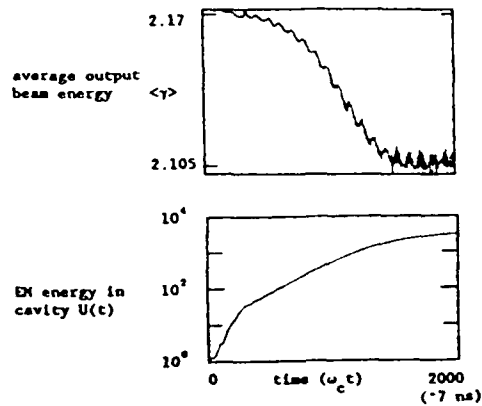
## COMPUTER MODEL

- Finite-length, nonuniform, 3-D cylindrical cavity.
- Considers TE<sub>61</sub> waveguide mode only.
- Includes self-consistent time and space dependence.
- No space charge effects.
- No wall dissipation.
- Injects seed wave to initiate CARM interaction.
- Cold electron beam assumed unless otherwise stated.

## SAMPLE OUTPUTS: 400 A OSCILLATOR

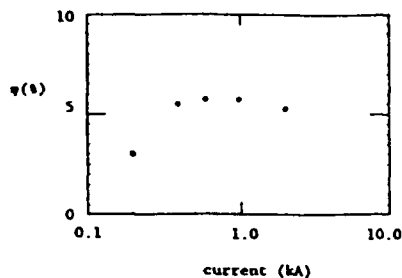


## SAMPLE OUTPUTS: 400 A OSCILLATOR

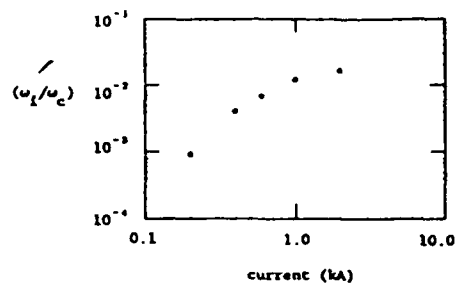


$\omega_c/2\pi$  is TE<sub>61</sub> cut-off frequency.

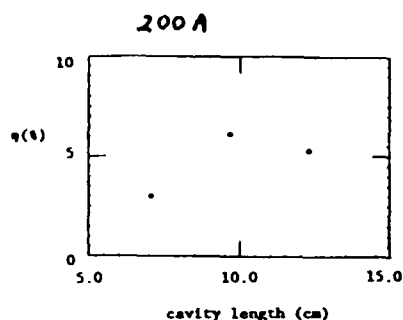
#### EFFICIENCY WITH BEAM CURRENT



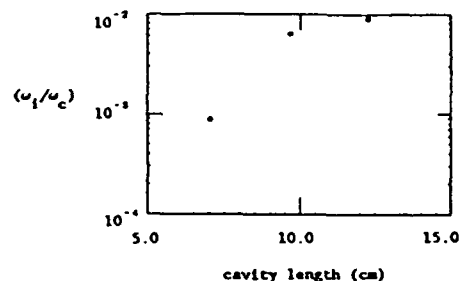
#### GROWTH RATE WITH BEAM CURRENT



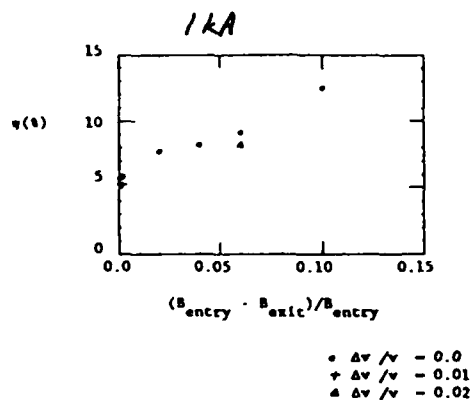
#### EFFICIENCY WITH CAVITY LENGTH



#### GROWTH RATE WITH CAVITY LENGTH



#### EFFICIENCY WITH MAGNETIC FIELD TAPERING AND AXIAL VELOCITY SPREAD



#### SUMMARY

From these tentative results, it appears that:

- The efficiency is low for the experimental parameters.
- Magnetic field tapering offers the most leverage in enhancing the efficiency.
- Axial velocity spread is not an important limitation here.

#### Reference

1. R.B. McGowan, A.V. Filiflet, S.H. Gold, V.C. Granatstein, and M.C. Wong, *Int. J. Electronics* **62**, 463 (1988).

#### Acknowledgements

This work is supported by the AFSOR 88-0027, the NSF, and the SDSC.

#### SPECULATION ON LOW EFFICIENCY OBSERVED IN SIMULATIONS

The low efficiency observed in these tentative results appears to be at odds with the theoretical prediction for the CARM oscillator.<sup>1</sup>

One explanation could be that reflected waves in the resonator significantly modify the CARM interaction.

**PROGRESS REPORT ON BEIJING FEL PROJECT**

J. Xie, J. Zhuang, Y. Wang, S. Zhong, R. Ying, C. Mao.

Institute of High Energy Physics, Academia Sinica  
P.O. Box 918, Beijing, China

**Abstract**

The progress of Beijing IR-FEL project carried out at IHEP will be reported. It includes some specific developments of software and hardware rather than striving for general coverage. First, computational studies of emittance and pulse-length effects to the small signal gain are presented. Then some experimental results of the microwave electron gun injector is given. Modifications of the beam transport system and the optimization and measurements of the NdFeB undulator are described. Finally, some aspects of the beam diagnostics and the spontaneous emission experiment are discussed.

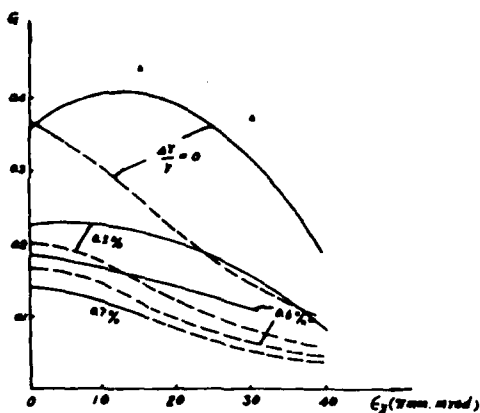


Fig. 1. SSG vs emittance with  $4\gamma/r$  as parameter. (Data points from ref. 3. solid line, simulation; dashed line, calculated according to ref. 1.)

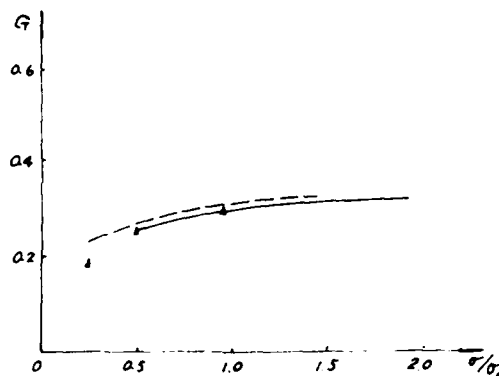


Fig. 2. SSG vs RMS pulse length ( $\sigma_0 = 1$  ps,  $I_p = 10$  A. Data points from ref. 3, solid line, simulation; dashed line, calculated according to ref. 1.)

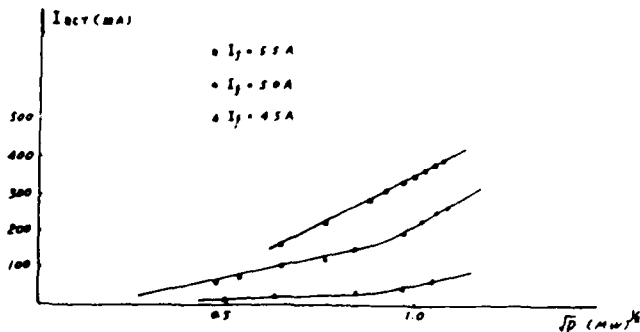


Fig. 3. Beam current vs square root of RF power.

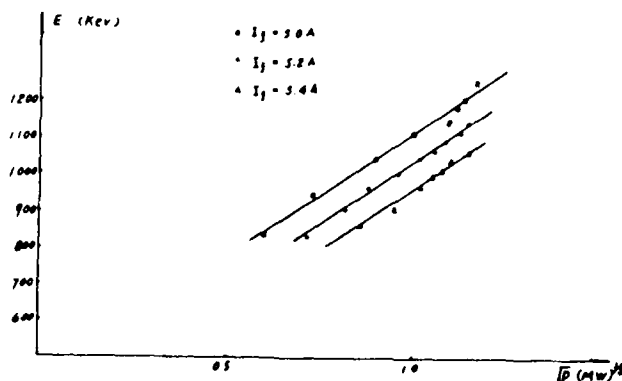


Fig. 4. Beam energy vs square root of RF power.



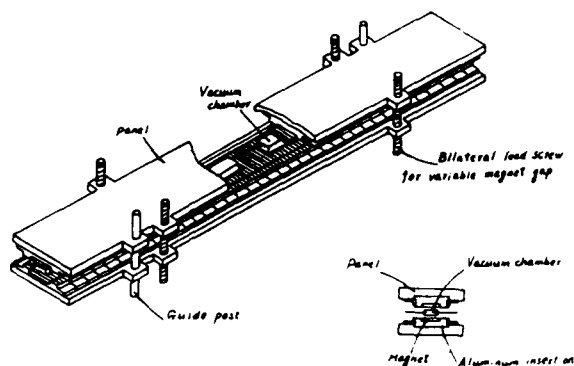


Fig. 9 Mechanical layout of the undulator

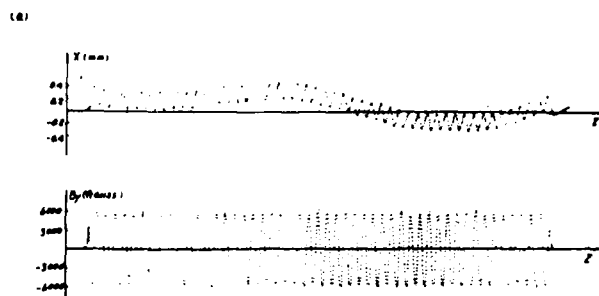


Fig. 10. Magnetic field distribution and electron trajectory (a) in a random undulator, (b) in the optimized undulator.

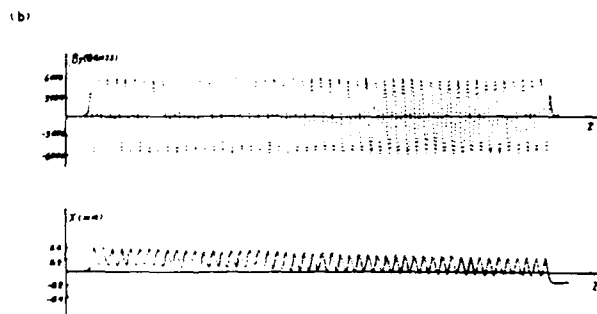


Fig. 10. Magnetic field distribution and electron trajectory (a) in a random undulator, (b) in the optimized undulator.

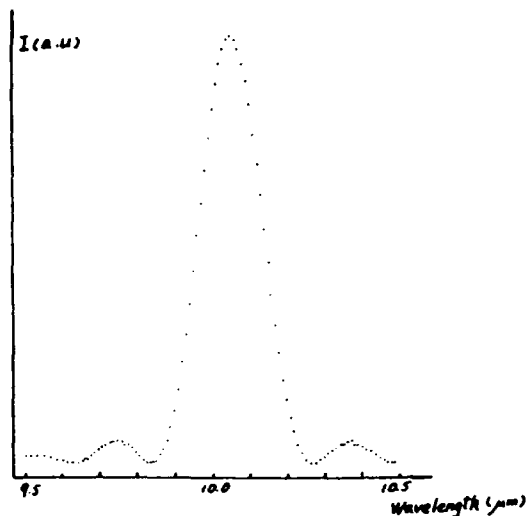


Fig. 11. Spontaneous emission of the optimized undulator.

#### References

- [1] G. Datolli, I. Latardi, J.M.J. Maday and A. Renieri, IEEE J. Quantum Electron. QE 20 (1984) 637
- [2] Xie Jialin, Zhuang Jiejia, Wang Youzhi and Zhong Shicai, Nuclear Instrument & Methods in Phys. Res. A 272 (1988) 40
- [3] J.C. Goldstein Private communication
- [4] G.A. Westenskow and J.M.J. Maday, Laser and Particle Beams, 2 (1984) 223
- [5] R.L. Sheffield, E.R. Gray and J.S. Fraser, Nuclear Instrument & Methods A 272 (1988) 222
- [6] Xie Jialin, Gao Jie, Huang Yongzhang, Zhang Renshar and Wang Youzhi, "Simulation and Experiment Study of the Microwave Gun", to be published
- [7] Halbach K., Nuclear Instrument & Methods, Vol.187, No.21 (1981) 109-117

# PI.21 THE VARIABLE DISPERSION ELECTRON SPECTROMETER AT THE SCAFEL

R. L. Swent, J. C. Frisch and T. I. Smith  
High Energy Physics Laboratory  
Stanford University  
Stanford, California 94305-4085

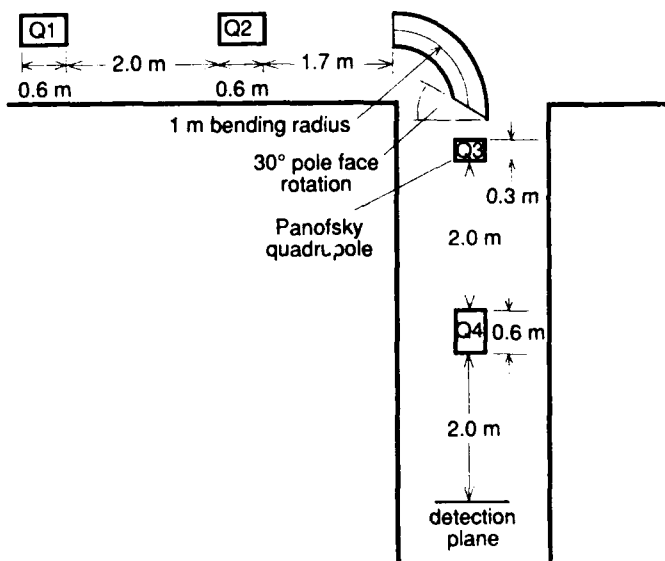
An electron spectrometer with dispersion variable between zero and 0.08%/mm has been installed on the SCA/FEL. At zero dispersion the energy acceptance is several percent. Spectral data can be acquired at a 30 kHz rate. Energy extraction by the FEL has been measured at 0.4%.

## VARIABLE DISPERSION GIVES FLEXIBILITY

DISPERSION	APPLICATION
High	Analyze SCA Beam with FEL off ( $\Delta E/E \leq 0.1\%$ )
Medium	Analyze spent beam from FEL ( $\Delta E/E = 2\% - 6\%$ )
Low	Beam "dump", independent of changes in SCA or FEL

## DESIGN PRINCIPLES

- 90° bending magnet provides energy discrimination
- Quadrupole pair before bend controls resolving power
- Quadrupole pair after bend controls dispersion
- Apertures at bending magnet exit determine acceptance



\* Supported by ONR Contract N00014-86-K-0118. Physical Layout of the System Components.

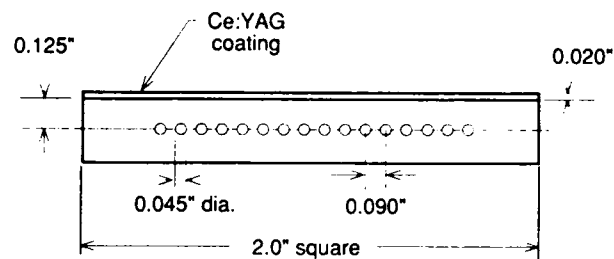
## DETECTORS

### Phosphor Screen and CCD Camera

- high resolution in energy
- low resolution in time (at present)
- Ce:YAG phosphor has 100 nsec relaxation time, so a gated intensifier could give time resolution comparable to a micropulse (but only one sample per macropulse)

### Wire Array

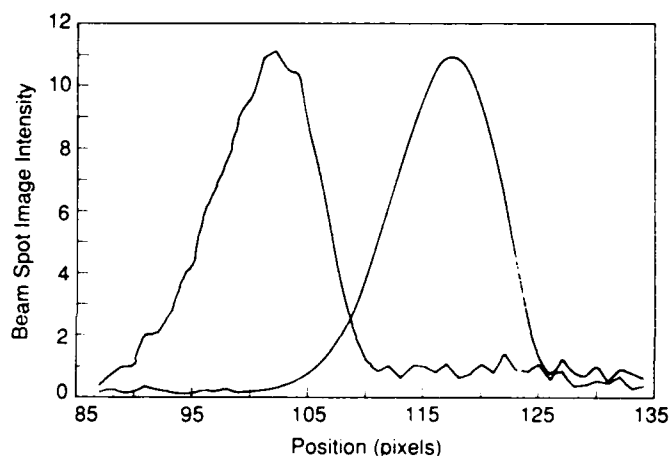
- moderate resolution in energy (16 wires)
- moderate time resolution (30  $\mu$ sec)
- many samples per macropulse



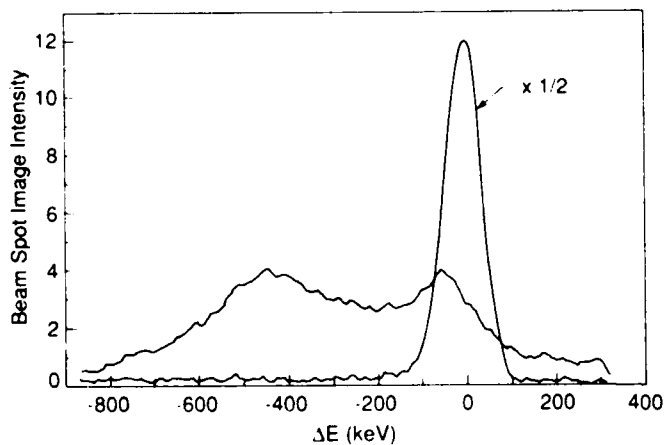
Arrangement of the Phosphor Screen and the Be Wire Array for Detecting Electrons.

## EXPERIMENTAL CONDITIONS

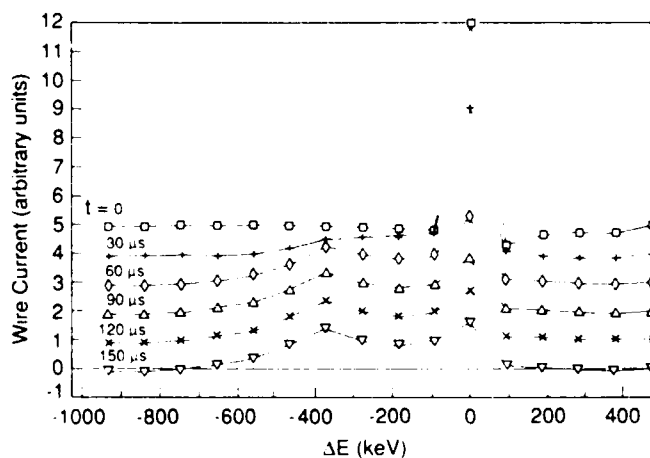
- Electron beam energy = 67 MeV
- Electron beam current = 210  $\mu$ A
- Optical wavelength = 1.54  $\mu$ m
- Optical power = 30 W (macropulse average)
- Macropulse length = 3 msec



Two Laser-Off Electron Spectra. Bending Magnet Current Differs by 0.1% between the two.



Laser-Off and Laser-On Electron Spectra. The Laser-Off Spectrum has been reduced by a factor of 2.



Electron Spectra From Wire Array, Taken as the Laser Turns On.

## Pl.22

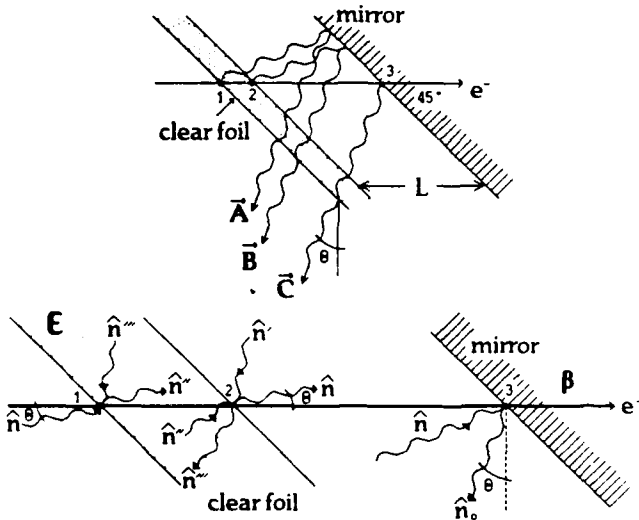
### COMPARATIVE ANALYSIS OF OPTICAL TRANSITION RADIATION BASED ELECTRON BEAM EMITTANCE MEASUREMENTS FOR THE LOS ALAMOS FREE-ELECTRON LASER

D. W. Rule and R. B. Fiorito  
Naval Surface Warfare Center  
Silver Spring, Maryland, USA 20903-5000

A. H. Lumpkin, R. B. Feldman and B. E. Carlsten  
Los Alamos National Laboratory  
Los Alamos, New Mexico 87545

We compare two methods to analyze OTR interference patterns in order to determine the electron beam emittance from the observed interference fringe visibility. The first method uses a simple analytical model assuming a Gaussian beam divergence. The second method is a numerical convolution of the beam phase space distribution with the OTR interference pattern.

#### Interferometer and OTR Amplitudes



#### Interferometer Intensity Distribution

$$\frac{d^2 I}{d\omega d\Omega} = \frac{e^2}{4\pi^2 c} \left| r_m (\vec{A} + \vec{B}) e^{-i\theta_{23}} - \vec{C} \right|^2, \theta_{23} = \frac{L}{L_v} = \frac{kL}{\beta} (1 - \beta \cos \theta)$$

Where, according to Wartski<sup>1</sup>,

$$\vec{A} = (1 - T e^{i\theta_{12}}) \frac{\vec{\beta} \times \hat{n}}{1 - \vec{\beta} \cdot \hat{n}} + R \frac{\vec{\beta} \times \hat{n}'}{1 - \vec{\beta} \cdot \hat{n}'}$$

$$\vec{B} = \frac{T}{t\sqrt{\epsilon}} (e^{i\theta_{12}} - 1) \frac{\vec{\beta} \times \hat{n}''}{1 - \sqrt{\epsilon} \vec{\beta} \cdot \hat{n}''} + \frac{T r'}{t\sqrt{\epsilon}} (e^{i\theta_{12}} - 1) \frac{\vec{\beta} \times \hat{n}''}{1 - \sqrt{\epsilon} \vec{\beta} \cdot \hat{n}''}$$

$$\vec{C} = \frac{\vec{\beta} \times \hat{n}_0}{1 - \vec{\beta} \cdot \hat{n}_0} + \frac{r_m \vec{\beta} \times \hat{n}}{1 - \vec{\beta} \cdot \hat{n}}$$

T, R are transmission and reflection coefficients across a foil  
t, r' are transmission and reflection coef. for inside the foil  
r<sub>m</sub> is the Fresnel reflection coefficient for mirror

#### Specializing to $\vec{E}$ in Plane of Observation

$\vec{E} = \vec{E}_{||}$  and  $\vec{\beta} \rightarrow \vec{\beta}_{||}$  component in plane of observation

Neglecting reflected clear foil amplitudes:

$$\vec{A}_{||} = \beta_{||} (1 - T_{||} e^{i\theta_{12}}) \frac{\sin \theta}{1 - \beta_{||} \cos \theta}, \vec{B}_{||} = \beta_{||} \frac{T_{||}}{t\sqrt{\epsilon}} (1 - e^{i\theta_{12}}) \frac{\sin \theta'}{1 - \sqrt{\epsilon} \beta_{||} \cos \theta'}$$

$$\vec{C}_{||} = \beta_{||} r_m \frac{\sin \theta}{1 - \beta_{||} \cos \theta} + \frac{\beta_{||} \cos \theta}{1 - \beta_{||} \sin \theta}$$

$\theta_{12}$  = phase of light from interface 1 wrt e<sup>-</sup> fields at interface 2. Note  $\theta_{12}$  and  $\theta_{23} \propto k$

$$\frac{d^2 I_{||}}{d\omega d\Omega} = \frac{e^2}{4\pi^2 c} \left| r_m (\vec{A}_{||} + \vec{B}_{||}) e^{-i\theta_{23}} - \vec{C}_{||} \right|^2 \leftarrow \text{Average this over filter's band width}$$

#### Average Interferometer Expression Over Bandwidth of Filter

$$\frac{d I(\theta)}{d\Omega} \equiv \int_{-\infty}^{\infty} F(k) \frac{d^2 I}{d\omega d\Omega} dk$$

#### Assume Lorentzian Bandwidth

$$F(k) = \frac{\Delta k}{2\pi} \frac{1}{(k - k_0)^2 + \left(\frac{\Delta k}{2}\right)^2}$$

#### Define Average Phase

$$\langle e^{i\theta} \rangle \equiv \int_{-\infty}^{\infty} F(k) e^{i\theta(k)} dk = e^{-\frac{\Delta k}{2k_0} |\theta(k_0)|} e^{-i\theta(k_0)}$$

Where  $\theta = (\theta_{12}, \theta_{23}, \theta_{12} + \theta_{23})$

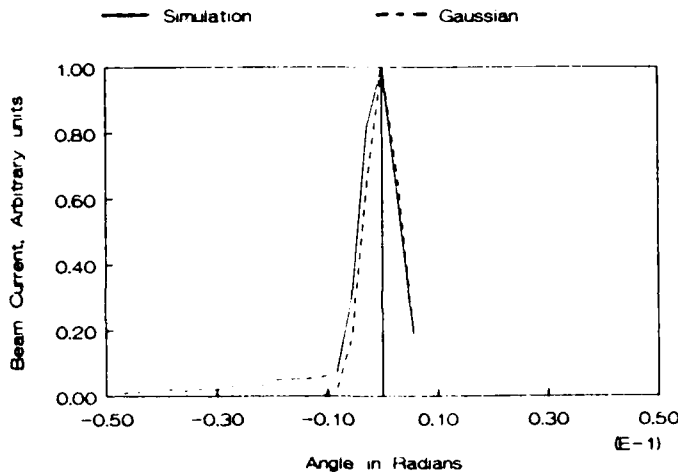
## Convolution of OTR Interferometer with Beam Phase Space Distribution

$$\frac{d^2 I}{d\omega d\Omega} = \int \frac{d^2 I_0(\theta_x - \alpha_x, \theta_y - \alpha_y, \gamma_z)}{d\omega d\Omega} f(\alpha_x, \alpha_y, \gamma_z) d\alpha_x d\alpha_y d\gamma_z$$

Where  $f$  is a Parmela  $f_p$  or Gaussian  $f_g$  Distribution

$$f(\alpha_x, \alpha_y, \gamma_z) = \begin{cases} \iint f_p(x, \alpha_x, y, \alpha_y, \gamma_z) dx dy \\ f_g(\alpha_x, \alpha_y) = \frac{1}{\sqrt{2\pi}\sigma_x^2} \frac{1}{\sqrt{2\pi}\sigma_y^2} e^{-\frac{\alpha_x^2}{2\sigma_x^2}} e^{-\frac{\alpha_y^2}{2\sigma_y^2}} \end{cases}$$

Beam Angular Distribution in X-Z Plane  
Standard Deviation of Gaussian = 3 mrad



## Moments of Distributions at Beam Waist

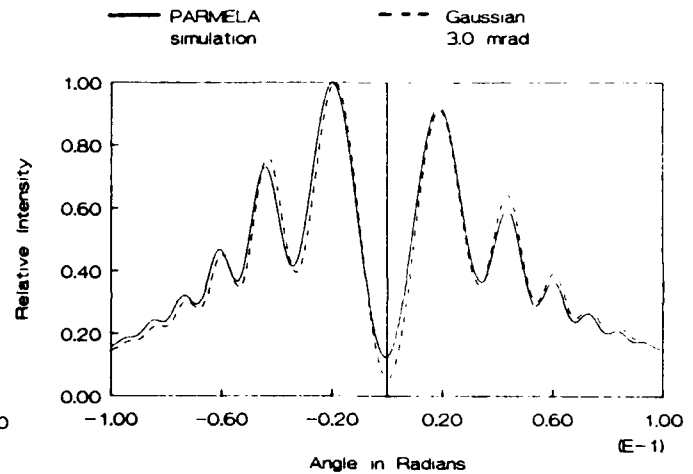
$$\sigma_x^2 = \langle \theta_x^2 \rangle, \quad \sigma_y^2 = \langle \theta_y^2 \rangle$$

$$\langle \gamma \rangle, \quad \langle x^2 \rangle, \quad \langle y^2 \rangle$$

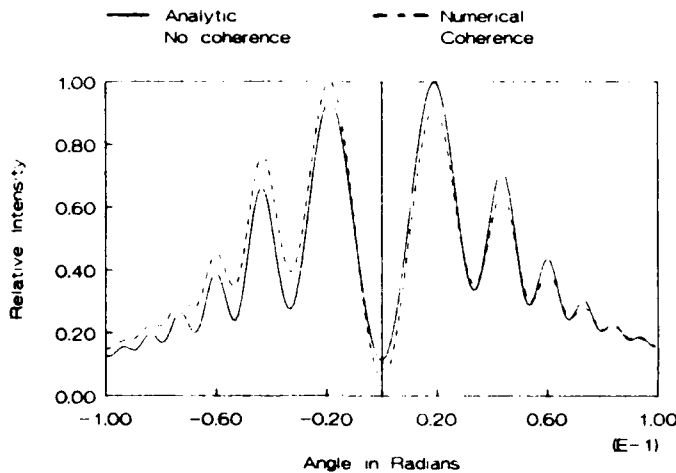
## Local RMS Emittance

$$\epsilon_x^2 = \langle x^2 \rangle \langle \theta_x^2 \rangle, \quad \epsilon_y^2 = \langle y^2 \rangle \langle \theta_y^2 \rangle$$

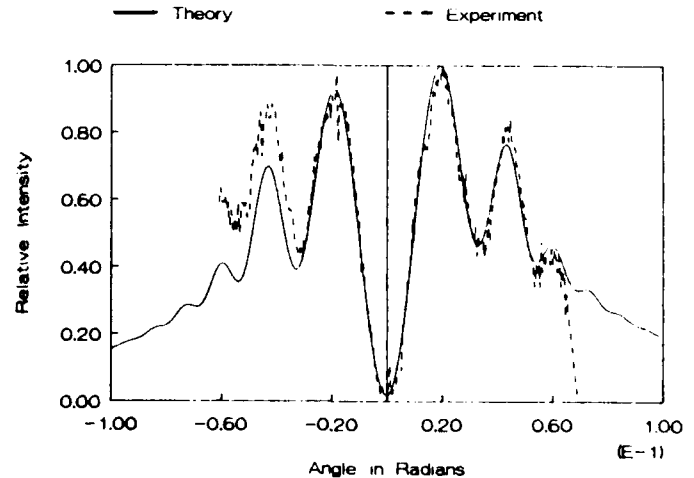
Comparison of Interference Patterns  
Beam Dist. from PARMELA vs Gaussian



Effect of Coherent Clear Foil Amplitudes  
Gaussian Distribution Std. Dev. = 3 mrad



Least Squares Fit of IPAR - IPERP  
SX=4.23 mrad, SY=3.60 mrad, E= 19.91 MeV



1. L. Wartski et al., J. Appl. Phys. 46 (1975) 3644.

## Design of a High Field Taperable Helical Wiggler

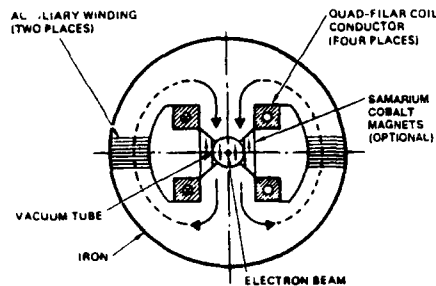
J. Vetrovec

TRW Inc., 1 Space Park, Redondo Beach, CA 90278  
(Now at Rockwell International, Rocketdyne Division, 6633 Canoga Avenue, Canoga Park, CA 91303, (818) 700-4875)

The paper discusses theoretical as well as practical aspects of an electromagnetic helical wiggler where the field strength and the taper are completely adjustable. Unique coil and core geometry together with a careful choice of materials make it possible to produce fields over 5 kG in a bore diameter of 2.5 cm.

### CONFIGURATION OF THE HELICAL WIGGLER

- Iron core and flux return
- Quad-filar coil provides main excitation
- Auxiliary winding for trimming and taper
- Assisting permanent magnets are optional



1

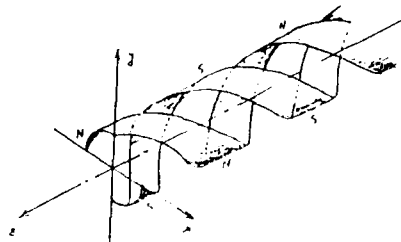
### REFERENCE DESIGN PARAMETERS

Parameter	Value
Wiggler wavelength	8 cm
Bore radius	1.25 cm
Nominal field	5 kG
Ampere turns (@ nominal field)	10 000
Dipole thickness	1 cm ( $\lambda_w/8$ )
Material	Oriented silicon steel
Ampere-turn loss in material	1%

2

### POLEFACE SURFACE

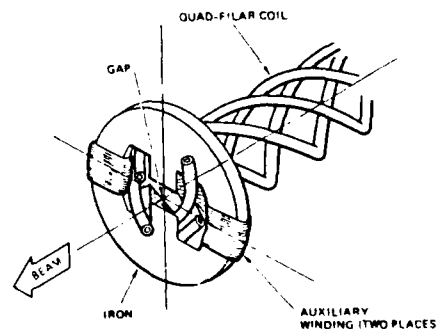
- Double threaded screw
- Surface shape defines Wiggler Field



3

### DEFINITION OF A HELICAL DIPOLE

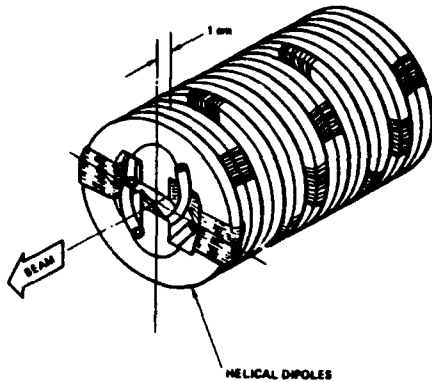
- Helical polefaces
- Core thickness =  $\lambda_w/n$  ( $n = 1, 2, 3, \dots$ )
- Main excitation from Quad-filar coil
- Field Trimming by auxiliary winding
- Flux returns are flattened to provide space for Aux. Winding and vacuum tube access



4

### WIGGLER ASSEMBLY

- Stack of Helical Dipoles rotated about z-axis
- Poleface surfaces are continuous

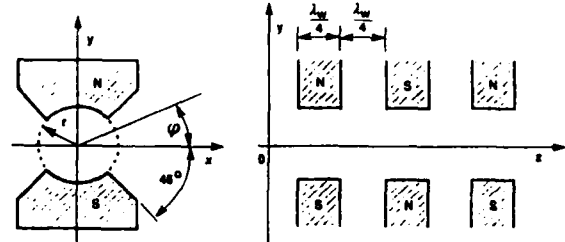


5

### WIGGLER FIELD DISTRIBUTION

- Scalar potential used in calculations
- Initial poleface assumed circular to simplify boundary conditions
- Solution can be generalized

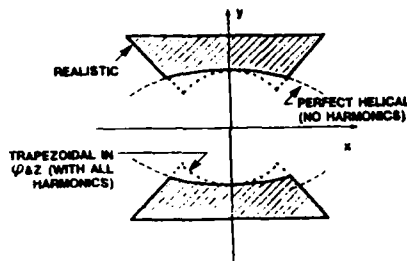
$$u(\rho, \phi, z) = \frac{8\sqrt{2}}{\pi^2} \sum_{n=0}^{\infty} (-1)^n (n+1)^{3/2} \frac{J_{2n+1}((2n+1)k_w \rho)}{J_{2n+1}((2n+1)k_w r)} \frac{\sin(2n+1)(k_w z + \phi)}{(2n+1)^2}$$



6

### HARMONICS-FREE POLEFACE

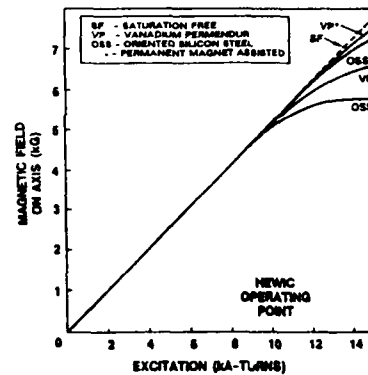
$$\phi = \arcsin \frac{f_1(k_w \rho)}{f_1(k_w r)} \cdot k_w z$$



7

### WIGGLER RESPONSE TO EXCITATION

- 5 kg Wiggler Field @ 1% H.d. loss
- Saturation first occurs in the root of the polepieces
- Permanent magnets can drive the material out of saturation

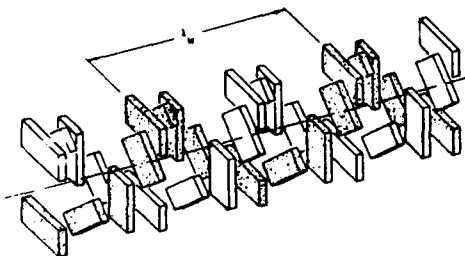


8

### STEERING-FREE TAPER

- Interpret helical wiggler as a superposition of linear wiggler formed by dipoles oriented at the same angle
- Apply Halbach's steering-free excitation patterns

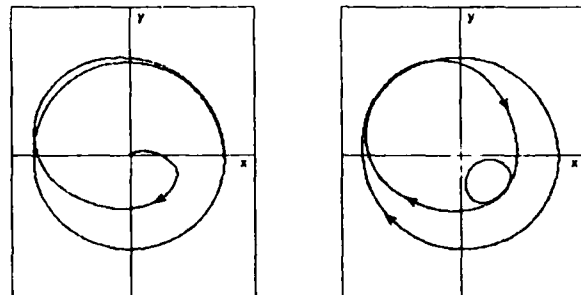
$$\begin{pmatrix} x(z) \\ y(z) \end{pmatrix} = \sum_{n=1}^{\infty} \sum_{j=1}^{\infty} v_{nj} \begin{pmatrix} \cos \\ \sin \end{pmatrix} \left( \frac{2\pi z}{\lambda} \right) [a_n + a_1 (j-1)n + i] + \dots \quad v_{ij} = \begin{pmatrix} K+2 \\ jn+i \end{pmatrix}$$



9

### TRANSVERSE PLANE TRAJECTORIES

- At wiggler entrance
- Due to 1 power supply "off"



10

# OPTICAL KLYSTRON CONFIGURATION FOR A HIGH GAIN X-RAY FREE-ELECTRON LASER

Juan C. Gallardo and Claudio Pellegrini

Brookhaven National Laboratory  
Upton, New York 11973

## ABSTRACT

We present theory and numerical simulations of the performance of an x-ray FEL in the amplified spontaneous emission mode with an optical klystron undulator configuration. This device can produce picosecond pulses of high brightness with a significantly shorter undulator than a conventional FEL.

## 1. INTRODUCTION

The amplified spontaneous emission (ASE) regime of an FEL can be used to produce coherent soft x-ray radiation in a long undulator ( $5 \leq L \leq 10 \text{ m}$ )<sup>1-4</sup>. In such a regime, the initial incoherent radiation, with an optical power proportional to the number of electrons, is amplified by the electron beam itself as it traverses the interaction region. This collective phenomena leads to exponential growth until the system reaches saturation<sup>5,6</sup>. To achieve this situation the undulator has to be made sufficiently long and the accelerator has to provide a high brightness electron beam, well above the values required for an oscillator experiment. However, the ASE has a number of advantages in comparison with an oscillator:

- good reflectivity soft x-ray mirrors are not needed;
- needs a single pulse traversing the undulator reducing the beam loading problem<sup>7</sup> in the electron beam accelerator.

In this work we discuss one possible alternative undulator configuration that will reduce its length keeping the total power output of the laser approximately constant. An optical klystron<sup>8-9</sup> consists of two undulators separated by a short dispersive magnet. This magnet configuration translates the energy spread created in the first undulator section (*modulator*) into significant changes in the electron phase  $\psi = (k + k_0)z - \omega t$  when the electron pulse arrives at the second undulator section (*radiator*). If these changes are arranged in a suitable manner we can achieve significant bunching and, consequently, a larger optical gain.

We first use a simple 1-D linearized theory to obtain an approximate estimate of the FEL field enhancement produced by the optical klystron magnet configuration; then, we numerically solve the complete non-linear set of 1-D FEL equations including both energy spread and emittance.

Our results show that an optical klystron is a very attractive alternative to achieve saturation in an

ASE FEL with less than half the undulator length of a conventional FEL and producing the same output power.

## 2. 1-D LINEARIZED MODEL

The spontaneous emission of the electron beam in combination with the undulator magnetic field, acts back over the electrons to introduce an energy modulation in the beam. This energy modulation is transformed into bunching of the electrons as they go through the dispersive section. The optimal position of the dispersive magnet occurs at the point where the laser power starts to grow exponentially which correspond to a gain length  $L_G$ , defined as the distance for e-folding of the laser power. This forced bunching results in a discontinuous jump of the gain as the electrons enter the radiator undulator.

The FEL dynamics are then described by defining three collective variables<sup>8</sup> for the laser field  $X$ , the bunching function  $Y$ , and the energy spread  $Z$

$$\begin{aligned} X &= a \\ Y &= \langle e^{-i\psi_0\theta} \rangle \\ Z &= \frac{1}{\rho} \langle e^{-i\psi_0\eta} \rangle \end{aligned}$$

where  $\psi_0$  is the initial electron phase,  $\theta = \psi - \psi_0$ ,  $\gamma_0$  is the initial electron energy and  $\eta = \frac{(\gamma - \gamma_0)}{\gamma_0}$ ,  $\rho = \left( \frac{K\lambda_0}{8\pi\gamma_0} \right)^{\frac{1}{2}} \left( \frac{4\pi r_e c^2 N_e}{\gamma} \right)^{\frac{1}{2}}$  is the FEL parameter with  $\lambda_0$  the wiggler period,  $K$  the undulator parameter;  $r_e$  is the classical electron radius and  $N_e$  is the particle density of the electron beam. In the limit of small  $\rho$  the FEL equations of motion<sup>8</sup> with initial conditions  $X(0) = Z(0) = 0$  and  $Y(0) = Y_0$  are,

$$\dot{X} = i\delta X + iY$$



$$\dot{Y} = Z$$

$$\dot{Z} = -X$$

here  $\delta$  is the detuning parameter  $\delta = \frac{\gamma_R^2 - \gamma_A^2}{2\gamma_A^2 \rho}$  and  $\gamma_R^2 = \frac{\lambda_R}{2\lambda} (1 + K^2)$  and  $\dot{X} = \frac{dX}{d\tau}$  with  $\tau = 4\pi\rho N$ ,  $N$  being the number of undulator periods.

The solutions in the high-gain self-spontaneous emission are

$$Y = \frac{1}{3} Y_0 e^{i\mu_1 \tau}$$

$$X = -\mu_1^* Y$$

$$Z = i\mu_1 Y$$

where  $\mu_1 = \left(\frac{1-i\sqrt{3}}{2}\right)$  and  $\mu_1^*$  is the complex conjugate.

The dispersive section can be taken as an instantaneous interaction at  $\tau_D$  with the following constraints on the dynamical variables ( $X_<$  and  $X_>$  denotes the values right before and after the dispersion interaction, respectively),

$$X_> = X_<$$

$$Y_> = Y_< - \mathcal{D}Z_<$$

$$Z_> = Z_<$$

where  $\mathcal{D} = \rho k D$  with

$$D = \left(\frac{e}{\gamma m c^2}\right)^2 \int_0^s dz' \left\{ \int_0^{z'} dz'' B_D(z'') \right\}^2.$$

Example of a dispersive section is

$$B_D(z) = \begin{cases} B_0 & 0 \leq z < \frac{s}{4} \\ -B_0 & \frac{s}{4} < z < \frac{3s}{4} \\ B_0 & \frac{3s}{4} < z \leq s. \end{cases}$$

This configuration gives  $D = \frac{1}{48} \left(\frac{eB_0}{m c^2 \gamma}\right)^2 s^3$  and satisfies the condition that the first and second integral over  $s$  of the magnetic field must vanish so as to have no transverse and angular beam displacements. The  $\mathcal{D}$  parameter turns to be  $\approx 2500$  for a 1 GeV electron beam,  $\rho = 1.9 \times 10^{-2}$ ,  $\lambda = 2.5$  nm,  $B_0 = 1$  T and  $s = 1$  m. After the dispersion section, the dynamical variables will evolve as in the first section but now with the initial conditions

$$Y_>(\tau_D) = Y_<(\tau_D)(1 - i\mu_1 \mathcal{D})$$

$$X_>(\tau_D) = X_<(\tau_D)$$

$$Z_>(\tau_D) = Z_<(\tau_D)$$

therefore we can write the laser field as,

$$X_>(\tau) = -\frac{1}{3} \mu_1^* Y_<(\tau_D)(1 - i\mu_1 \mathcal{D}) e^{i\mu_1(\tau - \tau_D)}$$

This last expression shows that the enhancement factor introduced by an optical klystron is given by the factor  $\approx \frac{1}{3} \mathcal{D}$  which for the parameters considered in our simulations is of the order of  $10^3$ . To obtain an equivalent growth in the field in the conventional FEL configuration, the length of the undulator can be estimated from  $e^{i\mu_1 \Delta \tau} \approx 10^3$  which for the value of  $\rho$  used corresponds to  $\approx 400$  magnet periods.

We have used a 1-D simulation code to solve the full set of FEL equations including energy spread and emittance and to calculate the output laser power of an ASE-FEL. To simulate a realistic electron beam with energy spread and emittance we use a uniform distribution in  $\psi_0$  and a product of a gaussian distribution in energy spread, transverse position and injection angle. As illustrated in Fig.1, the saturation power achieved by an optical klystron is larger than the one obtained with a standard wiggler and, more important, we observe significant power levels at less than half the undulator length. Although our results were obtained in the context of a 1-D theory, for the set of parameters used, the gain length of the device is shorter than the Rayleigh range of the laser and, consequently, 3-D effects will not significantly modify our conclusions<sup>10</sup>.

### 5. REFERENCES

1. J. Murphy and C. Pellegrini, J. Opt. Soc. Am. **B2**, 259 (1985).
2. C. Pellegrini, Nucl. Instrum. & Meth. **A272**, 364, (1988).
3. Kwang-Je Kim, Phys. Rev. Lett. **57**, 1871, (1986).
4. J. C. Goldstein, B. D. McVey and C. J. Elliott, Nucl. Instrum. & Meth. **A272**, 177, (1988).
5. R. Bonifacio, L. Narducci and C. Pellegrini, Optics Comm. **50**, 373 (1984).
6. J. Murphy, C. Pellegrini and R. Bonifacio, Optics Comm. **53**, 197 (1985).
7. P. B. Wilson and J. Griffin, *High Energy Electron Linacs; Applications to Storage Rings RF system and Linear Colliders*, Phys. of High Energy Particles Accelerators, R. A. Carrigan, F. R. Huson and M. Month Eds., AIP Conference Proc. **87**, 450 (1982).
8. W. B. Colson and I. Boscolo, Phys. Rev. **A31**, 2353 (1985).
9. A. S. Artamanov et al., Nucl. Instrum. & Meth. **177**, 247 (1980).
10. Li-Hua Yu and S. Krinsky, Phys. Rev. **A35**, 3406 (1987).

Figure 1: Laser power vs.  $z/L$  from the simulations for both standard undulator and optical klystron.  $\sigma_E = 0.0$  (solid);  $\sigma_E = 0.1\%$  (dash) and  $\sigma_E = 0.2\%$  (circle)

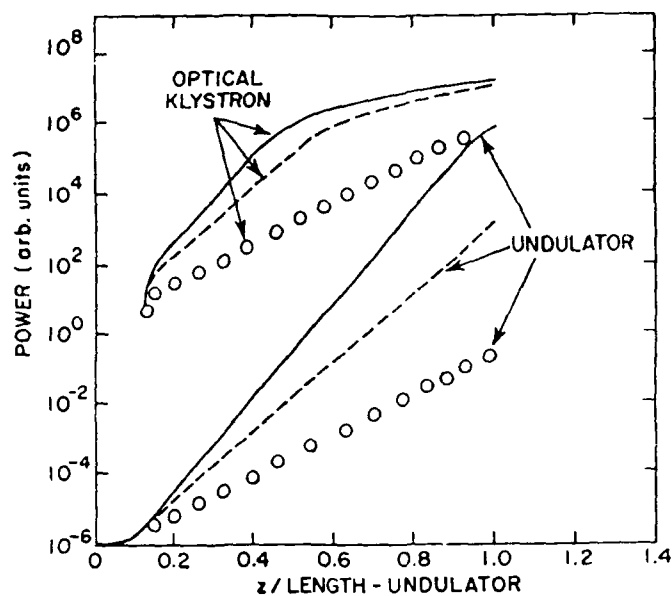


Table 1: Electron and undulator parameters used in the simulations

Parameters	
wavelength (nm)	2.5
energy (GeV)	1.02
$\rho \times 10^3$	1.2
L (m)	8.1
undulator period (cm)	1.0
gain length $L_G$ (m)	0.75
peak current (A)	400
normalized emittance (mm-mrad)	1.0
external focusing $\beta^*$ (m)	1.0

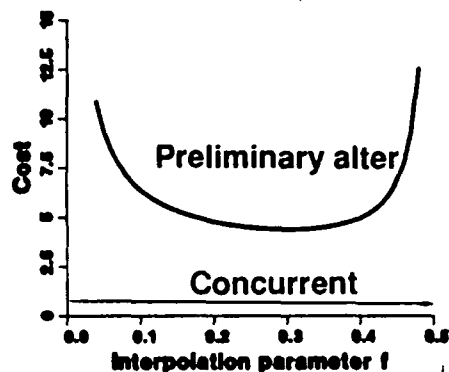
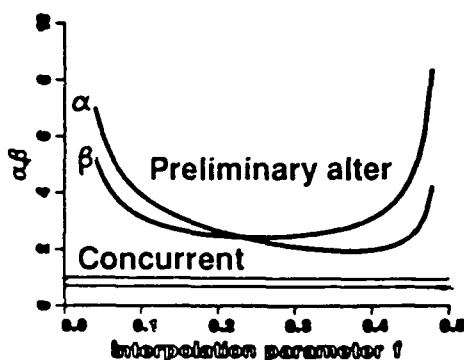
**P1.26**

## **ANALYTICAL TREATMENT OF ELECTRON TRAJECTORY STRAIGHTNER ISSUES IN FREE-ELECTRON LASERS**

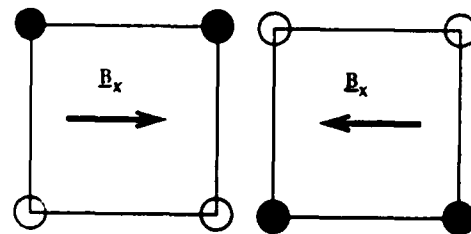
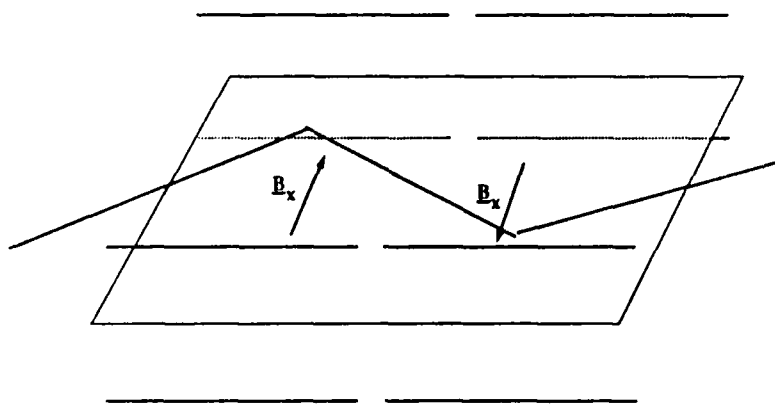
**C. J. ELLIOTT, Los Alamos Nat'l Laboratory, NM**  
**and**  
**D. C. Quimby, Spectra Technology, Inc., Bellevue, WA**

### **WE HAD A PROBLEM**

**ANALYSIS SHOWED THAT THE ALTERNATING  
SCHEME  
HAD MUCH TOO HIGH EFFECTIVE ERRORS**



### **MAGNETIC FIELD GEOMETRY OF THE CORRECTING COILS**





# TREATMENT OF FIELD-ERRORS AND CORRECTION SCHEMES IS EXTENDED IN SCOPE

- HIERARCHAL TREATMENT OF THE PROBLEM ON THREE LEVELS
- INCLUDE THE MAGNETIC FIELD ERRORS
- OBTAIN A BIVARIATE NORMAL DISTRIBUTION DESCRIPTION
- EXTEND THE INTERPOLATION SCHEME TO INCLUDE NON-LOCAL SYSTEMS
- EFFECTIVE FIELD ERROR LEVEL AND EFFECTIVE BPM PRECISION DESCRIBE THE PROBLEM

# COST FUNCTIONS MINIMIZED IN S

$$C_{min} = \frac{3}{2} [2\alpha_f \beta_f^2]^{1/3} \{ < \delta x^2 > [(\sigma_\theta^2)^{1/2}]^{1/3}$$

Preliminary concurrent\*

$$\alpha_f = 1/2$$

$$\beta_f = 1/3$$

Preliminary alternating\*

$$\alpha_f = 2.3$$

$$\beta_f = 2.3$$

Revised alternating\*

$$\alpha_f = 1/4$$

$$\beta_f = 17/48$$

\* Calculations are preliminary

# BEFORE BOOKKEEPING WAS HARD NOW IT IS EASY

BUT THE END RESULT OF THE MESS IS SIMPLE

THE DETAILS OF THE MOTION OVER A MICROSCOPIC INTERVAL ARE MESSY

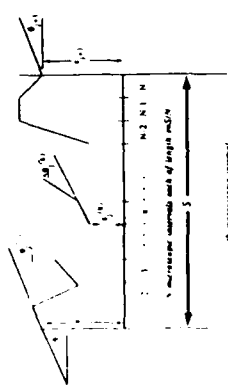
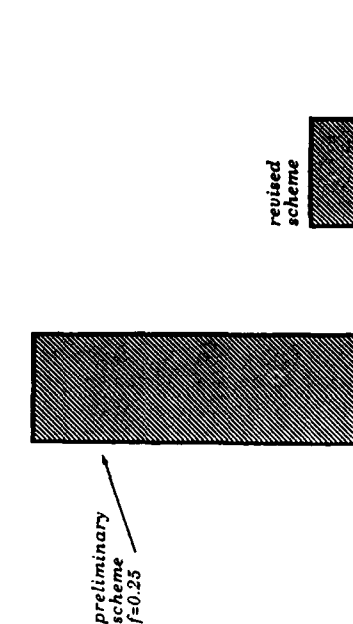


Fig. 1. The surface between the microscopic and macroscopic variables. The trajectory is an arc segment  $y_i$  and angle  $\theta_i$  and time  $t_i$  and  $y_{i+1}$  and  $\theta_{i+1}$ . The shaded region represents the number of the microscopic interval. The segment is at the beginning of the  $i$ -th microscopic interval  $y_i^{(1)}$  and the angle is  $\theta_i^{(1)}$ . The number will increase the angle in the interval  $\Delta\theta_i^{(1)}$ , which is applied at the end of that interval.

# COST FUNCTION COMPARISON FOR ALTERNATING SCHEMES



The revised scheme provides a substantial reduction of the angular variance

# $\Delta X_j$ AND $\Delta\theta_j$ FOLLOW A BIVARIATE NORMAL DISTRIBUTION

# A PROPOSED FEL INJECTOR AT IAE

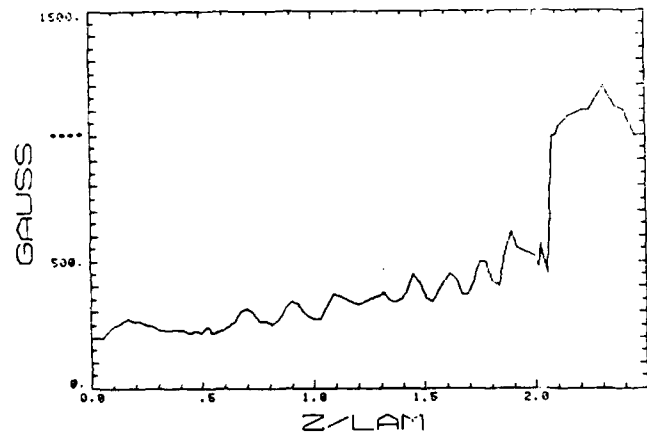
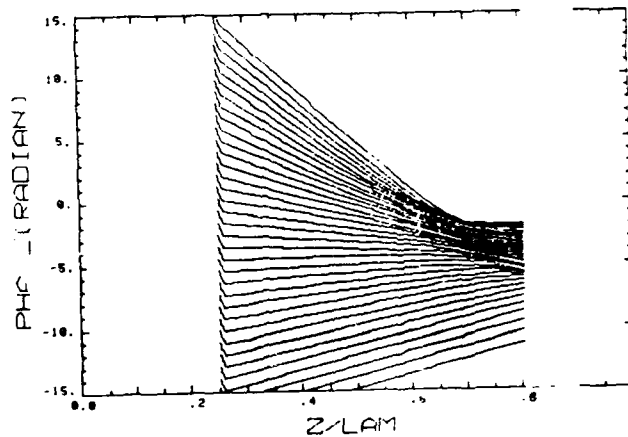
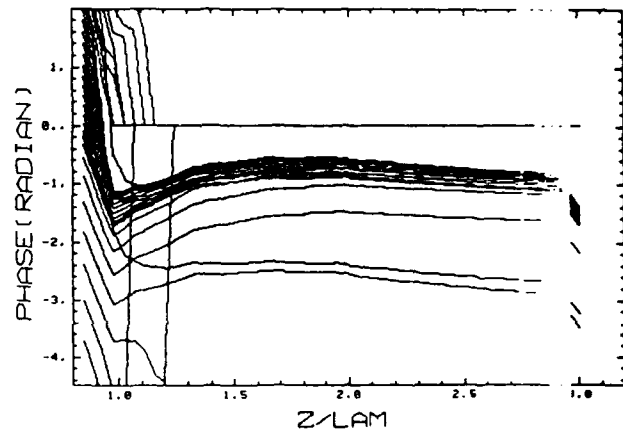
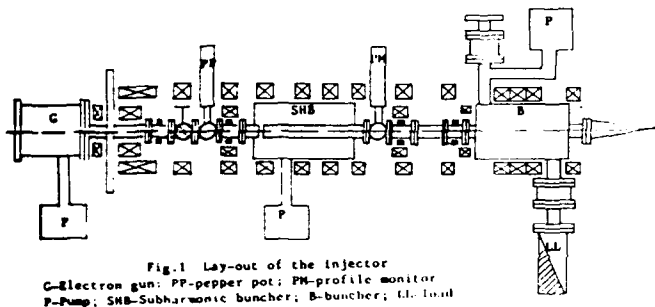
X. Zhai, W. Zhou, Z. Weng, T. Wu, C. Liu, Y. Lu, X. Shi, T. Yang.

Institute of Atomic Energy, P.O.Box 275(17)

Beijing 102413, China

## Abstract

For the purpose of scientific research, a L-band FEL injector at Institute of Atomic Energy (IAE) was proposed years ago and approved recently. It consists of a thermionic electron gun, a subharmonic buncher (108MHz), a fundamental buncher (1300 MHz), one accelerating section and diagnostic devices. The electron energy is about 20MeV, micropulse current is greater than 50A, macropulse length is 10-20ps. Now this project is in progress.



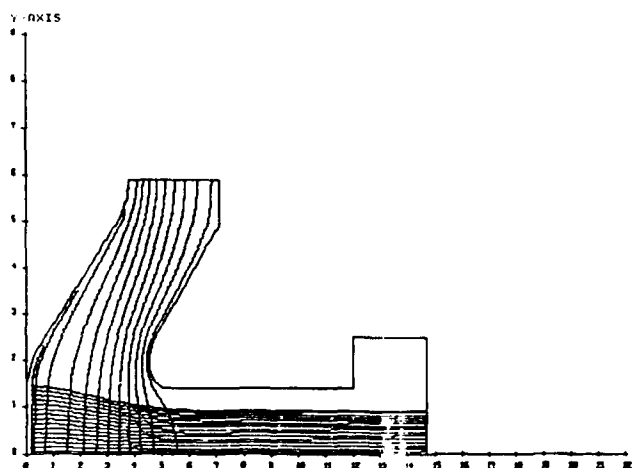


Fig. 5 Electron trajectories in the electron gun

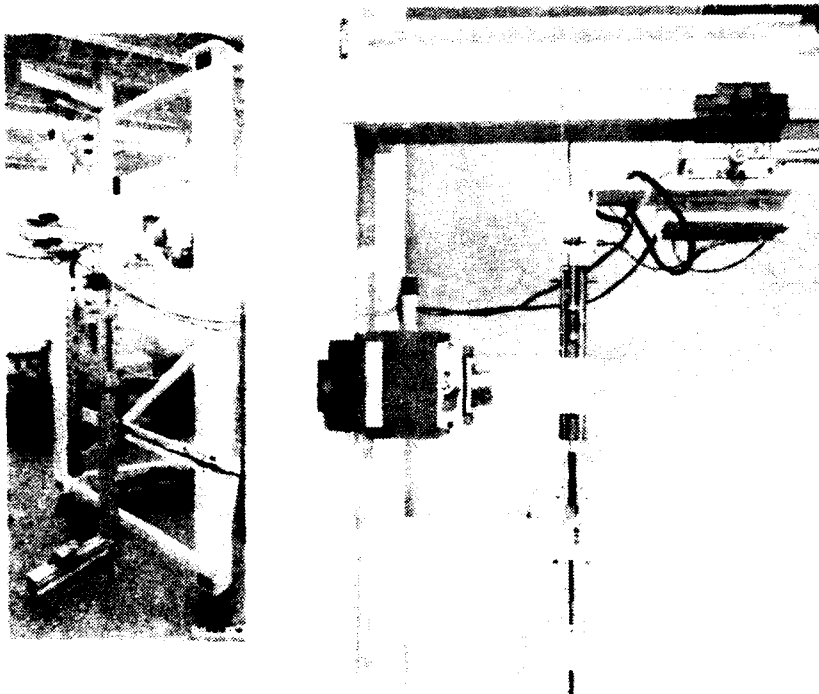
#### References

- 1, J. Adamski et al, Nucl. Instrum. & Metho.  
in Phys. Res. A 259(1987), P.49-55
- 2, D.W. Feldman et al, Proceedings of the  
Beijing FEL Seminar, Beijing University  
11-23 Aug. 1988 P.66
- 3, J.M. Watson, Nucl. Instrum. & Metho. in  
Phys. Res. A 250(1986), P.1-3

## PI.32 FULLY AUTOMATIC WIGGLER-FIELD TEST AND CORRECTION

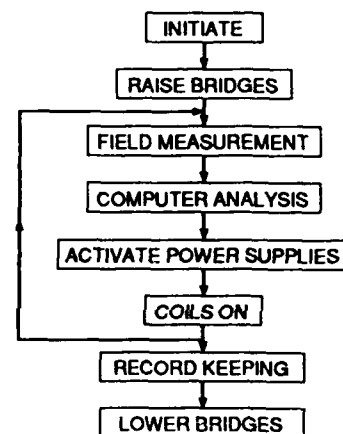
R. B. Feldman and R. W. Warren  
Los Alamos National Laboratory  
Los Alamos, NM 87545

The pulsed-wire field measuring technique has been integrated with a series of field-correcting dipole coils using computer control. The combined system performs a rapid, on-line, measurement of field errors in FEL wiggler magnets and their automatic correction.



Vertically-mounted wiggler with sensors, wire, bridges, and correcting coils.

### AUTOMATIC MEASUREMENT CORRECTION SYSTEM



### ON-LINE USE

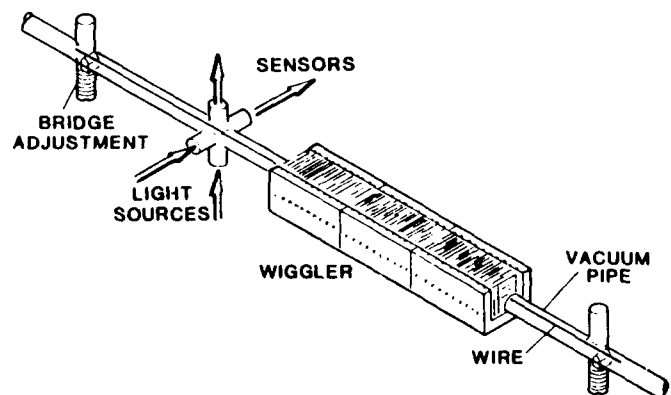
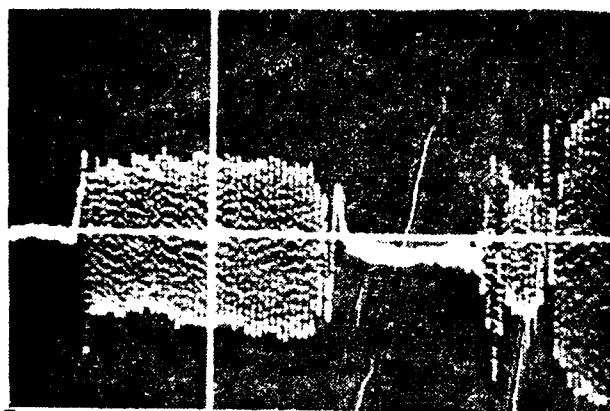
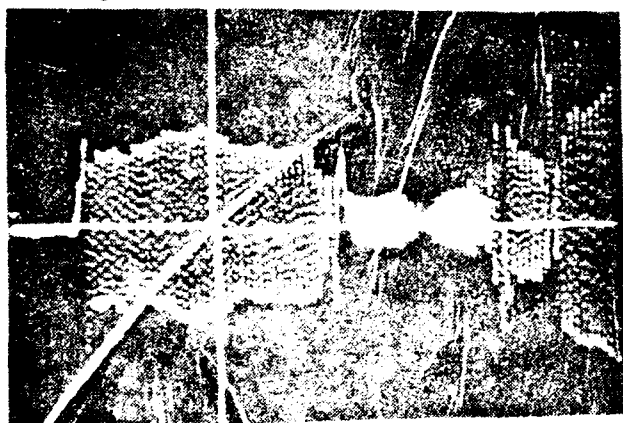


Diagram of on-line system showing the wiggler, sensors, wire, and bridges.

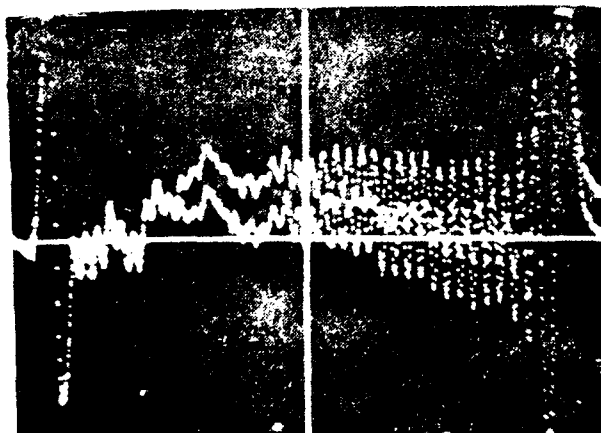




Signal from sensor, showing on the left, the field integral, and on the right, various reflections from the bridges.

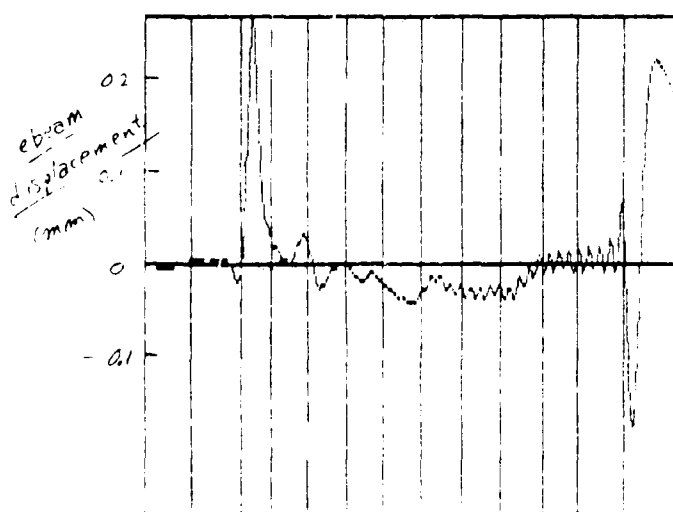
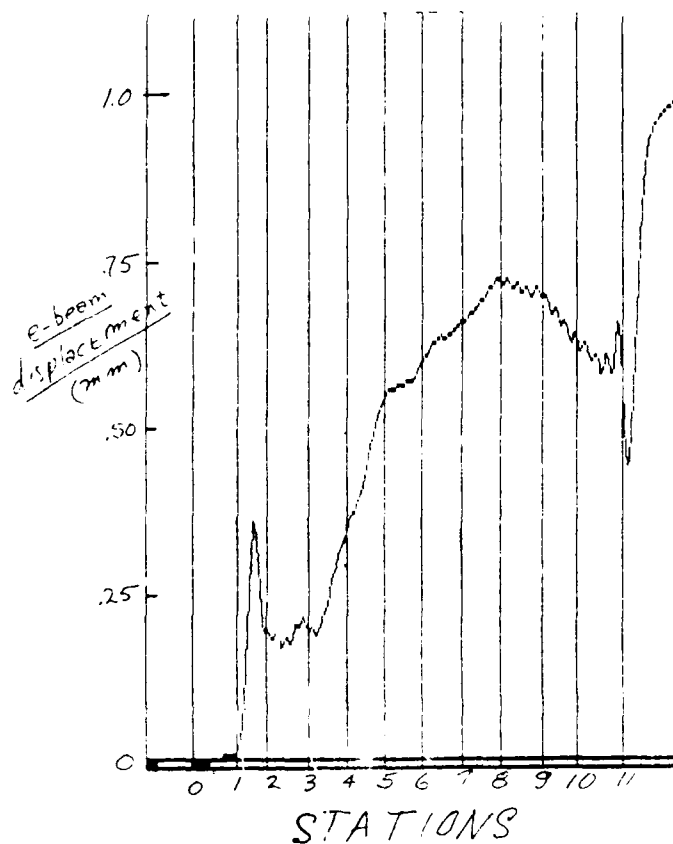


Signal from sensor when wire current is too large, generating large nonlinear signals



Expanded view of field integral where most of the high-frequency wiggles have been suppressed by employing a  $1 \lambda$  pulse. One curve has been displaced by activating a correcting coil.

Integral of signal showing displacement of e-beam in uncorrected wiggler.



Integral of signal showing displacement for corrected wiggler.

# PI.33

## TIME DEPENDENT MEASUREMENTS ON THE STANFORD SCA/FEL

J. C. Frisch

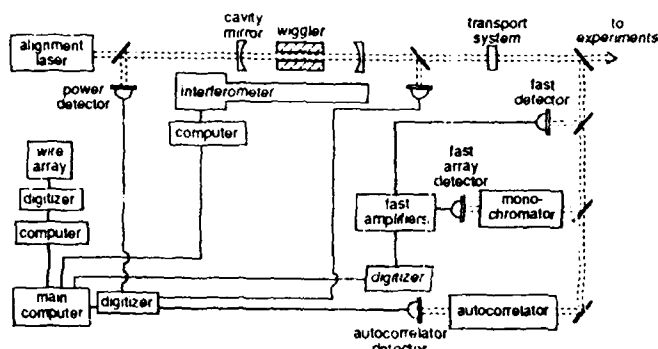
High Energy Physics Laboratory, Stanford University, Stanford, CA 94305-4085

and

J. E. Edighoffer

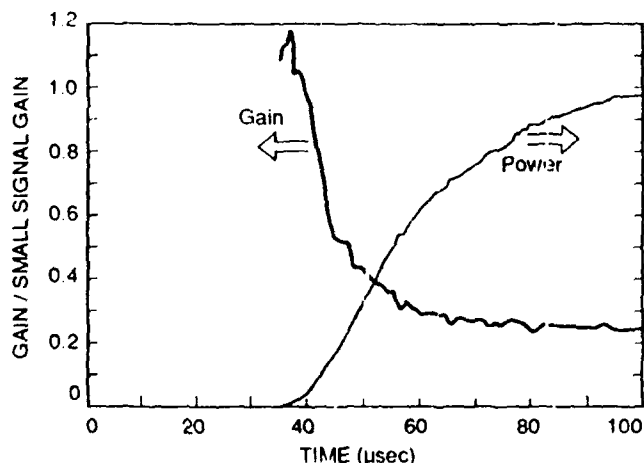
TRW, One Space Park, Redondo Beach, California 90278 U.S.A.

A new diagnostic system has made it possible to measure the time development of the optical electron beam spectra within a single macropulse. This system has allowed the measurement of several FEL effects, including the wavelength shift during laser startup, and the development of sidebands during high gain operation.



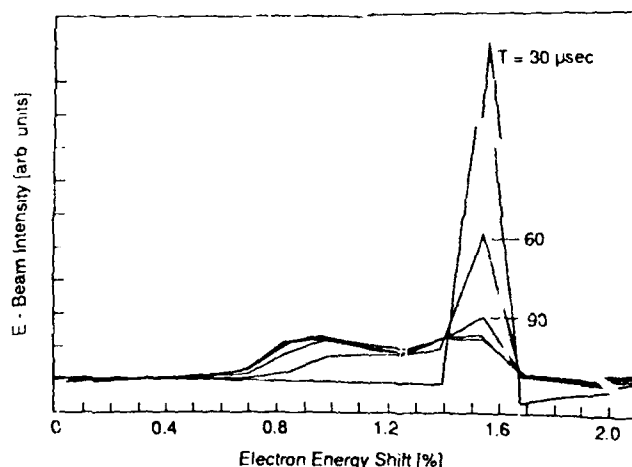
OPTICAL POWER AND GAIN DURING STARTUP

for 1.5  $\mu\text{m}$  Operation

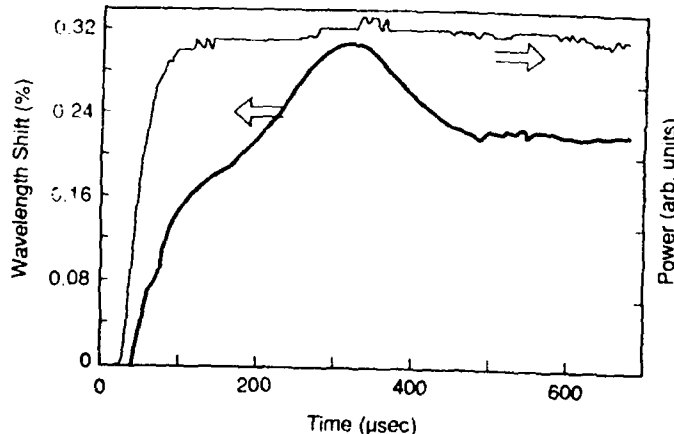


ELECTRON BEAM SPECTRA DURING STARTUP

Spectra Shown Every 30  $\mu\text{sec}$

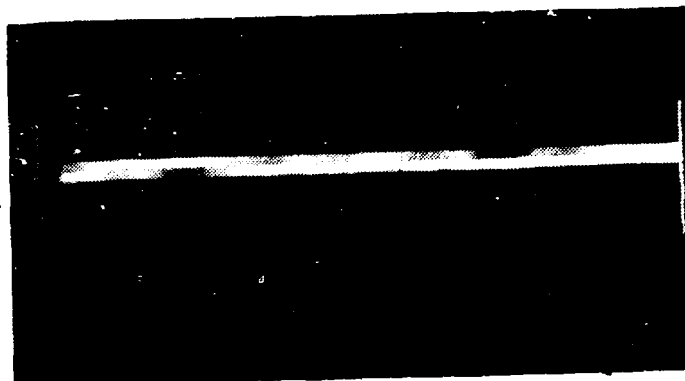
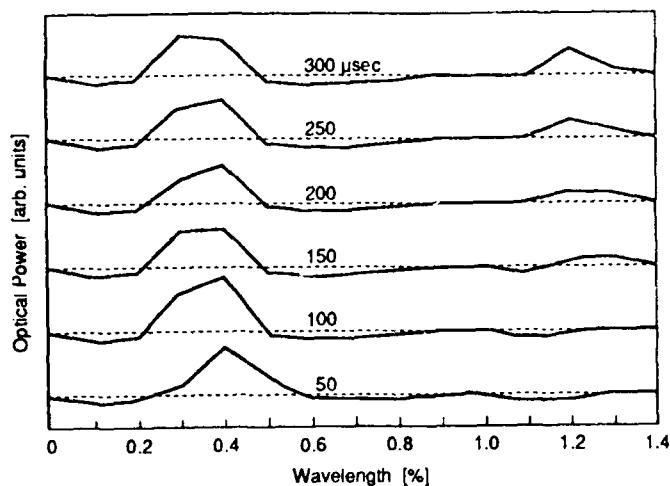


CENTER WAVELENGTH SHIFT DURING STARTUP



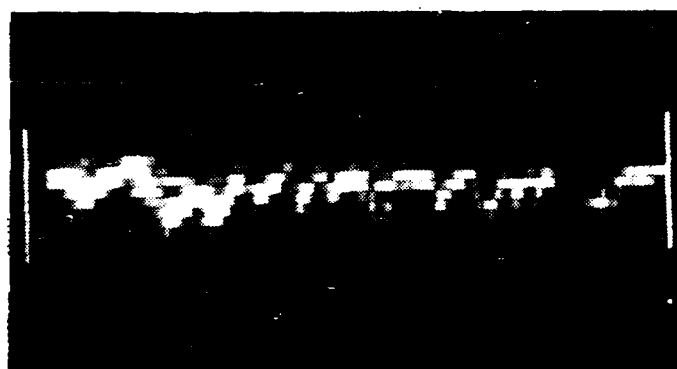
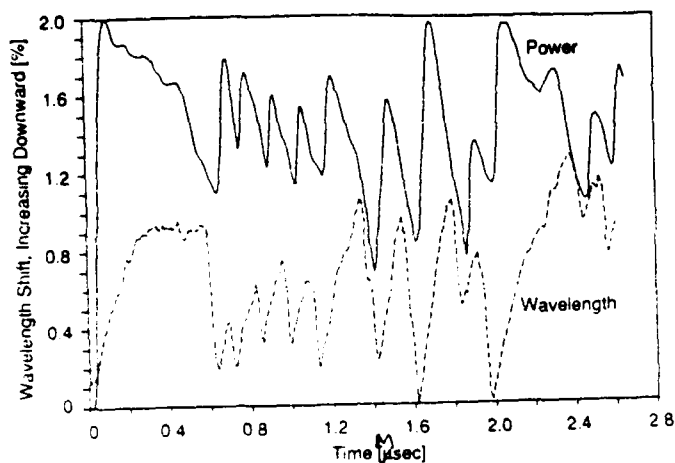
Works supported by ONR N00014-86-K-0118.

# **DEVELOPMENT OF SINGLE SIDEBAND** Pulses Shown Every 50 $\mu$ sec



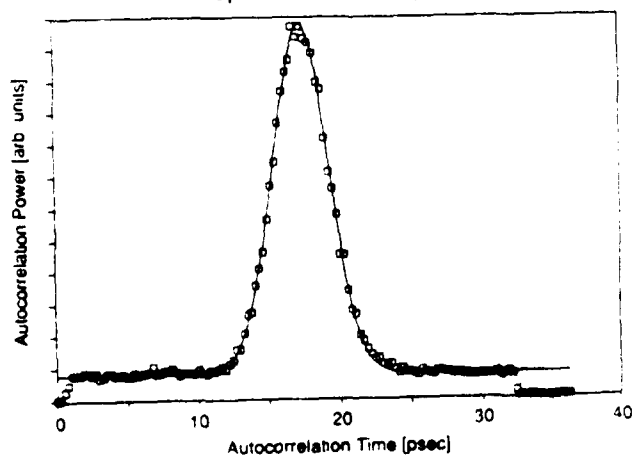
Time dependent spectrum of a stable macropulse.  
Time plotted horizontally 0-3 msec.  
Wavelength increasing downward, 0.1%/div.

## **POSSIBLE LIMIT CYCLE BEHAVIOR**



Time dependent spectrum  
of an unstable macropulse.

## **AUTOCORRELATION SIGNAL** Optical FWHM = 3.21 psec



# STABILITY REQUIREMENTS FOR RF LINAC-DRIVEN FREE-ELECTRON LASERS\*

William E. Stein, W. Joel D. Johnson, John F. Power, and Thomas J. Russell\*\*

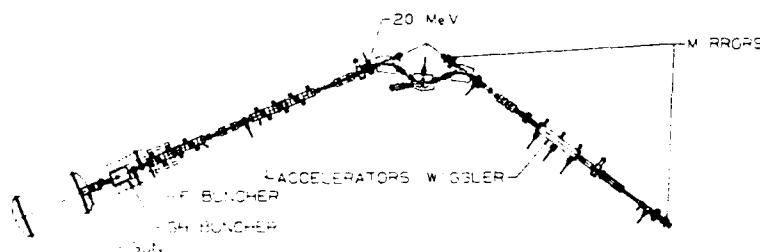
Los Alamos National Laboratory, MS J579  
Los Alamos, NM 87545  
505/667-1984

## ABSTRACT

The performance of free-electron lasers driven by an electron beam from a rf linac is strongly dependent on the stability of the electron energy, the charge per micropulse, and the time interval between micropulses. Effects of beam instabilities on lasing and the improvements made at the LANL and Boeing FELs are presented.

\* Work supported and funded by the US Department of Defense, Army Strategic Defense Command, under the auspices of the US Department of Energy.

\*\* Boeing Physical Science Research Center



LOS ALAMOS 10-MICRON FEL

Fig. 1. Configuration of the LANL FEL.

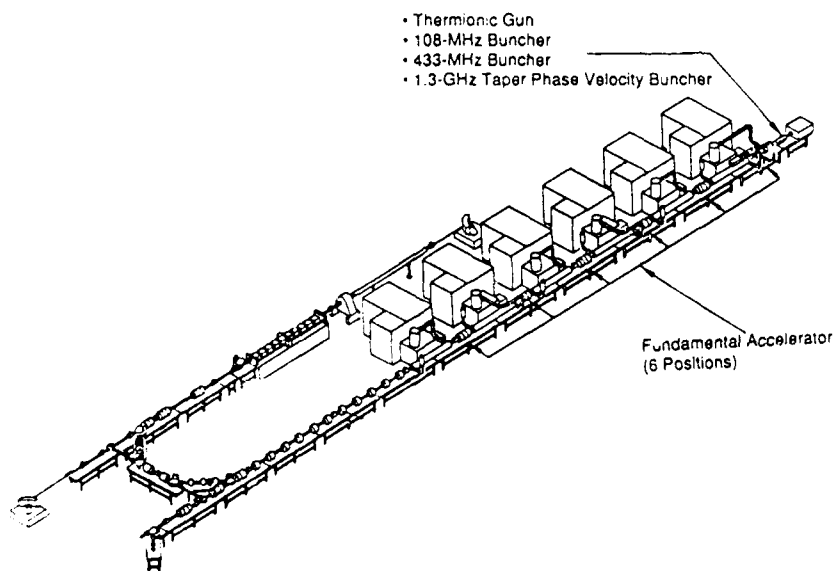


Fig. 2. Arrangement of the BPSRC FEL.

# SENSITIVITY OF LASING TO VARIATIONS IN RF PHASE AND AMPLITUDE IN THE LANL FEL

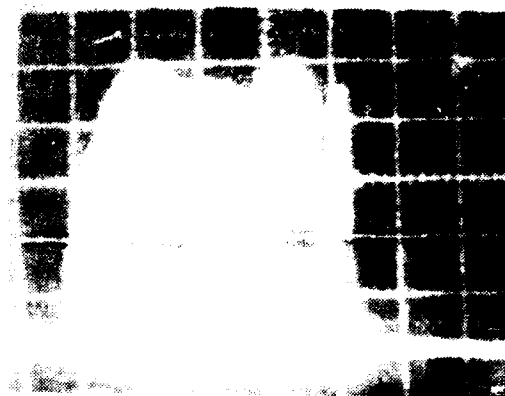
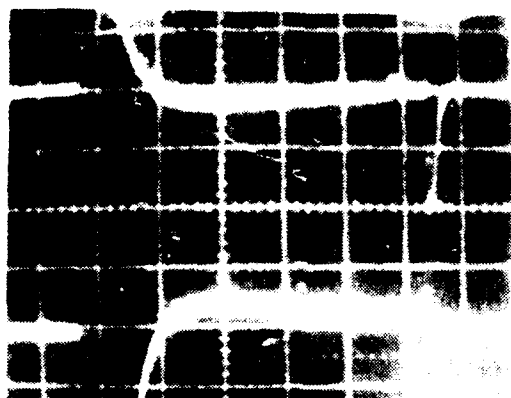


Fig. 4a. 0.5 and 1.3 degree rf phase shifts cause 20% and 40% change in laser power.

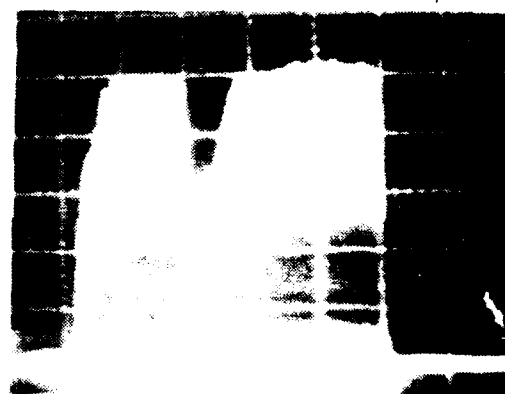
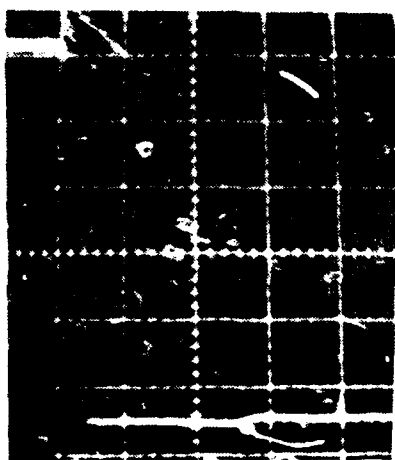


Fig. 4b. 0.6% change in electron energy causes 70% decrease in laser power.

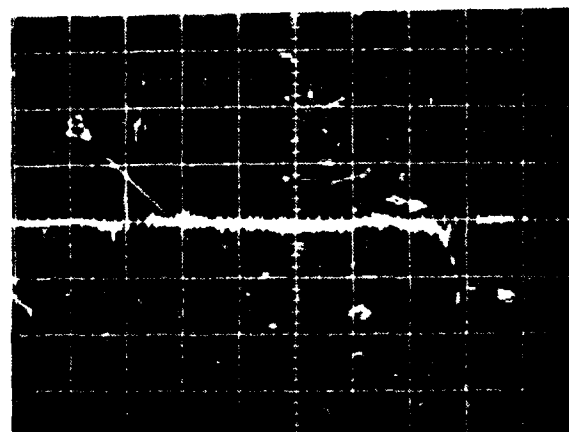
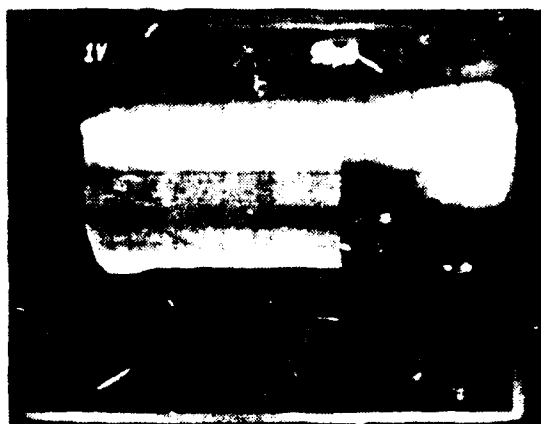


Fig. 5. BPSRC gun pulse. 1.25 nC per vertical division.

Fig. 6. BPSRC klystron rf phase. One degree per vertical division

A.A.Varfolomeev, Yu.Yu.Lachin  
Kurchatov Inst.of Atomic Energy  
Moscow, USSR

Abstract

FEL designs with the electron beam travelling through the undulator not along, but at some angle with respect to the laser beam have been analyzed. A general expression for small-signal gain is obtained. The noncollinear schemes can in some cases be preferable. They provide tunable laser operation, make two laser beams noncollinear interaction with electron beam possible within the same undulator, increase the acceleration rate and the upper limit of particle energies.

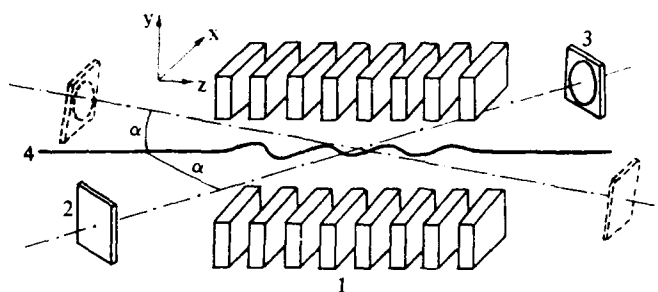


Fig.1 Noncollinear beam geometry in FEL:  
1 -undulator, 2,3-cavity mirrors, 4 -  
electron beam

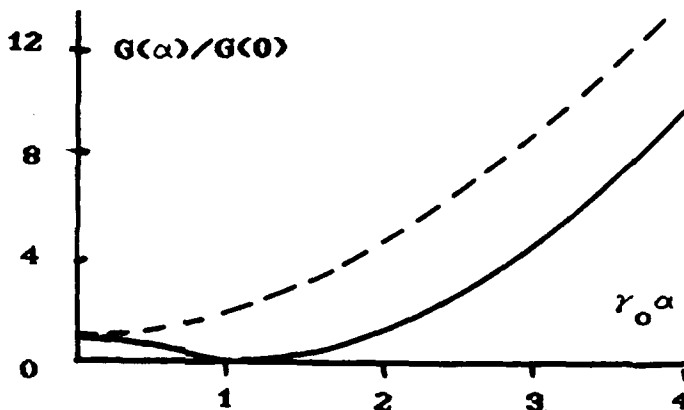


Fig.2 Gain enhancement in FEL with  
noncollinearity for different  
polarizations.

$$G_{\perp} = 4\pi^2 \frac{(N\lambda_w)^3}{r^5 \lambda_a} \frac{1K_w^2}{1_a S} \left( 1 + \frac{K_w^2}{2} + \alpha^2 \gamma_o^2 \right) f(\mu_o)$$

$$G_{\parallel} = 4\pi^2 \frac{(N\lambda_w)^3}{r^5 \lambda_a} \frac{1K_w^2}{1_a S} \left( 1 + \frac{K_w^2}{2} + \alpha^2 \gamma_o^2 \right) \left( \frac{1 + K_w^2/2 - \alpha^2 \gamma_o^2}{1 + K_w^2/2 + \alpha^2 \gamma_o^2} \right)^2 f(\mu_o)$$

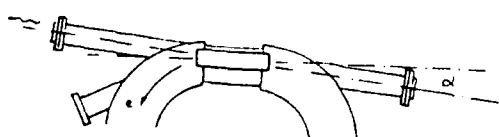


Fig.3 Noncollinear storage ring FEL  
scheme.

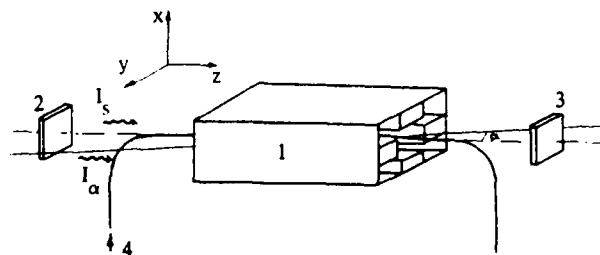


Fig.4 Harmonic generation with two-  
dimensional undulator: 1 - undulator,  
2,3 - mirrors, 4 - electron beam.

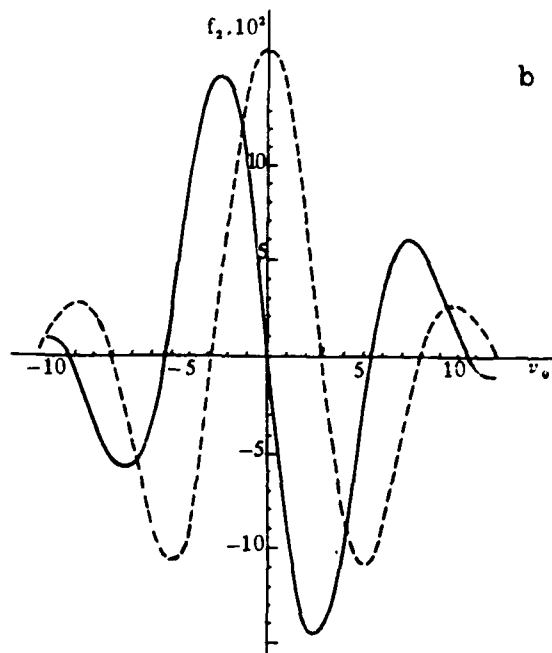
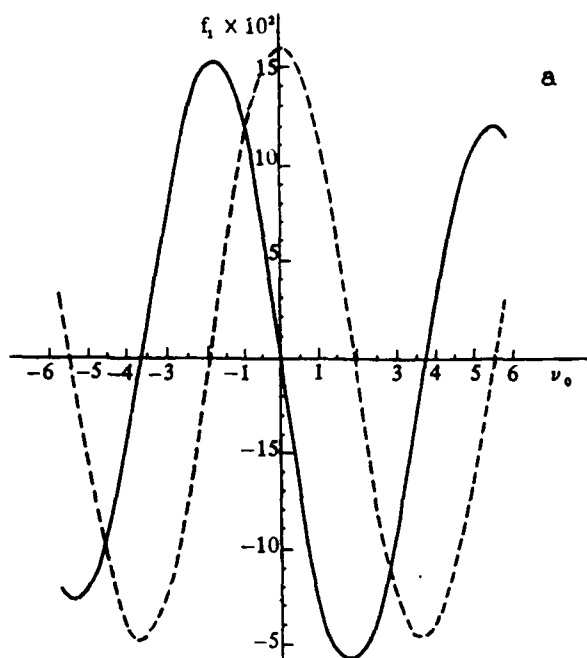


Fig.5 Second harmonic gain function  
(a)  $\mu_0=0$ ; (b)  $\mu_0=\nu_0/2$  for  $\phi = 0$  (solid curve) and  $\phi = \pi/4$  (dashed).  
 $\mu_0, \nu_0$ -detunings.

Second harmonic gain enhancement

$$\kappa = 2\pi^2 I_\alpha \lambda_s N^2 / \sqrt{I_s W_0}$$

$$W_0 = 1.38 \cdot 10^{10} \text{ W}$$

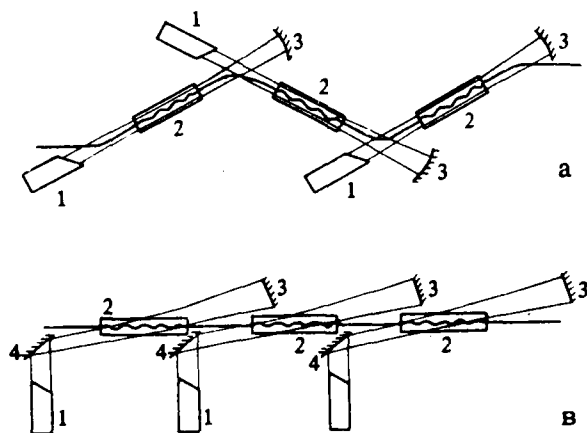


Fig.6 Collinear (a) and noncollinear (b) inverse FEL schemes. 1 - lasers, 2 - undulators, 3, 4 - cavity mirrors.

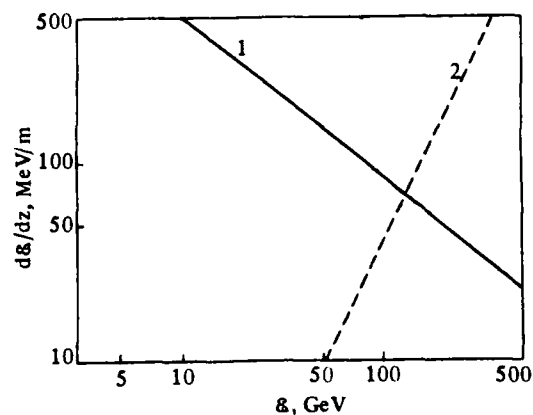


Fig.7 Maximum acceleration rate in collinear IFEL for the field  $10^{11}$  V/m and  $\lambda_\alpha = 1\mu$  (solid curve) and synchrotron radiation energy losses per unit length in bending magnet field 5 Tesla (dashed)

## PI.36

### DEVELOPMENT OF A HYBRID PERMANENT MAGNET UNDULATOR PROTOTYPE FOR FREE ELECTRON LASERS

F. Rosatelli, L. Barbagelata, A. Matrone, G. Ottonello, P. Prati, D. Tommasini  
ANSALDO RICERCHE - Corso Perrone 25, 16152 Genova (Italy)

F. Ciocci, A. Renieri, E. Sabia  
ENEA, Dip. TIB, U.S. Fisica Applicata, P.O. Box 65, 00044 Frascati (Italy)

#### Abstract

A hybrid permanent magnet undulator is under development in ANSALDO RICERCHE for the LISA FEL experiment.

The criteria adopted to optimize the magnetic and mechanical design of the undulator and the results of field measurements on an eight period prototype will be discussed.

The device used for measuring the permanent magnet blocks and the code developed for their sorting will be described.

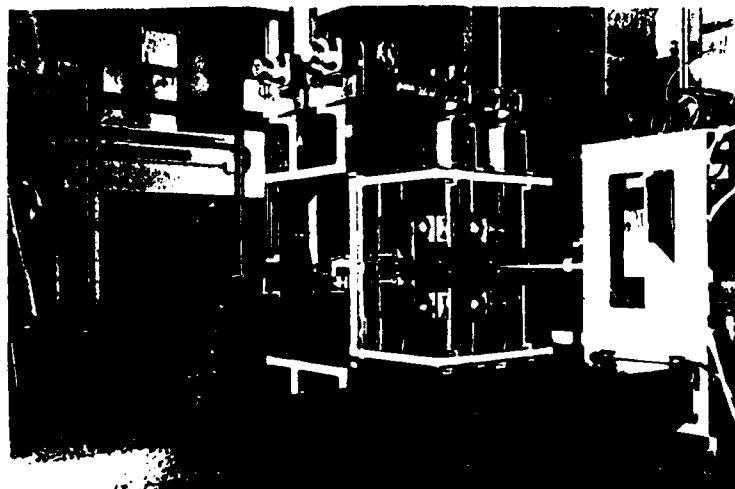


Fig. 1 : Eight period model of hybrid permanent magnet undulator.

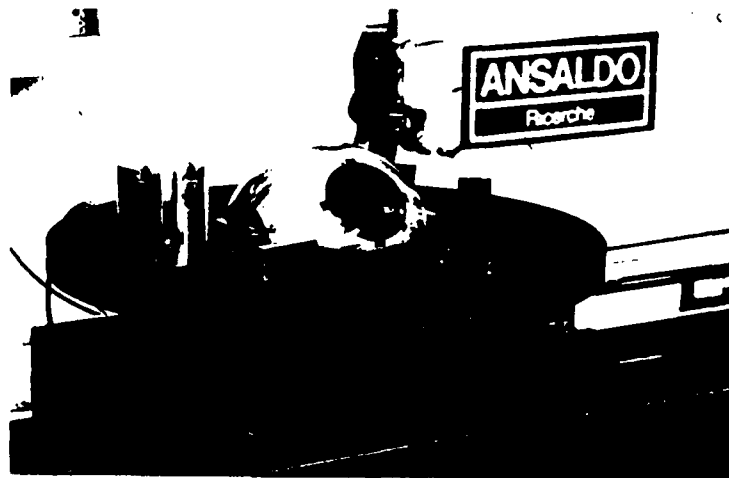


Fig. 3 : Equipment for measuring permanent magnet blocks.



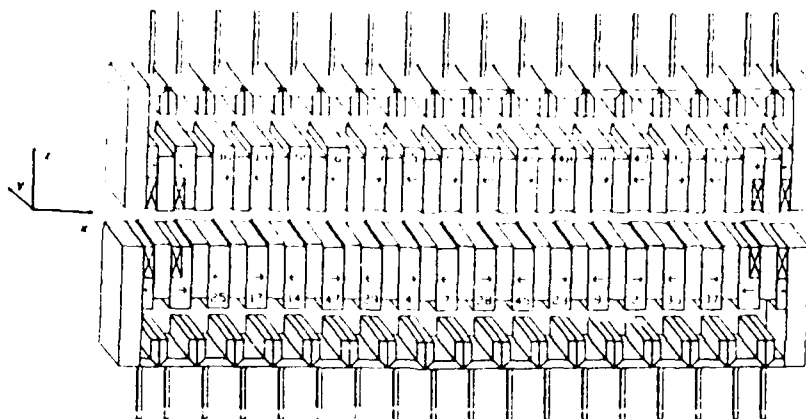


Fig. 2 - Magnetic structure of the model including tuning studs and correction coils

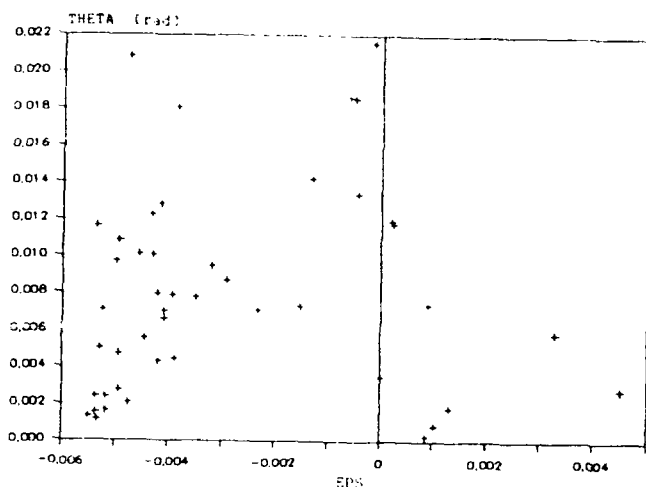


Fig. 4 - Measured permanent magnet blocks in the EPS-THETA plane. EPS = relative magnetization, THETA = angular deviation of the magnetic dipole

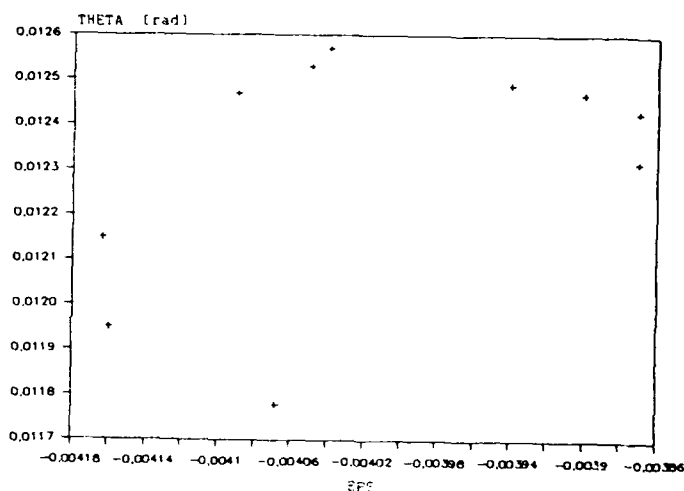


Fig. 5 - Results of 10 repeated measurements on the same permanent magnet block

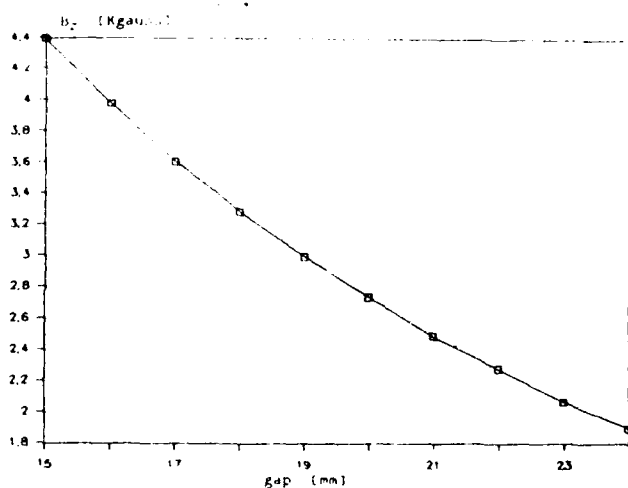


Fig. 6 - Peak magnetic field on the axis as a function of the gap

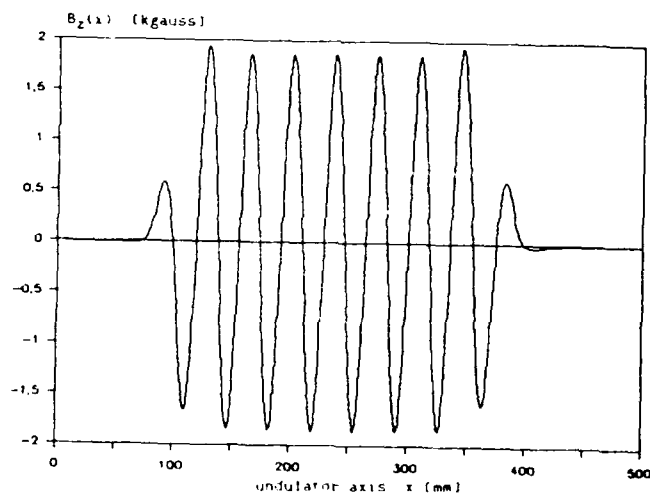


Fig. 7 - Magnetic field along the undulator axis : gap = 24 mm

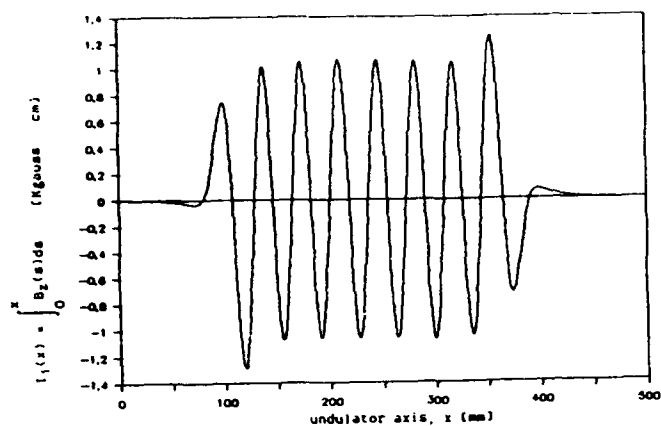


Fig. 8a : Field integral  $I_1$ ; gap=24 mm, coil left  $I_1 = 151.2$  mA, coil right  $I_1 = 77.8$  mA

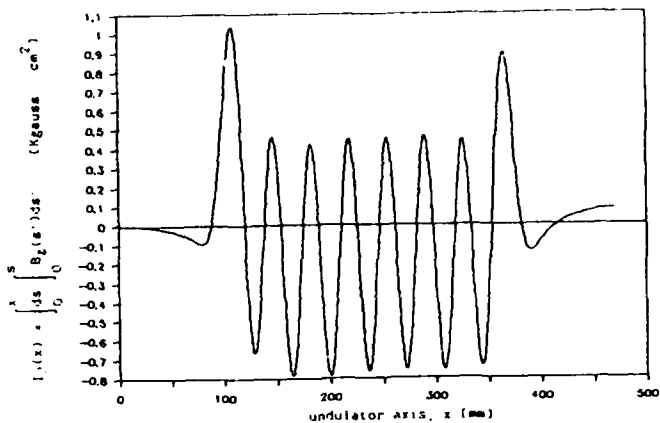


Fig. 8b : Field integral  $I_2$ ; gap=24 mm, coil left  $I_1 = 151.2$  mA, coil right  $I_1 = 77.8$  mA

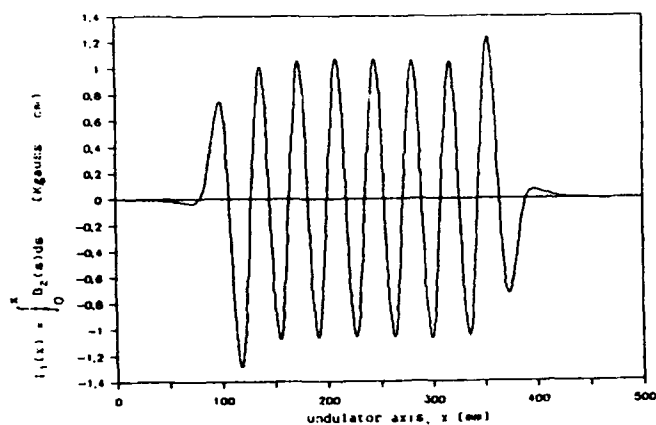


Fig. 9a : Field integral  $I_1$ ; gap=24 mm, coil left  $I_1 = 151.5$  mA, coil right  $I_1 = 77.9$  mA

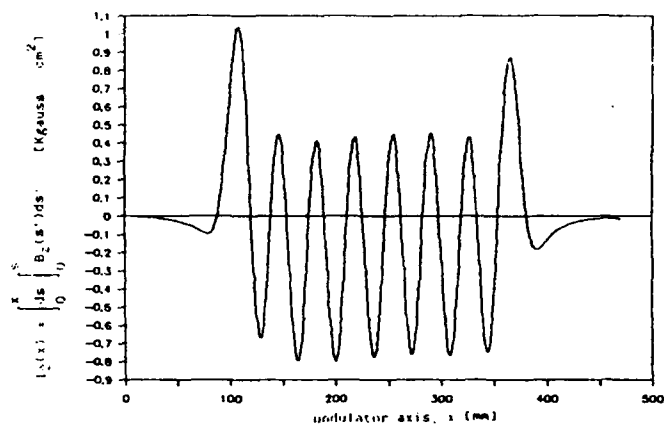


Fig. 9b : Field integral  $I_2$ ; gap=24 mm, coil left  $I_1 = 151.5$  mA, coil right  $I_1 = 77.9$  mA

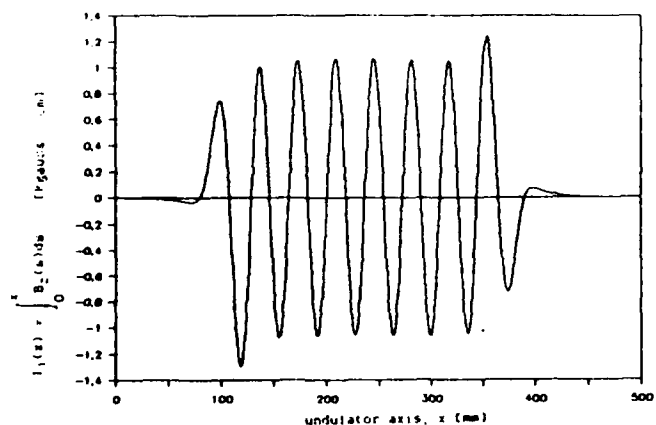


Fig. 10a : Field integral  $I_1$ ; gap=24 mm, coil left  $I_1 = 151.5$  mA, coil right  $I_1 = 68$  mA

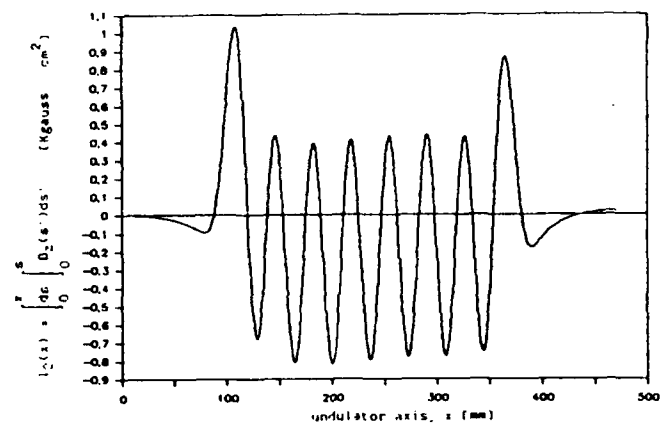


Fig. 10b : Field integral  $I_2$ ; gap=24 mm, coil left  $I_1 = 151.5$  mA, coil right  $I_1 = 68$  mA

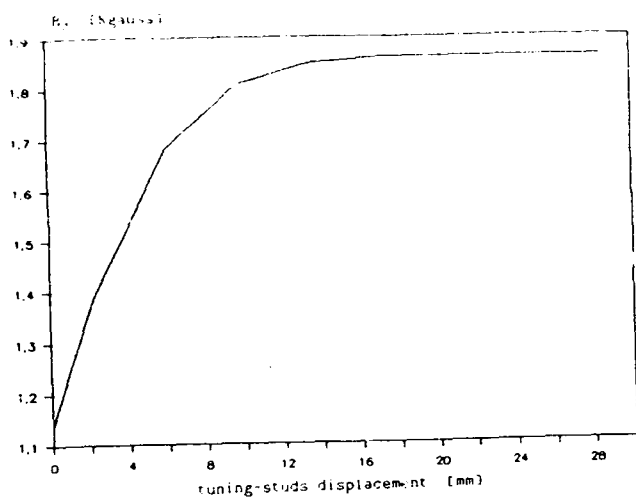


Fig. 11 - Magnetic field versus tuning-studs position; gap = 24 mm

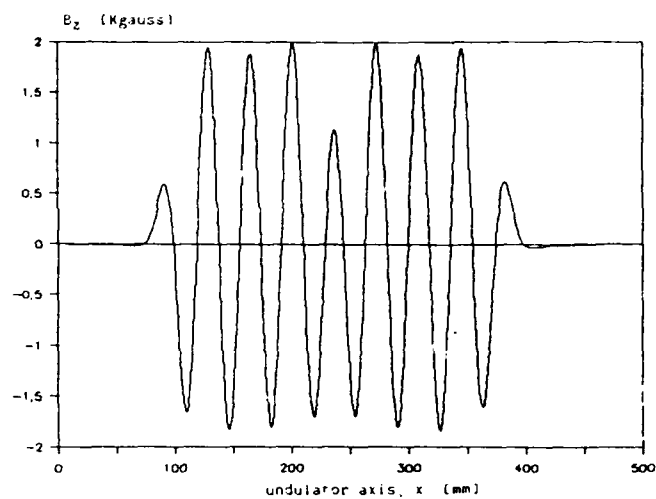


Fig. 12 - Maximum reduction of the magnetic field near a pole using tuning-studs; gap = 24 mm

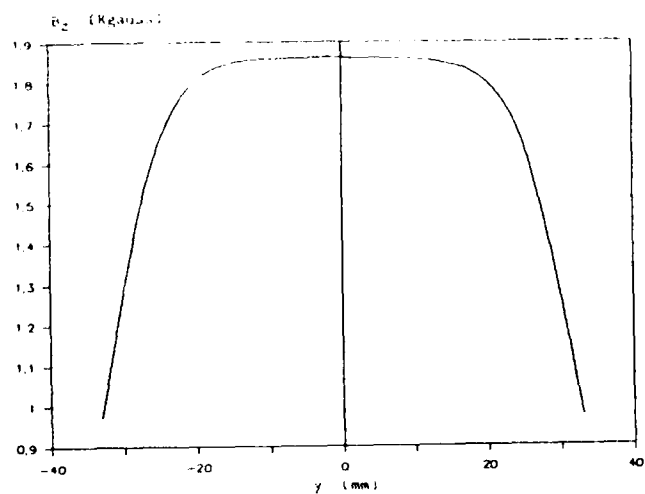


Fig. 13 - Magnetic field versus  $y$  at the undulator center; gap = 24 mm

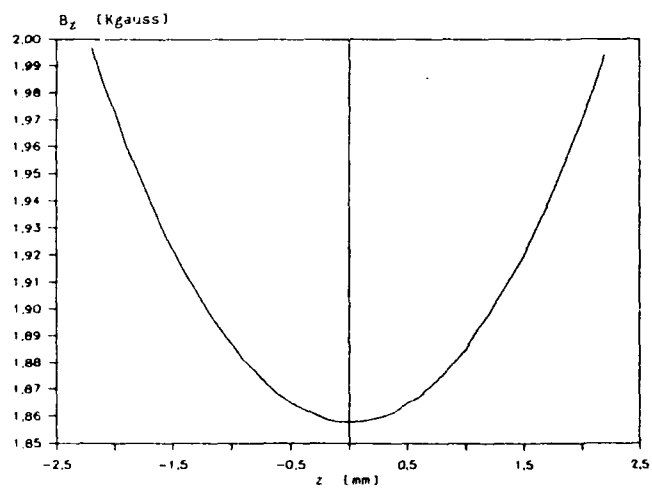


Fig. 14 - Magnetic field versus  $z$  at the undulator center; gap = 24 mm

**TUESDAY, AUGUST 29**

# EXI.1 Free Electron Laser Oscillation on the Super-ACO storage Ring at Orsay

M.E. Couprie\*, M. Billardon\*\*, M. Velghe\*\*\*, C. Bazin, J.M. Ortéga\*, R. Prazeres and Y. Petroff  
(LURE CNRS/CEA/MEN Univ. de Paris-Sud 91405 cedex Orsay FRANCE)

- \* CEA, IRF, DPhG, SPAS, 91191 cedex Gif-sur-Yvette
- \*\* ESPCI, 10 rue Vauquelin 75231 Paris cedex
- \*\*\* LPPM Univ. de Paris-Sud 91405 cedex Orsay

## ABSTRACT

The Free Electron Laser oscillation was obtained in February 1989 in the visible at Orsay. For such experiments, the Super-ACO Storage Ring is operated at 600 MeV with two opposite bunches, using the "low emittance" optics. It provides a gain of 2%. The general features of the laser are described.

## FREE ELECTRON LASER OSCILLATION ON THE SUPER-ACO STORAGE RING AT ORSAY

LURE CNRS/CEA/MEN  
Université de Paris-Sud  
91 405 cedex Orsay France

## PLAN

### I - Characteristics of the experiment

- 1) the storage ring
- 2) the optical klystron
- 3) the optical cavity

### II - Gain optimization

### III - The FEL features

- 1) spectral characteristics
- 2) temporal structure
- 3) laser modes
- 4) laser power

### conclusion

## OPTICAL CAVITY

- 1) Synchronism between the positrons and the light pulses  
cavity length = 18 m

- 2) Transverse overlap between the light and positron pulses

minimization of the transverse sizes of the optical modes along the optical klystron : "filling factor"

$R_c = 10$  m  $Z_c = 3$  m  
for the TEM<sub>00</sub> mode  
chromatic cond = 0.82 mm chromaticity = 2.4 mm at 630nm

### 3) Dielectric multilayers mirrors

Choices: material, top layer, substrate, deposition technology

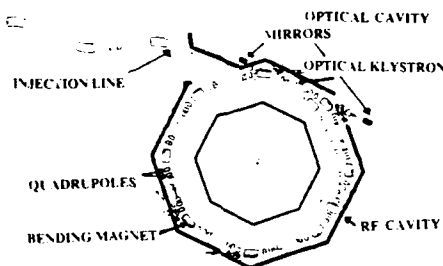
### 4) Mirror degradation

photons of the higher harmonics :  $\lambda_c \propto 1/\gamma E^2 \lambda$

Total emitted power :  $P \propto E^2 K^2$

E (MeV)	K	P.W. (100mA)	$\lambda_c$
800	5.75	25	60
600	4	9.4	120
400	3	2	240

## THE SUPER-ACO STORAGE RING



## CHARACTERISTICS OF SUPER-ACO AT 800 MeV (experimental)

number of bunches : 1-24 2 for the FEL  
current per bunch : 100 mA  
energy spread :  $5.3 \cdot 10^{-4}$   
Emittance: horizontal  $4 \cdot 10^{-8}$  m rad  
vertical  $2 \cdot 10^{-8}$  m rad  
Beam sizes: length 40 ps  
experimental threshold of anomalous bunch lengthening: 7mA  
horizontal 255  $\mu$ m vertical 125  $\mu$ m  
Energy range : 550 - 800 MeV  
RF frequency 100 MHz voltage : 150 MHz

## CHARACTERISTICS OF THE OPTICAL KLYSTRON DOMINO

**Magnet characteristics**  
dimensions :  $32 \times 32 \times 50$  mm<sup>3</sup>  
material : SmCo<sub>5</sub>  
manufacturer : UGIMAG (France)  
type : Recoma 22  
Remanent field : 0.9T

**Undulator characteristics**  
period : 12.9 cm  
number of periods : 10  
total length : 1.3m  
number of magnet layers : 1  
number of magnets/period : 16  
on-axis magnetic field : 0 - 0.48T  
K value : 0 - 5.75

**Dispersive section characteristics**  
length : 0.5m  
number of magnet layers : 2  
on-axis magnetic field : 0 - 0.5T

**Vacuum Chamber**  
inside gap : 50 mm  
outside gap : 38 mm

## CHOICE OF THE OPERATING POINT: Energy, optics...

### Energy

nominal energy 800 MeV energy range 800 - 400 MeV

### high energy

problems of mirror degradation  
thermal heating  
laser power enhanced

### low energy

less degradation  
reduced lifetime  
higher gains expected

### Desired spectral range

$K = 0 - 5.75$   
period length : 2.9cm  
 $\lambda = 633\text{nm} \Rightarrow E = 650\text{MeV}$   
choice : 800 MeV

### Gain optimization

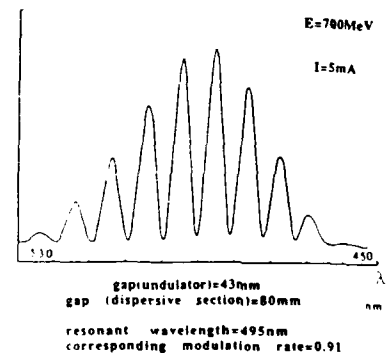
versus the current, the energy, the operating point

$$G \propto (N + N_d) \int \frac{1}{\sigma_z \sigma_r \sigma_e} \frac{1}{\gamma^3} \frac{1}{\gamma} \frac{1}{\gamma}$$

$$(N + N_d)_{\text{opt}} = \frac{1}{4\pi \sigma_r / \gamma}$$

↑ spontaneous emission spectrum  
↑ CCD camera  
↑ sampling a pick-up station signal or deduced from  $\sigma_r / \gamma$

## SPONTANEOUS EMISSION OF THE OPTICAL KLYSTRON

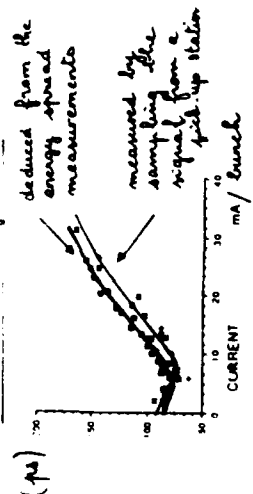


Example of spectrum  
 $\Rightarrow f(\lambda), \lambda_r, N + N_d, N$

## Energy Spread



## Bunch Length



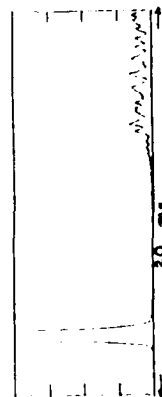
## Temporal structure

microtemporal structure :  
due to the revolution of the bunches (240 ns) inside the storage ring  
bunch length = 100 ps

"macrotemporal" structure (oscillations of relaxation)  
only with high fluctuations on the position beam or with vibrations of the mechanics of the optical cavity

Q-switched operation :  
enhancement of the peak power  
in situ measurements of the gain and optical cavity losses

laser generally "continuous"



Interpretation  
high first laser pulse starts from the non modified position  
bunch heating :  $\sigma_y/\gamma \neq 0 \Rightarrow G \neq P \Rightarrow$  the laser starts again  
stops  $\Rightarrow \sigma_y/\gamma$  relaxes with  $\tau_s \Rightarrow G = P \Rightarrow$  the laser starts again  
 $\Rightarrow$  noisy continuous regime



## FEL OPERATION

simultaneous adjustment of different parameters :

optical cavity length and RF frequency  
mirror lateral position and stored beam orbit  
undulators and dispersive section gap

laser oscillation at 630 nm, 600 and 650 MeV

during 2 hours, from 45 mA/bunch to 3 mA/bunch at 600 MeV  
during 3 hours, from 45 mA / bunch at 650 MeV  
 $\Delta E$  range > 300 Hz.

## Spectral characteristics

Spectral range: 633nm  
Tunability: at 10 mA / bunch = 390 Å  
at 600 MeV  
mirror bandwidth 350 Å at 0.3 dB  
Spectral width 1.2 Å  $\Delta \lambda / \lambda = 2 \cdot 10^{-4}$

narrowing gain is proportional to the local electronic density  
spontaneous emission accumulated at each pass  
"leakage"

Improvements:  
extension of the spectral range  
spectral narrowing

## Transverse laser modes

superimposed transverse modes  
with one main mode, being a TEM<sub>00</sub> with  $n = 0, 1, 2, 3$

depending on the mirror adjustment, the orbit position in the undulator and the RF frequency  
the energy contained in the large tail compared to the TEM<sub>00</sub> mode is not negligible

## CONCLUSION

1987 first beam in Super-ACO  
Jan 1988 installation of the optical klystron on the storage ring  
Feb 1989 insertion of the mirrors in the optical cavity  
Pumping  
July 1989 Lasing at 600 MeV at 630 nm  
Lasing at 650 MeV

Good quality of :  
the stored positron beam in Super-ACO  
the optical klystron  
the multilayers dielectric mirrors

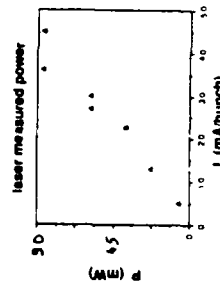
Third Storage ring Free Electron Laser  
after ACO (1983)  
VEPP 3 (1988, down to 240 nm)

Highest particle beam energy for an FEL.  
High average power extracted from a storage ring FEL.

## FUTURE DEVELOPMENTS:

- Study of the laser itself
  - transverse modes
  - dynamics
  - modulation rate, energy spread, position hum
- Improvements of its performances :
  - Q-switched operation
  - extension of the tunability range towards shorter  $\lambda$
  - enhancement of the output power

## LASER POWER



power transmitted at the center of the mirror  
5.1 W  
210 W  
90 mW  
65 mW  
165 mW  
26 W  
6.2 kW

average peak

transmitted through the mirrors  
absorbed in the mirrors  
initial extracted power  
intra cavity

## IMPROVEMENTS:

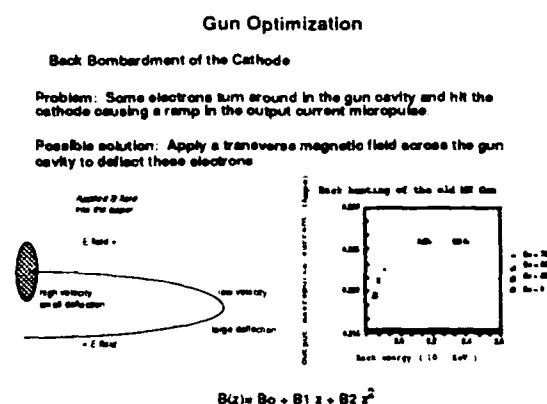
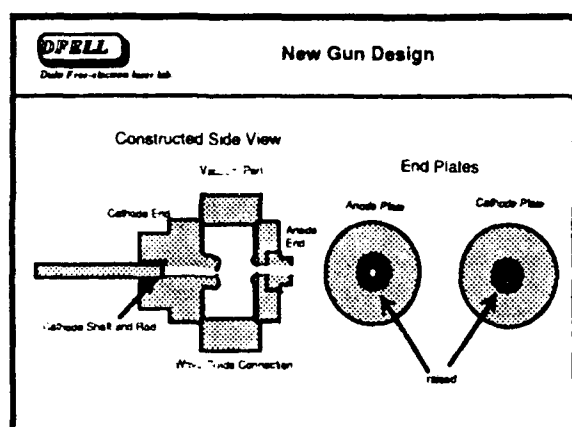
- With high positron beam energy  
enhancement of the average power
- Q-switched operation for the peak power

## EXI.2

### A Review of the Stanford Mark III Infrared FEL Program

Stephen V. Benson, Wun Shain Fann, Brett A. Hooper, John M. J. Madey, Eric B. Szarmes  
 Department of Physics, Duke University,  
 Durham NC 27706  
 Bruce Richman  
 Dept. of Applied Physics, Stanford Univ.  
 Stanford, CA 94305  
 Louis Vintro  
 Deacon Research,  
 Suite #203, 900 Welch Rd. Palo Alto CA 94305

The performance of Mark III infrared FEL with a new microwave gun will be reviewed. Operation of the accelerator is now close to design values. The Mark III has provided over 2000 hours of laser time to experiments in FEL physics, material science, and medical physics. Highlights of the experimental program will be presented.



**DFELL**  
 Duke Free-electron Laser Lab

**Electron Beam Performance**

Electron beam	
Macropulse length	9 $\mu$ sec
Micropulse length	2-3 psec
Micropulse repetition rate	2857 MHz
Beam energy	27-45 MeV
Macropulse energy spread	0.7%
Average current	100-200 mA
Peak current	20-40 A
Horizontal emittance(μm)	10x mm-mrad
Vertical emittance(μm)	4x mm-mrad
Repetition rate	30 Hz

Items in boldface meet or exceed design goals

**DFELL**  
 Duke Free-electron Laser Lab

**Laser Performance**

Tuning range	1-8 $\mu$ m
Demonstrated tuning range	1.4-8.1 $\mu$ m
Gain	20-100%
Energy per pulse	1-200 mJ
Repetition rate	Single shot-30 Hz
Peak power	0.5-2 MW
Macropulse length	0.5-8 $\mu$ sec
Micropulse length	0.5-3.0 psec
Spectral bandwidth	0.5-1.0% FWHM
Strehl ratio	>0.8

**Page / column number** Page 10 / column 1

### Mark III Applications

Ophthalmic Hazards	Josh Kearney, LAUR
Two photon absorption in Ge	John Seale, SPRS
Induced absorption of Butane on Sapphire	Steve George, Stanford Chem.
Star-Blocker compatibility of polyacrylates	Shahab Ezzamel, Butane
	Wen Shien Fan, SPRS
Sulfur formation in azobenzene	Laura Rothberg, AT&T Bell Labs
Laser surgery in hard and soft tissue	Richard Straight, Utah Laser Inst.
Hormonal Generation	Brett Haegele, SPRS, Utah Laser Inst.
Photodynamic Therapy	Brett Haegele and Richard Straight, ULI
Gallstone ablation and optical fiber propagation	Brett Haegele, John Olson, Utah
Amorphous Silicon LE	Craig Taylor, U. of Utah Physics
Peptide Formation	Michael Barry, Res. MARC

**DFLL**

**Date / registration form left**

## Harmonic Generation

<b>CRYSTAL</b>	AgGaIn <sub>2</sub>	LiNbO <sub>3</sub> (5.05)	Ba-Sr-Bi <sub>2</sub> O <sub>3</sub>
<b>DEVELOPMENT (mm)</b>	Scattering 1 inch long	Cyrtolens 1/8 inch	Scattering 2x 2x 1/8 inch
<b>FLUORESCENCE ANGLE (degrees)</b>	1) 90 2) 62.5	45	35
<b>FUNDAMENTAL WAVELENGTH (μm)</b>	1) 1.26-1.37 2) 1.30-1.3	1.03-1.05	0.94-1.25
<b>SECOND HARMONIC WAVELENGTH (μm)</b>	1) 1.26-1.66 2) 1.2-1.3	0.70-1.24	0.465-0.625*
<b>CONVERSION EFFICIENCY</b>	1) 17-45 % 2) 7-10%	10-40%	1-10%
<b>TEMPORAL WALKOFF (ps/cm²) -0.77</b>	1) 3.20	4.000	5.7
<b>SPATIAL WALKOFF (degrees)</b>	1) 0 2) 0.60	1.10	2.5

**DFELL**

2000

### Anomalous Conversion Efficiency

Due to the high average power in the FEL we are forced to operate with large area beams. This leads to the use of relatively long crystals to attain large conversion efficiency. The large spectral width of the picosecond pulses leads to large phase offsets. One therefore expects poor conversion efficiency due to large phase mismatch. This is not seen experimentally.

**DFELL**

**Only 7 free classes here!**

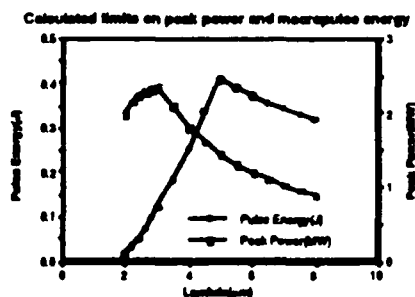
### Mark III machine physics projects

Optical transients made visible	John Latham, Dave Dawson
Gas Loaded operation	Richard Parcell, Alan Fletcher, et. al.
Coherent harmonic studies	Dave Dawson, Doug Sanford
Low Modulation and cavity dumping	John Wiley, Eric Szymanski, Reinhold
Dual PEI operation	Matt Curdin, John Wiley
Small signal MOPA	Luigi Vitro
Microwave guiding effects	Bruce Ruchman
Optical Damage Studies	Eric Szymanski, Ed Osborn
Continuously variable Tuner	Reinhold
Photocathode Induced Lasing	Reinhold

**DPRL**

**2017/2018**

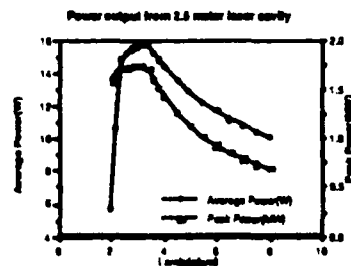
### Peak Power and Pulse Energy



**DP-ELL**

Date / re-evaluation later than

**Longer optical cavity can increase short wavelength power**





**DPFEL**

Duke Free-electron Laser Lab

### Possible Improvements (laser and optical systems)

#### Spectral or Temporal Intensity

Intracavity filtering should reduce spectral width to as little as 0.1%.  
Micropulse chirping could produce femtosecond pulses.

#### Output coupling

More efficient output coupling schemes could raise peak output power by a factor of four. Ring cavity would simplify output coupling.

#### Harmonic generation

More efficient harmonic generation would allow shorter wavelength operation.

#### Cavity dumping

By dumping stored cavity power, peak power as high as 100 MW is possible. The cavity dumper can also be used for loss modulation.

#### Custom spectral lineshapes

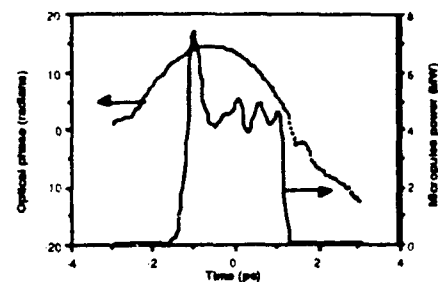
Intracavity optics can narrow the lineshape, phase-lock the microbunches, and stabilize the spectral output.

**DPFEL**

Duke Free-electron Laser Lab

### Pulse Compression— Energy slew causes chirped output

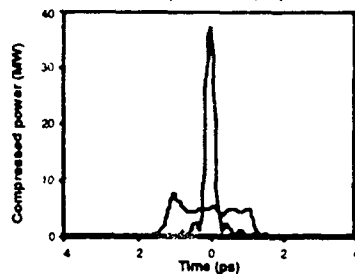
#### Chirped pulse output

**DPFEL**

Duke Free-electron Laser Lab

### Pulse Compression(cont.) Grating pair compresses pulse to 250 fs

#### Compressed pulse vs. output pulse

**DPFEL**

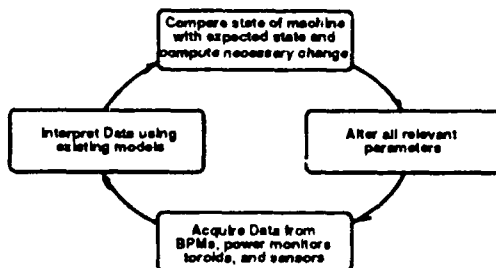
Duke Free-electron Laser Lab

### New Facility at Duke

**DPFEL**

Duke Free-electron Laser Lab

### Control system upgrade

**DPFEL**

Duke Free-electron Laser Lab

### Conclusions

"The new gun cavity has allowed us to operate the gun at design current for the full macropulse length allowed by the klystron modulator. Laser power at short wavelengths is limited by optical damage.

"The small size and flexibility of the system have allowed us to pursue many applications and machine physics projects.

"We are now entering an era where the optical cavity design will determine the FEL characteristics.

"New control systems should allow us to take advantage of the larger tuning range of the FEL.

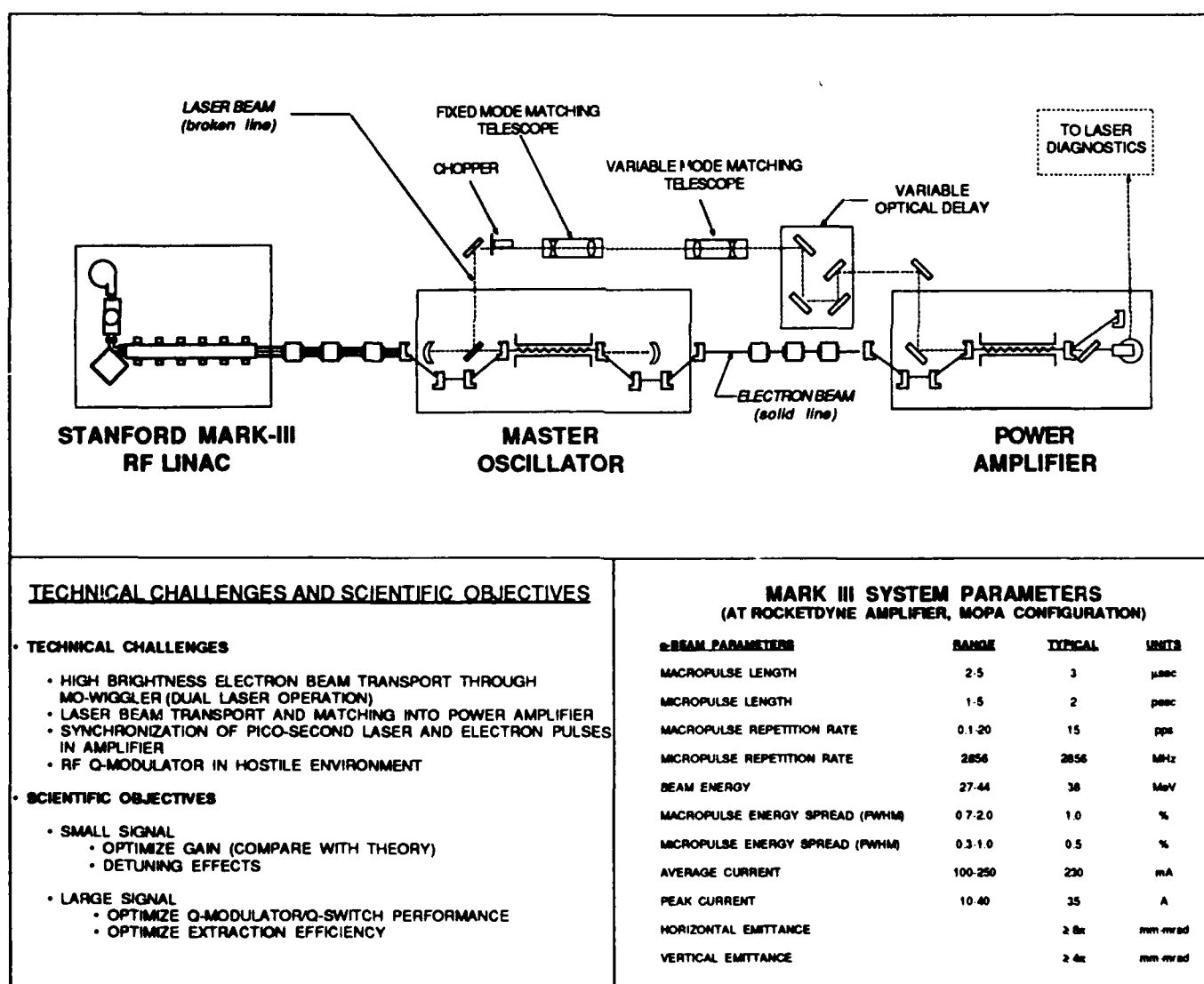
# EXI.4 INITIAL RESULTS FROM THE FREE-ELECTRON LASER MASTER OSCILLATOR/POWER AMPLIFIER EXPERIMENT

Anup Bhowmik, Mark S. Curtin, and Wayne A. McMullin

Rockwell International/Rocketdyne Division  
6633 Canoga Avenue, Canoga Park, CA 91303  
and

Stephen V. Benson [1], John M. J. Madey [1], Bruce A. Richman, and Louis Vintro [2]  
Stanford Photon Research Laboratory  
Stanford University, Stanford, CA 94305

We describe the first free-electron laser master oscillator and power amplifier experiment. The master oscillator and power amplifier are driven by time-sharing an electron beam from a single rf-accelerator. The optimized, small-signal gain spectrum realized in the untapered power amplifier is presented and additional Q-switched experiments are discussed.



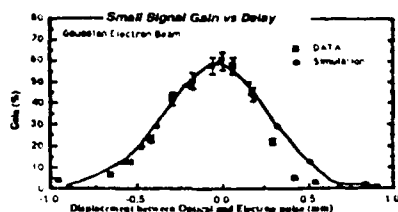
[1] Now at Duke University, Durham, NC 27706

[2] Now at Wharton School of Business, University of Pennsylvania, Philadelphia, PA 19104

### GAIN VS. DELAY

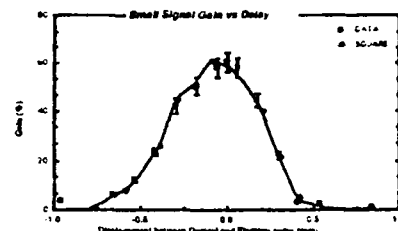
GAUSSIAN ELECTRON BEAM

Optical: 2ps  
Electron: 2ps



TOPHAT ELECTRON BEAM

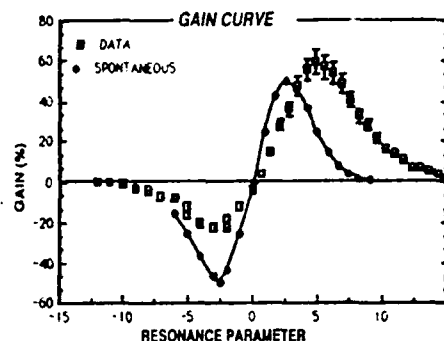
Optical: 2ps  
Electron: 2ps



### GAIN CURVE ASYMMETRY

Spontaneous Spectrum vs Gain Data

GAP OF AMPLIFIER WAS VARIED I.E. MAGNETIC FIELD WAS VARIED...



Note:  
Proportionality constant set using  
1-D gain calculation i.e. 50%

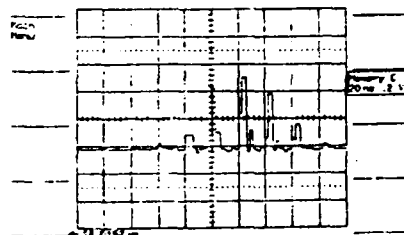
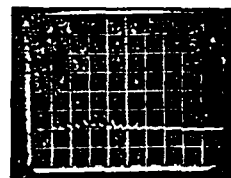
### FIRST DEMONSTRATION OF A Q-MODULATED/Q-SWITCHED FEL(\*)

- CdTe RF Q-MODULATOR/Q-SWITCH (23.8 MHz, EVERY 60TH  $\mu$  PULSE)
- CHALLENGES
  - DAMAGE -- SELF FOCUSING (CRYSTAL AREA, LENGTH) HIGH PEAK, AVERAGE POWER (CAVITY MODIFIED)
  - LOW INSERTION LOSS (AR COATED)
  - INFRARED ALIGNMENT (REMOVABLE CELL)
  - THERMAL DISTORTION (WATER COOLED/NOT USED)
  - HIGH VOLTAGE IN HIGH VACUUM
- OPERATED FEL IN BOTH Q-MODULATED/Q-SWITCHED MODES
- PROBLEMS
  - SURFACE CONTAMINATION/TRANSMISSION LOSS

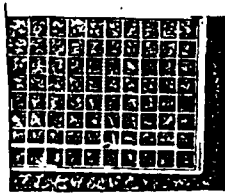
\*P15 S.V. BENSON, "DEMONSTRATION OF LOSS MODULATION/CAVITY DUMPING IN AN FEL"

### Loss Modulation and Cavity Dumping

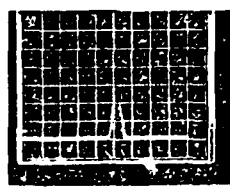
x10 power enhancement after 3 round trips



### Loss-Modulated Macropulses

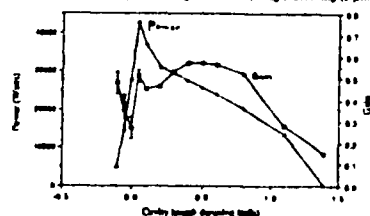


Maximum stable power



Power from shorter cavity

Computer simulations of power and gain vs. cavity length detuning (f  $\mu$ m)



### CONCLUSIONS

- FIRST DEMONSTRATION OF FEL-MOPA (SINGLE ACCELERATOR)
  - OPTIMIZED SMALL SIGNAL GAIN SPECTRUM
  - GAIN ASYMMETRY OBSERVED (INTERMEDIATE GAIN, 10% < G < 100%)
- FIRST DEMONSTRATION OF Q-MODULATED/Q-SWITCHED FEL
- HIGH POWER MOPA ATTEMPTED
  - CAVITY DUMPED PULSE TRANSPORTED TO AMPLIFIER
  - LASER BEAM QUALITY POOR
- EXPERIMENT SHUT DOWN / TO BE RESUMED AT DUKE

# EX1.5

## PALADIN Operation with a 25-m-Long Wiggler\*

T. J. Orzechowski, J. L. Miller, F. W. Chambers, Y. P. Chong,  
J. Edighoffer,† P. Lee, # D. Prosnitz, E. T. Scharlemann, and J. T. Weir

Lawrence Livermore National Laboratory  
University of California, Livermore, California 94550

The PALADIN free-electron laser amplifier operates at  $10.6 \mu\text{m}$ . The wiggler has recently been extended to 25 meters. We have measured exponential gain and saturation for various magnitudes of input signal. We have modeled the performance of PALADIN with the 3-dimensional simulation code FRED and will present both experimental results and simulations of the experiment.

\*Work performed jointly under the auspices of the US Department of Energy by the Lawrence Livermore National Laboratory under W-7405-ENG-48 and the DOD under SDIO/SDC-ATC MIPR No. W31RPD-9-D5007.

†TRW, Inc., Redondo Beach, CA

#General Atomics, San Diego, CA

### PALADIN Operation with a 25-meter Long Wiggler

T. J. Orzechowski, J. L. Miller, F. W. Chambers, Y. P. Chong,  
J. A. Edighoffer, P. Lee, D. Prosnitz,  
E. T. Scharlemann, and J. T. Weir

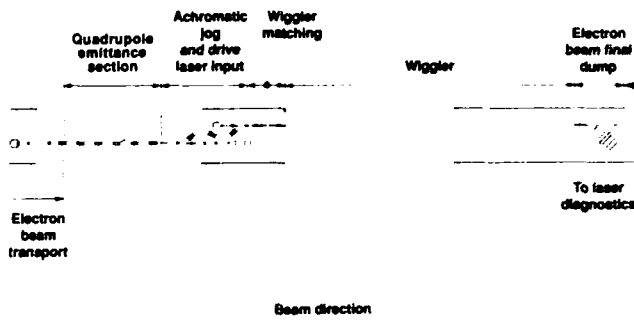


Presented at the  
11th International Conference on Free Electron Lasers  
Ritz-Carlton Hotel  
Naples, Florida

August 28 — September 1, 1990

### PALADIN phase four

Extended wiggler



### PALADIN Phase IV experimental parameters

Wavelength	10.6 $\mu\text{m}$
Beam Energy	44 MeV
Beam Current	500-800A
Beam Brightness	$10^8 \text{ A/(m-rad)}^2$ *
Wiggler period	8 cm
Wiggler length	25 m
Input signal power	18 kW, 3.6 MW, 400 MW

\* assumes uniformly filled acceptance of quadrupole emittance selector

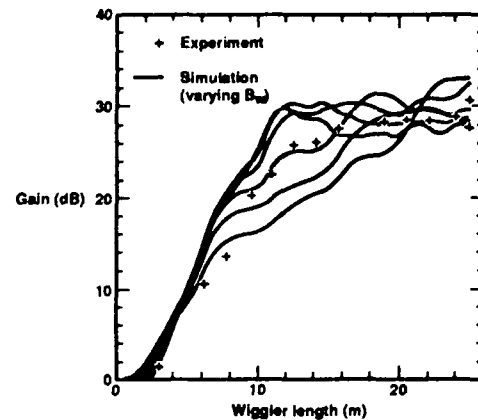
We have assumed a two-component phase space (core & halo) to model the beam incident on the QES

- Constraints (self-imposed)
  - Both components at a waist at first QES aperture
  - Each component is either a Gaussian or a uniformly filled ellipsoid
  - Both components have 7 mm radius ( $\geq 6.25$  mm aperture radius) at first QES aperture (edge radius for ellipsoid,  $1/e$  radius for Gaussian)
- Best fit (least squares) to  $\eta_{\text{para}}$  vs quadrupole gradient is
  - Core = 4D ellipsoid with  $\epsilon = 7.5 \text{ mm-mrad}$ ,  $\sim 300 \text{ A}$  [ $f = 1.4 \cdot 10^8 \text{ A/(m-rad)}^2$  or  $1.4 \cdot 10^5$  (old LLNL units)]
  - Halo = Gaussian with  $\epsilon_{1/e} = 30 \text{ mm-mrad}$ ,  $\sim 2700 \text{ A}$  [ $f$  (90% contour)  $\sim 4.6 \cdot 10^8 \text{ A/(m-rad)}^2$  or  $4.6 \cdot 10^5$  (old LLNL)]

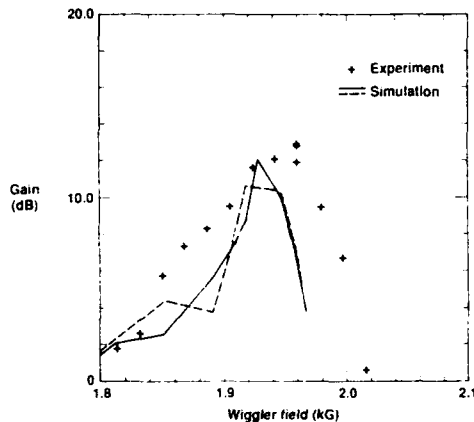
## Comparing the experiment to simulation

- The electron beam energy varied by  $\pm 1\%$  from shot-to-shot
- This energy variation caused large variations in the PALADIN output
- To model the FEL performance with FRED we choose the highest data point at any set of wiggler parameters and compare this to the upper envelope of a series of simulation runs where the wiggler field was varied by  $\pm 0.25\%$

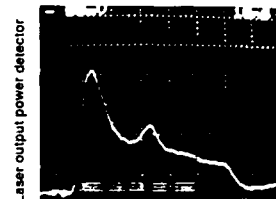
## Gain vs wiggler length, 18 kW input



## Gain vs. wiggler field, 3.6 MW input



Preliminary data indicates PALADIN has demonstrated 0.97% extraction from the electron beam



e<sup>-</sup> beam on

Wiggler parameters:

$B_{w, \text{peak}} = 1.80 \text{ kG}$   
17% linear taper starting at  $Z = 0$

At e<sup>-</sup> beam time:

$P_{\text{laser, in}} = 0.4 \text{ GW}$

$\frac{P_{\text{laser, out}}}{P_{\text{laser, in}}} - 1 = 0.533$

$P_{\text{extraction}} = 0.21 \text{ GW}$

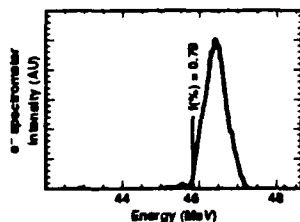
$E_{\text{beam}} = 44 \text{ MeV}$

$I_{\text{beam}} = 500 \text{ A}$

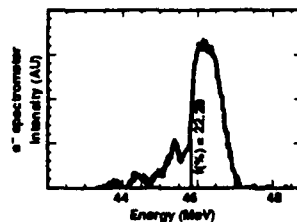
$P_{\text{beam}} = 22 \text{ GW}$

$\frac{P_{\text{extraction}}}{P_{\text{beam}}} = 0.97\%$

## Electron energy loss agrees with laser power gain



No input signal to FEL  
(unperturbed electron distribution)



400 MW input signal, 17% linear taper:  $\Delta\gamma/\gamma = 0.9\%$

## Conclusion

- PALADIN has demonstrated
  - sextupole transport of electron beam in wiggler (Y.P. Chong poster)
  - exponential gain (up to 31 dB – 2.5 dB/m exp gain)
  - saturation (0.6 GW)
  - optical gain guiding
  - 1% extraction with linear taper
- PALADIN results are in reasonable agreement with FEL simulations (3-D code FRED)
- PALADIN performance is currently limited by electron beam brightness
- PALADIN showed excellent power balance between optical power and electron beam power

## UNI.1 WORKSHOP RESULTS ON SMALL-PERIOD WIGGLER DESIGNS

Richard L. Sheffield, John H. Booske, Roger W. Warren, Klaus Halbach, Bruce Danly, Robert H. Jackson, Peter Walstrom, Jack Slater, and Arthur Toor  
Los Alamos National Laboratory, MS H825  
Los Alamos, NM 87545

A review of a workshop on small-period wiggler and undulator designs held at Los Alamos National Laboratory on April 13, 1989 will be presented. The wiggler designs are based on the following mechanisms: microwave fields, electromagnetic coils, miniature permanent magnets, current sheets, superconductive coils, and iron-free pulsed wire.

### WORKSHOP RESULTS ON SMALL-PERIOD WIGGLER DESIGNS

Richard L. Sheffield, John H. Booske, Bruce G. Danly, Robert H. Jackson, Jack Slater, Arthur Toor, Peter Walstrom, Roger W. Warren

Representing (in the order given above):  
Los Alamos National Laboratory  
University of Maryland  
Massachusetts Institute of Technology  
Naval Research Laboratory  
Spectra Technology  
Lawrence Berkeley Laboratory  
Grumman Space Systems  
Los Alamos National Laboratory

11th Int. Conf. on Free Electron Lasers  
August 28 - September 1, 1989  
Naples, Florida

### Why we are interested in small period wigglers.

Recent improvements in electron beam brightness has pushed the present limits on wiggler periods.

#### APPLICATIONS:

Where large gaps are required to reduce: wakefields, resistive wall instability, or beam interception.

Low-cost and/or high-efficiency FELs.

### SCALING LAWS FOR WIGGLERS Halbach, Slater, and Jackson

Permanent magnets:

$$a_w \sim 10^4 B_p(G) l_w(\text{cm}) e^{-(\pi l_{gap}/l_w)}$$

Electromagnets:

$$a_w \sim 10^4 J(A/\text{cm}^2) l_w^2(\text{cm}) e^{-(\pi l_{gap}/l_w)}$$

Resistance proportional to  $1/d$

Power proportional to  $d$

Cooling proportional to  $1/d$

### CURRENT SHEET SHORT-PERIOD WIGGLERS

John Booske, Univ. of Maryland

- For high average power mm-wave FELs.
- Wiggler periods to 0.5 to 1.5 cm.
- Electron beam is a sheet beam.
- Uses very thin iron laminations to reduce eddy current losses.

$$l_{ps} \sim H_0 [1 + (\text{thickness/skindepth})^2]$$

- Measured field errors less than  $\pm 2\%$  for cores with thicknesses within 4% and gap alignment within  $\pm 0.5$  to 1.0%

### ISSUES IN CURRENT SHEET SHORT-PERIOD WIGGLERS

---

- Field errors become important when the iron begins to saturate.
- Keeping the wiggler thermally stable by cooling must be considered for DC operation, for small wiggler periods this cooling will limit operation to a pulsed mode.
- Not compatible with external steering and/or focusing.
- Correction of end effects of the wiggler.
- Field errors become important when the iron begins to saturate.

### REDUCED EDGE EFFECTS LINEAR (REEL) WIGGLER

Bob Jackson, NRL

---

- Developed for 0.1 to 1 mm radiation.
- $a_w = 0.2$  to 1.0 for periods of 1 to 3 cm.
- Simple cheap fabrication and flexibility to vary the field intensity.
- Reduces uncompensated virtual bias currents at wiggler sides.
- Reduces excess field end effects.
- Microwiggler structures possible below 1 mm (to  $1 \mu\text{m}$ ) using wire-EDM or solid-state fabrication techniques.

### ISSUES IN REDUCED EDGE EFFECTS LINEAR (REEL) WIGGLER

---

- Field errors become important when the iron begins to saturate.
- Keeping the wiggler thermally stable by cooling must be considered for DC operation, for small wiggler periods this cooling will limit operation to a pulsed mode.
- Not compatible with external steering and/or focusing.

### ELECTROMAGNET COILS ON C-SHAPED IRON CORES

Bruce Danely, MIT

---

- 1 to 5 mm wiggler periods.
- Individual cores can be tuned to minimize wiggler errors during operation.
- Prototype devices have been built for 30 periods with 2.4 mm per period: 10 A for 160 turns per core,  $\sim 0.6$  kG peak fields, 3 mm gap.
- Next model is for 30 periods with 2.4 mm period: 2.5 A for 800 turns per core,  $\sim 1.3$  kG peak fields, 3 mm gap.
- Operation at low temperature or in pulsed mode gives  $\sim 3$  kG peak field.

### ISSUES IN ELECTROMAGNET COILS ON C-SHAPED IRON CORES

---

- To achieve high  $a_w$  requires pulsed mode operation.
- Not compatible with external steering and/or focusing.
- Field errors become important when the iron begins to saturate.

### MICROWAVE WIGGLERS

Bruce Danly, MIT

- Resonance gives extra factor of two:

$$\lambda = \lambda_0(1 + a_w^2)/(2(1 + k_{\text{period}}/k)\gamma^2).$$

- Less than 5 mm period and large bore.
- Experiment has given  $a_w \sim 0.006$  for 139 GHz at 325 kW drive power ( $k_{\text{period}}/k = 0.9$ ).
- Next experiment is designed to give an  $a_w \sim 0.049$  for 139 GHz at 4 MW drive power ( $k_{\text{period}}/k = 0.9$ ).
- equivalent wiggler period of 1.22 mm for above experiments.

### ISSUES IN MICROWAVE WIGGLERS

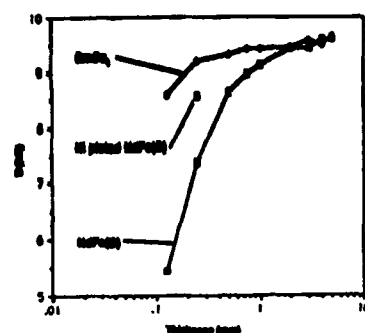
- Limited values of  $a_w$  for non-superconducting cavities.
- Broad-gain spectra and higher harmonics occurs for large  $a_w$ .
- Superconducting cavities are limited to  $a_w < 0.5$  because of cooling requirements.
- Large expense involved in purchasing and set-up of rf source.
- Very high rf drive powers required for appreciable ( $a_w > 0.1$ ) fields.

### SMALL-PERIOD PERMANENT MAGNETS

Art Toor, LL

- Permanent magnet wigglers with periods of 0.05 to 1 mm and up to  $10^4$  periods.
- Two types: one, machined solid blocks of permanent magnet material which is later magnetized and immersed in a reverse bias field and, two, extremely thin sliced wafers sliced wafers.
- Of the machined blocks, wigglers were built with periods of 62 to 700 microns and 32 to 250 total periods - gives more uniform fields and easier to fabricate.
- Of the sliced wafers, wigglers were built with 250 to 1000 microns and 50 to 250 periods.
- Gap to period ratios of 0.5 gave gap fields of 1 to 3 kG.

### MAGNETIC FIELD DECREASE WITH DECREASING PERIOD FOR PERMANENT MAGNET MATERIALS



### ISSUES IN SMALL-PERIOD PERMANENT MAGNET WIGGLERS

- The machined blocks have a field which is down by 2 and requires a bias field and thus cooling for dc operation.
- The sliced wafers less than 250 microns curled because of internal stresses; fabrication, handling, and controlling uniformity are very difficult for very thin wafers.
- Limited to small values of  $a_w$ .



### SUPERCONDUCTING WIGGLERS

Peter Walstrom, Grumman

- Superconducting wigglers give the highest cw field strengths on-axis for periods greater than 1 cm.
- Holmium inserts can increase the on-axis field by up to 50%.

- For example,

wiggler period = 1 cm,  
wiggler gap = 3 mm,

has

$$a_w = 1.1$$

### ISSUES FOR SUPERCONDUCTING WIGGLERS

- Alignment and correcting field errors when cold.
- Thermal expansion's effect on mechanical design.
- Cooling of wiggler tube.
- Expense of cryostat.
- Operating expense.
- Radiation effects on superconductor.
- Vacuum in wiggler tube.

### PULSED IRON-FREE COILS

Dodge Warren, LANL

- Goal is to keep  $a_w$  at 1 for sub-cm periods where operation is limited by wire failure.
- Uses no magnetic materials and therefore is not constrained by saturation effects.
- With room temperature cooling, pulse operation is limited to ~ 100  $\mu$ s for 3 mm period.
- Operation at 1-3 mm is possible for pulse lengths less than 10  $\mu$ s.
- High machining precision is possible.

### ISSUES IN PULSED IRON-FREE COILS

- Limited to pulsed operation.
- Skin and proximity effects become important for very short pulses (<10  $\mu$ s).
- Coil current generator must have very small amplitude variations.

### SUMMARY OF SMALL-PERIOD WIGGLER WORKSHOP

- Permanent magnet wigglers:  
initially more expensive;  
no operating costs;  
compatible with external steering and/or focusing.
- Hybrid wigglers:  
inherently smaller field errors;  
lower fields than pure permanent magnet wigglers.
- CW electromagnet:  
consume power;  
require cooling;  
flexible operation;  
relatively low cost.
- Superconducting wigglers:  
highest cw magnetic fields;  
for > 0.5 cm periods;  
very expensive to build and operate.

### SUMMARY OF SMALL-PERIOD WIGGLER WORKSHOP

- Microwave wigglers:  
wiggler periods of less than 5 mm;  
possible sub-mm periods;  
large wiggler gap;  
initial expense is high;  
for high  $a_w$  cavity cooling is an issue;  
requires high levels of rf power.  
compatible with external steering and/or focusing.
- Iron-free pulsed wire wigglers:  
give very high fields limited only by the cooling available;  
wiggler periods of 1 mm with an  $a_w$  of 1;  
compatible with external steering and/or focusing.

## UNI.2

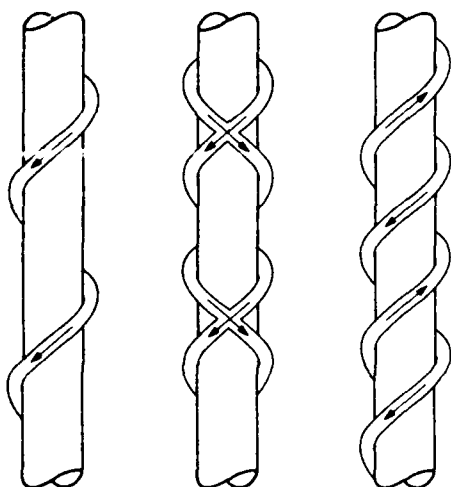
## PULSED-COIL MICROWIGGLERS

R. W. Warren, D. W. Feldman, and D. Preston\*

Los Alamos National Laboratory  
Los Alamos, NM 87545

\*California State University  
Hayward, CA 94542

Conventional wigglers made with periods of less than a few centimeters generate light of short wavelength, but usually have low gain because of their low fields. Iron-free electromagnets driven by high pulsed currents can generate the high fields needed. We will discuss the design and construction of such magnets.



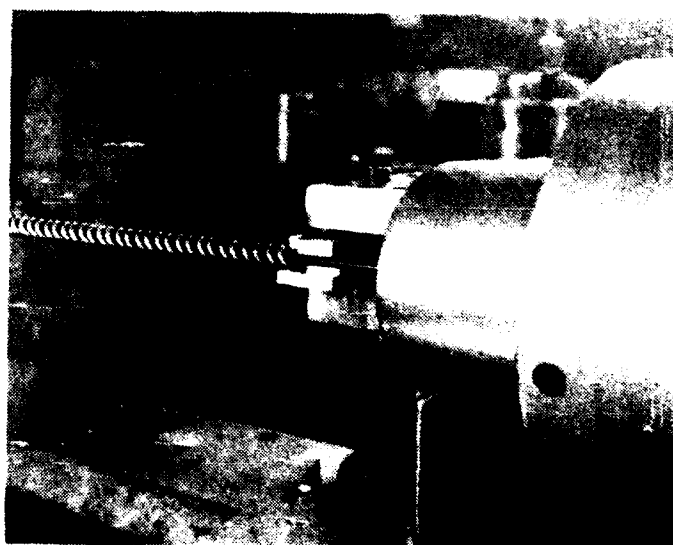
Different Coil Configurations

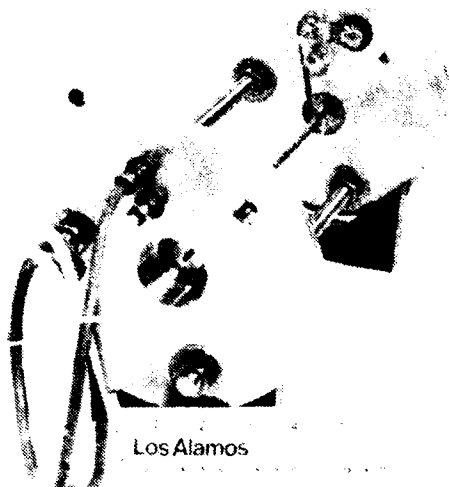


Winding double helixes of 8 mm period with 2 mm dia. tubing.

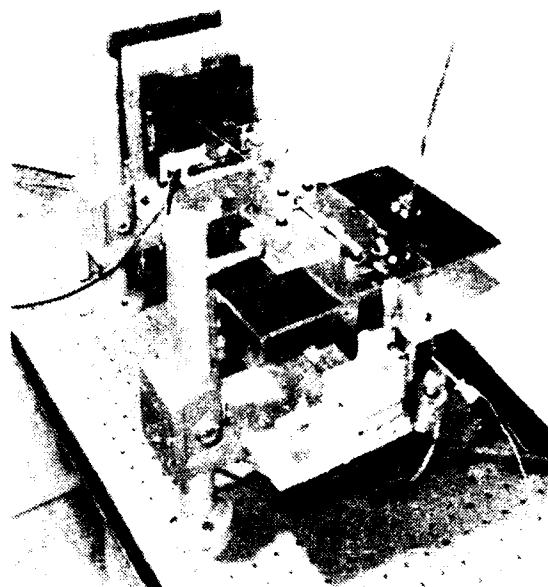
Wiggler	Period (mm)	Wire Diameter (mm)	Wire Resistance (mΩ)	Wire Inductance (pH)	Power @ 10 kA (kW)	Energy at 100 μs (Joules)	ΔT at 100 μs (°C)	ΔT at 10 μs (°C)
W 27	27	0.7	1.6	1.2	160	16	< 1	< 1
W 9	9	2.2	4.2	0.40	420	42	4	< 1
W 3	3	0.75	1.4	0.13	1,400	140	350	30
W 1	1	0.25	30	0.04	1,000	100	> 7m	> 7m

Properties of coils of different sizes

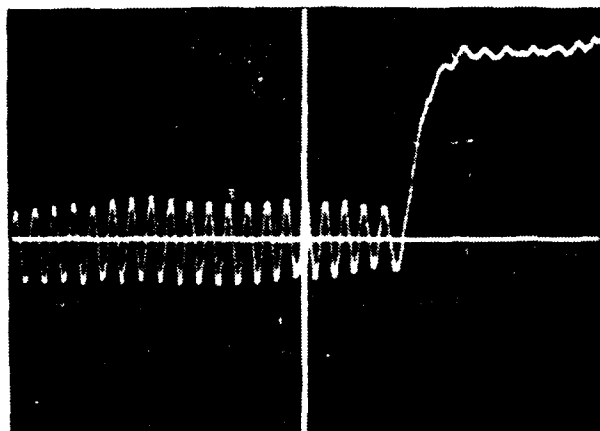




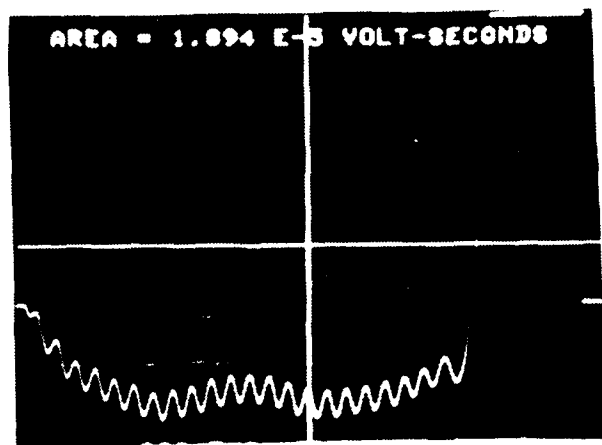
Completed wiggler



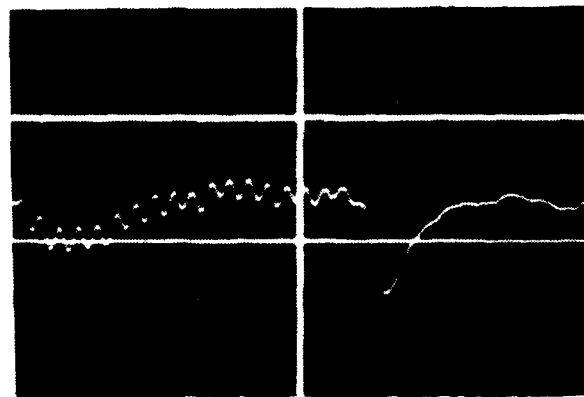
Field-measuring apparatus



integral of field



Double integral of field showing bad end effect.



Double integral of field showing good end effect.

Isidoro Kimel, Luis R. Elias

Center for Research in Electro-Optics and Lasers (CREOL)

University of Central Florida, Orlando, FL 32816

## ABSTRACT

Magnetic fields of several configurations for short period undulators made of permanent magnets, were studied analytically. These microundulators are made of blocks on which grooves are machined. First, the approximate two-dimensional fields were obtained by solving Poisson equation using Fourier transforms. The finite width corrections were added afterwards.

## 1. OVERVIEW

IT IS EXTREMELY HARD TO MAKE A VERY SHORT PERIOD (A FEW MM) UNDULATOR IN THE HALBACH CONFIGURATION.

OBJECTIVE OF THE WORK: Study different configurations of short period undulators made of permanent magnets in order to find the most convenient.

## STEPS.

- First consider two dimensional (large width) structures.
- Find a convenient way to calculate the fields.
- Use of rotation theorem plus translations.
- Analyze the best alternatives for microundulators.
- Calculate finite width effects.

$$= \int dz' dy' \bar{M}(z'y') \ln((z-z')^2 + (y-y')^2)$$

Taking the derivatives the potential comes out

$$\phi = \Re \left[ -\frac{\mu_0}{4\pi} \int dz' dy' \frac{M_x + iM_y}{(z-z') + (y-y')} \right]$$

$$= \Re \left[ -\frac{\mu_0}{4\pi} \int dz' dy' \frac{\mathcal{M}}{\xi - \xi'} \right],$$

with

$$\mathcal{M} = M_x + iM_y, \quad \xi = z + iy.$$

In a similar way the vector potential comes out

$$A_x = \Im \left[ -\frac{\mu_0}{4\pi} \int dz' dy' \frac{\mathcal{M}}{\xi - \xi'} \right].$$

It is then convenient to define

$$\psi = \phi + iA_x = -\frac{\mu_0}{4\pi} \int dz' dy' \frac{\mathcal{M}}{\xi - \xi'}.$$

As was done with the magnetization and coordinate, we can define the complex induction

## 2. THEORETICAL CONSIDERATIONS

An undulator consists of blocks in different positions in one period, each with the magnetization in a different direction. In calculating the total field, the fields from the different types of blocks have to be added. Fortunately, for two-dimensional structures, only the field of one type of block has to be explicitly calculated. Then, the fields of the other blocks can be obtained with the use of translations and the rotation theorem.

## 2.1. ROTATION THEOREM

Outside the magnets

$$\vec{B} = -\vec{\nabla} \phi, \quad \vec{B} = \vec{\nabla} \times \vec{A}.$$

In terms of the magnetization  $\vec{M}$

we have

$$\phi(x) = -\frac{\mu_0}{4\pi} \vec{\nabla} \cdot \int \frac{\vec{M}(x') d^3 x'}{|x - x'|}$$

$$\mathcal{B} = B_x + iB_y, \quad \mathcal{B}^* = B_x - iB_y.$$

A simple calculation shows

$$\begin{aligned} \mathcal{B}^* &= \frac{d}{d\xi} \left[ \frac{\mu_0}{4\pi} \int dz' dy' \frac{\mathcal{M}}{\xi - \xi'} \right] \\ &= -\frac{\mu_0}{4\pi} \int dz' dy' \frac{\mathcal{M}}{(\xi - \xi')^2}. \end{aligned}$$

A rotation of the magnetization by an angle  $\theta$  is described by

$$\mathcal{M} \rightarrow \mathcal{M}' = \mathcal{M} e^{i\theta}$$

and we have the ROTATION THEOREM:

When  $\mathcal{M}$  is rotated by  $\theta$ ,  $\mathcal{B}^*$  is also rotated by  $\theta$ .

Then  $\mathcal{B}$  is rotated by  $-\theta$ .

## 3. BASIC BLOCK CONFIGURATION

Let us calculate first, the fields (or potential) of simple periodic block structures like the upper and lower rows in Fig. 1. The source for the magnetic potential for the upper row, in one period, is

$$S_+ = \mu_0 M [\delta(y-h-g/2) - \delta(y-g/2)] \\ \times [\theta(z+a/2) - \theta(z-a/2)].$$

So the extended source is given by the Fourier series

$$S_+ = \frac{\mu_0 M}{2\pi} \int dp [e^{ip(y-h-g/2)} - e^{ip(y-g/2)}] \\ \times \sum_n \frac{2}{n\pi} \sin(nka/2) \cos(nkz).$$

The potential  $\phi_+$  in  $\nabla^2 \phi_+ = -S_+$

can be written as

$$\phi_+ = \frac{\mu_0 M}{2\pi} \int dp [e^{ip(y-h-g/2)} - e^{ip(y-g/2)}] \\ \times \sum_n \frac{2}{n\pi} F_n(p) \cos(nkz).$$

Poisson equation leads to  $F_n(p) = \sin(ka/2)/(p^2 + a^2 k^2/4)$ .

Then the potential is

can be obtained.

#### 4. HALBACH CONFIGURATION

For the orthodox Halbach configuration of Fig. 2 we have to add 8 Fourier series (one for each block in one period). But, the potential for each one can be simply obtained from the basic potentials obtained in the last section by rotation and translations. The potential for the upper row is

$$\psi_+ = \sum_{n=1}^4 \psi_n \left[ (m-1) \frac{\lambda}{4} - n(1/2 + (m-1)/4) \right] \\ = \frac{\mu_0 M}{\pi k} \sum_{n=1}^4 \left[ \sum_{m=1}^4 e^{in(m-1)(\lambda-1)/2} \right] \frac{C_n(\pi/4)}{n} e^{-n\pi y}.$$

and a similar expression for  $\psi_-$ . The total complex potential for the Halbach configuration is

$$\psi = \frac{i8\mu_0 M}{\pi k} \sum_{n=1}^4 \frac{C_n(\pi/4)}{n} \sin(nk\zeta).$$

From this is easy to derive the perpendicular field

$$B_y = \frac{2\mu_0 M}{\pi k} \sum_{n=1}^4 \frac{(-1)^{(n-1)/2}}{n} e^{-n\pi y/2} \\ \times (1 - e^{-n\pi h}) \sin(nk\zeta) \cosh(nky).$$

#### 6. FINITE WIDTH EFFECTS

The preceding analysis is strictly valid in the limit of infinity width. Finite width effects can be taken into account by multiplying the magnetic source by the function which is one inside the width and zero outside. Namely

$$f(x) = \frac{1}{2i\pi} \int dq \left[ \frac{e^{iq(\frac{x}{2} + i)} - e^{-iq(\frac{x}{2} + i)}}{q - i\epsilon} - \frac{e^{iq(\frac{x}{2} - i)} - e^{-iq(\frac{x}{2} - i)}}{q + i\epsilon} \right].$$

Introducing this function into the source yields a finite width correction factor given by

$$\left[ 1 - e^{-\frac{1}{2} \pi w} \cosh \sqrt{2} nkx \right].$$

$$\phi_+ = \frac{\mu_0 M}{\pi^2} \sum_n \frac{\sin(nka/2)}{n} \int dp \frac{(e^{ip(y-h-g/2)} - e^{ip(y-g/2)})}{(p^2 + a^2 k^2)} \cos(nkz) \\ = \frac{\mu_0 M}{\pi^2} \sum_n \frac{\sin(nka/2)}{n} \int dp e^{ip(y-g/2)} (1 - e^{-n\pi h}) \cos(nkz)$$

It is useful to introduce

$$C_n(ka) = \frac{1}{n} \sin(nka/2) e^{-n\pi h/2} (1 - e^{-n\pi h}).$$

and write the complex potential as

$$\psi_+(0, \pi/2) = \frac{\mu_0 M}{\pi k} \sum_n \frac{C_n(ka)}{n} e^{-n\pi y/2},$$

where the first argument indicates the first block is centered at  $z=0$  while the second corresponds to the magnetization being at  $\pi/2$  with the  $z$  axis. In a similar way the potential for the lower row in Fig. 1 is obtained as

$$\psi_-(0, \pi/2) = \frac{\mu_0 M}{\pi k} \sum_n \frac{C_n(ka)}{n} e^{n\pi y/2}.$$

From these potentials for the basic periodic block structure of Fig. 1, the potentials for several undulator arrangements

$$B_y = \frac{-8\mu_0 M}{\pi} \sum_{n=1}^4 \frac{(-1)^{(n-1)/2}}{n} (1 - e^{-n\pi h}) \cos(nk\zeta) \cosh(nky).$$

#### 5. MICROUNDULATORS

The microundulators we are considering are made up from magnetized blocks in which grooves have been machined. Let us consider the three structures shown in Figs. 3-5.

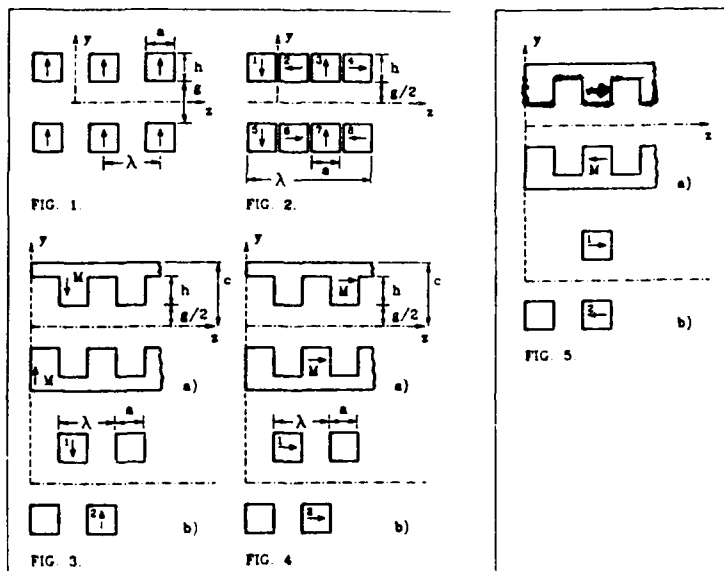
i) MU1. Consider the structure shown in Fig. 3a. If the blocks are large in the  $z$  and  $x$  directions, the field inside the gap is equal to the one produced by the blocks of Fig. 3b. The complex potential is

$$\psi = \frac{2i\mu_0 M}{\pi k} \sum_{n=1}^4 \frac{(-1)^{(n-1)/2}}{n} e^{-n\pi y/2} (1 - e^{-n\pi h}) \sin(nk\zeta).$$

ii) MU2. 3. For the structures of Figs. 4, 5 the complex potential is

$$\psi = \frac{2i\mu_0 M}{\pi k} \sum_{n=1}^4 \frac{(-1)^{(n-1)/2}}{n} e^{-n\pi y/2} (1 - e^{-n\pi h}) \cos(nk\zeta),$$

from which the perpendicular field comes out to be



# UNI.4

## In Search of a Meaningful Field Error Spec for Wigglers

B. Bobbs, G. Rakowsky, P. Kennedy, R. Cover and D. Slater  
Rockwell International, Rocketdyne Division  
6633 Canoga Avenue  
Canoga Park, CA 91303

Wiggler field quality is often characterized by its RMS deviation from the ideal. This deviation, however, is a poor predictor of actual system performance, particularly in light of the possibilities for optimized error ordering. An alternative field quality characterization in terms of trajectory wander and cumulative phase shake shows greatly improved correlation with performance.

### WIGGLER FIELD ERROR CHARACTERIZATION

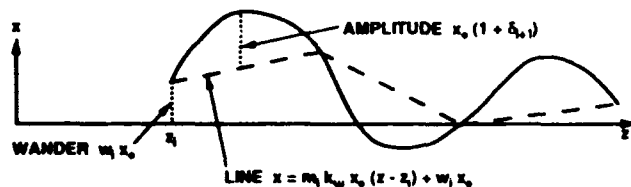
- CRITERIA FOR A USEFUL SPEC:
  - GOOD PREDICTOR OF PERFORMANCE
  - STRAIGHTFORWARD CALCULATION
  - INDEPENDENT OF ALL OR MOST OPERATING PARAMETERS
  - COMPUTATIONALLY QUICK
  - COMPENSATED FOR STEERING AND GAP TUNING
- RMS FIELD ERROR SATISFIES ALL OF THESE ... EXCEPT THE FIRST ONE!

### TRAJECTORY MODEL

- MODEL FIELD ERRORS BY A VARIATION IN SINE WAVE AMPLITUDE FROM ONE  $\lambda_w/2$  INTERVAL TO NEXT:

$$B(z) = -B_0 (1 + \delta_1) \sin(k_w z) \quad \text{for } z_{i-1} < z < z_i$$

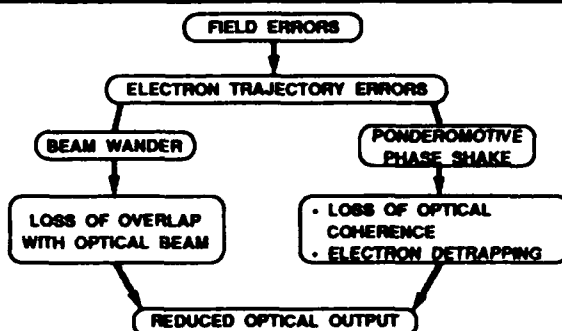
- INTEGRATE TWICE TO GET TRAJECTORY:



### ERROR COMPENSATION

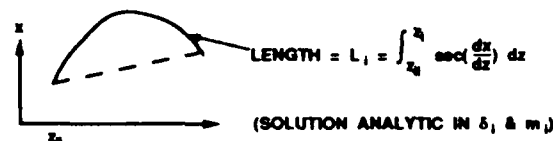
- NECESSARY TO AVOID UNDERESTIMATING PERFORMANCE WHEN FINE ADJUSTMENTS WILL BE MADE
- WANDER COMPENSATION - INITIAL STEERING
  - SET INITIAL SLOPE TO  $m_1 = 0$
  - REQUIRE FINAL WANDER RETURN TO ZERO:  $w_{2N} = 0$
- PHASE COMPENSATION - GAP TUNING
  - SCALE FIELD BY PARAMETER 1
  - REQUIRE FINAL PHASE SLIP RETURN TO ZERO:  $\psi_{2N} = 0$
- SOLVE FOR SELF-CONSISTENT SET OF VALUES FOR  $\delta$  AND 1 (ANALYTICAL SOLUTION)

### FIELD ERRORS AFFECT PERFORMANCE INDIRECTLY



### PHASE SHAKE CALCULATION

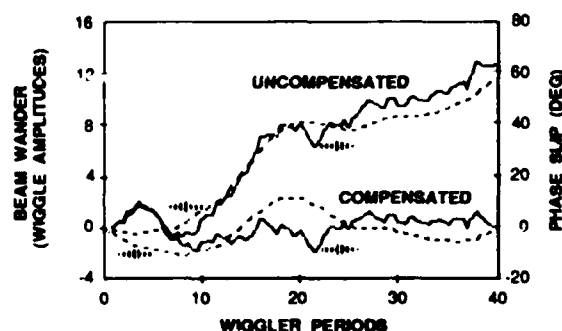
- COMPUTE DISTANCE TRAVELED BY  $e^-$  OVER ONE WIGGLE



- SLIP IN PONDEROMOTIVE PHASE:
 
$$\Delta\psi_1 = 2\pi/\lambda [L_1 - L(\text{NO ERRORS})]$$
- CUMULATIVE PHASE SLIP  $\psi_1 = \sum \Delta\psi_i$
- PHASE SHAKE = VARIATION IN CUMULATIVE PHASE SLIP

### TRAJECTORY ERROR EXAMPLE

- RANDOM 2% RMS FIELD ERROR

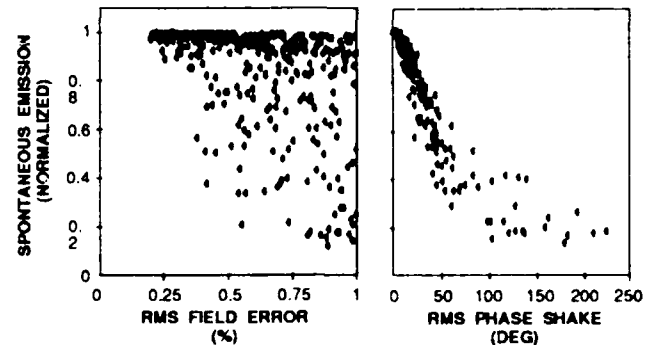


### 1-D FEL SIMULATION CODE

- COHERENT INTEGRATION OF OPTICAL EMISSION ALONG WIGGLER
- EVALUATE ON-AXIS QUANTITIES:
  - SPONTANEOUS EMISSION AT FIRST HARMONIC
  - OPTICAL SMALL SIGNAL GAIN
- SCAN SPECTRUM FOR PEAK VALUES
- FOR DETAILS SEE PAPER #P3.7 WEDNESDAY EVE (KENNEDY, *et al*)

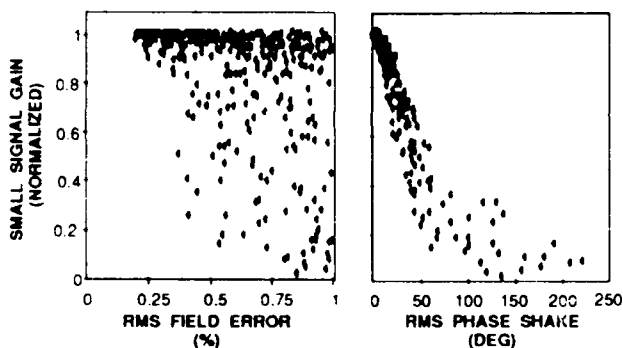
### ERROR / PERFORMANCE CORRELATION

- 400 RANDOM 84-PERIOD WIGGLERS



### ERROR / PERFORMANCE CORRELATION

- 400 RANDOM 84-PERIOD WIGGLERS

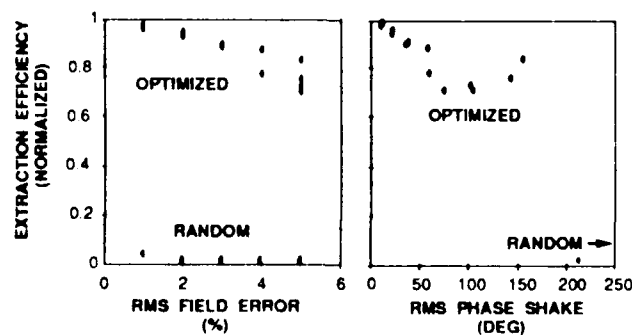


### 'FELOPT' - FEL SIMULATION CODE

- SOPHISTICATED 3-D SIMULATION
  - REALISTIC ELECTRON DISTRIBUTION
  - LORENTZ FORCE EQUATIONS FOR ELECTRON TRAJECTORIES
  - KROLL-MORTON-ROSENBLUTH EQUATIONS OF MOTION
  - PARAXIAL WAVE EQUATION FOR OPTICAL FIELD IN WIGGLER
- WIGGLER FIELD ERRORS ANALYZED USING KINCAID MODEL AS DEVELOPED BY ELLIOTT AND McVEY
- FOR DETAILS SEE PAPER #P2.25 TUESDAY EVE (COVER, *et al*)

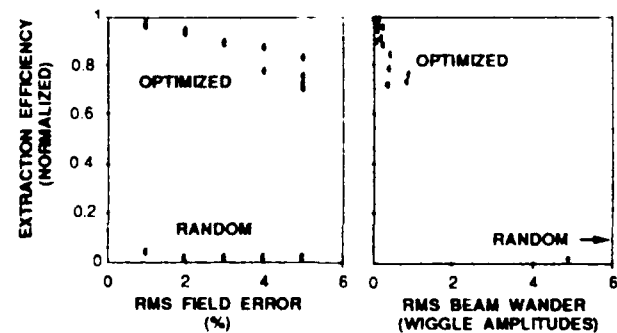
### ERROR / PERFORMANCE CORRELATION

- RANDOM AND OPTIMIZED 160-PERIOD TAPERED WIGGLERS



### ERROR / PERFORMANCE CORRELATION

- RANDOM AND OPTIMIZED 160-PERIOD TAPERED WIGGLERS



# UNI.5

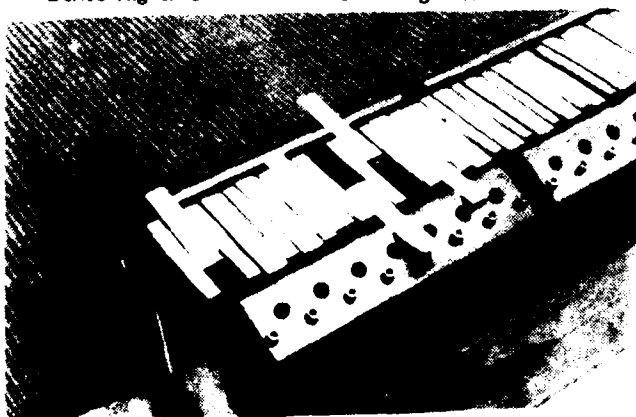
## Wiggler Error Reduction Through Shim Tuning

S.C. Gottschalk, D.C. Quimby, K.B. Robison, J.M. Slater  
Spectra Technology, Inc.  
2755 Northup Way  
Bellevue, Washington 98004-1495

A technique has been developed for reducing wiggler errors using shims placed on wiggler magnets. The measured shim fields are used by an optimization algorithm to determine the shim thicknesses. The RMS kick errors were reduced from 1.3% to 0.11% on a 50-cm test fixture.

### OVERVIEW

- Discuss Shims Placed Magnets With Uniform Dipole
  - Algorithm
  - Show results demonstrating correction to 0.1% from 1.3%
- Propose Placing Shims on Poles Instead of on Magnets
  - No need for external dipole
  - Shim by "inspection" without computer
- Discuss Transverse Dipole Shimming
- Derive Higher Order Moment Shimming Method

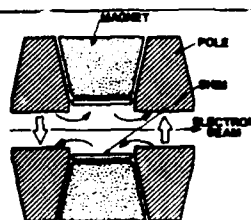


### SHIMMING PROCEDURE

- Measure Shim Field Signature
- Pre-Load Wiggler with Nominal Thickness Shims (e.g., 0.015")
- Measure Wiggler Field
- Use Optimizer to Find Shim Thicknesses
- Install Shims
- Re-Measure
- Repeat Thickness Calculation, if Needed

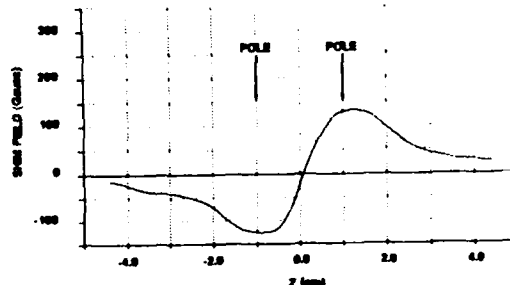
### FIELD SHIMMING CONCEPT

- Thin Iron Shims Placed Directly on Magnets
  - Reduces local field strength up to 1% rms
  - Shims produce no net steering
  - Self positioning, immediately changeable
- Shimming is Preferable Pole/Magnet Swapping
  - No movement of high-precision parts
  - Separation of magnet from pole errors is not required



### SHIM FIELD SIGNATURE

- Signature of 0.089 cm Thick Shim



- Measurements Show Simple Calibration of Shim Effect
  - Linear response with thickness
  - Additive with neighboring shim fields

### SHIMMING ALGORITHM

- Field is Addition of Effects of All Shims + Constant Steering. Spatial Frequency of Shim Field Allows all  $\lambda/2$  Integrals to be Corrected.
- Solve Using Constrained Optimization
 
$$M_{\text{tot}} = \int_{-L/2}^{L/2} dz \left[ \sum_{i=1}^N w_i (-1)^{i+1} B(z-z_i) + w_{N+1} + \text{err}(z) \right]$$

$$\min f(w_1, w_2, \dots, w_{N+1}) \text{ subject to constraints}$$

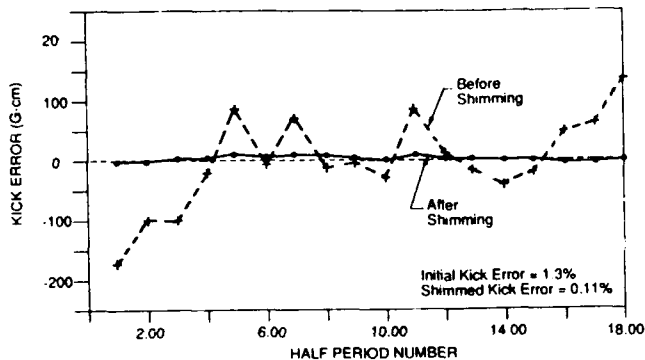
$$-L/2 \leq w_i \leq L/2 \quad i=1, \dots, N$$

$$-S \leq w_{N+1} \leq S$$

$$f(w) = \sum_{i=1}^K \text{err}_i^2 / K$$
- Method is Totally General. Any Target Function  $f(w)$  can be Minimized.

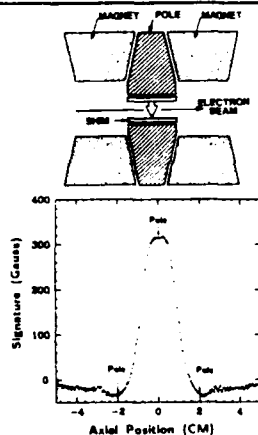


## STI SHIMMING DEMONSTRATES LOWEST WIGGLER ERRORS



## POLE SHIMS ELIMINATE NEED FOR EXTERNAL DIPOLE

- Pole Shims Adjust Local Gap



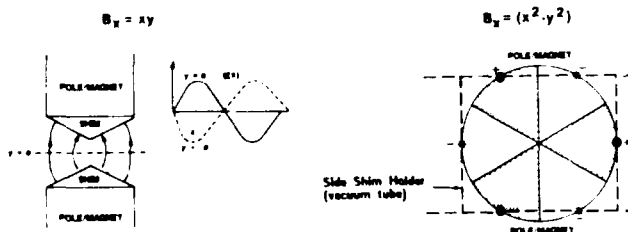
- Measured Signature Function is Very Narrow

- Large effect, 0.3%/mil. under pole
- Sidelobes < 10%

- Should be Able to Get to < 0.1% Error Without Computer. Better Still With a Computer

## HIGHER ORDER MOMENT SHIMMING

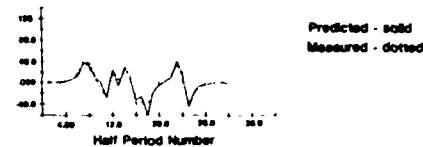
- Illustrate With Sextupole. Shims on Poles (Magnet case same principle)



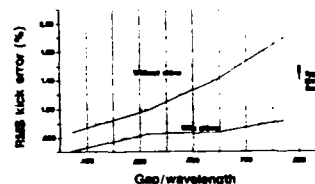
$$\begin{aligned} \langle D \rangle &= I_3 (h_w / \lambda) \cos(h_w z) \begin{cases} \cos 3\phi \\ \sin 3\phi \end{cases} \\ \langle D \rangle &= \text{const} @ \cos(h_w z) = \pm 1 \end{aligned}$$

## IMPROVED SHIMMING ON NISUS

- Predicted and Measured Shim Fields Agree to 0.09%. No Need to Iterate.

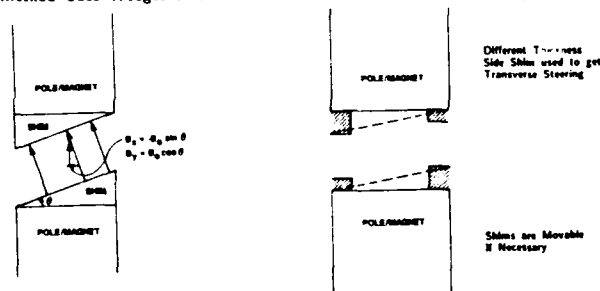


- Shim Reduces Gap Sensitivity of Field Errors



## TRANSVERSE DIPOLE CAN BE CORRECTED WITH SHIMS

- Transverse Errors can be as Large as Main Field Errors
- Method Uses Wedges to Affect a Local Rotation of Coordinator System



- Net Transverse Dipole With Pole Shims
- No Net Transverse Dipole With Magnet Shims

## CONCLUSIONS

- Shims on Magnets Have Demonstrated 0.1% Capability
- Shims on Poles Should Work as Well Without Need for External Corrector
- Long Correlation Length Errors Requires Tighter Control
  - Modify function being minimized
- Transverse Dipole Errors can be Corrected With Shims
- Method Found to Correct Higher Order Moment Errors as Well

# Dispersion Interference in the Pulsed Wire Measurement Method

O. Shahal  
N.R.C.- Negev, P.O.Box 9001, Beer-Sheva, Israel

B.V. Elkonin and J.S. Sokolowski  
Dept. of Nuclear Physics, The Weizmann Institute of Science, Rehovot, Israel

## Abstract

The magnetic profile of the wiggler to be used in the planned Weizmann Institute FEL has been measured using the pulsed wire method. The main transverse deflection pattern caused by an electrical current pulse in a wire placed along the wiggler was sometimes accompanied by minor faster and slower parasitic components. These components interfered with the main profile, resulting in distorted mapping of the wiggler magnetic field. Their periodical structure being very close to the main pattern could not be easily resolved by applying a numerical Fourier transform. A strong correlation between the wire tension and the amplitude of the parasitic patterns was found. Significant damping of these oscillations was achieved by applying high enough tension to the wire (close to the yield point), allowing to disregard their contribution to the measurement accuracy.

## Introduction

The pulsed wire magnetic profile measurements method which was first proposed by R.W. Warren [1] was applied for testing and adjustment of the TRW/Stanford wiggler [2]. This method enables measurements and adjustments of the magnetic profile in situ, it is very convenient for the conventional wigglers tests and becomes a real must for mapping of the electromagnetic pulsed wigglers.

## The Experimental Setup

The measuring setup was designed in such a way that it would allow for finding the best conditions for mapping and adjusting of the magnetic fields of our wiggler and also to enable us to investigate the behaviour of the system. The wiggler was 75 cm long, Halbach type ( $17 \times \lambda_w$ ,  $\lambda_w = 4.4 \text{ cm}$ ). In order to be able to observe the faster and slower components of the wire deflections we have chosen to use a 2.3 m long wire. Some measurements were performed with 5-wavelength wiggler or even 1-wavelength, in order to distinguish between the main pattern and the parasitic components.

The detection system used was similar to the one described in ref. [1,2].

## Results and Discussion

During the preparation and testing of the system for measuring and mapping of the wiggler magnetic field profile, we have encountered small amplitude oscillations which accompanied the main signal, quite often even quite distant from it. Thus, had we have used a short wire most probably we would not have realized the presence of these perturbations at all (see fig. 1).

The physical interpretation of these fast oscillations is not yet completely clear to us - we hope to reach full understanding of it after completion of these investigations.

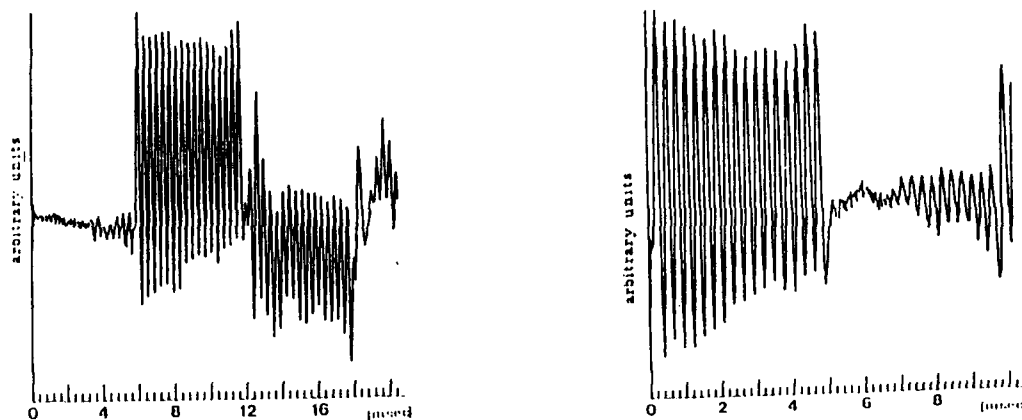


Fig. 1. The main full wiggler pattern ( $17 \lambda_w$ )

a) with its interference at  
 $1.6 \times 10^3 \text{ kg/cm}^2$  wire tension;

b) with its interference at  
 $3.1 \times 10^3 \text{ kg/cm}^2$  wire tension.

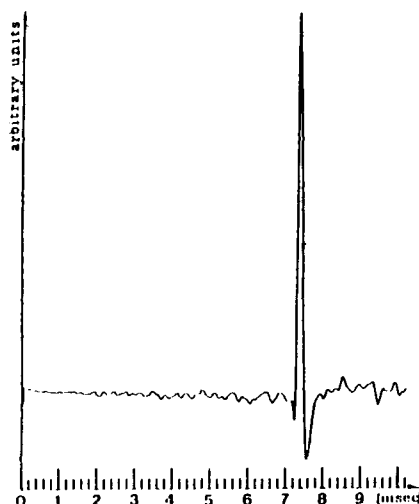


Fig. 3. The  $1\lambda$  pattern with interference  
at wire tension of  $4.7 \times 10^3 \text{ kg/cm}^2$ .

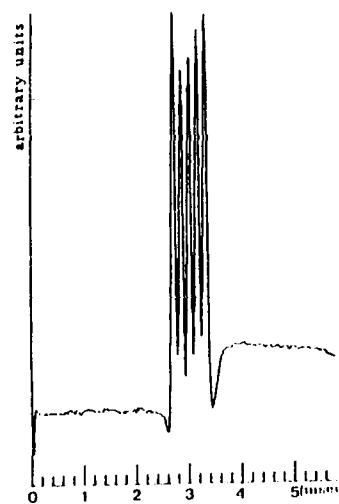


Fig. 4. The  $5\lambda_w$  main pattern at  
 $10.8 \times 10^3 \text{ kg/cm}^2$  wire tension.

The perturbation pattern seems to be rather continuous and does not resemble the basic main signal. This can be seen clearly in fig. 3.

Figure 4 (wire tension  $10.8 \times 10^3 \text{ kg/cm}^2$ ) shows that by increase of the wire tension one can decrease the amplitude of the parasitic signals very significantly.

### Conclusions

In spite of the perturbations described above this method is capable to give reliable, reproducible and accurate results. The necessary condition for this is relatively high tension of the wire (80% or more of the yield point for Be-Cu wire).

### References

1. R.W. Warren, Nucl. Instr. Meth. **A257**, (1988)257
2. O. Shahal and R. Rohatgi, Presented at the Tenth Intern. FEL Conference, Jerusalem, Israel. To be published in Nucl. Instr. Meth.
3. Harvey Fletcher, J. Acoust. Soc. of America **36** No.1, (1963)203.
4. E.R. Parker, "Materials Data Book" M Graw Hill, p.119, p.139.

## PR2.2 Status and Research Objectives of the Dutch Free Electron Laser for Infrared Experiments

P. W. van Amersfoort, R. W. B. Best, R. van Buuren, P. F. M. Delmee, B. Faatz,  
C. A. J. van der Geer, D. A. Jaroszynski, P. Manintveld, W. J. Mastop,  
B. J. H. Meddens, A. F. G. van der Meer, D. Oepts, J. Pluygers, and M.J. van der Wiel

*FOM-Institute for Plasma Physics 'Rijnhuizen', Association EURATOM-FOM,  
Edisonbaan 14, 3439 MN Nieuwegein, The Netherlands, Tel. 3402-31224*

We review the status and research objectives of the Free Electron Laser for Infrared Experiments (FELIX), which will be operated as a users facility for the far-infrared and microwave spectral regions. The spectral region between 8 and 80  $\mu\text{m}$  will be covered in the first stage of the project.

The accelerator for FELIX consists of a triode gun, a prebuncher, a travelling-wave buncher, and two travelling-wave linac sections. The beam can be bent into undulators at two locations: after the first (15-25 MeV) and after the second linac (25-45 MeV), see Fig. 1. In principle, two undulators can be placed at each location. By installing undulators with different periods this will, eventually, permit coverage of the wavelength range from 3 to roughly 300  $\mu\text{m}$ . Tuning will be achieved by varying the undulator gap width, rather than by varying the beam energy, so as to fulfil our first research objective, *rapid tunability*. We note that varying the energy would involve manipulation of a large number of bending and focusing elements.

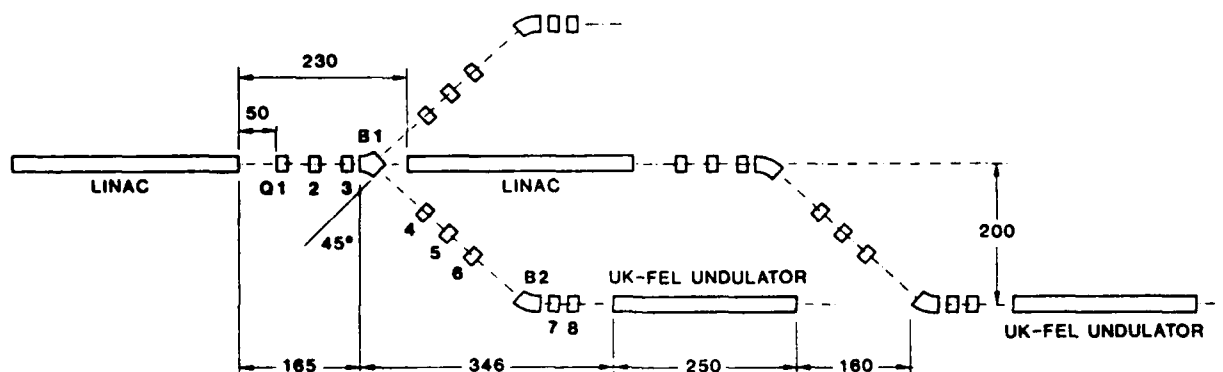


Figure 1. Basic layout of FELIX. Dimensions are in cm. In Stage I of the project, two sections of the UK-FEL undulator will be placed behind the first accelerating structure, and two sections will be placed behind the second structure. These cover the wavelength range from 5-30 and 17-80  $\mu\text{m}$ , respectively.

The design parameters for our accelerator are summarized in Table 1. The duration of the electron bunches emerging from the linac will be roughly 3 ps and thus, the duration of the optical pulse length

Table 1. Basic parameters for FELIX, Stage I.

$\gamma$	30-90	-	Lorentz factor
$\lambda_s$	5-80	$\mu\text{m}$	EM wavelength
$\lambda_u$	65	mm	Undulator period
B	< 4400	G	Peak undulator field on axis
N	38	-	Number of undulator periods
K	< 1.9	-	Undulator strength
$L_u$	247	cm	Undulator length
Q	194	pC	Charge per microbunch
I	70	A	Peak current
i	0.2	A	Average current during macropulse
$t_\mu$	3	ps	Micropulse length
$f_\mu$	1	GHz	Micropulse repetition frequency
$t_m$	20	$\mu\text{s}$	Macropulse length
$f_m$	10	Hz	Macropulse repetition frequency
$R_{x,y}$	1	mm	Rms electron beam radius
$\Delta_z$	2	mm	Rms microbunch length
$\sigma_e$	0.35	%	Energy spread
$\epsilon_n$	50	$\pi$ mm mrad	Normalized rms emittance

will also be in the ps-range. This fulfils our second objective, *the production of short pulses of IR radiation*. These have application in studies of lifetimes and relaxation phenomena. Simulations have shown that, by desynchronising the electron bunches and the optical pulses, the pulse length can be varied over nearly an order of magnitude.

Our third research objective is to obtain *narrow-band radiation*. This will be achieved via phase locking of the micropulses by means of an intracavity etalon, combined with external selection of a single cavity mode. This technique is only effective when there are a large number of circulating pulses in the cavity. For our microbunch repetition rate of 1 GHz, achieved by modulating the grid voltage of the electron gun, there are 40 circulating pulses.

During the past half year we have made an inquiry among potential users of FELIX, with the aim of collecting research proposals and making an inventory of user requirements. So far, fourteen proposals have been received, twelve on physics and two on chemistry. The proposals can be crudely categorized in (1) spectroscopy of adsorbed species, (2) semiconductor spectroscopy (3) reactive collisions in molecular beams, (4) ablation of biological material, and (5) FEL physics.

The status of the main components is as follows. Delivery of the electron gun (Hermosa Electronics), the bunching system (Interatom) and the accelerating sections (CGR-MeV) is expected in the fall of 1989. The 20-MW klystron (Thomson-CSF) powering the buncher and the accelerating sections has been delivered. The UK-FEL undulator has been shipped from East-Kilbride to Daresbury where it is being overhauled. The vault in which FELIX is to be placed is under construction and will be available by December 1989. Prior to that date, performance tests of the electron gun and the prebuncher will be done in the existing building.

**A MICROWIGGLER FREE-ELECTRON LASER  
AT THE BROOKHAVEN  
ACCELERATOR TEST FACILITY**

**K. Batchelor, I. Ben-Zvi, R. Fernow, J. Gallardo,  
H. Kirk, C. Pellegrini, A. van Steenbergen**

**Brookhaven National Laboratory  
Upton, New York 11973  
Tel. (516)282-3523, Fax. (516)282-3000**

**and**

**A. Blawie**

**Rockwell International /Rocketdyne Division  
6633 Canoga Avenue, MS/FA40  
Canoga Park, CA 91303**

**ABSTRACT**

We report the design and status of an FEL experiment at the Brookhaven National Laboratory Accelerator Test Facility. A 50 MeV high brightness electron beam will be utilized for an oscillator experiment in the visible wavelength region. The microwiggler to be used is a superferric planar undulator with a 0.88 cm period, 60 cm length and  $K = 0.35$ . The optical cavity is a 368 cm long stable resonator with broadband dielectric coated mirrors.

**BNL ATF**

**EXPERIMENTS**

- \* 50 MeV electron linac.
- \* Laser photocathode rf electron gun.
- \* Peak current 100A, 6ps pulse width.
- \*  $\epsilon_n \sim 6$  mm mrad.
- \* Energy spread  $3 \cdot 10^{-3}$ .
- \* e bunch separation 12.5ns.
- \* Measure FEL performance.
- \* Wide band tunability.
- \* Chirping for pulse compression.
- \* Shorter wavelength (higher energy / shorter  $\lambda_w$ ).
- \* Tapered microwiggler.
- \* Optical klystron.

## THE DESIGN PRINCIPLES

- \* Given the line emittance, we determine the shortest practical FEL wavelength  $\lambda$  given by:

$$\lambda \sim 2\pi e$$

- \* Given the line energy  $\gamma$  and the FEL wavelength, we have determined the undulator wavelength:

$$\lambda_u \sim 2\gamma^2\lambda$$

- \* Given the line energy spread, we determine the maximum wiggler length  $L_u \sim N_u \lambda_u$ :

$$N_u \sim \frac{\gamma}{2\delta\gamma}$$

- \* Given a minimum desired small signal gain  $G$ , we determine the wiggler magnetic field  $B$ :

$$B \sim \frac{218}{L_u} \sqrt{\lambda G/I}$$

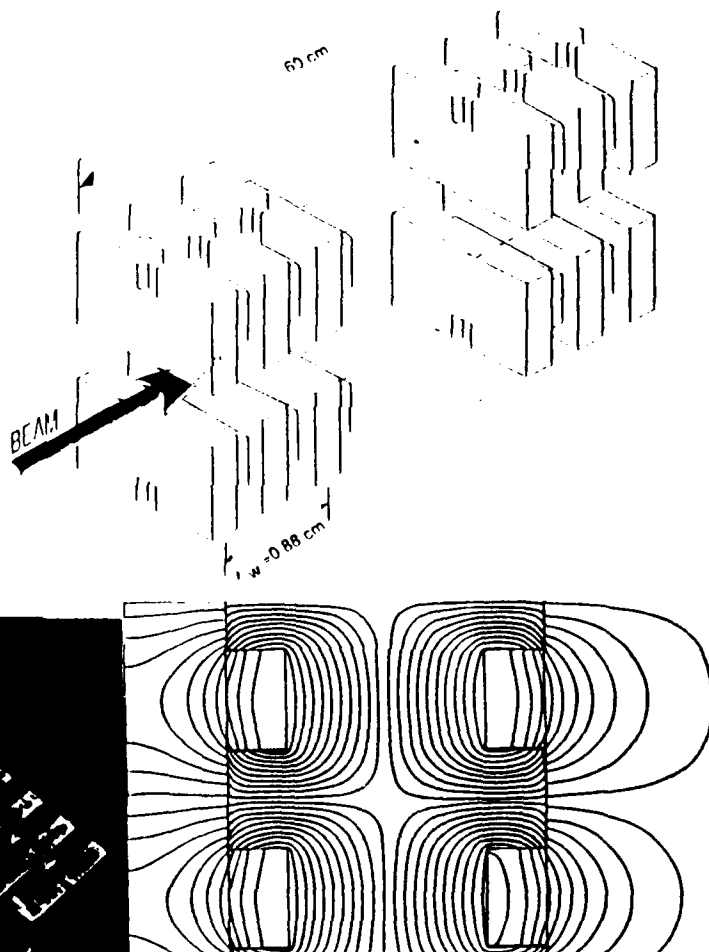
## THE MICROWIGGLER

- \* Microw wigglers ( $\lambda_u < 1\text{cm}$ ) can be readily made with electromagnets.
- \* The wiggler current adjustment is a convenient way to tune the wavelength.
- \* Series connected electromagnet wigglers can be made with high precision.
- \* Using a superconducting winding and a ferromagnetic yoke produces an attractive an.
- \* A superferric wiggler produces a stable field.
- \* This technology can be extended to shorter  $\lambda_u$ .



## THE RESONATOR

- \*  $\lambda = 470\text{nm}$ .
- \* Resonator length = 367.75cm.
- \* Mirror radius of curvature = 185.75cm.
- \* Beam waist = 0.016cm.
- \* Outcoupling fraction 5% (10%)
- \* Circulating power 216.5MW (115.0MW)
- \* Intensity at mirror 5.15MW/cm<sup>2</sup> (2.64MW/cm<sup>2</sup>)
- \* Peak output power 11MW



## P2.1

### Numerical Treatment Of Electron Trajectory Straightener Issues In Free-Electron Lasers

D.C. Quimby  
Spectra Technology, Inc.  
Bellevue, Washington

C.J. Elliott  
Los Alamos National Laboratory  
Los Alamos, New Mexico

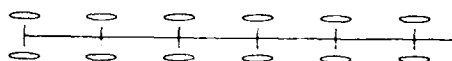
Requirements for e-beam trajectory alignment are examined for short-wavelength, high-efficiency FELs. Three-dimensional modeling is used to examine the sensitivity to e-beam wander resulting from wiggler field errors and inaccuracies in trajectory correction schemes. The performance of various geometric arrangements of trajectory diagnostics and correction coils is compared.

#### INTRODUCTION

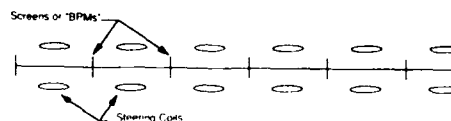
- Intra-Undulator E-Beam Position Diagnostics and Steering Coils are Often Required to Correct Trajectory Wander
- Examine Tradeoffs in Required Level of Undulator Field Errors and the Accuracy and Number of Trajectory Straighteners
- Compare Performance of Various Geometric Arrangements

#### NISUS UNDULATOR HAS DIFFERENT GEOMETRIC ARRANGEMENT FOR E-BEAM TRAJECTORY STRAIGHTENERS

Coincident or "THUNDER-type"

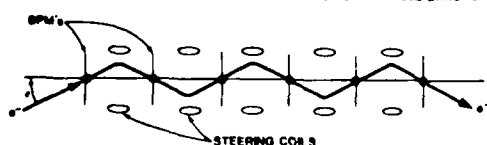


Alternating or "NISUS-type"

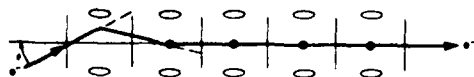


#### STRATEGY DEVELOPED FOR DAMPING ANGLE ERRORS IN ALTERNATING CONFIGURATION

- FORCING BEAM ON-AXIS AT EACH BPM DOES NOT DAMP ANGLE ERRORS

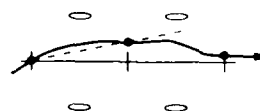


- ANGLE ERROR DAMPED BY IMAGING BEAM ONTO AXIS AT NEXT STEERING COIL

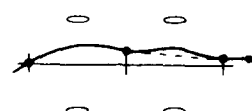


#### SEVERAL METHODS FOR ESTIMATING E-BEAM POSITION AT NEXT COIL HAVE BEEN EXAMINED

(a) EXTRAPOLATION



(b) INTERPOLATION



- Interpolation Gives Reasonable Correction for Range of Possible Steering Errors
- To Date Have Only Considered Simple Schemes Not Requiring Computer Optimization

This work was support in part by the U.S. Army Strategic Defense Command through Boeing Aerospace contracts HB1260 and HD4785.

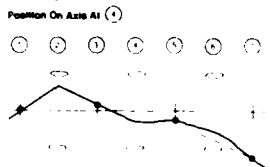


## MULTIPLE ITERATIONS MAY BE USEFUL

(1) Initial Random Trajectory

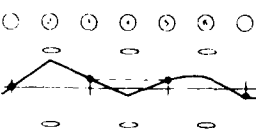


(2) Steer At (2) To Put Apparent e-Beam



(3) Steer At (4) To Put Apparent e-Beam

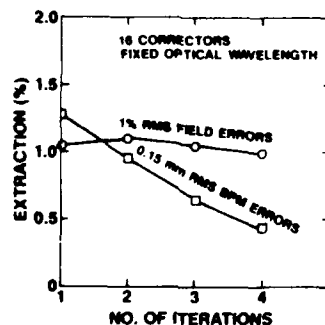
Position On Axis At (2)



(4) At This Point The Interpolated Position

Of The e-Beam At (2) Is No Longer On Axis. If Desired, One Can Repeat Steps (2) & (3) In An Iterative Manner

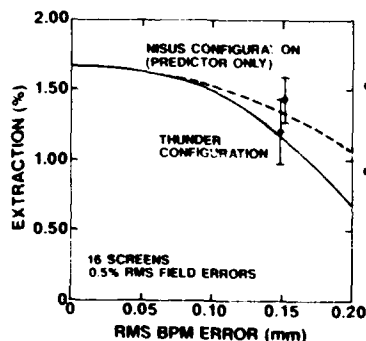
## OPTIMUM NUMBER OF ITERATIONS DEPENDS ON WHETHER FIELD ERRORS OR BPM ERRORS DOMINATE



- Fewest Number of Iterations Best When BPM Errors; Want to "Correct" These Fluctuating Trajectory Errors as Little as Possible

- Many Iterations Undesirable Because of Tendency Toward Oscillatory Steering

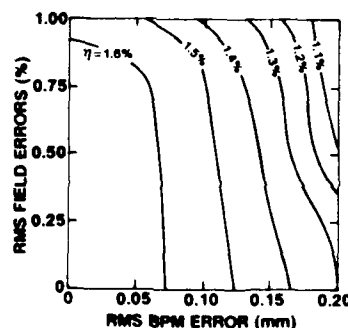
## NISUS-TYPE GEOMETRY LESS SENSITIVE TO BPM ERRORS



- Curves Based on One Sample Random Distribution of Errors

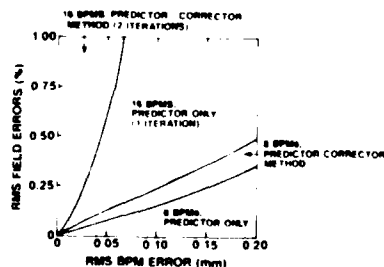
- Error Bars Denote One Standard Deviation for 8 Trial Random Distributions

## CONTOUR PLOT OF EXTRACTION ASSUMING BEST POSSIBLE STRATEGY USED IN EACH REGIME



16 BPMs AVAILABLE

## OPTION MAP SHOWS WHICH STRATEGY WORKS BEST DEPENDING ON LEVEL OF FIELD ERRORS AND BPM ERRORS



- When Field Errors are Small, the Impact of BPM Errors may be Reduced by Deactivating Every Other BPM

## CONCLUSIONS

- Alternating BPM/Corrector Geometry has Reduced Sensitivity to BPM Errors
- Undamped Angle Errors Can Be Readily Avoided
- Applicability of Model Has Been Illustrated by Quantifying the Required Number and Accuracy of E-beam Trajectory Diagnostics in the NISUS System

## P2.3

### The Hybrid Undulator for the NIST-NRL Free-Electron Laser

Ronald G. Johnson, David L. Mohr, and Mark A. Wilson  
National Institute of Standards and Technology  
Gaithersburg, MD 20899

Samuel Penner  
10500 Pine Haven Terrace  
Rockville, MD 20852

Francis C. Younger, Brian Ng, and Kenneth M. Thomas  
Brobeck Division, Maxwell Laboratories, Inc.  
1235 Tenth Street  
Berkeley, CA 94710

The NIST-NRL FEL will use a 3.64-m hybrid undulator that is being constructed at Brobeck Division of Maxwell Laboratories. Constructed of SmCo magnets and vanadium permendur pole pieces, the undulator has a period of 2.8 cm, a variable gap with a 1.0-cm minimum, and a peak magnetic field of 0.54 T.

Supported by the US SDIO through ONR Contract No. N00014-87-F-0066.

#### Undulator Design

- Hybrid undulator (SmCo permanent magnets; vanadium permendur poles)
- Number of periods - 130
- Period length - 2.8 cm
- Total length - 3.64 m
- Maximum magnetic field - 0.54 T
- Minimum gap - 1.0 cm
- Vacuum chamber aperture - 0.86 cm (vertical)  
1.6 cm (horizontal)
- Operation in full or half-length mode

Table 1. Parameters and dimensions of the magnetic design.

Peak field (T)	0.54
Minimum gap (mm)	10.0
Period (mm)	28.0
Pole width, Wp (mm)	5.0
Pole height, Hp (mm)	33.0
Pole length, Lp (mm)	50.0
Magnet width, Wm (mm)	9.0
Magnet height, Hm (mm)	40.0
Magnet length, Lm (mm)	60.0

• Permanent magnets are formed from two blocks each 30 mm in length.

#### Magnetic Design

- Dimensions of magnets and poles determined by the two-dimensional code POISSON. (Dimensions shown in Table 1)
- Dimensions re-calculated using a three-dimensional code. (Slightly smaller dimensions meet specifications)
- Full-scale, one-period models constructed and tested. (Confirms calculations)
- Conservative design selected. (Provides greater margin, especially for the peak field)
- Model test results shown in Table 2 and Figure 1.
- Steps undertaken to control magnetic field errors.
  1. Stringent magnetic and mechanical tolerances on permanent magnet blocks.
  2. Error minimization by sorting magnet blocks.
  3. Limiting deflections of the magnetic structure.
  4. Tight mechanical tolerances on pole pieces and holders.

Table 2. Specifications for the undulator magnetic field and model results.

	Specifications	Model Results
Peak Field (kG)	5.4	5.65
Maximum 3rd harmonic	10%	3.2%
5th harmonic	-	0.5%
7th harmonic	-	0.2%
Limit on transverse field variation (central 1.0 cm)	0.5%	0.3%
RMS error (G)	27	-
Vertical field integral error (G-cm)	23	-
Horizontal field integral error (G-cm)	23	-

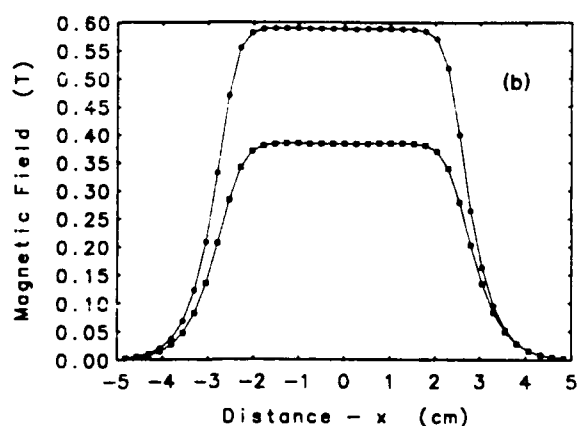
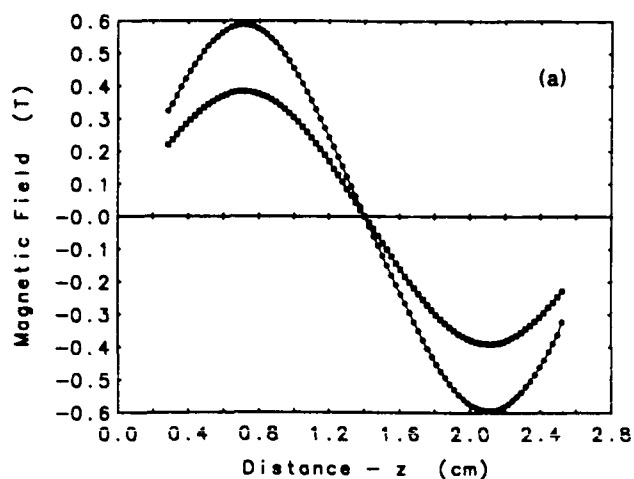


Fig. 1 Test results for the full-scale, one-period model of the magnetic structure. (a) Magnetic field along the axis. (b) Magnetic field transverse to the axis.

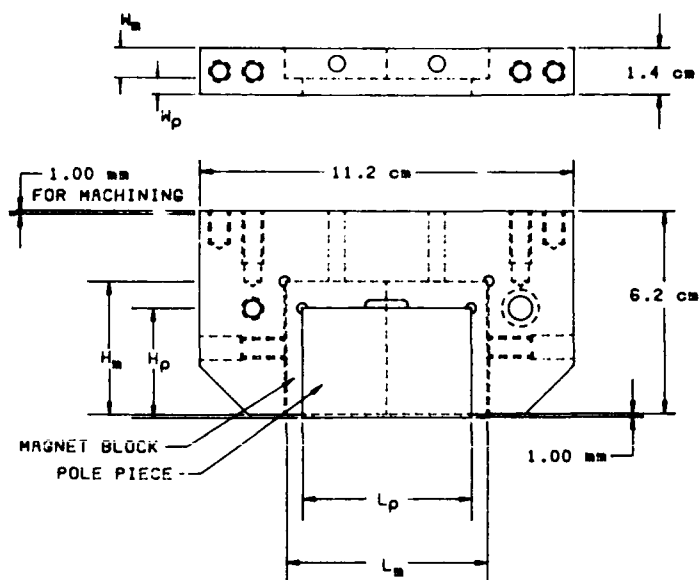


Fig. 3 Half-period magnet assembly.

## Mechanical Design

- Detailed mechanical structure is shown in Figure 2.

1. Sub-base
2. Half-length base
3. C-frame
4. Steel I-beam
5. Magnet assemblies
6. Gap adjustment mechanism
7. Air spring
8. Gap opening sensor
9. Vacuum chamber

- A half-period magnet assembly is shown in Figure 3.

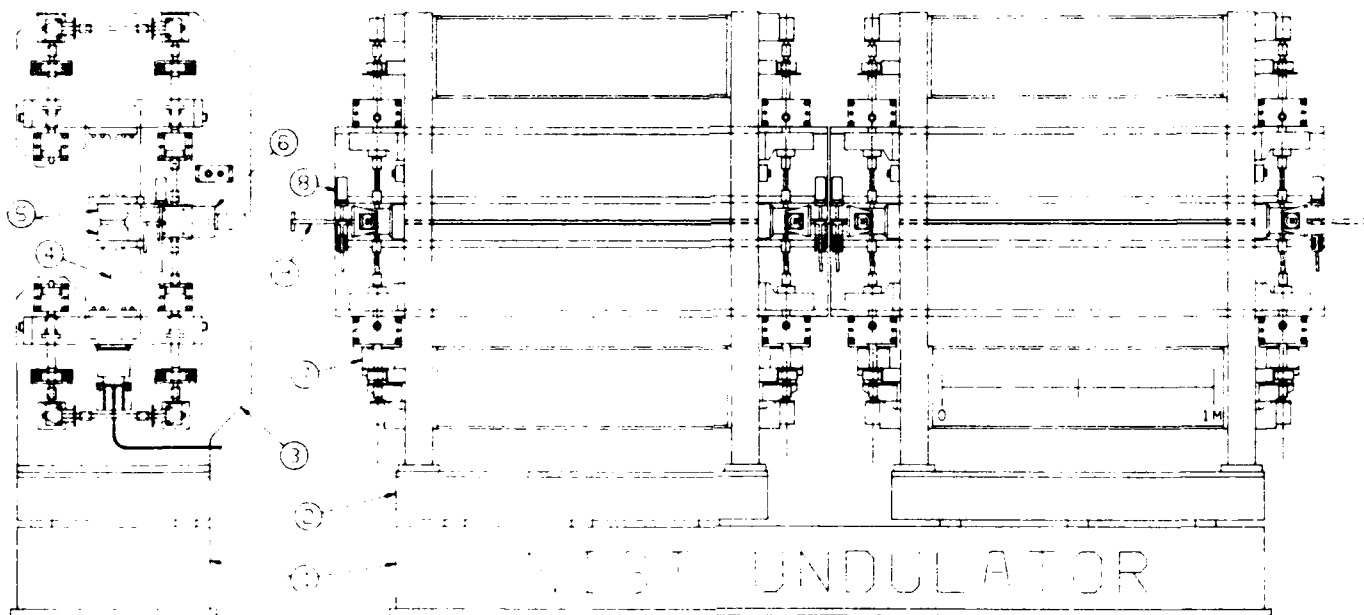


Fig. 2 Detailed mechanical structure of the undulator.

## P2.4

### INEX Simulations of the Los Alamos HIBAF Free-Electron Laser MOPA Experiment

John C. Goldstein, Bruce E. Carlsten, and Brian D. McVey

Group X-1, MS E531  
Los Alamos National Laboratory  
Los Alamos, NM 87545  
U. S. A.

We present results of Integrated Numerical Experiment (INEX) simulations of the performance of a 1-m oscillator driving a 2-m Rocketdyne amplifier for the new HIBAF (High Brightness Accelerator Free-Electron Laser) facility at Los Alamos. INEX simulations utilize a numerically-generated electron micropulse, from ISIS/PARMELA calculations of the photoinjector/linac/beam transport system in the 3-D FEL simulation code FELEX.

#### Introduction.

- A new free-electron laser facility, called HIBAF for High Brightness Accelerator Free-Electron Laser, is being constructed at Los Alamos.
- HIBAF will consist of a 40 MeV rf-linac with a photocathode injector, a 1-m-wiggler FEL oscillator, and a 2-m-wiggler FEL amplifier. The amplifier wiggler is being constructed, and will be supplied to Los Alamos, by Rocketdyne.
- This paper presents results of Integrated Numerical Experiment (INEX) simulations of the performance of the HIBAF Master Oscillator Power Amplifier (MOPA) FEL system. INEX consists of using the electron micropulse, generated from simulation of the accelerator system with the code PARMELA, in the FEL simulation code FELEX to calculate laser performance.

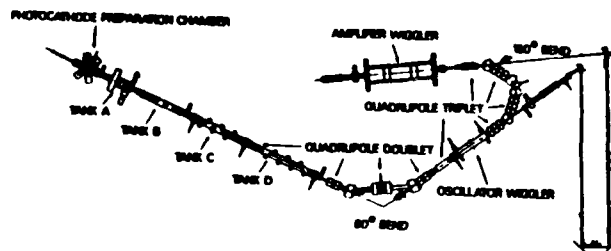
#### INEX simulations of free-electron laser performance.

- The HIBAF photoinjector/rf-linac/electron-beam transport system was designed with the code PARMELA which was used to simulate the performance of the entire beamline.
- INEX simulations use the numerically-generated electron-beam micropulse from PARMELA in the 3-D FEL simulation code FELEX to study the performance of the FEL MOPA system. In particular, the electron micropulse is propagated by PARMELA up to the entrance of the oscillator's 1-m wiggler where it is transferred to FELEX to be used in oscillator performance simulations.
- We have extended the INEX method to include returning the electron micropulse to PARMELA after a steady-state is reached in the FELEX oscillator simulation. The micropulse typically has been changed (the energy spread has been increased) due to its interaction with light in the oscillator. PARMELA is used to propagate the micropulse through the 150-degree bend magnet and focus it into the 2-m Rocketdyne wiggler. The electron pulse is then handed back to FELEX to simulate the performance of the FEL amplifier.

Los Alamos

Los Alamos

#### INEX modeling of HIBAF.



PARMELA

FELEX

Optical beam :

Los Alamos

#### HIBAF FEL components.

- The optical resonator is designed for an optical wavelength of  $3 \mu\text{m}$ . It will consist of two  $\text{CaF}_2$  mirrors of radii of curvature of 3 and 4 meters separated by about 6.93 m. Each mirror has a maximum reflectivity of about 99 % at  $3 \mu\text{m}$ . The lowest-order Gaussian mode has a Rayleigh range of 37 cm and is focused at the center of the wiggler. Relay optics will transport the light from the oscillator to the amplifier.
- The wiggler used in the oscillator will be 1-m long. Two possible choices are contemplated: (1) an untapered wiggler with  $B_w = 3214$  Gauss,  $\lambda_w = 2.73$  cm, thus giving  $a_w = 0.8184$ ; and (2) a 30 % parabolically-tapered ( $\ln k_w$ ) wiggler.
- The 2-m amplifier wiggler will be constructed and supplied by Rocketdyne. It will have a fixed wavelength of  $\lambda_w = 2.4$  cm but will have a variable gap to adjust the magnetic field strength. As an untapered wiggler, a full gap of about 1 cm will produce a magnetic field strength of  $B_w = 4548.7$  Gauss, thus giving  $a_w = 1$ . This wiggler can be linearly tapered in  $B_w$  by opening up the gap at the exit end; more complicated tapers, such as a parabolic taper, are not possible with this device.

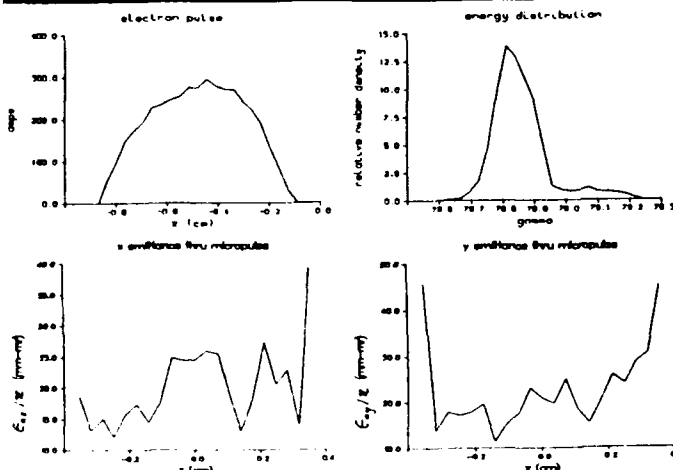
Los Alamos

## The sensitivity of amplifier performance to the oscillator-induced energy spread depends upon the wiggler configuration.

- For the 2-m Rocketdyne wiggler in an untapered configuration, we have found that the small-signal gain decreases by about a factor of two for an increase by a factor of two (from 0.25 % to 0.5 %) of energy spread.
- For the 2-m Rocketdyne wiggler with a 6 % taper in  $B_w$ , we have found that, with an incident optical power of 9.2 MW, the amplifier's gain and extraction efficiency drop by about a factor of two when the electron-beam energy spread increases by a factor of four (from 0.25 % to 1 %).
- Hence, the oscillator must be operated so as to increase the original electron-beam energy spread by about a factor of 2 to 6 (up to about 0.5% to 1.5 %). This clearly limits the power of the oscillator to quite low values, and it is hard to drive even a very modestly tapered wiggler to design performance with such meager input. This is particularly true since the Rocketdyne wiggler can only be linearly tapered. Note also that the tolerances estimated for allowable induced energy spread depend upon the shape of the induced energy spread; that is, the effect of increasing the rms energy spread by a factor of four will differ for distributions of different shape having the same rms spread.

Los Alamos

## Electron micropulse characteristics from PARMELA simulation.



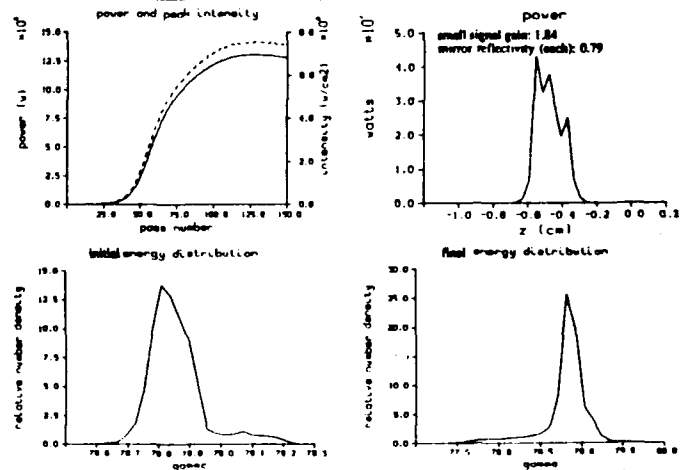
Los Alamos

## Controlling the oscillator operating power level.

- The calculated maximum small-signal gain of the oscillator with the uniform wiggler is about 550 %. Since the cavity losses are expected to be only about 2 %, this device will saturate at a very high optical intensity and induce an unacceptably large energy spread on the electron beam.
- The oscillator can be operated at low power by (a) reducing the small-signal gain and (b) increasing the cavity losses.
- A combination of methods can be used to control the oscillator:
  - The gain can be reduced by:
    - defocusing the electron-beam in the wiggler.
    - using a Littrow grating to tune the laser wavelength over the gain curve.
    - adjusting the cavity length for operation on the wing length tuning curve.
  - The cavity losses can be increased by adjusting the electron-beam energy so that the resonant wavelength falls in the lower reflectivity (higher transmission) region of the mirrors.
  - A combination of all of these methods can be used to produce stable oscillator operation at low power.

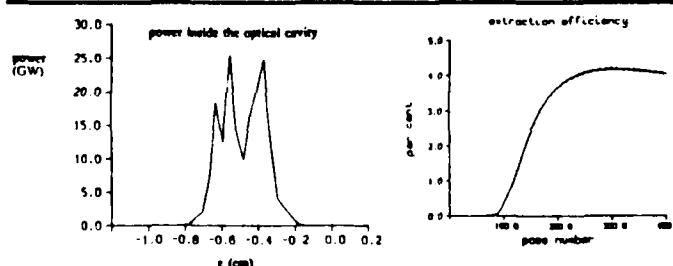
Los Alamos

## INEX results for the oscillator with a defocused electron beam.



Los Alamos

## INEX results for a high-power oscillator using the 1-m 30 % parabolically-tapered wiggler and the electron micropulse from PARMELA properly matched to the wiggler.



This simulation had 4 % total cavity loss and used the same near-concentric two-mirror resonator as the SAMOPA simulations. This will not be possible as the optical intensity on the mirrors will be exceeded; hence, a more complicated ring resonator will be required for high-power oscillator experiments in HIBAF.

Los Alamos

## Summary and conclusions.

- A new FEL facility named HIBAF is being built at Los Alamos. Among the various kinds of experiments planned are SAMOPA studies with a low-power oscillator and a 2-m amplifier wiggler to be supplied by Rocketdyne. High-power oscillator experiments are also planned; all of the FELs will operate at an optical wavelength of 3  $\mu$ m.
- We have studied various methods of operating the oscillator at low power so as not to unduly perturb the electron beam sent on to the amplifier. Defocusing the electrons in the oscillator's wiggler looks promising.
- We have studied the performance of HIBAF using INEX, and have extended INEX to include repeated exchanges of electron micropulses between the accelerator simulation code PARMELA and the FEL simulation code FELEX for the SAMOPA studies.
- The numerical simulations show that very large small-signal gain (>3000) is possible in the 2-m Rocketdyne amplifier wiggler if it is untapered; with a modest taper (6 %), gains of about 15 with 0.6 % extraction efficiency should be possible using the output from the low-power oscillator.
- A high-power oscillator needs a ring resonator and should be able to attain 20 GW power levels inside the cavity and 4 % extraction efficiency with a 1-m parabolically tapered wiggler.

Los Alamos

## P2.5

### Beam Profile and Position Diagnostic in the Advanced Test Accelerator (ATA) PALADIN FEL Experiment\*

Y. P. Chong, P. Lee,<sup>†</sup> T. J. Orzechowski, J. L. Miller, and J. T. Weir

Lawrence Livermore National Laboratory  
University of California, Livermore, California 94550

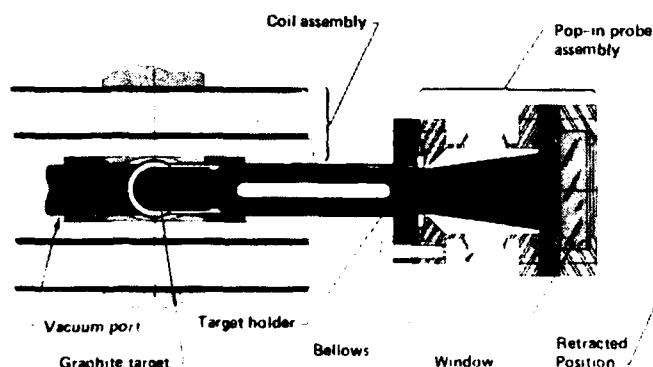
Performance of a free-electron laser is strongly dependent on the beam trajectory through the wiggler. A mismatched beam undergoing betatron oscillation through the wiggler results in reduced optical signal from the FEL. In order to monitor the electron beam in the PALADIN wiggler, we have designed an optical viewing probe to intercept the electron beam along its trajectory through the wiggler. Because access to the beam tube is severely restricted by the wiggler magnet poles, special care is required to produce a compact probe which does not perturb the wiggler magnet.

The 45-MeV electron beam, in the PALADIN wiggler, has a betatron wavelength of about 9 m. In order to measure the beam trajectory as carefully as possible and to help match the beam into the wiggler, we placed the probes every 1 to 1.5 m along the length of the 25-m-long wiggler. Thus, we had about six probes per betatron wavelength. We have observed both  $m = 1$  and  $m = 2$  oscillations of the electron beam.

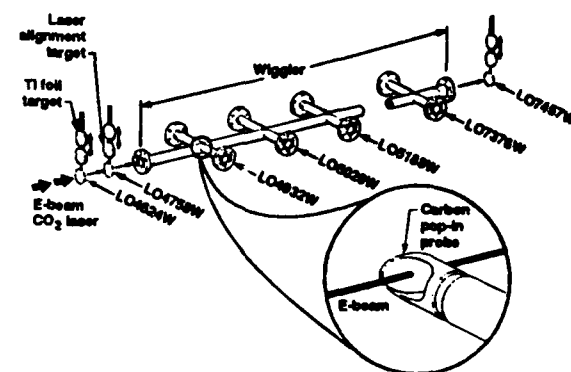
\* Work performed under the auspices of the US Department of Energy by the Lawrence Livermore National Laboratory under W-7405-ENG-48.

<sup>†</sup> General Atomics, San Diego, CA

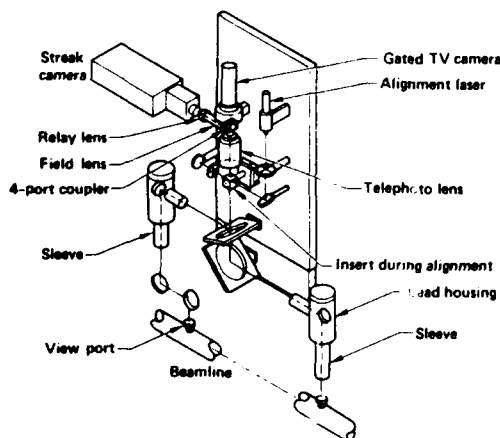
#### PALADIN Wiggler Diagnostics – "Pop-In Probe"



#### PALADIN wiggler optical lines of sight



#### Dual LOS arrangement with dual detectors – streak and gated TV camera



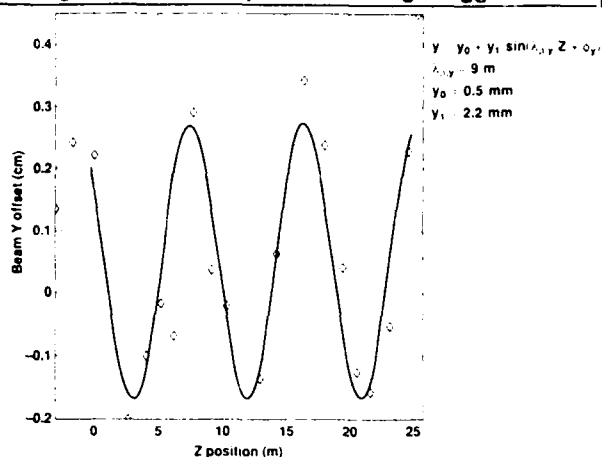
#### Beam transport through the wiggler is consistent with transport design

The PALADIN wiggler is designed to give equal focusing in the vertical and horizontal directions with

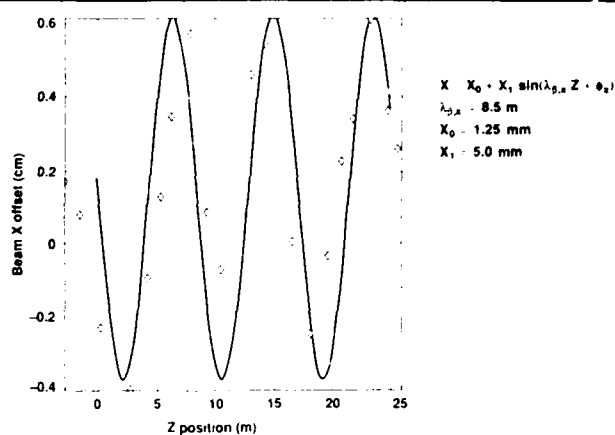
$$k_{\perp L} = \frac{eB_w}{2\gamma mc}$$

With a beam energy of 45 MeV ( $\gamma = 88$ ) and a wiggler field of 1.90 kG, we expect a betatron wavelength of 10 m. We have measured a betatron wavelength of 8.5 to 9 m.

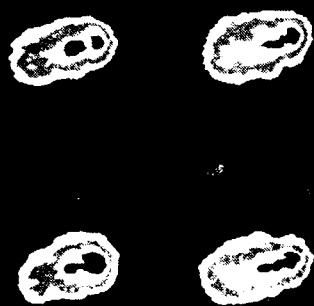
Average vertical beam position through wiggler



Average horizontal beam position through wiggler

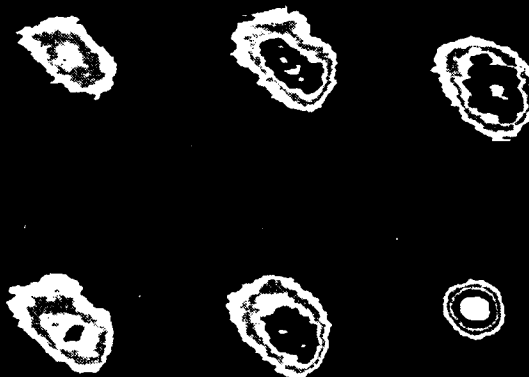


PALADIN Beam  $m=2$  oscillation  
Elongated in the Horizontal Plane



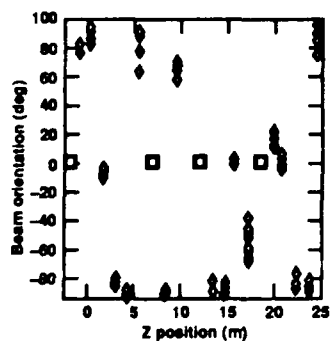
R9040A0B.RAS PIP 5188

PALADIN Beam  $m=2$  oscillation  
Elongated in the Vertical Plane  
1.5 Meters Downstream



R9040A0C.RAS PIP 5328

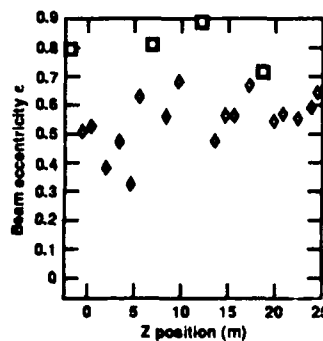
PALADIN IV beam shows  $m = 2$  oscillations  
in wiggler transport



Run Feb. 9, 1989  
Popin probe data

I  
E  
B<sub>w</sub>

PALADIN IV beam shape oscillation through wiggler



Run Feb. 9, 1989  
Popin probe data

I = 600 A  
E = 45 MeV  
B<sub>w</sub> = 1.9 kG

## P2.7

# "PAPA - A Particle Tracing Code in PASCAL"

Eltjo H. Haselhoff

Gerard J. Ernst

Nederlands Centrum voor Laser Research

P.O. Box 2662

7500 CR Enschede

The Netherlands

## Introduction

PAPA is a new PArticle tracing code in PAscal, developed at NCLR, the Dutch Center for Laser Research.

Keywords for the PAPA program are:

- o Modern, Clear and Consistent Programming Style
- o Accessibility for other users
- o Modular Setup - Flexibility
- o Ease in use
- o Good Documentation
- o PASCAL Compatibility

The current version of PAPA offers a solid base for a new, modern and convenient particle tracing code, to be used for simulations of all kinds of linear accelerator applications, including photo cathode injectors. It is intended to be a public domain code.

## Program Setup and Structure

Figure 1 shows a schematic picture of the program's hierarchy.

To achieve a good compatibility of the PASCAL source, we only used standard Pascal statements. This approach unfortunately cancels much of the power and charm of modern compilers. The action taken by PAPA is therefore restricted to the creation of an ASCII output file, which can be processed by arbitrary other routines. Currently we do the graphics on an IBM PC, using fast and convenient routines we wrote in Turbo Pascal. In the future we will probably also create C-versions in a UNIX environment, for use on a DECStation 3100. A fancy option is the creation of a red/green picture, which allows the user to see a stereoscopic 3D-view of the particle dynamics.

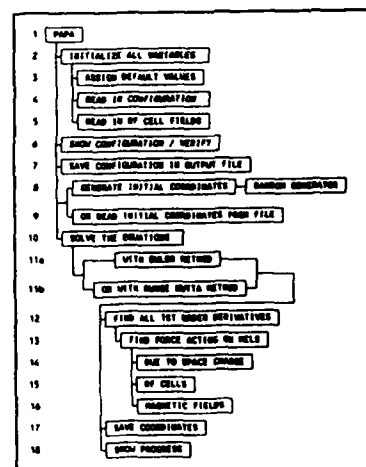


Figure 1. A simple sketch of PAPA's hierarchy.



## Mathematical Model

In the PAPA code, an electron pulse is represented by a limited number of uniformly charged, rigid but transparent clouds, called mels ('macro electron'). They have a spherical shape in the lab frame. Mels appeared to be a successful solution to the 'particle collision problem', since the repelling forces between them reduce to zero when they approach each other closely, see figure 2. Their radius is recalculated continuously, to prevent a limitation of the force interactions.

The equations of motion of  $N$  mels can be written as a set of  $6N$  first order DE's, which is solved in this general form, by either an Euler or a 4th order Runge Kutta routine. PAPA simulations showed that using the Runge Kutta routine in stead of the Euler routine allows a more than forty times larger step size, which results in a more than ten times faster speed, compared to many other particle tracing codes. The modular setup of PAPA allows very easy addition of other numerical routines.

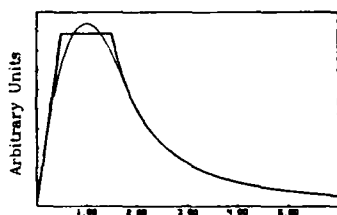
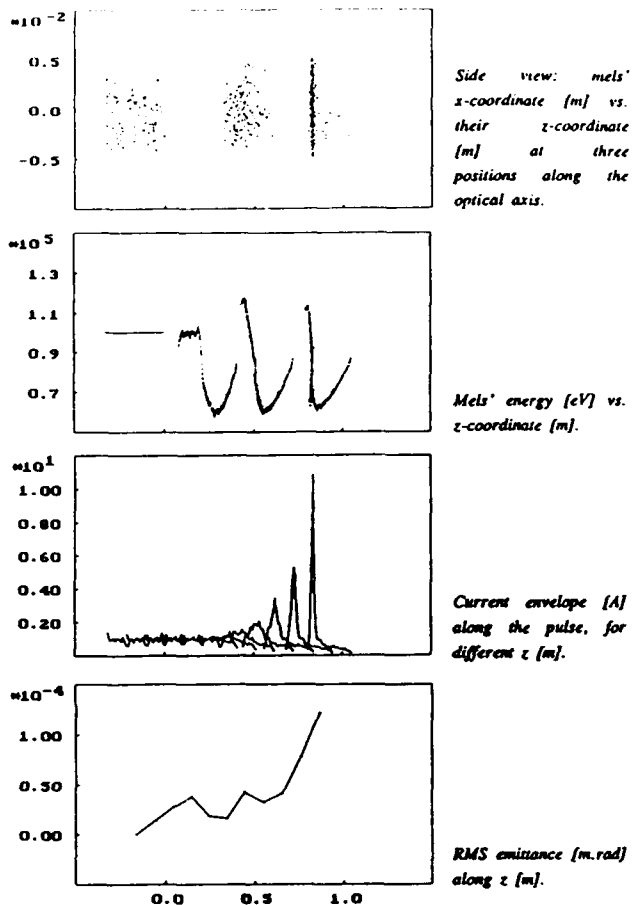


Figure 2. Thick line: repelling force [a.u.] between two charged spheres. Thin line: PAPA approximation.

## An Illustration

These plots show a typical result of a 1 A 100kV pulse which is bunched by a 40 MHz RF cell.



## Other Options

**Accessibility** The PAPA source code is well commented. Comments refer directly to the separate documentation.

**Input File Translation** PAPA can translate the code in the input file into a detailed hardware description in plain English on the computer screen. A useful help, which reduces errors.

**Cathodes** Optionally, all forces on the mels are ignored as long as their z-coordinate is smaller than zero. This allows the simulation of electrons emerging from a cathode surface. If the cell field files are filled with the electrostatic field distribution of a cathode-grid-anode configuration, PAPA could also be used as a sort of thermionic electron gun simulator, including pulse effects.

**Continued runs** Each cluster in the PAPA output file can easily serve as input for a continued run. This allows efficient and flexible simulations.

**Step Size Reduction** A step size reduction happens automatically as soon as one of the mels finds itself inside an RF cavity. The amount of reduction is specified by the user.

**Easy Cell Field Input** PAPA needs no information about the number of 'rows' and 'columns' in cell field files, since it finds this out by itself. The cell fields can be mapped on the screen.

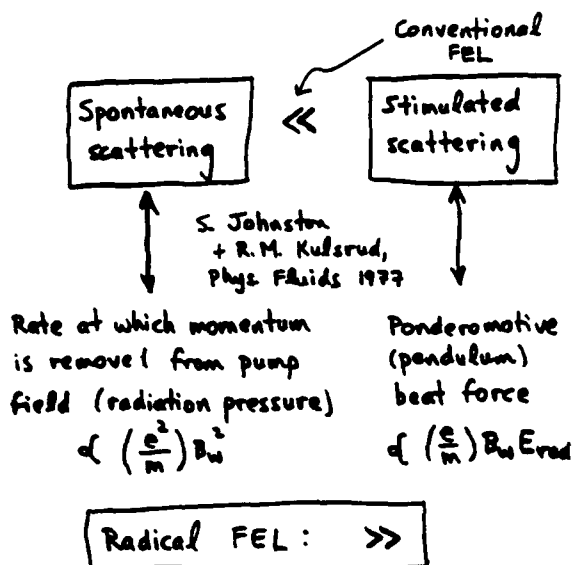
**Output** The format of the output file makes it both suited as a hard copy for direct reference, and as a plot file for graphic routines.

## P2.10

### Higher-Power Free-Electron Lasers

Shayne Johnston  
Jackson State University  
Jackson, Mississippi

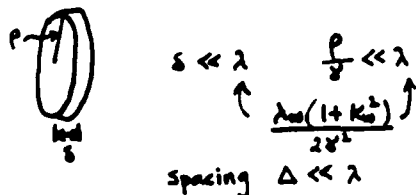
The dominant process is spontaneous emission, enhanced by prebunching on a length scale short compared with the wavelength, and sustained by a strong axial electric field. Generally speaking, the potential for very high power levels is achieved at the expense of phase coherence relative to the conventional free-electron laser.



\* Prebunch electron beam on length scale which is SHORT compared with  $\lambda$ .

Microbunches ( $N e^-$ ) with  $N \gg 1$ .

Train of disc-shaped macroparticles, each with  $N$  electrons.

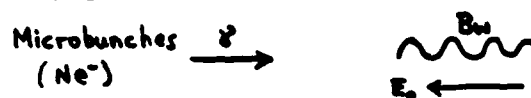


$$\frac{\gamma(\tau)}{\gamma_0} = \frac{e \Omega_e \tau}{\sqrt{1 + \left(\frac{\gamma_0}{\gamma_c}\right) (e^{2\Omega_e \tau} - 1 + \mu \Omega_e \tau)}}$$

Spontaneous-emission radiation source (a "laser"?)

$$\lambda = \frac{\lambda_w(1+K_w^2)}{2\gamma^2} \quad \gamma \gg 1 \quad K_w < 1$$

$$\frac{\Delta\omega}{\omega} \sim \frac{\pi}{2N_w} \quad \Delta\theta < \frac{1}{\gamma}$$



$$\gamma \rightarrow \gamma_\infty \text{ (constant) for } z > L_w$$

Self-regulating balance.

Accessible in laboratory for  $N \gg 1$ .

Work done by  $E_0$   $\xRightarrow{\text{efficiency}}$  Spontaneous radiation

$$\mu = \frac{2\Omega_e^2 - \Omega_w^2}{\Omega_e^2 K_w^2 c^2}$$

$$\gamma_0 = \sqrt{\frac{\Omega_e}{N \Omega_w^2 c^2}}$$

$$\gamma \rightarrow \gamma_\infty \text{ as } \tau \rightarrow \infty$$

$\uparrow$  independent of  $\gamma_0$

$$L_w = \frac{\gamma_\infty c}{\Omega_e} \ln \left( \frac{1 + \sqrt{1 - \gamma_0^2/\gamma_\infty^2}}{(1 + \gamma_0/\gamma_\infty)} \right)$$

### Relativistic - Dirac Equation

$$\frac{d\vec{u}}{dt} = -(\vec{\Omega}_0 \vec{u} + \vec{u} \times \vec{\Omega}_0) + \tau_0 \left\{ \frac{d^2 \vec{u}}{dt^2} - \left[ \left( \frac{d\vec{u}}{dt} \right)^2 - \left( \frac{d\vec{u}}{dt} \right)^2 \right] \vec{u} \right\}$$

where  $\vec{u} = \gamma \frac{\vec{v}}{c}$ ,  $\tau_0 = \frac{2}{3} \frac{e^2}{m_0 c^2} N$ ,  
 $\vec{\Omega}_0 = \frac{1e|\vec{E}|}{mc}$ ,  $\vec{\Omega}_0 = \frac{1e|\vec{B}|}{mc}$

### Exact Solution for $B_w, E_z$

$$\vec{E} = -E_0 \hat{z}, \quad \vec{B} = B_w (\hat{x} \cos k_w z + \hat{y} \sin k_w z)$$

$$\begin{cases} \hat{E}_x = -\hat{x} \sin k_w z + \hat{y} \cos k_w z \\ \hat{E}_y = -\hat{x} \cos k_w z - \hat{y} \sin k_w z \\ \hat{E}_z = \hat{z} \end{cases}$$

Seek solution for constant  $\gamma, u_1, u_2, u_3$ .

### Power radiated by train:

$$P = \frac{N' N |e| E_0 v_0}{(1 - v_0/c)}$$

$N' = \#$  of macroparticles whose radiation becomes superimposed during a wiggler transit time.

### Condition for neglect of ponderomotive force

$$E_r \lesssim \frac{2 \gamma_{\infty} E_0}{K_w}$$

### Length scale for macroparticle degradation

$$L_d = \frac{\gamma^2}{(1 + K_w^2)} \frac{v_1^2}{c^2} \int_{\delta_0}^{(\delta_0 + \Delta)} \frac{d\delta}{\left[ 2(\Delta \delta_0) + \int_{\delta_0}^{\delta} \frac{1e|\vec{E}(\delta')|}{mc^2} d\delta' \right]}$$

$\hat{E}(\delta) =$  longitudinal self electric field of the microbunch.

### Exact steady-state solution:

$$u_1 = -k_w \tau_0 u_2 u_3 (1 + u_1^2 + u_2^2)$$

$$u_2 - K_w = k_w \tau_0 u_3 (1 + u_1^2 + u_2^2)$$

For given  $u_3$ , cubic equation for  $u_1$  always has one real positive root.

$$\frac{\Omega_0}{k_w c} + K_w u_1 = k_w \tau_0 u_3^2 (u_1^2 + u_2^2)$$

Determines axial electric field.

$$\gamma \gg 1, \quad k_w \tau_0 \ll 1$$

$$u_1 \approx 0$$

$$u_2 \approx K_w$$

$$\Omega_0 = \gamma^2 \Omega_w^2 \tau_0$$

$$\text{cf. } F = \frac{I_0}{c}$$

- Balance is self-regulating and nonlinearly stable. Steady-state solution is an attractor.
- Prebunch electron beam on length scale small compared with radiated wavelength.

### Inclusion of guide magnetic field

Helical orbit condition

$$\frac{v_z^2}{c^2} = 1 - \frac{1}{\gamma^2} \left[ 1 + \frac{K_w^2}{\left( 1 - \frac{\Omega_0}{\gamma k_w v_z} \right)^2} \right]$$

- Condition for  $\frac{dv_z}{d\delta} \rightarrow 0$ :

(minimum axial degradation)

$$\frac{\Omega_0}{\gamma} = k_w v_z (1 + K_w^2) \quad \text{Strong field}$$

Type II orbit - Stable, on far side of magnetoresonance

- Condition for zero ponderomotive force: (immunity to saturation by trapping)

$$\frac{\Omega_0}{\gamma} = \frac{k_w v_z}{[1 - \beta_w^2 (\gamma_z^2 - 1)]}$$

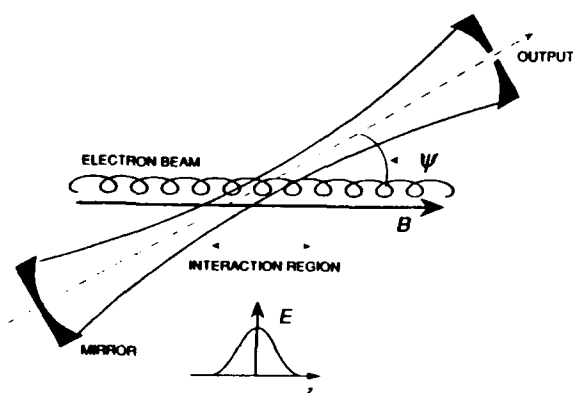
## P2.11

### Status and Design of the NRL IREC Maser Experiment

A. W. Fliflet, R. B. McCowan, W.M. Manheimer, and P. Sprangle  
Plasma Physics Division, Naval Research Laboratory,  
Washington, D.C. 20375-5000

A 500 kV, 280 GHz IREC maser experiment featuring an open mirror type resonator with the resonator axis tilted by  $\sim 20^\circ$  to the electron beam axis is underway at NRL. A high quality 100 A, 1  $\mu$ sec pulselength electron beam will be produced by thermionic cathode MIG type electron gun. Issues for the design of this FEL-like maser will be discussed.

### INDUCED RESONANCE ELECTRON CYCLOTRON QUASI-OPTICAL MASER OSCILLATOR



### Advantages of CARMs / IREC Maser

- Higher frequency potential with 0.5-1 MeV beam than FEL or gyrotron.
  - Frequency is doppler-upshifted from cyclotron frequency ( $\omega \sim \gamma \Omega_{ce}$ )
  - A 0.5 MV CARM with a 100 kG superconducting magnet can achieve 500 GHz.
  - The typical FEL wiggler period of 3 cm or longer limits a 1MV FEL to frequencies below 180 GHz.
- Efficiency potential of CARM is high (20-40%).
  - "auto-resonant" effect maintains beam-wave synchronism during interaction.
- Can operate at powers greater than 10 MW.

### Advantages of the Quasi-Optical IREC Maser

- Resonator and interaction volumes are large ( $\gg \lambda^3$ )
- Low ohmic losses independent of wave phase velocity.
- Does not support low frequency "gyrotron" modes.
- Effective transverse mode and phase velocity selection.
- Reduced sensitivity to electron beam temperature.
- Radiation output and e-beam collection are separated.

### MIG-type Gun for IREC Maser

Experiment requires a 500 keV, 100 Amp, 1  $\mu$ sec annular beam.

Temperature-limited MIG successfully developed for gyrotrons.

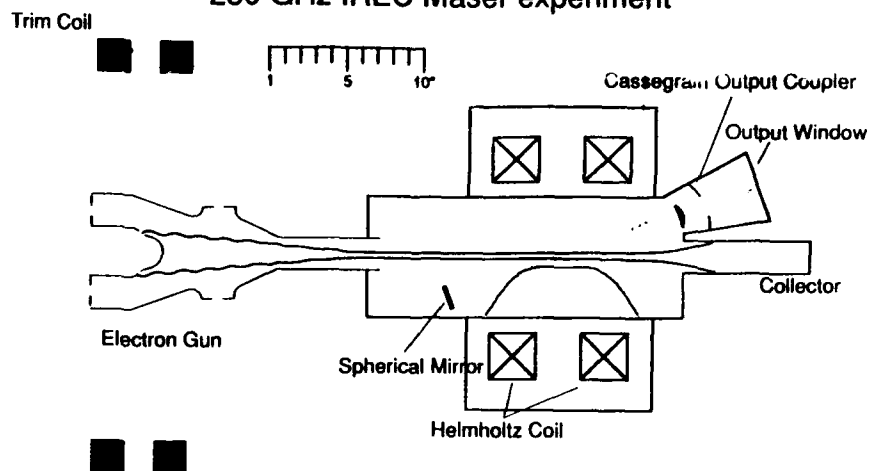
Design based on 500 kV MIG built for U. Maryland gyrokystron.

Variable mod-anode voltage allows control of  $v_a$  needed for voltage tuning of frequency.

Lower perveance and  $v_{\perp}/v_{\parallel}$  in CARM regime should allow high beam quality --- 1-3% axial velocity spread

High beam quality predicted by accurate 2-D simulations.

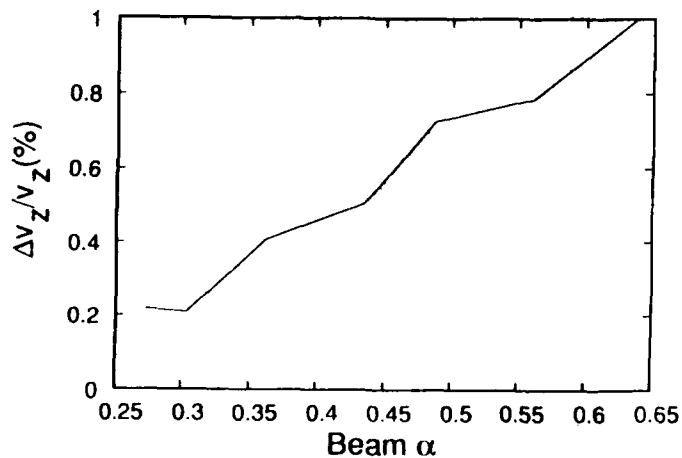
## 280 GHz IREC Maser experiment



## 280 GHZ IREC MASER PARAMETERS

Beam Voltage	500 kV	Resonator Angle	20°
Beam Current	150 A	Radiation Waist	8 mm
Magnetic Field	60 kG	Interaction Length	9.4 cm
Resonator Angle	20°	Mirror Separation	130 cm
Efficiency	35%	Mirror Diameter	8 cm
Pulse Length	1 $\mu$ sec	Peak Mirror Heating	110 kW/cm <sup>2</sup>
Power	26 MW	Output Coupling	3.5%
$\alpha \equiv v_{\perp}/v_z$	0.6	Required $\Delta v_z/v_z$	2.3%

## Electron Beam Quality from the 500 kV MIG



## IREC Maser Project Status

Engineering and fabrication of electron gun underway.

- Delivery expected in FY90.

500 kV, 200 Amp, 1  $\mu$ sec modulator ordered.

- Delivery expected in FY90

Design of superconducting magnet nearly complete.

- Procurement planned for FY90.

QO resonator and output coupler design in progress.

## P2.13

### The Investigation of an Optical Klystron

Ming Chang Wang, Shanghai Institute of Optics and Fine Mechanics, PO Box 8211 Shanghai, PR China; V.L. Granatstein, B. Levush, U. of Maryland, College Park, MD 20742

**Abstract:** The feasibility of developing an amplifier in the Optical Klystron (OK.) configuration at wavelength of 1-2 mm has been investigated. The effect of beam velocity spread on the efficiency and gain of OK. is taken into account. It is found that more sensitive to beam velocity spread for three cavities than two cavities.

The configuration of an OK. which can be used to improve the efficiency and gain of free electron lasers (FEL's) has been investigated[1]. Based on the concept of prebunching electron

beams, experimental and theoretical studies of the OK. have been carried out[2,3]. An attractive application by using OK. has been proposed[4]. For the FEL's employing small period wiggler (1 cm), and electron beam with modest parameters (375 KV, 100 A/cm<sup>2</sup>), an OK. has been designed to obtain the gain of 20-30 dB.

In this paper, the effect of velocity spread on the efficiency and gain is taken into account. We assume the velocity spread of the electron beams is of Gaussian distribution. For optimized gain and efficiency, the injection velocity of beams,  $B_i$  is slightly

above the resonant velocity as indicated by  $B_i = \alpha B_r$ , where  $\alpha$  is a detuning factor, which describes frequency deviation  $w$  from a resonant frequency  $w_s$ ,  $\alpha = w/w_s + 1$ . We optimized the injection radiation power  $P_{in}$  from 1 W to  $10^4$  W for the maximum efficiency. The maximum efficiency is 1.97% at  $P_{in} = 0.44 \times 10^3$  W, the corresponding gain at this point is 25.3 dB, the OK. works at a nonlinear region. For the same parameters: detuning factor  $\alpha = 1.001$ , beam energy  $\gamma = 1.73$ , each cavity length  $L_w = 0.20$  m, and the drift space  $L_d = 0.10$  m. A comparison of the efficiency for two cavities and three cavities with FEL's shows that the OK. configuration can improve not only the gain, but also the efficiency.

An OK. with three cavities has higher gain than an OK. with two

cavities, if we optimized the OK. parameters, and obviously has much higher gain than an FEL with a single cavity. Fig. 1 shows the efficiency and gain versus the  $Z$ , the wiggler distance for three cavities. The energy spread is about  $10^{-5}$ ,  $\alpha = 1.003$ , maximum efficiency is 1.96%, and the corresponding gain is 43.3 dB.

It is more sensitive to energy spread for three cavities than for two cavities. From Fig. 2, the efficiency doesn't change for all cases if the energy spread is less than  $10^{-4}$ . A limitation of energy spread is required. It is  $5 \times 10^{-4}$  for three cavities,  $7 \times 10^{-4}$  for two cavities,  $3 \times 10^{-3}$  for single cavity in our case.

The efficiency has been optimized for injection power.  $P_{in} = 4780$  W for single cavity,  $P_{in} = 450$  W for two cavities,  $P_{in} = 1$  W

for three cavities.

#### Reference

1. M.C. Wang, V.L. Granatstein and B. Levush, IEEE Trans. Plasma Sci. Vol.16, No.2, (1988) p.172.
2. R. Coisson, in Particle Accelerators (Gordon and Breach, 1981) Vol.II, pp.245-253.
3. M. Billardon, et al; in Proceedings of the Seventh International Conference on FEL's, E. T. Scharlemann and D. Prosnitz editors, (North Holland, 1986).
4. V.L. Granatstein, B. Levush and M.C. Wang, Innovative Science and Technology Symposium, Los Angeles, Jan. 12-14, 1988.

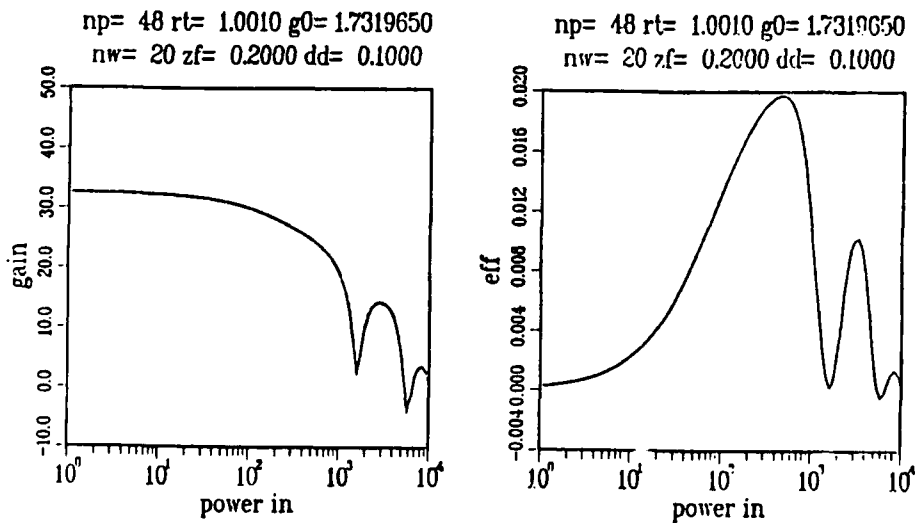


Fig. 1 The gain and efficiency of a two-cavity, 133 GHz O.K. versus input power from 1 W to  $10^4$  W for  $\Delta\gamma/\gamma = 10^{-5}$

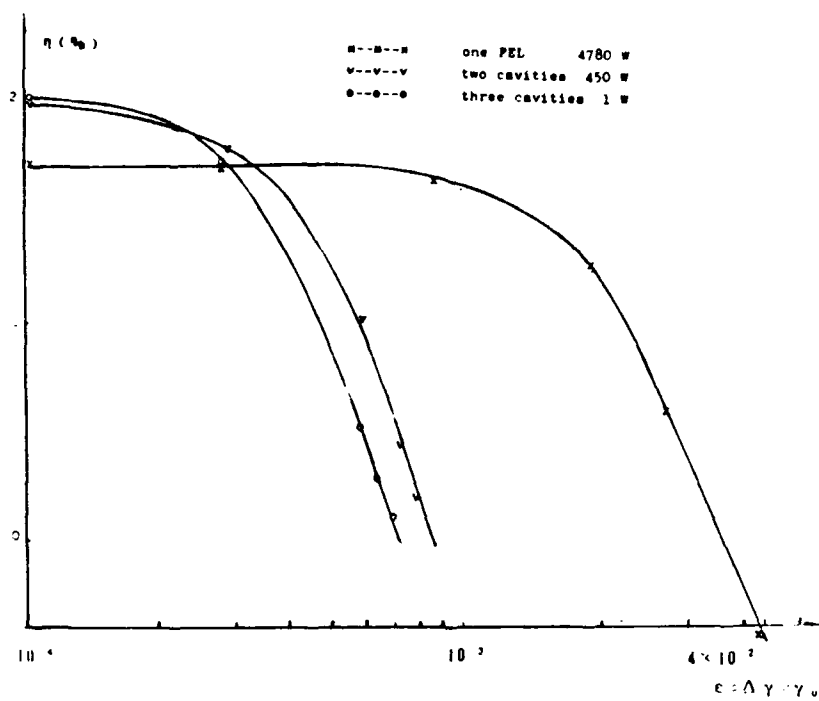


Fig. 2 The efficiency for different cavities O.K. vs. the beam velocity spread.



## P2.14

### High Performance Pure Permanent Magnet Undulators

G. Rakowsky, B. Bobbs, R. Burke, W. McMullin, G. Swoyer  
Rockwell International, Rocketdyne Division  
6633 Canoga Ave. FA38, Canoga Park, CA 91303

Pure permanent magnet designs that can match or exceed the on-axis field of PM hybrids are presented. Linearity and superposition of fields allows construction of undulators with minimized field error and optimized performance for both FEL and synchrotron radiation applications. Examples and performance data are given.

**INTRODUCTION:** Pure permanent magnet (PPM) undulators have been eclipsed in recent years by permanent magnet (PM) hybrid designs which offered higher peak on-axis fields and reduced sensitivity to variations in magnetic characteristics of PM materials. However, the application of simulated annealing (SA) to minimize the effects of magnet errors has revived interest in PPM undulator technology.

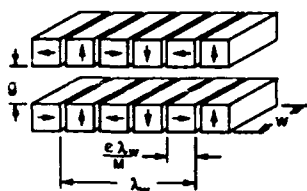
**BACKGROUND:** The Rocketdyne/Stanford 80 period, 2m long, PPM undulator was optimized by SA for minimum trajectory error. Trajectory straightness equivalent to random error of 0.055% was achieved, despite actual field errors of ~1%. [1]

#### OBJECTIVES OF THIS STUDY:

1. Push PPM technology to match PM hybrids;
2. Apply SA to optimize FEL performance directly;
3. Build a High-Performance PPM Undulator.

#### "Classical" Halbach PPM Undulator Configuration

(Rocketdyne/Stanford Undulator)



- Square Bar Magnets
- 4 Magnets / Period ( $M = 4$ )
- 90° Rotation / Magnet
- Packing Factor  $\epsilon = 0.8$
- Field is 53% of Limit

#### Examine Halbach's Formula for 2D Planar PPM Undulator:

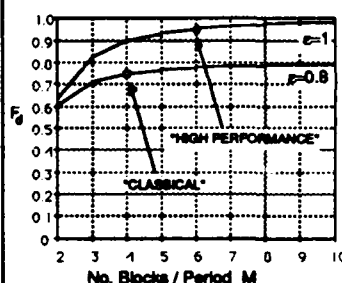
$$\text{Peak Field } B_p = 2B_r \left[ \frac{\sin(\pi/M)}{(\pi/M)} \right] \left[ 1 - e^{-2\pi h/\lambda_w} \right] \left[ e^{-\pi g/\lambda_w} \right]$$

$$= 2 \left[ \text{Remanence} \right] \times \left[ \text{Discretization Factor} \right] \times \left[ \text{Height Factor} \right] \times \left[ \text{Gap Factor} \right]$$

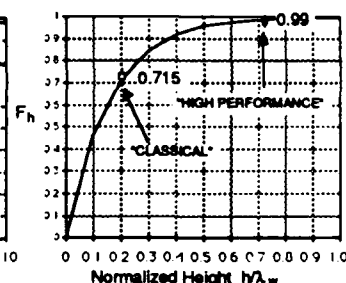
- Which factors can we "push" to increase  $B_p$ ?
- What is the practical limit?

#### Examine Discretization Factor $F_d$ and Height Factor $F_h$

Discretization Factor vs. M

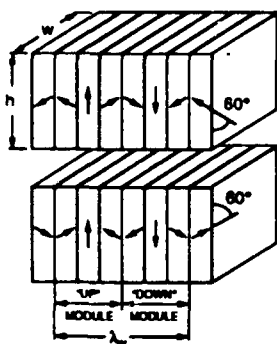


Height Factor vs. Magnet Height



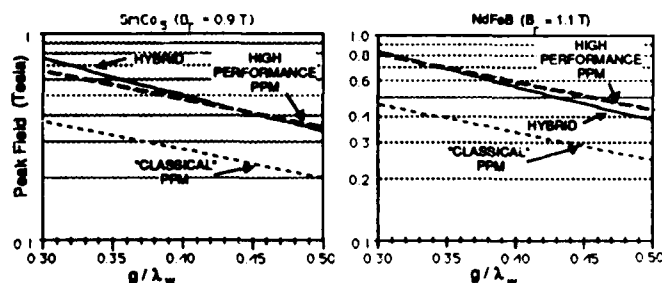
- Increase Discretization from 4 to 6 magnets/period.
- Increase Packing Factor from 80% to ~100%.
- Result -- Increase field = 27%
- Increase Magnet Height from  $0.2 \lambda_w$  to  $0.72 \lambda_w$
- Result -- Increase field = 38%

#### Rocketdyne High Performance PPM Design



- 6 Magnets / Period in Each Array ( $M = 6$ )
- 60° Rotation / Magnet
- Only 2 Polarization Angles Required: 0° & 60°
- Packing Factor  $\epsilon = 1$
- Half-period Symmetry
- Modular Geometry
- Suitable for Multi-parameter Optimization
- Field Achieved is 83% of Theoretical Limit.

#### PPM vs. Hybrid\*



\* Formulas: K. Halbach

**Rocketdyne's High Performance PPM Design  
Can Match or Exceed Field of Hybrid  
in Many Applications**

### Advantages of 6-Magnet PPM Configuration :

- Half-period symmetry & modularity lends itself to multi-parameter, multi-stage optimization by **Simulated Annealing (SA)**.
- X and Y trajectory errors can be largely decoupled.
- Half-strength end modules easily realized

### Advantages of Simulated Annealing:

- Can optimize FEL performance directly. [2], [3]
  - Can minimize RMS field error too, if desired.
- NOTE:** Minimizing field errors alone does *not* guarantee optimum, or even satisfactory performance! [4]
- Can also optimize performance of Synchrotron Radiation Insertion Devices.

### Rocketdyne High Performance 80-Period Undulator Will Be Optimized by 2-Stage SA Process

#### Stage 1 (COMPLETED)

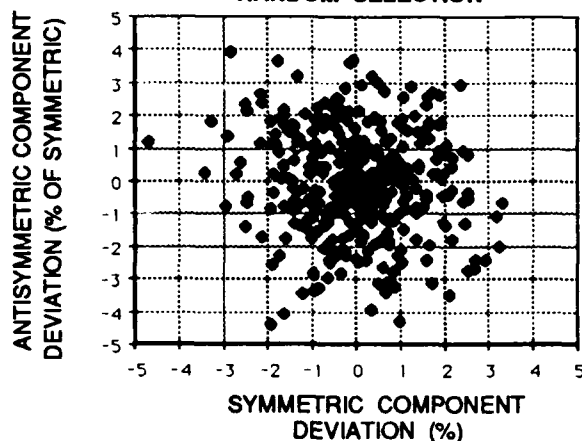
- Characterize each magnet in all possible orientations. (Map  $B_y$  vs.  $z$  as seen by electron)
- Apply SA to group magnets into half-period triplets with (nearly) equal & symmetric field profiles.

#### Stage 2 (IN PROGRESS)

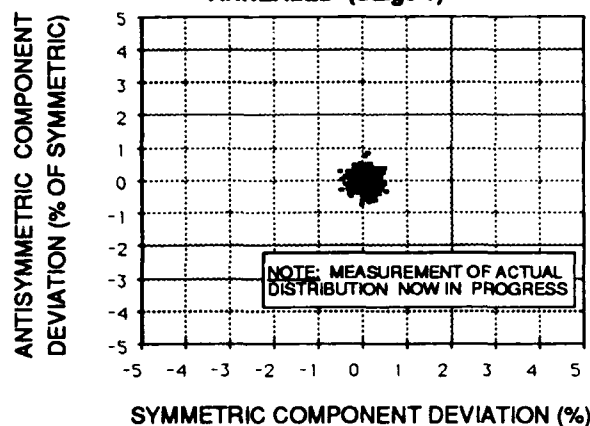
- Re-characterize assembled triplet modules. (Accounts for triplet assembly errors.)
- Apply SA again to find optimal ordering of modules for minimum phase and trajectory errors.

**Goal:** performance equivalent to random field error  $\leq 0.1\%$ .

PREDICTED DISTRIBUTION OF TRIPLET KICKS  
RANDOM SELECTION

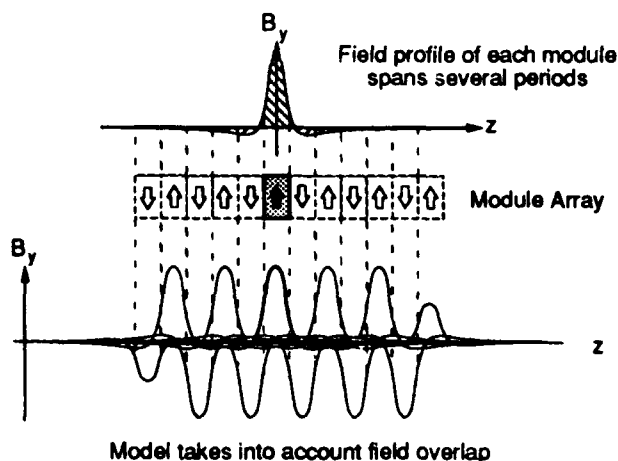


PREDICTED DISTRIBUTION OF TRIPLET KICKS  
ANNEALED (Stage 1)



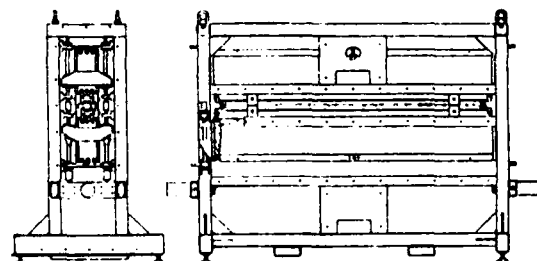
### Stage 2 : Evaluate trajectory & phase errors.

A realistic trajectory model is constructed from superposition of field data of individual half-period modules. Minimum trajectory & phase error yields maximum FEL performance. [3]



### Rocketdyne High Performance Undulator Design Parameters

Type - PPM	Minimum Gap - 0.76 cm
Structure - 6 Blocks / Period	Peak Field (max) - 0.65 T
Period - 2.4 cm	$K_u$ (max) - 1.47
Number Periods - 82	<u>Operating parameters for</u>
Length - 2 m	$\lambda_c = 3.0 \mu m, \gamma = 80$
Taper - Linear, Variable	Gap - 0.987 cm
Magnet Material - SmCo5	Peak Field - 0.489 T
Remanent Field - 0.97 T	$K_u$ - 1.096



Proposed application - as power amplifier in HIBAF at LANL [5]

Expected completion date - October 1989

- [1] M. Curtin et al., "A High Quality Permanent-Magnet Wiggler for the Rocketdyne/Stanford Infrared Free Electron Laser", Proc. IX Int'l. Free Electron Laser Conf., Nucl. Inst. Meth. A272 (1988) 187-191.
- [2] A. Bhowmik et al., "First Operation of the Rocketdyne/Stanford Free Electron Laser", Ibid., 10-14.
- [3] R. Cover et al., "FEL Performance with Pure Permanent magnet Undulators Having Optimal Ordering", this Conf.
- [4] B. Bobbs et al., "In Search of a Meaningful Field Error Spec for Wigglers", Proc. this Conference.
- [5] W.D. Cornelius et al., "The Los Alamos High-brightness Accelerator FEL (HIBAF) Facility," Proc. this Conference.

## P2.16

### Optical Resonator for the NIST-NRL Free Electron Laser

B. Carol Johnson, Ronald G. Johnson, David L. Mohr, and Marc S. Price  
National Institute of Standards and Technology, Center for Radiation Research  
Gaithersburg, Maryland 20899 USA

A 9-m linear optical cavity will be used in the NIST-NRL FEL. This FEL, which is driven by a racetrack microtron, is designed to lase from 0.2 to 10  $\mu\text{m}$ . The resonator must accommodate the large dynamic range in wavelength, low gain, high average power, and coherent harmonic emission of the laser. This work was supported by the US SDIO through ONR Contract No. N00014-87-F0066.

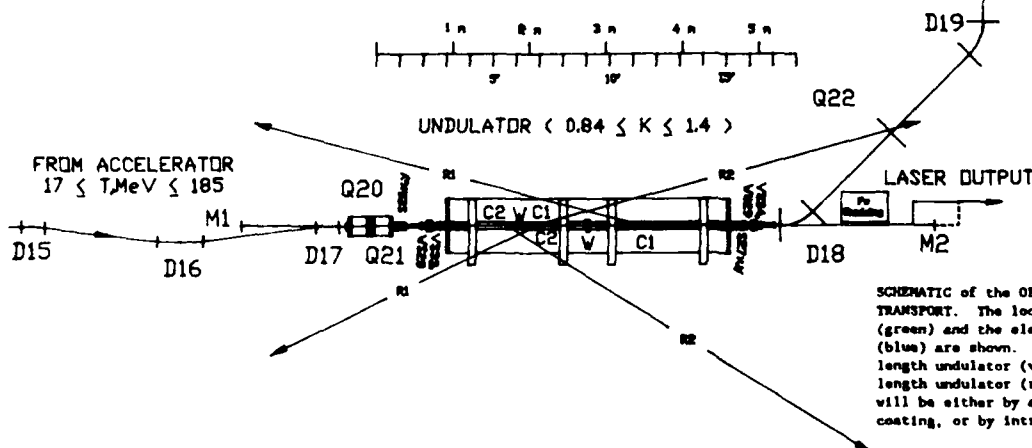
9-m NIST-NRL Cavity Parameters

Parameter	Full Length Undulator	Half Length Undulator
Wavelength	200 nm to $\approx 3 \mu\text{m}$	$\approx 2 \mu\text{m}$ to 10 $\mu\text{m}$
Mirror Separation, L	906.94 cm	906.94 cm
Rayleigh Length, $z_0$	182.00 cm	91.00 cm
$R_1$ to waist, $t_1$	453.47 cm	362.47 cm
Mirror Radius, $R_1$	526.51 cm	385.31 cm
Mirror Radius, $R_2$	526.51 cm	559.68 cm
Cavity stability, $g_1 g_2$	0.5220	0.8400
Separation of mirror center of curvature, d	146.09 cm	38.06 cm
Radius of mode at waist ( $e^{-2}$ intensity), $w_0(\lambda)$	0.34-1.32 mm	0.76-1.70 mm
Radius of mode at $M_1$	$2.68w_0(\lambda)$	$4.11w_0(\lambda)$
Radius of mode at $M_2$	$2.68w_0(\lambda)$	$6.07w_0(\lambda)$
Longitudinal mode spacing, $\Delta\nu$	16.5277 MHz	16.5277 MHz
Detuning length, $\delta L$	-0.65 $\mu\text{m}$ to -7.5 $\mu\text{m}$	
Normalized slippage, $A/\lambda$	0.03 to 0.16	0.13 to 0.65

NIST-NRL CAVITY PARAMETERS. Two cavity geometries are required for this FEL. The first, which maximizes the small-signal power gain by using the entire, or "full-length" undulator, will be used for UV, visible, and near-IR wavelengths. The second, which minimizes the diffraction losses by halving the length of the narrow-bore undulator, will be used for mid- and far-infrared wavelengths. The mirror separation remains the same, but the location of the intracavity waist and the Rayleigh length of the cavity mode changes. These cavity parameters were calculated under the assumption that free-space cavity modes are adequate. A schematic of the two systems is shown below.

Dipole magnets D15 to D17 are a chicane that provides achromatic transport around the first cavity mirror,  $M_1$ , and onto the cavity axis. The pair of quadrupole magnets Q20 and Q21 are part of a variable magnification telescope, for mode-matching the electron beam envelope to the fundamental cavity mode. The dipole magnet pair D18 and D19 extracts the electron beam from the optical cavity and directs it to a shielded electron beam collector. Q22 provides for achromatic transport to the beam collector or other experiments (dosimetry, transition radiation, etc). Electron beam steerers are labeled "S", alignment viewcreens "VS", and beam profile measurement devices, or wire-scanners, "WS". The three viewcreens that can be inserted inside the undulator are not shown, for reasons of clarity.

To Electron Beam collector



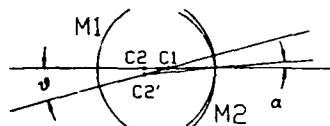
SCHEMATIC of the OPTICAL CAVITY and ELECTRON BEAM TRANSPORT. The locations of the cavity mirrors (green) and the electron beam transport magnets (blue) are shown. Cavity parameters for the full length undulator (violet) and those for the half length undulator (red) are also shown. Outcoupling will be either by a partially transmitting mirror coating, or by intracavity Brewster plates.

# ALIGNMENT SENSITIVITY and DIFFRACTION LOSSES

## PASSIVE CAVITY (no electrons or undulator field)

The optical axis of cavity contains the centers of curvature of spherical end mirrors. Small transverse displacements or rotations of the mirrors will rotate the optical axis with respect to the desired mechanical axis.

$$\theta_1 = \frac{1}{2} \frac{(1-g_1)}{(1-g_1g_2)}, \quad g_1 = 1 - L/R_1$$



If small intracavity apertures are present, (i.e., wiggler vacuum chamber), diffraction losses increase, since the perturbed cavity mode will be centered on the new optical axis. Cavities with well-separated centers of curvature are less sensitive to alignment errors. Also, if the electron beam is small, significant loss in gain will result from misalignment.

EXAMPLE: Half-Length Undulator at  $\lambda = 10 \mu\text{m}$ . One dimensional mirror tilt of  $90 \mu\text{rad}$  will increase the diffraction loss by a factor of 2.6.

# COMMERCIALLY-AVAILABLE MIRRORS for NIST-NRL FEL 450 nm to 850 nm

## Multi-layer Dielectric on Fused Silica

Bandwidth:  $\pm 50 \text{ nm}$   
Reflectivity: 0.9999  
Absorption: 10-20 ppm

## Distortion from Heating

- Observed to be negligible at  $250 \text{ kJ/cm}^2$  for cw dye lasers; we expect  $< 50 \text{ kJ/cm}^2$ , average
- Calculated distortion in steady state using finite element analysis method (see below)

## Dielectric Breakdown

- Damage threshold is  $20 \text{ J/cm}^2$  in  $1 \mu\text{s}$
- We expect  $0.25 \text{ J/cm}^2$  in  $1 \mu\text{s}$

## Damage from Harmonics

- From experience at other FELs, we expect absorption to increase
- We are calculating harmonic radiation (see Tang and Sprangle 1989)
- Deacon Research in Phase I of UV-induced damage study for multi-layer dielectrics that are designed for  $240 \text{ nm}$ . The planned work would complement the studies in the visible (see Deacon, Bakshi, and Cerece 1989).
- FEL operating parameters must be adjusted so that the harmonic content is minimized

# OUTPUT POWER

The total round-trip power losses,  $1-R^2$ , must be such that the lasing threshold is reached:

$$R_1 R_2 e^{-\delta} - R^2 > 1/(1+C_p)$$

where  $R_1$  is the mirror reflectivity,  $\delta$  represents intracavity losses, and  $C_p$  is the small-signal power gain. If the oscillator saturates by extracting the maximum power from the electron beam during the interaction, then the average intracavity power is

$$P_s = \eta P_0 R^2 / (1-R^2)$$

where  $\eta = 1/2M$ ,  $M$  is the number of periods, and  $P_0$  is the electron beam power ( $P_0$  is equal to the average current in A times the beam energy in eV). The minimum value for  $P_0$  is found from  $R^2 = 1/(1+C_p)$ . Finally, the output power is

$$P_o = \eta P_0 (T_1 + R_1 T_2) / (1-R^2)$$

where  $T_1$  is the mirror transmission. In the case where transmission dominates the round-trip losses, then  $P_o \approx \eta P_0$ . For the NIST-NRL,  $P_0 = 100 \text{ kW}$  at full energy, so  $P_o < 385(192) \text{ W}$  for  $M = 130(65)$ .

EXAMPLE:  $\lambda = 632.8 \text{ nm}$ ,  $K = 1.41$ ,  $T = 107 \text{ MeV}$ ,  $\langle I \rangle = 0.55 \text{ mA}$ ,  $C_p = 0.2$ ,  $\delta = 0$ ,  $T_1 = T_2 = 0.05$ ,  $R_1 = R_2 = 0.95$ , then  $P_s = 2.1 \text{ kW}$  and  $P_o = 161 \text{ W}$ .

# STEADY STATE THERMAL ANALYSIS

Cylindrical, Plane Mirror on Infinite Heat Sink  
Exposed to Gaussian Laser Beam

## BOUNDARY CONDITIONS

- 1) Constant potential, bottom:  $T=0$  at  $z=0$ ;
- 2) Constant field, edge:  $\frac{\partial T}{\partial r} = 0$ ;
- 3) Gaussian field, top:  $\frac{\partial T}{\partial z} = -\frac{2P}{\pi a^2} \exp(-\frac{2r^2}{a^2})$
- 4) Motion at  $z=0$  is constrained in  $r$ ,  $\theta$ , and  $z$ ;
- 5) Motion at  $r=0$  is constrained in  $r$  and  $\theta$ .

## MATERIAL AND PHYSICAL CONSTANTS

Mirror radius,  $a = 25.4 \text{ mm}$ , thickness,  $t = 9.525 \text{ mm}$ ;  
Absorbed power,  $P = 100 \text{ mW}$  (1 kW intracavity power & 100 ppm coating absorption);  
Node size on mirror,  $\omega = 1.626 \text{ mm}$ ;  
Fused silica substrate:  
 $\alpha = 1.38 \text{ W/m}^2\text{-degree}$  and  $\alpha = 5.5 \cdot 10^{-7} \text{ per degree}$   
 $E = 7.03 \cdot 10^{10} \text{ nt/m}^2$  and  $\nu = 0.17$

## METHOD

Finite element analysis, using the code ANSYS (Svan-son Analysis Systems) with 10 elements in  $z$ , 5 in  $r$ , and 12 in  $\theta$ . Nonuniform spacing in  $r$  and  $z$  was required.

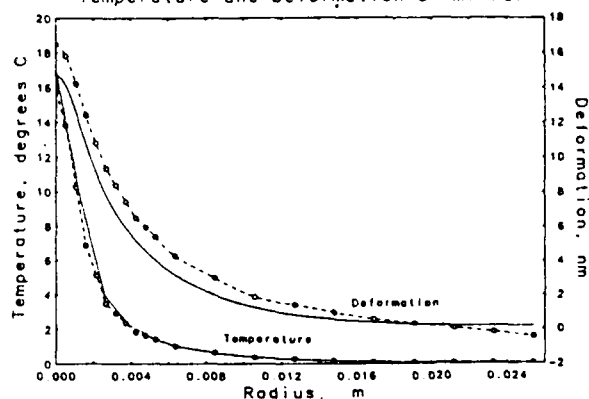
## PRELIMINARY RESULTS

- 1) Agreement with analytical formulation of Webb, Wieman, and Anderson (1988);
- 2) Temperature rise of  $16.5 \text{ degrees}$ ;
- 3) Deformation in  $z$  at  $r=0$ ,  $z-t$  is  $16.5 \text{ nm}$
- 4) Deformation in  $r$  at  $r=a$ ,  $z-t$  is  $1.7 \text{ nm}$

## FUTURE WORK

Radiative cooling; realistic mechanical boundary conditions; perturbation treatment of cavity modes; time dependence; elasticity effects; stress analysis

# Temperature and Deformation of Mirror



TEMPERATURE and DEFORMATION of MIRROR. The dashed lines are the finite element analysis solution for the temperature and deformation profiles on the mirror surface. The analytical solutions of Webb, Wieman and Anderson (1988) are the solid lines. The temperature profiles are in good agreement. The agreement in the deformation profiles is also reasonable, since the analytical solutions do not account for substrate elasticity.

# REFERENCES

- D.A.G. Deacon, M.H. Bakshi, and M. Cerece, "Measurements of UV Induced Absorption in Dielectric Coatings", this conference (1989).
- C.M. Tang and P. Sprangle, "The Analysis of Radiation Harmonics in the Free Electron Laser using the Source Dependent Expansion Method", this conference (1989).
- J.I. Webb, C.E. Wieman, and D.Z. Anderson, "New Mirror Absorption Measurement Technique using Substrate Surface Deformation", Optics News, 14, 207 (1988).

## P2.17

### APPLICATIONS OF HARMONIC GENERATION OF PICOSECOND PULSES FROM A FREE ELECTRON LASER

Brett A. Hooper<sup>1,2)</sup>, Stephen V. Benson<sup>2)</sup>, Richard C. Straight<sup>1)</sup> and John M.J. Madey<sup>2)</sup>

1) Utah Laser Institute, Department of Veterans Affairs and the University of Utah Medical Centers, Salt Lake City, Utah 84132

2) Department of Physics, Duke University  
Durham, North Carolina 27706

Using non-linear crystals we have produced harmonics of the Mark III Infrared Free Electron Laser from 495 nm to 2.1  $\mu\text{m}$ . Optimization of energy conversion efficiency as a function of group velocity walkoff, birefringent walkoff, finite linewidth and length will be discussed. Preliminary results on an optimized coated crystal system will be presented and compared to theory.

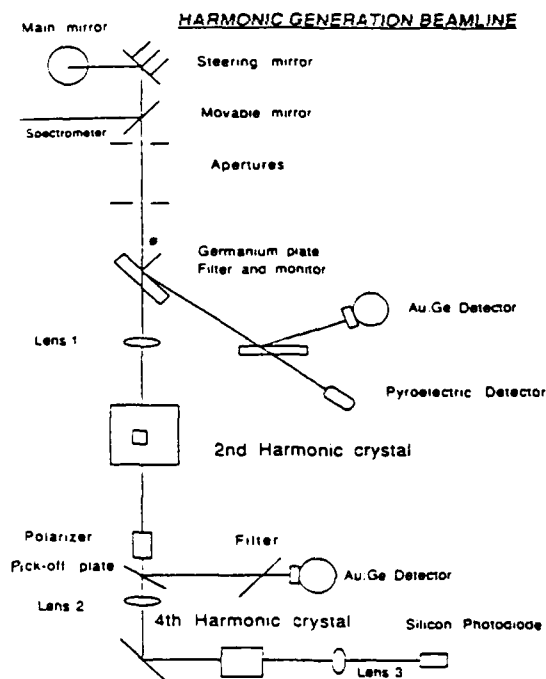
#### ABSTRACT

The Mark III Infrared Free Electron Laser has been used as a research tool by Utah Laser Institute and other investigators since September 1986. The Mark III IR FEL uses a Radio Frequency Linear Accelerator (RF Linac) to produce a 26-44 MeV electron beam. This allows operation of the laser in the spectral region 2 to 8  $\mu\text{m}$ .

The second and fourth harmonic wavelengths have been generated using non-linear crystals. The second harmonic has been generated from 0.99  $\mu\text{m}$  to 1.24  $\mu\text{m}$  using lithium niobate and 1.58  $\mu\text{m}$  to 1.64  $\mu\text{m}$  and 1.80  $\mu\text{m}$  to 2.1  $\mu\text{m}$  using silver gallium selenide. The fourth harmonic has been generated from 495 nm to 620 nm using a cascaded crystal system of lithium niobate and beta-barium borate.

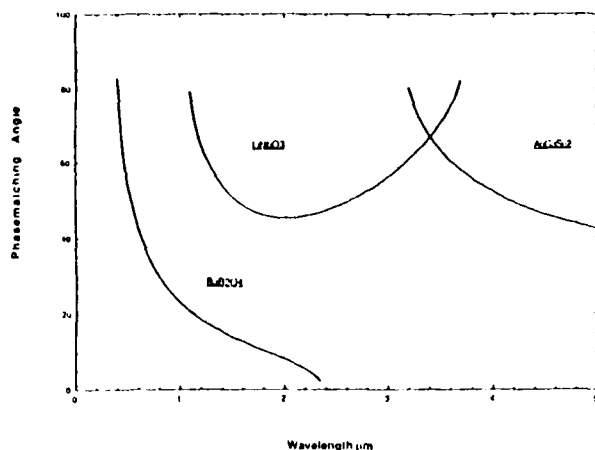
Optimization of energy conversion efficiency as a function of group velocity walkoff, birefringent walkoff, finite linewidth and length will be discussed. Preliminary results on an optimized coated crystal system will be presented and compared with theory. Conversion efficiencies of 1% and 25% were measured for the respective crystals. Poor conversion efficiencies on this first test may have been due to a poor Strehl ratio.

Work supported by SDIO/ONR MFEL contracts : N00014-86K-0823, N00014-86K-0256 and N00014-86K-0710



## FREQUENCY DOUBLING RESULTS USING THE MARK III IR FEL

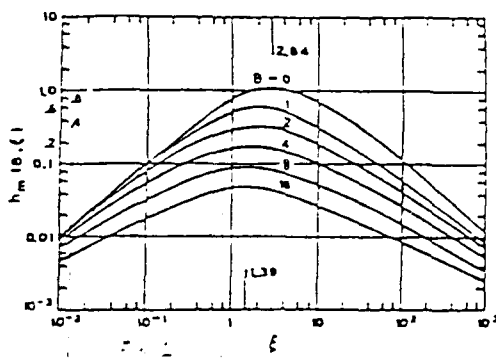
### SECOND HARMONIC GENERATION 0.5-5 $\mu\text{m}$



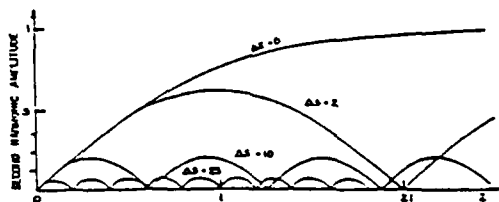
CRYSTAL	AgGaSe2 (1&2)	LiNbO3	$\beta$ -BaB2O4
DIMENSIONS (cm)	Rectangular 1x1x2 long	Cylindrical 1x3 long	Rectangular .5x.5x.8
PHASEMATCHING ANGLE (degrees)	1) 90 2) 52.5	45	22
FUNDAMENTAL WAVELENGTH ( $\mu\text{m}$ )	1) 3.15-3.27 2) 3.78-4.2	1.98-2.48	.99-1.24
SECOND HARMONIC WAVELENGTH ( $\mu\text{m}$ )	1) 1.58-1.64 2) 1.9-2.1	.99-1.24	.495-.630*
ENERGY CONVERSION EFFICIENCY	1) 17-41% 2) 7-10%	10-50%	1-10%
TEMPORAL WALKOFF (psec/cm)	1) -2.28 2) -0.77	-0.072	2.7
BIREFRINGENT WALKOFF (degrees)	1) 0 2) 0.64	1.93	2.9
COATING	1) AR coated 2) uncoated	AR coated	uncoated

\* Note the second harmonic wavelength for  $\beta$ -Barium Borate is the fourth harmonic of the FEL. Quadrupling the FEL from 1.98-2.48  $\mu\text{m}$  down to 0.495-0.630  $\mu\text{m}$  using LiNbO3 and  $\beta$ -BaB2O4.

### CONVERSION EFFICIENCY vs. FOCUSING



## PHASE VELOCITY MISMATCH



The growth of the second harmonic amplitude for varying degrees of phase velocity mismatch  $\Delta s \sim \Delta k l$ , where  $\Delta s$  and  $l$ , the characteristic length, are defined in J. Armstrong, N. Bloembergen, J. Ducuing and P. Pershan, *Phys. Rev.*, Vol.127, No.6, p. 1918(1962)

## APPLICATIONS OF HARMONIC GENERATION ON THE MARK III IR FEL

### PHOTOCHEMISTRY - PHOTODYNAMIC ACTION

Tunable visible light (0.495-0.530  $\mu\text{m}$ ) wavelengths were obtained from the FEL by harmonic generation. We studied the effect of wavelength and pulse structure on the one-photon excitation of porphyrins (Photofrin II) and zinc phthalocyanine sulfonate to photosensitize the oxidation of histidine in phosphate buffer [1]. This photosensitized oxidation reaction occurs when the photosensitizer is excited through a short lived (nanosecond) singlet excited state that undergoes an intersystem crossing to a long lived (microsecond) excited triplet state. The triplet state of the photosensitizer rapidly reacts with molecular oxygen and by energy transfer forms singlet oxygen. The singlet oxygen efficiently oxidizes histidine (imidazole nucleus) and other biological molecules [2]. This photosensitized oxidation is thought to be one of the important pathways involved in clinical laser photodynamic therapy of cancer. The efficiency of pulsed lasers for one-photon or two-photon excitation of porphyrins and phthalocyanines has not been well studied. This type of excitation of pigment and dye photosensitizers should be possible with the FEL but we have not yet studied it. The tunable IR FEL will be required for a wavelength study.

The preliminary results (Table 1) indicate that histidine was rapidly photooxidized with both photosensitizers when excited by pulsed FEL light at one-photon absorption bands. Neither photosensitizer was significantly destroyed or photobleached during the 10 minute exposure to the FEL light at the intensities shown. Table 1 compares the sensitized photooxidative destruction of histidine for two photosensitizers activated with the FEL as a function of wavelength and irradiance. The difference between the control histidine (2.00  $\mu\text{moles}$ ) and the amount of remaining histidine reflects the efficiency of FEL photooxidation shown in Table 1. The rate of histidine photooxidation with the FEL is similar to the rate found with continuous wave tungsten light photooxidation.

Table 1. Photodynamic Action. Mark III Free-Electron Laser photosensitized oxidation of histidine with Photofrin II (PF II) porphyrins and zinc phthalocyanine sulfonate.

SAMPLE	IRRADIANCE (nm)(mW/cm <sup>2</sup> )	TIME (min)	HISTIDINE ( $\mu\text{moles}$ )
Butter, phosphate (0.1 M, pH 7.6)			0.07
Histidine	532 42	10	1.96
PF II / Histidine	532 42	10	0.20
PF II / Histidine	577 21	10	1.10
PF II / Histidine	630 10.3	10	1.19
ZnPCs / Histidine	630 10.3	10	0.73

[1] S. Benson, J. Madey, R. Straight and B. Hooper, *Journal of Laser Applications*, in press.

[2] R.C. Straight and J.D. Sokas, *Singlet Oxygen: Polymers and Biomolecules*, Vol.4, A.A. Frimer, ed., CRC Press, Inc. Boca Raton FL, p. 91-143, 1985.

### EXCITATION SPECTROSCOPY OF $\alpha\text{-Si:H}$

The Mark III IR FEL has been used to measure the first photoluminescence excitation spectrum well below the optical absorption edge in a thin-film amorphous semiconductor [3]. This method should be useful for probing below-gap absorption mechanisms that contribute to photoluminescence (PL) in a wide class of amorphous semiconducting films.

An 8  $\mu\text{m}$  thick sample of  $\alpha\text{-Si:H}$  (hydrogenated amorphous silicon) was used in order to increase the absorption of light at energies well below the absorption edge. The PLE (Photoluminescence excitation) measurements, which covered the range from 1.0 to 1.23  $\mu\text{m}$  (1.01 to 1.24 eV), were performed using a lithium niobate crystal to generate second harmonics. For the frequency-doubled light the peak powers in the microjoules ranged from -20 to -250 kW, and the average power in the microjoules ranged from -0.2

## PHASE VELOCITY MISMATCH FOR SECOND HARMONIC GENERATION

CRYSTAL	$\lambda$ ( $\mu\text{m}$ )	$z$ (cm)	E-E-FIELD (MV/m)	$l^*$ (cm)	$\Delta k$ ( $\text{cm}^{-1}$ )	$\Delta s^*$	$\eta$
LiNbO <sub>3</sub>	3.2	0.2	156	0.170	53.7	0.6	5%
	3.2	1	89	0.314	53.7	16.9	5%
	3.2	1	46	0.606	53.7	32.5	10%
	2.8	3	38	0.44	0.219	0.1	50%
AgGaSe <sub>2</sub> (1&2)	1) 3.15	2.1	34	0.12	31.8	3.8	41%
	1) 3.15	2.1	11	0.36	31.8	12.1	20%
	2) 4.0	2.3	17	0.31	12.3	3.8	10%
B-BaB <sub>2</sub> O <sub>4</sub>	1.86	0.8	44	0.373	198	74	22%

where  $l$  is the characteristic interaction length evaluated at the fundamental wavelength and the phase velocity mismatch is given by  $\Delta s$ .

\*  $l = n\lambda/2\pi\Delta k$  and  $\Delta s = \Delta k l$

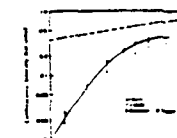
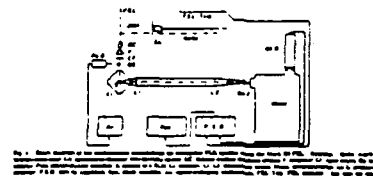
These are the results for the optimized coated crystal system with lithium niobate as the first stage in the cascaded system for quadrupling the Mark III IR FEL. The poor conversion efficiency was likely due to a poor Strehl ratio that was measured at less than 0.2 right after the harmonic generation experiments. A Strehl ratio of 0.2 means that the input electric field is smaller by a factor of  $\sqrt{2}$  therefore  $l$  and  $\Delta s$  are larger by the same factor of  $\sqrt{2}$ .

CRYSTAL	$\lambda$ ( $\mu\text{m}$ )	$z$ (cm)	E-E-FIELD (MV/m)	$l^*$ (cm)	$\Delta k$ ( $\text{cm}^{-1}$ )	$\Delta s^*$	$\eta$
LiNbO <sub>3</sub>	2.3	0.4	17	1.41	46	63	1%
	2.8	1	24	0.823	26.8	22	25%

to -2 kW. Using this system peak power densities at the  $\alpha\text{-Si:H}$  sample of -1 MW/cm<sup>2</sup> were generated. These high powers were necessary because the absorption in the thin film is very low ( $\alpha d < 10^{-2}$  where  $\alpha$  is the absorption coefficient and  $d$  is the sample thickness) at these wavelengths and the PL efficiency is probably also low ( $\eta < 0.1$ ) at the measurement temperature ( $T \sim 100$  K). Hence these experiments take advantage of the tunability and high power of the Mark III FEL.

The measured PLE spectrum in  $\alpha\text{-Si:H}$  exhibits an exponential falloff below -1.15 eV. This PLE spectrum is consistent with existing models for the PL process that attribute this radiative recombination to transitions between electrons in the conduction band tail states and the silicon dangling-bond defects.

[3] J. Ristein, B. Hooper, P.C. Taylor, *Journal of the Optical Society of America* B6, 1989, p. 1003



## DIRECT SPECTRAL MEASUREMENTS OF THE UCSB FEL

G. Ramian and J. Hu

Quantum Institute, University of California<sup>†</sup>  
Santa Barbara, CA 93106

S. G. Evangelides\*, T. S. Chu, B. G. Danly, R. J. Temkin, and T.G. Solner

Plasma Fusion Center, Massachusetts Institute of Technology<sup>‡</sup>  
Cambridge, MA 02139

Direct frequency-spectrum measurements of the FEL, in operation at the University of California at Santa Barbara (UCSB), have been made using a surface acoustic wave (SAW) spectrometer developed at MIT. A heterodyne converter, using a CW molecular laser as local oscillator, down-converted the FEL's 1.8 THz frequency to an IF frequency of 1 GHz to match the SAW device bandpass. This system had 10 MHz resolution over a 500 MHz bandwidth with a 100 ns sample window.

The need for a SAW spectrometer arises because the UCSB FEL is a repetitively pulsed device characterized by both a single-pulse linewidth and a wider average linewidth. This is due to both imperfect pulse-to-pulse regulation of the electrostatic-accelerators terminal voltage and inherently stochastic startup of the FEL itself. Each pulse ends up with a slightly different frequency. Further, during a pulse, a monotonically decreasing beam energy, characteristic of the electrostatic accelerator, limits the time of single frequency lasing to between 1 and 3  $\mu$ s. Conventional RF spectrometers cannot take a complete spectrum within that time and the frequency shifts prohibit the use of sampling techniques. On the other hand, the FEL operates at wavelengths too long for optical techniques. A grating spectrometer with sufficient resolution would be prohibitively large.

The UCSB FEL uses a waveguide Fabry-Perot type resonator of 7.14 m length. This results in a longitudinal mode spacing ( $c/2L$ ) of 21 MHz. While the SAW spectrometer resolution (10 MHz) was insufficient to measure the linewidth of a single mode, it could easily distinguish between lasing on a single and lasing on multiple modes. During the experiment, a large number of spectra were taken. A statistical analysis of these spectra is presented.

<sup>†</sup> Research sponsored under ONR/URI contract N00014-86-K-0692 and SDI-MFEL contract N00014-86-K-0110

<sup>‡</sup> Research sponsored under DOE contract DE-AC03-86SF16498

\* Presently at AT&T Bell Laboratories, Holmdel, NJ 07783

## Introduction

In a collaborative effort between the MIT and UCSB FEL groups, a real-time spectral analysis of the UCSB FEL has been performed. In recent theoretical work,<sup>1,2</sup> and past experimental work,<sup>3,4</sup> the mode spectrum has been studied. In past experimental work, the FEL radiation amplitude as a function of time was sampled with a fast detector, then this data was Fourier analyzed to obtain calculated spectral linewidths. Recent theoretical work by Antonsen and Levush<sup>1,2</sup> has suggested that FEL oscillators may produce a radiation field which has many spectral components for practical pulse durations but for which the amplitude is only weakly modulated. In this theory, a phase locking of neighboring resonator modes within the gain bandwidth is responsible for the greatly reduced amplitude modulations.

Here we report this first direct real-time spectral analysis of the UCSB FEL. This experimental work was carried out during October 1988 and March 1989. Both homodyne (Oct. 88) and heterodyne (March 89) receiver systems were employed. Results of this work are presented in this paper.

## MIT SAW Spectrometer System

- FEL radiation at 1.8 THz mixed with local oscillator (LO) signal ( $\sim 1.8$  THz) from FIR gas laser in Schottky diode to produce intermediate frequency (IF) centered at 1 GHz.
- If signal gated with 100 ns gate to produce IF pulse of appropriate length for SAW filter. Gate can occur at different times during FEL pulse to sample spectrum at different times.
- Gated IF signal is dispersed in a surface acoustic wave (SAW) filter with dispersion of 1  $\mu$ s/50 MHz and 500 MHz bandwidth. SAW transmission vs. frequency (see below) is unfolded from digitized spectra off line.

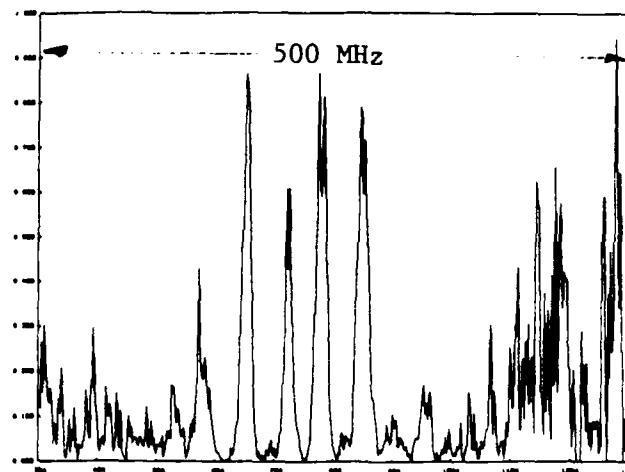
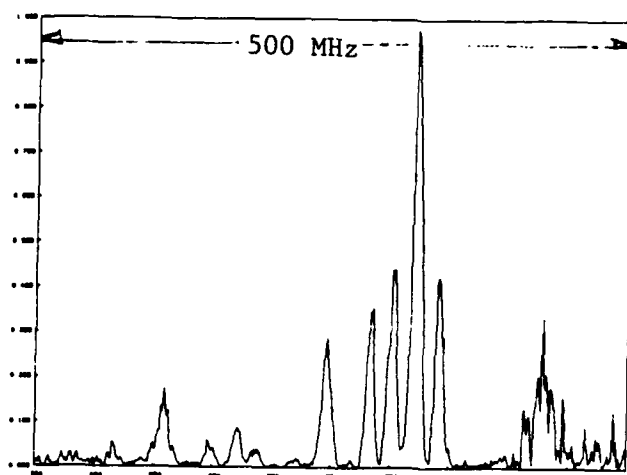
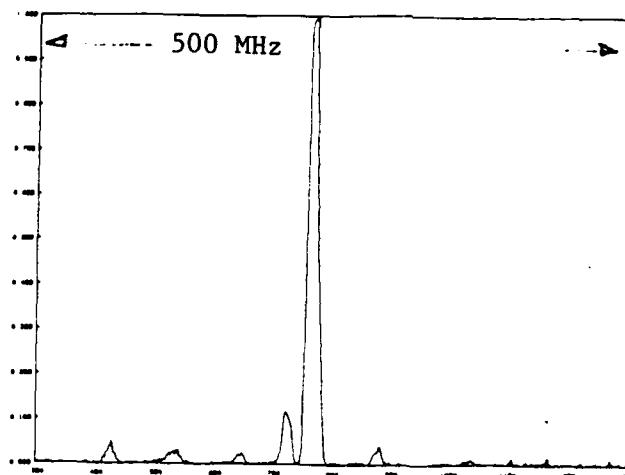
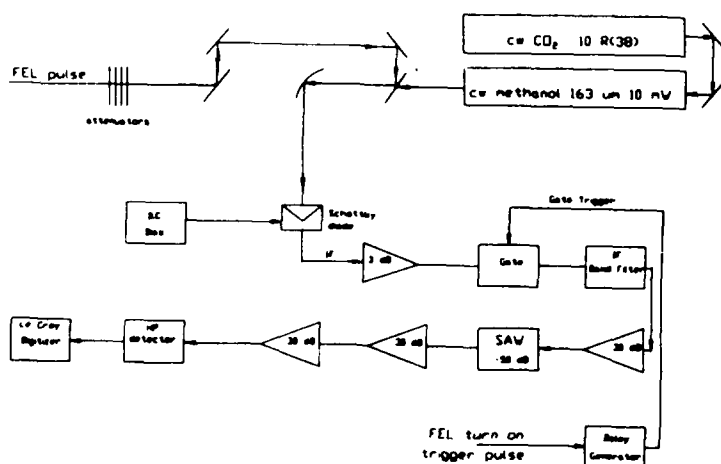


## Heterodyne Results (March, 1989)

- Heterodyne receiver operation obtained with ~10 mW CW 1.8 THz gas laser used as local oscillator (LO).
- Pressure broadened gain bandwidth of LO laser was much less than free spectral range of laser cavity resulting in monochromatic LO.
- Observed and recorded 90 spectra. Spectra obtained excitation of as few as one and as many as 10 FEL longitudinal cavity modes within the SAW filter bandwidth.
- Mode spectra show characteristic 20 MHz spacing of FEL cavity modes.
- Density of longitudinal modes excited within SAW bandwidth exhibited no correlation with temporal location of 100 ns SAW gate within FEL pulse.
- Samples of heterodyne, real-time spectra and histogram of mode density shown below. Complete catalog of spectra is appended to this paper.

## Conclusions

- A real-time spectral analysis of the UCSB FEL has been carried out using an MIT 1.8 THz heterodyne receiver system.
- Both homodyne and heterodyne receiver spectral data show excitation of multiple modes within the FEL cavity, and that such spectra are consistent with a field amplitude temporal structure which has only minor amplitude modulation.



## P2.20

### TECHNOLOGICAL REQUIREMENTS FOR A CONTINUOUS WAVE FREE ELECTRON LASER

D.J. Larson

Center for Research in Electro Optics and Lasers  
12424 Research Parkway, Orlando, FL 32826

**ABSTRACT** -- Recent progress in electron cooler technology has resulted in the operation of a 2 MeV 0.1 Ampere DC recirculating electron beam system. A similar system could be used to drive a continuous wave free electron laser (CW FEL). The requirements and feasibility of a CW FEL are discussed.

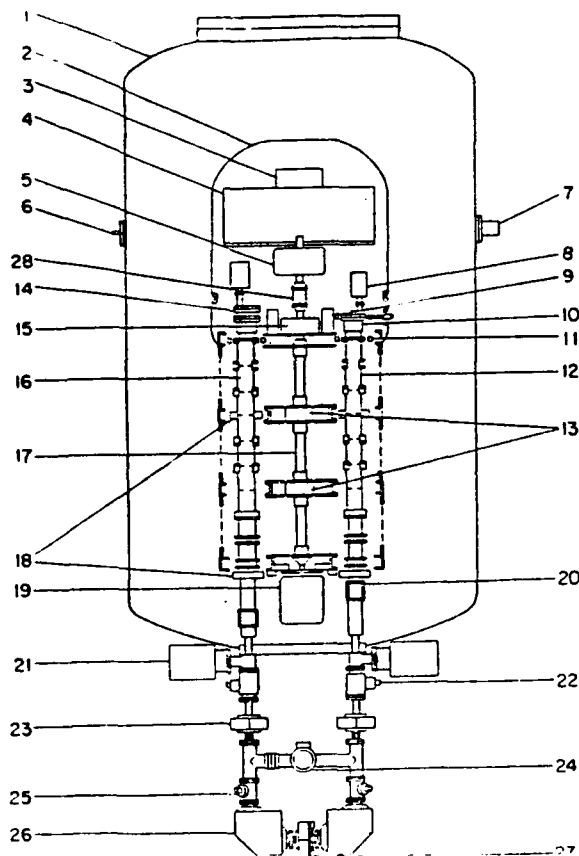


Figure 1. Diagram of the NEC electron cooler prototype that achieved 0.1 ampere DC currents of 2 MeV electron beams. 1) Accelerator Tank; 2) High Voltage Terminal; 3) Heat Exchangers; 4) Gun and Collector Electronics; 5) 10 KVA Generator; 6) Capacitive Pick Off; 7) Generating Volt Meters; 8) Ion Pump; 9) Electronics; 10) Electron Gun; 11) Steerers; 12) Acceleration Tube; 13) 200 W Generators; 14) Collector; 15) 1 KVA Generator; 16) Deceleration Tube; 17) Insulating Rotating Shaft; 18) Solenoids; 19) Motor; 20) Steerer; 21) Ion Pump; 22) Faraday Cup; 23) Quadrupole; 24) Ion Pump; 25) Beam Profile Monitor; 26) Dipoles; 27) Quadrupole; 28) Insulating Coupler.

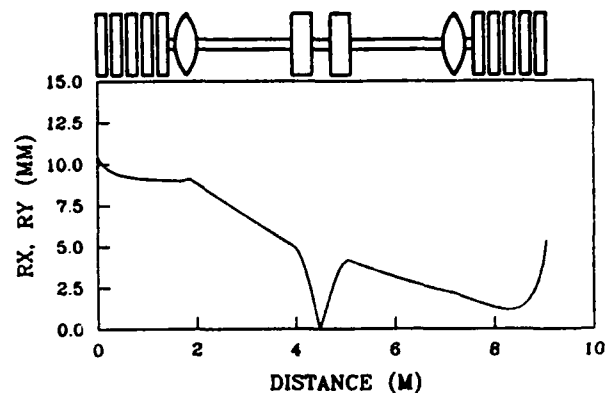


Figure 2. Calculated electron beam radius as a function of distance for the NEC electron cooler prototype.

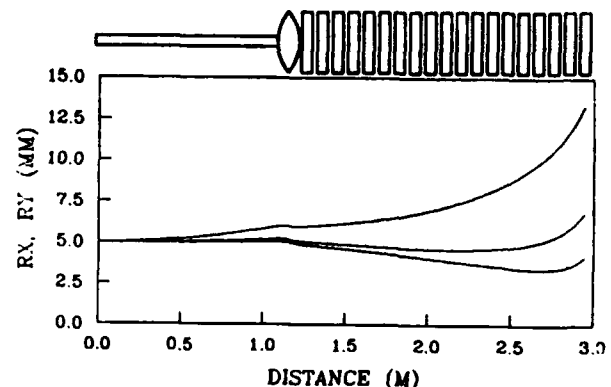


Figure 3. Calculated electron beam radius as a function of distance for the final beamline sections of a CW FEL. Beam radius is calculated for three values of emittance, thermal (normalized emittance  $e_n$  equal to 10 p mm-mr), ten times thermal ( $e_n = 100$  p mm-mr), and twenty times thermal ( $e_n = 200$  p mm-mr).

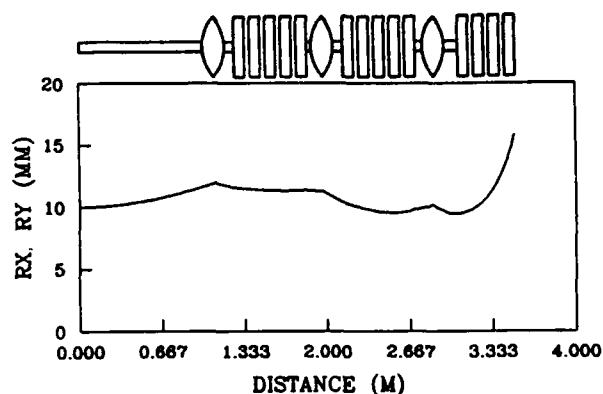


Figure 4. Calculated electron beam radius as a function of distance for the final beamline sections of a CW FEL ( $\epsilon_n = 1000 \text{ p mm-mr}$ ). Solenoidal focusing is used every 1 MV within the deceleration tube.

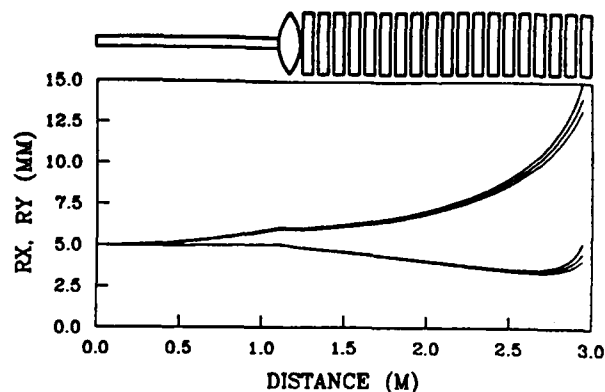


Figure 5. Calculated electron beam radius as a function of distance for the final beamline sections of a CW FEL. Beam radius is calculated for three values of emittance, thermal ( $\epsilon_n = 10 \text{ p mm-mr}$ ) and twenty times thermal ( $\epsilon_n = 200 \text{ p mm-mr}$ ), with energy loss in the FEL assumed to be 0, 50 KeV, and 100 KeV.

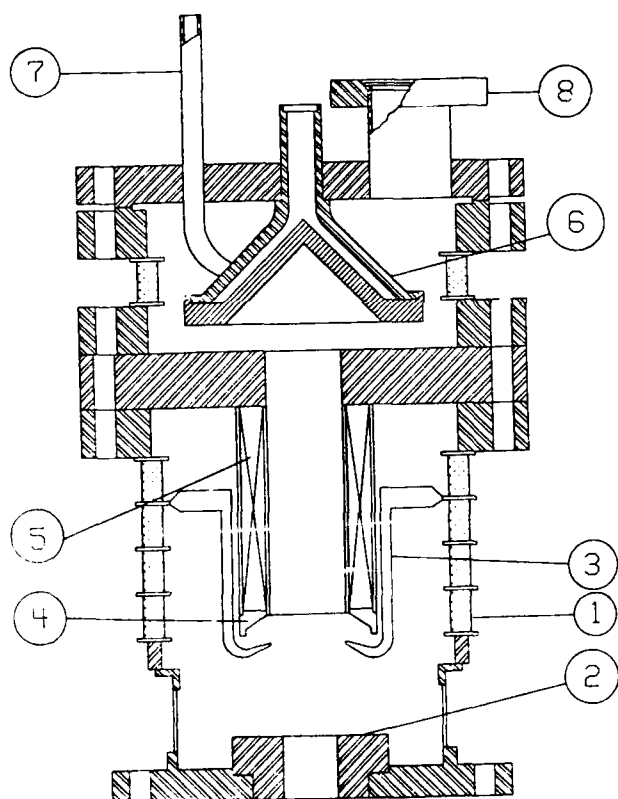


Figure 6. Diagram of the NEC magnetized collector: 1) Ceramic Housing; 2) Entrance Aperture; 3) Focus Electrode; 4) Pierce Geometry Electrode; 5) Solenoidal Coil; 6) Collection Cone; 7) Cooling Water Inlet; 8) Vacuum Port.

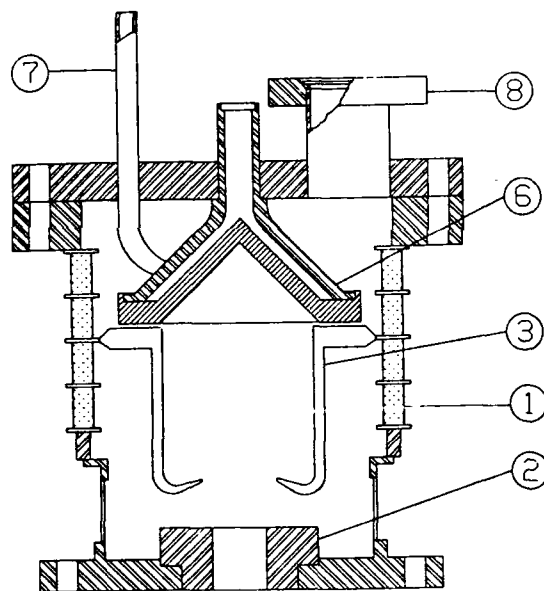


Figure 7. Diagram of the NEC nonmagnetized collector: 1) Ceramic Housing; 2) Entrance Aperture; 3) Focus Electrode; 4) Pierce Geometry Electrode; 6) Collection Cone; 7) Cooling Water Inlet; 8) Vacuum Port.

## P2.24

### A Micro-Fabrication Compatible Wiggler Design Scalable to Sub-Millimeter Periods\*

Robert H. Jackson and Hans Bluemel  
Code 6842  
Naval Research Laboratory  
Washington, DC 20375-5000

A linear wiggler design has been developed which is compatible with micro-fabrication techniques and is capable of producing uniform, multi-kilogauss fields at millimeter and sub-millimeter periods. It has implications for low voltage infrared free electron lasers.

#### Why Small Period Wigglers?

Free-Electron Lasers to-date have required high electron kinetic energy in order to generate high frequencies. This results in fairly large systems with heavy radiation shielding requirements.

$$\lambda = \frac{\lambda_w}{2\gamma^2}$$

Small period wigglers ( $\lambda_w \leq 10\text{mm}$ ) can lower the voltage requirements for operation at a given frequency, but other aspects of the FEL must be adjusted.

#### Advantages

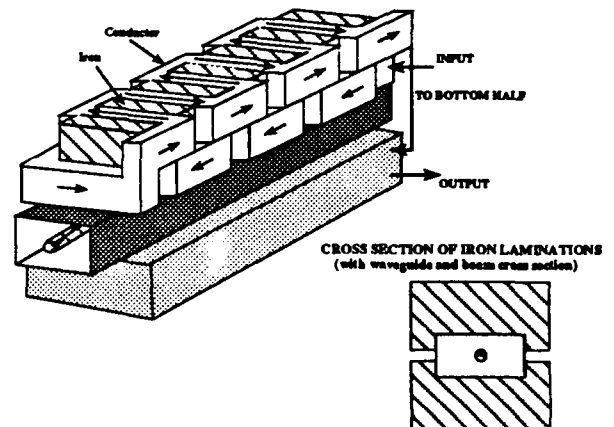
Voltage Reduction  $\propto \sqrt{\lambda_w}$   
Smaller Total System Size  
Lower Shielding Requirements

#### Disadvantages

Smaller wiggler period  $\rightarrow$  exponential drop in field unless wiggler gap is reduced  $\rightarrow$  drastic drop in gain  
Wiggler gap scaled by period reduction  $\rightarrow$  constant wiggler field, but smaller electron beams  $\rightarrow$  lower output power

However: Numerous Applications in the MM-Wave, Mid- & Far-IR Range Could Benefit From a Compact, Moderate Power, Tunable Source Based on Small Period Wigglers.

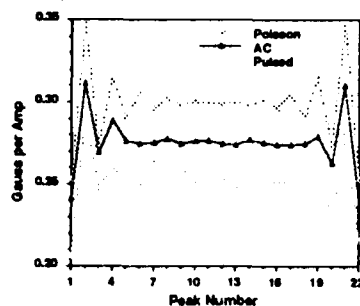
#### SCHEMATIC OF REDUCED EDGE EFFECTS LINEAR (REEL) WIGGLER



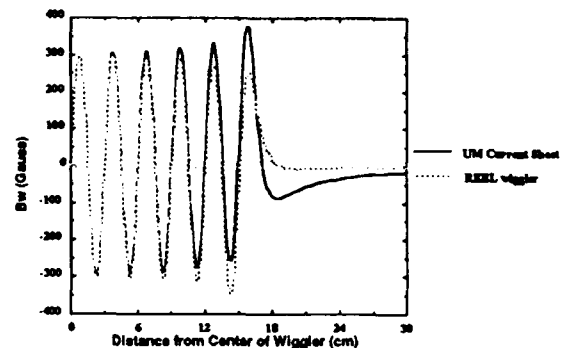
#### CHARACTERISTICS OF REEL WIGGLER DESIGN

- Simple design compatible with low cost, high accuracy fabrication
- 3D multilayer conductor winding pattern  $\rightarrow$ 
  - Current multiplication - adaptable to I-V parameters of power supply
  - Reduction of stray fields and field non-uniformities
    - cancellation of "side" currents
    - reduction of "end" effects
    - current leads attach to wiggler on same side
  - Inherent ability to taper entrance and exit wiggler sides
  - Series current path  $\rightarrow$  minimize control & monitoring systems
- Compatible with cooling  $\rightarrow$  DC, AC & Pulsed operation possible
- Capable of multi-kilogauss peak fields even for relatively large gap-to-period ratios
  - $B_{\text{peak}} \geq 2\text{kG}$  for gap/  $\lambda_w = 0.6$
- Winding pattern can be used with other iron core geometries and would be compatible with the use of multiple layers of thin film superconductors (if and when available!)

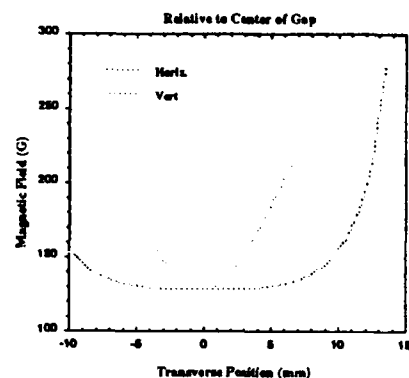
#### Comparison of Calculated & Measured Peaks



#### AXIAL PROFILE COMPARISON



#### Transverse Profiles



## Wiggler Parameter Scaling for Constant Gap to Period Ratio

Multiply all wiggler dimensions by a factor  $\epsilon$

Field — scales as  $1/\epsilon$  for constant current

Current — scales as  $\epsilon$  for constant field

Resistance — scales as  $1/\epsilon$

Voltage — constant for constant field

Power — scales as  $\epsilon$  for constant field

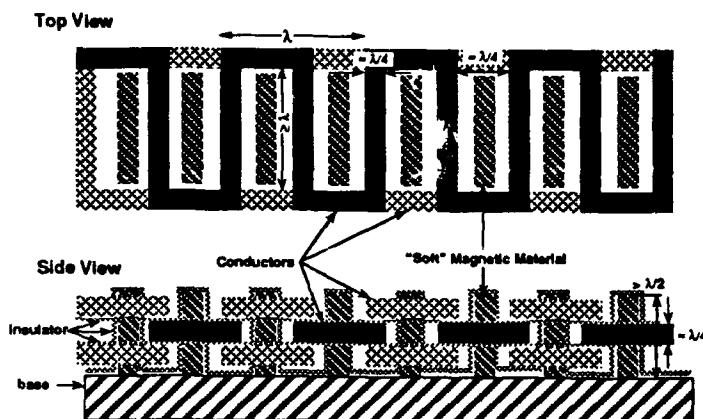
Power Density — scales as  $1/\epsilon^3$

Cooling — scales as  $1/\epsilon$  ( $\propto$  power density / surface-volume ratio)

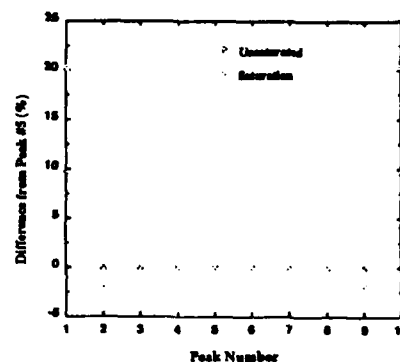
## $\mu$ REEL WIGGLER CHARACTERISTICS

- Use REEL wiggler winding pattern
  - Intrinsic field tapering and reduction of stray fields
  - reduced need for tuning coils and wiggler control systems
- Use **base & comb** configuration for pole pieces
  - base & comb can be fabricated as a single unit (note: the base & comb need not be of the same material)
  - Accurate & Reproducible Fabrication
  - Extended Structures Possible (i.e. 100's to 1000's of periods)
  - "Iron" base yields highly uniform wiggler field
- Calculations indicate uniform fields up to ~ 2kG can be generated with a 1mm period  $\mu$ REEL wiggler
- Fabrication: Existing methods provide reasonable cost and fabrication time
  - Wiggler periods down to ~ 1mm:
    - computer controlled machining and milling
    - computer controlled wire-EDM
  - Wiggler periods less than 1mm:
    - laser machining
    - reactive ion etching
    - ion milling

## Basic Concept for $\mu$ REEL Wiggler



Inherent Uniformity of  $\mu$ -REEL Wiggler



## $\mu$ REEL Based Proof-Of-Principle Experiment

**Experimental Goals:** Investigate low-voltage, high-frequency FEL operation utilizing small period wiggler

**Configuration:** oscillator  
sheet electron beam  
linear  $\mu$ REEL wiggler  
TE<sub>01</sub> waveguide mode interaction  
cavity structure unacidic

**Parameters:** current — 2A  
voltage — 250V  
wiggler period — 1.5 mm  
wiggler field — 2kG pulsed  
frequency — 350GHz  
pulse length — 1μsec  
PRF — 2-100 Hz

**Calculated Performance:** gain — 100% per pass for 100 μW  
(unoptimized) power — ≥ 2.5 kW extraction  
(zero velocity spread, untapered)

**Status:**  $\mu$ REEL test piece presently being fabricated  
calculations to optimize performance underway

## Summary

- A WIGGLER DESIGN SCALABLE TO MM- & SUB-MM PERIODS HAS BEEN DEVELOPED
- A PROTOTYPE WIGGLER HAS BEEN BUILT AND TESTED AND PERFORMANCE IS IN GOOD AGREEMENT WITH CALCULATIONS
- A  $\mu$ REEL WIGGLER TEST UNIT HAS BEEN DESIGNED WITH A 1.5 mm PERIOD AND IS BEING FABRICATED
- INITIAL CALCULATIONS FOR A LOW-VOLTAGE FEL EXPERIMENT BASED ON A  $\mu$ REEL WIGGLER INDICATE INTERESTING PERFORMANCE LEVELS ARE POSSIBLE IN THE MM-WAVE AND FAR-IR WITH EXTREMELY COMPACT SYSTEMS

\* Work supported by Office of Naval Technology and Office of Naval Research

† Laboratory for Plasma Research, University of Maryland, College Park, MD 20742

## P2.25

### FEL PERFORMANCE WITH PURE PERMANENT MAGNET UNDULATORS HAVING OPTIMIZED ORDERING

R. A. Cover, B. L. Bobbs, G. Rakowsky, S. P. Mills  
Rockwell International, Rocketdyne Division  
6633 Canoga Avenue  
Canoga Park, CA 91303

The degradation of FEL performance by field errors can be greatly mitigated in a pure permanent magnet undulator by appropriate ordering of magnets. Monte Carlo techniques have been used to obtain such optimized ordering for various systems. The resulting performance improvement has been evaluated using the Rocketdyne simulation code FELOPT.

<p><b>INTRODUCTION:</b> Pure permanent magnet (PPM) undulators are ideally suited to computer optimization because of the absence of high permeability pole pieces and because of their modular construction using interchangeable magnets. The cost function used to assess FEL performance during optimization must, however, be fairly simple to allow practical computation times. It is therefore important that realistic simulations be used to verify the effectiveness of the optimization.</p>	<p><b>SUMMARY:</b> The results show that optimized ordering generally results in substantial improvements in FEL performance, often yielding efficiencies almost as high as if magnet errors were absent.</p> <p><b>OUTLINE OF PAPER:</b></p> <ul style="list-style-type: none"> <li>• Structure of simulation code FELOPT</li> <li>• Error model</li> <li>• Results of simulations</li> </ul>
<p><u>Structure of Simulation Code FELOPT</u></p> <p>Electron parameters (<math>x, y, \beta_x, \beta_y, \gamma</math>) initiated by a random number generator consistent with a given emittance and energy spread.</p> <p>Electron Trajectory Equations:</p> $\frac{d(\gamma\beta_y)}{dz} = -\frac{a_w^2 k_{wy}^2}{2\gamma} y \quad \frac{dy}{dz} = \beta_y$ $\frac{d(\gamma\beta_x)}{dz} = -\frac{a_w^2 k_{wx}^2}{2\gamma} x \quad \frac{dx}{dz} = \beta_x$ <p>Magnetic Field</p> $B_y(\vec{r}) = B_y(0) \left( 1 + \frac{1}{2} k_{wy}^2 y^2 + \frac{1}{2} k_{wx}^2 x^2 \right)$	<p><u>FEL Equations of Motion</u></p> <p>Electrons</p> $\frac{d\gamma}{dz} = -\frac{1}{2\gamma} \frac{e}{mc^2} F_B a_w E_s \sin(\psi + \phi_s)$ $\frac{d\psi}{dz} = k_w - \frac{k_s}{2\gamma^2} \left[ 1 + \frac{a_w^2}{2} + (\gamma\beta_x)^2 + (\gamma\beta_y)^2 \right]$ <p>Optical Field</p> $\vec{E} = E_s(\vec{r}) \exp(i\phi_s(\vec{r}))$ $2ik_s \frac{\partial \vec{E}}{\partial z} + \nabla_{\perp}^2 \vec{E} = -\frac{4\pi}{c} F_B J_{aw} \left\langle \frac{\exp(-i\psi)}{\gamma} \right\rangle$ <p>Field resolved in <math>(r, \theta)</math>. Electron and optical field equations integrated using 4th order Runge-Kutta algorithm.</p>
<p><u>Error Model</u></p> <p>Kincaid Model [1]</p> $\Delta B_y = B \epsilon(z) \cos k_w z$ <p><math>\epsilon(z)</math> constant <math>\epsilon_n</math> over interval</p> $(2n-1)\pi/2 \leq k_w z \leq (2n+1)\pi/2$ <p><math>\epsilon(z)</math> has zero mean, <math>\sigma_{SD} = \text{RMS error}</math></p> $\Delta\beta_x = -\frac{e}{mc\gamma} \int \Delta B_y dz' = 2\epsilon(z) a_w/\gamma$ <p>over a given <math>\lambda_w/2</math> interval</p>	<p><u>Error Treatment in FELOPT</u></p> <p>Elliott and McVey [2]</p> $\frac{d\gamma\beta_x}{dz} = \left( \frac{d\gamma\beta_x}{dz} \right)_{\Delta B=0} + \frac{4 a_w}{\lambda_w} \epsilon(z) \sqrt{\frac{\lambda_w}{2\Delta z}}$ <p>where <math>\Delta z</math> is the integration step. Set of errors <math>\Delta B</math> are generated by annealing code [3] with a given seed. Set ordered in this work to minimize phase errors: errors in <math>\Psi</math> caused by <math>\Delta B</math>.</p> <p>[1] B. M. Kincaid, J. Opt. Soc. Am. B 2 (1985) 1294. [2] C. J. Elliott and B. D. McVey, "Analysis of Undulator Field Errors for XUV FELs," Conf. Undulator Magnets for Synchrotron Radiation and FEL's, Trieste (1987). [3] B. L. Bobbs et. al., "In Search of a Meaningful Field Error Spec for Undulators," this volume.</p>

Table 1

## FEL Parameters for 4 m Wiggler System

No intrinsic focusing in wiggler plane;  $k_{wx} = 0$ . Electron beam emittance-matched in y-z, focused to waist at center of wiggler in x-z.

Wiggler Length	4.0 m
Number of Periods	160
Optical Wavelength	0.8 $\mu\text{m}$
Magnetic Field	6.0 KG
Electron Energy	$\gamma = 175.3$
Optical Waist	0.054 cm
Emittance	$7.0 \times 10^{-8} \pi \text{ m-rad}$
Electron Waist	( $r_y = .02 \text{ cm}$ , $r_x = .03 \text{ cm}$ )
Optical Power	$2 \times 10^9 \text{ W}$
Current	500A
Resonant $\Psi$	$36^\circ$

Table 4

FEL Performance with Different Input Power  
WFE = 2%, Seed = 25

P (W)	$\eta$ (No Errors) (%)	$\eta$ (Errors) (%)
$2 \times 10^9$	7.8	7.6
$1 \times 10^9$	3.2	3.4
$5 \times 10^8$	0.9	1.1
$1 \times 10^8$	0.2	0.2

Optimization is not affected by operating at optical powers away from the design point.

Table 2

## FEL Performance for Different Sets of Errors

WFE (%)	Seed	Extraction Efficiency (%)
0	-	7.8
1	25 (Not Sorted)	0.3
1	25	7.8
1	99	7.8
1	75	7.7
2	25	7.6
2	75	7.4
3	25	7.2
3	75	7.1
4	25	6.2
4	75	7.0
5	25	5.7
5	75	5.8
5	99	6.7
5	50	6.0

WFE = RMS Wiggler Field Error

Table 5

Extraction Efficiency with Untapered Wiggler  
Seed = 25,  $\gamma = 175.5$ 

WFE (%)	Input Power = $10^7 \text{ W}$ Peak Extraction (%)	Input Power = $10^6 \text{ W}$ Peak Extraction (%)
0	0.52	0.54
1	0.50	0.56
2	0.40	0.43
3	0.32	0.37
4	0.33	0.30
5	0.19	0.12

Optimization effective in small signal as well as in high extraction regime.

Table 3

## FEL Performance with Retuning

WFE (%)	Seed	$\eta_1$ (%)	$\gamma'$	$\eta_2$ (%)
5	25	2.6	176.2	5.7
5	99	5.5	176.1	6.7
5	75	4.4	176.2	5.8
5	50	5.1	176.2	6.0
4	25	5.7	175.9	6.2
4	75	6.8	175.8	7.0

For larger WFE, optimum performance requires retuning system (changing  $\gamma$ , B,  $\lambda_w$ , or  $\lambda_s$ ) to compensate for phase error  $\Delta\Psi \sim \Delta(\gamma\beta_x)^2$ . For these cases no initial steering was necessary.

Table 6

## Wiggler Performance with Interpolated Field Errors

$L_w = 10 \text{ m}$ ,  $N_w = 500 \text{ Periods}$ ,  $\gamma = 289.2$ ,  $B = 8.5 \text{ KG}$ ,  
 $I = 100 \text{ A}$ ,  $\lambda_s = 0.3 \mu\text{m}$ ,  $P_o = 5 \times 10^9 \text{ W}$ , Seed = 75,  $\Psi_r = 10\text{-}30^\circ$

WFE (%)	0	1	2	3	4	5
$\gamma$	289.2	289.2	289.2	289.2	289.8	290.1
Initial Steering (mrad)	0	-.02	-.06	-.11	-.15	.08
Extraction Efficiency (%)	8.3	8.2	8.3	8.2	7.9	7.4

Fractional error  $\epsilon(z)$  in Kincaid model interpolated within half periods. Initial steering and retuning necessary for longer wiggler.

## P2.26

### INITIAL RESULTS OF OPERATING THE ROCKETDYNE UNDULATOR IN A TAPERED CONFIGURATION

Mark Curtin, Anup Bhowmik, Jeffory Brown, Phillip Metty and Wayne McMullin

Rockwell International, Rocketdyne Division  
6633 Canoga Avenue, Canoga Park, CA 91303  
and

Stephen V. Benson and John M. J. Madey  
Stanford Photon Research Laboratory  
Stanford University, Stanford, CA 94305

The near infrared Rocketdyne/Stanford free-electron laser uses a very high quality, precision undulator whose gap and magnetic field taper may be continuously varied. The FEL utilizes an electron beam supplied by the Mark III rf-linac at a nominal energy of 38 MeV. We have recently operated the FEL as an oscillator and observed sustained oscillations as the undulator B-field taper was continuously varied from 0 to 10%. Details of the experimental results will be presented.

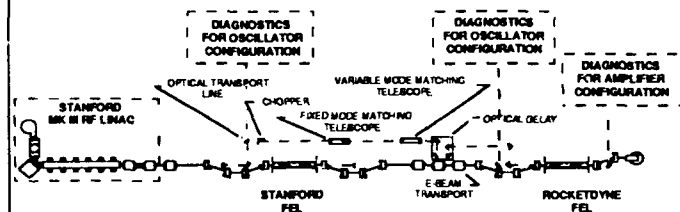
#### ROCKETDYNE UNDULATOR PARAMETERS

UNDULATOR TYPE	PURE REC HALBACH CONFIGURATION
MAGNET MATERIAL	SmCo <sub>5</sub> (Vacumax 170)
MAGNET DIMENSIONS	0.5 x 0.5 x 5.0 (cm)
UNDULATOR PERIOD	2.5 (cm)
UNDULATOR LENGTH	200 (cm)
# OF PERIODS	80
MAGNETIC FIELD RANGE	3.7 - 0.8 (kG)
MAGNETIC FIELD TAPER RANGE	0% - 75% (IN PEAK MAGNETIC FIELD)

- THE UNDULATOR CAN BE CONTINUOUSLY GAP TUNED BY OPENING BOTH ENDS OF THE UNDULATOR IN UNISON
- THE UNDULATOR CAN BE CONTINUOUSLY TAPER TUNED BY OPENING ONE END OF THE UNDULATOR RELATIVE TO THE OTHER

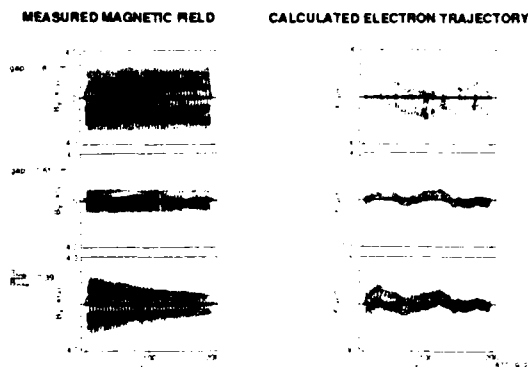
89-MSC-001

#### ROCKETDYNE FEL TESTBED AT THE STANFORD PHOTON RESEARCH LABORATORY



89-MSC-001

#### PURE PERMANENT MAGNET WIGGLER MAINTAINS ACCURATE ELECTRON TRAJECTORY OVER A WIDE RANGE OF GAP AND TAPER SETTINGS



#### ELECTRON BEAM PARAMETER TABLE

##### RF PARAMETERS

FREQUENCY	2857	MHz
REP. RATE	15	Hz
MACROPULSE LENGTH	5	μsec
MICROPULSE LENGTH	~ 2	psec

##### E-BEAM PARAMETERS

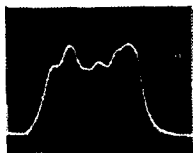
MACROPULSE CURRENT	200	mA
MICROPULSE CURRENT	35	A
NORMALIZED VERTICAL EMITTANCE	2π	mm-mrad
NORMALIZED HORIZONTAL EMITTANCE	10π	mm-mrad
ENERGY	38.5	MeV
ENERGY SPREAD	< 0.5	%

89-MSC-001



# PEAK INTRACAVITY POWER INCREASED BY A FACTOR OF 3.25 AS THE B-FIELD TAPER WAS INCREASED FROM 0 - 9.6%

MACROPULSE TRACE  
AU-GE DETECTOR  
FWHM = 2.75 MICROSEC

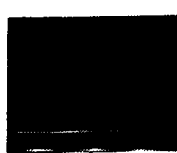


PYROELECTRIC DETECTOR  
ENERGY/MACROPULSE = 3.4 MJ



B-FIELD TAPER = 0%

MACROPULSE TRACE  
AU-GE DETECTOR  
FWHM = 0.80 MICROSEC



PYROELECTRIC DETECTOR  
ENERGY/MACROPULSE = 2.4 MJ



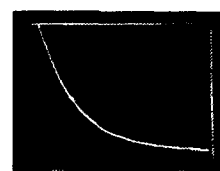
B-FIELD TAPER = 9.6%

99-MSC-009

A SMALL SIGNAL GAIN OF 55% PER PASS WAS MEASURED IN THE UNTAPERED CONFIGURATION AT THE END OF THE EXPERIMENT. A CAVITY RINGDOWN MEASUREMENT YIELDED 9.5% ROUNDTrip LOSSES.



Gap = 0.76 cm  
Taper = 0%  
50 nsec/div

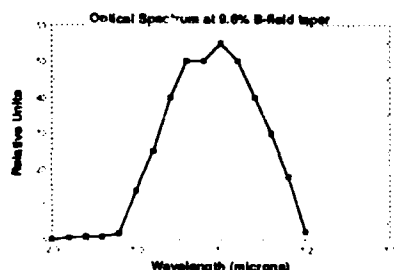


Gap = 0.76 cm  
Taper = 3%  
100 nsec/div

• CAVITY LOSSES OF 9.5% SUGGEST RESONATOR MIRROR DAMAGE WAS PRESENT FOR THIS RUN. [ CAVITY OUTCOUPLING = 0.5 % ]

99-MSC-009

## FEL LINESHAPE TAKEN AT A 9.6% MAGNETIC FIELD TAPER SETTING



99-MSC-009

## FELOPT CALCULATIONS FOR THE TAPERED UNDULATOR OSCILLATOR EXPERIMENT

### ELECTRON BEAM

Y	75.54
PEAK CURRENT (AMP)	35, 30, 25
ENERGY SPREAD (%)	0.5
RADIUS (CM)	0.04

### TAPERED WIGGLER

LENGTH (CM)	200
PERIOD (CM)	2.5
INITIAL MAGNETIC FIELD (KG)	3.7
MAGNETIC FIELD TAPER (%)	9.6

### OPTICAL RESONATOR

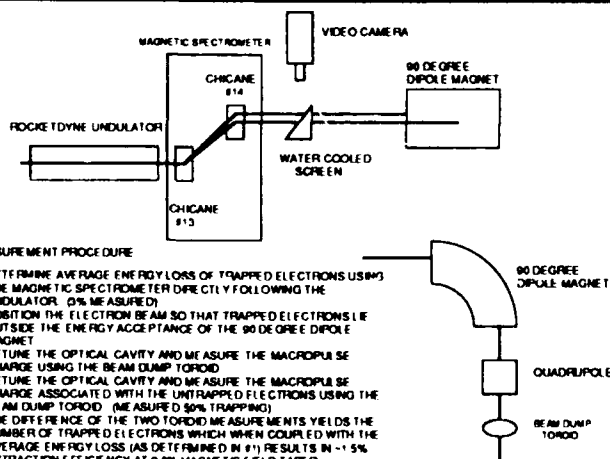
OUTPUT WAVELENGTH (μM)	3.0
RESONATOR LENGTH (CM)	314.8
MIRROR RADIUS OF CURVATURE (CM)	175.535
OPTICAL WAIST AT WIGGLER CENTER (CM)	0.0714
TOTAL RESONATOR LOSSES (%)	9.5

### RESULTS

PEAK INTRACAVITY POWER (MW)	184, 156, 128
EFFICIENCY (%)	1.52, 1.46, 1.40
GAIN (%)	11.2, 10.8, 10.5

99-MSC-009

## ENERGY EXTRACTION MEASUREMENT



99-MSC-007

## RESULTS FROM THE TAPERED WIGGLER EXPERIMENT

- DEMONSTRATION OF 1.5% EXTRACTION EFFICIENCY AT A MAGNETIC FIELD TAPER OF 9.6% FOR 140 MW CIRCULATING POWER
- DEMONSTRATION OF A 3.25 FOLD INCREASE IN INTRACAVITY POWER
- DEMONSTRATION OF CONTINUOUS LASING WHILE GAP TUNING THE UNDULATOR BETWEEN 3.7 KG AND 2.6 KG
- DEMONSTRATION OF CONTINUOUS LASING WHILE TAPER TUNING THE UNDULATOR BETWEEN 0% AND 10%

99-MSC-009

## P2.27

### Fundamental Mode Amplifier Performance of the NRL Ubitron\*

D. E. Pershing<sup>†</sup>, R. H. Jackson, H. Bluem<sup>††</sup>, and H. P. Freund<sup>†††</sup>

Naval Research Laboratory  
Washington, D.C. 20375

Operation of a ubitron/FEL amplifier using the fundamental wiggler harmonic interaction with the TE<sub>11</sub> circular waveguide mode is reported. Small signal gains as high as 17-19 dB have been observed in the 13-18 GHz frequency band. Gain, efficiency, and bandwidth results to date, including comparisons with theory, will be presented.

#### DESIGN FEATURES OF THE NRL UBITRON

- FULL INSTANTANEOUS BANDWIDTH AMPLIFIER
- DC AXIAL, PULSED WIGGLER MAGNETIC FIELDS
- REPETITIVE PULSE OPERATION
- HIGH QUALITY, HIGH CURRENT ELECTRON BEAM
  - \* MODIFIED SLAC KLYSTRON GUN
  - \* ADVANCED GUN
- HIGH GAIN PER FREE SPACE WAVELENGTH
- HIGH EFFICIENCY IN UNTAPERED CONFIGURATION
- VARIABLE POLARIZATION INPUT RF WAVE
- FUNDAMENTAL WAVEGUIDE MODE OPERATION WITH
- HELICAL WIGGLER WITH ADIABATIC ENTRANCE
- FLEXIBLE/MODULAR DESIGN FOR INTERACTION TAPERING

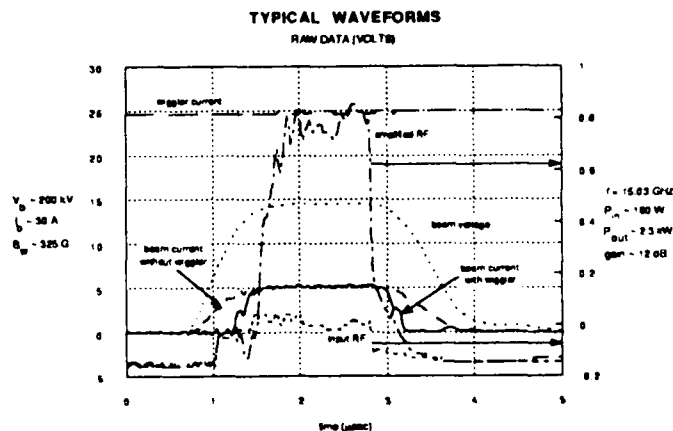
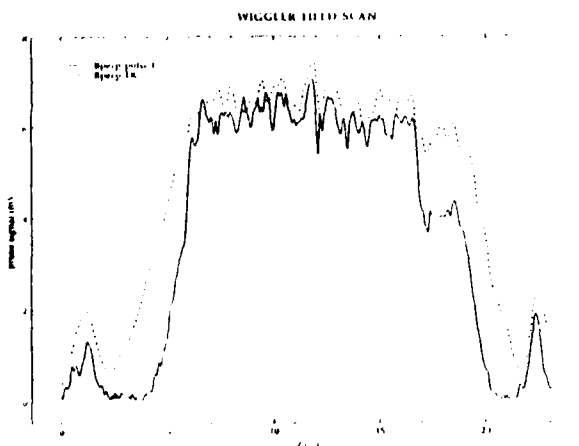
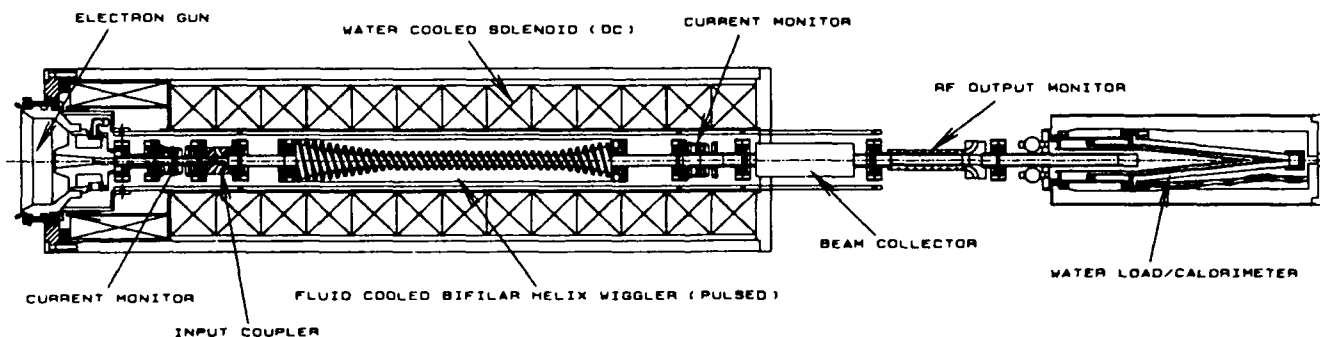
#### GOALS

TOTAL GAIN - 25-30 dB  
EFFICIENCY - > 15%  
BANDWIDTH - > 20%

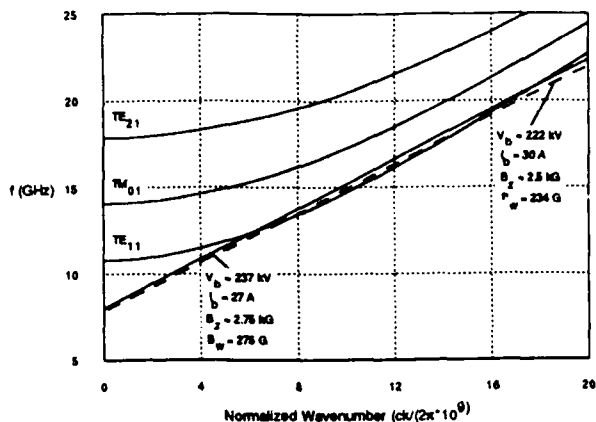
#### UBITRON EXPERIMENTAL PARAMETERS

	Present	Design
Voltage (kV)	190-250	250
Current (A)	0-37	30/100
Beam Radius (cm)	0.4	0.4
Pulse Length (μSec)	1	1
Repetition Rate (Hz)	3-30	1-100
Wiggler:		
Period (cm)	2.54	2.54
Entrance [DC, Pulsed] (periods)	5, 4	5
Uniform [DC, Pulsed] (periods)	12, 10	12
Exit [DC, Pulsed] (periods)	3, 5	3
Pulsed Field (Gauss)	575	1500
DC Field (Gauss)	140	500
Solenoid (kiloGauss)	1.8-2.8	1-3.2
Frequency (GHz)	13.5-17.4	12.4-18

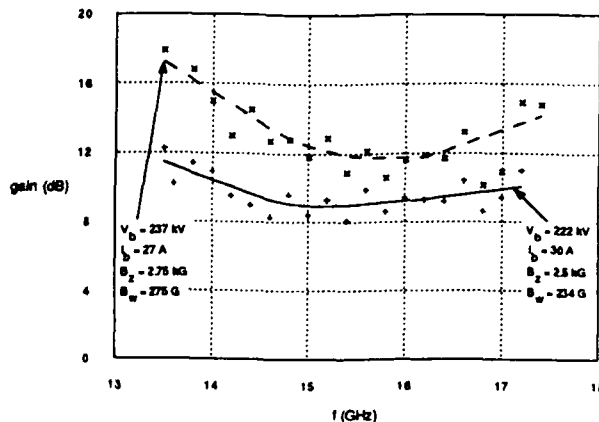
### NRL KU BAND UBITRON AMPLIFIER



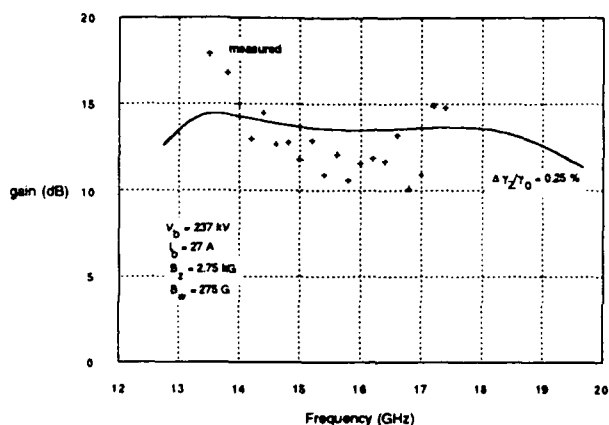
### UBITRON UNCOUPLED DISPERSION CURVES



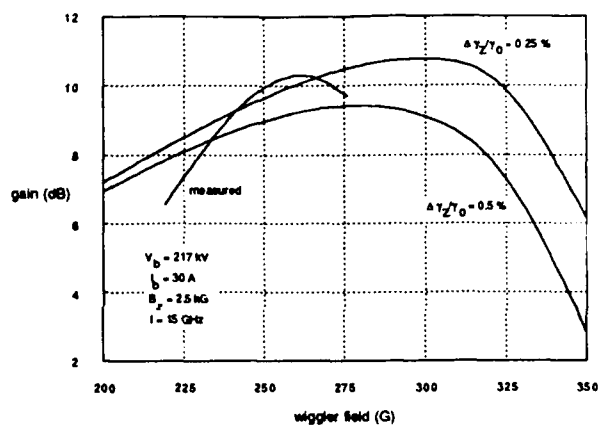
### UBITRON SMALL SIGNAL GAIN



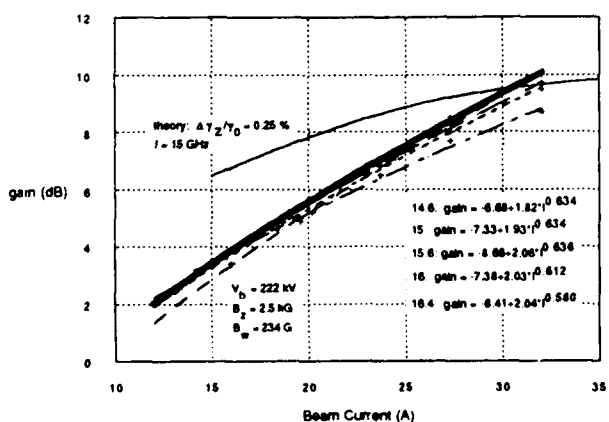
### COMPARISON: THEORY and EXPERIMENT GAIN vs. FREQUENCY



### COMPARISON: THEORY and EXPERIMENT GAIN vs. WIGGLER FIELD



### COMPARISON: THEORY and EXPERIMENT GAIN vs. BEAM CURRENT



### SUMMARY

#### Broadband Ubitron/FEL Amplification in Circularly Polarized TE<sub>11</sub> Mode

- Peak Gain = 19dB @ 17GHz
- Peak Gain / Free-Space Wavelength = 1.5dB/λ @ 13.5GHz
- Bandwidth ≥ 25%

#### Gain is Linear With Input RF Power

- no indication of saturation, anticipate requiring ~ 30dB to saturate with present RF drive power

#### Scaling Of Gain With Beam Current

- exponent ~ 0.6 - scaling is consistent with either  $I^{3/5}$  (strong pump) or  $I^{1/2}$  (Raman)

#### 3D Nonlinear Calculations Are In Good Agreement

- gains are in general agreement assuming ~ 0.25 % gamma spread
- differences in the shape of the gain curves indicate there are details which remain to be included or revised in the calculations; measured wiggler field profile is difficult to model

#### Measurements will Continue Over a Wider Parameter Range Using the Advanced Gun

\* Work supported by the Office of Naval Research and Office of Naval Technology

† Mission Research Corporation, Newington, VA 22122

†† Laboratory for Plasma Research, Univ. of Md., College Park, MD 20742

††† Science Applications International Corporation, McLean, VA 22102

Superconducting linacs provide beams with low emittance and low energy spread, comparable with a storage ring beam. This performance can be exploited in a FEL operating in the Optical Klystron configuration which was up to now taken into account mainly to increase the gain in storage ring FEL.

Moreover few constraints apply in the design of the transport optics for single pass devices, and uncommon layout are feasible.

### THE LAYOUT OF LISA DOK

The layout of the LISA FEL includes a chicane at both ends of the undulator to allow the insertion of a short optical cavity as shown in fig. 4.

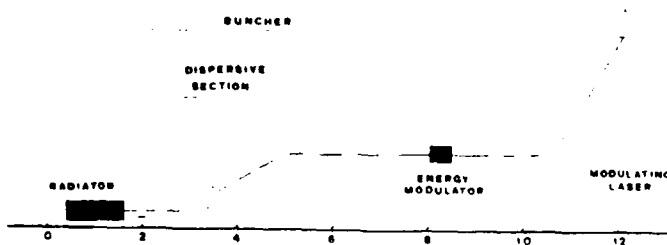


Fig. 4 - Location of the DOK elements on the LISA FEL layout

The modulating undulator is placed before the chicane in a straight section where the electron beam can be squeezed to interact with a focused laser beam and gain periodic energy modulation  $\delta\gamma = \delta\gamma_{mod} \sin \psi_0$ . In the path to the radiating undulator both the free space drift and the dispersion in the chicane cause the onset of longitudinal bunching at the laser wavelength  $\lambda_0$ .

### WAVELENGTH SHIFTING

Exploiting the distance between the modulator and the radiator an RF cavity can be inserted to add a linear energy variation to the beam already affected by the periodic energy modulation. The schematic is shown in fig. 5.

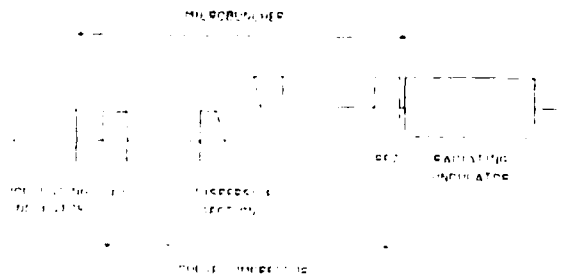


Fig. 5 - Layout of pulse compressor for wavelength shifting

We present a Distributed Optical Klystron (DOK) in which the modulator and the radiator undulator are far apart, allowing separate optimization of the interaction regions. This disposition allows the insertion of a pulse compressor, exploiting the dispersive section between the modulator and the radiator, which causes modulation stretching or shrinking. In this way the modulation is produced at fixed wavelength by an high power laser, and then shifted at the required wavelength before entering the radiation undulator.

### THE BEAM TRANSPORT AND THE BUNCHING PROCESS

The longitudinal modulation in a wavelength  $\lambda_0$  along  $z$  is described by

$$I(\psi) = I_0 \left( 1 + 2 \sum_{m=1}^{\infty} i_m \cos(m\psi) \right)$$

where

$$\psi = \psi_0 + \Psi \sin \psi_0 \quad (1)$$

and

$$\Psi = \frac{2\pi}{\lambda_0} \left( \alpha_t - \frac{z}{\gamma^2} \right) \frac{\delta\gamma_{mod}}{\gamma} \quad (2)$$

In the rhs of the above equation the terms

$$\alpha_t \frac{\delta\gamma_{mod}}{\gamma} = \int_0^z \frac{\eta}{\rho} ds \frac{\delta\gamma_{mod}}{\gamma} \quad \text{and} \quad \frac{z}{\gamma^3} \delta\gamma_{mod}$$

account respectively for the path length variation due to the magnetic dispersion and for delay due to the velocity modulation. The harmonic amplitude growth in the path from the modulator to the radiator is given by

$$i_m(z) = J_m(m\Psi)$$

The emittance causes path length variations uncorrelated with the energy modulation so the bunching will be smeared after a long drift space. The path lengthening due to emittance is given by

$$\delta l(\epsilon) = \int_0^z dl - z \approx \int_0^z \frac{\epsilon}{2\beta} \sin^2 \left( \frac{z}{\beta} \right) dz \approx \frac{\epsilon z}{4 < \beta >}$$

where the simplifications

$$\beta = < \beta > \quad \text{and} \quad < \sin^2 \left( \frac{z}{\beta} \right) > = \frac{1}{2}$$

have been used in the last expression.

In the layout shown in fig. 4 the distance  $z$  between the modulator and the radiator is  $\approx 8m$ ,  $< \beta_x > \approx 10m$  and  $< \beta_y > \approx 3m$ . The LISA normalized emittance is  $\gamma\epsilon = 10^{-5} m \cdot rad$  in both planes and the nominal energy is 25 MeV. The path length variations are

$$\delta z(\epsilon_x) = 4 \cdot 10^{-8} m \quad \text{and} \quad \delta z(\epsilon_y) = 13 \cdot 10^{-8} m$$

so their effect is always negligible in the IR range.

Assume a pulse of length  $l_p$ ; its center passes the RF cavity when the field is zero; the energy variation at the ends of the pulse is

$$\delta\gamma_{lin} \equiv \Gamma\delta\gamma_{mod} = e\hat{V} \sin\left(\frac{\omega_{PC}l_{pulse}}{2c\beta_0}\right) \approx \frac{e\hat{V}\omega_{PC}l_b}{2c\beta_0}$$

The energy modulation along the pulse is

$$\delta\gamma_T = \delta\gamma_{mod} \left( \Gamma \frac{\lambda_0\psi_0}{\pi l_p} + \sin\psi_0 \right)$$

In this case the dispersion of the chicane causes pulse lengthening or stretching while keeping the periodic modulation. A second RF cavity inserted after the chicane cancels the strong energy modulation impressed by the first one.

Assume that the RF cavities are just aside the undulators so that in the bunching process described by the eq. (1) it is possible to replace  $\delta\gamma_{mod} \rightarrow \delta\gamma_T$ ; then

$$\psi = \psi_0 + \Psi \left( \Gamma \frac{\lambda_0\psi_0}{\pi l_p} + \sin\psi_0 \right)$$

The final wavelength of the density modulation is

$$\lambda = \lambda_0 \left( 1 + \frac{\Psi\Gamma\lambda_0}{\pi l_p} \right)$$

In order to cancel in the cavity RF2 the modulation given by RF1 before the pulse compression their fields must be in the ratio

$$\frac{\hat{V}_{RF2}}{\hat{V}_{RF1}} = \frac{\lambda_0}{\lambda} = 1 - \frac{\Psi\Gamma\lambda_0}{\pi l_p + \Psi\Gamma\lambda_0}$$

#### HARMONIC COMPONENTS OF THE MODULATION

The profile and the harmonic components of the optical modulation of a pulse stretched or shrunk respectively at  $\Gamma = -200$  and  $\Gamma = 200$  are shown in figs. 8 and 9. The bunching parameter  $\Psi$  is kept fixed at the value which maximizes the fundamental harmonic of the modulating laser. The higher harmonic amplitudes in fig. 9 are unrealistic since the debunching due to the emittance has not been taken into account; moreover  $\delta\gamma_{mod} \gg \Delta\gamma_{spread}$  has been assumed.

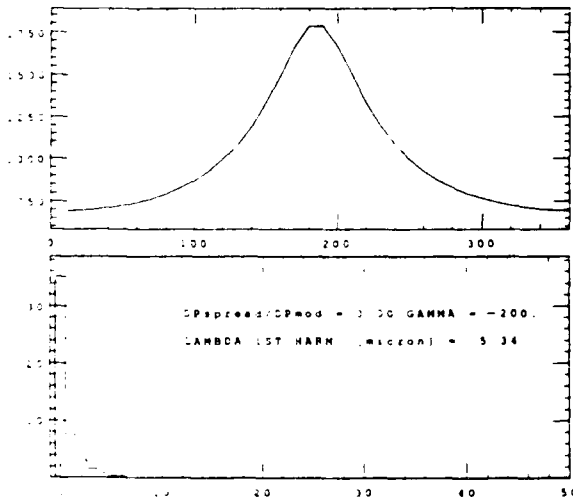


Fig. 8 - Profile and harmonic components of a pulse shrunk at  $\Gamma = -200$ .

The arriving time vs starting time from the modulator to the radiator is shown in fig. 6 for beams linearly modulated at  $\Gamma = 200, \Gamma = 0$  and  $\Gamma = -200$ . The corresponding arriving time distributions are shown in fig. 7.

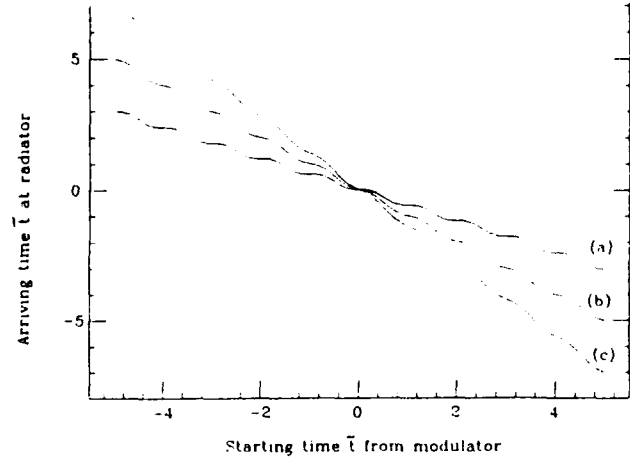


Fig. 6 - Arriving time vs starting time at  $\Gamma = -200$  (a),  $\Gamma = 0$  (b) and  $\Gamma = 200$  (c).

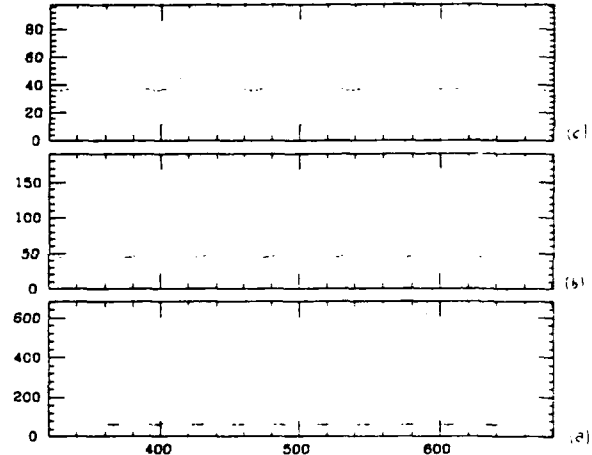


Fig. 7 - Distribution of arriving time at  $\Gamma = -200$  (a),  $\Gamma = 0$  (b) and  $\Gamma = 200$  (c).

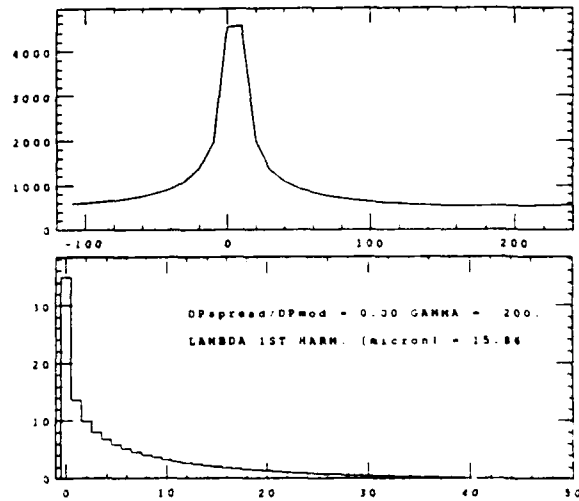


Fig. 9 - Profile and harmonic components of a pulse stretched at  $\Gamma = 200$ .

## P2.29

### A Proposed FIR-IR Metal-Grating FEL Experiment

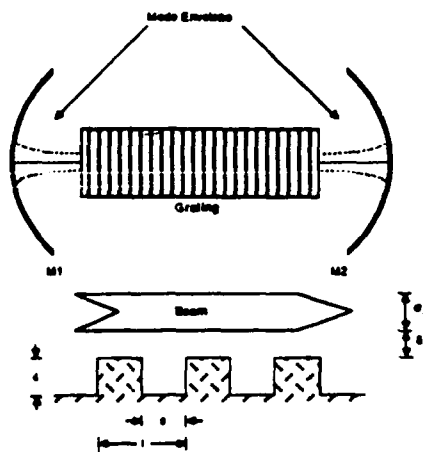
J. Walsh, E. Fisch, E. Marshall, E. Price, Y. Xu  
Department of Physics and Astronomy  
Dartmouth College  
Hanover, N.H. 03755, U.S.A.

G.P. Gallerano, A. Doria, A. Renieri  
Dip. T.I.B., ENEA  
Frascati 00044, ITALY

M.F. Kimmitt  
Department of Physics  
University of Essex  
Colchester, Essex CO4 3SQ, U.K.

A FIR-wavelength, RF-accelerator-driven, metal-grating (MG-FEL) experiment is proposed. The resonator will be an open planar structure, loaded with a narrow strip grating, and terminated with cylindrical section mirrors. Both continuous-grating and split (klystron) configurations will be considered.

The Metal Grating Free Electron Laser



#### Energy Storage and Power Flow

Poynting Theorem (Complex Form)

$$2i(\omega \mathbf{E} \cdot \mathbf{E} - \omega^* \mathbf{E} \cdot \mathbf{E}) + \frac{1}{2} \int_{\text{beam and losses}} \mathbf{J} \cdot \mathbf{E} dV = - \int_{\text{loading}} \mathbf{S} \cdot d\mathbf{A}$$

Energy Storage Capacity

$$\begin{aligned} \mathbf{E} \cdot \mathbf{E} &= \frac{1}{i6\pi} \int |\mathbf{E}|^2 dV \\ &= \frac{C}{4} \frac{V_0^2}{L} = \mathbf{E}_M \quad (\text{along } D = 0) \end{aligned}$$

$$C = \frac{\omega L}{4\pi} C \left( \frac{\omega L}{c} k L \right)$$

Beam Conductance

$$R_e \frac{1}{2} \mathbf{J} \cdot \mathbf{E} dV = \frac{G}{2} \frac{V_0^2}{L}$$

$V_0 = E_0 L$ ,  $E_0$  = slot field,  $L, w$  = grating length, width

#### The Operating Wavelength

Dispersion Curve

$$D \left( \frac{\omega L}{c}, k L, \frac{d}{L}, \frac{s}{L}, \frac{b}{L} \right) = 0$$

Synchronism

$$\omega = k v$$

Tuning

$$D_T \left( \frac{\omega L}{c}, k L, \frac{d}{L}, \frac{s}{L}, \frac{b}{L} \right) = 0$$

Wavelength Scaling

$$\lambda \sim L$$

$\omega$  = the angular frequency  $v$  = the beam velocity

$k$  = the axial wavenumber  $d$  = the slot depth

$L$  = the grating period  $s$  = the slot width

$b$  = the channel height

#### MG-FEL Scaling Relations

Compton-Collective Crossover ( $\alpha L = 1$ )

$$J_b \text{ (A/cm}^2\text{)} = \frac{I_0}{4\pi} \cdot \frac{L}{L^3} \cdot \frac{1}{F}$$

Spatial Gain (Collective Limit)

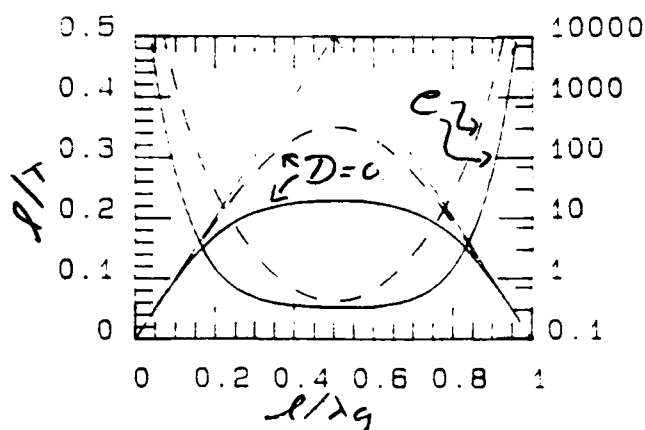
$$\alpha L = \frac{1}{2} \cdot \frac{4\pi J_b}{I_0} \cdot \frac{L^3}{L} \cdot \frac{1}{F}$$

Trapping Separatrix (Collective Limit)

$$\epsilon_{os} \text{ (cm}^{-1}\text{)} = \frac{1}{L} \left( \frac{J_b}{I_0} \right)^{5/3} \left( \frac{\omega L}{c} \right)^3 F^{-2/3}$$

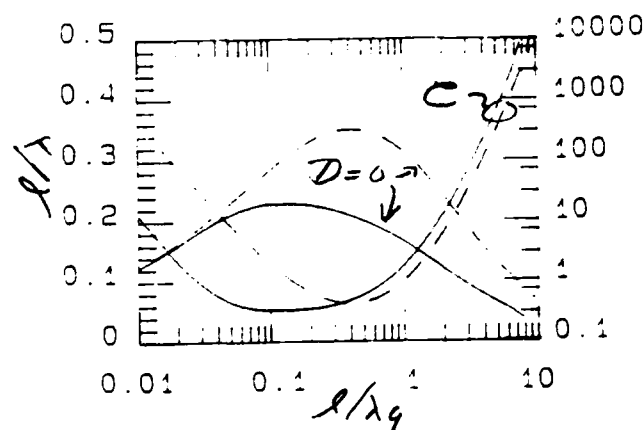
$$F = \frac{h e^2 \mu_e (1 - e^2 \mu_e)}{2 \gamma^2 (\omega L/c)^2 e} \quad h = \text{the space harmonic amplitude}$$

$$\mu_e = \frac{4\pi(\sigma_h \text{ or } \delta)}{13\gamma}$$



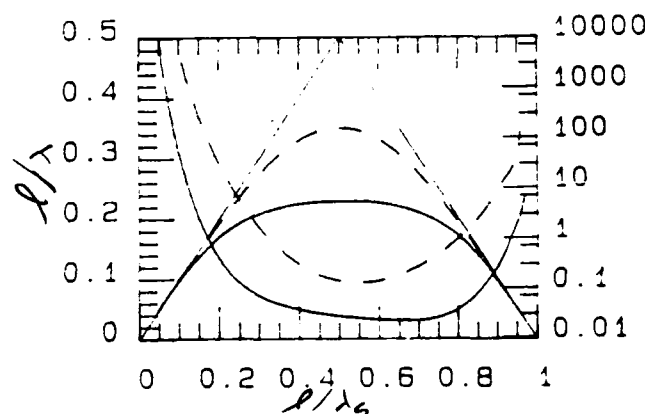
### Dispersion and Relative Capacitance

The curves defined by  $D = 0$  with  $d/l = 0.4, 0.8$  are displayed for an open-topped resonator (right axis). The associated relative capacitance (left axis) curves are also shown.



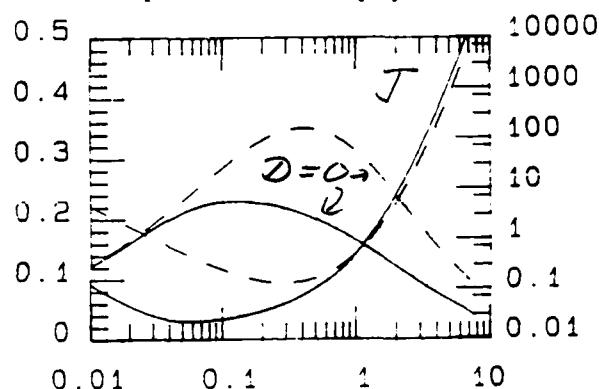
### Tuning and Relative Capacitance

The function  $D = 0$  evaluated along the line defined by  $\omega = kv$ , where  $v$  is the beam velocity is displayed as a function of the beam's relative kinetic energy. The parameters are the same as those in the dispersion plot and the relative capacitance is also displayed.



### The Start Current Density: 1

The current density required for threshold at the point where the exponent in the spatial gain ( $\alpha L$ ) is unity is displayed as a function of the phase shift per slot.



### The Start Current Density: 2

The current density required for threshold is displayed as a function of the beam's relative kinetic energy.

## Accelerators\*

### 2.3 MeV Linac

$$E_E - 2.3 \text{ MeV}; \quad \tau_M - 4 \mu\text{s} \text{ (macropulse)}$$

$$I - 200 \text{ ma (avg.) } (J_b = 254 \text{ A/cm}^2)^{**}$$

### 5.0 MeV Microtron

$$E_E - 5.0 \text{ MeV}; \quad \tau_M - 2 \mu\text{sec}$$

$$I - 100 \text{ ma } (J_b = 127 \text{ A/cm}^2)$$

\* The radio frequency gun (K. Batchelor et al., NSLS pub. BNL 41766) might also make an excellent beam for MG-FEL investigations.

\*\* Assuming  $\sigma_{bx} = 0.1 \text{ mm}$ ,  $\sigma_{by} = 1.0 \text{ mm}$  in an elliptical spatial distribution.

## P2.30

### Prospects for a Soft X-Ray FEL Powered by a Relativistic Klystron-High Gradient Accelerator (RK-HGA)\*

H. D. Shay, W. A. Barletta, S. S. Yu, E. T. Scharlemann, R. Schlueter, and G. A. Deis

Lawrence Livermore National Laboratory  
University of California, Livermore, California 94550

Recent advances in the technologies of high gradient linear accelerators driven by relativistic klystrons, of high brightness electron injectors, and wigglers with small random field errors and with accurate beam steering suggest the possibility of developing a soft x-ray FEL based on the architecture of single pass simplification from spontaneous noise. This paper examines the selection of x-ray wavelength and FEL power for several applications and the implications in the technology requirements. Relatively compact designs are proposed which balance the requirements for small electron beam emittance, small energy slewing, high energy, high current, and small wiggler field errors. Other authors have previously considered similar architectures, but without the proposed use of high gradient acceleration. We also show the influence of 3D effects on the choice of designs.

\* Work performed under the auspices of the US Department of Energy by the Lawrence Livermore National Laboratory under W-7405-ENG-48.

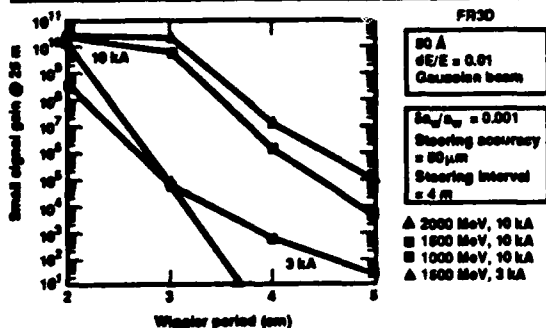
#### Architecture under consideration:

- High brightness injector
  - emittance = 15-40 mm-mrad demonstrated in photoinjector (LANL)
  - pulse compression to ~ 1 ps may result in peak currents of 1-10 kA
- Relativistic klystron RF high gradient accelerator
  - 100-200 MeV/m  $\Rightarrow$  accelerator length ~ 10 m
  - ~ 100 MeV/m already demonstrated (LLNL/SLAC)
- Single pass, wiggler amplifier
  - linearly polarized
  - short period  $\Rightarrow$  may require superconducting coils and/or cryogenic rare earth pole types
  - no tapering of magnetic field required: in exponential gain
- Growth from spontaneous noise
  - beam noise level  $\leq 1$  W
- $\lambda = 45\text{\AA}$ , near carbon edge
  - for holography,  $\lambda \leq 45\text{\AA}$ , require  $P_{\text{peak}} \geq 1\text{-}10$  MW, single pulse of  $\tau = 1\text{-}10$  ps

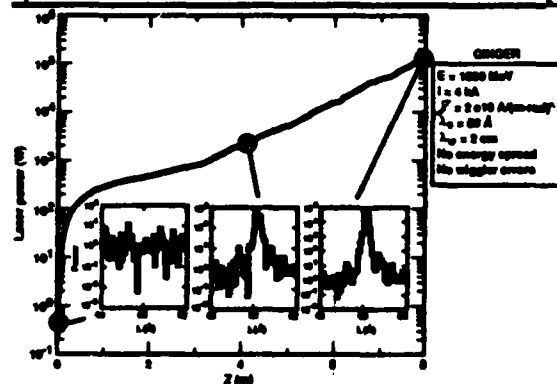
#### Design parameters and issues:

- E 1/2 - 2 GeV
  - with RK-HGA,  $L_{\text{acc}} = 10$  m
- $\epsilon_N$  1 - 100 mm-mrad
- I 0.300 - 10 kA
  - with pulse compression
- $\delta E/E$ , energy spread  $\leq 10^{-3}$
- $L_{\text{wiggler}}$  10 - 25 m
- $\lambda_w$  1 - 8 cm
- $B_0$  < Halbach limit @ 30°C  
 $\leq 2 \times$  Halbach limit @ cryogenic temperatures
- ( $\delta B/B$ ) rms, field errors  $\leq 10^{-3}$
- $\Delta x$ , steering errors  $\Delta x/r_{\text{lube}} \leq 10^{-2}$
- Spatial beam jitter <  $\Delta x$

#### Short wiggler period results in higher gain

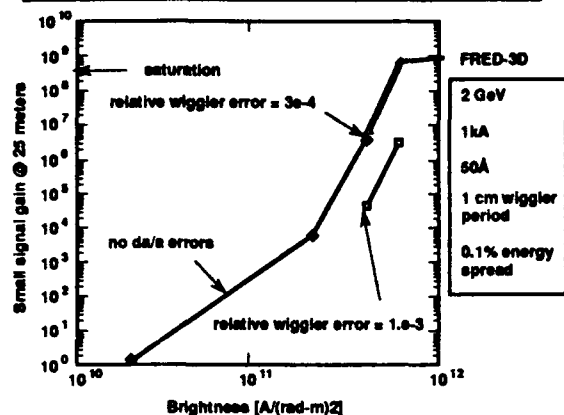


#### Growth from beam noise shows characteristic spectral evolution

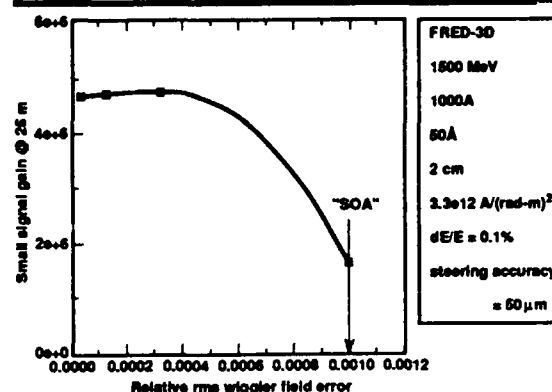




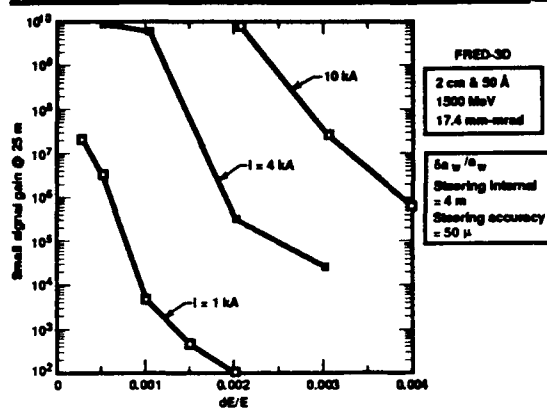
## Gain vs. brightness



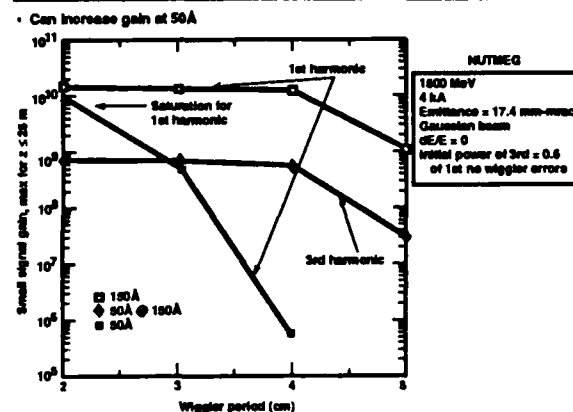
## Gain vs. wiggler field error



## FEL is more tolerant of electron energy spread at higher current

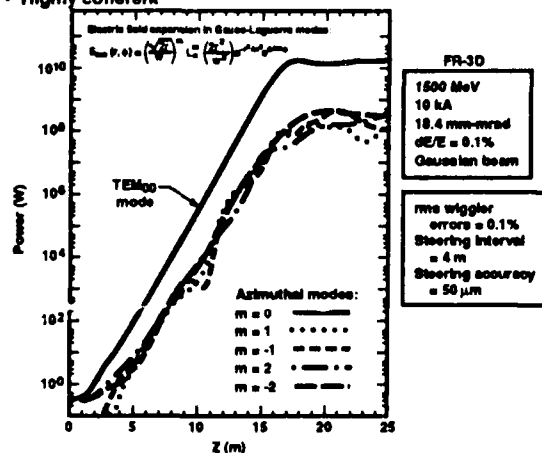


## Tuning for 150 A and using 3rd harmonic



## About 95% of power in TEM<sub>00</sub> spatial mode

### Highly coherent



## Output characteristics of FEL permit x-ray holography

- $\lambda = 50 \text{ \AA}$ ;  $\Delta\lambda/\lambda = 0.2\%$ ; fully tunable in  $\lambda$
- Instantaneous power =  $10^8 - 10^9$  W
- Beam radius at exit of FEL =  $100 \mu\text{m}$
- Beam divergence at exit of FEL =  $20 \mu\text{rad}$
- Spectral brilliance =  $2 \times 10^{29} - 2 \times 10^{30}$  photons/(sec · mm<sup>2</sup> · mrad<sup>2</sup> 0.1% BW)
- Pulse length = 1-10 ps
- = 0.1-1 mJ/pulse ( $2.5 \times 10^{12} - 10^{13}$  photons — pulse)
- Highly coherent
  - Transverse coherence: = 85% in TEM<sub>00</sub> mode
  - Longitudinal coherence:  $l_c = \frac{\lambda^2}{\Delta\lambda} = 2.5 \mu\text{m}$
- Completely linearly polarized
- Repetition rate = 1-10 Hz

## P2.31

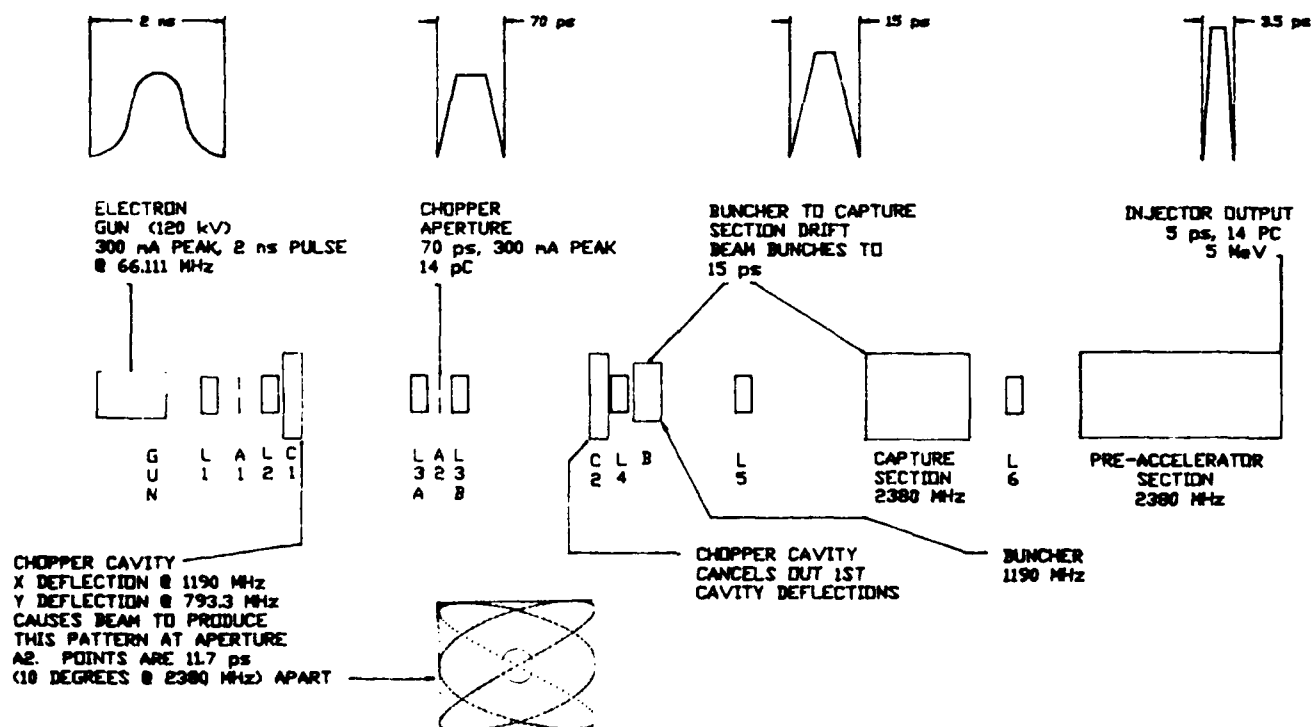
### DESIGN OF A HIGH-CURRENT INJECTOR FOR THE NIST-NRL FREE ELECTRON LASER\*

R. I. Cutler and E. R. Lindstrom  
National Institute of Standards and Technology  
Gaithersburg, Md 20899  
(301)-975-5607

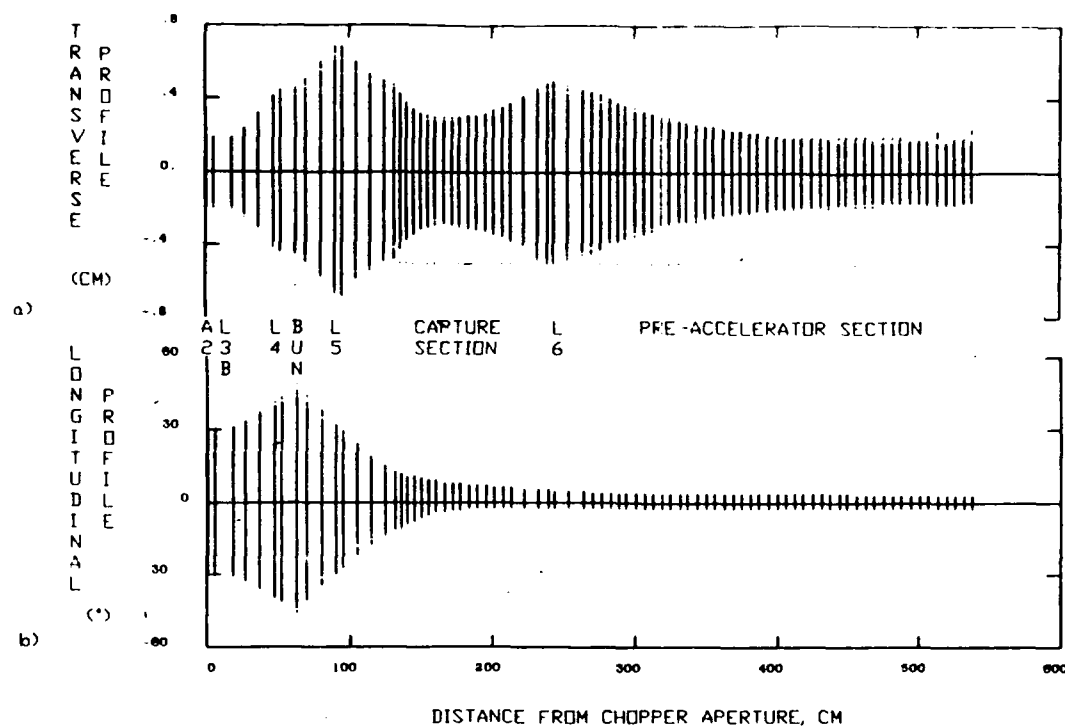
S. Penner  
10500 Pine Haven Terrace  
Rockville, Md 20852

The electron beam of the NIST-LANL Racetrack Microtron (RTM) is to be used to drive a free electron laser and for other applications. We have designed a new injector for the RTM to provide the 3.5 long, 7-14 pC electron beam pulses required for lasing. The new injector consists of a pulsed, 120-keV thermionic electron gun, a subharmonic chopping and bunching system, and the existing 5-MeV RTM injection linac. It has been designed to produce a continuous train of electron pulses at 5 MeV with a normalized transverse emittance of 5 mm-mr and a longitudinal emittance of 20 keV-degrees for 95% of the beam (for 7 pC) at repetition rates of 66.111 or 16.528 MHz. These two frequencies are subharmonics of the fundamental accelerator frequency of 2380 MHz. The new injector will also produce lower emittance beams at lower peak currents at the fundamental frequency.

## INJECTOR SCHEMATIC



# PARMELA-CALCULATED BEAM PROFILES



## OUTPUT EMITTANCES FROM PARMELA FOR 95% OF BEAM PARTICLES

CHARGE PER PULSE pC	TRANSVERSE EMITTANCE, (NORMALIZED) mm-mr	LONGITUDINAL EMITTANCE, keV-DEGREES
0.25	0.7	5
7	4.3	17
14	6.1	34

## P2.32

### TWFEL - a hybrid TWT/FEL interaction

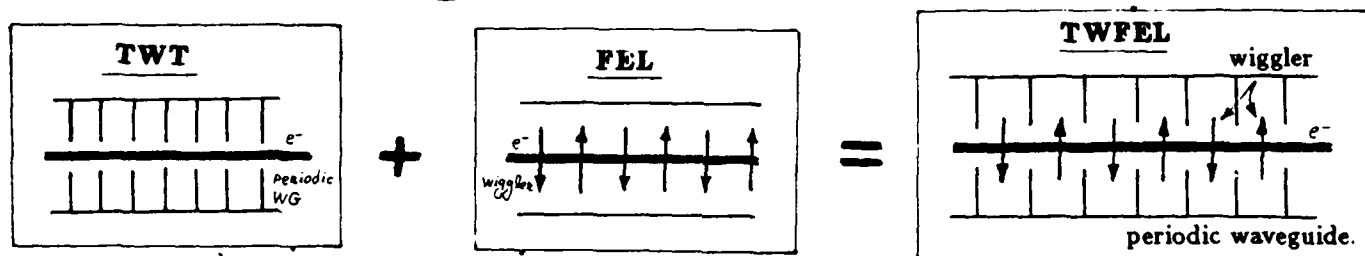
Eli Jerby

Faculty of Engineering, Tel-Aviv University, 69978, ISRAEL \*

#### ABSTRACT

A concept of an hybrid TWT-FEL device, operating in the *mm wave* range with low energy e-beam, is presented. The TWFEL consists of both periodic waveguide (with period  $\lambda_p$ ) and a planar wiggler (with period  $\lambda_w$ ). It is shown that when  $\lambda_w = \lambda_p$ , the parametric interaction is composed of a double FEL interaction and a TWT interaction, all of which are in resonance with three different spatial harmonics. Simpler TWFEL schemes are presented for  $\lambda_w = 2\lambda_p$  (two harmonic interaction) and for  $\lambda_w \gg \lambda_p$  (single harmonic interaction). A 2D model was derived to analyze the TWFEL features in the various regimes. A conceptual TWFEL scheme is proposed on the base of a folded-foil wiggler which functions also as a periodic waveguide.

#### hybrid

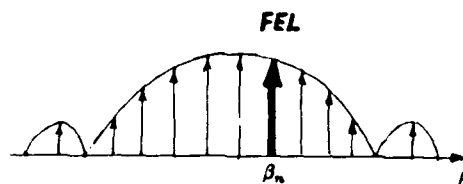
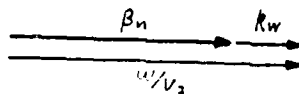


Three operating regimes are distinguished,

#### A. $\lambda_w \gg \lambda_p$ FEL interaction with one harmonic

the FEL synchronism with the  $n^{\text{th}}$  harmonic is

$$\frac{\omega}{\langle v_z \rangle} - \beta_n - k_w \sim 0,$$



the coupling parameter with the  $n^{\text{th}}$  harmonic is

$$\kappa_n = \frac{k^2 V_W^2}{4\beta_n c^2} \cdot "JJ_n",$$

$$"JJ_n" = \frac{\alpha_{n,n} \beta_n^2 e_{zn}^2 / \gamma_n^2}{\sum_m \alpha_{m,m} \beta_m^2 e_{zm}^2 / \gamma_m^2}$$

(The spatial equivalent of the FEL known JJ term for higher harmonic)

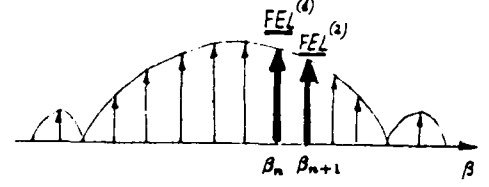
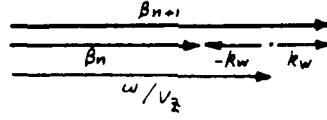
Though the interaction occurs with one harmonic, the amplified power is divided to all the harmonics and therefore the net gain is smaller. However, the advantage of this scheme, as the other higher harmonic schemes, is that the e-beam energy can be smaller as the order of the harmonic is higher. Moreover, some reduction of the e-beam energy can be achieved also with the fundamental harmonic, depending on the specific dispersion condition (similar to the Gas-Loaded FEL [4]).

\* Present address - Res. Lab. of Electronics, MIT, Cambridge, MA 02139

### B. $\lambda_W = 2\lambda_p$ FEL interaction with two harmonics

$$\text{FEL 1 : } \frac{\omega}{\langle \bar{v}_z \rangle} - \beta_n - k_W \sim 0,$$

$$\text{FEL 2 : } \frac{\omega}{\langle \bar{v}_z \rangle} - \beta_{n+1} + k_W \sim 0,$$



the coupling parameter includes now the contribution of two harmonics as follows :

$$\kappa_{n,n+1} = \frac{k^2 V_W^2}{4\beta_n c^2} \left[ \sum_m \alpha_{m,m} \frac{\beta_m^2}{\gamma_m^2} e_{zm}^2 \right]^{-1} \cdot \left[ \alpha_{n,n} \frac{\beta_n^2}{\gamma_n^2} e_{zn}^2 + \alpha_{n,n+1} \frac{\beta_n^2 + \beta_n \beta_{n+1}}{\gamma_n \gamma_{n+1}} e_{zn} e_{z_{n+1}} + \alpha_{n+1,n+1} \frac{\beta_{n+1}^2}{\gamma_{n+1}^2} e_{z_{n+1}}^2 \right]$$

One may identify in the coupling expression terms for each harmonic, and also a cross term for the coupling between the harmonics due to the FEL interaction.

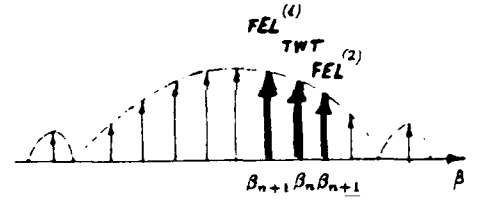
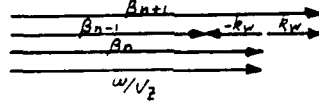
### C. $\lambda_W = \lambda_p$ TWFE interaction with three harmonics

When  $\lambda_W = \lambda_p$ , the TWFE interaction is composed of a double FEL interaction and a TWT interaction, all of which are in resonance with three different spatial harmonics.

$$\text{FEL 1 : } \frac{\omega}{\langle \bar{v}_z \rangle} - \beta_{n-1} - k_W \sim 0,$$

$$\text{TWT : } \frac{\omega}{\langle \bar{v}_z \rangle} - \beta_n \sim 0,$$

$$\text{FEL 2 : } \frac{\omega}{\langle \bar{v}_z \rangle} - \beta_{n+1} + k_W \sim 0,$$



The coupling parameter for the TWFE interaction includes the contribution of three harmonics as follows :

$$\kappa_{n-1,n,n+1} = \left[ \sum_m \alpha_{m,m} \frac{\beta_m^2}{\gamma_m^2} e_{zm}^2 \right]^{-1} \cdot \left\{ \frac{k^2 V_W^2}{4\beta_n c^2} \left[ \alpha_{n,n} \frac{\beta_n^2}{\gamma_n^2} e_{zn}^2 + \alpha_{n,n+2} \frac{\beta_n^2 + \beta_n \beta_{n+2}}{\gamma_n \gamma_{n+2}} e_{zn} e_{z_{n+2}} + \alpha_{n+2,n+2} \frac{\beta_{n+2}^2}{\gamma_{n+2}^2} e_{z_{n+2}}^2 \right] + \alpha_{n+1} \beta_{n+1} e_{z_{n+1}}^2 \right\}$$

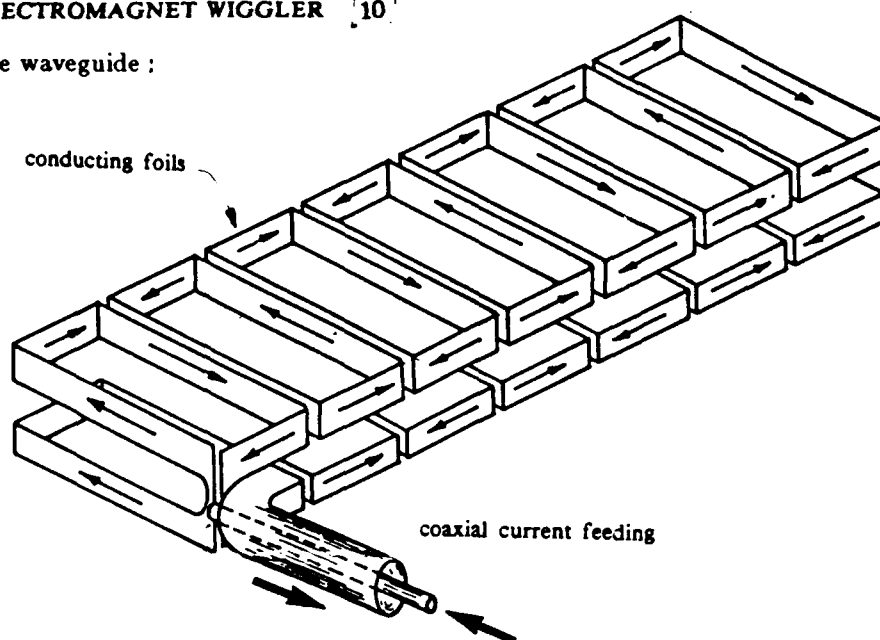
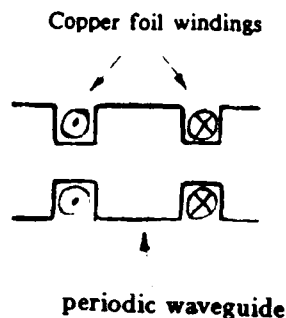
The additional last term in the coupling expression in this case is equivalent to the TWT gain parameter, accepted in the Pierce equation [3,5] (which is essentially the denominator of the gain dispersion equation (12b)). As in the previous cases, the TWFE interaction requires lower energy e-beam. The coupling is emphasized by the three harmonic interaction, thus a lower current is needed to acquire the same amplification.

## The TWFE interaction and the miniature wiggler concept

### COAXIALLY FED FOLDED FOIL ELECTROMAGNET WIGGLER [10]

functions also as a periodic structure waveguide :

(  $\lambda_w = 2\lambda_p$  scheme )



A 2-D model of the TWT-FEL interaction is presented in Ref.[11]. The features of the TWFE are analysed in the various regimes. A conceptual design of a TWFE is presented,

## REFERENCES

1. R. M. Philips, *IRE Trans. ED-7*, 231 (1960) also in *Nucl. Instrm. and Methods*, **A272**, 1 (1988).
2. L. R. Elias, W. Fairbank, J. Madey, H. A. Schwettman, and T. Smith, *Phys. Rev. Lett.*, **36**, 717 (1976).
3. J. R. Pierce, *Travelling Wave Tube*, Princeton, NJ: Van Nostrand, 1950.
4. R. H. Pantel, J. Feinstein, A. S. Fisher, T. L. Deloney, M. B. Reid, and W. M. Grossman, *Nucl. Instrm. and Methods*, **A250** 39 (1986)
5. W. Gewartowski and G. Watson, *Microwave Tubes*, McGraw Hill, 1965.
6. E. Jerby and A. Gover, *Phys. Rev. Lett.*, **63**, 864 (1989).
7. E. Jerby, *Nucl. Instrm. and Methods* **A272**, 457 (1988).
8. A. Gover and P. Sprangle, *IEEE J. Quantum Electron.*, **QE-17**, 1196 (1981); also in E. Jerby and A. Gover, *ibid* **QE-21** 1041 (1985).
9. W. B. Colson, G. Dattoli, and F. Ciocci, *Phys. Rev. A*, **31** 828 (1985).
10. A. Sneh and E. Jerby, "Coaxially fed folded foil electromagnet wiggler", to be published in the Proc. of the 10<sup>th</sup> Int. FEL Conf., Jerusalem. (1988).
11. E. Jerby, to be published.

## P2.34

### Status of the JAERI FEL System

M.Ohkubo, M.Sugimoto, M.Sawamura, K.Mashiko  
E.Minehara, M.Takabe, J.Sasabe\* and Y.Kawarasaki

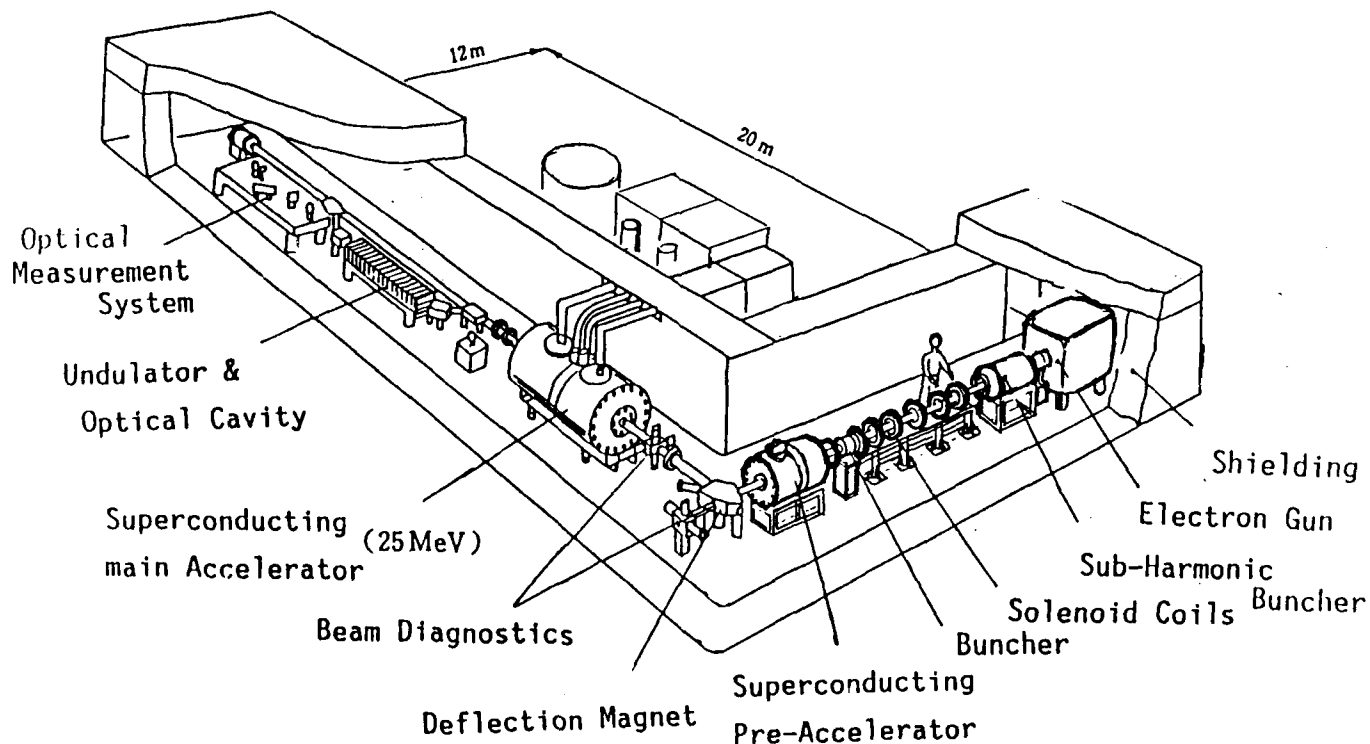
Japan Atomic Energy Research Institute  
Tokai-mura, Ibaraki-ken, 319-11 Japan

\* Hamamatsu Photonics Co.

#### Abstract

An overview of the JAERI FEL program and the status are described. Design and construction of the JAERI FEL system based on a superconducting linac are continued aiming at FEL oscillation in 10 20  $\mu\text{m}$  infrared wavelength. A part of vacuum system, a sub-harmonic buncher and a buncher have been fabricated.

### JAERI FEL System (Phase I, 1987-'92)



## P2.35

### Energy Measurement of the Electron Beam Beyond the PALADIN Wiggler\*

T. J. Orzechowski, J. A. Edighoffer,<sup>†</sup> P. Lee,<sup>#</sup> T. E. Smith,  
Y. P. Chong, A. C. Paul, and J. T. Weir

Lawrence Livermore National Laboratory  
University of California, Livermore, California 94550

An electron beam spectrometer has been deployed at the exit of the PALADIN wiggler. The dispersed electron beam is monitored by observing the Cerenkov light emitted as the electron beam passes through a quartz foil. We present energy spectra under lasing and nonlasing conditions and compare them to the FEL optical energy gain.

\*Work performed jointly under the auspices of the US Department of Energy by the Lawrence Livermore National Laboratory under W-7405-ENG-48 and the DOD under SDIO/SDC-ATC MIPR No. W31RPD-9-D5007.

<sup>†</sup>TRW, Inc., Redondo Beach, CA

<sup>#</sup>General Atomics, San Diego, CA

#### Energy Measurement of the Electron Beam Beyond the PALADIN Wiggler

J. A. Edighoffer, T. J. Orzechowski, P. Lee, T. E. Smith,  
Y. P. Chong, A. C. Paul, and J. T. Weir



Presented at the  
11th International Conference on Free Electron Lasers  
Ritz-Carlton Hotel  
Naples, Florida

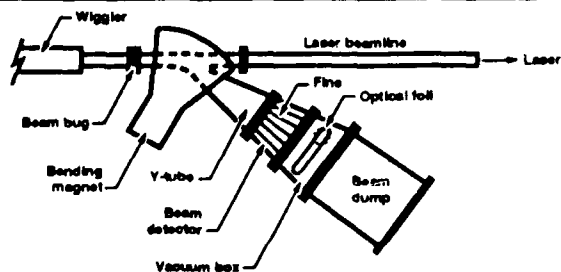
August 28 — September 1, 1989

#### Energy measurement of the electron beam beyond the PALADIN wiggler

Ted Orzechowski, J. Edighoffer  
Ping Lee, Tom Smith, Yee Ping,  
Art Paul, and John Weir

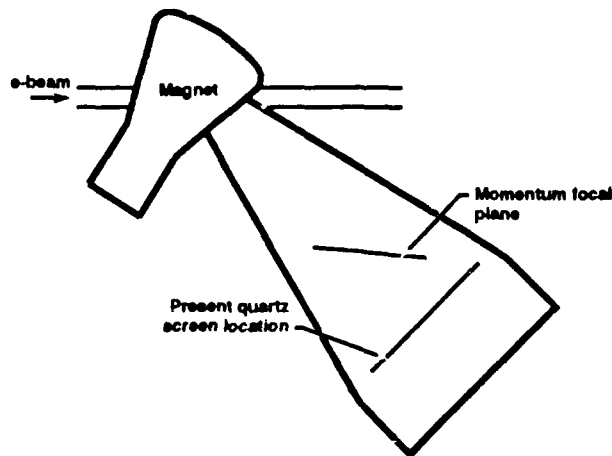
Initial measurements of the energy loss during FEL amplification. Cerenkov light emission from a quartz screen viewed with gated camera with 5 ns temporal resolution. With the present configuration, the energy resolution of  $\frac{\Delta E}{E} = 0.2\%$  was observed and coverage of  $\frac{\Delta E}{E} = 8\%$ . Comparison of lasing and non lasing electron energy spectra will be presented and compared with FEL optical energy gains.

#### Electron beam spectrometer measures effect of FEL interaction on electron beam

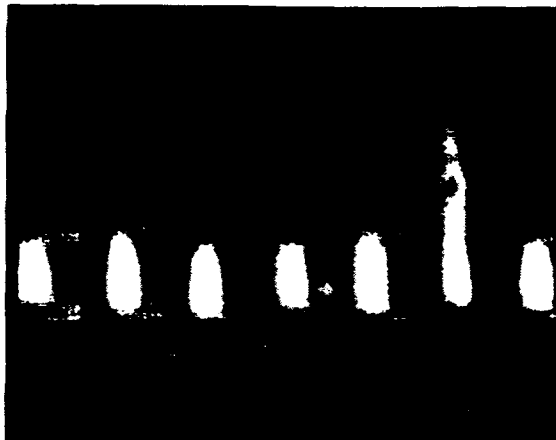


- Electron beam is deflected out of beamline at end of wiggler into spectrometer
- Dispersed electron beam is monitored on Cerenkov foil
- Resolution of spectrometer = 0.2%

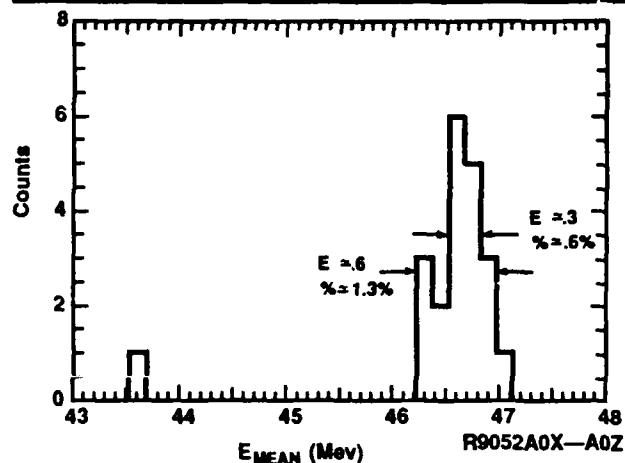
#### Spectrometer magnet



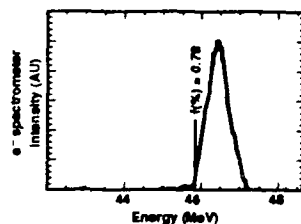




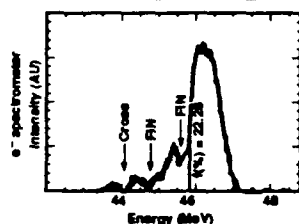
#### PALADIN SPECTROMETER: CO<sub>2</sub> OFF



#### Electron energy loss agrees with laser power gain



No input signal to FEL  
(unperturbed electron distribution)



400 MW input signal, 17% linear  
taper:  $\Delta\gamma/\gamma = 0.9\%$

#### Conclusion

- High Resolution Electron Spectrometer achieved 0.2% resolution
  - mod. location will provide 0.1% resolution
- Measured 0.9% extraction efficiency

**WEDNESDAY, AUGUST 30**

## EX2.1

### The NIST-NRL Free-Electron Laser Facility

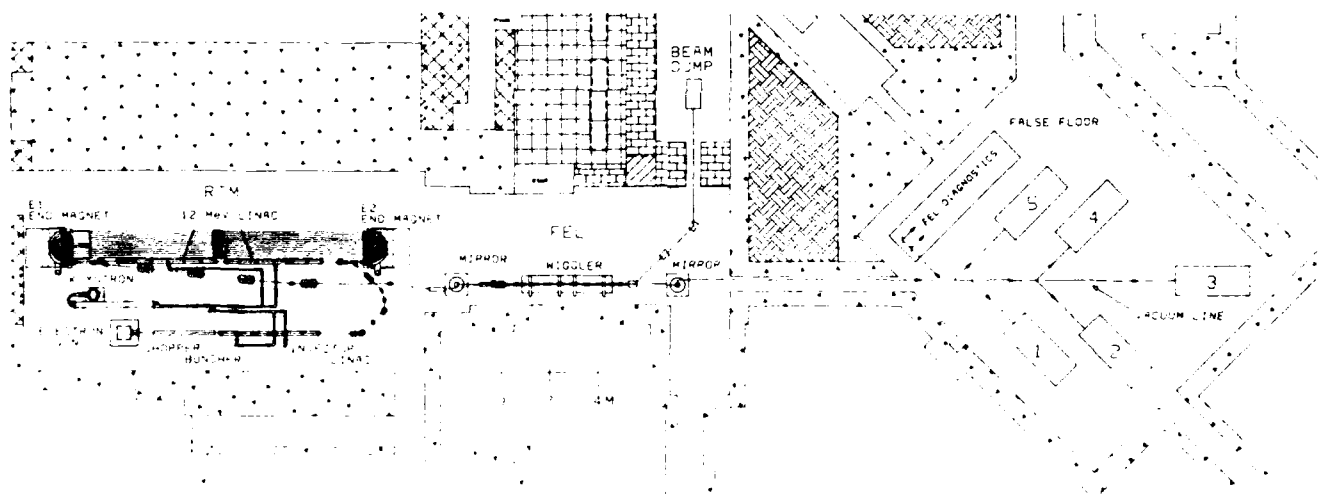
R.G. Johnson, R.L. Ayres, J.B. Broberg, R.I. Cutler, P.H. Debenham,  
B.C. Johnson, E.R. Lindstrom, D.L. Mohr, J.E. Rose,  
J.K. Whittaker, N.D. Wilkin, and M.A. Wilson  
National Institute of Standards and Technology  
Gaithersburg, MD 20899

S. Penner  
10500 Pine Haven Terrace  
Rockville, MD 20852

C.-M. Tang and P. Sprangle  
Naval Research Laboratory  
Washington, DC 20375

A FEL facility is being constructed at NIST in collaboration with NRL. The FEL will provide a powerful, tunable light source for research in medical and materials science. The FEL will lase over wavelengths from 200 nm to 10  $\mu\text{m}$  with a continuous train of 3-ps pulses at 66 MHz and with average power of 10 W to 200 W.

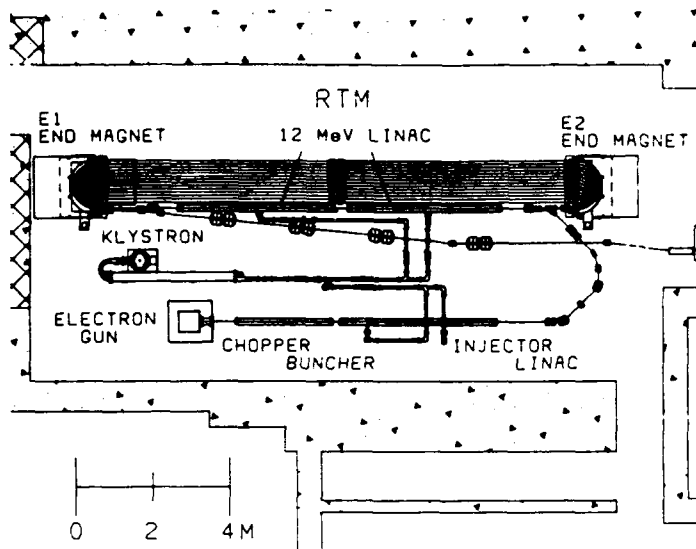
Supported by the US SDIO through ONR Contract No. N00014-87-F-0066.



Plan view of the NIST-NRL FEL facility.

#### OUTPUT LIGHT PROPERTIES

WAVELENGTH	200 nm - 10 $\mu\text{m}$	PHOTON FLUENCE	$3 \cdot 10^{13}$ - $6 \cdot 10^{15}$ phot $\text{cm}^{-2}$ (1 mm-diam spot)
AVERAGE POWER	10 - 200 W	SPECTRAL RESOLUTION	$1.4 \cdot 10^{-4}$ - $7 \cdot 10^{-3}$
PULSE WIDTH	3 ps	POLARIZATION	LINEAR
REPETITION RATE	66.111 MHz	SPATIAL MODE	TEM <sub>00</sub>
PEAK POWER	40 - 1000 kW	BEAM DIAMETER (at 1/e amplitude)	0.4 - 1.6 mm
PEAK ENERGY	0.1 - 3.0 $\mu\text{J}$	BEAM DIVERGENCE (full angle)	0.3 - 5 mrad
PHOTON FLUX	$10^{25}$ - $2 \cdot 10^{27}$ phot $\text{cm}^{-2}\text{s}^{-1}$		



Schematic diagram of the NIST RTM.

#### NIST-RTM Performance

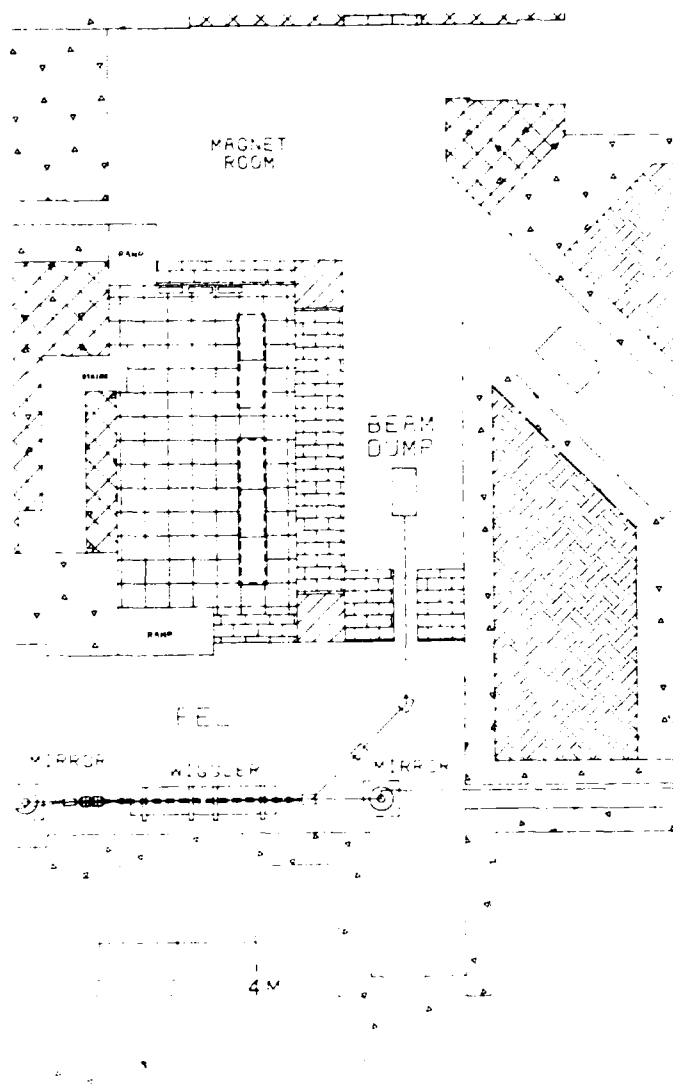
	Original Design	Measured 2/87	Measured 5/89	New Gun Design
Energy (MeV)	17-186	5.5	17	17-186
Average current (μA)	550 max cw	630 max cw	300 pulsed	550 max cw
Micropulse length (ps)	3.5	-	-	3.5
Micropulse frequency (MHz)	2380	2380	2380	66.1
Macroscopic duty factor (%)	100	100	0.6	100
Energy spread (keV)	40	5	18	40
Normalized emittance (μm)	10	0.7	2.4	10

#### Advantages of the RTM as a FEL driver

- Good emittance - short wavelengths and uniform filling factor
  - Low energy spread - transform limited linewidth and enhances gain
  - Good energy and phase - wavelength and power stability
  - Continuous pulse train - no pulse to pulse start-up problems
  - Electrons not recirculated - no constraints on undulator
  - Broad energy range - broad wavelength range
- 
- Limited peak current - low gain

#### OUTPUT EMITTANCES FROM PARMELA FOR 95% OF BEAM PARTICLES

CHARGE PER PULSE pC	TRANSVERSE EMITTANCE, (NORMALIZED) mm-mr	LONGITUDINAL EMITTANCE, keV-DEGREES
0.25	0.7	5
7	4.3	17
14	6.1	34



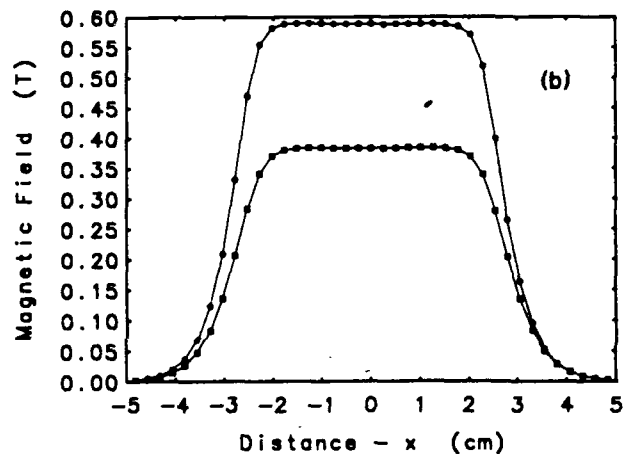
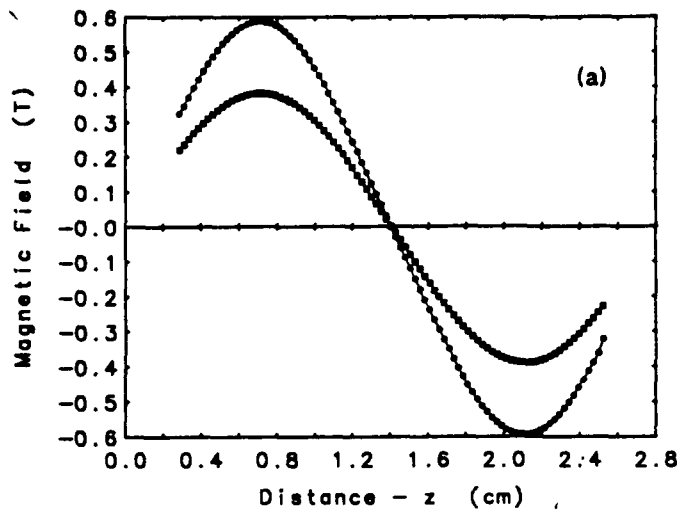
Plan view of the FEL area including the undulator (wiggler), mirror positions, beam stop, shielded equipment room, and area for electron beam experiments.

## Undulator Design

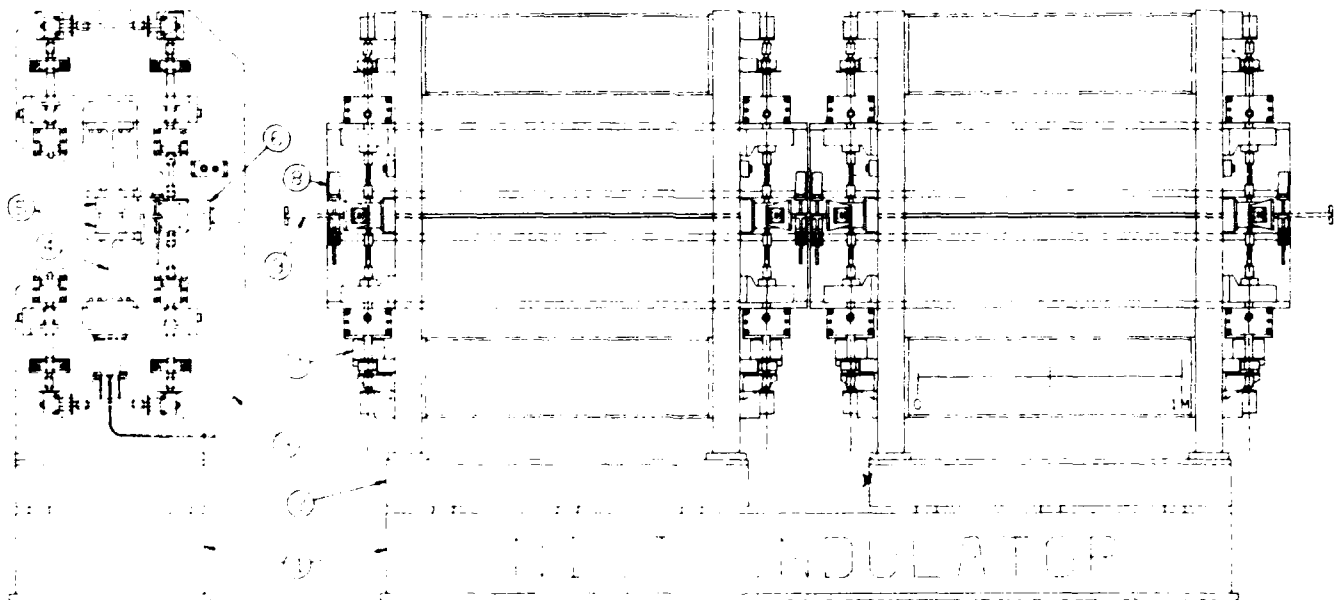
- Hybrid undulator (SmCo permanent magnets; vanadium permendur poles)
- Number of periods - 130
- Period length - 2.8 cm
- Total length - 3.64 m
- Maximum magnetic field - 0.54 T
- Minimum gap - 1.0 cm
- Taper - 0.5 mm/m
- Vacuum chamber aperture - 0.86 cm (vertical)  
16 cm (horizontal)
- Operation in full or half-length mode

### Specifications for the undulator magnetic field and model results

	Specifications	Model Results
Peak Field (kG)	5.4	5.65
Maximum 3rd harmonic	10%	3.2%
5th harmonic	-	0.5%
7th harmonic	-	0.2%
Limit on transverse field variation (central 1.0 cm)	0.5%	0.3%
RMS error (G)	27	-
Vertical field integral error (G-cm)	23	-
Horizontal field integral error (G-cm)	23	-



Test results for the full-scale, one-period model of the magnetic structure. (a) Magnetic field along the axis. (b) Magnetic field transverse to the axis.



Detailed mechanical structure of the undulator.

# COMMERCIALLY-AVAILABLE MIRRORS for MIST-NRL FEL 450 nm to 850 nm

## Multi-layer Dielectric on Fused Silica

Bandwidth:  $\pm 50$  nm

Reflectivity: 0.9999

Absorption: 10-20 ppm

## Distortion from Heating

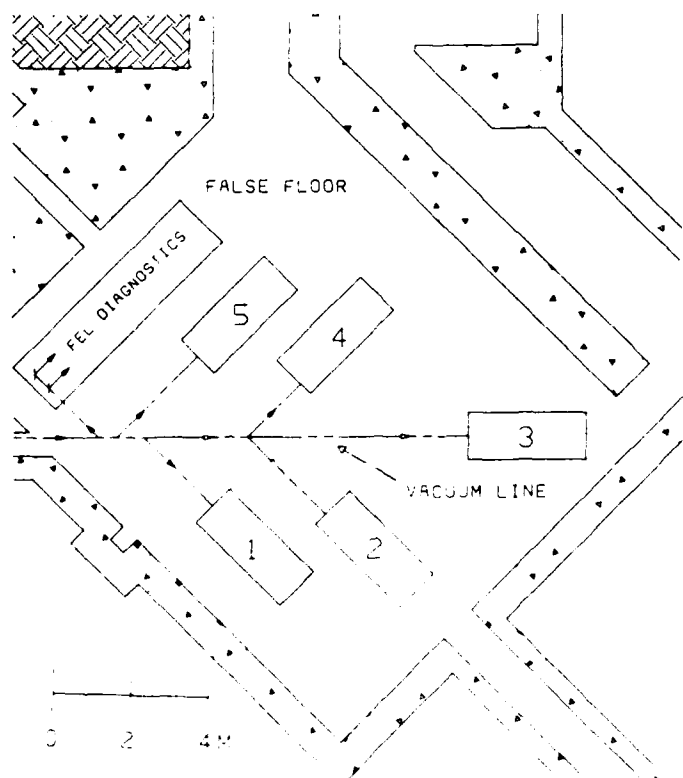
- Observed to be negligible at  $250 \text{ kW/cm}^2$  for cw dye lasers; we expect  $< 50 \text{ kW/cm}^2$ , average
- Calculated distortion in steady state using finite element analysis method

## Dielectric Breakdown

- Damage threshold is  $20 \text{ J/cm}^2$  in  $1 \mu\text{s}$
- We expect  $0.25 \text{ J/cm}^2$  in  $1 \mu\text{s}$

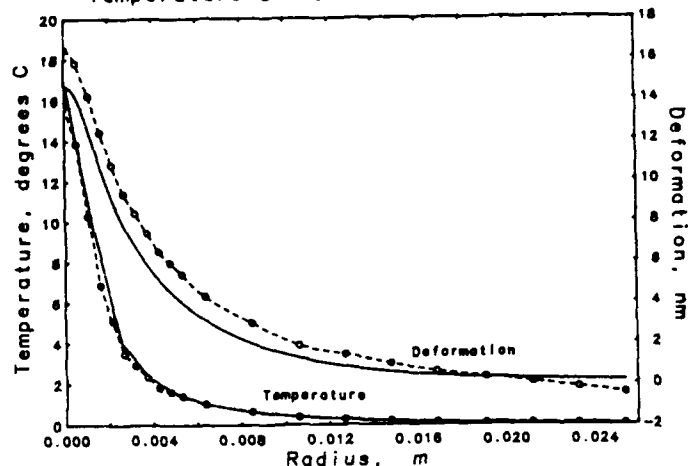
## Damage from Harmonics

- From experience at other FELs, we expect absorption to increase
- We are calculating harmonic radiation
- Deacon Research in Phase I of UV-induced damage study for multi-layer dielectrics that are designed for 240 nm
- FEL operating parameters must be adjusted so that the harmonic content is minimized

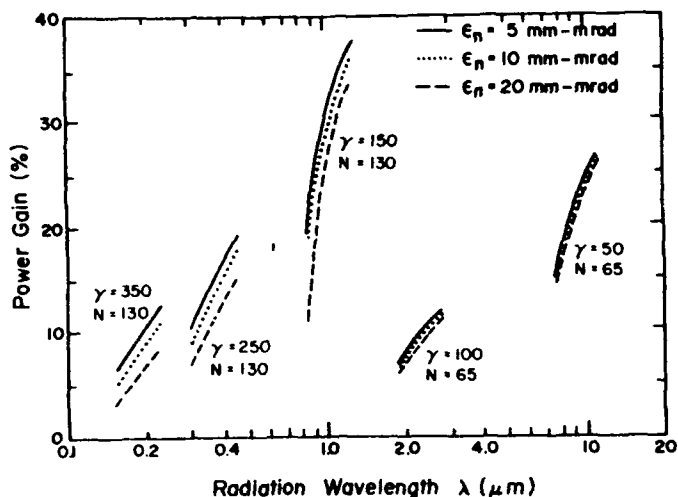


Proposed layout for the FEL user facility.

## Temperature and Deformation of Mirror



Temperature and deformation at the surface of a mirror from thermal absorption. Dashed line - finite element analysis. Solid line - analytical solution.



FEL power gain vs wavelength. (Shown as functions of the energy and emittance of the electron beam, and the magnetic field of the undulator.)

## FEL Studies

- Dynamic tuning by adjusting the undulator gap
- Lasing mode and gain studies vs electron beam focusing
- Dynamic variation of outcoupling to study saturation and to maximize output power
- Measure coherent harmonics
- Dynamic variation of taper to maximize output power
- Power and frequency stabilization by feedback

## EX2.2

### SCA/FEL Status\*

T. I. Smith, J. C. Frisch, R. Rohatgi, H. A. Schwettman and R. L. Swent

High Energy Physics Laboratory  
Stanford University  
Stanford, California 94305-4085 U.S.A.

#### Abstract

During a 3-week run in May-June, 1989, the SCA/FEL provided 18 days of FEL beam at 16-18 hours/day. The FEL operated at 3.5  $\mu\text{m}$ , and in a 20% band centered at 1.54  $\mu\text{m}$ . 30 W of optical power was extracted in 3 ms macropulses with a 0.15% linewidth and a 3 ps micropulse.

During a 3-week run in May-June 1989, the SCA/FEL provided 18 days of FEL beam at 16-18 hours/day. Most of the operation was at a wavelength of 1.54  $\mu\text{m}$ , but the tunability of the dielectric mirrors was tested by varying the wavelength from 1.39  $\mu\text{m}$  to 1.65  $\mu\text{m}$  by changing the linac energy. In addition, changing mirrors allowed a demonstration that the SCA/FEL can successfully oscillate at wavelengths at least as long as 3.5  $\mu\text{m}$ .

At 1.5  $\mu\text{m}$ , 30 W of optical power was extracted during 3 ms macropulses repeating at a 10 or 20 Hz rate. The linewidth of the radiation was 0.15%, consistent with the transform limit of the 3 ps micropulse length. The micropulse power was 700 KW. The separation between micropulses was 84.6 ns.

Two independent groups of experimenters successfully doubled the light into the visible, and used the doubled light in materials science experiments studying picosecond processes. One of the groups took advantage of the SCA/FEL's long micropulse separation to select individual micropulses from the pulse train, and was successful in observing a photon echo in a dye molecule/glass system. Another group of experimenters, pursuing the concept of a gas loaded FEL (GFEL), filled the wiggler with 5 torr of hydrogen and observed the expected decrease in lasing wavelength. They also demonstrated that FEL problems due to electron beam induced plasma in the gas were much less severe with the 85 ns pulse separation than in previous experiments with a 350 ps pulse separation.

New electron beam and optical beam diagnostic systems allowed collection of data which had previously been unavailable. As an example, when the optical cavity length was adjusted for maximum average power out (significantly greater than the 30 W quoted above), time resolved optical spectra clearly showed the growth of sidebands as the power built up at the beginning of each macropulse. The presence of sidebands was consistent with the rather chaotic nature of the optical power level within the macropulse. As expected, when the cavity length was adjusted for stable power output (30 W) during the macropulse, the spectrum of the pulse consisted of a single transform limited line. Time resolved electron beam spectral data allow the evolution of the energy spread of the electron beam to be studied, as well as allowing a comparison to be made between the photon power extracted and the electron beam power lost. With 30 W in the photon beam, 56 W was measured lost from the electron beam. (At present we don't understand the discrepancy). As a final set of examples, emittance can now be measured before and after the wiggler. After passing through the wiggler, the normalized emittance of the 5.6 A peak current beam was measured to be 20  $\pi$  mm mr. Before the wiggler it was 8  $\pi$  mm mr.

#### Optical Spectra in Stable and Unstable Modes at 1.5 Microns

- Macropulse averaged spectra (top figure)
- Micropulse spectra (bottom figure)
- Unstable mode has higher power ( $2 \times$  or  $3 \times$ ), broader spectrum. Usable power in narrow bandwidth is higher in the stable mode
- Absence of wavelength jitter or slew is demonstrated by the fact that the (stable mode) macropulse spectrum is just as narrow as the micropulse spectrum

#### USERS' EXPERIMENTS IN JUNE 1989

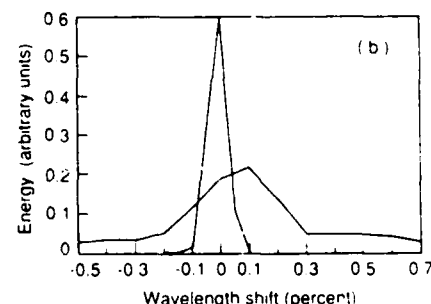
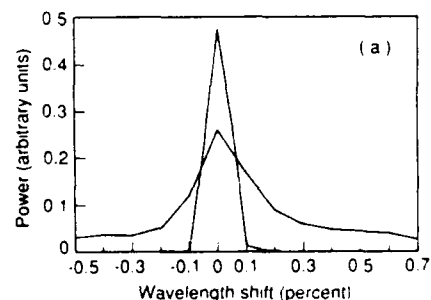
- Photon echos from dyes in glasses (Stanford)
- Non-linear optics (Princeton)
- Gas-loaded FEL (Stanford)

#### Electron Beam:

Energy	66 MeV
Energy Resolution	.05%
Macropulse Current	200 $\mu\text{A}$
Macropulse Duration	3 ms
Macropulse Repetition Rate	10 Hz
Micropulse Duration	3 ps
Micropulse Current	5.6 A
Normalized Emittance	8 $\pi$ mm mr

#### Extracted Optical Beam:

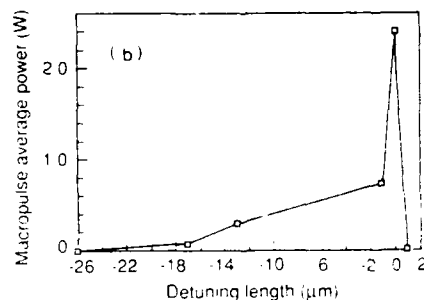
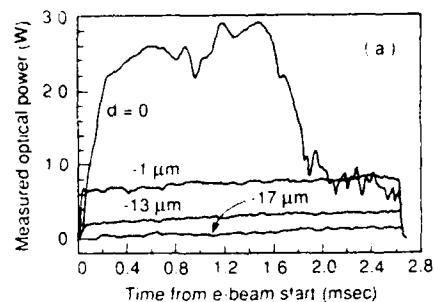
Wavelength	1.54 $\mu$
Spectral Width	.15%
Macropulse Power	24 W
Macropulse Duration	3 ms
Repetition Rate	10 Hz
Micropulse Power	700 Kw
Micropulse Length	2.25 ps
Time Between Micropulses	84.6 ns



<sup>1</sup> Work supported by ONR N00014-86-K-0118

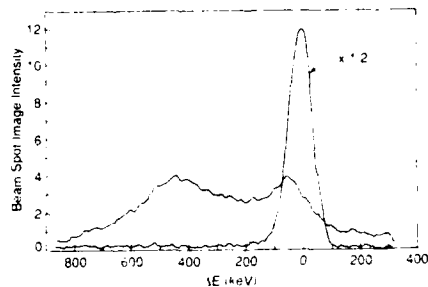
## DETUNING BEHAVIOR AT 3.5 MICRONS

- Power vs. time for several optical resonator detuning lengths (top figure)
- Macropulse average power vs. optical resonator detuning length (bottom figure)
- Zero detuning ( $d=0$ ) is defined as the length for maximum power
- Unstable power vs. time (such as  $d=0$ ) is associated with a broad spectrum and/or discrete sidebands



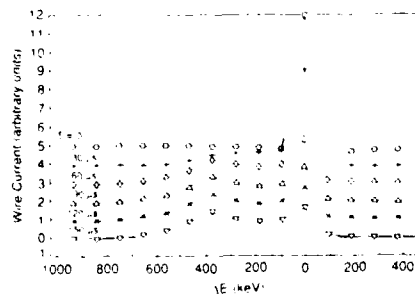
## TIME-AVERAGED ELECTRON BEAM ENERGY SPECTRA

- Data obtained from phosphor screen/TV camera (integrates whole macropulse)
- Narrow peak (reduced by  $2 \times$ ) is the spectrum with the laser off.  $E = 67 \text{ MeV}$
- Broad spectrum is with laser producing  $30 \text{ W}$  at  $1.5 \text{ microns}$
- Centroid shift gives energy extraction of  $0.4\%$ . The TRW wiggler used has 120 periods, so  $1/2 N$  is  $0.42\%$ .



## TIME RESOLVED ELECTRON SPECTRA DURING LASER TURN-ON

- Data taken from 16-wire array
- Spatial Resolution is lower than that of the phosphor, but temporal resolution is  $30 \mu\text{sec}$
- Turn-on is essentially complete after  $90 \mu\text{sec}$
- During stable operation, the wire array data agree well with the phosphor, indicating that the macropulse averages are meaningful
- During unstable operation, the wire array gives valuable information on the electron dynamics





## EX2.3

### Cyclotron Autoresonance Maser Experiments A. DiRienzo, G. Bekefi, C. Leibovitch, B. Danly Massachusetts Institute of Technology Cambridge, MA 02139

Studies of a 35 GHz, 1.4 MeV, 260 Amp cyclotron autoresonance maser (CARM) amplifier are presented. A bifilar helical wiggler is used to impart perpendicular energy. Radiation is generated in a wiggler-free region. A small signal gain of 91 db/m has been observed with a saturated power output of 10 MW (electronic efficiency of 3%). Methods of improving efficiency are presented.

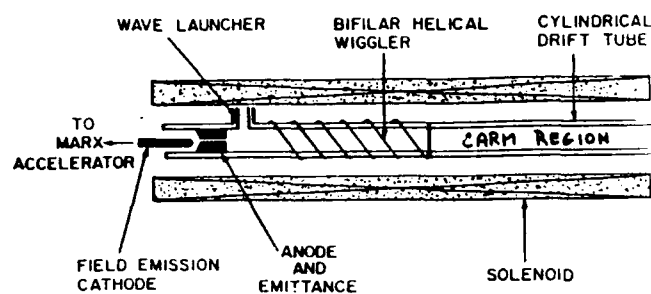


Fig. 1. Schematic of CARM Experiment

$$\text{Brightness } B_n = \frac{e^2 \gamma^3}{(4\pi)^2 (\delta^2 V)}$$

where  $\delta^2 V = \frac{e^2 \gamma^3}{8\pi^2 r_p^2}$  and  $r_p$  = emittance selector radius

Normalized Emittance  $\epsilon_{rms}^2 = \frac{2\delta I}{9B_n}$   
for a uniform phase space distribution

$$\frac{\Delta \gamma_{\parallel}}{\gamma_{\parallel}} = \frac{\epsilon_{rms}^2 (r_{ms})}{2r_p^2}$$

FOR  $B_{axial} = 7.0 \text{ KG}$

$r_p$ (cm)	$\delta I$ (Amps)	$B_n$ ( $\frac{\text{Amps}}{\text{cm}^2 \cdot \text{rad}^2}$ )	$\epsilon_{rms}$ (cm - rad)	$\frac{\Delta \gamma_{\parallel}}{\gamma_{\parallel}}$
.0762	8.4	$9.50 \times 10^4$	$4.43 \times 10^{-3}$	$1.69 \times 10^{-3}$
0.254	260	$2.38 \times 10^4$	$49.3 \times 10^{-3}$	$1.88 \times 10^{-3}$

Fig. 3. Beam Parameters

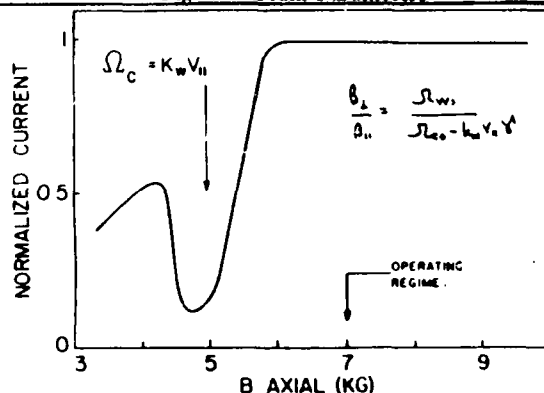


Fig. 5. Beam current transmitted through wiggler region, as a function of axial magnetic field.  
N.B. Resonance at 5 kG.

Beam Energy	1.5 MeV
Total Current	20 kA
Pulse Length	30 ns
Current into CARM	260 A
Axial Solenoid Field	7 kG
Wiggler Type	Bifilar Helical
Wiggler Period	7 cm
Adiabatic Uptaper Length	42 cm
Untapered Length	14 cm
Termination at Exit of Wiggler	Single Loop
Wiggler Field	460 G
$v_{\perp}/c$	$\sim 0.3$
Wiggler Free Region	86 cm
Waveguide Radius	.79 cm
Waveguide Mode	$TE_{11}$

Fig. 2. Operating Parameters

#### WIGGLER FIELD COMPONENTS

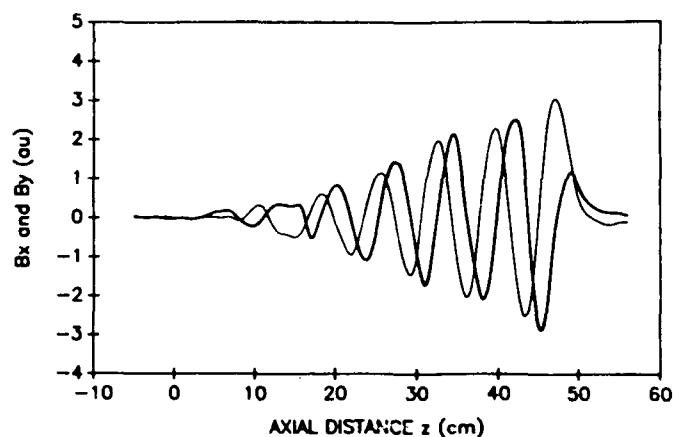


Fig. 4. Bifilar Helical Wiggler Field Components

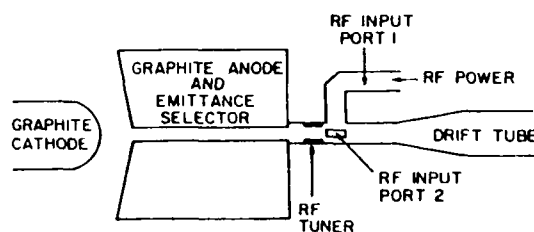


Fig. 6. Schematic of Microwave Input Coupler

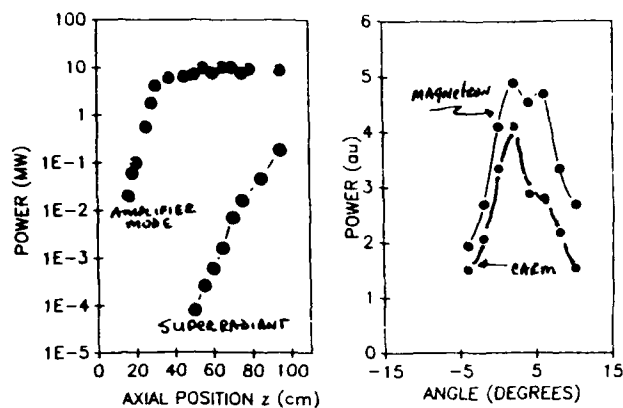


Fig. 7. (Left) Amplified and superradiant power generated by CARM as a function of axial position. (Right) Angle scan of input microwave signal (above) and amplified signal (below) to show similarity.

### FUTURE WORK

- To Improve:
- Perpendicular Velocity Spread
  - Operation at Beam Resonance
  - Efficiency
  - Tapering of the Axial Magnetic Field

Fig. 9. Future Work

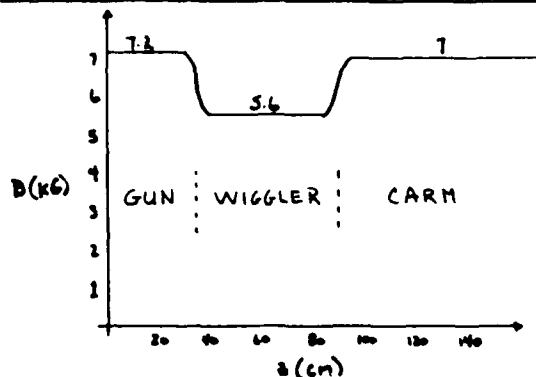


Fig. 11. Axial magnetic field to allow for high current generation as well as operation near wiggler resonance.

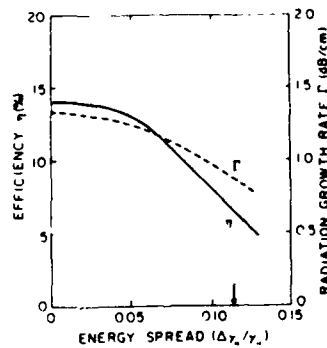


Fig. 8. Computed efficiency and growth rate as a function of energy spread. Experimental results shown by arrow on abscissa.

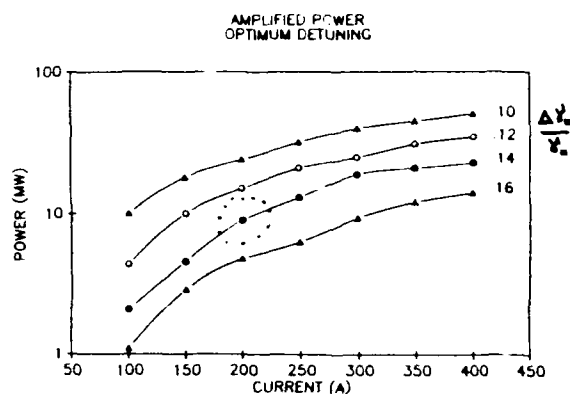


Fig. 10. Calculated power as a function of current and energy spread. Dotted area is experimental value.

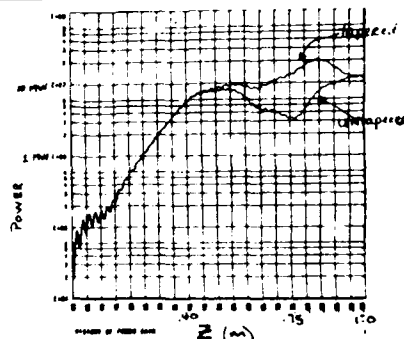


Fig. 12. Calculated effect of optimal tapering of the axial magnetic field in the non-linear CARM region.

Conclusion: First successful operation of a high power (10 MW), single pass amplifier CARM. Future increases in efficiency of power planned.

Reference: G. Bekefi, A. DiRienzo, C. Leibovitch, and B. Danly. *95 GHz Cyclotron Autoresonance Maser Amplifier*, Appl. Phys. Lett. 54, 3 April 1989.

## EX2.4

### Bandwidth Narrowing by Seed Injection of a Free-Electron Laser

Avner Amir, J. Finn Knox-Seith and Michael Warden

Center for Free-Electron Laser Studies

Quantum Institute

University of California, Santa Barbara, Ca. 93106

We show recent results from an injection seeding experiment at the UCSB FEL in which a low power molecular laser was used to seed the FEL. Narrowing of the pulse-to-pulse frequency bandwidth as well as earlier startup of the pulse have been observed.

#### THE UCSB FEL:

ELECTROSTATIC ACCELERATOR  
WITH BEAM RECOVERY

=> quasi-cw pulses

1-10 ns

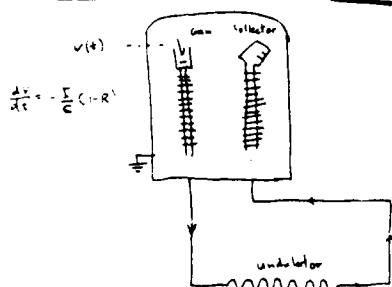
rep. rate 0.3 Hz - 1 Hz

E. beam Energy = 4.67 MeV

Wavelength 184  $\mu\text{m}$

(1630 GHz)

Spectral characteristics are  
determined by voltage variations



(a) Terminal Voltage fluctuations (pulse-to-pulse)

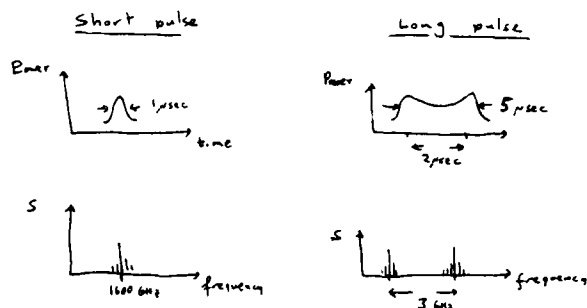
$$\frac{1}{V} \langle \Delta V \rangle_{rms} = 0.5\%$$

(b) Terminal Voltage drop

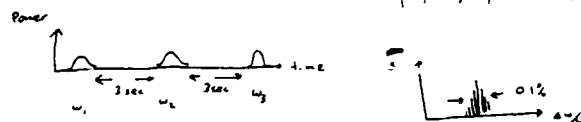
$$\frac{1}{V} \frac{dV}{dt} = -\frac{I}{C}(1-R) \frac{1}{V} = 0.06\% / \mu\text{sec}$$

For  $I = 2 \text{ A-p}$   
 $C = 150 \text{ pF}$   
 $R = \text{Recovery} = 80\%$   
 $V = 5 \text{ MeV}$

(a) Voltage drop causes frequency jump during the pulse

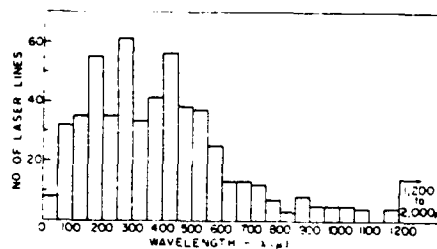


(b) Voltage fluctuations cause pulse to pulse frequency fluctuations



CO<sub>2</sub> - pumped molecular lasers  
cover most of FIR

10 - 1000  $\mu\text{m}$



CW { Typical power < 10 mW  
Strong lines ~ 100 mW

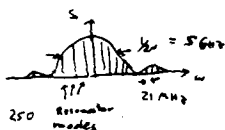
pulsed { energy ~ 1 mJ  
pulse width ~ 200 ns

## INJECTION SEEDING:

START FEL FROM EXTERNAL  
SOURCE RATHER THAN ITS  
OWN SPONT. EMISSION

### 1) FEL SPONT. EMISSION

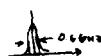
$$\text{Power} / \text{Bandwidth} = 1.6 \mu\text{W}/\text{GHz}$$



### 2) Pulsed molecular laser

$$P_{\text{pulsed}} \gg 1.6 \frac{\mu\text{W}}{\text{GHz}} \times 0.6 \text{ GHz} = 0.96 \mu\text{W}$$

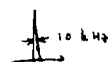
(13 μW in experiment)



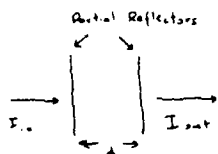
### 3) CW molecular laser

$$P_{\text{CW}} \gg 1.6 \mu\text{W}/\text{GHz} \times 1 \text{ kHz} = 16 \mu\text{W}$$

(30 μW in experiment)



## SPECTRUM MEASUREMENT WITH FABRY-PEROT INTERFEROMETER (FPI)



$$\text{Kinetic} \quad \frac{u}{\lambda/2} = f$$

$$\text{Order (fringe)} = \frac{d}{\lambda/2} = n$$

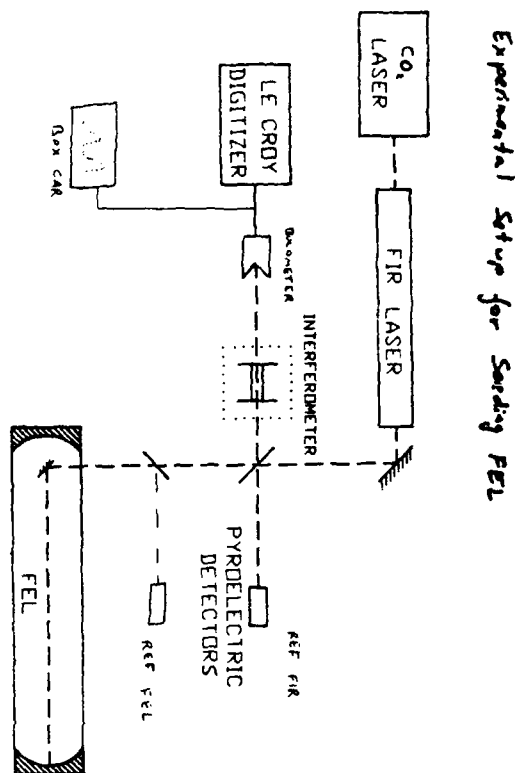
$$\text{Transmission } T = \frac{I_{\text{out}}}{I_{\text{in}}} \approx \frac{1}{1 + \left(\frac{2F}{\pi}\right)^2 \sin^2(kd)}$$

At a given spacing, frequency fluctuations  
cause intensity fluctuations  
which will broaden the  
curve



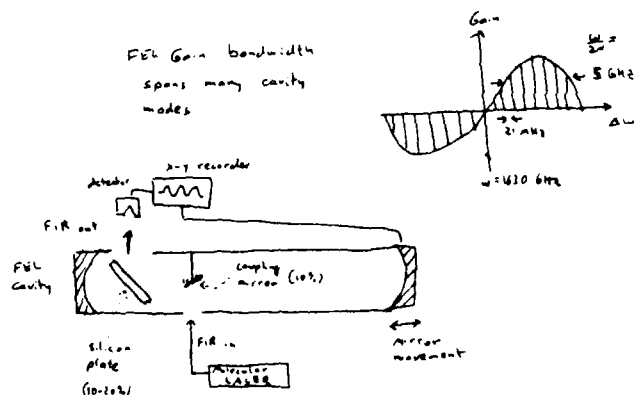
$$\text{At } kd = \pi/4, F \gg 1$$

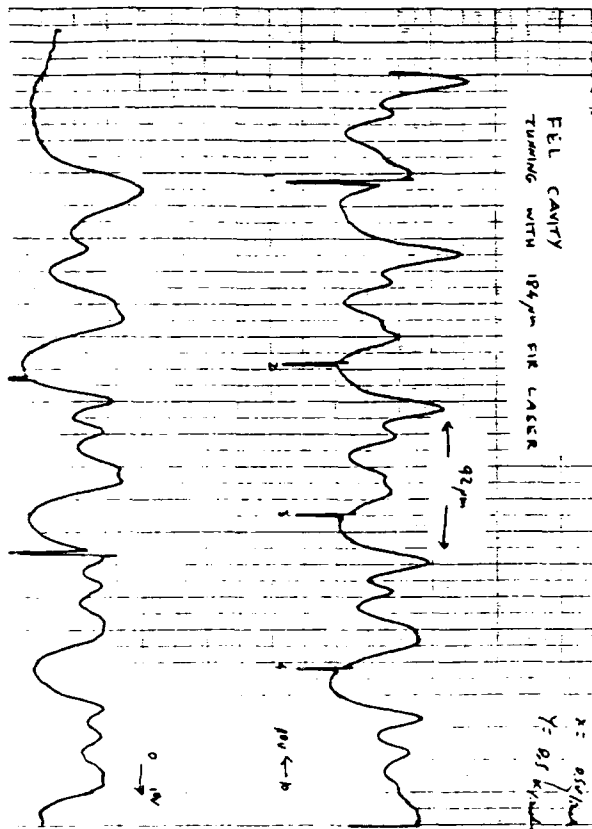
$$\frac{\Delta u}{u} \approx 2\pi n \frac{\Delta r}{r}$$



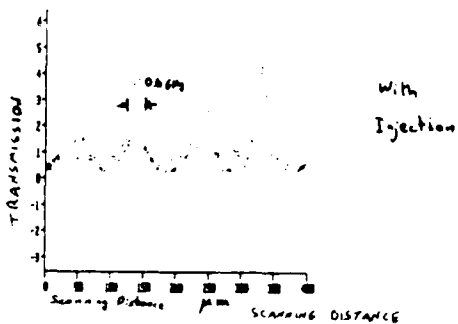
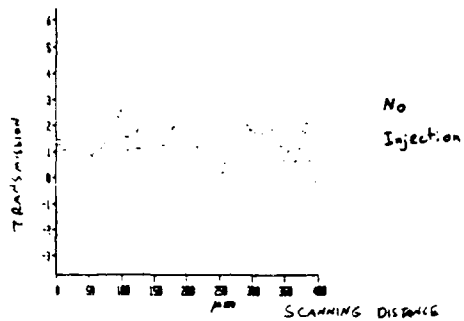
## How to get the two lasers on exactly the same line

- Set FEL to energy given by  $\lambda = \sqrt{\frac{\lambda_u}{2\lambda}}$
- Set Fabry-Pérot to peak transmission on the molecular laser
- Fine tune FEL energy by maximize transmission through Fabry-Pérot
- Tune FEL cavity to molecular laser line



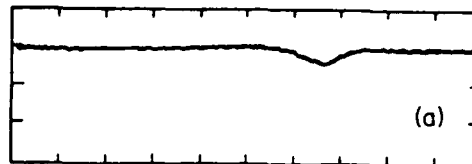


PULSE-TO-PULSE  
BANDWIDTH NARROWING USING EXTERNAL INJECTION  
(PULSED FIR LASER)

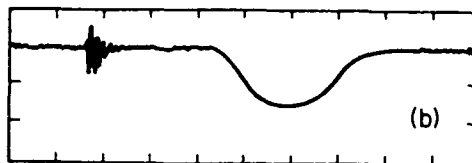


# OPTICAL AND ELECTRON BEAM PULSES

UN-  
SEEDED  
OPTICAL  
PULSE



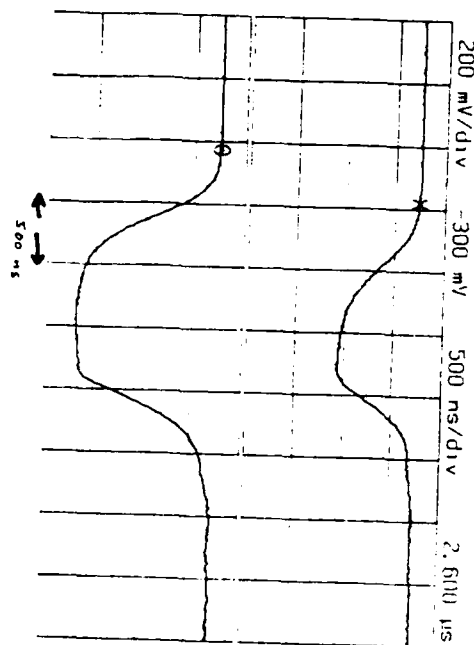
SEEDED  
OPTICAL  
PULSE



ELECTRON  
BEAM



1 μs/div.

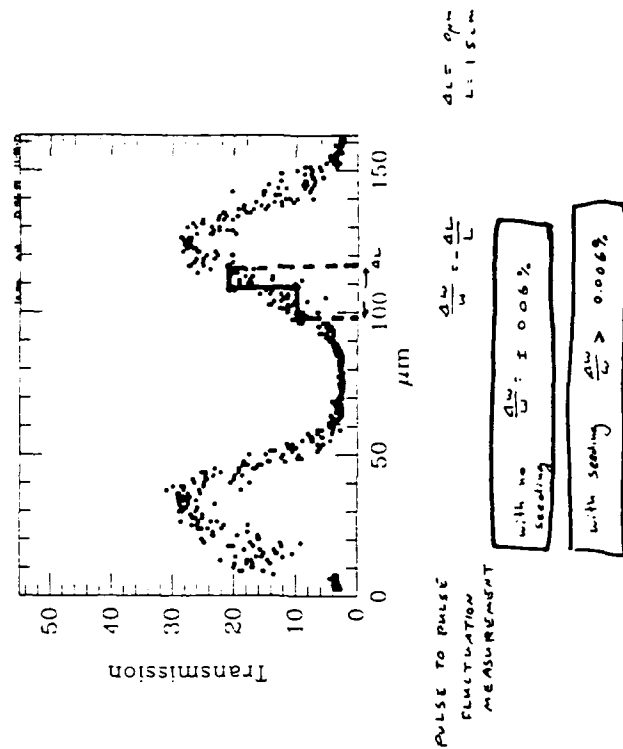
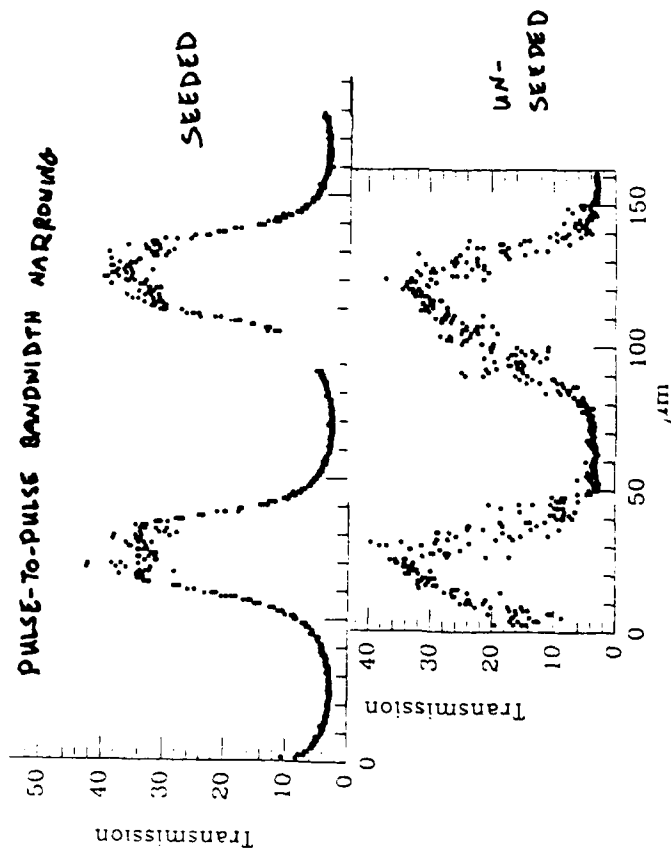
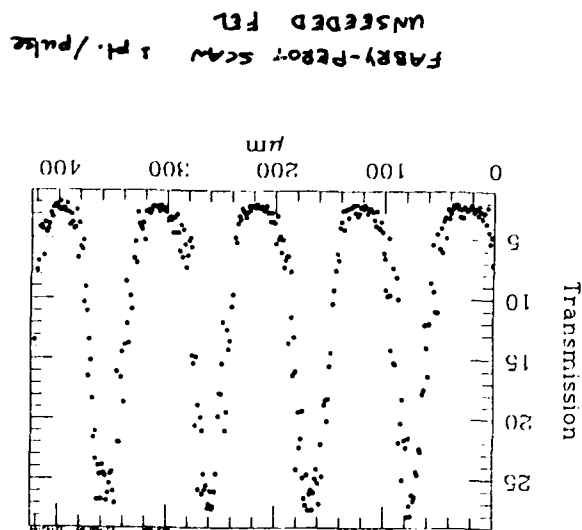
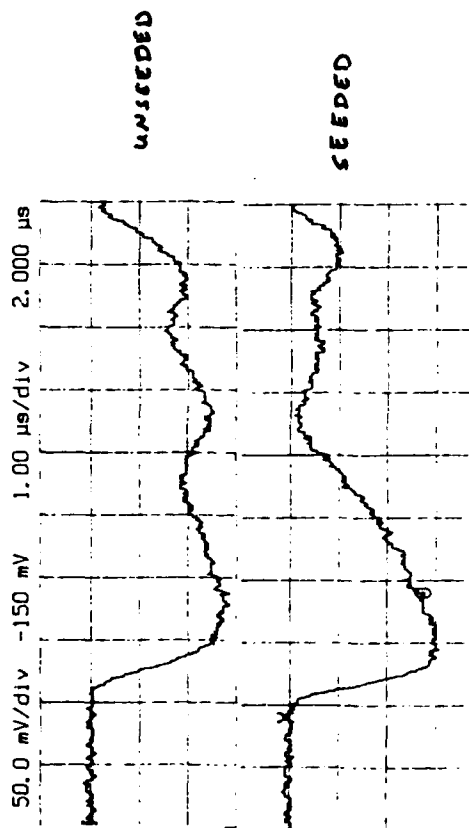


OPTICAL PULSE TIME STRUCTURE  
(SEEDING WITH CW FIR LASER)

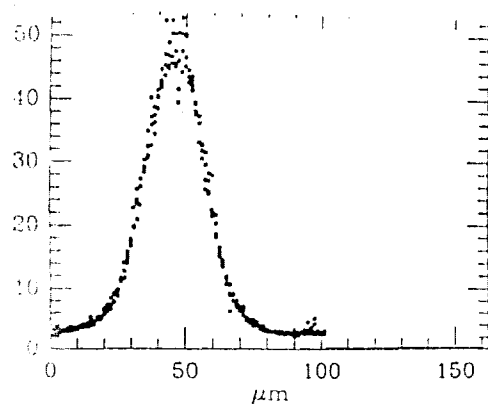
SEEDED

UNSEEDED

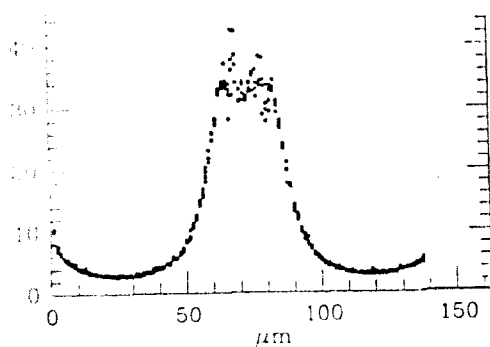
# SEEDING IN A LONG PULSE



# "FLAT TOP" MYSTERY

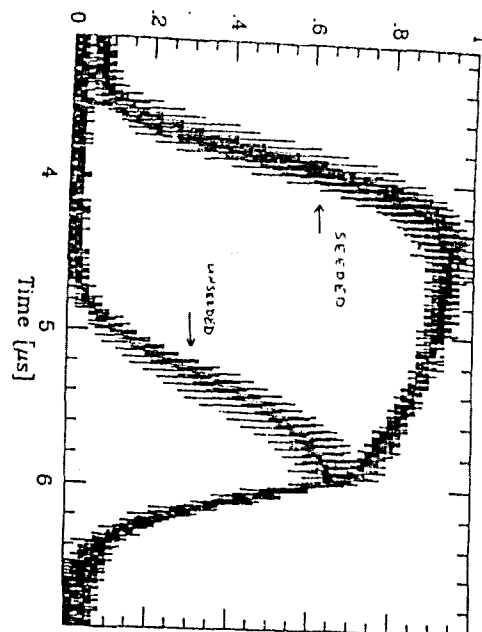


1  $\mu\text{sec}$   
pulse



1.5  $\mu\text{sec}$   
pulse

## Normalized Laser Amplitude



Free Electron Laser Power versus Time

(SEEDING WITH PULSED LASER)

## RESULTS OF SEEDING WITH CW LASER

- (1) Early start up 1-2  $\mu\text{sec}$
- (2) Pulse-to-pulse bandwidth  
narrowing 0.06%  $\rightarrow$  0.006%

## Multimode Simulations

J. Finn Knox-Seith  
AVNER AMIR

LONG PULSE  $E(z,t)$  is simulated in the space time domain.

Following Colson, we average over the carrier frequency and look at the evolution of the envelope  $a(z, \tau)$  of the field over many passes.

Electron dynamics is governed by pendulum Eq.

$$\frac{d\phi}{d\tau} = ka \cos(S\tau\phi)$$

$$\frac{da}{d\tau} = j\langle e^{-i\phi} \rangle$$

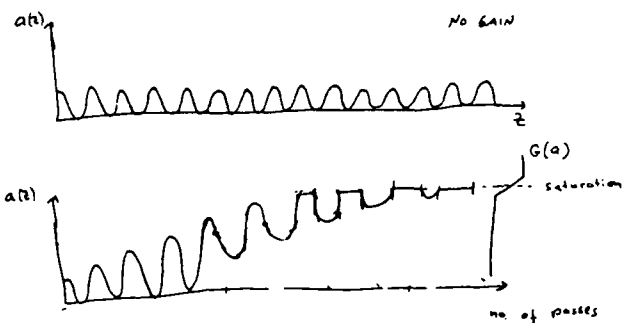
Electron at phase  $S(z, \tau)$  interacts with field  $a(z + \tau, \tau)$

Fourier Transform with respect to  $\tau$ , gives the mode composition

Periodic boundary conditions are imposed over a light segment of length  $L_w$

### Saturation of two modes

The envelope shows the beating frequency  
 $a = a_0 + a \cos(\Delta\omega z)$

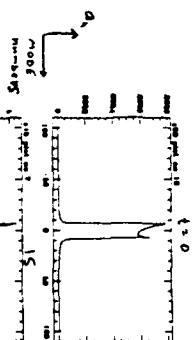
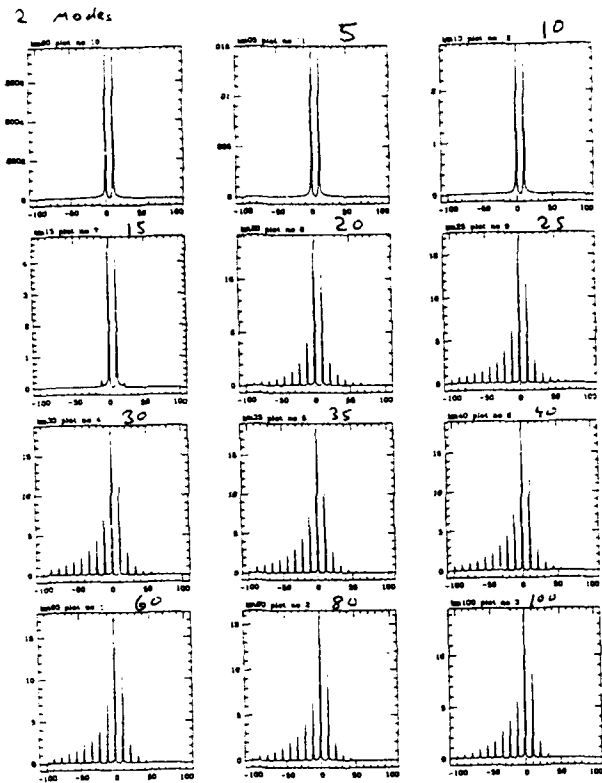
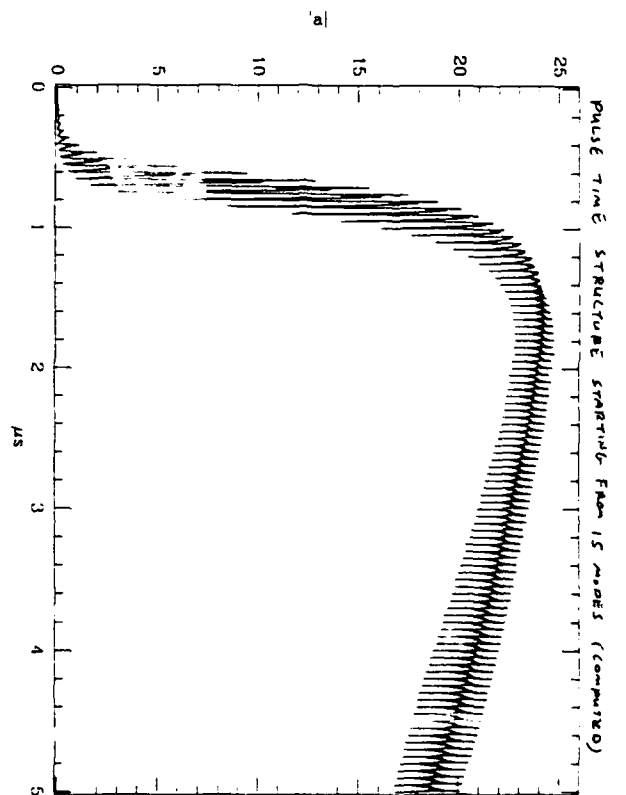
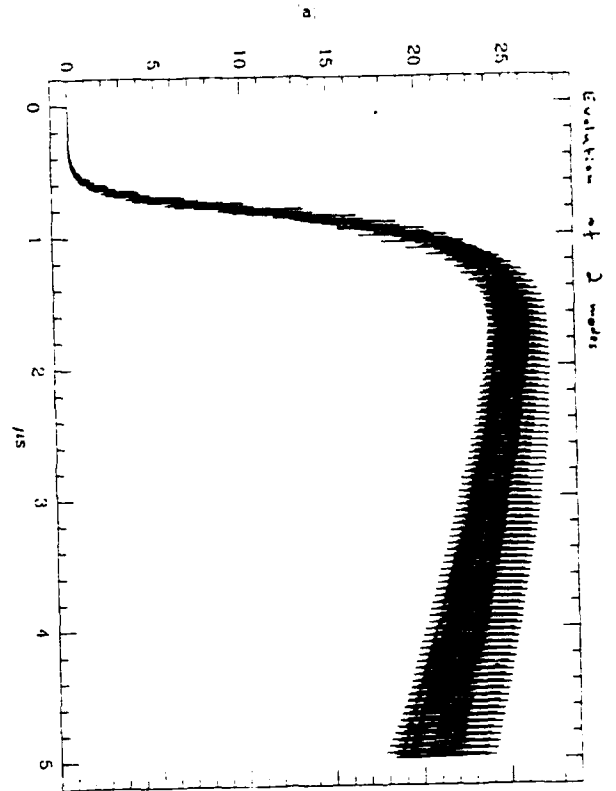


The peaks saturate first } increase in  
The 'dips' are then filled up } the D.C. component

"corners" shows up as multipoles of the beat frequency

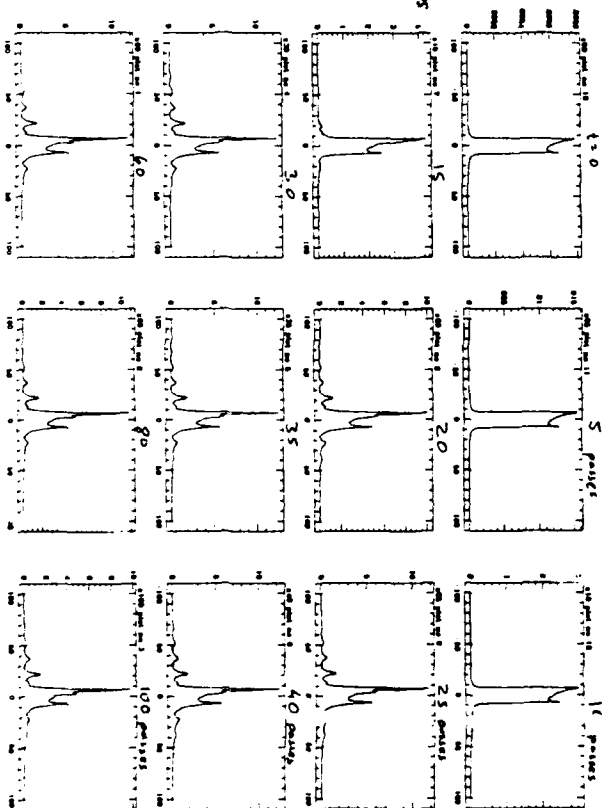






1 pulse = 50 ns

MODES DEVELOPMENT IN TIME



## EX2.5

### 140 GHz Microwave Experiments in ELF-II\*

A. L. Throop, R. A. Jong, D. P. Atkinson, J. C. Clark, B. Felker,  
S. W. Ferguson, M. A. Makowski, W. E. Nexsen, B. W. Stallard, and W. C. Turner

Lawrence Livermore National Laboratory  
University of California, Livermore, California 94550

We describe the modeling, the experimental set-up, and initial operating results for ELF-II, an induction-linac based free-electron laser designed to produce up to 2 GW of peak power at 140 GHz. ELF-II is the initial configuration of an FEL system which will eventually produce up to 2 MW of average power at a frequency of 250 GHz, for use in plasma heating experiments in the Microwave Tokamak Experiment at the Lawrence Livermore National Laboratory.

\* Work performed under the auspices of the US Department of Energy by the Lawrence Livermore National Laboratory under W-7405-ENG-48. ETA-II accelerator development is part of SDIO/SDC's induction free-electron laser science and technology program.

#### The ELF-II experiment will provide an initial evaluation of an Induction-Linac microwave FEL for plasma heating

##### Objectives

- Evaluate present ETA-II beam quality as driver for microwave FEL
  - Beam current, brightness, and energy flatness
- Use ELF-II to verify FEL simulation codes
  - High peak-power (2 GW) at high frequency (140 GHz)
  - High amplifier gain (77 dB)
- Evaluate quasi-optical microwave transmission over long distances
  - Transmission efficiency
  - Microwave breakdown
  - Alignment and vacuum issues
- Qualitative evaluation of nonlinear plasma coupling
  - Plasma absorption
  - Backscatter instabilities

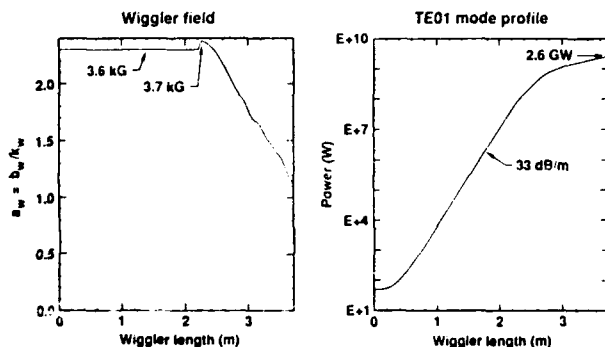
Subsequent upgrades will allow experiments at high powers (8 GW peak, 1-2 MW average) and higher-frequencies (250 GHz)

#### Design parameters for ELF-II experiment

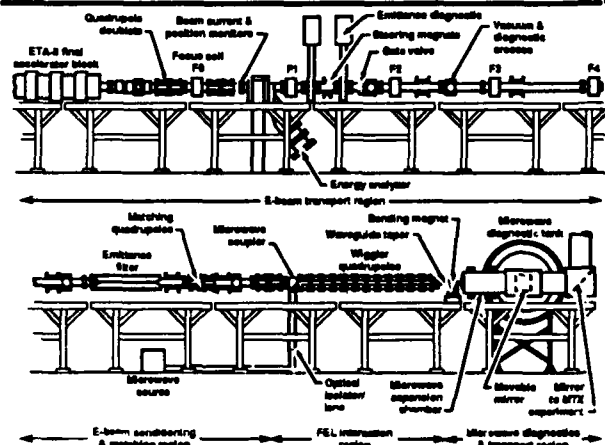
ETA-II Accelerator	ELF air-core wiggler	FEL Interaction
$V_a = 6 \text{ MeV}$	$\lambda_w = 9.8 \text{ cm}$	140 GHz
$I_a = 2.5 \text{ kA}$ (25% margin)	$L_w = 4.0 \text{ m}$	$I_{a, \text{wiggler}} = 2 \text{ kA}$
$J = 1.0 \pm 8 \frac{\text{A}}{(\text{m} \cdot \text{r})^2}$	$B_w = 3.7 \text{ kG}$	$P_{in} = 50 \text{ W}$
$\tau_p > 20 \text{ ns}$	$\frac{\Delta B_w}{B_w} \text{ taper} = 54\%$	$P_{TET} = 2.5 \text{ GW}$
$\frac{\Delta \gamma}{\gamma} = \pm 1\%$	$\text{PRF} = 0.5 \text{ Hz}$	3 x 6 cm waveguide
$\Delta r < 1 \text{ mm}$		TE01 mode

#### Calculated wiggler-field and -gain profiles for ELF-II at 140 GHz

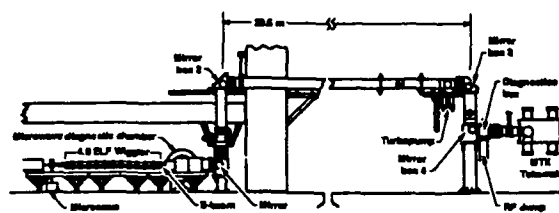
6 MeV, 2 kA,  $1.0 \times 10^8 \text{ A}/(\text{m} \cdot \text{r})^2$ , 50 W, errors =  $\pm 1\%$ , 1 mm, 0.5%



#### Diagram of 6 MeV Electron Laser Facility (ELF-II)



## ELF-II and microwave system for initial 140 GHz experiments with MTX



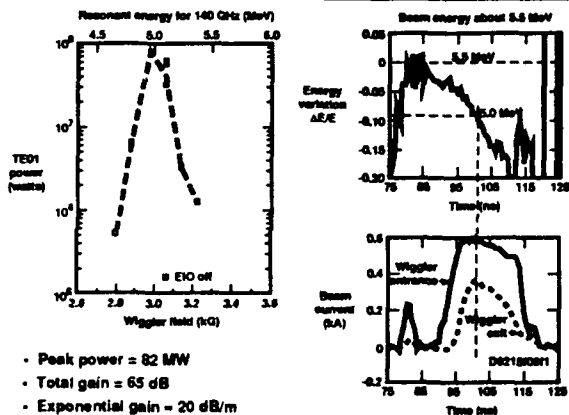
- Quasi-optical microwave transport
  - 4 transport mirrors ( $\sim 17 \times 24^\circ$ )
  - Windowless transport
  - Tokamak port =  $4 \times 30$  cm
- Field strength  $\sim 32$  MV/m
- Beam centering tolerance  $\pm 4$  mm (0.2 mrad)
- Calculated TEO1 transmission loss  $< 13\%$

## Status of ETA-II accelerator for ELF-II experiments\*

\* See W. E. Nassen et al. for detailed report (poster session P 3.18)

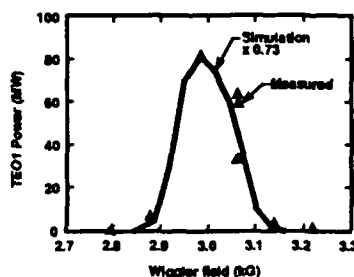
Parameter	ELF-II requirement	Present status
Accelerator current	2.5 - 3.0 kA	3.2 kA at 4.2 MeV,
Beam energy	6.0 MeV	1.7 kA at 6 MeV (routine)
Beam brightness	0.3 - 3.0	$> 3.0$ at 1.7 kA, 6 MeV
	$\left[ \times 10^6 \frac{\text{A}}{(\text{m} \cdot \text{r})^2} \right]$	
Energy sweep	$\leq \pm 1\%$ over	$\pm 1\%$ over 10 ns
Pulse width	$\geq 20$ ns	
Beam spatial offset	$< 1$ mm	2 - 4 mm
Beam angular offset	$< 10$ mrad	10 - 20 mrad

## Measured detuning curve and beam energy on ELF-II



- Peak power = 82 MW
- Total gain = 65 dB
- Exponential gain = 20 dB/m
- Spontaneous noise = 1-10 mW/GHz

## Comparison of FRED simulation code with measured detuning curve on ELF-II

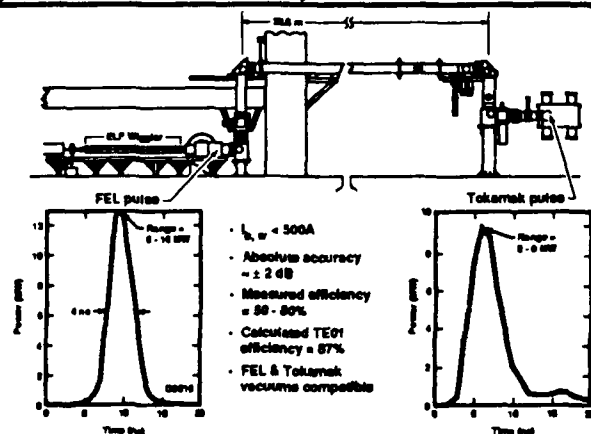


### Simulation

- 5.2 MeV
- 550 A
- Gain = 22 dB/m
- 80% TEO1

To within experimental error, FRED simulation code shows good agreement with measured curve

## Initial microwave transport experiments indicate good transmission efficiency into Tokamak



- $I_e = 500$  A
- Absolute accuracy  $\sim \pm 2$  dB
- Measured efficiency = 50 - 60%
- Calculated TEO1 efficiency = 67%
- FEL & Tokamak vacuum compatible

## Summary and plans

- ETA-II
  - Can achieve 3 kA, 1 MeV injector
  - Can achieve required brightness
  - Energy sweep identified and being resolved
- ELF-II
  - Low-current experiments to date ( $< 600$  A)
  - Peak power = 80 MW
  - Overall gain = 65 dB
  - Agreement with simulations
- Microwave transmission
  - First measurements indicate good transmission efficiency
  - Alignment and vacuum compatibility are not major issues
- Near-term plans
  - High-current accelerator operation
  - High-power, tapered-wiggler operation
  - High-power plasma heating experiments
- Upgrades during early FY 90
  - ETA-II to 5 kV, 10 ns operation
  - Install DC electromagnet wiggler
  - IMP experiment: 3 - 4 GW at 140 GHz, 5 kHz burst

# TH2.2 ANALYTICAL STUDY OF MULTIMODE COMPETITION

Isidoro Kimel and Luis R. Elias  
Center for Research in Electro-Optics and Lasers (CREOL)  
University of Central Florida, Orlando, FL 32816

## ABSTRACT

A theoretical analysis of multimode competition in FELs is performed. The system is mathematically described by a set of coupled differential equations (one for each mode). The coupling coefficients in the equations are obtained from a perturbation expansion of the current. The result is that the only asymptotically stable solutions are single mode.

### 1. INTRODUCTION

GIVEN A CHOICE: WOULD A FEL OPERATE  
SINGLE OR MULTIMODE?

PURPOSE OF THE WORK:

ANALYTICALLY STUDY MODE  
COMPETITION IN FELs

ITEMS:

- Perturbation theory
- Linear term
- Nonlinear terms
- Two-mode competition
- Three modes
- Many modes

The usual small signal gain and other linear properties follow from this first order term.

### 4. NONLINEAR TERMS

Saturation effects start with the third order terms. These are of the form

$$J_q^{(3)} = -\frac{1}{2} S a_q \left[ a_q^2 + u \sum_{s \neq q} a_s^2 \right], \quad (u = 2).$$

The derivation of which, as well as the value of the saturation parameter  $S$ , are given in previous work. There are two types of saturation effects: i) Self saturation with the intensity of a mode reducing its own growth. ii) And crossed saturation whereby the intensity of a mode reduces the growth of other modes. An important feature is that FELs are systems with strong coupling in which the crossed saturation is twice as strong as the self saturation ( $u=2$ ).

### 2. PERTURBATION THEORY

After introducing the radiation field written in terms of optical modes into the wave equation, one obtains the evolution equation for the mode  $q$  with amplitude  $a_q$  and phase  $\phi$

$$\frac{da_q}{d\tau} + i a_q \left( \frac{d\phi}{d\tau} - \frac{\alpha}{2} \right) = J_q,$$

where  $\alpha$  represents the losses per pass and  $J_q$  is the reduced current that drives the mode  $q$ . This current is, of course, a nonlinear function of the mode fields; and the idea is to perform a perturbation expansion in powers of the amplitudes as in

$$J_q = J_q^{(1)} + J_q^{(2)} + J_q^{(3)} \dots$$

### 3. LINEAR TERM

The linear term in the perturbation expansion is

$$J_q^{(1)} = i G_0 \int_0^{\tau} d\tau_1 \int_0^{\tau_1} d\tau_2 e^{-i\omega_q(\tau-\tau_2)} \chi_q(\tau_2),$$

where  $\chi_q = a_q e^{i\phi}$ .

### 5. TWO-MODE COMPETITION

Two mode competition is described by the system of coupled differential equations

$$\frac{da_1(\eta)}{d\eta} = \frac{1}{2} a_1 [\Gamma - S(a_1^2 + u a_2^2)],$$

$$\frac{da_2(\eta)}{d\eta} = \frac{1}{2} a_2 [\Gamma - S(a_2^2 + u a_1^2)].$$

In order to see what is the composition of the stable states, it is convenient to transform to polar coordinates

$$a_1(\eta) = r(\eta) \cos \theta,$$

$$a_2(\eta) = r(\eta) \sin \theta,$$

$$r^2 = R.$$

In terms of the new variables the system of equations is

$$\frac{dR(\eta)}{d\eta} = R(\eta) \left\{ \Gamma - S R(\eta) \left[ 1 + \frac{1}{2} (u-1) \sin^2(2\theta) \right] \right\},$$

$$\frac{d\theta(\eta)}{d\eta} = -\frac{1}{8} (u-1) S R(\eta) \sin[4\theta(\eta)].$$

For  $u=1$  any  $\Theta$  is possible. For other  $u$  values the only equilibrium points are  $\Theta=0, \pi/4$  and  $\pi/2$ . The stable equilibrium points are:

$$\text{Weak coupling } (u < 1) \Rightarrow \Theta = \frac{\pi}{4}$$

$$\text{Strong coupling } (u > 1) \Rightarrow \begin{cases} \Theta = 0, \text{ pure mode 1} \\ \Theta = \frac{\pi}{2}, \text{ pure mode 2} \end{cases}$$

## 6. THREE MODES

For three modes the situation is, of course, more complicated and we have now the set of three coupled equations

$$\frac{d\alpha_1(\eta)}{d\eta} = \frac{1}{2}\alpha_1\{\Gamma - S[\alpha_1^2 + u(\alpha_2^2 + \alpha_3^2)]\},$$

$$\frac{d\alpha_2(\eta)}{d\eta} = \frac{1}{2}\alpha_2\{\Gamma - S[\alpha_2^2 + u(\alpha_1^2 + \alpha_3^2)]\},$$

$$\frac{d\alpha_3(\eta)}{d\eta} = \frac{1}{2}\alpha_3\{\Gamma - S[\alpha_3^2 + u(\alpha_1^2 + \alpha_2^2)]\}.$$

Transform to cylindrical coordinates

$$i) \Theta = 0 \text{ (pure mode 1).}$$

ii)  $\Theta \neq 0$ , then  $\sin 4\Phi = 0$  again leading to  $\Phi = 0$  (no mode 3),  $\pi/2$  (no mode 2) or  $\pi/4$ ; only the first two being stable for  $u > 1$ . With  $\sin 4\Phi = 0$  the second equation simplifies to

$$\frac{d\Theta(\eta)}{d\eta} = -\frac{1}{8}(u-1)RS \sin 4\Theta.$$

Since in this case  $\Theta \neq 0$  the only stable point is  $\Theta = \pi/2$  (no mode 1).

Thus we see that also in the case of three competing modes, only single mode states are stable.

## 7. MANY MODES

For  $n$  modes the set of equations is (with  $i=1, \dots, n$ )

$$\frac{d\alpha_i(\eta)}{d\eta} = \frac{1}{2}\alpha_i\left\{\Gamma - S\left[u\sum_{j=1}^n \alpha_j^2 - (u-1)\alpha_i^2\right]\right\}.$$

The mode amplitudes can be parametrized as

$$\alpha_i(\eta) = r(\eta) \cos(\Theta_i),$$

$$\cos \Theta_{n-2} \frac{dR}{d\eta} - 2R \sin \Theta_{n-2} \frac{d\Theta_{n-2}}{d\eta} + 2R \cos \Theta_{n-2} \sum_{j=1}^{n-2} \cot \Theta_j \frac{d\Theta_j}{d\eta}$$

$$= R \cos \Theta_{n-2} \left\{ \Gamma - RS \left[ u - (u-1) \cos^2 \Theta_{n-2} \sum_{j=1}^{n-2} \sin^2 \Theta_j \right] \right\}.$$

$$\sin \Theta_{n-2} \cos \Theta_{n-1} \frac{dR}{d\eta} + 2R \cos \Theta_{n-2} \cos \Theta_{n-1} \frac{d\Theta_{n-2}}{d\eta}$$

$$- 2R \sin \Theta_{n-2} \sin \Theta_{n-1} \frac{d\Theta_{n-1}}{d\eta} + 2R \sin \Theta_{n-2} \cos \Theta_{n-1} \sum_{j=1}^{n-2} \cot \Theta_j \frac{d\Theta_j}{d\eta}$$

$$= R \sin \Theta_{n-2} \cos \Theta_{n-1} \left\{ \Gamma - RS \left[ u \right. \right.$$

$$\left. \left. - (u-1) \sin^2 \Theta_{n-2} \cos^2 \Theta_{n-1} \sum_{j=1}^{n-2} \sin^2 \Theta_j \right] \right\}.$$

$$\sin \Theta_{n-2} \sin \Theta_{n-1} \frac{dR}{d\eta} - 2R \cos \Theta_{n-2} \sin \Theta_{n-1} \frac{d\Theta_{n-2}}{d\eta} - 2R \sin \Theta_{n-2}$$

$$\times \cos \Theta_{n-1} \frac{d\Theta_{n-1}}{d\eta} + 2R \sin \Theta_{n-2} \sin \Theta_{n-1} \sum_{j=1}^{n-2} \cot \Theta_j \frac{d\Theta_j}{d\eta}$$

$$= R \sin \Theta_{n-2} \sin \Theta_{n-1} \left\{ \Gamma - RS \left[ u - (u-1) \sin^2 \Theta_{n-2} \sin^2 \Theta_{n-1} \sum_{j=1}^{n-2} \sin^2 \Theta_j \right] \right\}$$

$$\alpha_1(\eta) = r(\eta) \cos(\Theta),$$

$$\alpha_2(\eta) = r(\eta) \sin(\Theta) \cos(\Phi),$$

$$\alpha_3(\eta) = r(\eta) \sin(\Theta) \sin(\Phi),$$

$$r^2 = R.$$

With these, the differential equations turn into

$$\frac{dR(\eta)}{d\eta} = R(\Gamma - uRS) + (u-1)R^2S$$

$$\times \{\sin^4 \Theta [\sin^4 \Phi (\sin^4 \Phi - \cos^4 \Phi) + \cos^4 \Phi]\},$$

$$\frac{d\Theta}{d\eta} = -\frac{1}{4}(u-1)RS \left[ \frac{1}{4} \sin^2 \Theta (\cos 4\Phi + 3) - \cos^2 \Theta \right] \sin 2\Theta,$$

$$\frac{d\Phi(\eta)}{d\eta} = -\frac{1}{8}(u-1)RS \sin^2 \Theta \sin 4\Phi.$$

The stable equilibrium states have a fixed ratio of the different modes. That corresponds to the derivatives of the angles being equal to zero at points of minima. From the last equation we see that the derivative of  $\Phi$  vanishes in the following cases

$$\alpha_2 = r \sin \Theta_1 \cos \Theta_2,$$

$$\alpha_3 = r \sin \Theta_1 \sin \Theta_2,$$

$$\alpha_{n-1} = r \sin \Theta_1 \dots \sin \Theta_{n-2} \cos \Theta_{n-1},$$

$$\alpha_n = r \sin \Theta_1 \dots \sin \Theta_{n-2} \sin \Theta_{n-1},$$

$$r^2 = R.$$

A generic amplitude is

$$\alpha_i = r \cos \Theta_i \sum_{j=1}^{i-1} \sin \Theta_j, \quad (\Theta_n = 0).$$

Suppose we are interested in knowing whether three given modes can coexist in FEL radiation (either with or without other modes); assuming that we know that at least one of the modes exists. All the possible modes can be labeled in such a way that the three in question are  $(n-2)$ ,  $(n-1)$  and  $n$ . In the new parametrization the evolution equations for these three modes are

Combining these equation with appropriate coefficients the evolution equations for the angles are derived. They read

$$\frac{d\Theta_{n-2}}{d\eta} = -\frac{1}{4}(u-1)RS \left( \sum_{j=1}^{n-2} \sin^2 \Theta_j \right) \times \left[ \frac{1}{4} \sin^2 \Theta_{n-2} (\cos 4\Theta_{n-1} + 3) - \cos^2 \Theta_{n-2} \right] \sin 2\Theta_{n-2}.$$

$$\frac{d\Theta_{n-1}}{d\eta} = -\frac{1}{8}(u-1)RS \left( \sum_{j=1}^{n-2} \sin^2 \Theta_j \right) \sin^2 \Theta_{n-2} \sin 4\Theta_{n-1}.$$

If at least one of the three modes exist then

$$\sum_{j=1}^{n-2} \sin^2 \Theta_j \neq 0,$$

which, naturally, is positive.

It is easy to see that the discussion for only three modes also holds for any three chosen modes out of  $n$ . Meaning that only one of these chosen modes can exist. This, of course, indicates that the FEL operates single mode.

F. Hartemann and G. Mourier  
Thomson-CSF/DTE, 78111, Vilizy, France

Recent experimental [1] and theoretical [2,3] results have suggested that the stimulated refraction effect, also referred to as "optical guiding", in a Free-Electron Laser (FEL) may have a strong influence on both the mode content and the gain of millimeter-wave FELs.

In this paper, we first present a formal method allowing to reduce the system of linearized equations of evolution of the microwave field from 8 equations in the 4-vector potential  $A_\mu$  and current density  $j_\mu$  to a canonical system of 4 PDEs in  $A_\mu$ . This formalism is very general and can be used for small-signal analysis of any beam-wave interaction.

We then specialize this set of equations to the study of a FEL with axial guide field and helically polarized wiggler, operating with a cylindrical waveguide interaction region, by defining the appropriate fluid equilibrium and boundary conditions. At this point, the 3-dimensional analysis can be performed according to two different formal methods. One can either find the eigenmodes of the system, which yields both the gain of the system and the radial intensity distribution of the interacting waves, or expand the microwave field into vacuum waveguide modes and make use of the orthonormality of these modes to study their coupling. In the latter case, the guiding appears as an active mode conversion effect.

We finally apply the eigenvalue analysis to the design study of a millimeter-wave FEL and show that for some parameters the gains can be improved by optical guiding effects.

[1] F. Hartemann, K. Xu, G. Bekefi, J.S. Wurtele and J. Fajans, Phys. Rev. Lett. **59**, 1177 (1987).

[2] A. Fruchtman, Phys. Rev. **A37**, 2989 (1988).

[3] J. Fajans and J.S. Wurtele, PFC Report JA89-15 (1989).

\* Present address: Plasma Fusion Center, MIT, Cambridge MA. 02139, USA.

### 3-D Theory with Optical Guiding

• Region 1 (vacuum) :  $r_b < r < a$ ,  $[\omega_p(r) = 0]$

$$\delta A_\theta(r, \theta, z, t) = [AJ_1'(\chi_1 r) + BY_1'(\chi_1 r)] \exp[i(\omega_1 t - k_1 z + l_1 \theta)].$$

Vacuum Dispersion Relation  $[D_1(k_1, \chi_1) = 0]$

$$\frac{\omega_1^2}{c^2} - k_1^2 - \chi_1^2 = 0.$$

• Region 2 (beam) :  $0 < r < r_b$ ,  $[\omega_p(r) = \omega_{p0}]$

$$\delta A_\theta(r, \theta, z, t) = CJ_1'(\chi_2 r) \exp[i(\omega_2 t - k_2 z + l_2 \theta)].$$

Beam Dispersion Relation  $[D_2(k_2, \chi_2) = 0]$

$$\left[ \frac{\omega_2^2}{c^2} - \beta_{||}(k_2 + k_w) - \frac{\omega_{p0}^2}{\gamma_{||} c^2} \sqrt{\phi} \right] \left[ \frac{\omega_2}{c} - \beta_{||}(k_2 + k_w) - \frac{\omega_{p0}^2}{\gamma_{||} c^2} \sqrt{\phi} \right] \\ \left[ \frac{\omega_2^2}{c^2} - k_2^2 - \chi_2^2 \right] = \beta_{||}^2 \frac{\omega_{p0}^2}{c^2} \frac{\phi}{\beta_{||}} k k_w.$$

• Boundary Conditions

1.  $\delta A_\theta(r = a) = 0$ , (waveguide wall)
2.  $\Delta \delta A_\theta(r = r_b) = 0$ , (no  $\propto$  B-fields)
3.  $\Delta \partial_r \delta A_\theta(r = r_b) = 0$ , (no surface currents)

Condition (2) must be verified  $\forall t, z$  and  $\theta$  :

$$\omega_1 = \omega_2 = \omega, \quad k_1 = k_2 = k, \quad l_1 = l_2 = l.$$

Upon elimination of the amplitudes  $A, B$  and  $C$ , we obtain a third equation

$$D_0(\chi_1, \chi_2) = 0.$$

Solving the nonlinear system of 3 equations

$$D_0(\chi_1, \chi_2) = 0, \quad D_1(k, \chi_1) = 0, \quad D_2(k, \chi_2) = 0.$$

for the 3 complex variables  $k, \chi_1$  and  $\chi_2$  yields both the growth rate and mode profile of the FEL interaction, including guiding effects, plasma frequency reduction, EM-wave filling factors etc...

### General Formalism

• Maxwell's Equations (Linearized Source Terms)

$$\left[ \nabla^2 - \frac{1}{c^2} \frac{\partial^2}{\partial t^2} \right] \delta \vec{A} = \mu_0 e [n_0 \delta \vec{v} + \vec{v}_0 \delta n], \\ \left[ \nabla^2 - \frac{1}{c^2} \frac{\partial^2}{\partial t^2} \right] \delta \phi = \frac{1}{\epsilon_0} e \delta n, \\ \frac{1}{c^2} \partial_t \delta \phi + \vec{\nabla} \cdot \delta \vec{A} = 0.$$

• Linearized Equations of Fluid Dynamics

$$[\partial_t + \vec{v}_0 \cdot \vec{\nabla}] \delta \vec{v} + [\delta \vec{v} \cdot \vec{\nabla}] \vec{v}_0 = - \frac{e}{\gamma_0 m_0} \left\{ - \vec{\nabla} \phi - \partial_t \delta \vec{A} + \delta \vec{v} \times \vec{B}_0 \right. \\ \left. + \vec{v}_0 \times \vec{\nabla} \times \delta \vec{A} + \frac{\vec{v}_0}{c^2} (\vec{\nabla} \delta \phi + \partial_t \delta \vec{A}) \cdot \vec{v}_0 - \frac{\gamma_0^2}{c^2} (\vec{v}_0 \cdot \delta \vec{v}) (\vec{v}_0 \times \vec{B}_0) \right\}$$

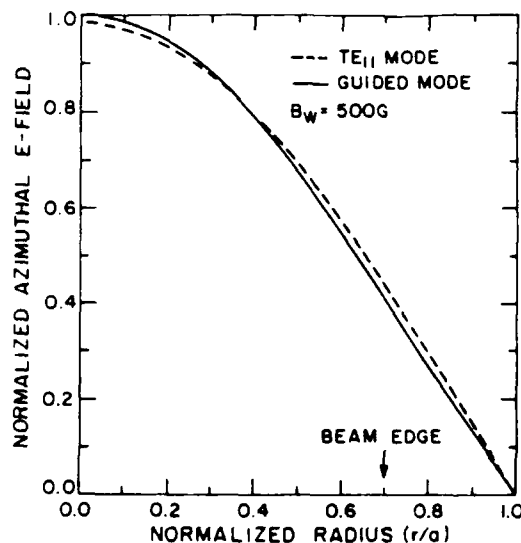
• Canonical System in  $A_\mu$

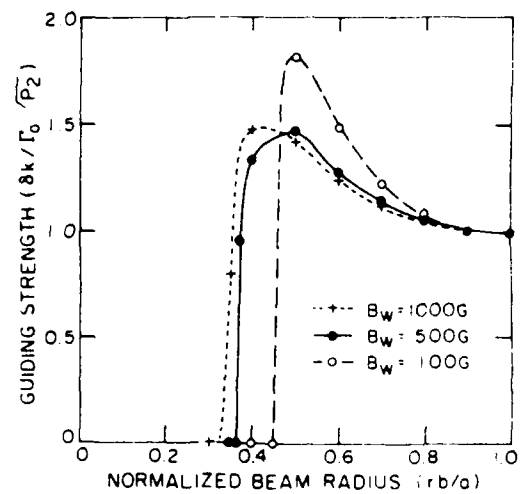
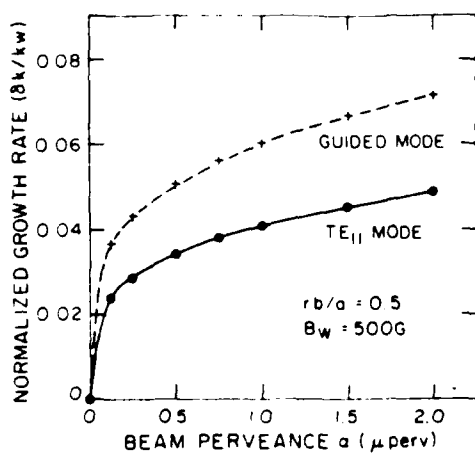
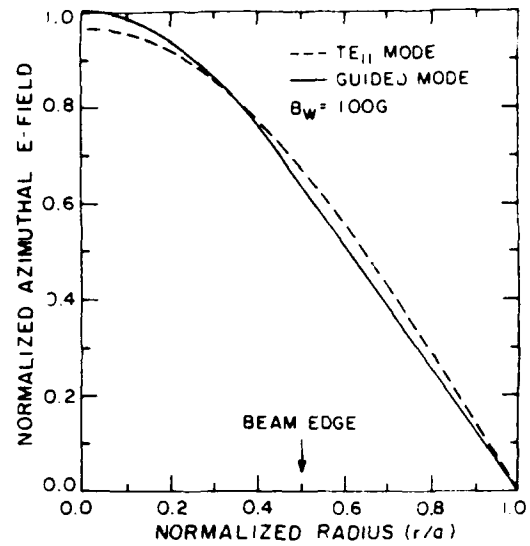
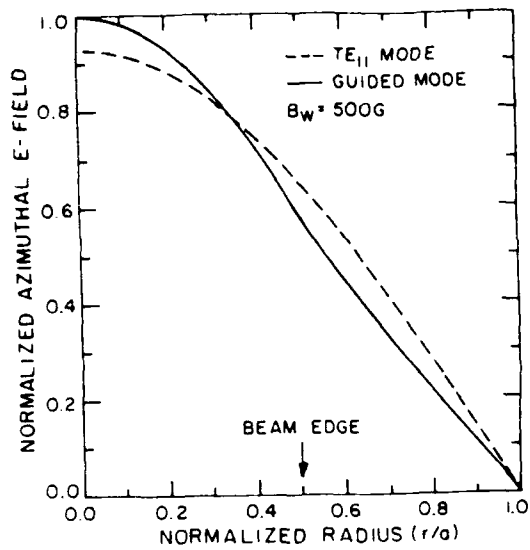
$$[\partial_t + \vec{v}_0 \cdot \vec{\nabla} + \vec{\nabla} \cdot \vec{v}_0 - \vec{\Omega}_0 \times + \gamma_0^2 (\vec{\Omega}_0 \times \vec{\Omega}_0) \cdot \vec{\Omega}_0] \left( \square \delta \vec{A} - \vec{\Omega}_0 \square \frac{\delta \phi}{c} \right) \\ + \left[ \left( \square \delta \vec{A} - \vec{\Omega}_0 \square \frac{\delta \phi}{c} \right) \cdot \vec{\nabla} \right] \vec{v}_0 \\ + \frac{\omega_p^2}{c^2} \left\{ - \vec{\nabla} \delta \phi - \partial_t \delta \vec{A} + \vec{v}_0 \times \vec{\nabla} \times \delta \vec{A} + \vec{\beta}_0 (\vec{\nabla} \delta \phi + \partial_t \delta \vec{A}) \cdot \vec{\Omega}_0 \right\} = 0, \\ \frac{1}{c^2} \partial_t \delta \phi + \vec{\nabla} \cdot \delta \vec{A} = 0.$$

"0" refers to the fluid equilibrium and we define

$$\vec{\Omega}_0 = \frac{e \vec{B}_0}{\gamma_0 m_0}, \quad \frac{\omega_p^2}{c^2} = \mu_0 \frac{n_0 e^2}{\gamma_0 m_0}, \quad \vec{\beta}_0 = \frac{\vec{v}_0}{c}.$$

A specific system is characterized by its fluid eq. and boundary conditions.





# AC1.2 ACCELERATOR DESIGN AND CALCULATED PERFORMANCE OF THE LOS ALAMOS HIBAF FACILITY

Bruce E. Carlsen, Lloyd M. Young, Michael E. Jones, Barbara Blind, Ernest M. Svaton, K. C. Dominic Chan, and Lester E. Thode  
Los Alamos National Laboratory, MS H825 Los Alamos, NM 87545

The HIBAF 40-MeV accelerator and beam transport have been designed and studied with ISIS and PARMELA simulations. The nominal beam parameters for a 5-nC pulse are an emittance of 40 n-mm-mrad, 300-A peak current, and an energy spread of 0.25%. We will discuss the major design issues and report on performance expectations.

The HIBAF (High Brightness Accelerator FEL) facility is the new FEL accelerator upgrade at the Los Alamos National Laboratory currently being commissioned. Although it includes components from the previous accelerator, it is virtually a new design, rather than a modification of the old one. It incorporates recent theoretical ideas on maintaining beam quality, and also insights learned from studying problem areas in the old machine. The new accelerator uses a photocathode to replace the previous subharmonic bunching system, and four standing-wave accelerator tanks to accelerate the beam to 40 MeV. After acceleration, the beam is first bent 60° by an isochronous bend, passes through an FEL oscillator, and then is bent 150° by another isochronous bend before it encounters an FEL amplifier. This way the FELs can be operated in a MOPA (Master Oscillator Power Amplifier) configuration.

	old 20 MeV	new 40 MeV
electron source	thermionic gun	photocathode
emittance	160 n-mm-mrad	40 n-mm-mrad
energy spread	0.5 %	0.2 %
charge per bunch	5 nC	5 nC

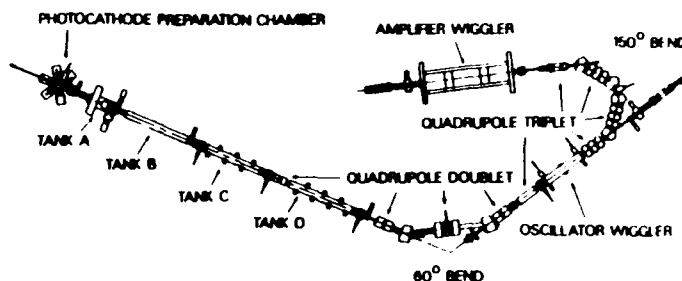
## INSIGHTS ON VELOCITY BUNCHING FROM PREVIOUS STUDIES

- Thermionic guns should be planar, and not focus the beam down to a narrow waist. The time dependent nature of the space charge inside the pulse causes different expansion rates.
- For charges of 5 nC or more, velocity bunching to 20 ps or less allows significant amounts of particles to escape, leading to a large energy variation and interception by the beam wall.
- Velocity bunching also introduces an energy spread into the beam which becomes thermalized.
- Different parts of the beam scallop with different periods in the long drift required, and get out of phase if there are significant current variations, leading to emittance growth.

## INSIGHTS ON PHOTOCATHODES FROM PREVIOUS STUDIES

- No appreciable beam interception is allowed near the cathode.
- The beam edges may develop large emittances, although the center remains extremely bright.
- A single external solenoid can both provide good downstream focusing and allow for compensation of the nonlinear space charge forces to regain whole beam brightness.
- The solenoid must be relatively small in diameter.
- The gradient in the first cell must be matched to the cell and solenoid size. Either too small or too large a gradient will interfere with the compensation process.

## HIBAF BEAMLINE



## INSIGHTS ON WAKEFIELDS FROM PREVIOUS STUDIES

- Wakefields for 5 nC bunches can easily be 100 kV.
- Even relatively small wakefields in a bend can make it extremely nonchromatic.
- Beampipes in bends must be large enough so that the wall currents associated with the bunch do not see interruptions in the walls.
- Nonisochronous bends can lead to emittance growth just from the potential redistribution in the bunch, which changes the particles' kinetic energy.
- Effects of wakefields scale as the inverse of the beam energy.

## PHOTOINJECTOR DESIGN CONSIDERATIONS

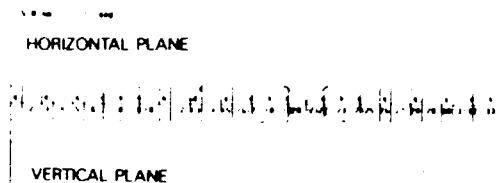
- The design must use a small diameter solenoid and a smaller bucking coil.
- RF focusing can ease the size requirement on the coils, but it reduces the gradient on the cathode and introduces strong nonlinear radial RF forces.
- Longitudinal space charge forces are partially compensated by the change in RF phase the beam ends see.
- Varying the initial phase effectively varies the amount of RF focusing and gradient, but not the beam expansion.
- A smaller cathode helps keep the emittance generated by RF fields down, but increases effects from space charge.



## OUR PHOTOINJECTOR DESIGN

- We stayed at 13 GHz so we could use our old klystrons
- Breakdown field for a 100  $\mu$ s pulse is about 60 MV/m
- We chose an intermediate RF focusing case for maximum flexibility
- A half wavelength long first cell provided the right phase delay for the second cell in a  $\pi$  mode structure
- Two external solenoids were positioned around the first tank to provide effective position control
- Only six cells could be driven in the first tank, accelerating the beam to 6 MeV
- We expect good performance from both a 5 and 6 mm cathode

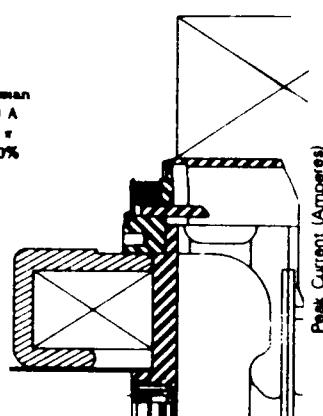
## 150° BEND OPTICS



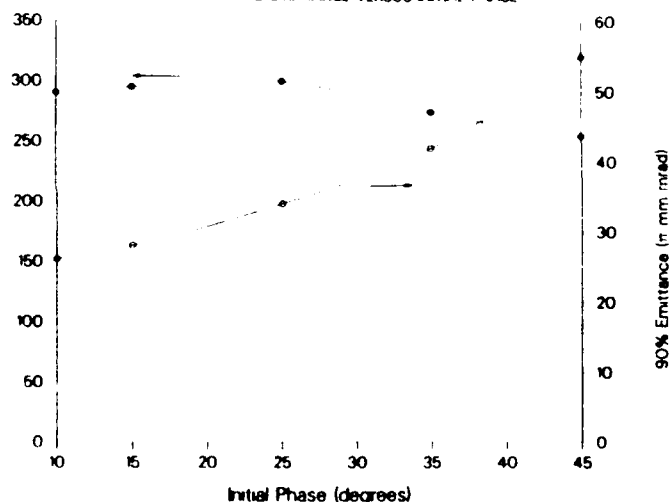
NOMINAL PERFORMANCE FOR 5 AND 6 MM CATHODES

5 mm		6 mm	
Flat Top	Gaussian	Flat Top	Gaussian
290 A	300 A	320 A	330 A
21 $\mu$	26 $\mu$	27 $\mu$	32 $\mu$
0.35%	0.35%	0.30%	0.30%

FIRST CAVITY DESIGN



PEAK CURRENT AND EMITTANCE VERSUS INITIAL PHASE



## DESIGN SENSITIVITIES

Nominal stability of the RF is  $\pm 1^\circ$  of phase and 0.1% in amplitude.

Here we show the effects on energy spread, emittance and peak current from various errors.

Error	Mean Energy	Energy Spread	Emittance	Peak Current
none	39.8 MeV	0.25%	33 $\mu$ mm mrad	300 Amperes
10% more charge	39.8	0.30%	36 $\mu$	270
10% less charge	39.8	0.25%	31 $\mu$	300
0.5% higher rf fields	40.0	0.25%	36 $\mu$	2
0.5% lower rf fields	39.6	0.35%	36 $\mu$	270
2.5° phase advance	40.0	0.65%	31 $\mu$	300
2.5° phase delay	39.6	0.65%	35 $\mu$	300

## DESIGN IMPROVEMENTS

- Not so much RF focusing is needed, and less would improve the emittance.
- Alternative shapes for the first cell have a higher ratio of cathode field to peak surface field. The gradient we used is probably quite a bit smaller than the optimum.
- A quad singlet after tank B would provide better focusing for the OTR measurements after tank D

## AC1.3

# A Development of a Tandem Electrostatic Accelerator Quasi-CW FEL

**A. Gover, E. Jerby and H. Kleinman**

Faculty of Engineering, Tel Aviv University, Ramat Aviv, Israel

**I. Ben-Zvi, B.V. Elkonin, A. Fruchtman and J.S. Sokolowski**

Dept. of Nuclear Physics, The Weizmann Institute of Science, Rehovot, Israel

**B. Mandelbaum, A. Rosenberg and J. Shiloh**

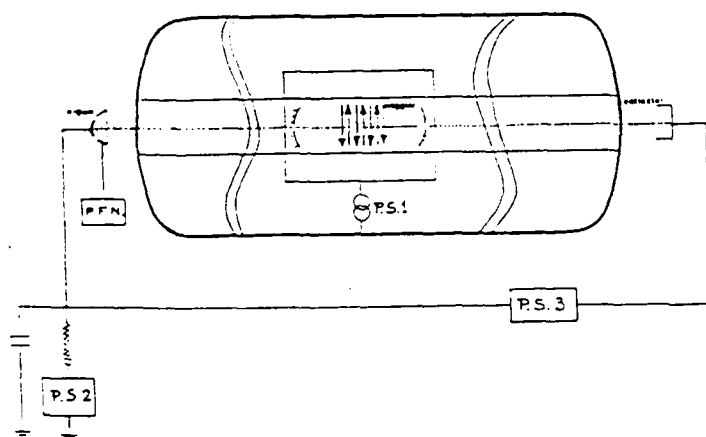
Dept. of Applied Physics, Rafael, P.O.Box 2250, Haifa, Israel

**G. Hazak and O. Shahal**

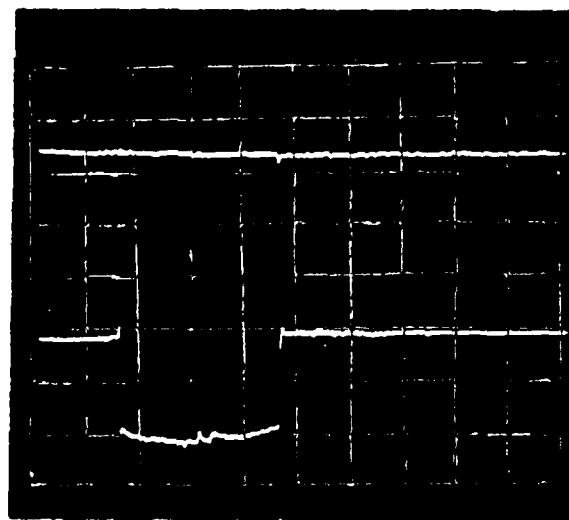
N.R.C.- Negev, P.O.Box 9001, Beer-Sheva, Israel

### ABSTRACT

The EN Tandem Electrostatic Accelerator at the Weizmann Institute of Science has been converted into an electron accelerator with beam power recovery. We report on the design and performance of the accelerator as well as on a new approach to stable, long pulse operation of this class of machines. The long pulse mode of operation offers interesting possibilities for the operation of Free Electron Lasers, in particular studying of high coherence, single mode operation.



A simplified schematic of the tandem accelerator including the FEL.



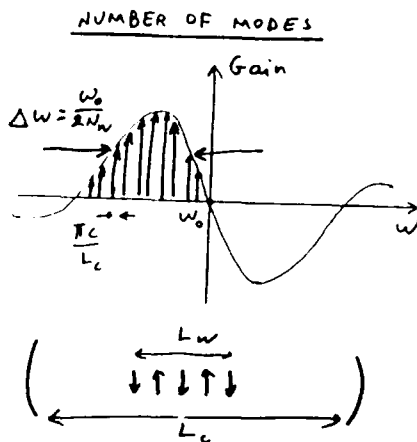
The terminal voltage behaviour as a result of a short ( $65 \mu\text{sec}$ ) beam pulse (upper trace);  $V_0 = 2.7 \text{ MV}$ ; vertical scale =  $6.4 \text{ kV/box}$ ; horizontal scale =  $20 \mu\text{sec/box}$ . The lower trace represents the collector current - vertical scale =  $100 \text{ mA/box}$

Table 5-1 FEL Experiments with Tandem FEL

Experiment	Type of FEL	E	$\lambda_w$	$\Delta$	Gain	Loss	net
Internal waveguide							
(1)mm	resonator	5 MeV	4.4 cm	3 mm	100%	20%	80%
Internal waveguide							
(2)FIR	resonator	5.5 MeV	4.4 cm	300 $\mu$ m	45%	15%	30%
External open							
(3)MIR	resonator, Optical klystron	5.5 MeV	4 mm	15 $\mu$ m	70%	5%	65%

Table 5-2 Mode Competition Parameters of FEL Experiments

Experiment	$\chi$	$\frac{1}{\epsilon}$	$\frac{1}{\epsilon^2}$	$t_d$	$t_{coh}$	$t_{SM}$
(1) mm	1-5	-17	278	3-12 ns	51-200 ns	0.8-3.3 $\mu$ s
(2) FIR	1-3	147	$2.1 \times 10^4$	5-15 ns	.7-2.2 $\mu$ s	100-300 $\mu$ s
(3)MIR	1-14	1875	$3.5 \times 10^8$	43-600 ns	.08-1.1 ms	.15-2.1 s



$$N_{mode} = \frac{\Delta\omega}{\pi \frac{c}{L_c}} = \frac{\omega_0 / 2N_w}{\pi c / L_c} = \frac{L_c}{L_w} \frac{\lambda_w}{\lambda} \gg 1$$

MODE COMPETITION PARAMETERS

$$\chi = \frac{I}{I_{th}}$$

$$\epsilon = \frac{L_w / \sqrt{3} - L_w / \sqrt{2}}{L_c / \sqrt{2}} \quad (= \frac{1}{N_{modes}})$$

$\beta = 0$        $\beta = \omega / \omega_2$        $\beta = L_w$

$$t_c = \frac{Q}{\omega}$$

$$t_{coh} = \frac{L}{\sqrt{3}} \frac{1}{\epsilon}$$

$$t_{sm} = t_c \frac{1}{\epsilon^2}$$

## Reference

1. E. Jerby, A. Gover, S. Rushin, H. Kleinman, I. Ben-Zvi, J.S. Sokolowski, S. Eckhouse, Y. Goren and J. Shiloh, Nucl. Instr. and Meth. **A259**, 263(1987).

# P3.1

## Mode Stability in a Sheet-beam Free Electron Laser with Sidewalls

Edward R. Stanford and T.M. Antonsen, Jr.

Laboratory for Plasma Research,

University of Maryland at College Park, College Park, MD 20748

**Abstract:** A nonlinear time-evolution equation for the transverse mode structure of the radiation amplitude in a sheet beam FEL is derived. Equilibria of this equation are found numerically. Equilibrium mode stability for such FEL's is investigated both numerically and analytically, determining stability ranges for single and double mode FEL operations.

Figure 1a: General Layout, End View

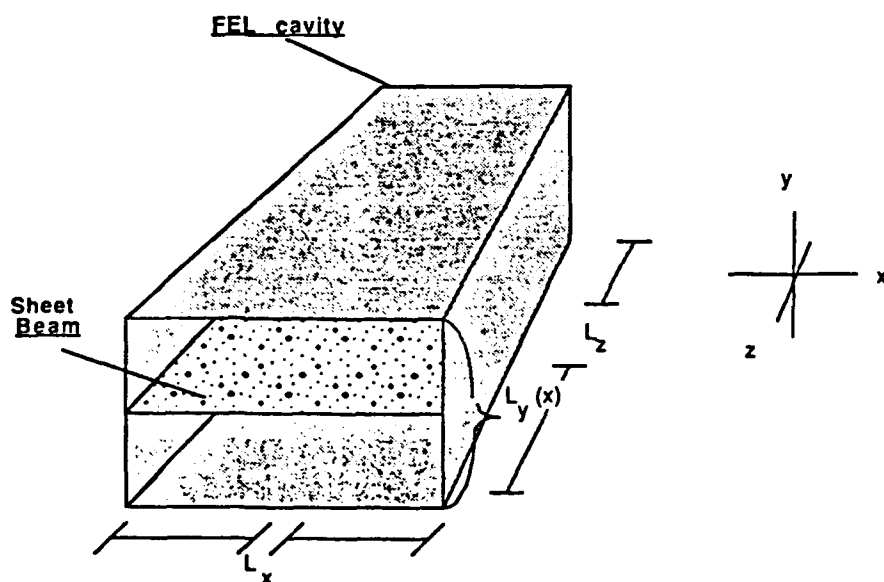


Figure 1b: General Layout, Top View

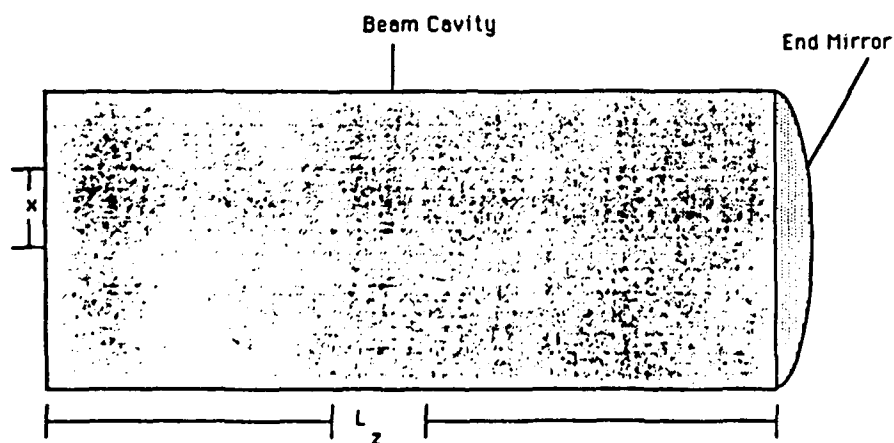


FIGURE 2: The Hybrid Mode

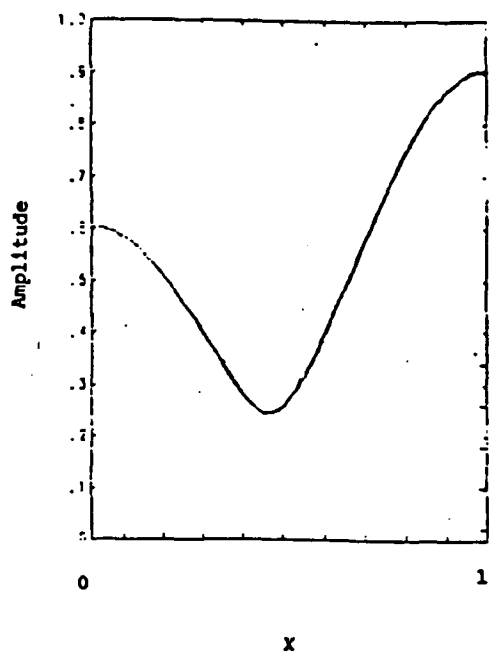


Figure 3: Regions of Stability

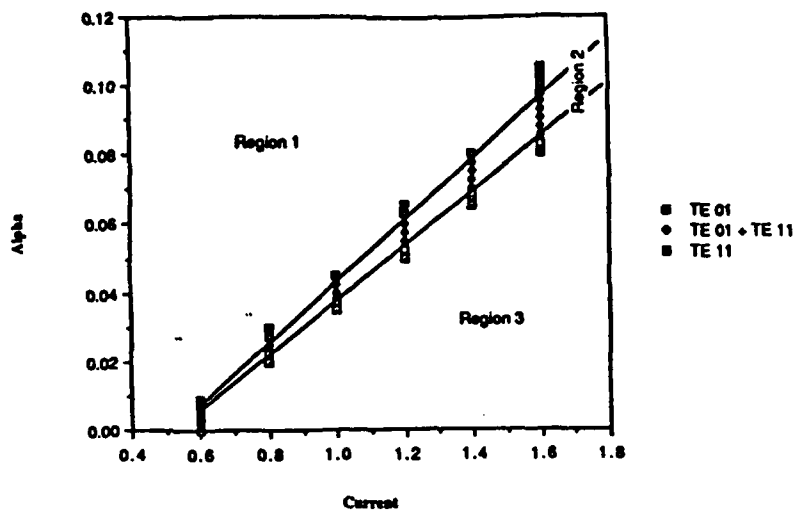
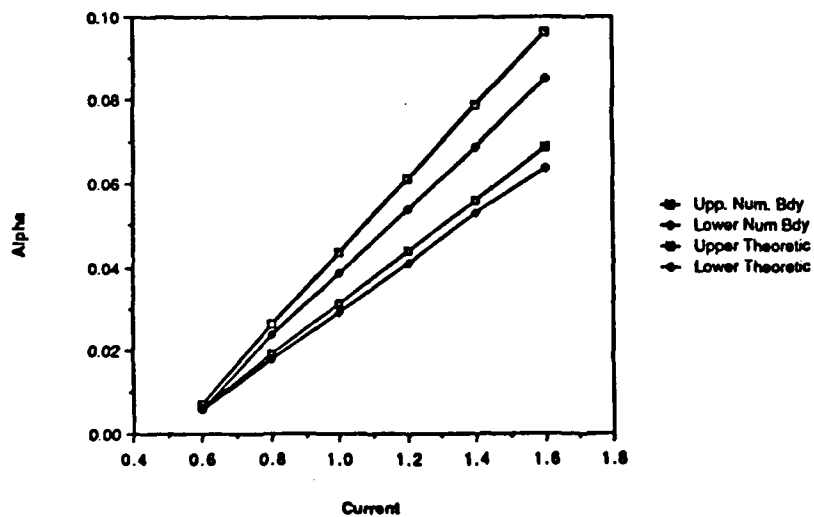


Figure 4: Regional Boundaries



## P3.2

### Resonator Mode Matching for Free-Electron Laser Optical Guiding

K. C. Sun

Rocketdyne Division of Rockwell International, Canoga Park, CA 91303

B. D. McVey and R. L. Tokar

Los Alamos National Laboratory, Los Alamos, NM 87545

The FELEX code is used to evaluate optical guiding on a grazing incidence resonator at Boeing's FEL facility. The results indicate that a high brightness e-beam requires a resonator which is "mode matched" to curvature changes caused by optical guiding. However, mode matching is not necessary for a low brightness e-beam.

**INTRODUCTION:** Optical guiding produces a mismatch between the laser beam curvature and resonator focal lengths. This mismatch can cause a major reduction in power extraction. However, this mismatch can be eliminated by refocusing the resonator via a process called mode matching. Resonator mode matching is by either two deformable mirrors or repositioning (i.e., despace) two paraboloid mirrors.

**BACKGROUND:** Boeing's 0.63  $\mu\text{m}$  wavelength FEL experiment has a 100 MeV RF linac accelerator, a 5-m wiggler and a 60-m long grazing incidence ring resonator. The experiment has already been designed, fabricated and installed at Seattle. Various effects may cause lower electron beam brightness. The resonator does not have deformable mirrors but we can despace the paraboloids.

**PROBLEM:** What is the impact of a lower brightness electron beam? How effective is paraboloid despace?

**RESULTS:** High brightness electron beam requires mode matching by paraboloid despace.

Paraboloid despace gives same mode matching performance as deformable mirrors.

Mode matching may not be required for low brightness electron beam

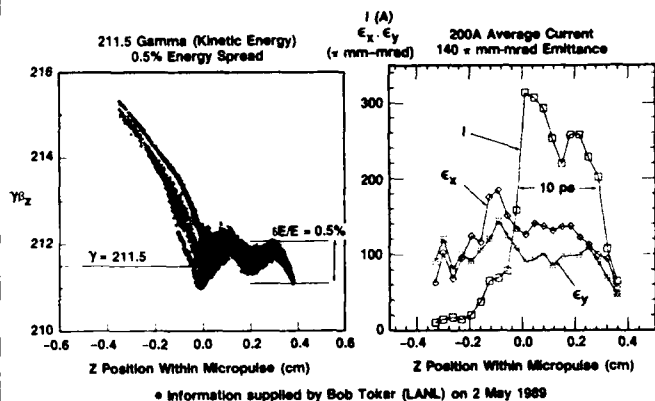
**OUTLINE:**

1. Gain Medium Parameter
2. Resonator Description
3. Single Pass Amplifier
4. Resonator with High Brightness Electron Beam
5. Resonator with Low Brightness Electron Beam

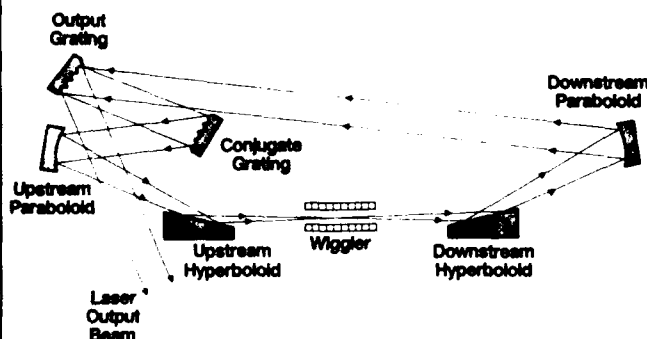
#### Gain Medium Parameters

Gain Parameters	Case 1 (High Brightness)	Case 2 (Low Brightness)
Average Current (A)	300	200
Kinetic Energy	211.2	211.5
Energy Spread (%)	1.0	0.5
X-Emittance (cm-rad) ( $\pi$ mm-mrad at 90%)	37	140
Y-Emittance (cm-rad) ( $\pi$ mm-mrad at 90%)	37	100
Relative Brightness	15.3	1.0
Wiggler Length (cm)	500	same
Wiggler Period (cm)	2.18	same
Max. Magnetic Field (G)	8755	8700
Energy Taper (%)	7.7	3.9

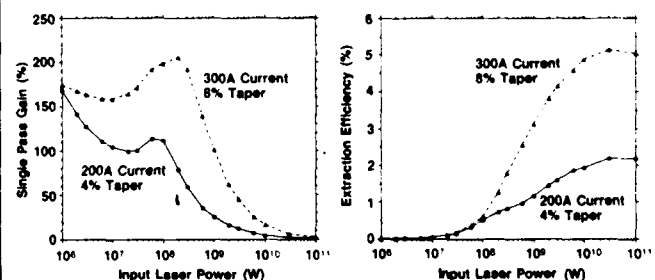
#### INEX Code Predicts Electron Beam Performance



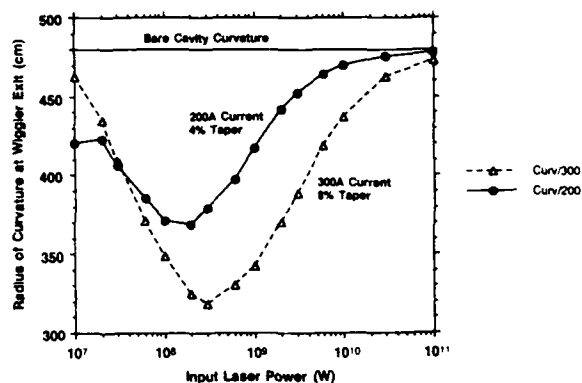
#### Grazing Incidence Ring Resonator with Grating Rhomb



#### Reduced (200A) Current Yields Lower Gain and Extraction

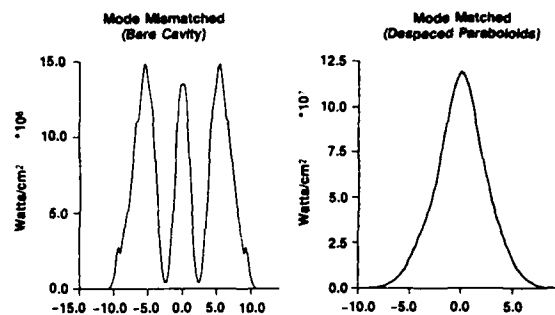


### Optical Guiding is Proportional to Electron Beam Current



89d-11-104  
648

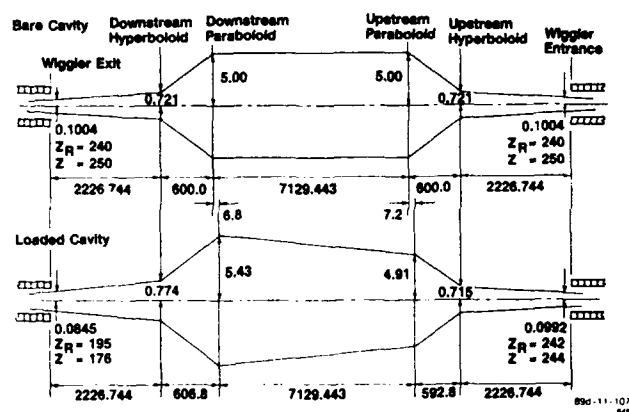
### 300A Current and 8% Taper Requires Mode Matching



- Efficiency Increase = 2.5% to 3.9%
- Outcoupled Power Increase = 659 to 1253 MW
- Outcoupling Fraction (Loss) = 30%

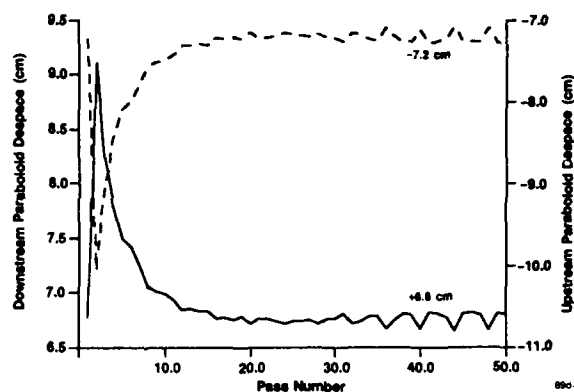
89d-11-106  
649

### Gaussian Beam Parameters for Ring Resonator



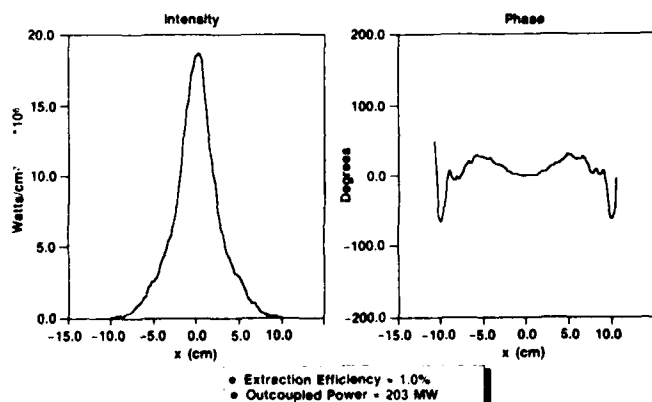
89d-11-107  
649

### Paraboloid Despace Changes During Mode Build-Up



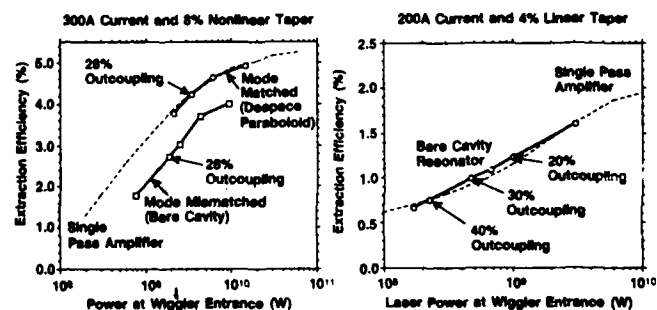
89d-11-108  
649

### Bare Cavity Yields Gaussian Mode With 200A Current and 4% Taper



89d-11-109  
649

### Mode Matching is Not Required for Lower (200A) Current



89d-11-110  
649

# THREE-DIMENSIONAL SIMULATIONS OF SIDEBAND IN A MILLIMETER-WAVE FREE ELECTRON LASER

Yang Zhenhua   Tian Shihong   Jiang Youming  
Institute of Applied Physics and Computational Mathematics  
P.O.Box 8009, Beijing 100088  
Beijing, People's Republic of China

*In this paper, we presented a three dimensional physical model and simulating technique for sideband instability in a millimeter wave free electron laser. With this 3-D code, we investigated the effects of various parameters on and the quantitative conditions for producing sideband instability in a rectangular waveguide FEL.*

We presented a three dimensional physical model and simulating technique for sideband instability in a millimeter wave FEL. A millimeter FEL must operate in a waveguide because the wavelength of the radiation is long and diffraction is very strong, here we choose a rectangular waveguide. Like LLNL's FRED<sup>[1]</sup>, our equations include that the electron energy's and pandermotive phase's evolving equations in terms of

averaged single-particle derived by KMR<sup>[2]</sup>, and the field equation based on paraxial wave equation, and the electron betatron equation.

Physically sideband instability results from the slippage between the light pulse and the electron pulse in FEL. The slippage is customarily considered to occur because the microwave travels at  $V_\phi$ , while the electron travels at some  $V_\parallel < V_\phi$ . The slippage couples different longitudinal slice of electron beam, but different slices of electron beam is just possess of different phase about synchrotron oscillation of electrons in buckets. It is possible that the slippage couples different longitudinal slices of electron beam, and can lead to growing modulation in light intensity.

The equations simulating sideband instability are

$$\frac{\partial \gamma_i}{\partial z} + \frac{1}{V_{\parallel i}} \frac{\partial \gamma_i}{\partial t} = - \frac{a_w(\vec{r}_i) e_i(\vec{r}_i)}{\beta_{\parallel i} \gamma_i} f_{\parallel} \sin(\theta_i + \Phi_i) \quad (1)$$

$$\begin{aligned} \frac{\partial \theta_i}{\partial z} + \frac{1}{V_{\parallel i}} \frac{\partial \theta_i}{\partial t} = & k_w + \delta k - \frac{\omega_p}{\gamma_i c} - \frac{\omega_s / c}{\beta_{\parallel i} (1 + \beta_{\parallel i}) \gamma_i^2} \left[ 1 + a_w^2(\vec{r}_i) + a_s^2(\vec{r}_i) \right. \\ & \left. - 2 a_w(\vec{r}_i) a_s(\vec{r}_i) f_{\parallel} \cos(\theta_i + \Phi_i) + \langle \gamma_i^2 \beta_{\perp i}^2 \rangle \right] \end{aligned} \quad (2)$$

$$\left( \frac{\partial e_i}{\partial z} + \frac{1}{V_s} \frac{\partial e_i}{\partial t} \right) = \frac{2\pi e \omega_s}{mc^4 k_s} \frac{I}{NS_0} \sum_{i=1}^N a_w(\vec{r}_i) f_{\parallel} \cos(k_s y_i) \frac{\sin(\theta_i + \Phi_i)}{\gamma_i} \quad (3)$$

$$e_i \left( \frac{\partial \Phi_i}{\partial z} + \frac{1}{V_s} \frac{\partial \Phi_i}{\partial t} \right) = \frac{2\pi e \omega_s}{mc^4 k_s} \frac{I}{NS_0} \sum_{i=1}^N a_w(\vec{r}_i) f_{\parallel} \cos(k_s y_i) \frac{\cos(\theta_i + \Phi_i)}{\gamma_i} \quad (4)$$



Where, the electron position  $\vec{r}_e$  is described by betatron equations and  $V_g = c \left[ 1 + k_{\perp}^2 / k_z^2 \right]^{-\frac{1}{2}}$  is the group velocity of the microwave in the waveguide.

In order to deal with the slippage between the light pulse and the electron pulse, we divide the microwave pulse and the electron beam pulse by  $n$  respectively, that is light pulse to consist of by a series of  $n$  light points and electron beam to consist of by  $n$  slices (groups). Every light point and electron slice are respectively described by equations (1)–(4). For a fixing light point, it will interact with the slice which has same delayed-time as the light point. Finally, the spatial

Fourier transform of the light pulse at the end of wiggler is calculated and electric field amplitude versus wavelength is given. The special conditions producing the sideband instability will be given in details on the paper for proceedings.

- [1] T.J.Orzechowski, E.T.Scharlemann, B.Anderson et al., IEEE J.Quantum Electronics, QE-17(7) 831 (1985).
- [2] N. M. Kroll, P. L. Morton, and R. Rosenbluth, IEEE J.Quantum Electronics, QE-17(7) 1436 (1985)

# **P3.4 DEVELOPMENTS IN ON-LINE, ELECTRON BEAM EMITTANCE MEASUREMENTS USING OPTICAL TRANSITION RADIATION TECHNIQUES**

R. B. Feldman, A. H. Lumpkin, D.W. Rule\*, R.B.Fiorito\*

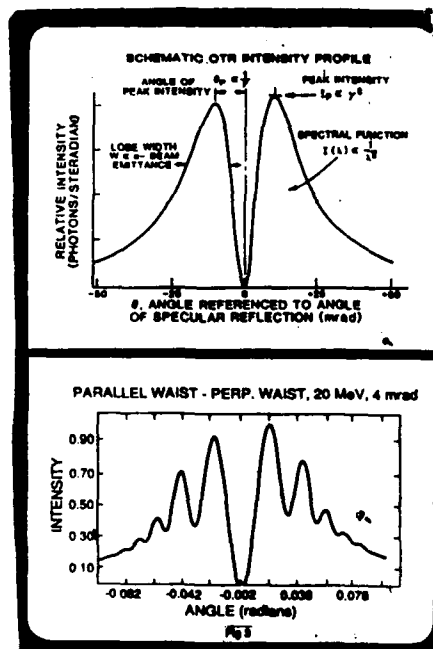
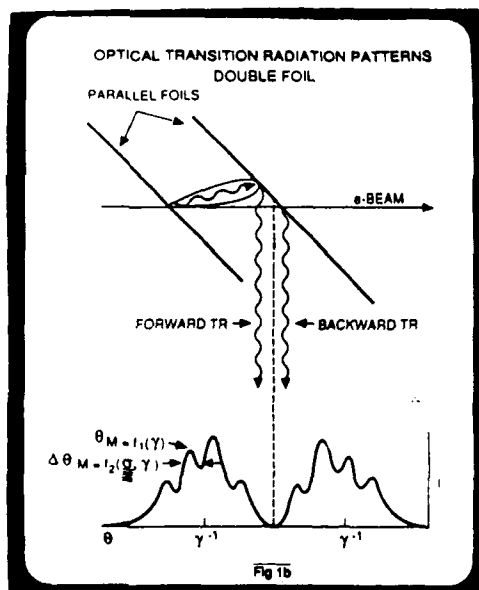
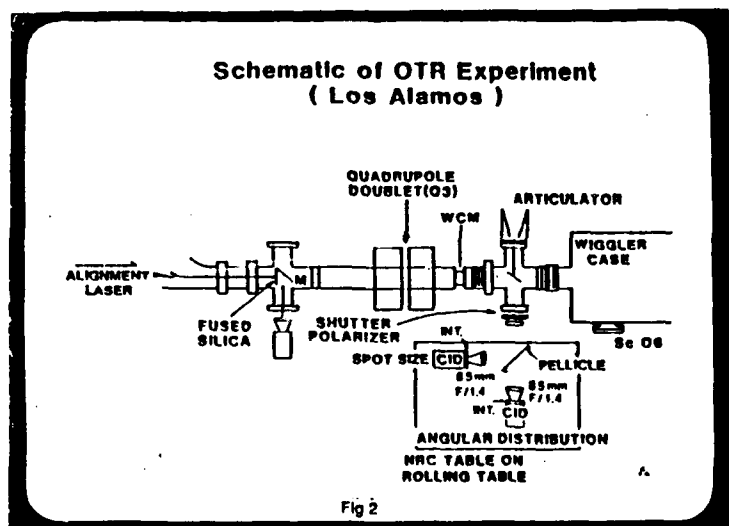
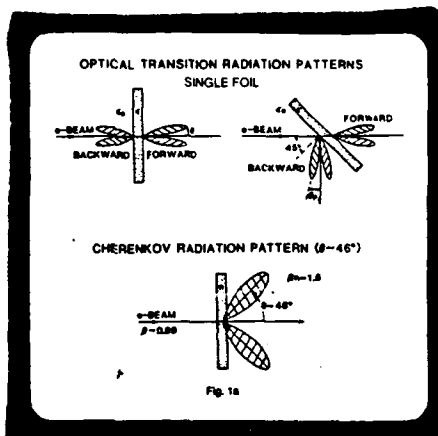
Los Alamos National Laboratory

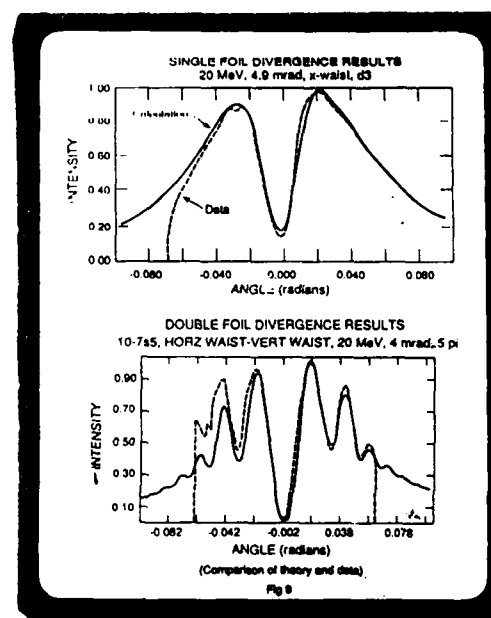
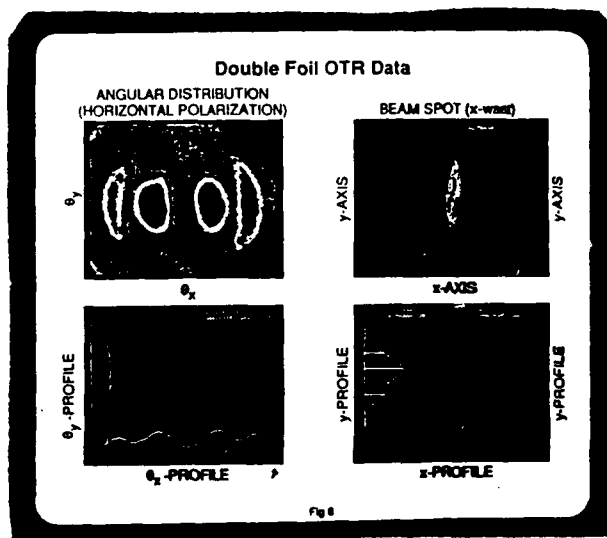
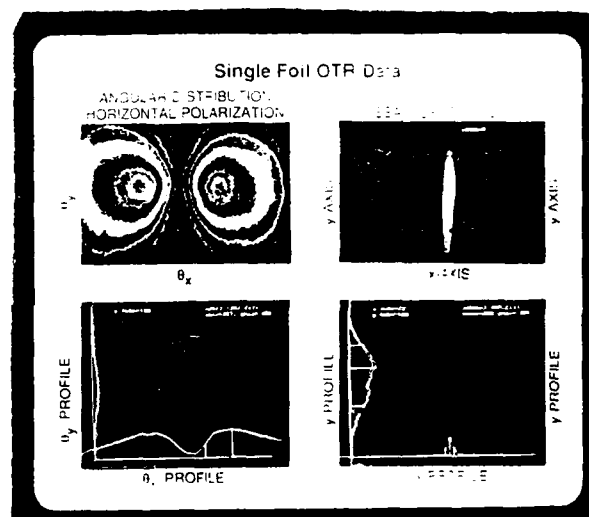
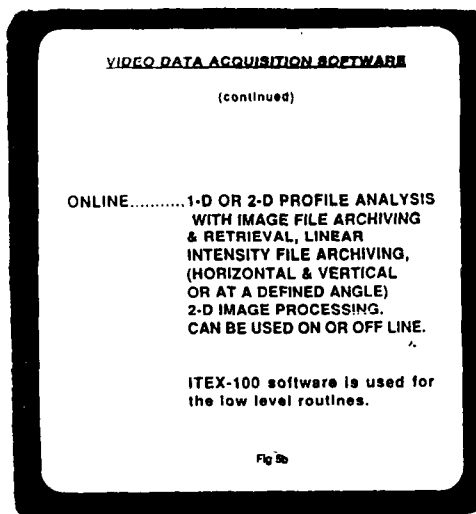
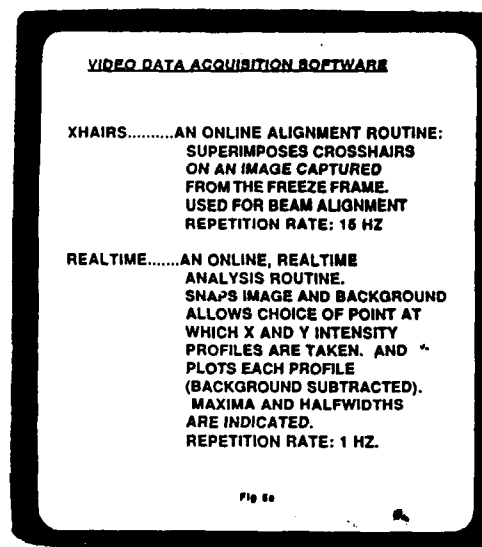
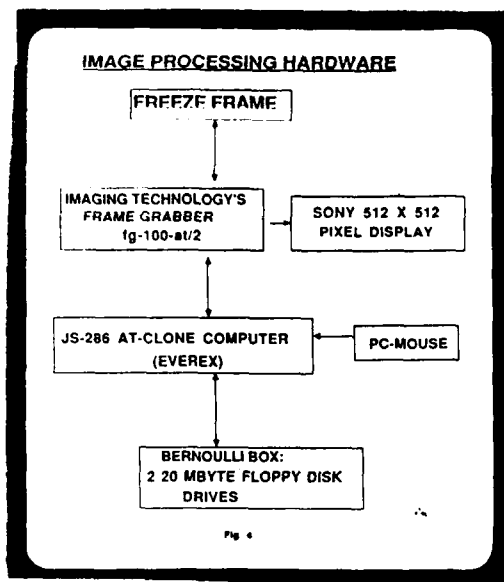
Los Alamos, New Mexico 87544, USA

\*Naval Surface Warfare Center

\*Silver Spring, Md. USA

On-line monitoring of electron beam emittance can facilitate optimization of free electron laser performance and provide critical input data for FEL simulation programs. Using optical transition radiation techniques, we simultaneously record both beam spot and divergence information from a single macropulse. Our system provides real-time qualitative and on-line quantitative emittance measurements.





## P3.5

### Optical Design and Performance of an XUV FEL Oscillator

John C. Goldstein, Brian D. McVey, and Brian E. Newnam

Group X-1, MS E531  
Los Alamos National Laboratory  
Los Alamos, NM 87545  
U. S. A.

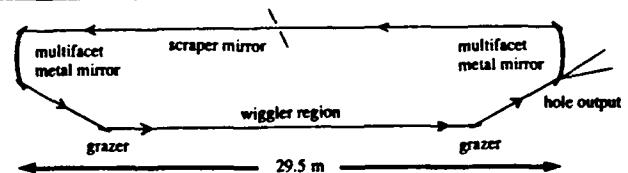
*A study by numerical simulation of the performance of a multifacet metal mirror ring resonator FEL oscillator is presented for several XUV wavelengths. Laser performance in the presence of mirror aberrations and thermal distortion is calculated for two different output coupling methods, a scraper mirror and a hole.*

#### Outline.

- We describe some of the characteristics of the ring optical resonator which was used to calculate the performance of an XUV FEL at four different wavelengths: 100 nm, 50 nm, 12 nm, and 4 nm.
- We then present the results of the laser performance simulations at each of the four optical wavelengths.
- We next present some results on the effects of spherical aberration on one of the mirrors of the ring resonator. This represents a first attempt to characterize the tolerable level of mirror aberrations in these devices. In this study, we limit ourselves to spherical aberration only.
- Finally, we discuss some preliminary findings on the effects of thermal distortion of the mirrors on the operation of these XUV FELs.

Los Alamos

#### General properties of the ring optical resonator for XUV FELs.



- The resonator consists of two multifacet metal end mirrors and two grazing-angle-of-incidence mirrors ("grazers"). Each grazer has a reflectance of 98.2 % and a focal length of -2 m. Each metal retroreflector has 6 facets, 5 of which are flat and one of which is a paraboloid. The curvatures of the paraboloidal elements are chosen to yield a lowest-order Gaussian mode with the desired Rayleigh range. The Rayleigh range is typically chosen to equal about 1/2 of the wiggler's length, and this varies with the operating optical wavelength as does the total reflectance.
- The outcoupling is accomplished either with a scraper mirror placed in the middle of the back leg, or a hole in the first flat mirror of the downstream retroreflector.
- The roundtrip optical path length in the unloaded resonator is almost exactly 60 m. The width of the resonator, 1.37 m, is not shown to scale in the schematic.

Los Alamos

#### Simulation results for an optical wavelength of 100 nm.

- Electron-beam parameters:
  - mean energy: 184.46 Mev ( $\gamma = 361.685$ )
  - peak current: 300 A
  - fractional energy spread ( $\delta\gamma/\gamma$ ): 0.155 %
  - "90 %" normalized transverse emittance  $\epsilon_n = 31 \pi \text{ mm-mr}$
- Optical parameters:
  - reflectance of each multifacet metal mirror: 90 %
  - empty cavity Rayleigh range: 1.5 m
- Wiggler length  $L_w = 3 \text{ m}$
- Calculated performance: maximum small-signal gain 11.21 at  $\lambda = 100.05 \text{ nm}$ ; threshold gain 1.28.
- Maximum output power of 58 MW with a scraper mirror of radius 0.575 cm; lower output powers were obtained with hole coupling apparently because the hole caused the optical mode to diverge through the wiggler and thus to be considerably larger than the optical spot in the wiggler using the scraper mirror.

Los Alamos

#### Simulation results for an optical wavelength of 50 nm.

- Electron-beam parameters:
  - mean energy: 261.4 Mev ( $\gamma = 511.5$ )
  - peak current: 300 A
  - fractional energy spread ( $\delta\gamma/\gamma$ ): 0.155 %
  - "90 %" normalized transverse emittance  $\epsilon_n = 31 \pi \text{ mm-mr}$
- Optical parameters:
  - reflectance of each multifacet metal mirror: 70 %
  - empty cavity Rayleigh range: 2 m
- Wiggler length  $L_w = 5 \text{ m}$
- Calculated performance: maximum small-signal gain 12.0 at  $\lambda = 49.96 \text{ nm}$ ; threshold gain 2.1163.
- Maximum output power of 21.5 MW with hole-coupling; hole radius 0.225 cm. Scraper mirror output did not exceed 14.5 MW.

Los Alamos

### Simulation results for an optical wavelength of 12 nm.

- Electron-beam parameters:
  - mean energy: 534.3 MeV ( $\gamma = 511.5$ )
  - peak current: 300 A
  - fractional energy spread ( $\delta\gamma/\gamma$ ): 0.1 %
  - "90 %" normalized transverse emittance  $\epsilon_n = 23.4 \pi$  mm-mr
- Optical parameters:
  - reflectance of each multifacet metal mirror: 60 %
  - empty cavity Rayleigh range: 5 m
- Wiggler length  $L_w = 12$  m
- Calculated performance: maximum small-signal gain 14.04 at  $\lambda = 11.94$  nm; threshold gain 2.88.
- Maximum output power 9.5 MW with hole-coupling; hole radius 0.0578 cm.

Los Alamos

### Simulation results for an optical wavelength of 4 nm.

- Electron-beam parameters:
  - mean energy: 919.8 MeV ( $\gamma = 1800$ )
  - peak current: 400 A
  - fractional energy spread ( $\delta\gamma/\gamma$ ): 0.1 %
  - "90 %" normalized transverse emittance  $\epsilon_n = 10 \pi$  mm-mr
- Optical parameters:
  - reflectance of each multifacet metal mirror: 35 %
  - empty cavity Rayleigh range: 6 m
- Wiggler length  $L_w = 12$  m
- Calculated performance: maximum small-signal gain 14.3 at  $\lambda = 4.026$  nm; threshold gain 8.465.
- Maximum output power 4.89 MW with hole-coupling; hole radius 0.0263 cm.

Los Alamos

### Effects of spherical aberration on the performance of XUV FELs.

- We have introduced third order spherical aberration into the phase front of the light via the Zernike polynomial Z13 in the following way: the optical phase  $\phi$  is written as  $\phi = \phi_0 + (2\pi\alpha/\lambda) Z13$ , where  $\alpha$  is the magnitude of the aberration in waves and  $Z13 = 6\rho^4 - 6\rho^2 + 1$ . Here  $\rho = r/r_n$ , where  $r_n$  is a "normalization radius" which defines the actual radial scale of the aberration.
- We calculated the effects of introducing the aberration only at the first paraboloidal mirror of the ring resonator.
- We have reached the following conclusions:
  - (1) The scale size  $r_n$  is crucial: if  $r_n \gg$  spot size, the magnitude of the aberration is small over the optical beam radius and the effects are small. We calculated for the 50 nm oscillator that for  $r_n = 4$  cm, the output power was reduced by 0.5 relative to the unaberrated case; for  $r_n = 2.46$  cm (3 times the optical spot size in the unaberrated case), the output power dropped by a factor of 0.15 (for  $\alpha = 0.5 \lambda$ ).
  - (2) For  $r_n = 3 \times$  unaberrated spot size, we found for all four XUV wavelengths that an amplitude of  $0.2 \lambda$  reduced the output by a few percent,  $0.5 \lambda$  reduced the output by a large factor (70-85 %), and  $1.0 \lambda$  prevented laser action entirely.

Los Alamos

### Compensation of aberration.

- We attempted to compensate for the presence of spherical aberration by changing various elements of the resonator from their values in the unaberrated case.
- We reduced the outcoupling to reduce the total cavity losses. We found small improvement in the case of  $0.5 \lambda$  of spherical aberration, but this method did not succeed at all with  $1.0 \lambda$ .
- We refocused the curved mirrors of the resonator in the following sense: the radius of curvature of the first paraboloid was changed so as to recover, approximately, the same spot size on the second paraboloid as in the unaberrated case; the curvature of the second paraboloid was changed so as to recover, approximately, the same Rayleigh range of the light after reflection from that mirror as in the unaberrated case. We found that this scheme worked well for a modestly strong aberration ( $0.5 \lambda$  with  $r_n = 4$  cm for the 50 nm oscillator) in the sense that almost the full output power of the unaberrated case was recovered in steady-state.
- We have yet to try to compensate for the aberration by leaving the radii of curvatures of the paraboloids unchanged but slightly moving their positions so as to accomplish the same beam adjustments as described above. We believe that this will prove to be a successful method of compensation as well.

Los Alamos

### Preliminary results on the effects of thermal distortion.

- Because absorption in the XUV is high, thermal distortion of the mirrors was anticipated to be a potentially serious problem.
- Thermal distortion of mirrors is being calculated by R. D. McFarland, J. H. Vernon, and M. E. Marshall at Los Alamos. Calculations have been performed for the 12 nm oscillator assuming an axially-symmetric optical beam of specified intensity incident on a resonator mirror. The nonnormal incidence of the real problem is not an axially-symmetric problem, but, as a first attempt, it has been approximated by averaging the power absorbed from an elliptical footprint over a circular spot. The thermal calculations assume a Gaussian intensity distribution on the mirror, and they produce as results plots of the vertical displacement,  $d$ , of the mirror surface as a function of radius.
- The displacement function ( $2d/\lambda$ ) is then expanded in a series of Zernike polynomials and introduced into FELEX.
- Qualitative conclusions from a preliminary study:
  - (1) Radial scale size of the distortion is again crucial.
  - (2) It appears that any coefficient in the Zernike expansion must be smaller than  $0.5 \lambda$  in order not to extinguish the laser.
  - (3) Increasing the number of mirror facets may be an effective way to reduce the absorbed power and, hence, the thermal distortion effects.

Los Alamos

### Summary and conclusions.

- We have calculated the output power of FEL oscillators at four XUV wavelengths using electron-beam and mirror reflectivity data believed to be achievable at this time. Steady-state peak output powers, from multiple-pass self-consistent resonator simulations using the code FELEX, were found to be: 58 MW at 100 nm, 21.5 MW at 50 nm, 9.5 MW at 12 nm, and 4.9 MW at 4 nm.
- We have made a preliminary study of the effect of third-order spherical aberration on one of the paraboloidal mirrors of the ring resonator. In general,  $0.5 \lambda$  reduces the output very substantially, and  $1.0 \lambda$  extinguishes the laser totally. These aberration magnitudes are in the phase front of the wave normal to the direction of propagation; defects on the mirror surface which lead to this aberration are reduced in their effect on the wave by the cosine of the angle of incidence (here, 75 degrees). We have proposed a mode-matching technique, by either recurving or repositioning the mirrors, to compensate for the aberration and restore the performance to the unaberrated level.
- We have started to study the effects of thermal distortion of the mirrors due to the large absorption of XUV mirrors. Thermal expansion calculations have been done to predict surface distortion, and that distortion has been included in FELEX as phase-front distortion. These effects, which may be particularly serious at the shorter optical wavelengths, might be substantially reduced by increasing the number of facets of the multifacet metal retroreflector mirrors.

Los Alamos

John J. Barnard

Lawrence Livermore National Laboratory  
University of California, Livermore, California 94550

**Abstract:** We calculate the trajectory of an electron in an FEL, including non-linear, off-axis focusing terms in the equations of motion. We obtain a set of two coupled second order differential equations for the particle guiding center position, having the form of two weakly coupled harmonic oscillators. We estimate the emittance growth due to the non-linear terms.

\* Work performed jointly under the auspices of the US Department of Energy by the Lawrence Livermore National Laboratory under W-7405-ENG-48, for the Strategic Defense Initiative Organization and the U. S. Army Strategic Defense Command in support of SDIO/SDC-ATC MIPR No. W31RPD-8-D5005.

### Introduction

When the wiggler magnets are designed with curved pole pieces, the guiding center equations for the  $x$  and  $y$  positions are to lowest order those of independent harmonic oscillators (ref. 1). Higher order terms are in  $x$  and  $y$  are small and are usually neglected when computing the particle motion. The question addressed in this poster session is: Can the higher-order terms (in the small quantities  $k_x x$  and  $k_y y$ , where  $k_w$  is the wiggler wavenumber) have a secular effect on such parameters as beam position or emittance over the length of a wiggler? In light of the desire to use very long wigglers in current designs for high power FELs, it is useful to understand such secular effects.

### Specification of the Magnetic Field

We make the following five assumptions about the wiggler magnetic field  $\mathbf{B} = (B_x, B_y, B_z)$ :

- (1) The field is well approximated by a vacuum field

$$\nabla \times \mathbf{B} = \nabla \phi \times \mathbf{h} = 0$$

So that,

$$\mathbf{h} = \nabla \chi \quad \text{and} \quad \nabla \chi \cdot \mathbf{h} = 0$$

Here  $\chi$  is the magnetic potential

- (2) Along the wiggler axis ( $x = y = 0$ ) the field is that of a perfect wiggler, with no harmonics of the wiggler wavenumber  $k_w$  present:

$$\frac{\partial \chi}{\partial x} = 0, \quad \frac{\partial \chi}{\partial y} = 0, \quad \frac{\partial \chi}{\partial z} = 0, \quad \frac{\partial \chi}{\partial x} = 0, \quad \frac{\partial \chi}{\partial y} = 0, \quad \frac{\partial \chi}{\partial z} = 0, \quad \frac{\partial \chi}{\partial x} = 0, \quad \frac{\partial \chi}{\partial y} = 0, \quad \frac{\partial \chi}{\partial z} = 0$$

### Magnetic Field Specification - continued

- (3) Reflection symmetry about  $x = 0$

$$\chi(x, y, z) = \chi(-x, y, z)$$

- (4) Reflection anti-symmetry about  $y = 0$

$$\chi(x, y, z) = -\chi(x, -y, z)$$

- (5)  $\chi$  may be expanded as a Taylor Series about  $x = y = 0$

$$\chi = \sum_{i,j} \sum_{k,l} M_{ijkl} x^i y^j z^k$$

The above five assumptions allow the following form for the first six terms of the Taylor Series for the magnetic potential  $\chi$

$$\chi = \frac{b}{k_w} \cos Z \left[ Y + dX^2 Y + \frac{1}{6} \frac{d}{dZ} Y^3 + eX^4 Y + \frac{d}{dZ} 2eX^2 Y^3 + \frac{1}{20} \frac{1}{6} \frac{d}{dZ} \frac{2}{3} d^2 Y^5 \right] + fZ$$

Here  $X = k_w x$ ,  $Y = k_w y$ , and  $Z = k_w z$ . The potential of reference (1)

$$\chi = \frac{1}{k_w} \cosh k_x x \sinh k_y y \cos Z = -\frac{k_y^2 + k_z^2}{k_w^2} x^2 y^2 \cos Z \quad (1)$$

is a special case of eq. (1). If we choose  $d = -k_y^2/k_w^2$  and  $e = -k_z^2/k_w^2$  then eq. (1) is the fifth order expansion of eq. (1). For equal harmonic focusing in the  $x$  and  $y$  directions,  $k_x = k_y = k_w/2$  so that  $d = -1/4$  and  $e = -1/4$ . Equation (1), however, allows an arbitrary  $d$ , even for equal harmonic focusing in the two directions.

### The Equations of Motion

When the independent variable is  $Z$  rather than  $z$  (time), the equations of motion become

$$\ddot{X} = -\frac{W}{k_w} \left( 1 + \frac{1}{2} Y^2 \right) \cos Z, \quad \ddot{Y} = -\frac{W}{k_w} \left( 1 + \frac{1}{2} X^2 \right) \cos Z$$

$$\ddot{X} = -\frac{W}{k_w} \left( 1 + \frac{1}{2} Y^2 \right) \cos Z, \quad \ddot{Y} = -\frac{W}{k_w} \left( 1 + \frac{1}{2} X^2 \right) \cos Z$$

$$\ddot{X} = -\frac{W}{k_w} \left( 1 + \frac{1}{2} Y^2 \right) \cos Z, \quad \ddot{Y} = -\frac{W}{k_w} \left( 1 + \frac{1}{2} X^2 \right) \cos Z \quad (III)$$

Here  $\dot{\phantom{x}}$  indicates a derivative with respect to  $Z$  ( $\dot{\phantom{x}} = d/dZ$ ), where the dot indicates derivative with respect to time.  $W = k_w^2 (1 - \beta^2) / (1 - \beta^2 \cos^2 \theta)$ ,  $\beta = v/c$ ,  $\theta = Z/k_w$  parallel velocity at  $Z = 0$ , and  $\mathbf{h} = \nabla \chi$ .

### Guiding Center Equations

Let  $X = X_0 + X_1$  and  $Y = Y_0 + Y_1$  where  $X_0, Y_0$  vary on scales of order  $Z^2$  and  $X_1, Y_1$  vary on scales greater than or of order of  $Z^2$ .  $W = B$  was assumed that  $X_0$  and  $Y_0$  are first order quantities and that  $W$  is a second order quantity (ref. 2).

$$\ddot{X}_0 = -\frac{B}{k_w} \left( 1 + \frac{1}{2} Y_0^2 \right) \cos Z, \quad \ddot{Y}_0 = -\frac{B}{k_w} \left( 1 + \frac{1}{2} X_0^2 \right) \cos Z$$

We find that through fourth order integration of the first component of eq. (III) yields

$$X_0 = \frac{1}{k_w} \left( 1 + \frac{1}{2} Y_0^2 \right) \cos Z + \frac{1}{k_w} B \cos Z$$

$$Y_0 = \frac{1}{k_w} \left( 1 + \frac{1}{2} X_0^2 \right) \cos Z$$

Above, the slow quantities were treated as constant during the integration, and higher harmonics in  $Z$  were ignored ( $n = 0$  through fourth order). When these solutions for  $X_0$  and  $Y_0$  are substituted into eq. (III), and when averages over the short length scale are taken the result is two coupled second order differential equations for  $X_1$  and  $Y_1$  (through seventh order)

$$\ddot{X}_1 = -\frac{B}{k_w} \left( 1 + \frac{1}{2} Y_1^2 \right) \cos Z, \quad \ddot{Y}_1 = -\frac{B}{k_w} \left( 1 + \frac{1}{2} X_1^2 \right) \cos Z \quad (IV)$$

Here,

$$Y_1 = \frac{1}{k_w} \left( 1 + \frac{1}{2} X_1^2 \right) \cos Z$$

$$X_1 = \frac{1}{k_w} \left( 1 + \frac{1}{2} Y_1^2 \right) \cos Z$$

$$Y_1 = \frac{1}{k_w} \left( 1 + \frac{1}{2} X_1^2 \right) \cos Z, \quad X_1 = \frac{1}{k_w} \left( 1 + \frac{1}{2} Y_1^2 \right) \cos Z$$

When the ordering is such that

$$X_1 = X_0 Y_0 W^2, \quad Y_1 = Y_0 X_0 W^2$$

then eqs. (IV) are still obtained with the following modifications

$$X_1 = \frac{1}{k_w} \left( 1 + \frac{1}{2} Y_1^2 \right) \cos Z + \frac{1}{k_w} B \cos Z, \quad Y_1 = \frac{1}{k_w} \left( 1 + \frac{1}{2} X_1^2 \right) \cos Z + \frac{1}{k_w} B \cos Z$$

(Eq. IV had been independently derived previously in ref. (2) for the case of the potential of ref. (1) and the limit when  $B$  is a second order quantity.)

# Equations for the Betatron Amplitude and Phase

Let,

$$\begin{aligned} X_n &= X_0 \cos(A^{1/2} W_0^2 Z + \phi_x) \\ Y_n &= Y_0 \cos(B^{1/2} W_0^2 Z + \phi_y) \end{aligned} \quad (V)$$

Then substitution of eqs. (V) into eqs. (IV) yields,

$$\begin{aligned} X'_0 &= -\frac{A^{1/2} D W_0^2}{8} X_0 Y_0^2 \sin 2\Delta\phi \\ Y'_0 &= \frac{B^{1/2} E W_0^2}{8} Y_0 X_0^2 \sin 2\Delta\phi \\ \phi'_x &= \frac{A^{1/2} W_0^2}{8} (3C X_0^2 + (2 + \cos 2\Delta\phi) D Y_0^2) \\ \phi'_y &= \frac{B^{1/2} W_0^2}{8} ((2 + \cos 2\Delta\phi) E X_0^2 + 3F Y_0^2) \end{aligned} \quad (VI)$$

# Analytic Solution - continued

Above,

$$C_1 \equiv C + V; \quad C_2 \equiv U V (1 + \cos 2\Delta\phi)$$

are constants of the motion and

$$\alpha = 1 - \frac{2C_1}{C_2^2}; \quad K_1 = \frac{(2C_2)^{1/2}}{8} W_0^2; \quad \Delta\phi_0 = \Delta\phi(z=0);$$

$$\theta = \sin^{-1} \left( 1 + \frac{16C_1}{\alpha(C_2^2 + 1 + \cos 2\Delta\phi_0)} \right)$$

The analytic solution is of interest because it provides the scaling for the betatron "precession" rate  $K_1$  and the change in the betatron wavenumber  $\Delta K_1$ .

$$K_1 = \frac{1}{4\sqrt{2}} X_0 Y_0 (1 + \cos 2\Delta\phi)^{1/2} W_0^2$$

$$K_1 = \frac{W_0^2}{2} + \Delta K_1$$

$$\text{where } \Delta K_1 = \left( X_0^2 + Y_0^2 + X_0 Y_0 (2(1 + \cos 2\Delta\phi))^{1/2} \right) \frac{W_0^2}{16}$$

There are two major effects of the non-linearity: (1) The betatron frequency becomes amplitude dependent so that phase mixing results. (2) The X and Y amplitudes are coupled and thus energy is exchanged. Phase mixing and finalization results in a final state such that

$$X = Y = 0; \quad \Delta X^2 = \frac{\Delta Y^2}{K_1^2}; \quad \Delta Y^2 = \frac{\Delta X^2}{K_1^2}$$

Thus  $E_{\text{final}} = 2(1 + K_1^2) \Delta X^2 + \Delta Y^2 + \Delta X^2 + \Delta Y^2 = H/2$  so that

$$E_{\text{final}} = \frac{1}{\sqrt{2}} K_1 H$$

The emittance grows due to the phase mixing. The growth length  $L$  is defined by

$$\Delta K_1 L = \pi$$

Here  $\Delta K_1$  is the difference in betatron frequencies between the outer most particle and a central particle. Thus the rate of emittance growth is roughly given by

$$\frac{dE}{dZ} = \frac{\Delta K_1}{\pi} (E_{\text{final}} - E_0)$$

# Analytic Solution for a Special Case

For the magnetic potential treated in ref. 1, for the case of equal harmonic focusing in the X and Y directions, and when  $W_0^2$  is regarded as a second order quantity, the constants  $c, d$  and  $A$  through  $F$  take on particularly simple values:

$$d = \frac{1}{4}; \quad c = \frac{1}{96}; \quad A = B = \frac{1}{4}; \quad D = E = 1; \quad C = F = \frac{1}{3}$$

Then the amplitude and phase equations become

$$\frac{d}{dz} X = -\frac{W_0^2}{8} U V \sin 2\Delta\phi$$

$$\frac{d}{dz} Y = \frac{W_0^2}{8} U V \sin 2\Delta\phi$$

$$\frac{d}{dz} \Delta\phi = -\frac{W_0^2}{16} (1 - \cos 2\Delta\phi) (U - V) \quad (VII)$$

Here  $U \equiv X_0^2$ ,  $V \equiv Y_0^2$ , and  $\Delta\phi = \phi_y - \phi_x$ . These have the solutions:

$$X_0^2 = \frac{C}{2} \left( 1 + \frac{\alpha}{2} (1 - \sin(2K_1 Z + \theta_0))^{1/2} \right)$$

$$Y_0^2 = \frac{C}{2} \left( 1 + \frac{\alpha}{2} (1 + \sin(2K_1 Z + \theta_0))^{1/2} \right)$$

$$\Delta\phi = \frac{1}{2} \cos^{-1} \left( \frac{2 - 3\alpha + \sin(2K_1 Z + \theta_0)}{2 - \alpha + \sin(2K_1 Z + \theta_0)} \right) \quad (VIII)$$

# Emittance Growth Due to Anharmonic Effects in FELs

The emittance is defined such that in the absence of anharmonic terms, the linear focussing would result in constant emittance:

$$E_x \equiv \langle \Delta X^2 \rangle \langle \Delta X'^2 \rangle - \langle \Delta X \Delta X' \rangle^2$$

$$E_y \equiv \langle \Delta Y^2 \rangle \langle \Delta Y'^2 \rangle - \langle \Delta Y \Delta Y' \rangle^2$$

$$E \equiv (E_x^2 + E_y^2)^{1/2}$$

where,

$$\Delta X \equiv X_i - X_0; \quad \Delta Y \equiv Y_i - Y_0; \quad \Delta X' \equiv X'_i - X'_0; \quad \Delta Y' \equiv Y'_i - Y'_0;$$

$$X_0 \equiv \langle X_i \rangle; \quad Y_0 \equiv \langle Y_i \rangle; \quad X'_0 \equiv \langle X'_i \rangle; \quad Y'_0 \equiv \langle Y'_i \rangle.$$

Here  $N$  = the number of simulation particles,  $i$  indicates the  $i$ th particle, and  $\langle \dots \rangle = (1/N) \sum_{i=1}^N$ .

We may estimate the emittance growth rate from the non-linear terms: Energy conservation implies:

$$H_0 \approx \frac{1}{2} (X_0^2 + \langle \Delta X^2 \rangle + \frac{X_0^2}{K_1^2} + \frac{\langle \Delta X'^2 \rangle}{K_1^2} + Y_0^2 + \langle \Delta Y^2 \rangle + \frac{Y_0^2}{K_1^2} + \frac{\langle \Delta Y'^2 \rangle}{K_1^2})$$

$H_0$  is an approximate constant of the motion. (The higher order terms have been neglected in this expression). Here  $K_1 = W_0^2/2$ . For a rotationless beam

$$E = (\langle \Delta X^2 \rangle \langle \Delta X'^2 \rangle + \langle \Delta Y^2 \rangle \langle \Delta Y'^2 \rangle)^{1/2}$$

# Summary and Conclusions

We have reanalyzed the transverse equations of motion for an electron traversing a wiggler including terms higher-order in the small quantities  $k_x, x, k_y, y$ , and  $\sqrt{2}a_w$  that had not previously been included. We find that the equations for the guiding center particle coordinates  $x$  and  $y$  can be expressed as a pair of weakly coupled harmonic oscillator equations. The resulting motion is approximately harmonic betatron motion, but with amplitudes and phases which precess on a relatively long length scale. The precessing phase implies an effective correction to the betatron wavenumber. The length scale increases linearly with  $\gamma$  and the inverse square of the beam radius, both factors indicating that the effects of the included higher order terms will diminish for high power, high frequency FELs. When ensembles of particles are examined the non-linear terms cause the emittance to grow. This is due to the phase mixing caused by the amplitude dependent betatron frequency. A beam with an initial offset of the beam centroid is thus converted into a beam with a larger radius and higher emittance. Simulations with the FEL code FRED indicate that the fractional change in final power produced is small when the initial beam mismatch is small, however.

# References

- [1] Charlemann, E. T. (1985), "Wiggle Plane Focusing in Linear Wigglers," J. Appl. Phys. 58, 2154
- [2] Nguyen, K. T. and Uhm, H. S. (1986), "Parabolic Pole Faces Focussing in Long Linear Wiggler FEL," presentation at A. P. S. Meeting in Baltimore, MD, December 1986, (Abstract in Bull. A. P. S. 31, 1538, (1986)).

## P3.7

### Statistical Variation of FEL Performance Due To Wiggler Field Errors

P. Kennedy, B. Bobbs, G. Rakowsky, and R. Cover  
Rockwell International/Rocketdyne Division  
6633 Canoga Avenue, Canoga Park, CA 91303

Numerical simulations are used to demonstrate that large statistical variations in peak spontaneous emission and small signal gain are obtained for FEL wigglers with the same rms field error, but different error distributions. Results demonstrate the need for a wiggler spec which reflects the effect of error ordering on FEL performance.

**INTRODUCTION:** A previous study found that reordering of field errors produced wide variations in the harmonic emission spectra of undulators for synchrotron light sources [1]. We examine the effect of random field error ordering on FEL wiggler performance and find large statistical spreads in peak first harmonic emission and peak small signal gain.

#### Baseline FEL Parameters

Period Length	$\lambda_w = 2.4$ cm
Number Periods	$N = 168$
Wiggler Length	$L = 403.2$ cm
Peak Field	$B_0 = 3.5$ kG
Vector Potential	$a_w = 0.785$
RMS Field Error	$\sigma = 0.5\%$
E-Beam Energy	$\gamma = 80$
Resonant Wavelength	$\lambda_0 = 2.4527$ $\mu\text{m}$

#### Field Error And Emission Models

- Random Field Error Model [2] -  $B_y(z) = C_n(z) B_0 \cos(kz)$ 
  - $C_n(z) = C_n \approx 1 + \epsilon_n = \text{Constant in } n\text{th } 1/2 - \text{Period}$
  - $C_n$  Randomly Chosen from Gaussian Distribution
  - Mean = 1, RMS Deviation =  $\sigma$
- On-Axis Emission Model [3] -  $d^2W/d\Omega d\omega = e^2 \omega^2 / 4\pi^2 c |Q|^2$ 

$$Q = (1/c) \int_0^L \beta_n(z) \exp[-i\phi(z)] dz$$

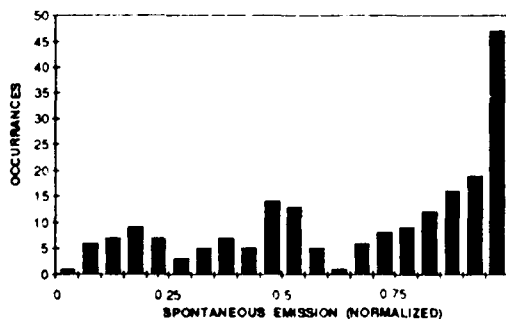
$$\phi(z) = (\omega/c) \int_0^z [1 - \beta_n(z')] dz'$$

$$\beta_n(z) = (e/mc^2 \gamma)^2 B_y(z) dz'$$
- On-Axis Small Signal Gain: Madey's Theorem [3]
$$G = -\omega_0^2 / 2 |dQ/d\gamma|^2$$

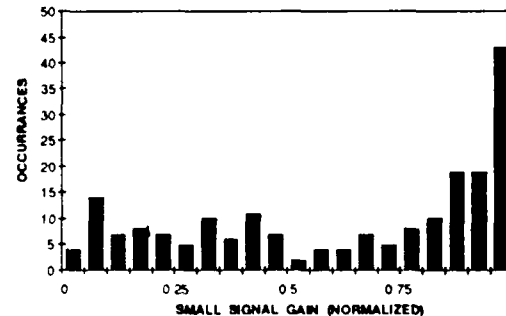
#### Statistical Effect of Error Ordering On Baseline FEL Performance

- Ensemble of 200 Wiggler Configurations
  - Same set of random field errors ( $N = 168, \sigma = 0.5\%$ )
  - Different error ordering
- For Each Configuration Compute
  - Peak first harmonic emission and peak S.S. gain
  - Normalize by ideal peak values ( $\sigma = 0$ )
- Statistical Distribution of Peak Values Ranges From Near-Ideal to Quite Poor
- Full Spectra For Three Sample Configurations Show Varying performance and Wiggler Quality

#### Statistical Distribution of Normalized Peak Spontaneous Emission ( $N = 168, \sigma = 0.5\%$ )

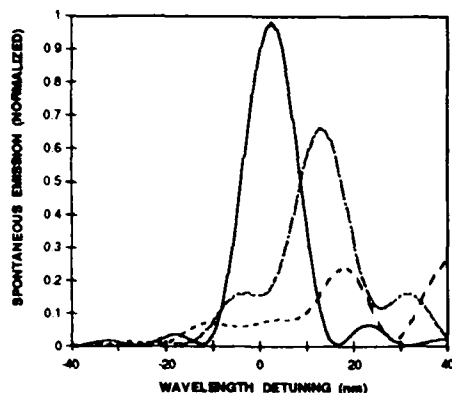


#### Statistical Distribution of Normalized Peak Small Signal Gain ( $N = 168, \sigma = 0.5\%$ )

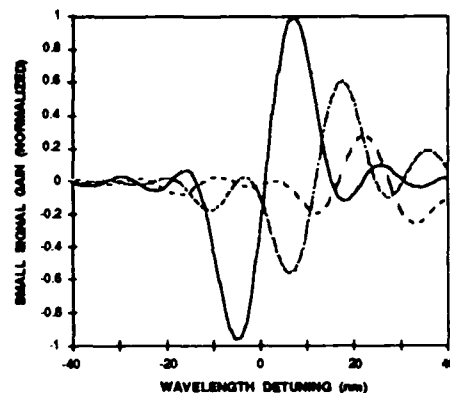




### Normalized Spontaneous Emission Spectrum Three Sample Configurations ( $N = 168, \sigma = 0.5\%$ )



### Normalized Small Signal Gain Spectrum Three Sample Configurations ( $N = 168, \sigma = 0.5\%$ )



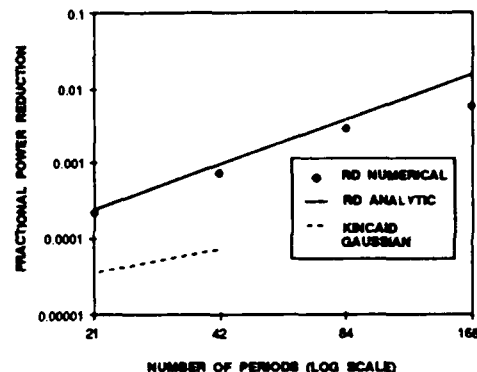
### Reduction in RMS Emission (Power) with Length and RMS Field Error

- RMS Peak Emission Computed for
  - $\sigma = 0.1\%$  ,  $N = 168, 84, 42, 21$
  - $\sigma = 0.5\%$  ,  $N = 168, 84, 42, 21$
- Analytic scaling relationship for fractional power reduction (from ideal value,  $\sigma = 0$ )

$$[|Q_P^2 - |Q_P^2|] / |Q_P^2| \approx (8/3) [\sigma^2 / (1 + \sigma^2/2)]^2 N^2$$

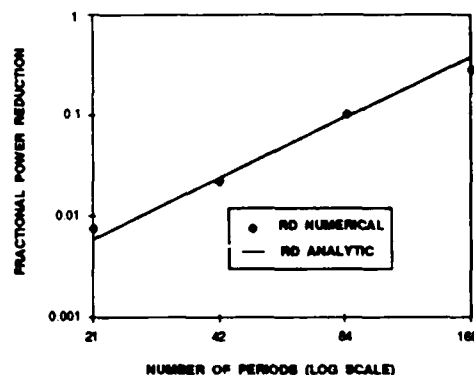
- Good agreement with numerical results for all  $N, \sigma$
- Gives better fit to our data in Gaussian limit ( $\sigma^2 N^2 \leq 1/7$ ) than corresponding Kincaid [2] formula

### Fractional Power Reduction vs. Number Periods ( $\sigma = 0.1\%$ )



**CONCLUSION:** Results show that rms field error is not a reliable indicator of wiggler quality and demonstrate the need for a wiggler spec which reflects the effect of error ordering on FEL performance [4]. They also indicate the importance for pure permanent magnet wigglers [5], of obtaining an optimized magnet ordering [6].

### Fractional Power Reduction vs. Number Periods ( $\sigma = 0.5\%$ )



#### REFERENCES:

- [1] B. Diviacco and R. P. Walker, "The Effect of Magnetic Field Errors on the Radiation Spectrum of ELETTRA Undulators," Proc. Particle Accelerator Conf., Chicago (1989).
- [2] B. M. Kincaid, J. Opt. Soc. Am. B, 2, pp. 1294-1306, (1985).
- [3] C. C. Shah and M. Z. Capom, Phys. Rev. A, 26, pp. 438-450 (1982).
- [4] B. Rebbe, et al., "In Search of a Meaningful Field Error Spec for Wigglers," Proc. this Conference.
- [5] G. Rakowsky, et al., "High Performance Pure Permanent Magnet Undulators," Proc. this Conference.
- [6] R. Cover, et al., "FEL Performance with Pure Permanent Magnet Undulators Having Optimal Ordering," Proc. this Conference.

## P3.8

### Minimized Emittance Growth with Elliptical Beam Pipes in FEL

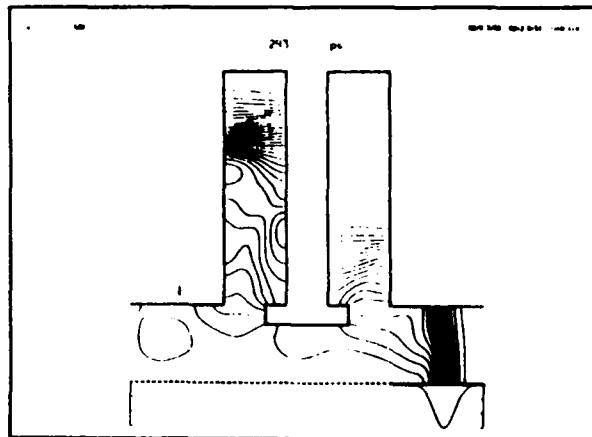
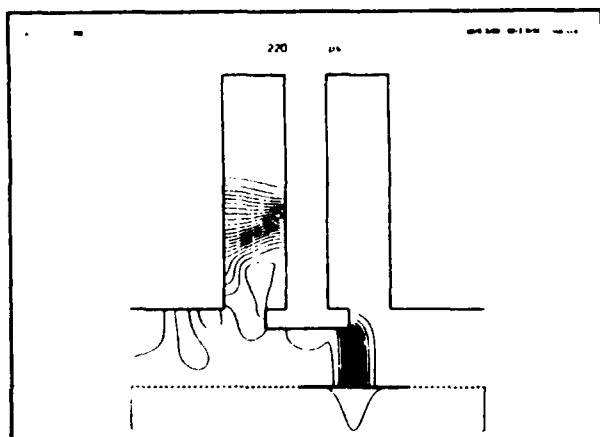
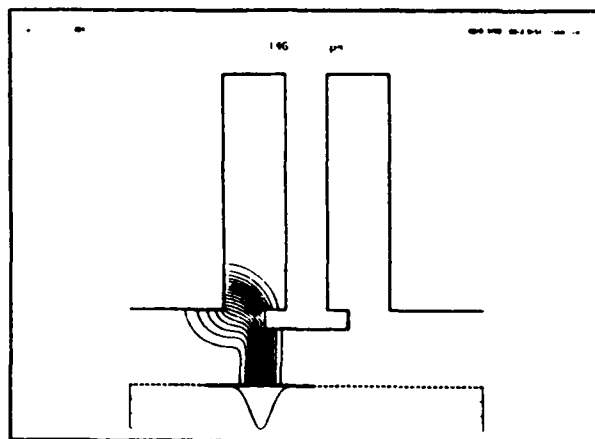
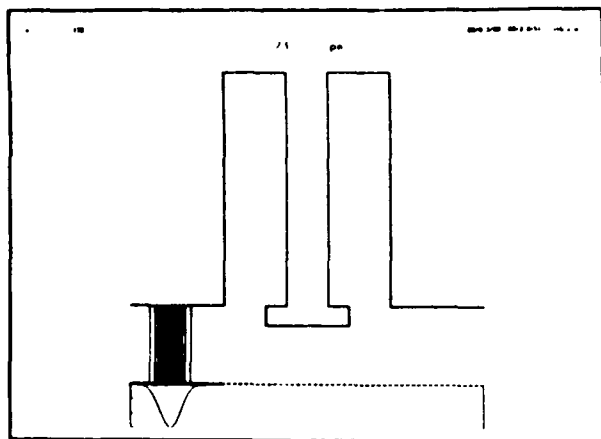
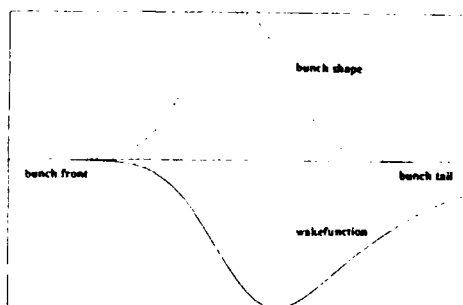
K. C. D. Chan

Los Alamos National Laboratory, H829, Los Alamos, NM87545

#### Abstract

Deleterious wakefield effects caused by openings along the beam pipes can be effectively reduced by using beam pipes of elliptical cross sections with large ratios of major to minor axes. Such beam pipes can be matched to existing circular beam pipes on accelerators without introducing additional wakefields using a concept based on energy-conservation considerations.

#### Wakefield effects cause emittance growth



Emittance growths are minimized by using elliptical/rectangular beam pipes

Wakefield emittance growth caused by discontinuities along the beam pipe (Fig. 1a) can be reduced by increasing the cross-sectional area of the beam pipe. A beam-pipe cross section can be increased either by increasing both (Fig. 1b) or only one (Fig. 1c) of the two transverse dimensions.

Figure 2 shows that wakefield effects decrease with the increased transverse dimensions to a power of 1.5 (dashed curve) for the scheme in Fig. 1b and exponentially (solid curve) for the scheme in Fig. 1c. This indicates that wakefield effects can be reduced more effectively by using a rectangular or elliptical beam pipe.

Figure 1  
Lengths of beam pipes with two openings on the sides as typical beam-pipe discontinuities

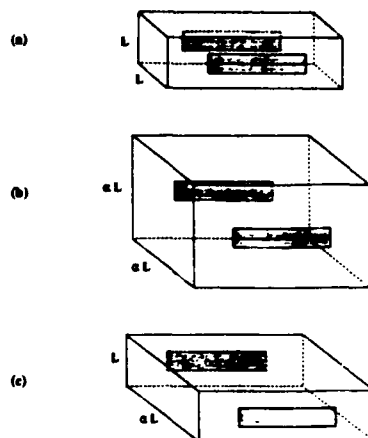
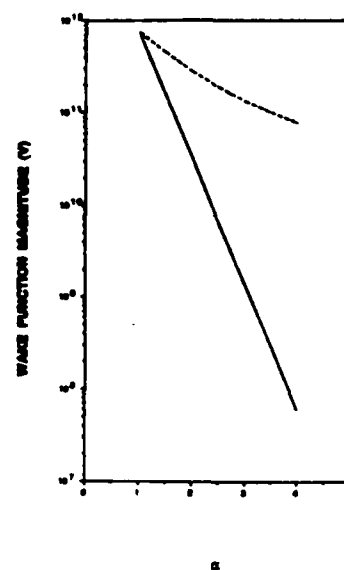


Figure 2



An elliptical beam pipe can be joined to a circular beam pipe without introducing wakefield

To employ an elliptical beam pipe after the circular aperture in an accelerator, a wakefield-less transition is necessary. Such a 'matched' transition can be made by observing energy-conservation considerations.

First, a slow taper should be used to eliminate energy transfer to generate scattered waves. Second, the elliptical cross section along the transition should be designed such that the electro-magnetic field energy of the beam is always equal to that of the initial circular pipe.

Figure 3 shows that a wakefield-less transition can reduce wakefield by better than a factor of ten.

Typical Matched Transition

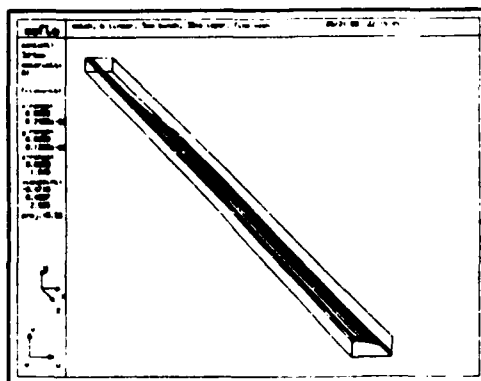
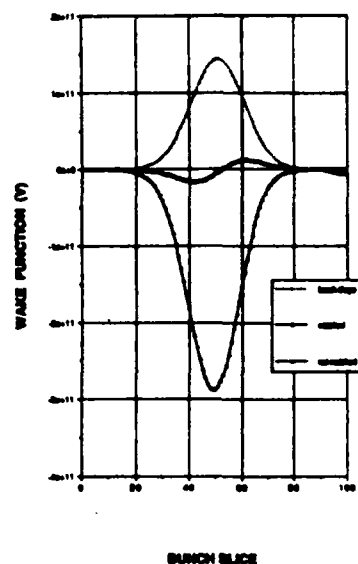


Figure 3



## P3.9

### PULSE COMPRESSION ON THE MARK III FEL USING ENERGY CHIRPING

E.B. Szarnes, S.V. Benson, and J.M.J. Madey.

#### ABSTRACT

We have performed preliminary numerical simulations of the optical pulse formation in an FEL using micropulses with a linear energy dependence on time. The simulations are based on a one-dimensional code assuming Gaussian modes and including shot noise for parameters appropriate to the Mark III FEL. The optical micropulses are allowed to oscillate near the synchronous cavity length to a point just short of full saturation to prevent distortion of the optical envelope and phase by the sideband instability. The pulses are then numerically propagated in the frequency domain through a quadratic dispersive delay line. Preliminary simulations have varied both the sign and magnitude of the energy chirp as well as the slippage parameter (via the pulse width), and have demonstrated optical frequency chirps agreeing fairly well with those obtained analytically by assuming that the resonance condition determines the lasing wavelength during the pulse ( $\delta\lambda/\lambda = 2\delta\gamma/\gamma$ ). Slight deviations from this condition are observed which depend on the sign of the chirp. In a typical case, we project pulse compression by a factor of 13.3, from an initial pulsewidth of 3.13 ps to a final pulsewidth of 236 fs, at a wavelength of 3.35 microns and an electron micropulse energy chirp of +2% (energy increasing towards the back of the pulse). Note that this represents an optical pulse less than half as short as the slippage length of 47 magnet periods for this wavelength. Proposed experiments using the Mark III FEL are discussed.

#### NUMERICAL SIMULATIONS

- 1) Optical pulses build up from noise to a point just short of full saturation using the coupled Maxwell-Lorentz equations
- 2) One-dimensional simulation with a complex filling factor for the transverse resonator modes (TEM<sub>00</sub>)
- 3) Includes shot noise via electron beam density modulations on a tophat pulse
- 4) Electron energy chirp is introduced by linear variation of the electron resonance parameter along the electron pulse
- 5) Simulations investigate dependence on
  - i) sign and magnitude of energy chirp
  - ii) electron pulse width
  - iii) cavity length detuning
- 6) Parameters appropriate to the Mark III FEL

Graph showing average macropulse power vs. Cavity length detuning

Parameters:	$\lambda$	= 3.35 $\mu\text{m}$
	Electron energy	= 42.5 MeV
	Electron energy chirp	= +2%
	Micropulse peak current	= 20 Amps
	Micropulse width	= 4.0 ps
	Number of passes	= 100(1.2 $\mu\text{s}$ )
	Cavity losses	= 7.3%
	Net gain	~ 45%

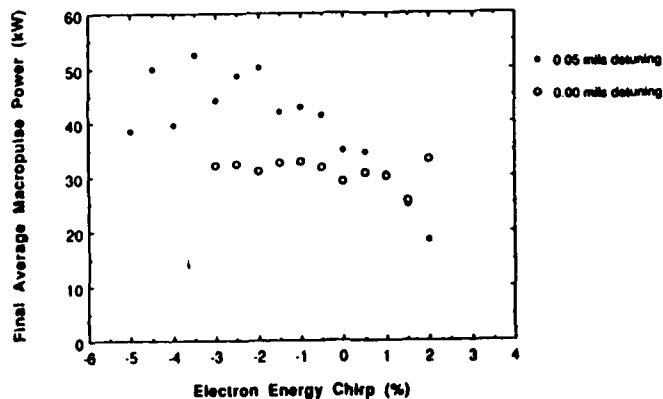
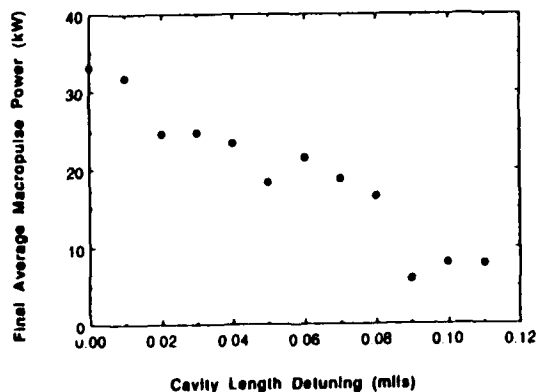
NOTE: POSITIVE CHIRP = HIGHER ENERGIES AT TRAILING EDGE

Graph showing average macropulse power vs. Electron energy chirp for zero and finite cavity length detunings

Parameters:	$\lambda$	= 3.35 $\mu\text{m}$
	Electron energy	= 42.5 MeV
	Micropulse peak current	= 20 Amps
	Micropulse width	= 4.0 ps
	Number of passes	= 100(1.2 $\mu\text{s}$ )
	Cavity losses	= 7.3%
	Net gain	~ 45%

(The curve for zero cavity length detuning remained flat even for 170 passes - well into saturation)

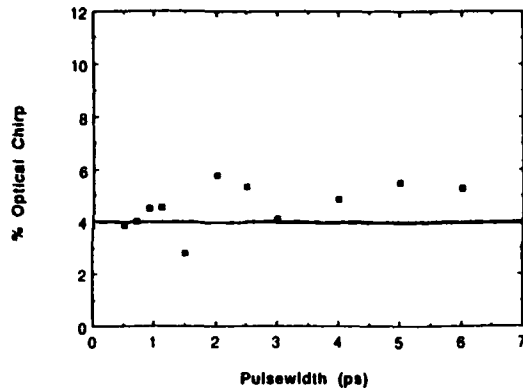
Macropulse Power vs. Cavity Length Detuning      Macropulse Power vs. Electron Energy Chirp



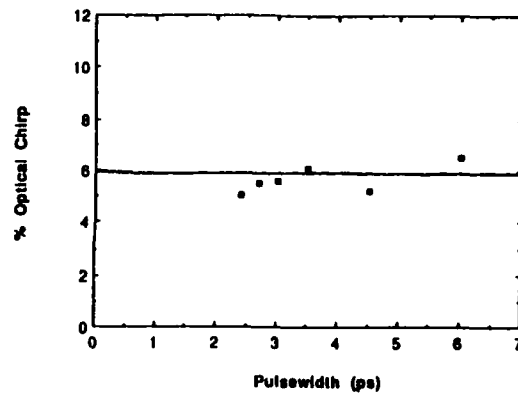
**Graphs showing % Optical Chirp Induced by the given % Electron Energy Chirps**

Parameters:	+2% chirp	-3% chirp
$\lambda$	3.35 $\mu\text{m}$	3.0 $\mu\text{m}$
Electron energy	42.5 MeV	42.5 MeV
Micropulse peak current	20 Amps	-
Micropulse charge	-	75 pC
Number of passes	100(1.2 $\mu\text{s}$ )	60(0.74 $\mu\text{s}$ )
Cavity length detuning	0 mils	0 mils
Cavity losses	7.3%	7.3%
Net gain	45%	20% - 55%

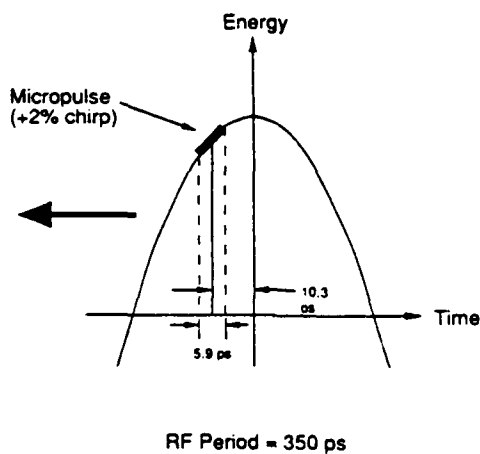
**% Optical Chirp Induced by +2% Energy Chirp**



**% Optical Chirp Induced by -3% Energy Chirp**

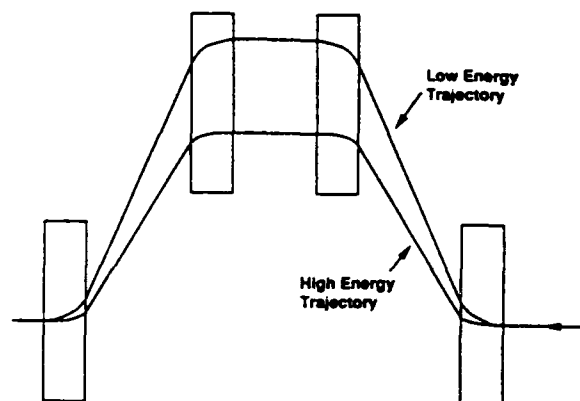


**Preferred Relative Phase Offset Between Electron Micropulse and Accelerator RF Field (greatly exaggerated)**



**Four-dipole Chicane Serving as an Electron Pulse Compressor**

for electron pulses with higher energies at the trailing edge



Dispersion ~ 1 picosecond per percent energy spread in the Mark III FEL

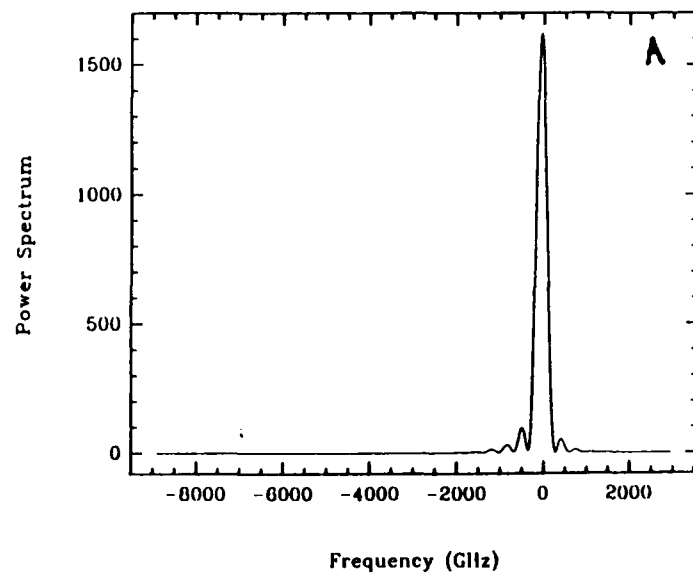
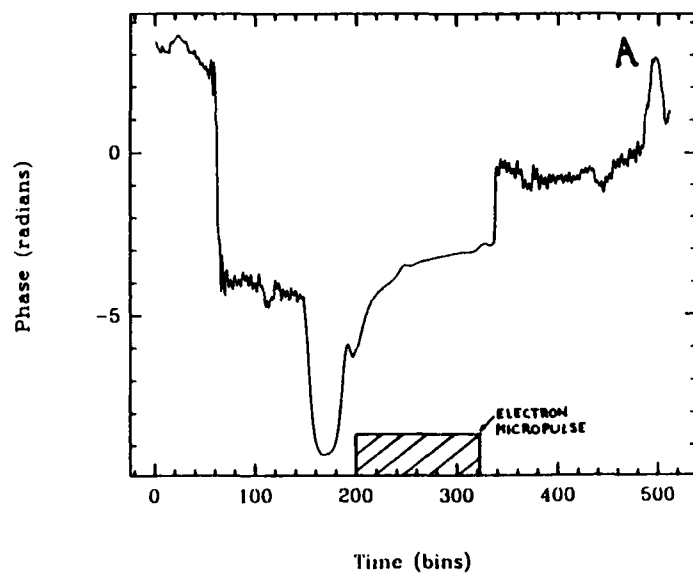
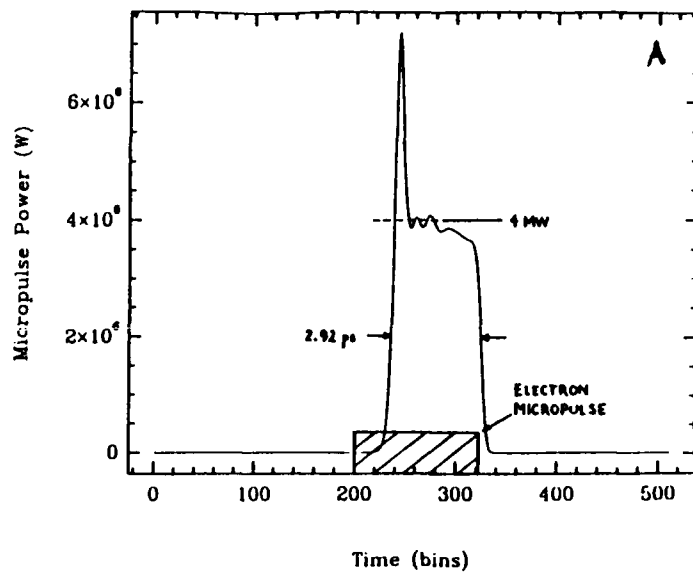
**Computer simulations showing:**

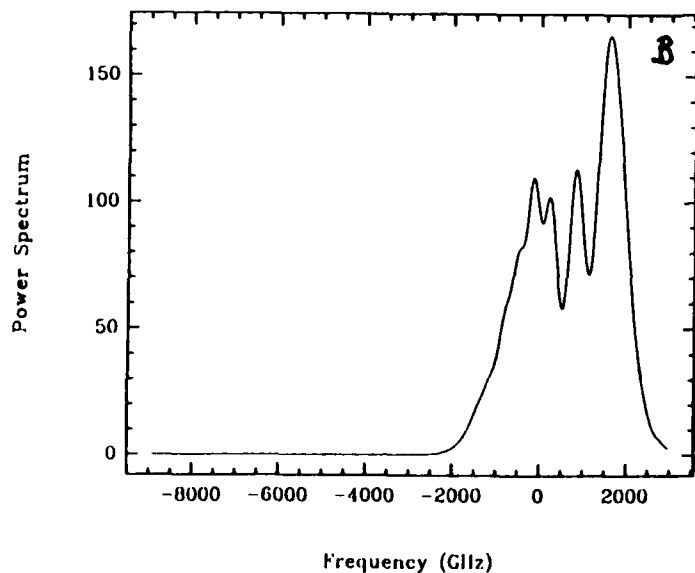
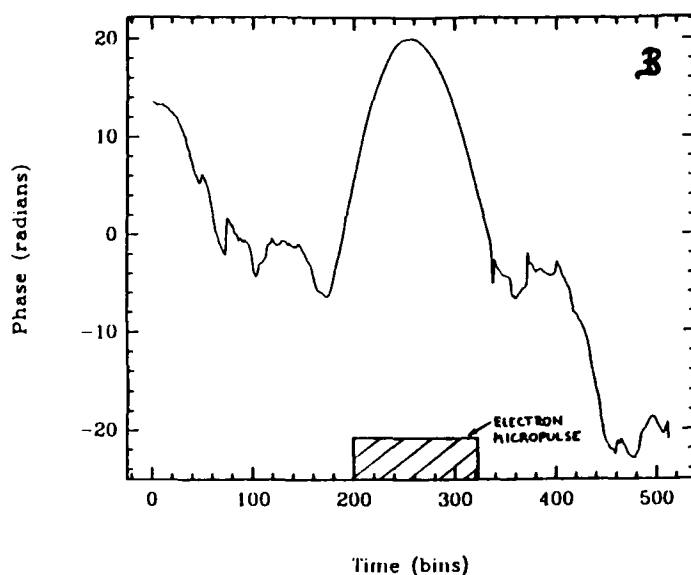
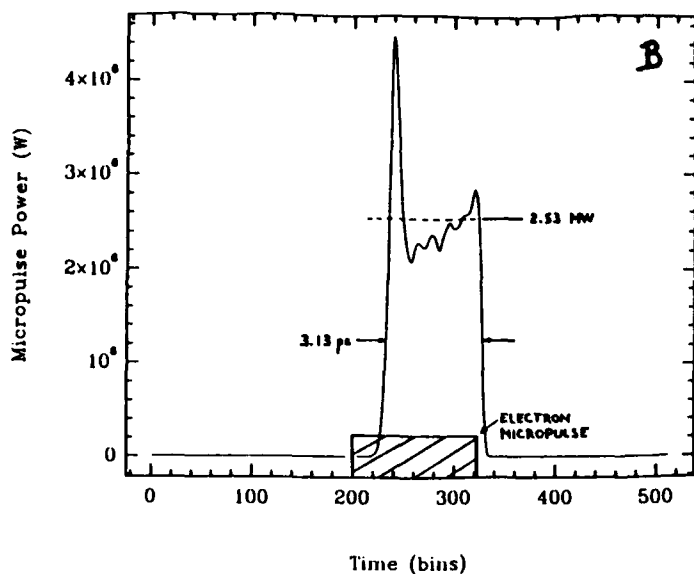
A) Optical micropulse power, phase, and spectrum in the absense of energy chirp in the electron beam (0.05 mils detuning)

B) Optical micropulse power, phase, and spectrum with a +2% energy chirp in the electron beam (0.04 mils detuning)

Other parameters:

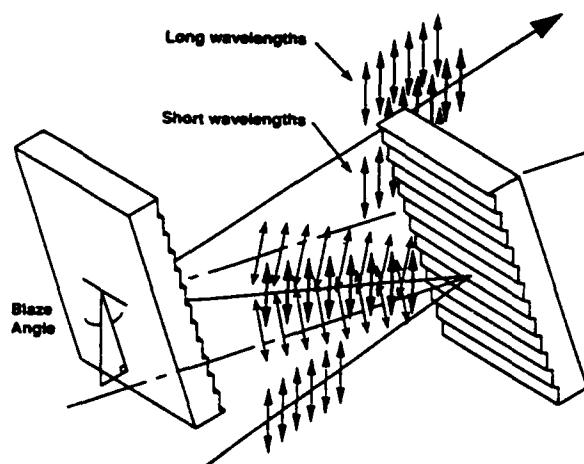
$\lambda$	= 3.35 $\mu\text{m}$
Electron energy	= 42.5 MeV
Micropulse peak current	= 20 Amps
Micropulse width	= 4.0 ps
Number of passes	= 100 (1.2 $\mu\text{s}$ )
Cavity losses	= 7.3%
Net gain	= 45%





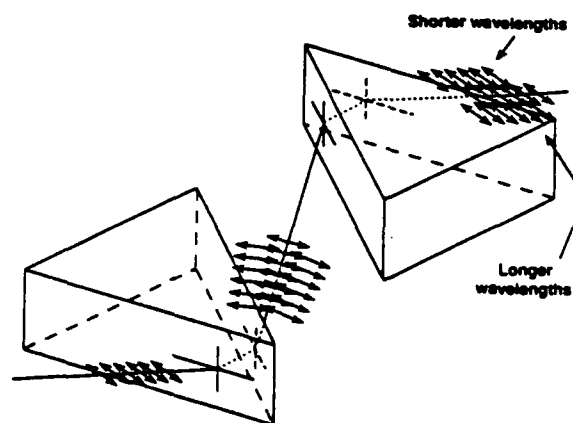
### Grating Pair in the Littrow Configuration Serving as a Pulse Compressor

for optical pulses with higher frequencies at the trailing edge



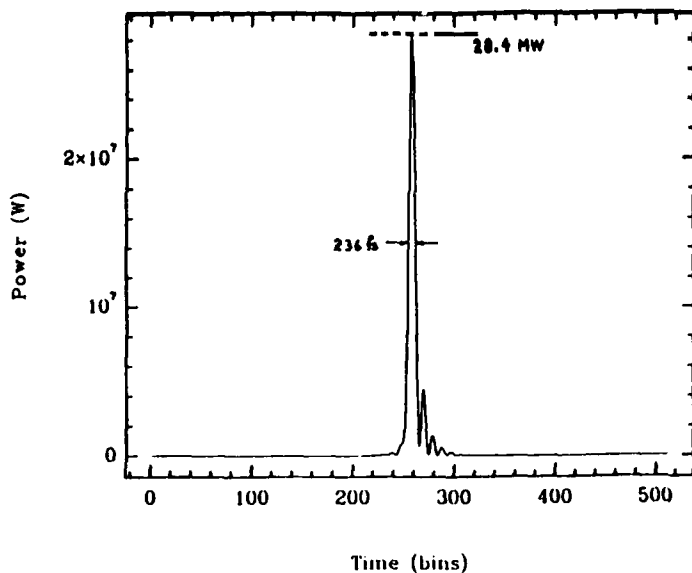
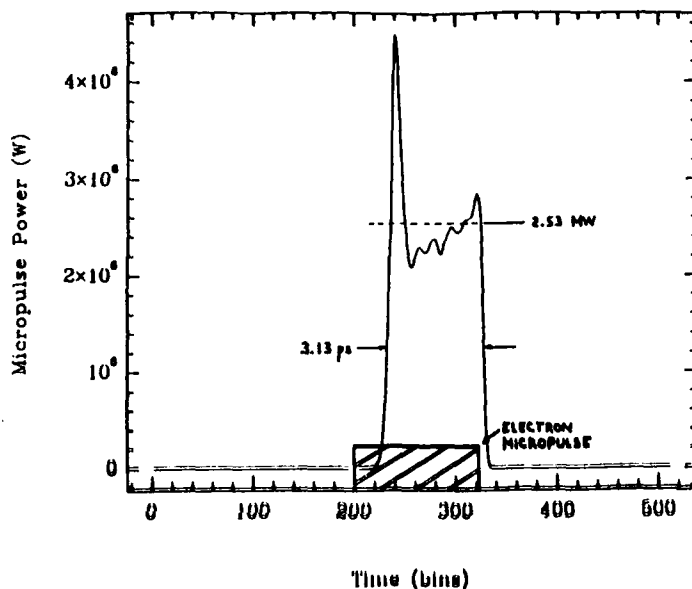
### Minimum Deviation, Brewster Angle Prism Pair Serving as a Pulse Compressor

for optical pulses with higher frequencies at the trailing edge



# Comparison Between Chirped Input Pulse and Compensated Output Pulse

(Note change of scale on vertical axis)



## CONCLUSIONS

Computer simulations on realistic FEL configurations have demonstrated substantial pulse compression ratios for modest electron micropulse energy chirps.

Negatively chirped pulses show increased optical powers for finite cavity length detunings, but slightly lower optical chirps than predicted by the FEL resonance condition.

Positively chirped pulses show decreased optical powers for finite cavity length detunings, but slightly larger optical chirps than predicted by the FEL resonance condition.

Have proposed an experiment using 4 ps electron micropulses with a +2% energy chirp.



# P3.11

## SPECIFIC OPTICAL PROPERTIES OF MULTILAYER MIRRORS FOR S.R. FEL EXPERIMENTS

LURE CNRS/CEA/MEN - Batiment 209D - Université Paris-Sud  
91405 ORSAY CEDEX FRANCE

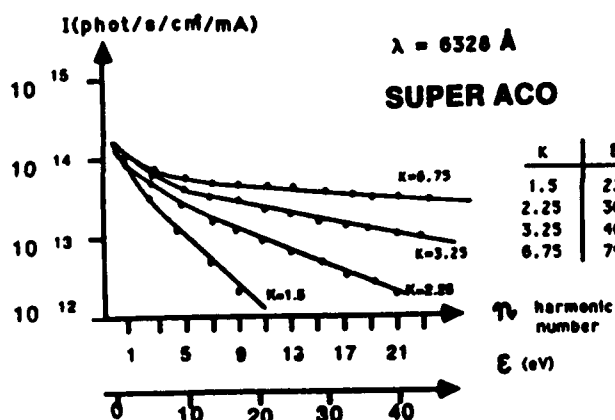
M.F. VELGHE<sup>\*</sup>, M.E. COUPRIE<sup>\*\*</sup>, M. BILLARDON<sup>\*\*\*</sup>

<sup>\*</sup> Laboratoire de Photophysique Moléculaire, Bât. 213, Université Paris-Sud  
91405 ORSAY CEDEX, FRANCE

<sup>\*\*</sup> CEA, IRF DPHG-S.P.A.S.  
91191 GIF-SUR-YVETTE, FRANCE

<sup>\*\*\*</sup> Ecole Supérieure de Physique et Chimie, 10 rue Vauquelin  
75231 PARIS CEDEX 05, FRANCE

**ABSTRACT.** Mirror degradation is a crucial drawback for the F.E.L. experiments in the visible and UV range. This degradation is due to the high X ray flux of the spontaneous emission. In the present paper, we summarize new results from the multilayer dielectric mirrors and the mirrors temperature measurements.

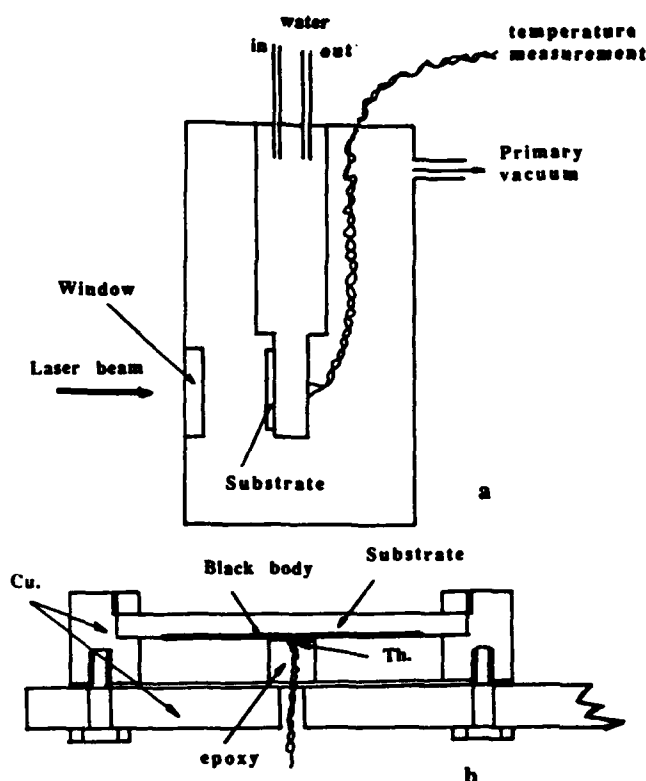


Mirror	Init. losses	Irrad. (A.h)	Current (A)	Losses after irr.	Losses after clean.
S1	0.028 %	0.266	0.08	0.216 %	0.072 %
	0.072	0.35	0.13	0.27	
K1	0.15	0.3	0.06	0.22	0.12
	0.12	0.37	0.08	0.17	0.15
	0.15	0.34	0.135	1.1	0.39
V8	0.138	0.52	0.088	0.28	
	0.28	0.35	0.101	0.39	0.15
S3	0.12	0.23	0.084	0.21	0.136
	0.136	0.72	0.103	0.186	0.147
S5 *	0.077	0.755		0.29	0.153

\* this mirror was used for the FEL oscillation

Table of the mirrors losses evolution versus irradiation, before and after cleaning

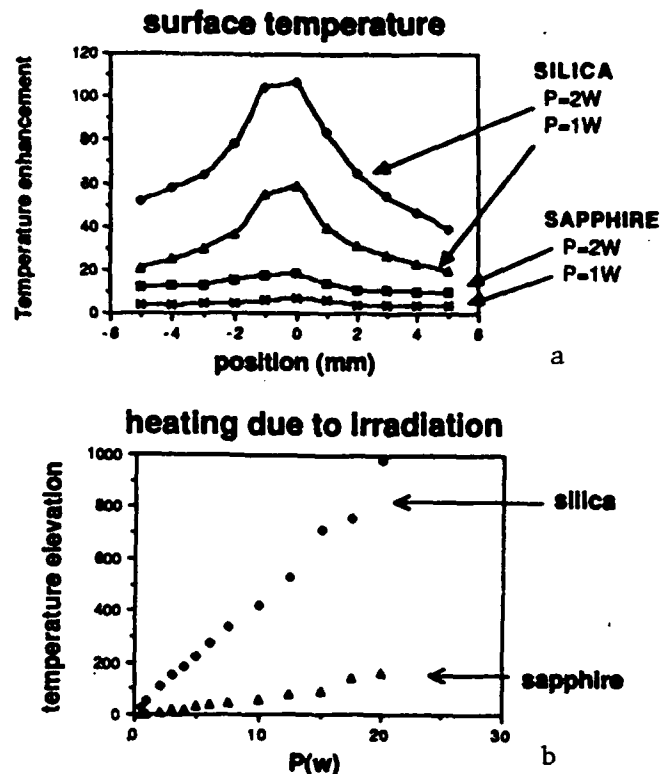
## EXPERIMENTAL LAY-OUT



Temperature measurement device

a General view

b Detail of the substrate holder



Results of the temperature measurements with sapphire and silica substrates

a Surface heating at two laser powers

b Central heating versus of the laser power

## REFERENCES

- (1) N.A. VINOKUROV, V. LITVINIENKO. "Visible and Ultraviolet lasing in optical klystron on VEPP-3 storage Ring", to be published in the Proceedings of SR88 Conference in Novossibirsk (Aug. 88).
  - (2) M. VELGHE, P. ELLEAUME. "F.E.L. optics test device", in Proceedings of the 8th International FEL Conference, Glasgow (Sept. 86).
  - (3) M.E. COUPRIE, M. BILLARDON, M. VELGHE, C. BAZIN, M. BERGHER, H. FANG, J.M. ORTEGA, Y. PETROFF, R. PRAZERES. "Optical properties of multilayer mirrors exposed to synchrotron radiation". Nucl. instr. and Meth. Proceedings of the 9th International FEL Conference, Williamsburg, A272, n°1-2, 166 (1988).
- J.M. HERBELIN et al. "Sensitive measurement of photon lifetime and true reflectances in an optical cavity by a phase-shift method". Appl. Opt., 19, 144 (1980).
- N.A. VINOKUROV, V.N. LITVINENKO. "Method for measuring reflection coefficients near unity". Preprint INP 79-24 (Institute of Nuclear Physics, 630090, Novosibirsk, URSS).
- M. BILLARDON, M.E. COUPRIE, J.M. ORTEGA, M. VELGHE. "Fabry-Perot effects in the exponential decay phase-shift reflectivity measurement methods", submitted to Applied Optics.

## P3.12 Numerical Studies On Mode Competition In Long-Pulse FELs

R. Hajima, H. Ohashi and S. Kondo  
Nuclear Engineering Research Laboratory,  
University of Tokyo, JAPAN.

**ABSTRACT:** A multi-mode FEL simulation has been made for the analysis of laser mode competition in long-pulse FELs. The development of each mode has been calculated from particle motion in the potential of many modes. The ratio between self-saturation and cross-saturation has been estimated in both shallow and deep saturation.

### Spectrum of FELs

- (1) Fourier transform limit  $\Delta f = 1/\Delta t$ .  
→ Dominant in short pulse FELs.
- (2) Mode selecting by the resonator cavity.
- (3) Mode competition ( mode dynamics ).  
→ Dominant in long pulse FELs.

● In this study, we have investigated the mode competition in long pulse FELs. The theory of the mode competition, the simulation method and the calculation results are presented.

### Laser Mode Analysis

van der Pol equation for single mode lasers

$$\frac{dE}{dt} = (G - L - S|E|^2) E$$

G: Gain, L: Loss, S: Self-Saturation

for two mode lasers

$$\frac{dE_1}{dt} = (G_1 - L - S|E_1|^2 - C|E_2|^2) E_1$$

$$\frac{dE_2}{dt} = (G_2 - L - S|E_2|^2 - C|E_1|^2) E_2$$

C: Cross-Saturation

- If  $C/S > 1$ , then only single mode is stable.  
If  $C/S < 1$ , then both two modes are stable.
- For the FEL,  $C/S=2$  has derived using a perturbation analysis of the third-order in the radiation field.  
( third-order theory )
- van der Pol equations cannot be applied to the cases of more than three modes. We have, therefore, developed a numerical code for the mode dynamics simulation.

### Multi-Mode FEL Simulation

$$(\nabla^2 - \frac{1}{c^2} \frac{\partial^2}{\partial t^2}) E = \mu_0 \frac{\partial}{\partial t} J$$

- The radiation field and the current terms are expanded into the series of plane-wave modes.

$$E_x(z, t) = \sum_q e^{i(k_q z - \omega_q t + \phi_q)} E_q(z)$$

$$J_x(z, t) = \sum_q e^{i(k_q z - \omega_q t + \phi_q)} J_q(z)$$

- The slowly varying approximation and the orthogonal relation between the modes are used.

$$(\frac{\partial}{\partial z} + \frac{1}{c} \frac{\partial}{\partial t}) E_q = -\frac{1}{2} \mu_0 c \operatorname{Re}(J_q)$$

$$E_q (\frac{\partial}{\partial z} + \frac{1}{c} \frac{\partial}{\partial t}) \phi_q = -\frac{1}{2} \mu_0 c \operatorname{Im}(J_q)$$

- The Fourier transform of the current term gives the each modal current.

$$J_q(z) = \int_{-\infty}^{\infty} J_x(z, t) e^{-i(k_q z - \omega_q t + \phi_q)} dt$$

- A periodic boundary condition is introduced.

$$J_q(z) = -\frac{cen_s}{N} \sum_j \beta_{qj} e^{-i(k_q z - \omega_q t + \phi_q)}$$

- The real and the imaginary part of the current term are expressed as

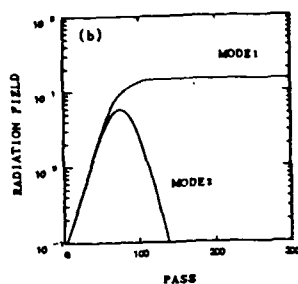
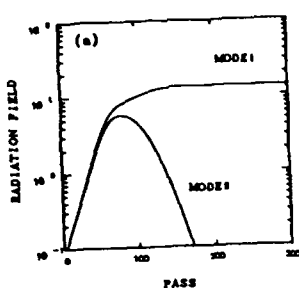
$$\operatorname{Re}(J_q) = -\frac{\sqrt{2}cen_s K}{N} \sum_j \frac{\sin \Psi_{qj}}{\gamma_j}$$

$$\operatorname{Im}(J_q) = -\frac{\sqrt{2}cen_s K}{N} \sum_j \frac{\cos \Psi_{qj}}{\gamma_j}$$

$$\Psi_{qj} = (k_q + k_w) z_j(t) - \omega_q t + \phi_q$$

- The kinetic equation of an electron is given by

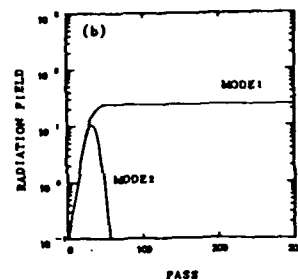
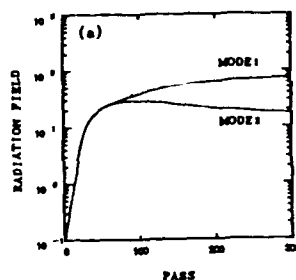
$$\ddot{z}_j = -\frac{e^2 B_w (1+K^2)}{2k_w \gamma_j^4 m_0^2 c} \sum_q E_q \sin \Psi_{qj}$$



The results of two mode analysis in the shallow-saturated region.

(a) Simulation code (b) Third-order theory  
Resonator loss = 20%  
 $\mu = 2.6$  (mode 1) and  $\mu = 2.3$  (mode 2)

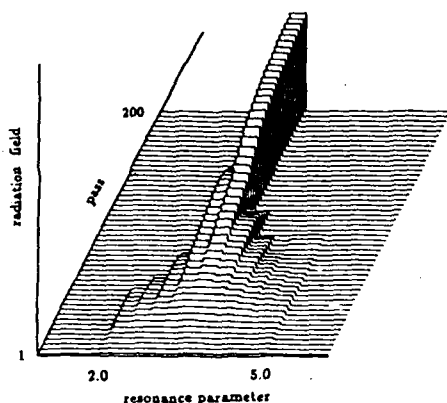
- The field cannot reach deep saturation because of the large loss of the resonator.



The results of two mode analysis in the deep-saturated region.

(a) Simulation code (b) Third-order theory  
Resonator loss = 0%  
 $\mu = 2.6$  (mode 1) and  $\mu = 2.3$  (mode 2)

- The numerical analysis shows that both two modes are stable at steady state, which is inconsistent with the third-order theory predictions. This is because the third-order theory was obtained from an analysis of the third order perturbation in the radiation field and perturbation terms of higher order are neglected, whereas the simulation code includes all nonlinearity of the radiation field. In this figure, the field grows up into deep-saturated region because of no resonator loss. Thus, the simulation code gives precise results even in the large amplitude region.



Ten-mode analysis including beam energy spread  
 $\Delta E/E = 2\%$ , resonator loss = 20%

- The oscillation wavelength is up-shifted by the beam energy spread.

## Conclusions

The mode competition in a long-pulse free-electron laser was calculated using a multi-mode FEL simulation code. It was found that the radiation field reaches the deep-saturated region and the mode selectivity becomes considerably deteriorated when the loss of the resonator cavity is small. Two-mode calculations showed that the cross saturation parameter is equal to the self saturation parameter in the deep-saturated region. In the shallow-saturated region the code and the third-order theory predicted the mode competition behavior well for the two-mode case. The simulation code is also applicable to the multi-mode calculations over three modes.

## References :

- [1] R.A.Jong and E.T.Scherlemann, Nucl. Instr. and Meth., A259(1987) 254-
- [2] P.Ringy, Nucl. Instr. and Meth., A239(1985) 432-
- [3] D.Oepts, A.F.G. van der Meer, R.W.B.Best, P.W. van Amersfoort and W.B.Colson, Proc. of the 10th International FEL conference, to be published
- [4] I.Kimel and L.R.Elias, Phys. Rev. A35(1987) 3818-

# P3.13

## CONSEQUENCES OF SHORT ELECTRON BEAM PULSES IN THE FELIX PROJECT

D.A. Jaroszynski,\* D. Oepts, A.F.G. van der Meer, P.W. van Amersfoort  
FOM-Instituut voor Plasmafysica 'Rijnhuizen', Associatie EURATOM-FOM,  
Edisonbaan 14, 3439 MN Nieuwegein, Nederland

W.B. Colson  
Berkeley Research Associates, 125 University Avenue, Berkeley, CA  
94710, USA\*\*

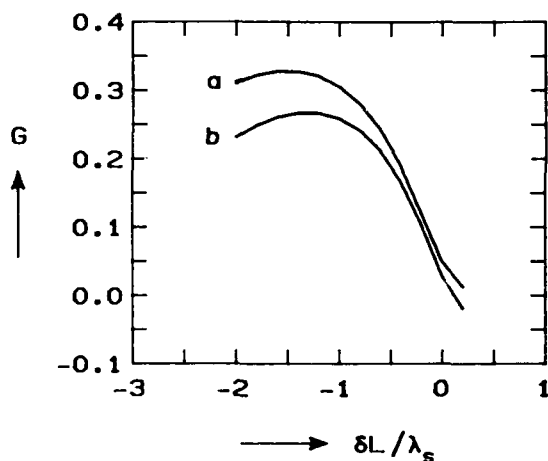
\*Permanent address: Heriot-Watt University, Riccarton, Edinburgh EH144AS, United Kingdom

\*\*Present address: Physics Dept., Naval Postgraduate School, Monterey, CA 93940, USA

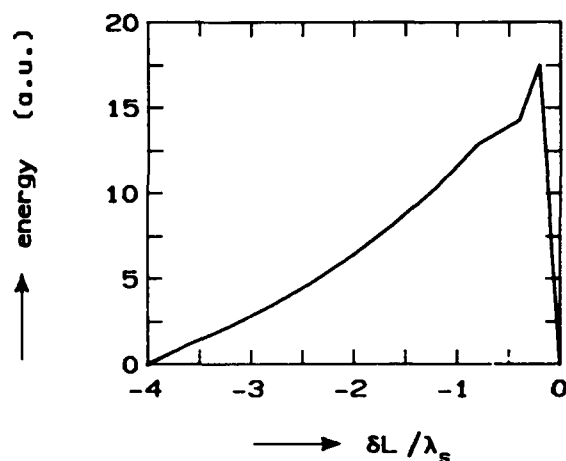
### Abstract

We discuss the consequences of short micropulses on the output of infra red and far infra red free electron lasers with special reference to the FELIX project which operates with 3 ps long electron pulses.

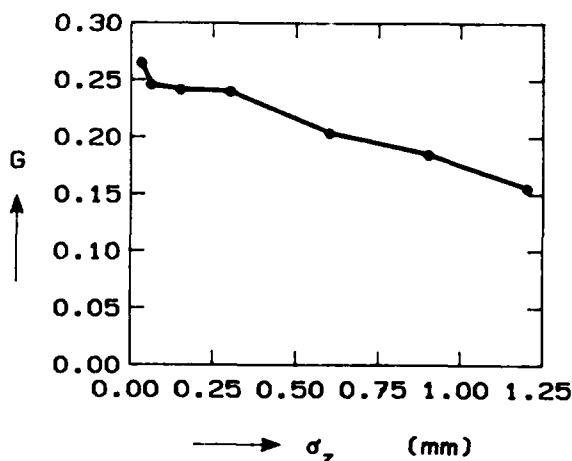
Desynchronism: small signal gain



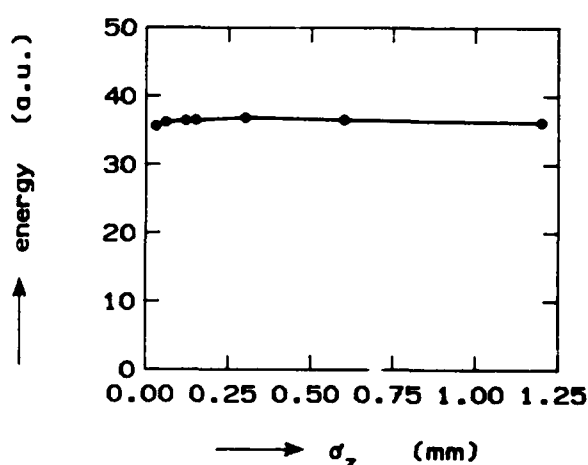
Desynchronism: saturated pulse energy

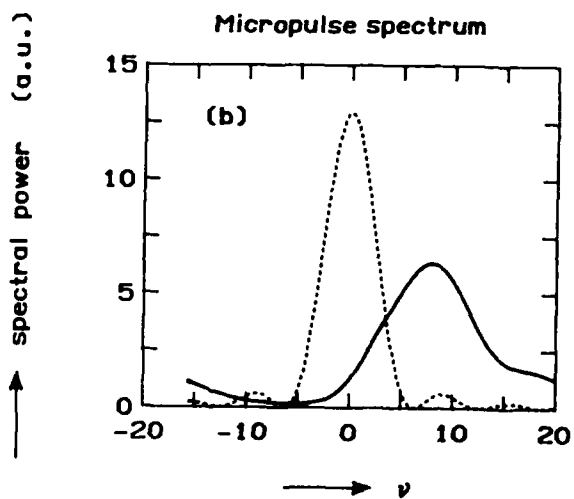
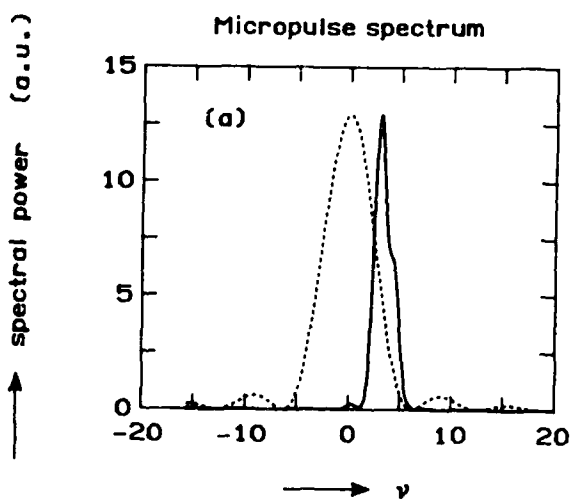
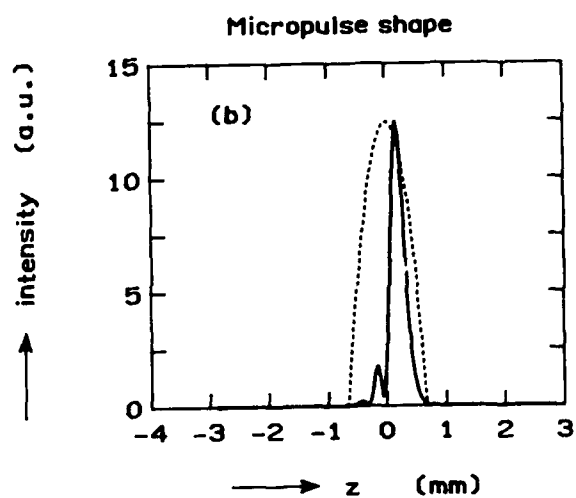
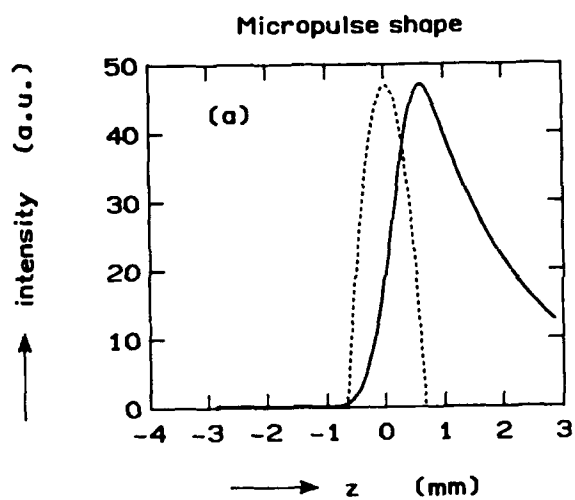
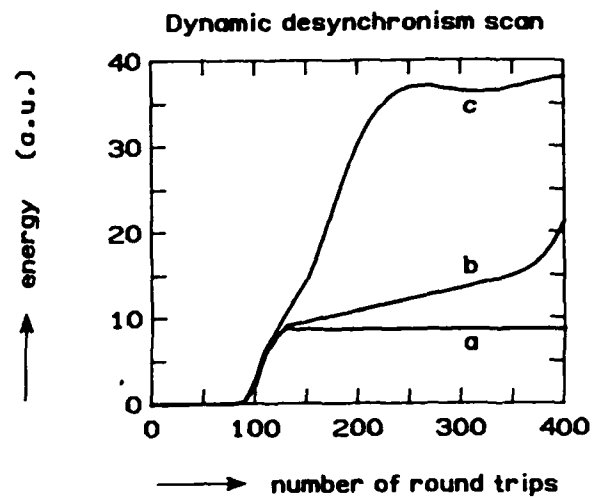
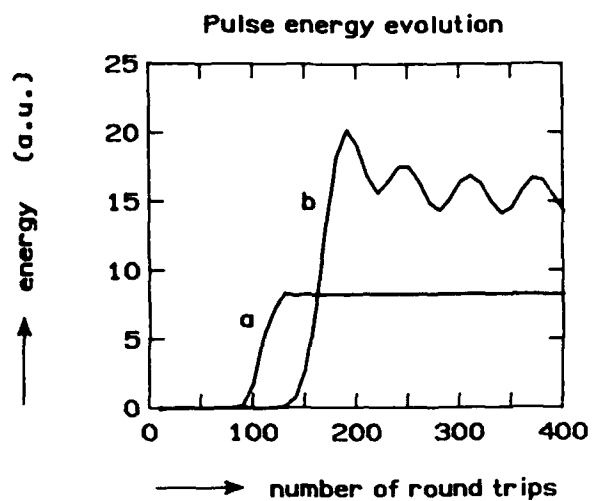


Small signal gain vs pulse length



Saturated energy vs e-pulse length





#### 4. Conclusions

We have shown that the desynchronism curves for the FELIX project, where the micropulses have an rms length of 0.3mm, are of the order of one wavelength wide for the first stage of the project where the laser will be operating around 27 $\mu$ m. We have also shown that for long wavelength FELs, where lethargy effects are important, the gain per pass in the small signal regime and the saturated pulse energy, as a function of  $\sigma_z$ , are constant when the charge in the electron micropulse is maintained constant. Finally, we have shown preliminary results of numerical work studying the feasibility of dynamic scanning of the desynchronism as a function of time through the macropulse to optimise both the growth rate and the final power at saturation. We have also shown that this method is useful for altering the pulse shape at saturation controlling the spectra.

## PARAMAGNETIC AND DIAMAGNETIC CORRECTIONS TO THE ELECTRON DYNAMICS IN A FREE-ELECTRON LASER WITH GUIDE FIELD

F. Hartemann, MIT Plasma Fusion Center, Cambridge, MA.

### FEL Cyclotron Resonance

#### Paramagnetic and Diamagnetic Corrections to the Electron Dynamics in a Free-Electron Laser with Guide Field

F. Hartemann\*, MIT Plasma Fusion Center, Cambridge MA.

- Introduction : FELs, CARMs
- Review of Single-Particle Model
- Fluid Model with Space-Charge
- Numerical Example : MIT 140 GHz CARM
- Higher-Order Effects : Axial Energy Spread
- Conclusions

\* Permanent address : Thomson-CSF/DTE, Vélizy, France

#### Theory with Space-Charge

- Total Magnetic Field

$$\vec{B} = B_0 + (1 + \chi) B_w [\hat{r} \cos \psi + \hat{\theta} \sin \psi]$$

$\chi$  : diamagnetic or paramagnetic correction to the wiggler field.

- Fluid Equation of Motion

$$(\vec{v} \cdot \vec{\nabla}) \vec{v} = -\frac{e}{\gamma_0 m_0} \vec{v} \times \vec{B}$$

- Fluid Velocity Field

$$\vec{v} \approx \hat{z} v_{||} + \hat{r} v_{\perp} \cos \psi + \hat{\theta} v_{\perp} \sin \psi$$

We find

$$J_{\perp} = \frac{J_0 (1 + \chi) \Omega_w}{\Omega_0 - \gamma_0 k_w J_0 c} \quad (1)$$

- Single-Particle Theory :

$$J_{\perp} = \frac{J_0 \Omega_w}{\Omega_0 - \gamma_0 k_w J_0 c}$$

- Energy Conservation :

$$\frac{1}{\gamma^2} = 1 - J_0^2 - J_{\perp}^2$$

- 1-D Wiggler Field :

$$\vec{B} = B_0 + B_w [\hat{r} \cos \psi + \hat{\theta} \sin \psi]$$

$B_0$  : guide field strength.

$B_w$  : pump field amplitude.

$\psi = k_w z - \theta$ , where  $\ell_w = \frac{2\pi}{k_w}$  is the wiggler period.

- Ampère's Theorem

$$\vec{\nabla} \times \vec{B} = -e \mu_0 n \vec{v}$$

$\hat{r}$  and  $\hat{\theta}$  components yield

$$\chi = J_{\perp} \frac{\omega_p^2}{\Omega_w k_w c} \quad (2)$$

- Volume currents of the wiggling electrons generate a dia/paramagnetic correction to the wiggler field.

Combine Eqs. (1) and (2) to obtain self-consistent  $J_{\perp}$

$$J_{\perp} = \frac{J_0 \Omega_w}{\Omega_0 - k_w J_0 c \left( \gamma_0 + \frac{\omega_p^2}{k_w^2 c^2} \right)}$$

- Resonance is shifted towards higher  $B_0$ , lower  $J_0$

- Group I ( $\Omega_0 < \gamma_0 k_w J_0 c$ )  $J_{\perp}, \chi < 0$ , the beam is diamagnetic.

- Group II ( $\Omega_0 > \gamma_0 k_w J_0 c$ )  $J_{\perp}, \chi > 0$ , the beam is paramagnetic.



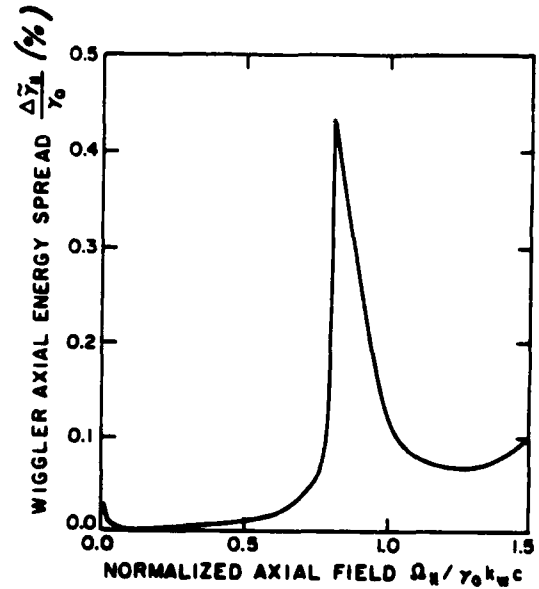
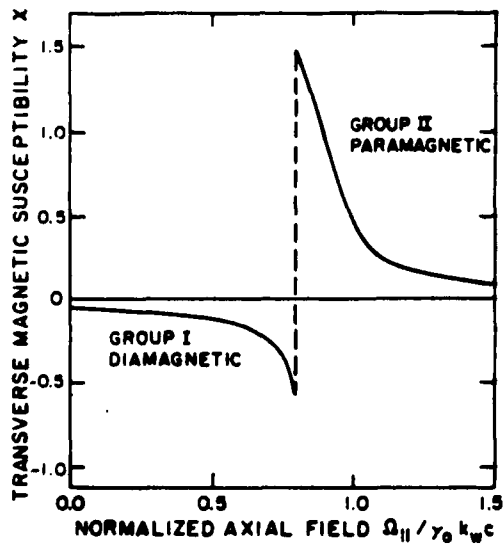
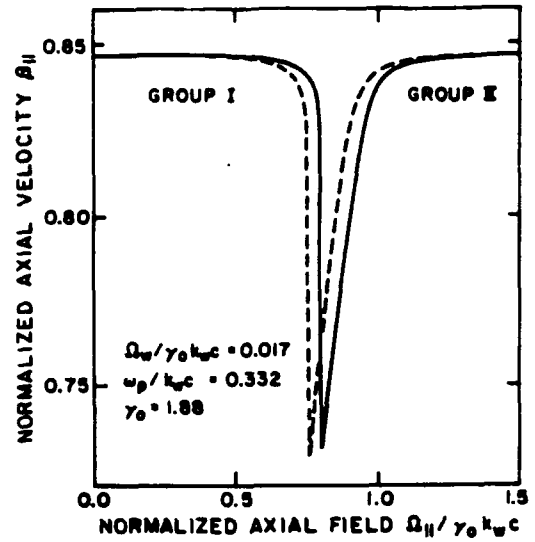
# 140 GHz CARM Design Parameters

## • Design Parameters

Beam Energy :	$V = 450 \text{ kV}$
Beam Current :	$I_b = 30 \text{ A}$
Beam Radius :	$r_b = 2.5 \text{ mm}$
Wiggler Period :	$\ell_w = 7.0 \text{ cm}$
Wiggler Amplitude :	$B_w = 50 \text{ G}$
Guide Field :	$B_1 = 2.5 \text{ kG}$

## • Normalized Parameters

$\epsilon = \Omega_w / \gamma_0 k_w c$	0.01734
$\sigma = \omega_p / k_w c$	0.3318
$\lambda = r_b / \ell_w$	0.03571
$\mu = \Omega_H / \gamma_0 k_w c$	0.877
$(\pi \sigma \lambda)^2$	0.138%



# P3.15

## DESIGN OF A 12 MEV RECIRCULATING BEAM ELECTROSTATIC ACCELERATOR FEL

D.J. Larson and Luis R. Elias  
Center for Research in Electro Optics and Lasers  
12424 Research Parkway, Orlando, FL 32826

The design of a 12 MeV electrostatic accelerator FEL is presented. The system will use recirculation of the electron beam in order to obtain ampere currents from an electrostatic system. Energy variability, coupled with the use of a microundulator, will allow continuous tunability of the system over wavelengths between 5 and 500 microns.

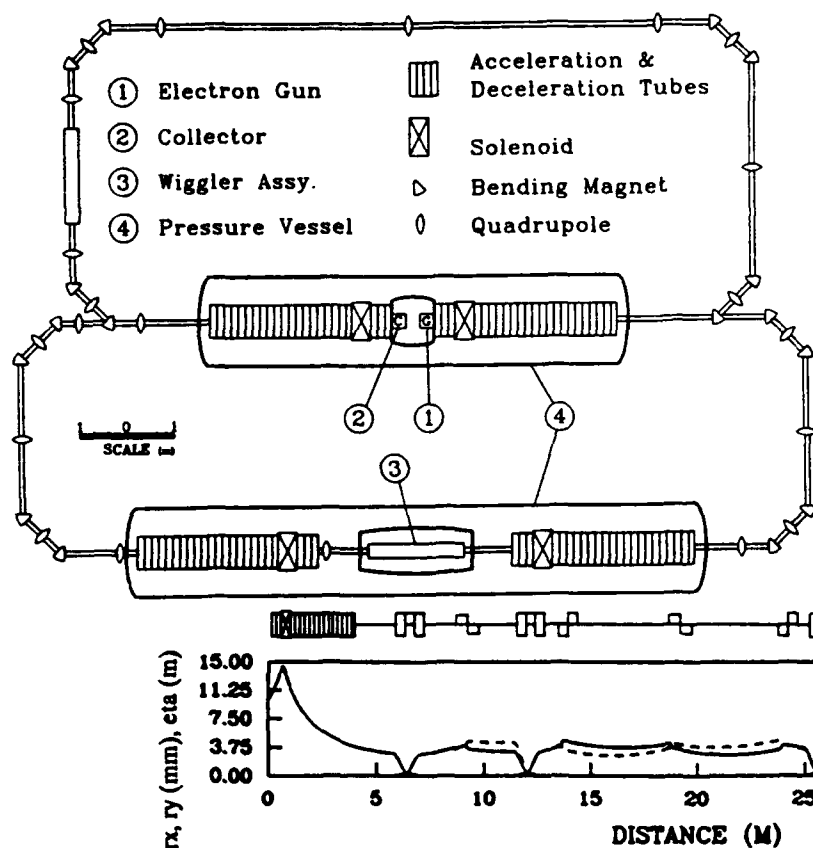


Figure 1. Design of a 6 and 12 MeV Electrostatic FEL system. Electron beam is accelerated from a negative 6 MV terminal, and can either go to an undulator at ground potential, or be accelerated to a positive 6 MV terminal that contains an undulator. System design uses achromatic 90 degree bends, resulting in a flexible, error forgiving design, at the cost of many additional magnetic components.

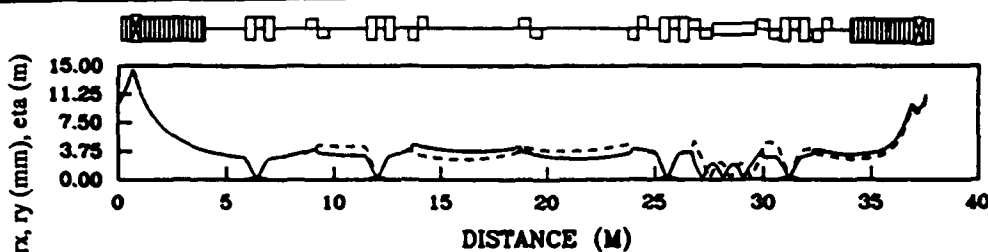


Figure 2. Beam size and dispersion as a function of distance along the 6 MV path of the system shown in Figure 1. Upper solid trace shows horizontal (bend plane) beam profile, dashed trace shows vertical profile, lower solid trace shows dispersion function.

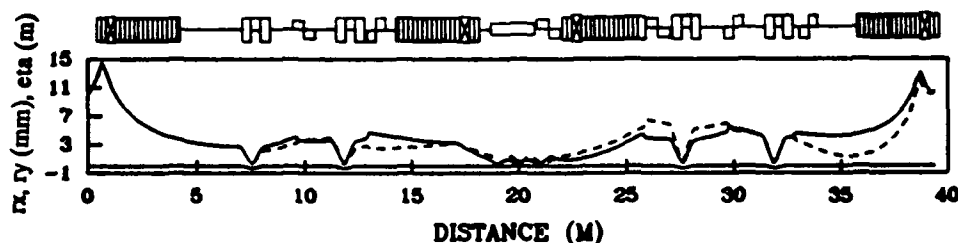


Figure 3. Beam size and dispersion as a function of distance along the 12 MV path of the system shown in Figure 1. Upper solid trace shows horizontal (bend plane) beam profile, dashed trace shows vertical profile, lower solid trace shows dispersion function.

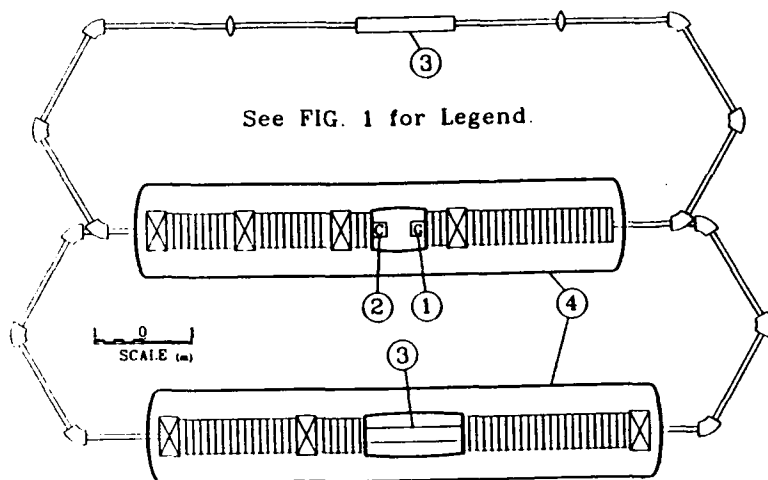


Figure 4. Design of a 6 and 12 MeV Electrostatic FEL system. Electron beam is accelerated from a negative 6 MV terminal, and can either go to an undulator at ground potential, or be accelerated to a positive 6 MV terminal that contains an undulator. System design uses three 60 degree chromatic bends for the 180 degree achromat, resulting in a design with very few magnetic components, at the cost of an inflexible, low tolerance design.

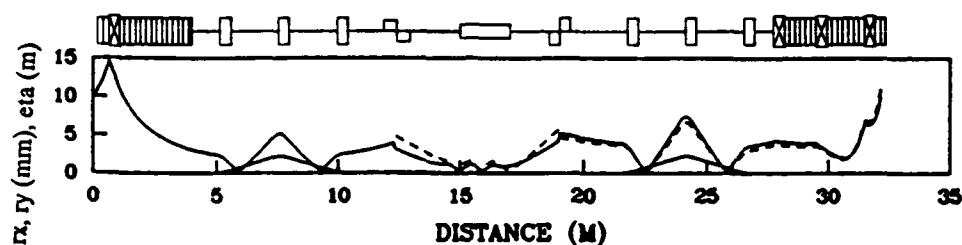


Figure 5. Beam size and dispersion as a function of distance along the 6 MV path of the system shown in Figure 4. Upper solid trace shows horizontal (bend plane) beam profile, dashed trace shows vertical profile, lower solid trace shows dispersion function.

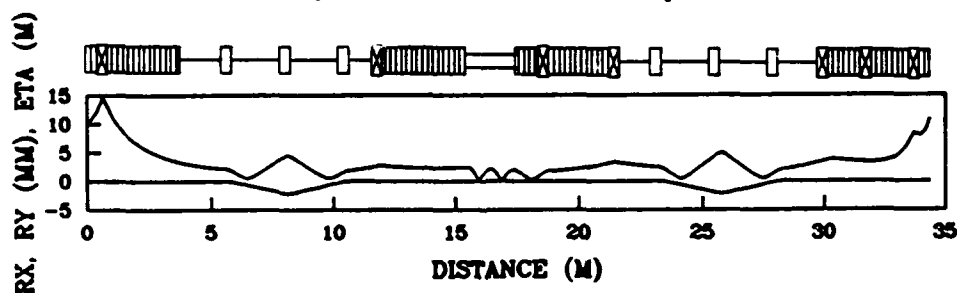


Figure 6. Beam size and dispersion as a function of distance along the 12 MV path of the system shown in Figure 4. Upper solid trace shows horizontal (bend plane) beam profile, dashed trace shows vertical profile, lower solid trace shows dispersion function.

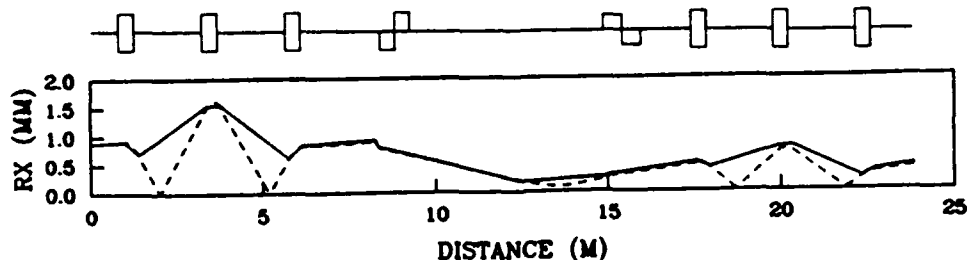


Figure 7. The above figures use the code SCAAT for beam optics calculations. SCAAT can include space charge. Here, the dashed trace shows the SCAAT calculation in the absence of space charge for the 6 MV horizontal beam profile of the system of figure 4. The solid trace is a TRANSPORT calculation of the same beamline. The undulator has been removed, and the matching conditions changed to allow for code comparison. (TRANSPORT only shows the profile from element to element, and does not show waist development between elements. TRANSPORT does not have an undulator element, requiring the modification of input.)

# P3.16

## A COMPARISON OF THEORY AND EXPERIMENT IN AN ALL FEL MASTER OSCILLATOR/POWER AMPLIFIER SYSTEM

Stephen V. Benson, John M. J. Madey  
Department of Physics, Duke University,  
Durham NC 27706

Bruce Richman  
Dept. of Applied Physics, Stanford University  
Stanford, CA 94305

Louis Vintro  
Deacon Research,  
Suite #203, 900 Welch Rd. Palo Alto CA 94305  
and

Anup Bhowmik and Wayne McMullin  
Rockwell International, Rocketdyne Division  
6633 Canoga Ave. Canoga Ave. 91305

Using the simulation code FELIX we have modelled the performance of an all FEL master oscillator/power amplifier. The results of the code are compared with the experimental results from the Stanford/Rockwell MOPA experiment. Excellent agreement is seen.

### Abstract

Extensive data has been accumulated on the operation of an all FEL master oscillator/power amplifier (MOPA) in the small signal regime. Gain was studied as a function of wavelength detuning, optical waist position, electron beam position and delay. Both the electron and the optical beam were well characterized by means of an electron beam spectrometer, emittance measurements, Strehl Ratio measurements, optical spectral measurements, and autocorrelation measurements. Using measured parameters for the electron and optical beam in the simulation code FELEX at Los Alamos National Lab, we have derived theoretical curves for the dependence of MOPA gain on all the parameters listed above. Excellent agreement was found. The extra information present in the simulation data allowed us to explain several curious features in the data. The results exemplify a number of special features of FEL operation at intermediate and high gain including the asymmetry of gain and absorption and optical mode distortion.

### Motivation

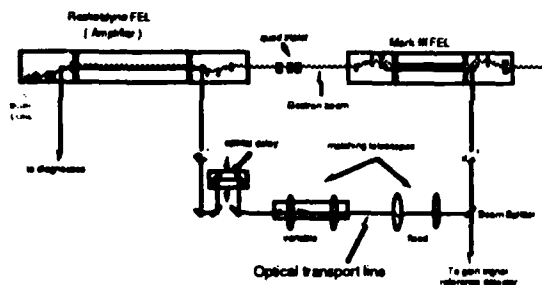
Early FEL master oscillator/power amplifiers (MOPAs) used a conventional laser as the master oscillator. The oscillator was not well matched in time and space to the amplifier though due to the different characteristics of conventional lasers and FELs. An all FEL MOPA solves this problem but makes the spatial and temporal overlap problem more acute. High gain effects make it difficult to match into the amplifier. The matching problem can be studied using simulation codes such as FELEX (developed at Los Alamos Natl. Labs) but these codes should be bench-marked against experimental results using realistic initial conditions. The electron beam and the optical output from the oscillator should be well characterized for the code bench-marking.

We have carefully measured the optical and electron beam characteristics of the Mark III FEL and accelerator and have matched the experimental results to the FELEX simulations.



Duke Free-electron laser lab.

### MOPA Schematic



Duke Free-electron laser lab.

### Experimental Electron Beam Parameters

Electron energy	30 MeV
Peak Current	35 A
Energy Spread (FWHM)	0.5%
Horiz. Emittance (μm)	10x mm-mrad
Vert. Emittance (μm)	4x mm-mrad
Micropulse length	2 psec.
Macropulse length	3 μsec.
Micropulse rep. rate	2857 MHz
Macropulse rep. rate	15 Hz

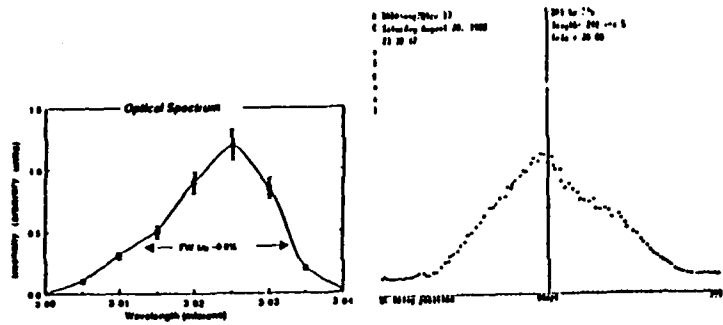
**DFELL**

Data Free-charge beam lab.

## Experimental Optical Beam Parameters

Wavelength	3.0 $\mu\text{m}$
Wavelength Spread(PW1%)	0.8%
Micropulse length	1.8 psec.
Macropulse length	2 $\mu\text{sec}$ .
Rayleigh Range(amplifier)	100 cm
Waist size	1 mm
Strehl Ratio	>0.7
Macropulse energy	3 mJ
Peak power at Small Signal	3 kW

## Optical Spectrum and Autocorrelation Function



Optical Spectrum at Small Signal

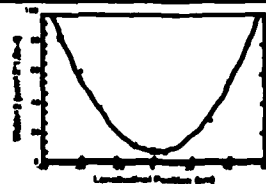
Autocorrelation Function at Small Signal showing Top-hat micropulse length. Micropulse length inferred from this measurement is 1.8 psec.

**DFELL**

Data Free-charge beam lab.

## Strehl Ratio Measurement

OPTICAL WAIST AT WIGGLER CENTER:  
S = 0.8  $\pm$  0.05



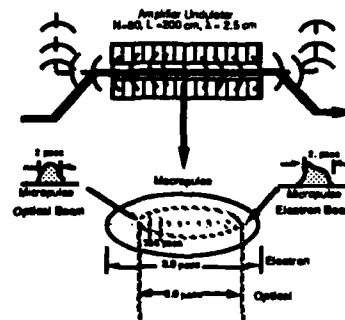
OPTICAL WAIST AT 40 CM FROM WIGGLER CENTER:  
S = 0.7  $\pm$  0.05



**DFELL**

Data Free-charge beam lab.

## Time Structure in Amplifier



**DFELL**

Data Free-charge beam lab.

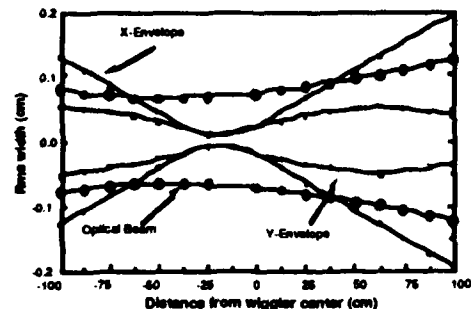
## FELEX Input Parameters

$\gamma$	70
$\delta\gamma/\gamma$	0.5%
Peak Current	30 A
Normalized Horiz. Emittance	30 nm-mrad
Normalized Vert. Emittance	50 nm-mrad
Magnetic Field in Amplifier	3.7 kG
Amplifier period	2.5 cm
Amplifier length	300 cm
Oscillator Wavelength	3.0 $\mu\text{m}$
Optical Waist Position	20 cm upstream of undulator center.

**DFELL**

Data Free-charge beam lab.

## Electron-Optical Beam Overlap



Beam envelopes used in simulation code

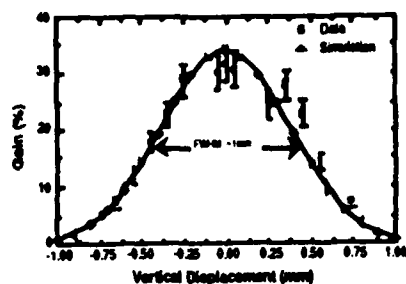
## Matching Results

The gain vs. horizontal and vertical beam position agrees well with simulations. Vertical overlap is consistent with the optical waist size. The horizontal overlap is less critical due to the larger beam size in that dimension. The gain vs. horizontal position was skewed. This is consistent with an electron beam tilted by 0.1 mrad. This is the alignment tolerance in the horizontal plane. We were able to get better alignment in another run which produced a wider, more symmetric curve. The gain vs. waist position agrees only when the waist is near the undulator center. This may be due to vignetting effects downstream when the waist is small and far upstream. The optimum match was seen to be when the electron beam and optical beam waists overlapped. Considering the gain, this is surprising but it does agree with the simulation.

DFELL

Sub: Free-electron laser lab.

## Gain vs. Vertical Displacement



SIMULATION FWHM: ~1mm

DFELL

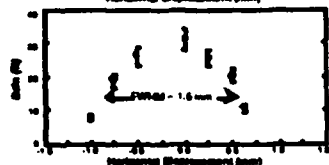
Sub: Free-electron laser lab.

## Gain vs. Horizontal Displacement

SCAN WITH SKEWED BEAM



ALIGNED BEAM

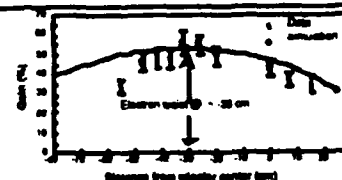


DFELL

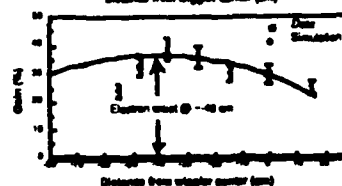
Sub: Free-electron laser lab.

## Gain vs. Waist Position

CASE I:  
Electron Beam  
Waist at -30 cm



CASE II:  
Electron Beam  
Waist at -40 cm



DFELL

Sub: Free-electron laser lab.

## Gain vs. Optical Delay

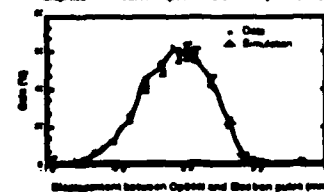
GAUSSIAN  
ELECTRON  
BEAM

Optical Delay  
Electron: 3ps



TOPHAT  
ELECTRON  
BEAM

Optical Delay  
Electron: 3ps



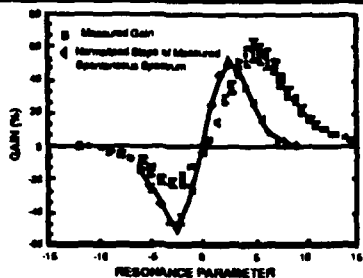
## Three Dimensional High Gain Effects

One expects an asymmetric gain curve which violates the gain-spread theorem at high gain. When three dimensional effects are taken into account, the effect occurs in the intermediate gain regime. The experimental gain curve is in strong disagreement with the slope of the spontaneous curve. It is in reasonable agreement with the simulations however (the agreement would probably be even better if a less conservative assumption had been made concerning the beam brightness). The strong asymmetry can be seen when the three dimensional gain is plotted vs. detuning for currents of 10 A, 35 A, and 100A with the peak gain normalized to unity. The loss part of the curve almost vanishes for the 100 A case. This is due to a distortion in the optical mode which produces a "hole" on axis and decouples the loss interaction. The gain curve is enhanced by the narrowing of the mode size caused by the interaction. This is seen as an enlargement of the beam in the far field.

DFELL

Date: Free electron laser lab.

### Madey Theorem Violated Due to Guiding Effects



Notes:

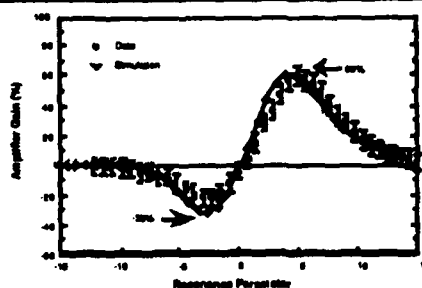
Resonance parameter was varied by changing the Magnetic field.

Proportionality constant set using 1-D gain calculation i.e. 50%

DFELL

Date: Free electron laser lab.

### Gain vs. Resonance Parameter



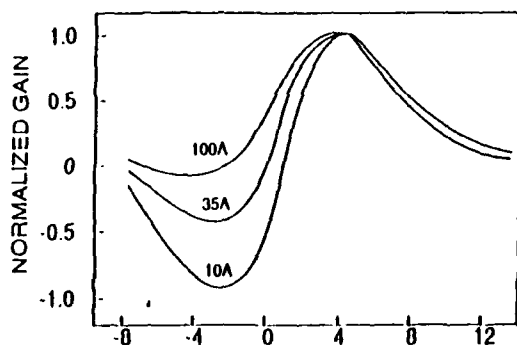
Simulation is from FELEX FEL code from  
Los Alamos National Laboratory

DFELL

Date: Free electron laser lab.

### Simulated Gain Curves vs. Electron Beam Current

FELEX simulations for low, intermediate and high gain for  
the Rockwell/Stanford MOPA parameters.  
Curves are normalized to the peak gain



DFELL

Date: Free electron laser lab.

### CONCLUSION

1. Gain maximized
2. Good agreement with simulations  
(short pulse effects, mode evolution)
3. Low vs. High gain:
  - a. Optical waist must overlap electron  
waist to maximize gain (low gain effect)
  - b. Asymmetry in gain curve cannot be explained  
by low gain Madey theorem
  - c. Simulation results of intensity distributions  
and iris experiment show qualitative agreement  
w.r.t mode evolution

DFELL

Date: Free electron laser lab.

### Mode Distortion at High Gain

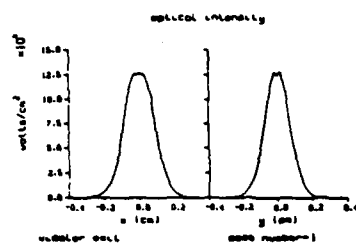


Figure 6-11(b) Transverse mode profile for 35A (intermediate gain)

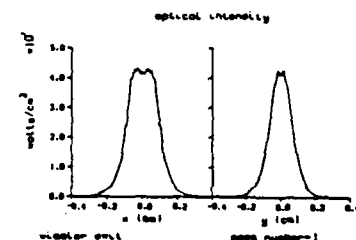


Figure 6-11(c) Transverse mode profile (high gain simulation)

# P3.17 Computer Simulation Of Cathode Heating By Back Bombardment In The Microwave Electron Gun

C. B. McKee and John M. J. Madey  
Department of Physics, Duke University  
Durham, N.C. 27706, 919-684-8144

An electron beam with low normalized emittance,  $2.5 \times 10^{-6}$  m rad, can be achieved by using a microwave electron gun as an injector for a RF linac. However, cathode heating caused by back bombarding electrons causes a ramp in the macropulse electron current structure. A transverse magnetic field can be applied at the cathode to reduce this effect. The simulation finds the optimum magnetic field.

Computer Simulation of Cathode Heating by Back Bombardment  
in the Microwave Electron Gun

C. B. McKee and John M. J. Madey  
Department of Physics, Duke University, Durham, N.C. 27706  
919-684-8144

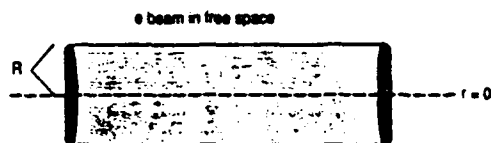
The electron beam emittance greatly affects the gain of a FEL. If the electron beam radius is comparable to or larger than the optical waist, the effectiveness of coupling between the electrons and the optical mode is reduced. In addition, transverse momentum spread increases the spontaneous inhomogeneous linewidth of the beam. To achieve a high gain, one needs a low emittance electron beam.

Lieville's Theorem states that in a system with a conserved Hamiltonian the microscopic emittance of a beam cannot be changed without losing some particles. However, the macroscopic emittance is increased by aberrations and nonlinear forces in the electron transport system. Therefore, the electron beam must be produced with the lowest possible beam emittance. The beam must also be transported and accelerated such that aberrations and nonlinear forces do not drastically increase the emittance.

Due to space charge and other effects at the cathode, the linear charge density of electron beams tends to increase with radial distances. Consider a charged particle beam whose particle density increases linearly with the radial distance up to a distance  $R$  and is zero beyond  $R$ .

Let all particles in the beam have a velocity of  $\beta$  parallel

to the  $z$  axis and no initial transverse velocity. Also let the beam be in a vacuum.



$N$  - particle density per unit length

By Gauss's Law, the electric field in the particle's rest frame for  $r < R$  is

$$E_r' = q N r^2 / (2 \epsilon_0 \pi R^3).$$

The fields in the lab frame are:

$$E_r = \gamma E_r'$$

$$= \gamma q N r^2 / (2 \epsilon_0 \pi R^3)$$

$$B_\phi = -\gamma \beta / c (\beta \times E_r')$$

$$= -\gamma q N r^2 \beta / (2 \epsilon_0 \pi R^3)$$

The force on one particle in the beam due to the rest of the beam is

$$F_r = (1 - \beta^2) N q^2 r^2 \gamma / (2 \epsilon_0 \pi R^3)$$

$$= r^2 / \gamma$$

Since a force that is proportional to  $r^2$  will increase the macroscopic emittance,  $\gamma$  needs to be as high as possible.



The electron beam emittance growth from a RF linac can be minimized by using a microwave electron gun instead of the traditional DC gun as the injector. By using a microwave field, the electric field near the cathode can be increased without generating arcs in the cavity or at the cathode. With the increased field, the electrons are accelerated quickly to relativistic velocities, thereby minimizing the effects of space charge forces.

The microwave electron gun was developed by S. A. Westenskow, John M. J. Maday, L. C. Vintro, and S. V. Benson. Using it as an injector, the Mark III RF linac at Stanford University achieved a normalized emittance of  $2.5 \times 10^{-6}$  m rad, with a brightness of  $5 \times 10^{11}$  A/m<sup>2</sup> rad<sup>2</sup>.

The microwave accelerating field in the RF gun can cause cathode heating during the current macropulse. A significant number of electrons that are emitted late in the RF period are not fully across the cavity before the accelerating field reverses direction. A number of these electrons are accelerated back towards and hit the cathode. These impacting electrons raise the temperature of the cathode. The raised temperature then increases the number of electrons emitted, causing a ramp in the current macropulse.

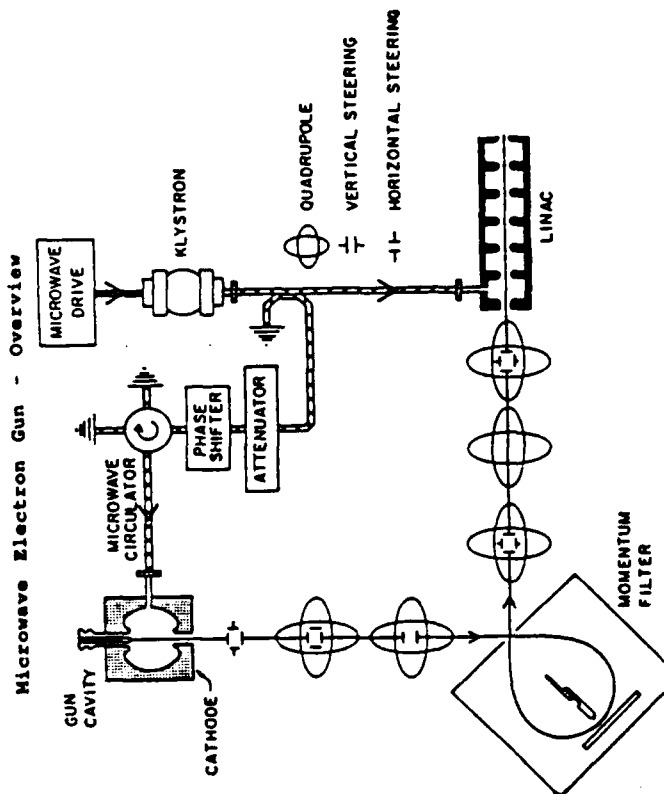
If one applies a transverse magnetic field across the cavity, some of the back bombarding electrons are deflected away from the cathode. However, the forward current is also affected by the applied magnetic field. The optimum field is one that deflects the back bombarding electrons, while having the least effect on the usable forward current (current of electrons with energy above 780 KeV) and

emittance.

The computer simulation is an effort to find this optimum magnetic field. By the use of simple electromagnetic formulas and an iterative process, the trajectories of the electrons through the cavity are calculated. Different possible applied transverse magnetic fields are simulated and the usable forward current and back bombarding energy for each is calculated.

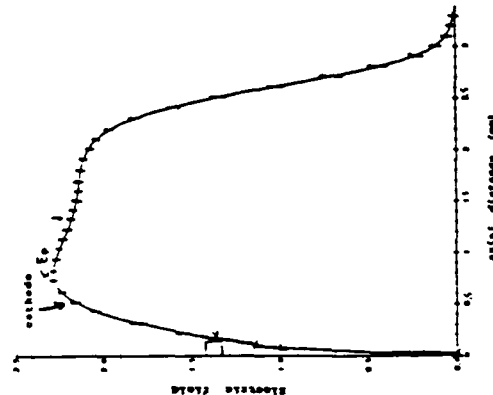
The initial simulation approximates the gun cavity to be a right cylindrical cavity in a perfect conductor. Only the TM<sub>010</sub> is excited. However, the time independent constant axial electric field for the TM<sub>010</sub> mode is replaced by  $E_0(z)$ , the electric field on axis given by the LALA computer code. The radial electric field is assumed to be zero and the magnetic field is found from  $\text{curl } E = -\partial B/\partial t$ . The total energy of the electrons that hit the cathode is calculated to be  $2.4 \times 10^{11}$  KeV/macropulse for the above fields. The optimum applied transverse magnetic field is a constant 50 gauss across the cavity. This applied field deflects 12% of the back heating energy, while leaving the usable forward current virtually constant.

The present simulations use a more accurate field and the dimensions of the new gun cavity. The fields are calculated from the Maxwell equations and the wave equation, given the field on the z axis from the LALA code. Results from these simulations should be available in the next few months.

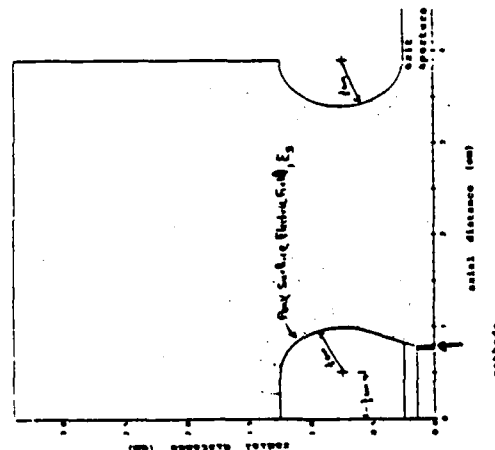


Microwave fields in the gun cavity

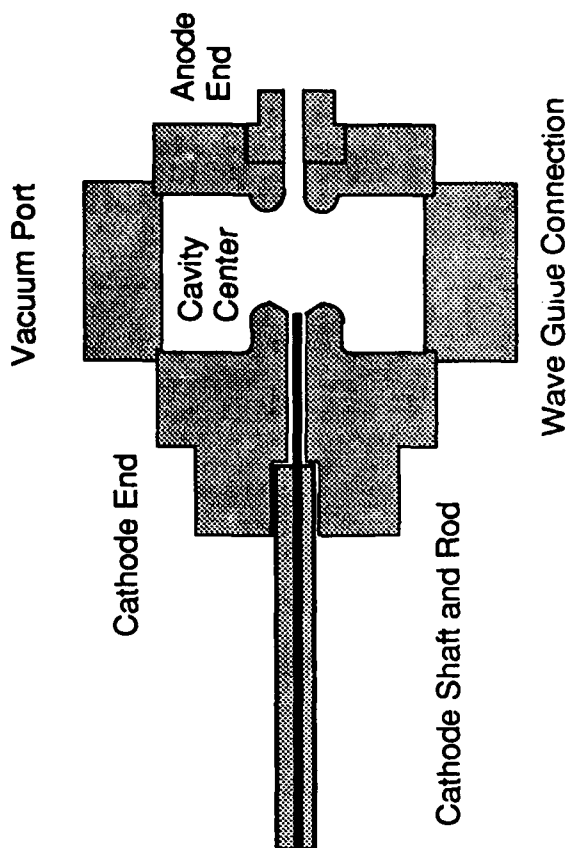
Axial Dependence



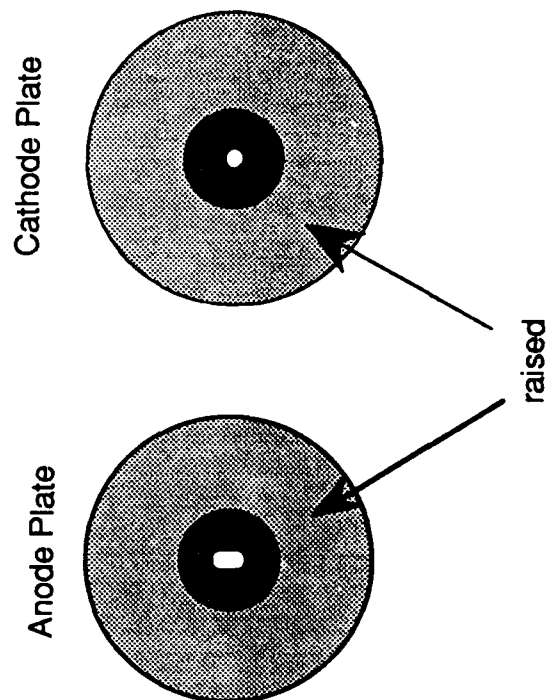
Radial Dependence



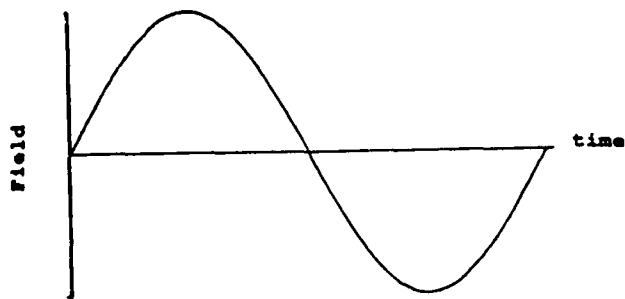
# Constructed Side View



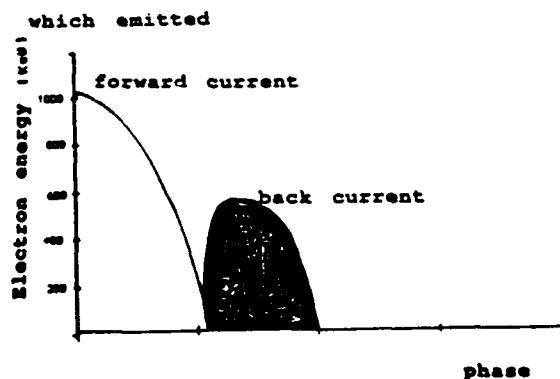
# End Plates



Back bombarding electrons  
Electric field versus time

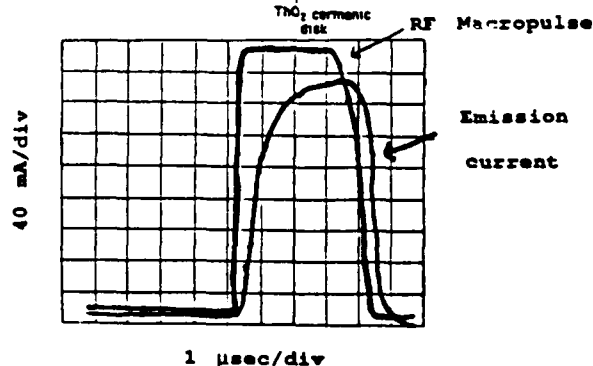
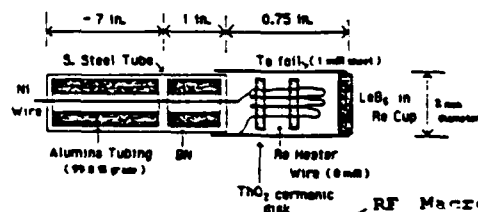


Electron energy versus phase in



# Cathode Heating

The power available to the cathode for electron emission is 4.62 watts. This results assumes the computer simulation prediction of the total energy of the back bombarding electrons of  $2.4 \times 10^{11}$  KeV per micropulse or 4.11 watts continuous. However, since the back heating energy is not continuous, the temperature of the cathode will vary with time. So as the back bombarding electrons hit the cathode, the temperature of the cathode increases causing a ramp in the micropulse current.



## A Possible Solution - Apply a transverse magnetic field

Consider only the microwave electric field and a constant applied transverse magnetic field. When

$$E(x,t) = 0,$$

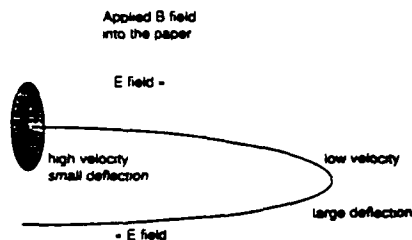
then

$$F = q(v \times B) \\ = mv^2/R,$$

where  $R$  is the radius of curvature of the deflection. Thus

$$R = mv / (qB).$$

Electrons at lower velocities are deflected more than electrons at higher velocities.



## Computer Simulation

### Assumptions

- No electron-electron interaction
- Electrons are not radiating
- No image charges

### Calculations of the fields

#### First simulation

$$E_z(x,z,t) = E_0(z) J_0(k_0 z/R) e^{-i\omega t} \\ E_0(r=0,z) \text{ given by LALA} \\ R \text{ given by the equation for resonance frequencies for TM cylinder modes.} \\ E_r(r,z,t) = 0 \\ B_\theta(r,z,t) \text{ from curl } E = -\partial B/\partial t$$

#### Present simulation

$$\text{Single frequency } \omega \\ E_0(r=0,z) \text{ given by LALA} \\ E_z(x,z,t) \text{ from wave equation} \\ E_r(x,z,t) \text{ and } B_\theta(r,z,t) \text{ Maxwell's equations using } E_z(x,z,t) \text{ as calculated above}$$

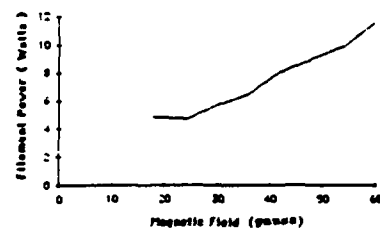
### Relativistic treatment

$$dp_H / dt = q v_H F_{EH}(z) \\ du_H = q / m v_H F_{EH}(z) dt \\ \text{For small time periods, } \Delta t \\ u_H^2 - u_0^2 = q/m v_H F_{EH}(z) \Delta t \\ u_H^2 - u_0^2 = u_H \Delta t$$

## Experimental data

Experimental data was taken to measure the filament power needed for a given output current for various applied magnetic fields. As the applied field increases, more of the back bombarding electrons are deflected from hitting the cathode. To keep the output current constant, the filament power has to be increased to make up for the power lost by deflecting the electrons from hitting the cathode. In addition, the applied magnetic field deflects some of the normal output current. The temperature of the cathode must be increased to compensate for this lost current.

The first computer simulation predicts that a 60 gauss field deflects about 23% of the back energy. The current of electrons with energies above 780 KeV is not affected. However, the experimental data uses the total current. The lower energy electrons are deflected more than the high energy ones.

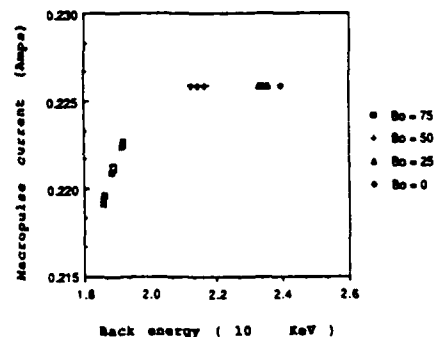


## Results

Assume the applied field depends only on  $x$ . Taylor series expansion about  $x = 0$ .

$$B(x) = B_0 + (dB/dx|_{x=0}) x + (d^2B/dx^2|_{x=0}) x^2 \\ = B_0 + B_1 x + B_2 x^2$$

### Back heating of the old MW Gun



Only the usable electrons, those with energy above 780 KeV, are included in the output current.

NOTE: The above data is from the first simulation.

## References

Colson, Classical Free Electron Laser Theory. To be published in Free Electron Laser Handbook.

Griffiths, David J., Introduction to Electrodynamics. Englewood Cliffs, N.J.: Prentice-Hall Inc., 1981.

Humphries, Stanley Jr., Principles of Charged Particle Acceleration. New York: John Wiley & Sons, 1986.

Jackson, J. D., Classical Electrodynamics. New York: John Wiley & Sons, 1975.

Johnson, C. C., Field and Wave Electrodynamics. New York: McGraw-Hill Inc., 1965.

Marshall, Thomas G., Free-Electron Lasers. New York: Macmillan Publishing Company, 1985.

Roberson, C. W., and P. Sprangle, "A Review of Free-Electron Lasers," Phy. Fluids B 1, Jan. 1989.

Westenskow, G. A., J. M. J. Madey, L. C. Vintro, and S. V. Benson, Owner's Manual for the Microwave Electron Gun. 1986.

## P3.18

### The ETA-II Induction Linac as a High Average Power FEL Driver\*

W. E. Nexsen, D. P. Atkinson, D. M. Barrett, Y.-C. Chen, J. C. Clark, L. V. Griffith,  
H. C. Kirbie, M. A. Newton, A. C. Paul, S. Sampayan, A. L. Throop, and W. C. Turner

Lawrence Livermore National Laboratory  
University of California, Livermore, California 94550

The Experimental Test Accelerator-II (ETA-II) is the first induction linac designed specifically to power an FEL. It is intended to demonstrate accelerator technology by driving 140 and 250 GHz FELs which will be used for plasma heating experiments in the Microwave Tokamak Experiment (MTX) at LLNL.

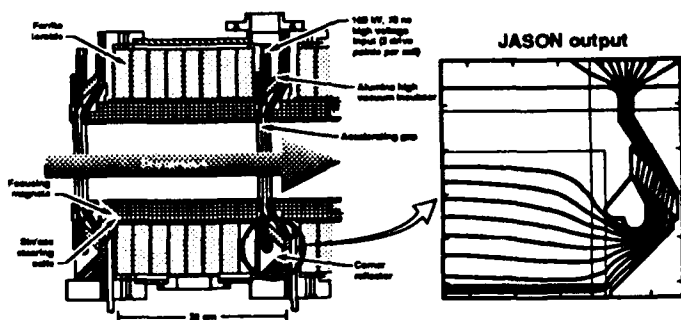
\* Work performed under the auspices of the US Department of Energy by the Lawrence Livermore National Laboratory under W-7405-ENG-48. ETA-II accelerator development is part of SDIO/SDC's induction free-electron laser Science and Technology Program.

#### ETA-II is a testbed for high power IFEL technology

Parameter	ETA-II Goal	Date
Brightness ( $A/m^2 \text{ rad}^2$ )	$>2 \times 10^9$	11/88
Current (kA)	2.2 3.0	1/89 6/89
Beam energy (MeV)	6 10	4/89 1/91*
Energy sweep (head to tail)	$\pm 1\%$ , 50 ns	4/89
Energy stability (pulse to pulse)	$\pm 0.1\%$	7/89
Flux line alignment ( $\mu m$ )	$\pm 100$	11/89
Centroid displacement ( $\frac{\Delta x}{x}$ )	$\pm 1 \text{ mm}$ , 50 ns	4/89
Rep rate (kHz)	5	5/89(0.01 sec)
Duration (sec)	0.5	10/91*

#### ETA-II Induction Cell Design

- Designed to minimize beam breakup (BBU) instability.
- Ferrite loading looks like transmission line.
- Uniform electric field along surface of insulator less than 50 kV/cm. Field stress in gap less than 200 kV/cm.

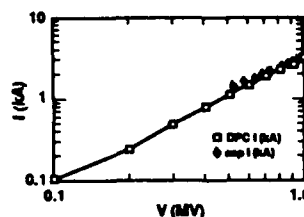
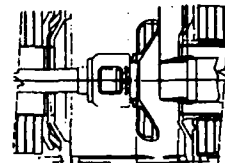


- No evidence of the BBU seen at up to 3 kA beam current.
- High voltage breakdown across the vacuum surface of the insulator is an intermittent problem. Cause is under investigation.

#### The ETA-II 3 kA Injector Design

- Injector required to supply 3 kA beam current at an A-K voltage of 1 MV.
- DPC code used to design diode injector configuration.

Cathode Type "M"  
Diameter 12.7 cm  
Radius of curvature 36.5 cm  
A-K gap 7.6 cm



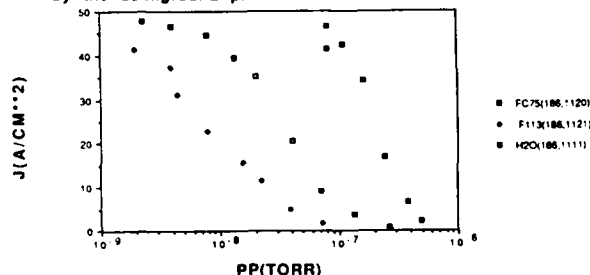
- The experimental I-V data agrees well with the predictions of the DPC code.

#### ETA-II Injector Operation Requires High Vacuum

o FEL experiments will require 3 kA, 50ns beam pulses at a 5 kHz PRF for 0.5 sec.

o A "M" type dispenser cathode capable of pulse current densities greater than 50 A/cm<sup>2</sup> is used.

o In early operation the cathode emission was poisoned by the background pressure of Freon113.

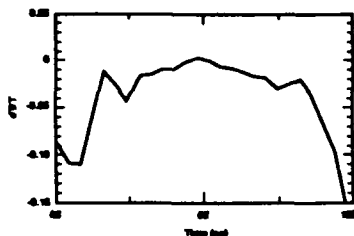
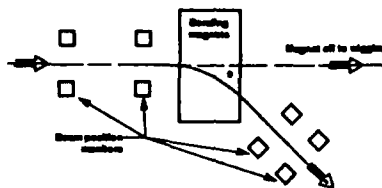


o Use of Fluorinert(FC75) and Viton O-rings in the induction cells produced low 10<sup>-8</sup> Torr base pressures (residual gases are mainly water vapor and CO) and eliminated the poisoning.

o Using a 5" diameter type "M" cathode we have met our requirements for a 3 kA, 50 ns pulse width, beam.

### ETA-II Beam Energy Measurements

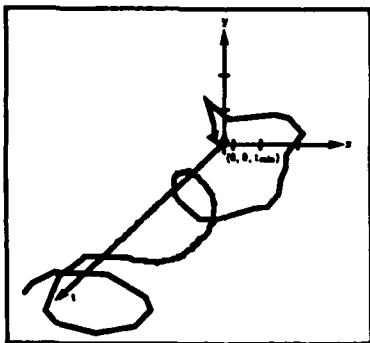
- Energy analyzer uses beam position monitors to measure bending angle. Energy variation of 0.1% can be resolved.



- Efficient FEL operation requires beam energy regulation within  $\pm 1\%$ . In present operation the energy variation is within this range for about 10 ns.

### Corkscrew Mode

- Field line tilt plus energy variation cause corkscrew motion of the beam

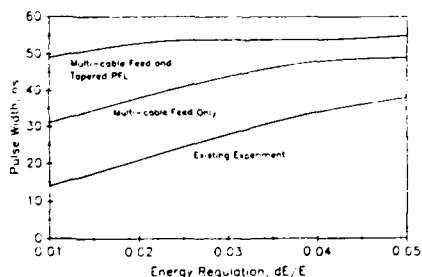


- Corkscrew at the exit of ETA-II accelerator for one set of conditions is shown above
- Efficient FEL operation requires corkscrew amplitude  $< 1$  mm and 0.1 mm alignment of the magnetic axis

### Meeting the Energy Regulation Goals

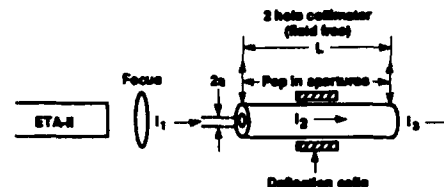
- ETA-II energy regulation goal is  $\pm 1\%$  for 50 ns.
- Reconfiguration of cell power feed plus passive compensation is required.
  - Present feed distorts high voltage pulse.
  - Response of cell ferrites is ignored.
- Multi-cable feed will eliminate distortion.
- Tapered PFL will compensate for ferrite response

### ETA-II Energy Regulation Simulation Results



- Model predicts energy regulation goal can be met.

### ETA-II brightness is measured with a two hole collimator



$$J = \text{brightness} = \frac{1}{(2a)^2} \frac{I_2}{V_0} \frac{1}{L}$$

$$V_0 = \text{phase space 4-volume} = \pi^2 a^4 L^2$$

$$\delta = \text{space charge correction} = (2\pi L I_2 / a^2 V_0) \delta L$$

$$a = 0.15 \text{ cm}$$

$$L = 67.5 \text{ cm}$$

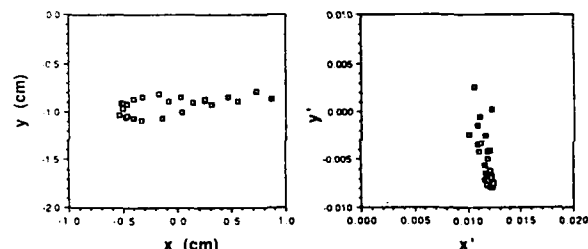
Energy (MeV)	$I_1$ (A)	$I_2$ (A)	$I_3$ (A)	$J$ (A/m-rad) <sup>2</sup>	$\delta$	Date
6	1372	46	0.4	$3 \times 10^8$	0.94	DB171F0200

### ETA-II Magnetic Alignment

- Correction coil current ratios for producing a cell block magnetic axis straight to within 0.1 mm of the mechanical axis were obtained by low energy electron (LEEP) mapping.

- Cell blocks were optically aligned with respect to each other.

- Intercell solenoids were mechanically aligned. Field errors produce corkscrew.



- Above corkscrew caused by  $\pm 2\%$  energy variation is predicted to cut FEL power in half.

- LEEP gear for aligning the complete accelerator is under construction.

### ETA-II Program Summary

- As a test bed for high average power technology ETA-II and associated experiments have satisfied their initial goals.

- Magnetic alignment and energy flatness are perceived as the most important problems faced in meeting the future goal of high average power.

- Solutions for these problems are ready to be implemented and tested on ETA-II.

- LEEP will be used for magnetically aligning the entire accelerator.

- Replacement of present cell block pulse power feeds with multi-cable feeds plus passive compensation should give required energy flatness.

- These changes are scheduled for the next year.

## P3.19 Final Design and Cold Tests for a Harmonic Ubitron Amplifier Experiment\*

H. Bluem,\*\* R.H. Jackson, D.E. Pershing†  
Naval Research Laboratory, Code 6840  
Washington, D.C. 20375

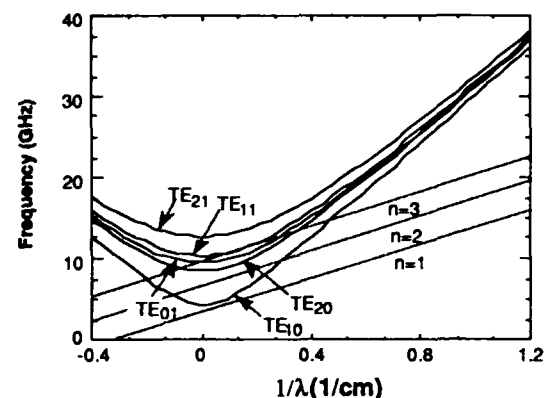
J.H. Booske and V.L. Granatstein  
Lab. for Plasma Research, University of Maryland  
College Park, MD 20742

The experiment will examine harmonic operation in a Ku band Ubitron. Three dimensional nonlinear simulations of the interaction predict untapered efficiencies of 3% for the third harmonic and 7% for the second harmonic periodic position. The project is presently in the cold test and assembly stage.

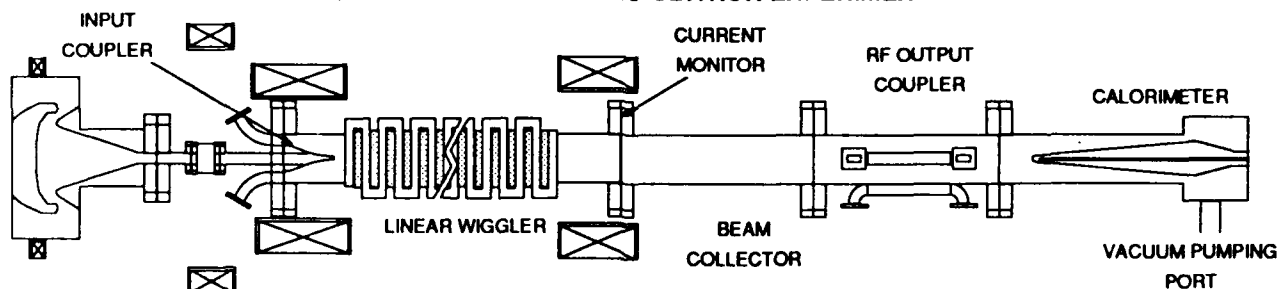
### Introduction

- Ubitrons/FELs are high voltage devices,  $V > 100$  kV.
- For many applications higher frequencies at lower voltages are desired.
- Harmonic operation of the ubitron is a possible way to increase the frequency while keeping the voltage low and the wiggler period large enough to be practical.
  - For a given frequency and wiggler period the voltage reduction scales as  $n^2$  as voltage goes to zero and  $\sqrt{n}$  at high voltages.
  - In waveguide configurations, cutoff properties and grazing incidence operation can be utilized to control the possible interactions.
  - However, lower gain, bandwidth, and greater restrictions on axial velocity spread are also characteristic of harmonic operation.

### UNCOUPLED DISPERSION CURVES



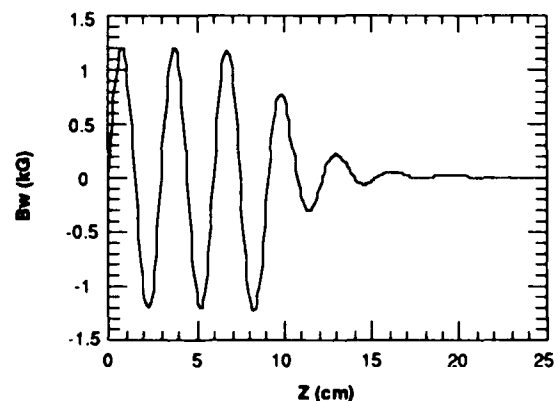
### SCHEMATIC OF HARMONIC UBITRON EXPERIMENT



### Harmonic Ubitron Experimental Parameters

harmonic no.	1	2	3
waveguide mode	TE <sub>01</sub>	TE/TM <sub>11</sub>	TE <sub>01</sub>
voltage (kV)	250	120	55
current (A)	25	15	10
Bw (kG)	1.5	1.5	1.0
calc. efficiency (%)	>15	7	3
waveguide height (cm)		1.58	
waveguide width (cm)		3.48	
Rb (cm)		0.25	
lw (cm)		3	
frequency (GHz)	12.4-18		

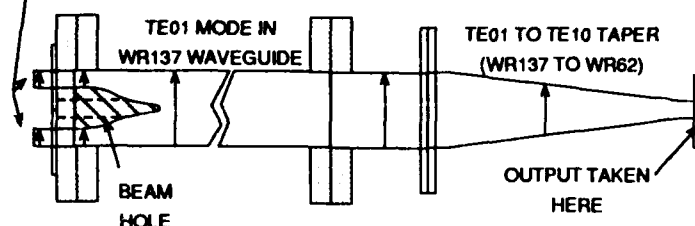
### ON AXIS FIELD OF 8 LAYER WIGGLER



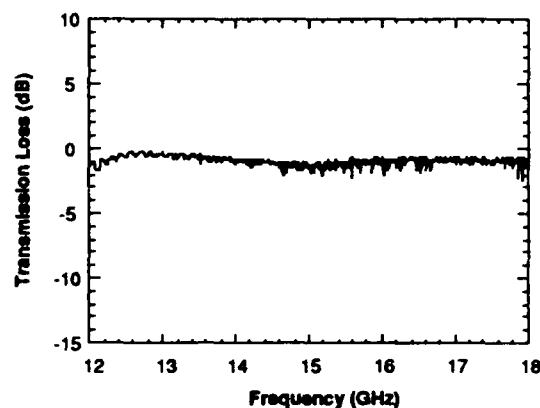
## INPUT COUPLER COLD TEST CONFIGURATION

TWO EQUAL AMPLITUDE,  
IN PHASE INPUT SIGNALS,

TE<sub>10</sub> MODE IN WR62



## Frequency Response of Input Coupler to TE<sub>01</sub> Mode



## PERFORMANCE OF RF INPUT COUPLER

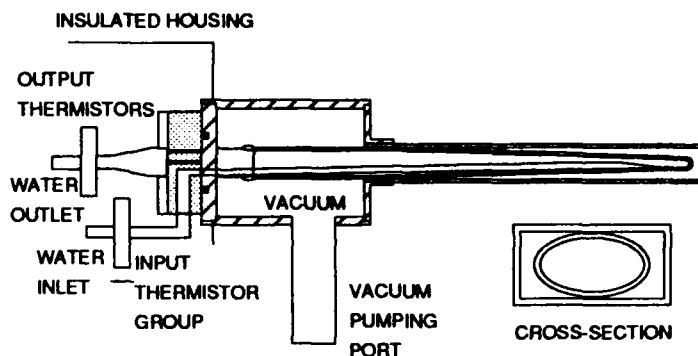
Efficiently launches a TE<sub>01</sub> mode into oversize waveguide  
(losses ~ 1 dB)

Mode purity is good (spurious modes are at least 10 dB below  
desired mode, TE<sub>10</sub> is >20 dB below)

Beam hole contributes to mode conversion below 16 GHz, but  
has very little effect above 16 GHz

Phase difference between input ports is critical

## SCHEMATIC OF CALORIMETER



## CALORIMETER PARAMETERS

Flow rate: 100-1500 ml/min

Temperature Difference Resolution:  $\leq 0.01^\circ\text{C}$

Range of  $\Delta\text{Temp.}$ :  $0.1 - \geq 1.0^\circ\text{C}$

Pulse width:  $1\mu\text{s}$

Repetition rate: 10 - 60 Hz

Range of Measurable Average Power:  $< 1 - > 100\text{ W}$

Range of Measurable Peak Power: 10 kW - 10 MW

## SUMMARY

An experiment has been designed to study the feasibility of utilizing harmonics  
to lower the operating voltage of ubtrons

Operation at several harmonics will be achieved through voltage tuning

Third harmonic operation gives a factor of 5 voltage reduction

An eight layer REEL wiggler will provide fields up to 2kG with good uniformity

A higher order mode input coupler has been designed which couples efficiently  
over the entire waveguide band with mode control

A calorimeter design which provides flexible handling of average and peak  
power has been developed and is under construction

Complete assembly and operation are expected soon

\* Work supported by the Office of Naval Research

\*\* Laboratory for Plasma Research, Univ. of Md., College Park, MD 20742

† Mission Research Corp., Newington, VA 22122



## P3.20

ONDINE : Studies About A High Power Microwave F.E.L. At C.E.S.T.A.

H. BOTTOLLIER-CURTET, J. BARDY, C. BONNAFOND, C. BRUNO, J. DELVAUX, A. DEVIN  
P. EYL, J. GARDELLE, G. GERMAIN, J. LABROUCHE, J. LAUNSPACH  
P. LE TAILLANDIER, G. PITEL

Commissariat à l'Energie Atomique  
Centre d'Etudes Scientifiques et Techniques d'Aquitaine  
P.O.box 2 - 33114 LE BARP (France)

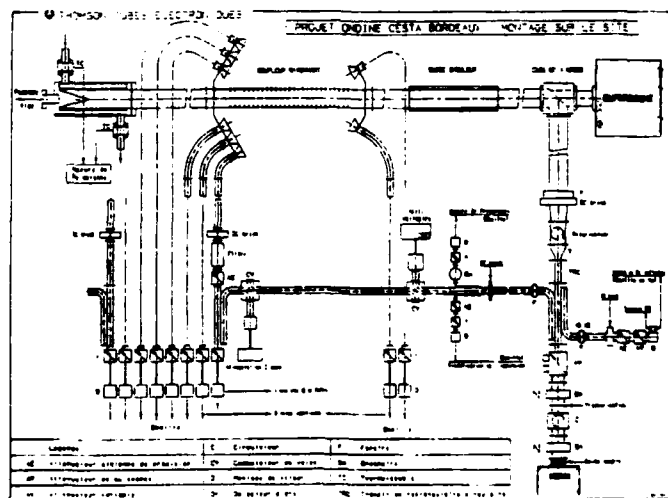
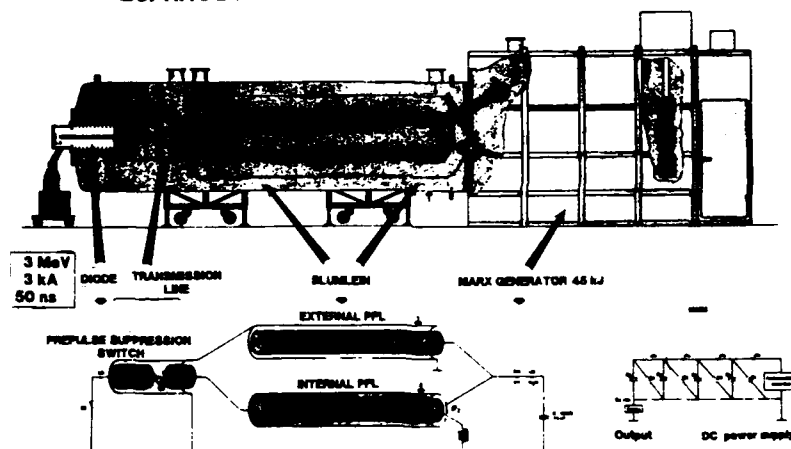
An Intense Relativistic Electron Beam Device (Marx generator + Pulse forming network + Hot cathode : 3 MV, 1 kA) is completed for investigation of a single pass amplifier at 35 GHz.

A bifilar helical wiggler with an adiabatic entrance immersed in a guiding magnetic field will be used and a tapered output is planned.

A wave number spectrometer has been carefully designed to give a precise multimode analysis in an oversized waveguide.

F.E.L. output is expected to be at several hundreds of MW.

### EUPHROSINE : A PULSED POWER ACCELERATOR



## ONLINE CHARACTERISTICS

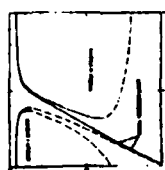
- $F = 35 \text{ GHz}$  ( $\lambda_p = 8.6 \text{ mm}$ )
- SINGLE PASS AMPLIFIER
- HOT CATHODE GUN
- $1.5 - 3 \text{ MV}$  B.A.  $70 \text{ ns}$  PUMP
- BIPOLAR HELICAL WIGGLER
- $A_w = 12 \text{ cm}$   $L_w = 3 \text{ m}$   $B_w = 25 \text{ T}$
- AXIAL MAGNETIC FIELD  $B_z = 1 \text{ T}$
- EFFICIENCY ENHANCEMENT
- INPUT SIGNAL  $50 \text{ mW}$  relating  $TE_{10}$  mode
- $\approx 8 \text{ cm}$  diameter guide

## PRECISE MULTIMODE ANALYSIS



## WIGGLER PARAMETERS FOR 35 GHz

Axial Magnetic Field  $B_z$



Steady-state trajectories

$$\begin{aligned} \dot{y}_0 &= \frac{1}{2} \frac{\partial \omega_p}{\partial y} / (1 - \beta^2)^{3/2} \\ \dot{y}_0^2 &= \frac{1}{2} \frac{\partial^2 \omega_p}{\partial y^2} / (1 - \beta^2)^{3/2} \\ y_0 &= \frac{1}{2} \frac{\partial \omega_p}{\partial y} / (1 - \beta^2)^{3/2} \end{aligned}$$

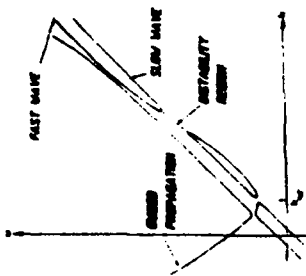
## FREQUENCY DETERMINATION

$$\begin{aligned} \omega_{ce} &= (k + k_0) \gamma_0 \frac{2 \pi \omega_p}{\omega_{ce}} / \gamma_0 \frac{1}{\gamma_0} \\ \omega_{ce} &= \frac{1}{2} \frac{\partial^2 \omega_p}{\partial y^2} / (1 - \beta^2)^{3/2} \\ y_0 &= \frac{1}{2} \frac{\partial \omega_p}{\partial y} / (1 - \beta^2)^{3/2} \end{aligned}$$

## Example

$$\begin{aligned} E_0 &= 3 \text{ MeV} & A_w &= 12 \text{ cm} & B_w &= 25 \text{ T} & B_z &= 1 \text{ T} \\ I &= 1 \text{ mA} & r_0 &= 5 \text{ mm} \\ r_0 &= 3 \text{ cm} & L_w &= 3 \text{ m} & F &= 35 \text{ GHz} \end{aligned}$$

## LINEAR GAIN AND EFFICIENCY



## 1D COLD BEAM THEORY

VLASOV - MAXWELL LINEARIZED

$$\Rightarrow \partial(\omega, k) = 0$$

$L_w$  Estimation of  $\Gamma, \eta$

STUDIES ABOUT FEL REGIME (RAMAN/COMPTON)

EXPERIMENTAL VERIFICATION

## MICROWAVE APPARATUS

### INJECTION LINE

- MAGNETRON LITTON L404-A  
 $34.85 \text{ GHz}$   $125 \text{ kW}$   $\Delta f = 800 \text{ ns}$
- VARIABLE CALIBRATED ATTENUATOR  $0-20 \text{ dB}$
- $TE_{10}$   $\square$  feed  $\rightarrow TE_{10}$   $\bigcirc$  rotating oversized  $\phi_0 = 60 \text{ mm}$
- WIRE MESH REFLECTOR ( $10 \text{ or } 16 \text{ I}$ )  
thickness:  $5 \mu$   
wire:  $10 \mu$   
space:  $200 \mu$
- $\Rightarrow$  EXPECTED MAXIMUM INJECTED POWER  $50 \text{ kW}$

## DIAGNOSTICS

- SPECTRUM ANALYSIS  
FERRETEC YIG FILTERS  $F_0 = 32 - 36 \text{ GHz}$   $\Delta F = 100 \text{ MHz}$
- MODE ANALYSIS  
NEAR FIELD MEASUREMENT OF A  
LEAKY WAVE ANTENNA  
coupling:  $-60 \text{ dB}$   
8 receiver antennas  
MEASUREMENT OF  $TE_{10}$ ,  $TE_{11}$ ,  $TM_{10}$ , MODES

## ELECTRON BEAM

$$\begin{aligned} V &= 1.5 \text{ to } 3 \text{ MV} \\ I &= 1 \text{ mA} \\ \Delta t &= 20 \text{ ns} \end{aligned}$$

## HF SOURCE: MAGNETRON

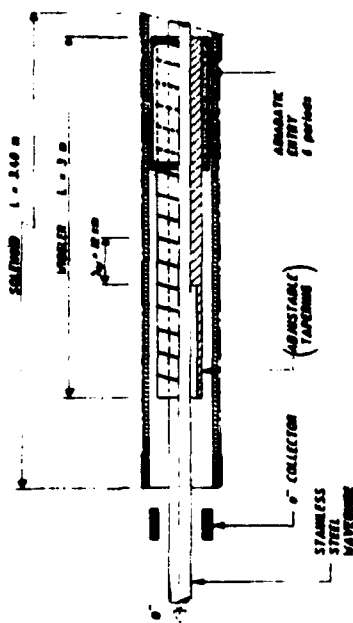
$$\begin{aligned} F &= 35 \text{ GHz} (\lambda = 8.6 \text{ mm}) \\ P_e &= 125 \text{ kW} \end{aligned}$$

## WIGGLER

$$\begin{aligned} A_w &= 12 \text{ cm} \\ L_w &= 3 \text{ m} \\ B_w &= 25 \text{ T} \end{aligned}$$

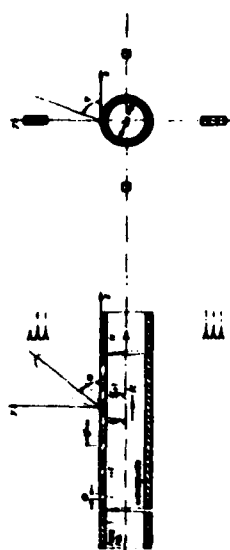
## GUIDING MAGNETIC FIELD

$$B_z = 1.2 \text{ T}$$



## NEAR FIELD MEASUREMENT OF A LEAKY WAVE ANTENNA

- 200 MELES
- $15 \times \phi = 2.5 \text{ mm}$  Gaussian Distribution
- $d = 3.5 \text{ mm}$ ,  $2\sigma = 30 \text{ mm}$
- $\phi_0 = \arccos \frac{d}{2\sigma}$ ,  $k_1$  = wave number of the mode,  $k_0 = \frac{2\pi}{\lambda}$
- 8 receiver antennas



## P3.21

### INTERACTION BETWEEN A RELATIVISTIC ELECTRON BEAM AND A RELATIVISTICALLY STRONG ELECTROMAGNETIC PUMP WAVE

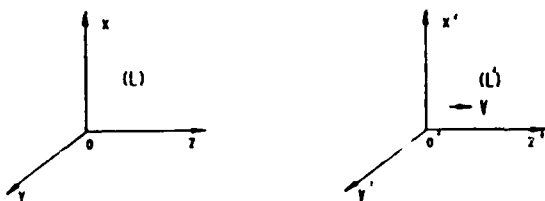
A. BOURDIER\*, J.M. BUZZI

Laboratoire de Physique des Milieux Ionisés, UPR 287 du CNRS  
Ecole Polytechnique, 91128 Palaiseau Cedex (France)

\* Also in Centre d'Etudes de Limeil-Valenton, BP 27,  
94190 Villeneuve-St-Georges Cedex (France)

We replace the wiggler by a strong electromagnetic pump wave. In a frame in which the propagation of the wave is time dependent only, we show that an electromagnetic wave can be amplified due to relativistic effects. The pump wave can propagate either along or perpendicularly to the beam.

We replace the wiggler by a strong electromagnetic pump wave which can propagate either along or perpendicularly to the beam. We show that, in the first case, the treatment of the interaction is greatly simplified by making a Lorentz transformation to a frame,  $L'$ , in which the spatial variable for the pump wave propagation no longer appears.



If we consider a superluminal wave propagating in the  $z$ -direction with the general form

$$\vec{A}(\vec{r}, t) = \vec{A}_0 f(\theta), \quad \theta = \omega_0 t - k_0 z$$

$$\omega_0 t - k_0 z = \gamma \left[ \omega_0 \left( t' + \frac{v}{c} z' \right) - k_0 (z' + vt') \right]$$

This quantity depends on time only in a frame  $(L')$  such as [1, 2, 3].

$$\frac{v}{c} = \frac{k_0 c}{\omega_0} = \frac{c}{v_\phi}$$

$v_\phi$  is the phase velocity of our wave in the lab-frame. Then in  $(L')$

$$\theta = \omega_0' t'$$

$$\text{with } \omega_0' = \frac{\omega_0}{\gamma}$$

If we wish to use the dipole approximation in the beam frame  $(F)$ , we must have [2]

$$(F) \sim (L')$$

which means  $(F)$  moves very slowly with respect to  $(L')$ . The condition which has to be respected is

$$v v_\phi \approx c^2$$

$v$  is the speed of the beam in the lab-frame.

Then it has a physical meaning to neglect the spatial dependence of the pump wave.

When our condition applies in  $(F)$ , the electric field of the pump is given by

$$\begin{aligned} E'_x &= \frac{1}{\gamma} E_x \\ E'_y &= \frac{1}{\gamma} E_y \\ E'_z &= E_z \end{aligned} \quad \vec{B}'_0 = 0$$

Here we assume there is no constant magnetic field.

Considering a pump wave propagating along the  $z$ -axis, we can obtain [4] (working in  $(F)$ ) a Mathieu eq. for the perturbation of the magnetic field. This situation is not very interesting as the factor  $\gamma$  can be very high.

We study in detail the more interesting case when the pump propagates perpendicularly to the beam (in  $(F)$ ). The electric field  $\vec{E}_0$  is assumed to be in the  $z$ -direction. We start with Maxwell's and Lorentz's Eqs.. Combining the zeroth order Eqs. we determine the form of the pump wave in  $(F)$  [3,5,6].

Then we linearize these equations and perform a Fourier transformation on space. We take the cross product with  $\vec{k}$  of one of

Maxwell Eqs. and of Lorentz Eqs. we combine the two Eqs. obtained. This leads to the following expression governing the magnetic field of the perturbation [1, 4, 6].

$$\left[ \frac{\partial^2}{\partial t^2} + \Omega^2 \left( 1 - \frac{\eta}{4} \cos 2\omega_0 t \right) \right] H_1 = 0$$

$$\Omega^2 = \omega_p^2 \left( 1 - \frac{1}{4} + \frac{c^2 k^2}{\omega^2} \right)$$

$$\eta = \frac{\epsilon}{1 - \frac{\epsilon}{4} + \frac{c^2 k^2}{\omega^2}}$$

$$\epsilon = v_0^2 = \left( \frac{eE_0}{m\omega c} \right)^2$$

as a consequence

$$\gamma_{\max} = \frac{1}{16} \frac{\omega}{p}$$

Let us consider for instance a beam such as

$$\frac{\omega}{p} = 10^{10} \text{ s}^{-1}$$

then, when  $v_0 = 0.3$  ( $\epsilon = 9 \cdot 10^{-2}$ )

$$\gamma_{\max} = 5.6 \times 10^7 \text{ s}^{-1}$$

In the very relativistic situation when  $v_0 = 0.91$ , ( $\epsilon = 0.83$ ), we have

$$\gamma_{\max} = 5.18 \times 10^9 \text{ s}^{-1}$$

Now, we must take into consideration a constant magnetic field  $H_0$  in our model.

#### References.

1. B.B. Winkles, Ph.D. thesis (University of Tennessee, 1972), available on University Microfilms, #12914.
2. A. Bourdier, G. Di Bona, and P. Gerllanoux, Phys. Lett. A 21, 2 (1975).
3. A. Bourdier, Thèse d'Etat, Université de Paris-Sud, Centre d'Orsay (1978).
4. N.L. Tsintsadze, Zh. Eksp. Teor. Fiz. 52, 1251 (1970) [Soviet Phys. JETP, 11, 684 (1971)].
5. A. Bourdier, D. Bamonneau, G. Di Bona and X. Fortin, Phys. Rev. 18, 1194 (1978).
6. A. Bourdier, G. Di Bona, X. Fortin, and C. Masselot, Phys. Rev. 11, 887 (1976).

## GAS LOADED FEL

$$\text{AT } \lambda = 600 \text{ \AA}$$

Meric Özcan  
Stanford University  
Electrical Engineering Dept.  
Stanford, CA 94305

Co-workers : R.H. Pantell  
J. Feinstein  
A. Ho  
H.D. Duman

The work is supported by National Science Foundation

### THE GAS LOADED FEL:

- Operating an FEL at short wavelengths is expensive as it requires a storage ring to provide very high energy electrons. The gas-loaded FEL is designed to obtain short wavelengths without the necessity of very expensive facilities.

- In a vacuum FEL, the electrons propagate with velocity;  
 $v_e = \beta c$ , where  $c$  is the vacuum velocity of light and  $\beta < 1$

Introducing a dielectric medium with refractive index  $n$  slows the light wave but does not significantly effect the velocity of the electrons.

The synchronism condition becomes:

$$(n-1) \pm \frac{\lambda}{\lambda_w} = \frac{1+\alpha_w^2}{2\gamma^2}$$

Thus a lower wavelength satisfies the synchronism condition for a given set of beam and wiggler parameters than in the vacuum case.

It is now possible to achieve net gain with the electron slipping or advancing by one optical period per wiggler period, as indicated by the plus or minus sign in the synchronism equation.

The advantages to adding a gas are:

1-The ability to tune the FEL over a large bandwidth. Wavelength shift from the vacuum wavelength:

$$\Delta\lambda = -\lambda_w(n-1)$$

2-A reduction in the cost and size of the accelerator for a given wavelength.

3-An increased gain per unit length.

### Potential problems with the GFEL:

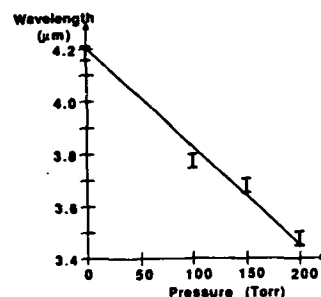
1-Alterations in the electron beam because of the scattering in the gas and the containing foil.

2-Plasma effects due to the ionization of gas molecules.

### GFEL EXPERIMENTS IN MARK III:

-GFEL first operated in MARK III. By introducing 200 Torr of gas we obtained 7300 Å wavelength shift in the infrared.

The plasma generated from the ionization of the hydrogen molecules diminished the oscillator gain, but this effect was eliminated by the addition of an electron attachment gas,  $C_4F_8$ . Gain was also reduced by multiple scattering of the beam electrons but this effect was not severe for a one meter of wiggler length. Also it was very sensitive to energy spread and focusing of the beam.



Tuning curve of GFEL in MARK III experiments.

### EXPERIMENTS IN STANFORD SUPER CONDUCTING ACCELERATOR:

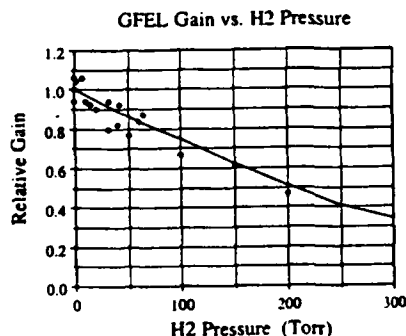
At the present time, GFEL experiments are conducted in Stanford Super Conducting Accelerator (SCA).

With an electron beam of 66 MeV, we obtained 350 Å wavelength shift from vacuum wavelength of 1.6 μm, with 5.8 Torr of hydrogen.

Future experiments are planned at SCA:

Goals are:

- Improve the gain.
- Lase at shorter wavelengths.
- Increase the gas pressure.



Theory  
Experiment

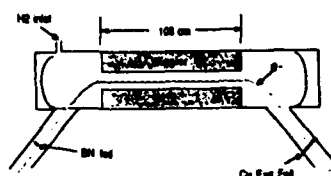


Diagram of wiggler and gas chamber for GFEL experiments in MARK III

### GFEL AT 600 Å:

-Near the electronic resonance of helium, which occurs at  $\lambda=584$  Å, the index of refraction becomes large, so it is possible to use low gas pressures, hence less degradation of the electron beam quality.

-With  $\gamma=220$ , and using typical electron beam parameters, 15 Torr of helium is sufficient to oscillate at  $\lambda=600$  Å with enough gain to overcome the mirror losses.

-Some small wavelength tuning is possible by changing gas pressure. For example, with 27 Torr of helium, oscillation wavelength becomes 615 Å.

-Other schemes to operate around  $\lambda=600$  Å, requires much higher energies, and have much more stringent requirements on the electron beam quality.

-In contrast to the vacuum FEL, here the wave falls behind the electron micropulse, since the operation near resonance leads to a reduction in group velocity for the wave, and in turn, this sets a limit on the wiggler length.

-Micropulse separation must be high enough (several tens of nanoseconds) in order for the plasma, which is produced by the collisions of electrons with gas atoms, to diffuse away.

-A helical wiggler is used to avoid the gain reduction resulting from the Bessel function coefficient.

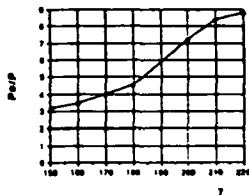
-Around 600 Å, mirror reflectivity is very low, this necessitates the use of a ring cavity with six or more multifaceted aluminum mirrors, which has round trip reflectance in excess of 50%.

-Absorption loss in helium is not as significant as mirror losses.

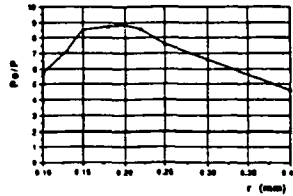
TABLE I

FEL operating parameters for helium loaded FEL

Wiggler length, $L_w$	115 cm
Wiggler period, $\lambda_w$	2.3 cm
Wiggler type	helical
Wiggler parameter, $a_w$	1
Electron energy, $\gamma$	220
Normalized beam emittance	$7 \pi$ mm mrad
Electron beam energy spread	0.2 - 0.4 %
Electron beam radius	0.2 mm
Peak current	100 A
Micropulse duration	6 psec
Micropulse repetition period	80-100 nsec

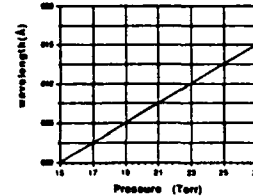


Single pass power gain vs beam energy at  $\lambda = 600$  Å

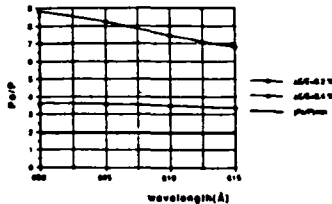


Single pass power gain vs electron beam waist size.

[  $\gamma=220$ ,  $\epsilon = 7 \pi$  mm mrad  
 $\Delta E/E = 0.2\%$  ]



Wavelength vs helium pressure,  $\gamma=220$ ,  $a_w=1$ ,  $\lambda_w=2.3$  cm.



Single pass gain vs wavelength for helium loaded GFEL.

(Po/P) denotes the single pass small signal gain. Since the gain is quite high it is evaluated at the exponential regime.

For  $\Delta E/E = 0.2\%$ , at  $\lambda = 600$  Å signal is amplified by a factor of 9, or 9.5 dB!

(Po/P)<sub>min</sub> is minimum required gain for the signal to build-up. It has a very high value because of the low reflectivity of the mirrors at these wavelengths.

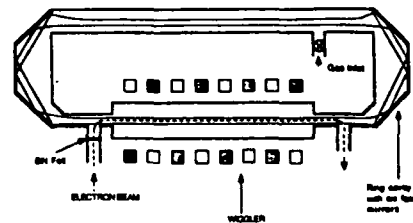


Diagram of proposed 600 Å GFEL; a helical wiggler with a ring cavity

A boron nitride foil is used inline with the electron beam, in order to prevent the gas entering the accelerator.

## P3.23

### Microwiggler Free Electron Laser Experiment

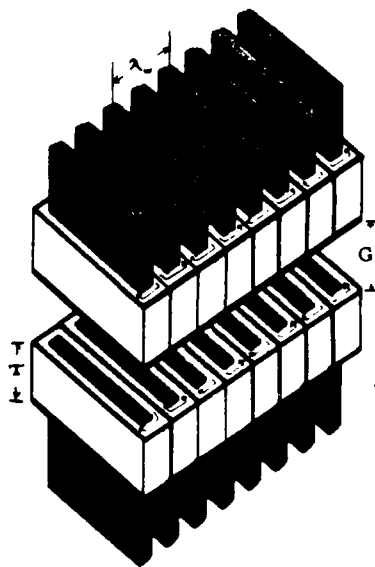
R. Stoner, S.C. Chen, and G. Bekefi

Department of Physics, Plasma Fusion Center, and Research Laboratory of Electronics  
MIT, Cambridge, MA 02139

We present experimental and computational results of several microwiggler structures having periods of 2.4–10 mm. Good tunability and precision of wiggler field are demonstrated. A peak field on axis of greater than 5 kG is achieved with a 5 mm gap. We also describe our microwiggler FEL experiment, (under construction) driven by a 450 kV Marx and a thermionic gun.

MIT Microwiggler Test Pieces — Physical Characteristics

	MW-1	MW-2	MW-3
Period	2.4 mm	8.4 mm	10.2 mm
Gap	3.0 mm	5.1 mm	5.1 mm
$B_{max}$	~800 G	~800 G	>4.6 kG
Number of Periods	30	5	4
Number of Coils Per Period	4	4	4
Number of Turns Per Coil	160 (40 AWG)	85 (32 AWG)	50 (32 AWG)
Ferro-Core $B_{sat}$	$\geq 10$ kG	>16 kG	>16 kG
Gauss per (ampere per coil) in linear regime	125	120	150
Tunability	—	Each half period independently tunable	—



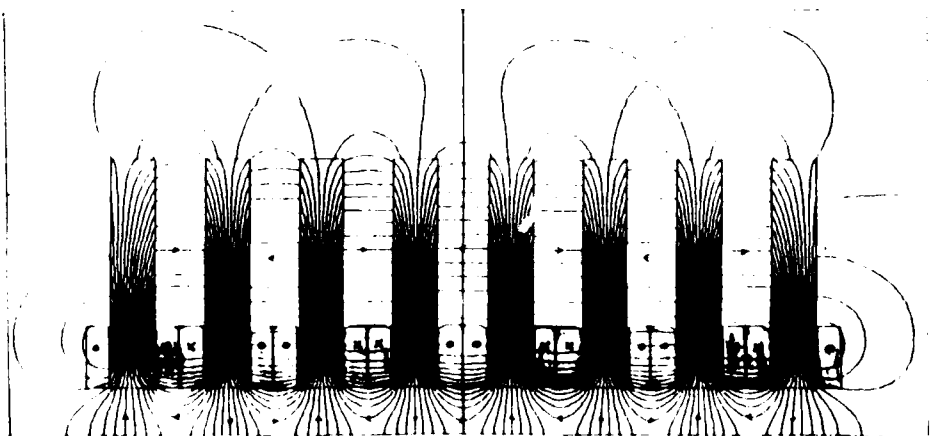
MIT Microwiggler MW-3

#### Goals of the MIT Microwiggler Project

- Design and build a tunable 50-period wiggler with a period  $\leq 1$  cm, peak field amplitude of 3 kG, and of better than 1% precision of periodicity.
- Design and implement a tuned wiggler field amplitude profile with random field amplitude errors of  $\leq 1\%$ .
- Develop e-beam optics for SLAC-style Pierce thermionic gun to obtain a beam of  $\sim 2$  mm radius.
- Integrate microwiggler, 450 kV Marx accelerator, and thermionic gun to produce/amplify  $\leq 1.8$  mm microwave radiation.

#### MW-3 Design Greatly Increases Flux Density Delivered Across the Gap

- We placed the current windings as close as possible to the gap, and shortened and widened the poles pieces (as compared to MW-2):  
 $\Rightarrow$  MW-3's magnetic field per input current density is increased, and saturation field is many times larger than that of MW-2.
- $\Rightarrow$  "End effects" even at saturation-level fields are very small.
- We eliminated flux return paths and greatly simplified the core geometry:  
 $\Rightarrow$  Fabrication is made much easier, and the wiggler can be made very physically compact.

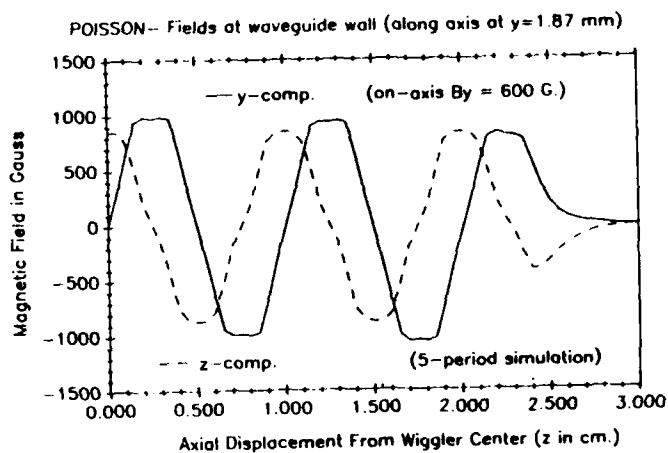
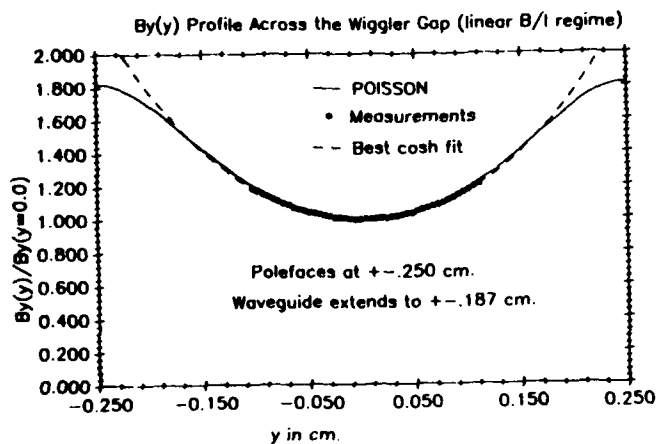
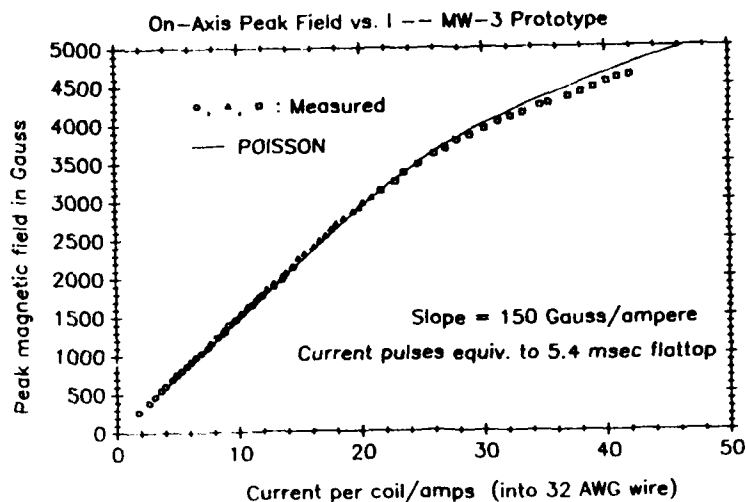


MW-3 MAGNETIC FLUX MAP (computed, POISSON)

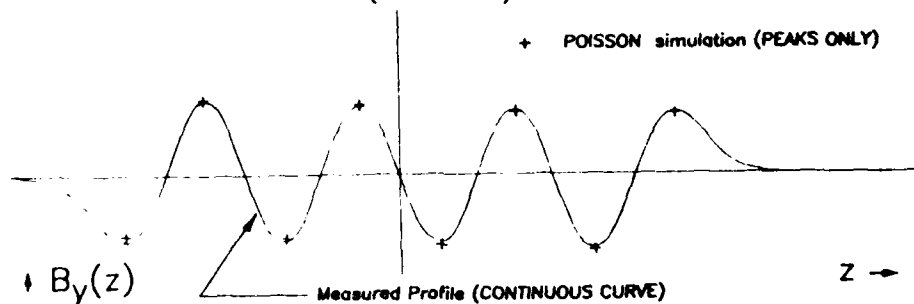
### Field Properties of the MW-3 Prototype

The following illustrations describe field properties of the MW-3 prototype:

- Peak field (on axis) vs. input current at a location near the middle of the wiggler (MEASURED).
- Wiggler field profiles along the wiggler axis — untuned, and tuned to a flat amplitude profile (MEASURED).
- Transverse field profile (MEASURED).
- Off-axis wiggler and axial field (CALCULATED, using POISSON).



### MW-3 MEASURED ON-AXIS FIELD (UNTUNED)





### A "Copper-Only" Pulsed-Wire Wiggler Concept Provides a Basis for the MW-3 Design

- We have derived an analytical expression for a 2-d pulsed-wire structure (see next page for geometry): it is

$$B_y(y, z) = \frac{8j\lambda}{\pi c} \sum_{\text{odd } n > 0} \left\{ \frac{1}{n^2} \left( 1 - e^{-\frac{j\pi n y}{\lambda}} \right) e^{-\frac{\pi n z}{\lambda}} \sin \frac{n\pi}{2} \right. \\ \left. \times \sin \frac{n\pi C}{\lambda} \cosh \frac{2\pi n y}{\lambda} \cos \frac{2\pi n}{\lambda} z \right\}$$

( $j$  = current density in conductors) for the field inside the wiggler gap.

- Lowest harmonic: the  $\left( 1 - e^{-\frac{j\pi n y}{\lambda}} \right)$  dependence means diminishing returns from extending conductors in the  $y$ -direction; and the  $e^{-\frac{\pi n z}{\lambda}}$  dependence means keep  $G/\lambda$  as small as possible (a general result, of course).
- Hence, for MW-3 — crowd as much current (conductor-borne and magnetization-induced) as close to the polefaces as possible. Windings therefore extend right to the polefaces and fill up the spaces between the ferro-cores.

### MIT Microwiggler FEL Experiment is Currently Under Development

- e-beam:
  - 1.5 mm radius,  $\Delta\gamma/\gamma < .01$
  - 10 Amperes at 450 kV:  $\gamma = 1.88$ ,  $\beta = 0.847$
  - SLAC-style Pierce thermionic gun/Marx bank
  - Axial guide field (2-plane wiggler focussing may also be feasible)
- Wiggler:
  - 1 cm period, 50 periods
  - 5 mm gap/planar geometry
  - B/I linear to 3 kG, max. field  $\gtrsim 5$  kG achieved by prototype MW-3
- Waveguide:
  - Cylindrical, 3.75 mm diameter
  - Cutoff frequency = 61.2 GHz
  - Serves also as electron drift tube and axial guide field magnet core
- FEL output
  - $\lambda_w = 1$  cm,  $\beta = .847 \Rightarrow$  Output  $\lambda = 1.81$  mm
  - $\Rightarrow$  Output  $f = 166$  GHz (fits in waveguide)
  - Single-pass gain  $\gtrsim 100\%$  (amplifier, linear regime)
  - Power output  $\geq 50$  kW (oscillator)

### Scaling MW-3 to a 5 mm Period/2.5 mm Gap

- To produce a given field amplitude as a 10 mm period/5 mm gap design, the 5 mm period/2.5 mm gap design requires twice the input current density. Therefore, to maintain a given field amplitude and a given conductor temperature increase per shot, field pulse durations must be reduced by a factor of 4.
  - A 5 mm period/2.5 mm gap design has the same saturation field as the 10 mm/5 mm system.
  - A 5 mm period/2.5 mm gap design has  $\frac{1}{4}$  the (L/R) rise-time of the 10 mm/5 mm system.
  - A 5 mm period/2.5 mm gap design has  $\frac{1}{4}$  the characteristic conduction cooling time of the 10 mm/5 mm structure: hence (4  $\times$  repetition rate) ( $\frac{1}{4} \times$  pulse length)
- $\Rightarrow$  Same duty factor is attainable with 5 mm/2.5 mm geometry as with 10 mm/5 mm design.

### Summary

- We have constructed a microwiggler prototype, MW-3, which has produced long-pulse (equivalent to  $\gtrsim 5$  msec flat-top) magnetic field amplitudes of nearly 5 kG. MW-3 produces a field amplitude linear in input current to about 3 kG.
- A 3 kG shot heats MW-3's copper conductors by  $\lesssim 2^\circ\text{C}$  per msec. A repetition rate of 1 Hz for 1 msec, 3 kG pulses should be attainable with air cooling only.
- General scaling laws show that a 5 mm period/2.5 mm gap, scaled-down version of MW-3 could operate at the same magnetic field duty factor as the full-sized version.
- We are developing a proof-of-concept microwiggler FEL experiment to produce/amplify 1.8 mm radiation.

### Reference

- [1] S.C. Chen, G. Bekefi, S. DiCecca, and R. Temkin, "Tunable microwigglers for free-electron lasers", Appl. Phys. Lett. 54 (14), 1299 (1989)

## P3.25

### MICRO-UNDULATOR RESEARCH AT UCSB

K.P. Paulson, Quantum Institute, University of California, Santa Barbara, CA 93106

Micro-undulator blocks made of Nd-Fe-B 100mm in length with a period of 4mm have been tested at the University of California at Santa Barbara. The measurements have shown that there are several problems dealing with micro-undulators. Methods to cope with them have been developed. Chief among them are large end fields due to the unique structure of the micro-undulator. As a possible solution a flux return path is used to overcome the end field. Other problems and solutions will be discussed. Field plots will be introduced.

#### FIGURES

- Figure 1. Micro-Undulator block made of Nd-Fe-B (Vacodym 370 by Vacuumschmelze). Polarized along the long (100mm) direction. The 2mm by 2mm grooves provide a 4mm period. The material left other than the crests is the bulk magnet
- Figure 2. The field created by a micro-undulator block in the absence of ferrous material. The large end fields need to be reduced.
- Figure 3. The flux return path used in the experiment. The hatched section is made of steel. The endcaps also cover some of the crest to provide some field tailoring.
- Figure 4. First integral of one of the blocks. The dotted line is for a measurement about 1mm from the crests, the solid line is taken 3mm away. Since the two lines agree this indicates that the problem is due to the bulk field. Note fluctuations in the angle. This is due to easy-axis rotation and is best solved by a thin bulk field along with steering coils and/or correction magnets.
- Figure 5. Micro-Undulator block field corrected using ferrous shims. The rms error is 0.5%. However 0.5mm further from the crests the error jumps to 3.7%. Therefore the correction due to the shims is localized in y. The corrections shouldn't be based only on rms error and correction methods shouldn't be localized in y. Methods to correct the field include steering coils and/or correction magnets on the back side of the bulk magnet.
- Figure 6. Dotted line is the first integral of Figure 5. The solid line is the first integral of the field without shims present. Note that even with 0.5% rms error the first integral still wanders. Again rms error does not give a good measure of field error.

#### CONCLUSION

The problems and solutions are:

- 1) Large end field: Correct by using flux return path
- 2) Easy-axis rotation: Correct by having thin bulk magnet along with steering coils and/or correction magnets
- 3) Peak field errors: It is best not to worry about rms error and correct the field as in 2)
- 4) Block to block variations: Correct by thin bulk field and method 2)

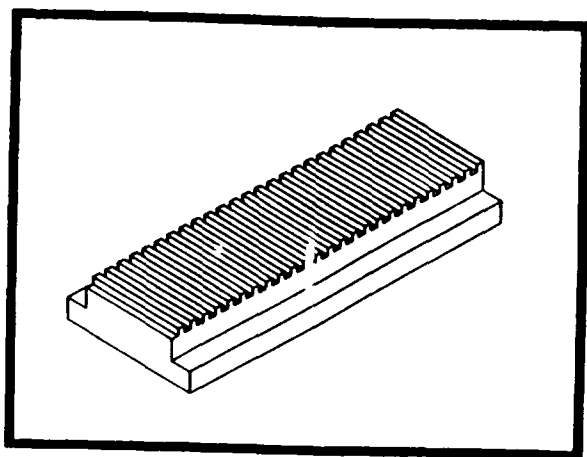


Figure 1

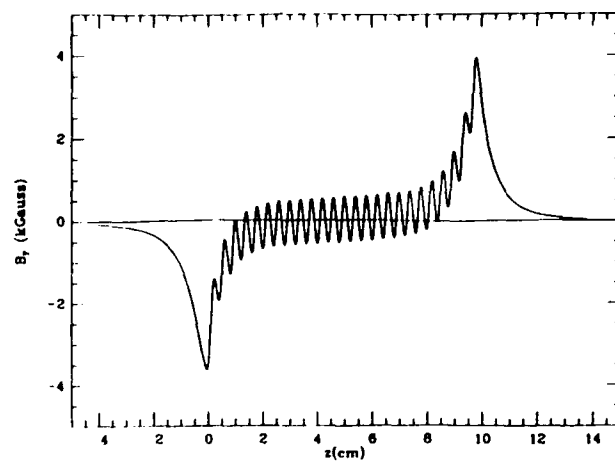


Figure 2

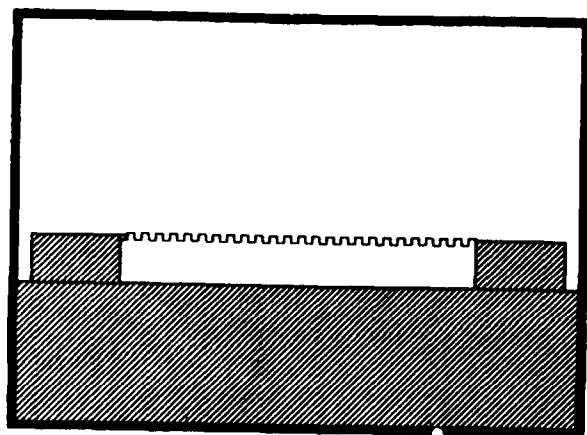


Figure 3

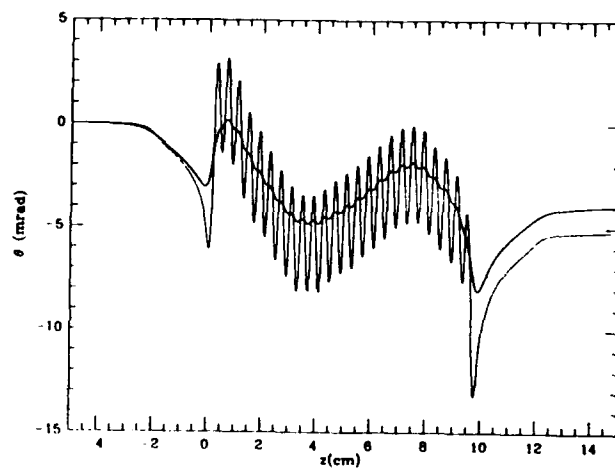


Figure 4

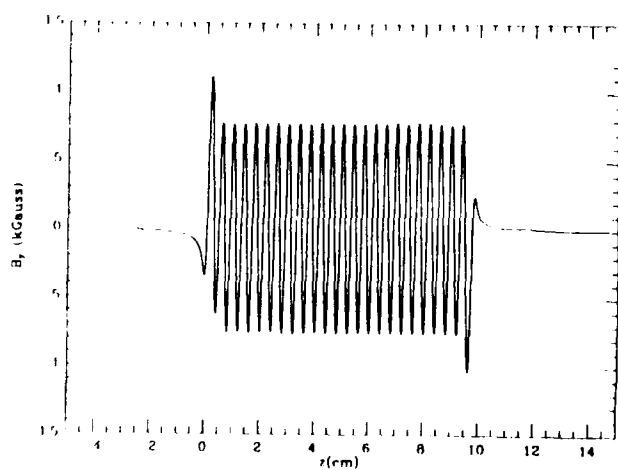


Figure 5

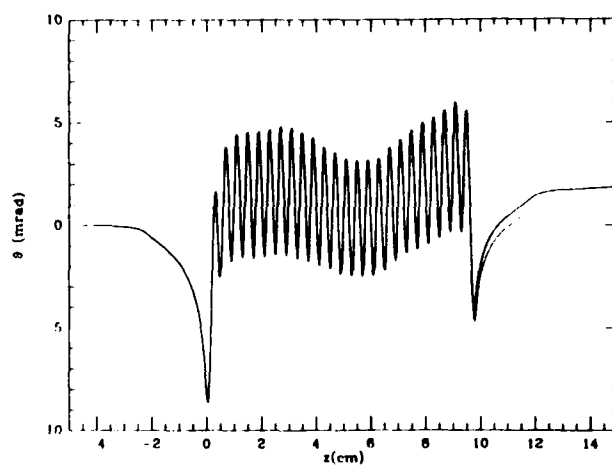


Figure 6

## P3.26

### LELIA : Induction Accelerator Studies For High Peak Power FEL Application at the Centre d'Etudes Scientifiques et Techniques d'Aquitaine (C.E.S.T.A.)

J. LAUNSPACH, J.M. ANGLES, M. ANGLES, P. ANTHOUARD, J. BARDY,  
C. BONNAFOND, H. BOTTOLIER-CURTET, G. BOUQUET, C. BRUNO, J. DELVAUX  
A. DEVIN, P. EYHARTS, P. EYL, J. GARDELLE, G. GERMAIN, J. LABROUCHE,  
P. LE TAILLANDIER, Y. PRENVEILLE, W. STADNIKOFF, M. THEVENOT

Commissariat à l'Energie Atomique  
Centre d'Etudes Scientifiques et Techniques d'Aquitaine  
P.O.box 2 - 33114 LE BARP (France)

A survey of the FEL program using a linear induction accelerator (L.I.A.) is presented.

In a first step, we use EUPHROSYNE re-designed to perform research on high brightness electron beam injectors.

A microwave FEL amplifier experiment (35 GHz), using the electron beam from EUPHROSYNE into a helical undulator is also in progress. At the same time we are developing a magnetic energy compression generator that will produce short (80 nsec), high voltage (150 kV) pulses to drive a LIA at a repetition rate of about 1 kHz.

At C.E.S.T.A. we are developing an FEL program based on a linear induction accelerator. Studies are conducted on two ways. On the one hand, we want to acquire the knowledge on induction accelerator technology as LIME has been using for a long time. That is the LELIA program which consists of 3 steps.

#### First Step : Basic technology studies

- design and fabrication of induction cells
  - high voltage pulse generator (150 kV, 80 ns) to drive cells
- As we are interested in high mean power FEL, the pulse generator has to work at a high repetition rate.
- A magnetic energy compression generator working at 1 kHz will be presented. The main components of the modulator are:
- A 30 kV power supply
  - A 2  $\mu$ F storage capacitor
  - A 1-10 step up transformer
  - A 20 nF water capacitor and a 2 Ohm, 40 ns water line
  - A magnetic switch and a output magnetic switch
  - A load comprises by twenty-four 50 Ohm output cables
- High brightness injector studies are performed using a classical intense relativistic electron beam device called EUPHROSYNE ( Marx Generator + Pulse Forming Line + cold Cathode, 3 MV, 80 kA, 50 ns, single shot pulse ). This device has been modified for that purpose and now consist of:
- A concave thermionic oxide cathode
  - An intermediate electrode
  - A hollow anode with a magnetic guiding channel.
- The choke is matched by means of carbon resistors shunting most of the 80 kA current to give a 3MV, 1 kA, 10 ns flat top pulse. We are associated with the CEA/Limeil for our numerical and theoretical efforts. Hence the device design has been done using a modified version of E-GUN installed at the Limeil Computer Center. There are also plans to perform numerical studies of the device using several full electromagnetic codes.

**Second Step** (89-91) Construction of a high brightness induction injector (15 MV - 1 to 3 kA - 1 kHz -  $10^{10}$  A/m<sup>2</sup>rad<sup>2</sup>)

**Third Step** (90-92) Construction of a 10 MV - 1 kHz induction accelerator

On the other hand, the second part of the program is devoted to an FEL experiment called OMDNE. It will be presented in greater details in a companion paper (poster presentation).

**In a first step** : (89-90) the electron beam delivered by EUPHROSYNE will be coupled with a bifilar helical wiggler with an adiabatic entrance in order to study the amplification of a microwave source at 35 GHz.

**In a second step** : (91-92) this experiment will be carried on using the induction injector instead of EUPHROSYNE.

#### Induction Accelerators used for high average power FEL applications means :

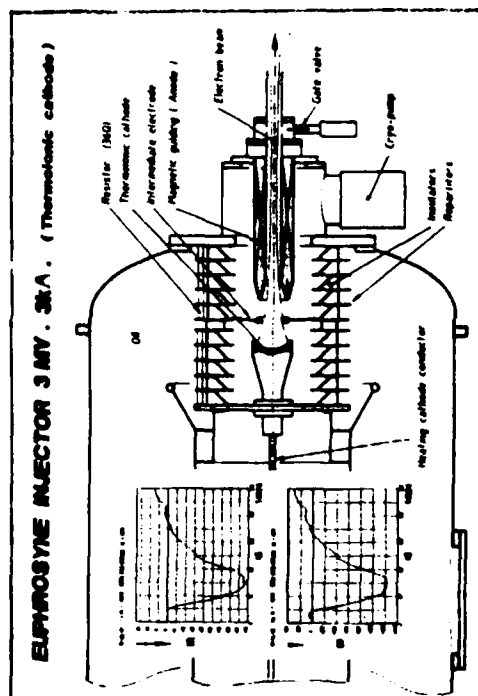
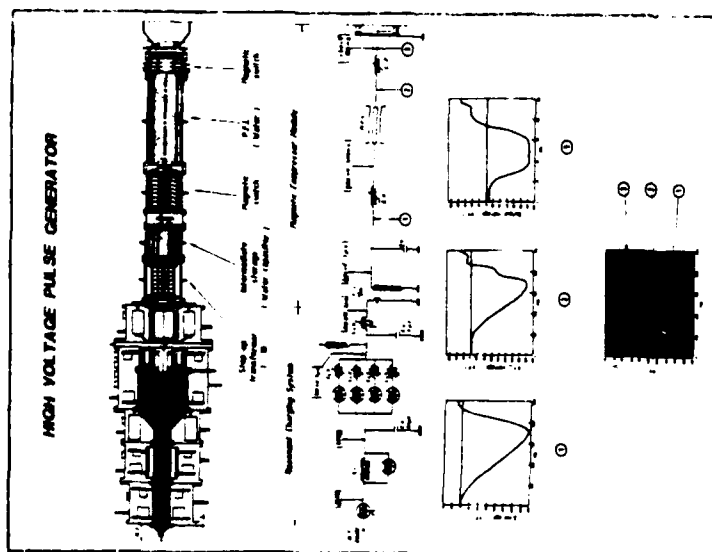
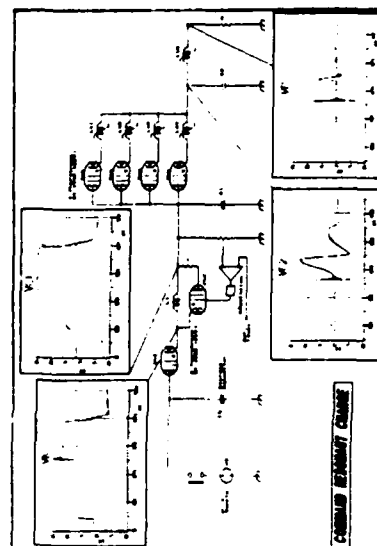
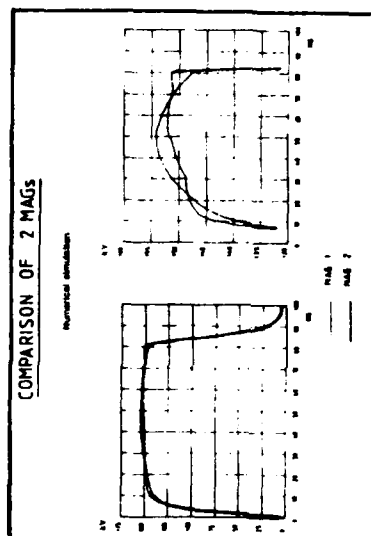
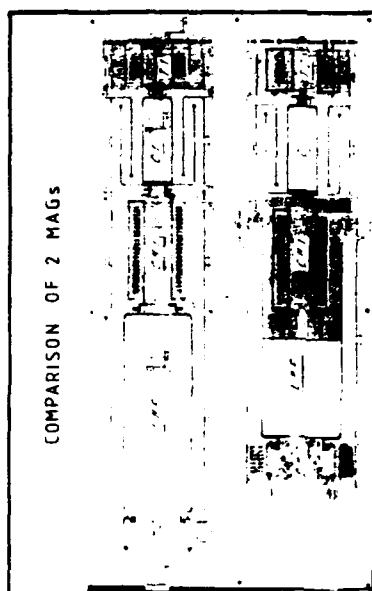
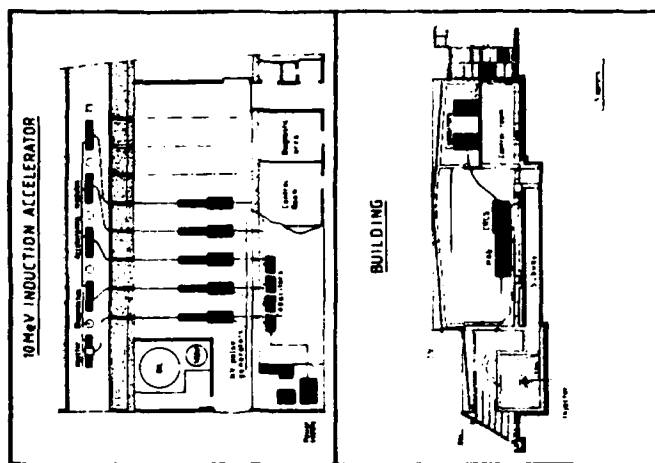
##### 1 High brightness injectors

Injector studies using  
" EUPHROSYNE "

##### 2 High repetition rate

$$\langle P \rangle = \eta UI f \Delta t$$

High voltage pulse generator  
uses magnetic compressor (MAG)



# P3.29

## STUDIES ABOUT APPLICATION OF FREE ELECTRON LASER TO INERTIAL CONFINEMENT FUSION

K. Imasaki, T. Akiba\*, K. Ohi,\*\*, S. Kuruma, K. Mima\*,  
T. Yamanaka\*, S. Nakai\*, and C. Yamanaka

Institute for Laser Technology,

\*Institute of Laser Engineering, Osaka University

\*\*Faculty of Engineering, Kansai University,  
Suita, Osaka, Japan

Application of free electron laser to inertial confinement fusion has been studied. conceptual design for 10 MJ system with beam accelerator, FEL and beam recovery system was studied. Efficiency of total system including laser extraction, e-beam acceleration and recovery was investigated.

The results implies FEL was promising for reactor energy driver for inertial confinement fusion.

Conceptual Diagram of ICF Reactor System

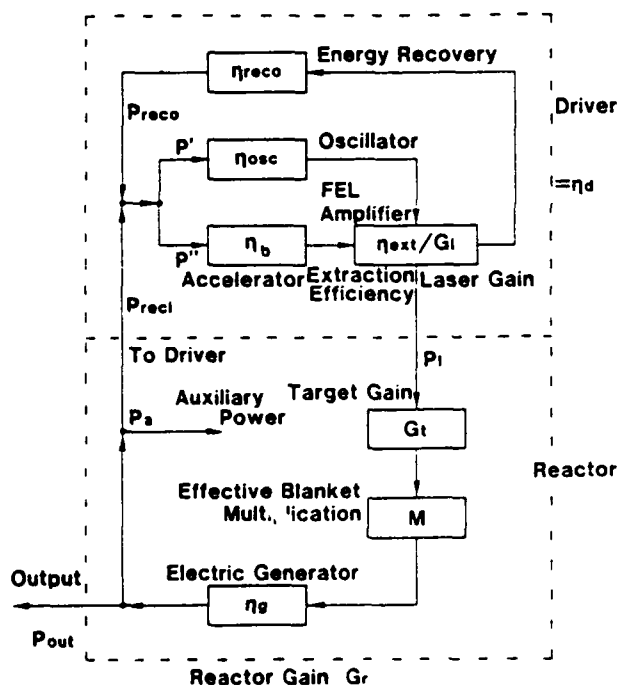
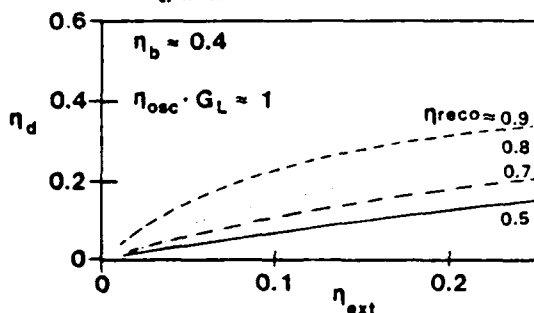


Fig. 1 Conceptual diagram of reactor system using FEL as the energy driver.



Reactor Gain:  $G_R$

$$G_R = \frac{P_{out} + P_{reci} + P_A}{P_{reci}} = \eta_D G_t M \eta_G \quad 1)$$

where

$\eta_D$ : driver efficiency,  $G_t$ : target gain

$M$ : effective blanket multiplication factor,

$\eta_G$ : electric generator efficiency

For Commercial reactor

$$\eta_G = 0.4, \quad M = 1.2, \quad G_t = 100,$$

$$G_R > 10, \quad P_{out} > P_{reci} > P_A$$

Requirement

$$P_L = 4 \sim 8 \text{ MJ} / \tau_p$$

$$\tau_p = 10 \text{ ns (laser pulse length)}$$

$$\text{Laser wavelength } 5000 \sim 2000 \text{ \AA for a good coupling}$$

$$\eta_D > 20 \%$$

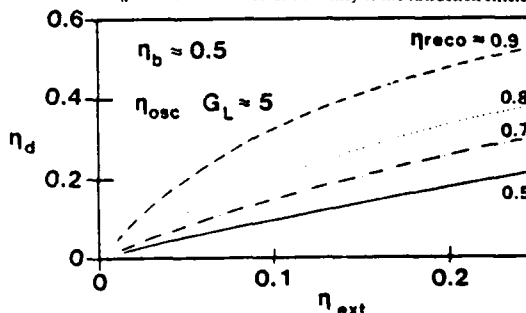
Driven Efficiency  $\eta_D$

$$\eta_D = \frac{P_D}{P_{reci}} = \frac{\eta_b \eta_{ext}}{1 + R - (1 - \eta_b \eta_{ext}) \eta_{reco}}$$

$$\text{where } R = \frac{\eta_b \eta_{ext}}{\eta_{osc} G_L}$$

Fig. 2. Reactor gain, requirements for the driver and driver efficiency

Fig. 3. Calculated driver efficiency to the extraction efficiency.



# Computer Simulation for extraction efficiency FUELNODES

- 3D code including laser and e-beam coupling in space.
- calculate multimode and wave amplification.

## Simulation Parameters

Beam Energy	$E_b$ : 200 MeV ~ 2 GeV
Beam Current	$I_b$ : 20 KA ~ 50 KA
Beam Size	$D_b$ : 3mm
Laser Size	$D_L$ : 3mm
Wave Length	3500 Å
Wiggler	constant / linear and nonlinear tapered

length 105 m  
K ~ 5

Results on nonlinear taper wiggler gave a maximum efficiency and gain. Trapping efficiency is the most important to improve FEL efficiency on tapered wiggler.

## Limitations for Window

- Experimental emittance scaling<sup>5)</sup>

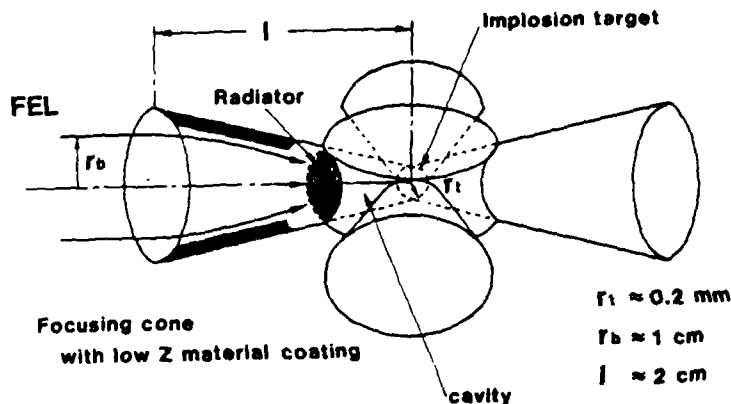
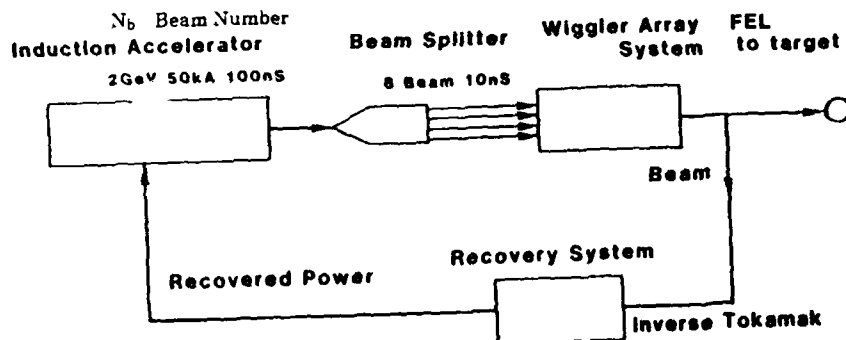
$$I_b = 1.1 \times 10^{11} (\gamma \epsilon)^2$$

- BBU Instability

$$\Gamma = \frac{I_b}{I_A} \frac{W_0 Z_0}{K_B} \frac{\gamma^2}{\Delta E_g} \text{ mc}^2$$

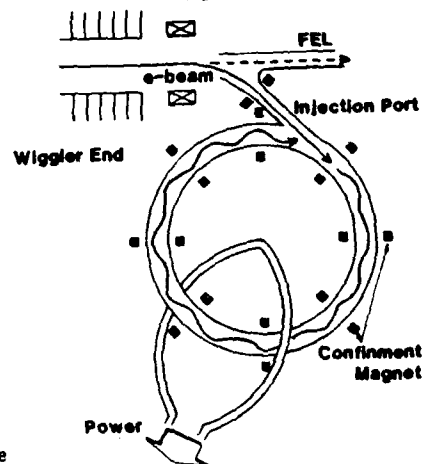
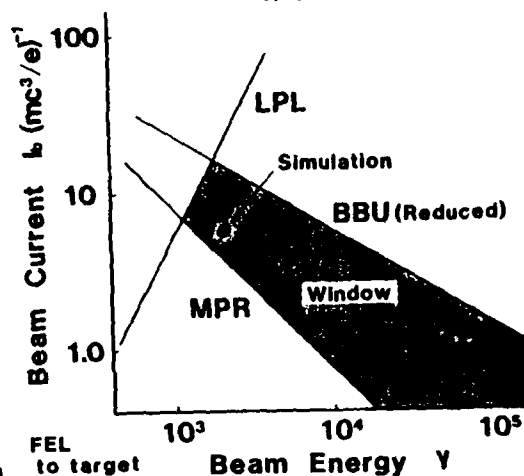
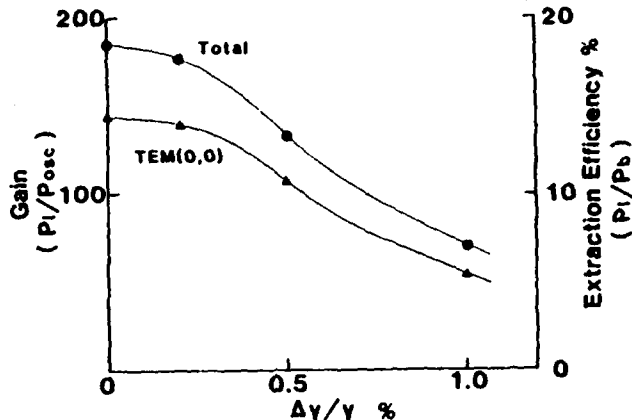
## Minimum Power Requirement for E-beam<sup>4)</sup>

$$I_b \cdot E_b \cdot N_b \cdot \eta_{\text{ext}} = P_L > 400 \text{ TW}$$



## Energy Spread Effect to FEL Gain and Extraction Efficiency

(nonlinear tapered wiggler) 100GW Laser Injection  
2GeV, 50kA



## Reference

- 1) S. Segall: KMSF-U 806 (1975)
- 2) C. Yamanaka edit: ILE Int. Rep. Conceptual Design for ICF Reactor (1979)
- 3) D. Prosnitz: LLNL UCRL-92095 (1984)
- 4) K. Imasaki et al. Rev. Laser Engin. 17 (1989) 71
- 5) J. D. Lawson: The Physics of Charged Particle Beams Oxford, England (1977) 178
- 6) R. J. Briggs: IEEE NS-28 (1981) 3360

## P3.31

## COMPACT RF-LINAC FREE-ELECTRON LASERS

John C. Goldstein, Richard L. Sheffield, Bruce E. Carlsten, and Roger W. Warren  
Group X-1, MS E531  
Los Alamos National Laboratory  
Los Alamos, NM 87545

The use of high currents and excellent beam quality produced by a photoinjector combined with a short-period wiggler leads to a new generation of smaller FELs.

### *Outline.*

- We present a preliminary design for a compact rf-linac-driven free-electron laser oscillator and evaluate its performance using the 3-D simulation code FELEX and the INEX method.
- The design is based upon two technological advances:
  - (1) A very high brightness electron beam generated with a laser-illuminated photocathode injector for the linac.
  - (2) A short-period (3 mm to 9 mm), high-field ( $a_w = 1.0$ ) wiggler made with pulsed-wire techniques.
- We limit the linac to 15 MeV to reduce the shielding requirements for the device.
- The theoretical performance of the laser is expected to reach several percent extraction efficiency, which corresponds to macropulse-averaged optical power output of tens of kilowatts and long-time-averaged output of several watts.

### *Simulations of compact FEL performance.*

- Fully 3-D simulations were performed with the code FELEX. The code includes 3-D motion of electrons, energy spread, diffraction, mode overlap, etc.
- The calculations are single-wavefront (single frequency); no pulse effects were included.
- Single-pass gains were calculated to determine small-signal gain and saturated gain as a function of the optical wavelength and the wiggler parameters.
- Multiple-pass single-wavelength calculations were performed to determine the self-consistently-calculated steady-state resonator solutions.

### *Optics parameter values in the simulations.*

- The optical resonator was taken to be a simple stable two-mirror near-concentric cavity of a fixed length: 277.777 cm.
- The Rayleigh range was always chosen to be equal to one-half of the wiggler's length. This is the condition for minimum vignetting losses at the ends of the wiggler.
- The center of the wiggler coincides with the central focus of the resonator.
- Output coupling was taken to be 10% mirror transmission (total for both mirrors). The mirrors were much larger than the optical spot sizes so that no losses occurred on those elements. Vignetting losses at the ends of the wiggler were included by putting apertures of a size equal to the gap of the wiggler at the ends of the wiggler.
- Wigglers with two different wavelengths were considered. Since the same electron beam was used to drive each wiggler, two different radiation wavelengths arose in these simulations: about 8  $\mu\text{m}$  and about 2.7  $\mu\text{m}$ .

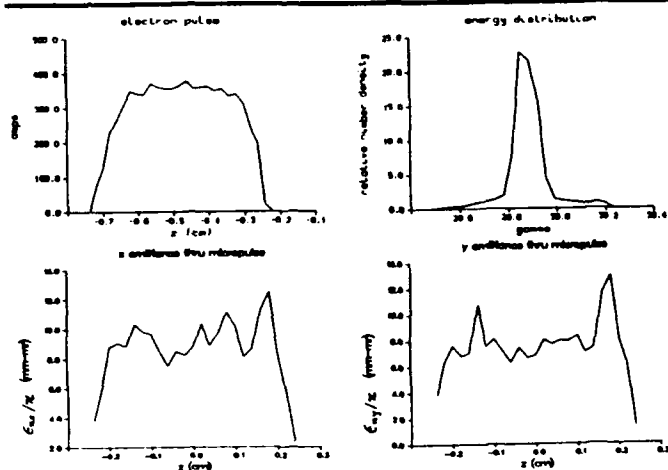
### *The performance of a compact FEL with two different wigglers was simulated.*

Wiggler	Wavelength, cm	Magnetic field, T	$a_w$	Full gap, cm
1	0.9	1.1911872	1.0	0.3
2	0.3	3.5735616	1.0	0.1

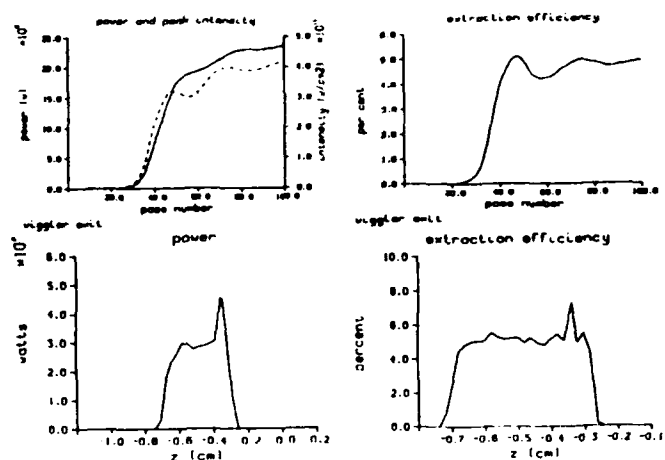
The FEL performance with various lengths of these two wigglers was evaluated.



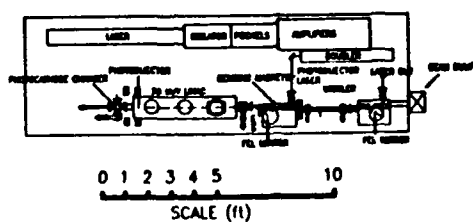
### Electron-beam properties from PARMELA simulation.



### Results of INEX simulation of compact FEL with wiggler 1.



### COMPACT FEL DESIGN USING PHOTOINJECTOR



20 MeV, 10  $\mu$ S MACROPULSE, 20  $\pi$ -mm-mrad  
350 A, PEAK SURFACE FIELD = 60 MV/m

### Summary and conclusions.

- We have presented a design of a compact free-electron laser oscillator and evaluated its performance theoretically using the INEX simulation method.
- The design is made possible by the existence of two significant technological advances:
  - (1) The laser-illuminated photocathode injector for the rf-linac makes possible very high-brightness electron beams. The accelerator design makes use of other techniques to maintain the brightness as the beam propagates through the accelerator and beam transport system. The accelerator design was done with the code PARMELA.
  - (2) The pulsed-wire technique can be used to make short-period (3 mm to 9 mm) high field ( $a_w = 1.0$ ) wigglers.
- The very bright electron beam together with a high-field wiggler produces ample gain in the 2.5 - 9.0  $\mu$ m spectral region. To increase the saturated laser power we reduce the wiggler length to 10 - 14 periods while maintaining an optical Rayleigh range equal to one-half of the wiggler's length. This produces a large enough optical spot on the mirrors to avoid damage.
- We expect such compact FELs to be capable of producing up to ten watts of average power.

## P3.34 The Impact of Field Error Reduction Techniques on FEL Performance

W. P. Marable, E. Esareya<sup>a)</sup> and C. M. Tang<sup>a)</sup>  
 Department of Physics and Astronomy  
 University of Maryland  
 College Park, Maryland

There have been extensive studies on the effects of intrinsic field errors on the operation and performance of free electron lasers (FELs) based predominately on simple models for the spatial form and statistical properties of the field errors. In the present study we consider the effects of i) compensation magnets, ii) general spatial forms which are more realistic models of experimental wigglers and iii) statistical correlations of the field errors. This theoretical study has resulted in a quantitative means of measuring the relative merit of these experimental techniques for reducing wiggler field error effects.

### Simple Model(Un-Correlated Errors)

$$B_y(z) = (\epsilon_{Ny}(z) + B_w) \sin k_w z,$$

$$B_x(z) = (\epsilon_{Nx}(z) + B_w) \cos k_w z,$$

$$\epsilon_{Ny}(z) = \delta B_y \epsilon_i^y \delta_{i,n} H\left(\frac{l_w}{4} + z_{yi}\right) H\left(\frac{l_w}{4} - z_{yi}\right),$$

$$\epsilon_{Nx}(z) = \delta B_x \epsilon_i^x \delta_{i,m} H\left(\frac{l_w}{4} + z_{xi}\right) H\left(\frac{l_w}{4} - z_{xi}\right),$$

$$\{x^2\}^{Ens} = \left(\frac{\alpha_x}{k_{\beta x}}\right)^2 \left(z - \frac{\sin 2k_{\beta x} z}{2k_{\beta x}}\right),$$

$$\{x^{1/2}\}^{Ens} = \alpha_x^2 \left(z + \frac{\sin 2k_{\beta x} z}{2k_{\beta x}}\right),$$

### Micro-Scaled Field Error Correlations

$$B_x = B_w \cos k_w z + \left\{ \sum_{p=1}^3 \delta B_x^{(p)} \mathfrak{I}^{(p)}(z) f_x^{(p)}(i) \right\} \delta_{i,m} \\ \times H\left(\frac{l_w}{4} + z_{xi}\right) H\left(\frac{l_w}{4} - z_{xi}\right),$$

$$B_y = B_w \sin k_w z + \left\{ \sum_{p=1}^3 \delta B_y^{(p)} \mathfrak{I}^{(p)}(z) f_y^{(p)}(i) \right\} \delta_{i,n} \\ \times H\left(\frac{l_w}{4} + z_{yi}\right) H\left(\frac{l_w}{4} - z_{yi}\right),$$

$$\mathfrak{I}^{(1)}(z) = \cos k_w z,$$

$$\mathfrak{I}^{(2)}(z) = \sin 2k_w z,$$

$$\mathfrak{I}^{(3)}(z) = \cos k_w z - \delta \sin^2 2k_w z.$$

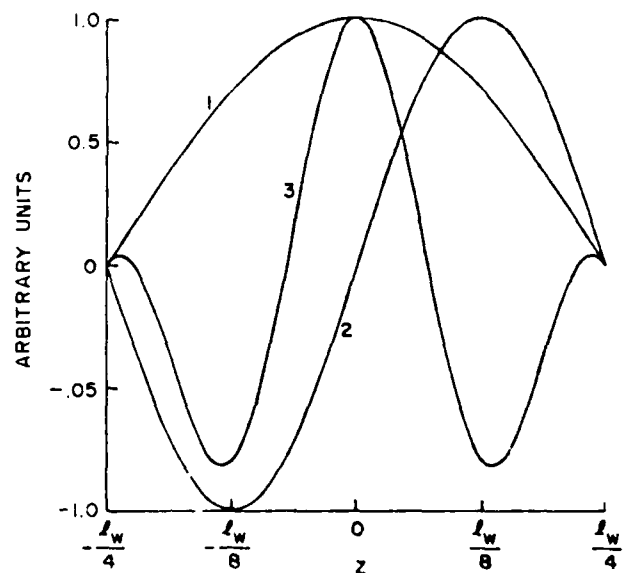
### Macro-Scale Field Error Correlations

$$\epsilon_{Ny}(z) = \delta B_y f_y(\epsilon_i^y) \delta_{i,n} H\left(\frac{l_w}{4} + z_{yi}\right) H\left(\frac{l_w}{4} - z_{yi}\right),$$

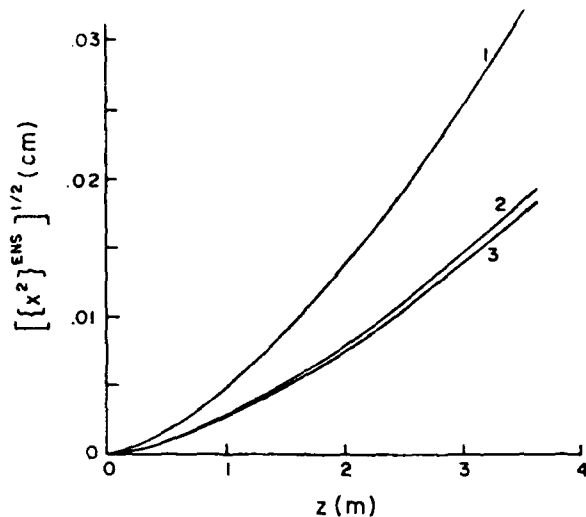
$$\epsilon_{Nx}(z) = \delta B_x f_x(\epsilon_i^x) \delta_{i,m} H\left(\frac{l_w}{4} + z_{xi}\right) H\left(\frac{l_w}{4} - z_{xi}\right).$$

$$\alpha_y^2 = \left(\frac{a_w k_w}{\gamma \beta_{so}}\right)^2 \left(\frac{\delta B_y}{B_w}\right)^2 \frac{l_w \sin(k_{\beta} l_w / 2)}{8\pi^2 k_{\beta} l_w / 2} S_y,$$

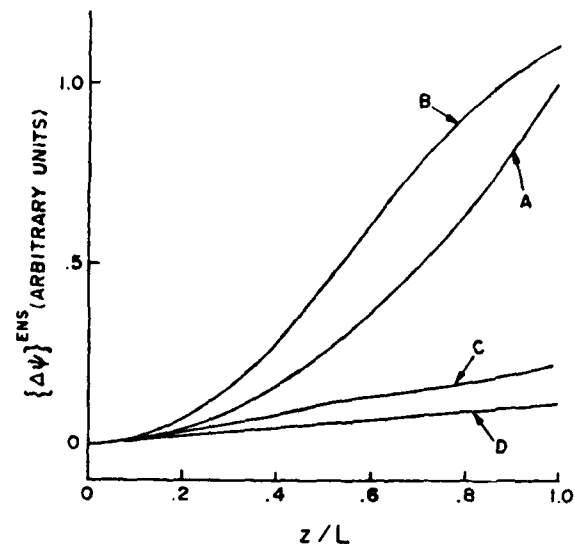
$$S_y \equiv 4\{f_y^2(i-1)\}^{Ens} - 4\{f_y(i-1)f_y(i-2)\}^{Ens} \\ - 4\{f_y(i)f_y(i-1)\}^{Ens} + \{f_y^2(i-2)\}^{Ens} \}^{Ens} \\ + 2\{f_y(i)f_y(i-2)\}^{Ens} + \{f_y^2(i)\}^{Ens},$$



The spatial forms used to model micro-correlations,  $\delta = 1.5$ .



Transverse displacement,  $\sqrt{\{x_p^2\}^{ENS}}$ , for micro-correlations with A) spatial form (1), B) spatial form (2) and C) spatial form (3) with  $\delta = 1.5$ . No macro-correlations  $\alpha = 0 = \beta$ .



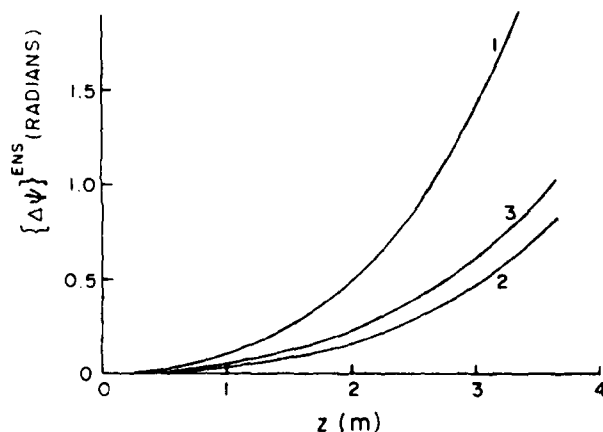
Relative phase shake for focusing strength  $k_B L = 5.0$  and steering rates  $L/\ell_f = 0, 1, 2, 3$ . (A, B, C, D)

### Multi-Steering Theory

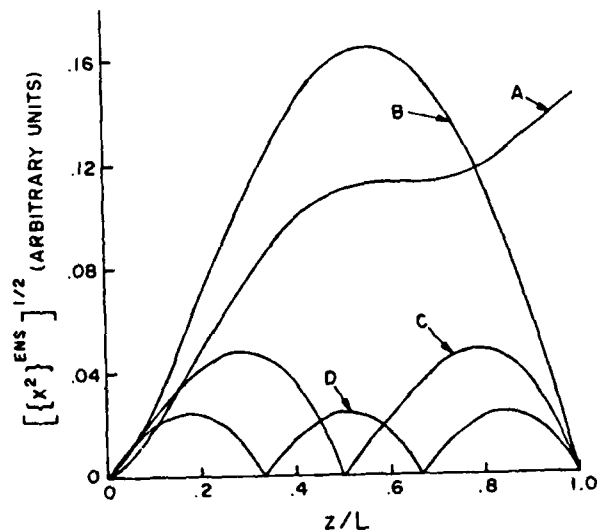
$$x_p'(z) = \Delta\beta_z^{(i)} + \int_{(i-1)l_f}^z d\tilde{z} h_x(\tilde{z}) \cos k_{\beta z}(\tilde{z} - z),$$

$$x_p(z) = x^{(i)} + \Delta\beta_z^{(i)}[z - (i-1)l_f] - \frac{1}{k_{\beta z}} \int_{(i-1)l_f}^z d\tilde{z} h_x(\tilde{z}) \sin k_{\beta z}(\tilde{z} - z),$$

$$\Delta\beta_z^{(i)} = \frac{x^{(i+1)} - x^{(i)}}{l_f} + \frac{1}{k_{\beta z} l_f} \int_{(i-1)l_f}^{il_f} d\tilde{z} h_x(\tilde{z}) \sin k_{\beta z}(\tilde{z} - il_f),$$



Phase shake for micro-correlations with A) spatial form (1), B) spatial form (2) and C) spatial form (3) with  $\delta = 1.5$ . No macro-correlations,  $\alpha = 0 = \beta$ .



Relative transverse displacement for focusing strength  $k_B L = 5.0$  and steering rates  $L/\ell_f = 0, 1, 2, 3$ . (A, B, C, D)

### Case of Inexact Steering

$$\{\Delta\psi\}^{ENS} = \{\Delta\psi\}^{ENS} (old) + \frac{\omega}{\beta_{soc}} \left[ \frac{\sigma_z^2}{l_f^2} z + k_{\beta z}^2 \sigma_z^2 \times \left[ z - \frac{(i-1)l_f}{3} - l_f \left( \frac{z - (i-1)l_f}{l_f} \right)^2 + \frac{2}{3} \left( \frac{z - (i-1)l_f}{l_f} \right)^3 \right] \right]$$

The condition for non-perfect steering to yield negligible effects with regard to beam walk-off and phase shift, as compared to perfect steering, can be expressed as,

$$\frac{\sigma_z^2}{l_f^2} < \frac{1}{24} \left( \frac{a_w}{\gamma \beta_{so}} \frac{\delta B(max)}{B_w} \right)^2 \frac{l_f}{l_w}$$

# P3.36

## Waveguide Effects in Superradiant Free-Electron Lasers\*

W. M. Sharp and S. S. Yu  
Lawrence Livermore National Laboratory  
Livermore, California 94550, USA

A quasi three-dimensional time-dependent particle simulation has been developed to model slippage effects in a single-pass microwave FEL. The code is used here to model the large-amplitude "superradiant" signal that can develop in the slippage region of constant-current beams. Results are presented for single-mode and multiple-mode cases, and the effects of the waveguide dimensions, detuning, energy spread, and the initial power in the modes are discussed.

\* Performed jointly under the auspices of the US DOE by LLNL under W-7405-ENG-48 and for the DOD under SDIO/SDC-ATC MIPR No. W31RPD-8-D5005.

### WHAT IS FEL SUPERRADIANCE?

TERM BORROWED FROM ATOMIC PHYSICS  
DESCRIBES RADIATED INTENSITY FROM  
N OSCILLATORS THAT SCALES LIKE  $N^2$   
SEEN IN COHERENTLY PHASED  
CONVENTIONAL LASERS (DIODE SUPERRADIANCE)

BY ANALOGY, FEL SUPERRADIANCE IS  
EMISSION WITH INTENSITY SCALING LIKE  
 $I_s^2$ , RATHER THAN USUAL  $I_s^{1/2}$

$$|A_s|^2 \sim I_s^2$$

### WHEN DOES IT OCCUR?

STANDARD FEL TREATMENT ASSUMES  
AXIAL UNIFORMITY  
FRED FOLLOWS SINGLE BUCKET  
GINGER FOLLOWS PERIODIC STRING OF BUCKETS

APPROXIMATION GOOD WHEN  
SCALE LENGTHS  $\gg$  PERIODIC LENGTH  
FAILS IN 'SURFACE REGION' AT BEAM TAIL  
 $u \approx 3 - \sqrt{2} + \sqrt{2} \approx 2.5(2-1)$

SUPERRADIANCE OCCURS IN THAT REGION  
SURFACE REDUCES PHOTON REABSORPTION  
MORE ENERGY LOST TO WAVE ON AVERAGE



### WHAT ARE THE MAIN FEATURES?

LARGE AMPLITUDE  
PEAK PULSE HIGHER THAN SATURATION LEVEL  
REQUIRES  $L_s \gg L_u (1-\beta)$

NON-RESONANT  
WEAKEST NEAR FEL RESONANCE  
BUNCHING NOT REQUIRED

NON-SATURATING  
PEAK AMPLITUDE GROWS EXPONENTIALLY IN  $z$   
LENGTH BEHAVES LIKE  $A_s^{1/2}$

RELATIVELY ROBUST  
SURVIVES ENERGY SPREAD, DETUNING, NOISE, I-D

DIFFICIENT  
F & 1/2 FOR TAILORING PARAMETERS  
BETTER IN MICROWAVE RANGE

UNDERSTOOD ANALYTICALLY AT SMALL AMPLITUDE  
DOES NOT INVOLVE USUAL FEL RESONANCE  
OCCURS AT SPONTANEOUS EMISSION FREQUENCY

### WHAT'S DIFFERENT IN A WAVEGUIDE?

#### MULTIPLE MODES

$$A_s(z, t) = -\frac{e}{m} \sum_k A_k(z, t) [S_k(z, t) \cos \phi_k - \dot{S}_k(z, t) \sin \phi_k]$$

$$\phi_k = \omega_k t - k z - \phi_0$$

$$\dot{\phi}_k = (\frac{\omega_k}{c} - k) \dot{z}$$

$$\dot{\phi}_k = [(\frac{\omega_k}{c} - k) \dot{z}]^2 \quad \text{FOR } T_{E-}, T_{H-}$$

#### MODE VELOCITY SPREAD

$$\dot{\phi}_k = \frac{\omega_k}{c} \dot{z}$$

#### AXIAL $E_z$ FOR TM MODES

#### NO DIFFRACTION

### ASSUMPTIONS IN WAVEGUIDE MODEL

#### HIGH ENERGY

$$\beta \omega / \gamma \ll 1$$

#### SMALL SIGNAL

$$|A_s| \ll |A_u|$$

#### SMALL $(\gamma - \langle \gamma \rangle) / \langle \gamma \rangle$

SAME  $\frac{1}{\gamma}$  FORM FOR ALL ELECTRONS

#### SLOWLY VARYING AMPLITUDE AND PHASE

NO 2ND DERIVATIVES IN FIELD EQUATIONS

SIMPLER ELECTRON EQUATIONS

#### IDEAL LINEAR WIGGLER

$$A_u = \frac{e}{m} \cos(k_z z) \hat{z}$$

#### LOW BEAM EMITTANCE

NEGLECTABLE ROTATION MOTION

SMALL  $\gamma - \langle \gamma \rangle$

1-D PARTICLE PUSH

#### LOW BEAM DENSITY

NEGLECTABLE ELECTROSTATIC FORCE

COMPTON-RESCINING OPERATION

#### CENTERED BEAM

$$\text{WIGGLE-AVERAGED } \langle x \rangle = 0 \text{ AND } \langle y \rangle = 0$$

### FIELD EQUATION DERIVATION

#### LORENTZ - CAUSE FIELD EQUATION

$$(\nabla^2 - \frac{\partial^2}{\partial t^2}) A_s = \frac{e}{m} \sum_k A_k$$

#### SUBSTITUTE $A_s = \frac{1}{2} A_s e^{i(\omega t - k z)}$

DISCARD 2ND DERIVATIVES

SEPARATE COMPONENTS USING ORTHOGONALITY

AVERAGE OVER A BUCKET TO REMOVE HIGH FREQUENCIES

SUBSTITUTE  $x = \frac{z}{L_u} = \frac{z}{L_u} \sin(\omega t)$

$$z = \frac{L_u}{2} + \frac{L_u}{2} \sin(2\pi x)$$

EXPAND FLUCTUATING QUANTITIES IN POWER SERIES

RETAIN ONLY 1st AND 3rd TERMS

AVERAGE OVER WIGGLE MOTION

#### FINAL EQUATION FORM

$$(\frac{\partial^2}{\partial t^2} - \frac{\partial^2}{\partial z^2}) A_s = \frac{e}{m} \sum_k A_k \langle \frac{\partial^2}{\partial t^2} \cos(k_z z) \rangle$$

$$A_s (\frac{\partial^2}{\partial t^2} - \frac{\partial^2}{\partial z^2}) = \frac{e}{m} \sum_k A_k \langle \frac{\partial^2}{\partial t^2} \cos(k_z z) \rangle$$

$$A_s = (1 + \frac{L_u}{2}) (1 - \frac{L_u}{2})$$

$$\frac{\partial^2}{\partial t^2} = \frac{\partial^2}{\partial z^2} \quad \text{TM MODE WIGGLER}$$

$$= \frac{\partial^2}{\partial z^2} \quad \text{TM MODE WIGGLER}$$

$$\frac{\partial^2}{\partial t^2} = (\frac{\partial^2}{\partial z^2} - \frac{\partial^2}{\partial x^2}) = \frac{\partial^2}{\partial z^2}$$

# COUPLING COEFFICIENTS

MODE	$\beta_1$	$\beta_2$
$TE_{01}$	$-\frac{1}{2} [Z(0) - Z(0)]$	0
$TE_{10}$	$\frac{1}{2} [Z(0) - Z(0)]$	0
$TM_{01}$	$\frac{1}{2} [Z(0) - Z(0)]$	$-\frac{1}{2} [Z(0) - Z(0)]$
$TE_{00}$	$\frac{1}{2} [Z(0) - Z(0)]$	0
$TE_{10}$	$\frac{1}{2} [Z(0) - Z(0)]$	0
$TM_{10}$	$\frac{1}{2} [Z(0) - Z(0)]$	$\frac{1}{2} [Z(0) - Z(0)]$

$$Z = \frac{1}{2} \frac{d^2}{dz^2} \frac{1}{\epsilon}$$

$$Z = \frac{1}{2} \frac{d^2}{dz^2} \frac{1}{\epsilon}$$

# ELECTRON EQUATIONS

NEGLECT SPACE CHARGE  $\rho = 0$   
 NEGLECT BEAM DISTURBANCE  $\nabla \cdot \mathbf{E} = \nabla \cdot \mathbf{E}_0 = 0$   
 ASSUME  $|E_0| \gg |E_1|$

RELATIVISTIC KHR HAMILTONIAN

$$H_1 = \frac{1}{2} m_0 c^2 \left[ 1 + \frac{1}{c^2} (\mathbf{v} \cdot \mathbf{v}) \right] - e \phi$$

$$H = H_0 + H_1 = \frac{1}{2} m_0 c^2 \left[ 1 + \frac{1}{c^2} (\mathbf{v} \cdot \mathbf{v}) \right] - e \phi$$

HAMILTONIAN EQUATIONS OF MOTION

$$\frac{d\mathbf{r}}{dt} = \frac{\partial H}{\partial \mathbf{p}}$$

$$\frac{d\mathbf{p}}{dt} = -\frac{\partial H}{\partial \mathbf{r}}$$

EQUATIONS FOR  $\mathbf{r}$  AND  $\mathbf{p}$  IN  $(x, y, z)$  COORDINATES

$$\frac{dx}{dt} = \frac{1}{m_0} \frac{\partial H}{\partial v_x} = \frac{1}{m_0} \frac{1}{\sqrt{1 + \frac{v^2}{c^2}}} v_x$$

$$\frac{dy}{dt} = \frac{1}{m_0} \frac{\partial H}{\partial v_y} = \frac{1}{m_0} \frac{1}{\sqrt{1 + \frac{v^2}{c^2}}} v_y$$

$$\frac{dz}{dt} = \frac{1}{m_0} \frac{\partial H}{\partial v_z} = \frac{1}{m_0} \frac{1}{\sqrt{1 + \frac{v^2}{c^2}}} v_z$$

$$\frac{dp_x}{dt} = -\frac{\partial H}{\partial x} = -e \frac{\partial \phi}{\partial x}$$

$$\frac{dp_y}{dt} = -\frac{\partial H}{\partial y} = -e \frac{\partial \phi}{\partial y}$$

$$\frac{dp_z}{dt} = -\frac{\partial H}{\partial z} = -e \frac{\partial \phi}{\partial z}$$

AVERAGE OVER WAVELENGTH

$$\frac{dx}{dt} = \frac{1}{m_0} \frac{\partial H}{\partial v_x} = \frac{1}{m_0} \frac{1}{\sqrt{1 + \frac{v^2}{c^2}}} v_x$$

$$\frac{dy}{dt} = \frac{1}{m_0} \frac{\partial H}{\partial v_y} = \frac{1}{m_0} \frac{1}{\sqrt{1 + \frac{v^2}{c^2}}} v_y$$

$$\frac{dz}{dt} = \frac{1}{m_0} \frac{\partial H}{\partial v_z} = \frac{1}{m_0} \frac{1}{\sqrt{1 + \frac{v^2}{c^2}}} v_z$$

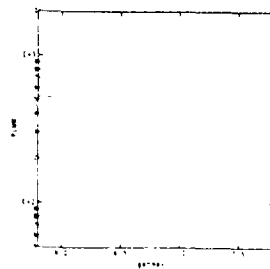
$$\frac{dp_x}{dt} = -\frac{\partial H}{\partial x} = -e \frac{\partial \phi}{\partial x}$$

$$\frac{dp_y}{dt} = -\frac{\partial H}{\partial y} = -e \frac{\partial \phi}{\partial y}$$

$$\frac{dp_z}{dt} = -\frac{\partial H}{\partial z} = -e \frac{\partial \phi}{\partial z}$$

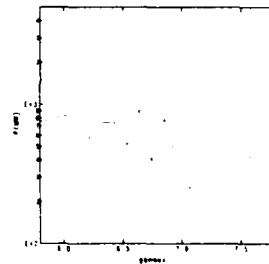
# EFFECT OF DETUNING: $TE_{01}$ ONLY

ELF PARAMETERS  
 200 PARTICLES/GRIDPOINT



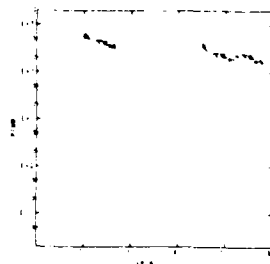
# EFFECT OF DETUNING: $TE_{01}$ , $TE_{10}$ , $TM_{01}$

ELF PARAMETERS  
 200 PARTICLES/GRIDPOINT  
 INITIAL MODE WEIGHTS 1:1:1:0.1



# EFFECT OF WAVEGUIDE HEIGHT

ELF PARAMETERS  
 $A = 10 \text{ cm}$



# TENTATIVE CONCLUSIONS

BEHAVIOR OF  $TE_{01}$  ALONE IS SIMILAR TO 1-D CASES  
 HIGHER MODES CAN PROVIDE OR SUPPLEMENT STANDING SUPERGRADIENT SIGNAL  
 PEAK SUPERGRADIENT POWER HORIZONTAL DECREASES WITH INCREASING  $A$  OR  $b$   
 MULTI-MODE SIMULATIONS ARE MUCH MORE SENSITIVE TO STATISTICAL NOISE  
 PRESENT CODE CANNOT MODEL STREAM PERTURBATION USING WAVEGUIDE SIZE

**THURSDAY, AUGUST 31**

## EX3.2

### Harmonic Generation-Strength and Mode Shape\*

Brian E. Newnam, Roger W. Warren, Donald W. Feldman, and William E. Stein  
Los Alamos National Laboratory, MS J564  
Los Alamos, New Mexico 87545

We have measured the intensities and mode shapes of the light produced at the second-, third-, and fifth harmonics of the Los Alamos free-electron laser oscillator operating near 10  $\mu\text{m}$ . The strengths and shapes could be changed markedly by slight shifts in system parameters. We present explanations for these unexpected effects.

\*Work supported in part by the U.S. Army Defense Command and Los Alamos National Laboratory Institutional Supporting Research funds, and conducted under the auspices of the U.S. Department of Energy.

#### FEL OPERATING PARAMETERS

WAVELENGTH	10 - 12 $\mu\text{m}$ , mainly 10.5 $\mu\text{m}$
PEAK CURRENT	400 - 600 A
ENERGY SPREAD	- 1 - 2%
BEAM EMITTANCE	- 2x mm-mr, FWHM
UNDULATOR GAP	6.0 mm or 8.8 mm
UNDULATOR PARAMETER	$K = 1.0$ or $0.76$
RESONATOR MIRRORS	REAR: Cu ( $R=99\%$ ) OUTPUT: ZnSe/ThF <sub>4</sub> on ZnSe ( $R=98\% - 99\%$ at 10 - 12 $\mu\text{m}$ )
SPECTRAL WIDTH	- 0.5%, SINGLE LINE

#### OVERVIEW OF RESULTS

- CAVITY LENGTH DETUNING DEPENDENCE:  
HARMONIC POWER DETUNING CURVES SIMILAR TO FUNDAMENTAL, EXCEPT WHEN NEAR LASING THRESHOLD FOR 3RD HARMONIC.
- SPATIAL DISTRIBUTIONS:  
FUNDAMENTAL: SINGLE LOBE - GAUSSIAN  
SECOND HARMONIC: DOUBLE LOBE WITH AXIAL NULL OR QUASI DONUT.  
- VERY SENSITIVE TO BEAM & MIRROR ALIGNMENT.  
THIRD HARMONIC: MAJOR CENTRAL LOBE WITH TWO MINOR LOBES.

#### OVERVIEW OF RESULTS

##### HARMONIC EFFICIENCIES VS RESONATOR Q:

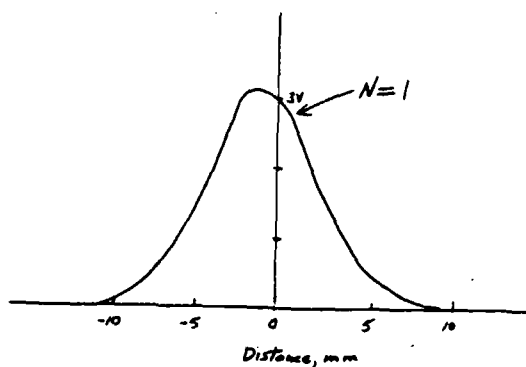
ORDER	$P_N/P_1$ (LOW Q)	$P_N/P_1$ (HIGH Q)
2	$10^{-5}$ ( $7 \times 10^{-5}$ theory)	—
3	$10^{-5}$ ( $5 \times 10^{-6}$ " )	$10^{-4} - 10^{-2}$ (LASE)
4	$< 10^{-7}$ ( $4 \times 10^{-8}$ " )	—
5	$10^{-7}$ ( $3 \times 10^{-8}$ " )	$5 \times 10^{-5} - 2 \times 10^{-4}$

- HARMONIC EFFICIENCY VS CURRENT: LITTLE EFFECT  
(BEAM EMITTANCE INCREASES WITH CHARGE)

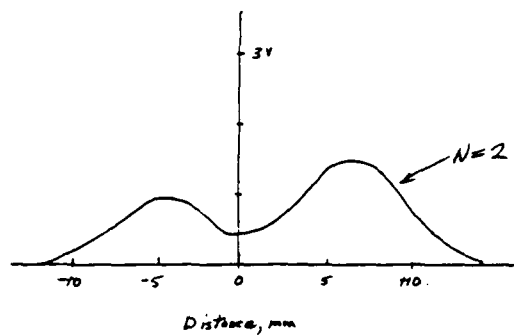
#### SUMMARY

- EFFICIENCY OF HARMONIC GENERATION FOR LAML FEL IS LESS THAN MEASURED FOR STANFORD FEL - PROBABLY DUE TO GREATER EMITTANCE.
- HARMONIC SPATIAL PROFILES ARE SENSITIVE TO ALIGNMENT OF ELECTRON BEAM AND MIRROR TILT. SECOND HARMONIC WAS MOST SENSITIVE.
- LARGE ENHANCEMENT CAN ARISE FROM LOW-LOSS RESONATOR AT HARMONIC WAVELENGTHS.
- COHERENT ADDITION OF ELECTRIC FIELDS CAN EXPLAIN LARGE POWER INCREASE OF ORDER -100.
- $10^3$  ENHANCEMENT REQUIRES FURTHER ANALYSIS

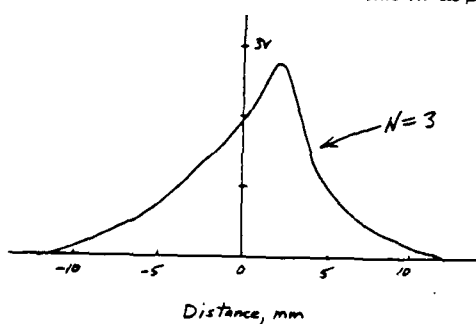
SPATIAL PROFILE OF THE FUNDAMENTAL AT 10.5  $\mu\text{m}$



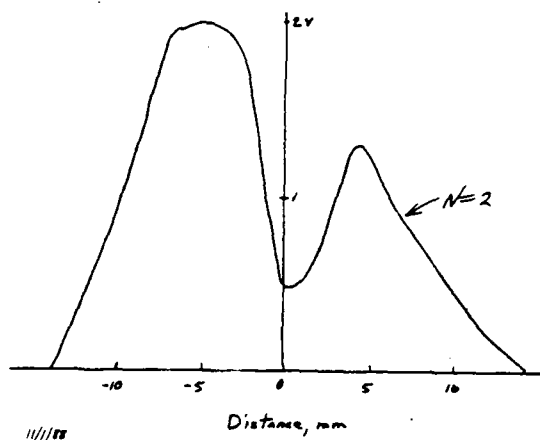
SPATIAL PROFILE OF THE SECOND HARMONIC AT 5.25  $\mu\text{m}$



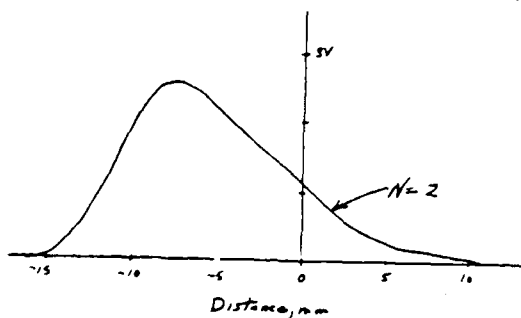
SPATIAL PROFILE OF THE THIRD HARMONIC AT 3.5  $\mu\text{m}$



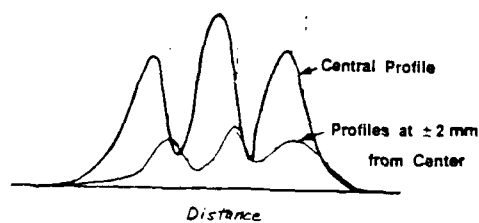
LOPSIDED PATTERNS WERE SEEN FOR CERTAIN ELECTRON-BEAM POSITION OR FOCUS ADJUSTMENTS



PEAKING OF THE FUNDAMENTAL POWER SOMETIMES RESULTED IN ONLY ONE LOBE FOR THE 2ND HARMONIC

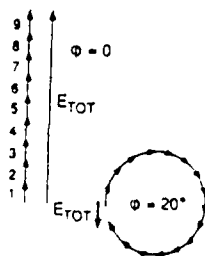


NEARLY EQUAL THREE-LOBE, THIRD-HARMONIC PROFILES RESULTED FROM CERTAIN ELECTRON-BEAM ALIGNMENTS

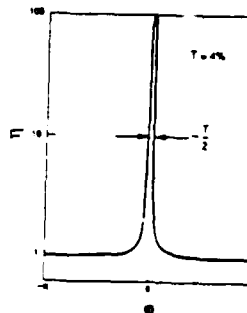


APERTURE SCANS OF THE THIRD HARMONIC AT  $\pm 2$  mm FROM BEAM CENTER

PHASE OF ADDED FIELDS IS IMPORTANT



EFFICIENCY CAN BE GREATLY ENHANCED FOR  $\phi \cong 0^\circ$





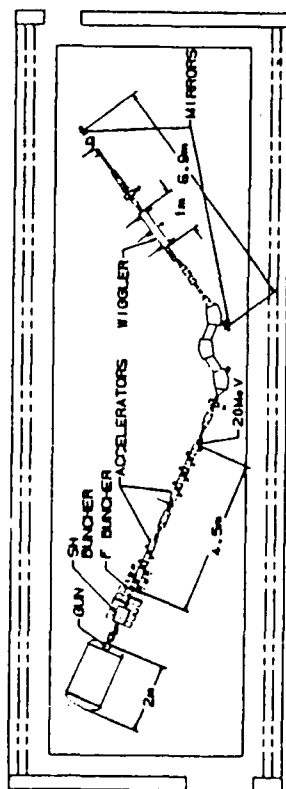
## EX3.3

### THE LOS ALAMOS HIGH-BRIGHTNESS ACCELERATOR FEL (HIBAF)

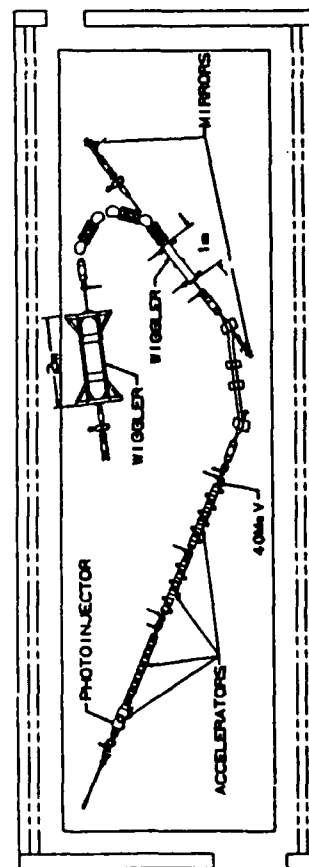
W. D. Cornelius, S. Bender, K. Meier, L. E. Thode, and J. M. Watson  
Los Alamos National Laboratory, Los Alamos NM 87545

The 10  $\mu\text{m}$  Los Alamos FEL facility is being upgraded. The conventional electron gun and bunchers have been replaced with a much more compact 6 MeV photoinjector accelerator. By re-using existing parts from previous experiments, the primary beam energy will be doubled to 40 MeV. With the existing 1 meter wiggler ( $\lambda_w = 2.7 \text{ cm}$ ) and resonator, the facility can produce photons with wavelengths from 3 to 100  $\mu\text{m}$  when lasing on the fundamental mode and produce photons in the visible spectrum with short-period wigglers or harmonic operation. After installation of a  $150^\circ$  bend, a second wiggler will be added as an amplifier. The installation of laser transport tubes between the accelerator vault and an upstairs laboratory will provide experimenters with a radiation-free environment for experiments. Although the initial experimental program of the upgraded facility will be to test the single accelerator-master oscillator/power amplifier configuration, some portion of the operational time of the facility can be dedicated to user experiments.

Previous Los Alamos FEL Facility



LOS ALAMOS HIBAF  
HIGH BRIGHTNESS ACCELERATOR FEL



## Previous Los Alamos FEL Experiments:

1981-82 **Amplifier Experiment**  
4% extraction efficiency with tapered wiggler  
optical gain measured

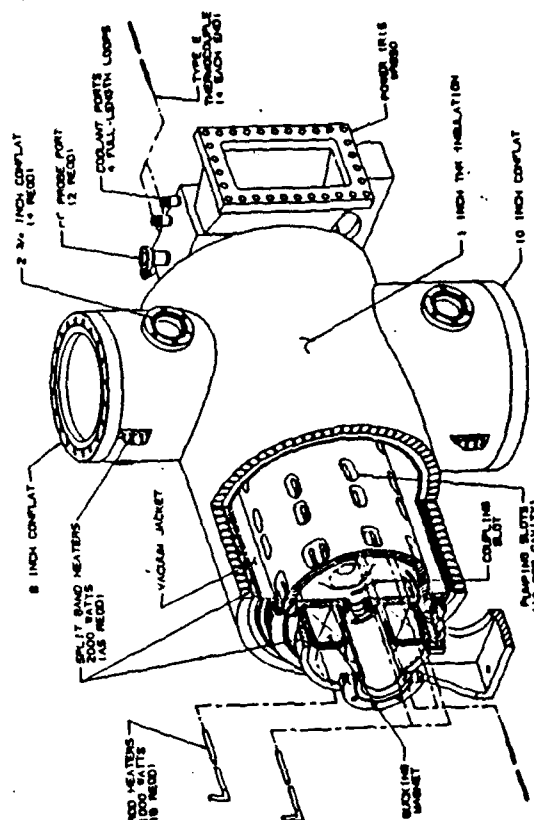
1983-84 **Oscillator Experiment**  
10 kW output at 10  $\mu\text{m}$   
"Perfect" optical quality  
Tunable from 9-35  $\mu\text{m}$

1985-86 **Energy Recovery Experiment (ERX)**  
70% of electron beam energy recovered  
FEL operation stable during recovery  
2% extraction efficiency in oscillator

**Photoelectric Injector Demonstrated**  
600 A/cm<sup>2</sup> emission from 1 cm<sup>2</sup> Cs<sub>3</sub>Sb cathode  
3 Amp average current produced at 1 MeV  
Good emittance demonstrated (40  $\pi$  mm-mRad  
at 8 nCoul)

1987-88 **FEL Experiments Demonstrated**  
Sideband suppression using Littrow grating  
6% efficiency using prebuncher  
Validation of computer codes  
Lasing on 3<sup>rd</sup> harmonic (4  $\mu\text{m}$ )  
Harmonic measured to 7<sup>th</sup> harmonic

**Photoelectric Injector**  
Durability of Cs<sub>3</sub>Sb cathode  
3 MeV operation  
600 Amp peak current in 22 ps pulses



## SUMMARY OF PHOTOINJECTOR PROPERTIES:

### PHOTOCATHODE DRIVE LASER:

Nd-YLF Oscillator and Amplifiers  
Laser Wavelength: 527 nm  
Laser Power: 230 W/A% QE

Modelocked Frequency: 100.33 MHz  
Micropulse Repetition Rate: 21.67 MHz  
Macropulse Repetition Rate: 1.00 Hz

### PHOTOCATHODE:

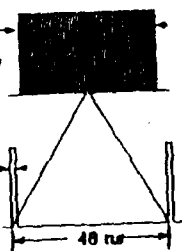
Cs<sub>3</sub>Sb Quantum Efficiency: 1% at 527 nm  
CsK<sub>2</sub>Sb Quantum Efficiency: 4% at 527 nm  
Cathode Area: 1 cm<sup>2</sup>

### ELECTRON MACROPULSE:

Pulsewidth: 10-100  $\mu\text{s}$   
Average Current: 0.1 A  
Output Energy: 6.0 MeV

### ELECTRON MICROPULSE:

Pulsewidth: 17 ps  
Charge per Pulse: 5 nC  
Peak Current: 300 A



## Conclusions:

HIBAF will be a unique facility for continued development of FEL technology.

1. High quantum efficiency photocathode rf gun.
2. Production and transport of high-current, high-brightness electron beams.
3. Develop, validate, and calibrate electron beam diagnostics.
4. Validate and calibrate "integrated" numerical design codes (INEX).
5. Test new concepts.
6. Demonstrate maintenance of electron beam quality through large-angle bends.
7. Demonstrate technologies needed for the next generation FEL.

## EX3.4 FIRST DEMONSTRATION OF A FREE-ELECTRON LASER DRIVEN BY ELECTRONS FROM A LASER IRRADIATED PHOTOCATHODE

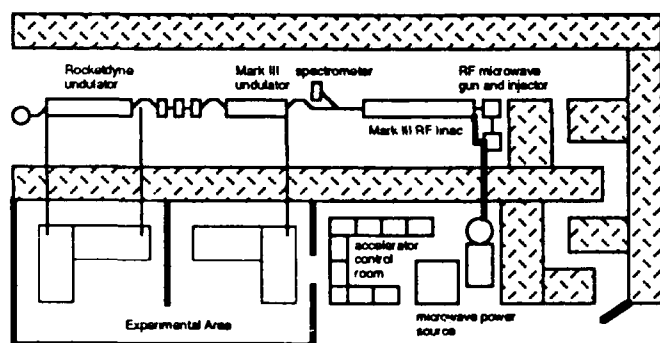
Mark Curtin, Glenn Bennett, Anup Bhowmik, Robert Burke and Phillip Metty  
Rockwell International, Rocketdyne Division  
6633 Canoga Avenue, Canoga Park, CA 91303

and

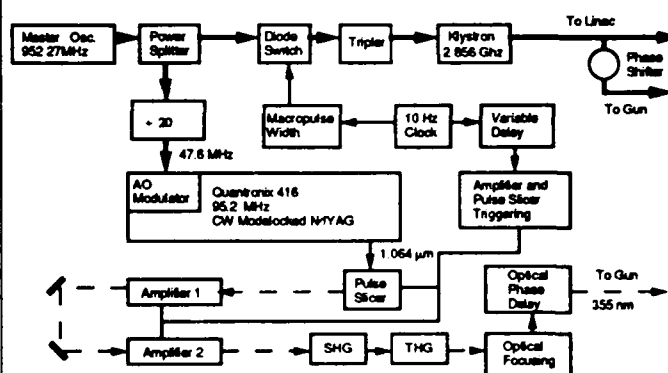
Stephen V. Benson and John M. J. Madey  
Stanford Photon Research Laboratory  
Stanford University, Stanford, CA 94305

We report the results from the first operation of a free-electron laser driven by electrons from a laser irradiated photocathode. A tripled Nd:Yag mode-locked drive laser was used to irradiate a LaB<sub>6</sub> cathode positioned within a microwave gun to produce 700 pC micropulses. Peak currents in excess of 125 Amp were observed for electron beams having an energy spread of 0.8% (FWHM) at 38.5 MeV and an emittance, at the undulator, comparable to that observed for thermionic operation of the cathode. Preliminary estimates for beam brightness deliverable to the undulator range from  $3.5 \times 10^{11}$  (A/m<sup>2</sup>) to  $5.5 \times 10^{11}$  (A/m<sup>2</sup>).

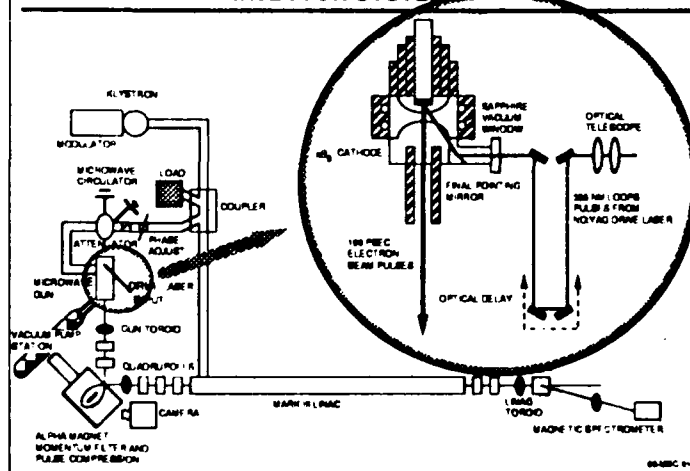
LAYOUT OF THE STANFORD PHOTON RESEARCH LABORATORY



PHOTOCATHODE DRIVE LASER / RF LINAC TIMING



LAYOUT OF THE MARK III MICROWAVE GUN AND INJECTOR SYSTEM



SYSTEM PARAMETERS FOR THE LASER-DRIVEN PHOTOCATHODE EXPERIMENT

### DRIVE LASER PARAMETERS

FREQUENCY	95.2 MHz
REP. RATE	10 Hz
MACROPULSE LENGTH	10 μsec
MICROPULSE LENGTH	100 psec
WAVELENGTH	355 nm
MICROPULSE ENERGY	40 μJ

### INJECTOR/LINAC PARAMETERS

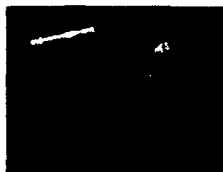
FREQUENCY	2857 MHz
REP. RATE	10 Hz

### E-BEAM PARAMETERS

MACROPULSE CURRENT	15 mA
MACROPULSE LENGTH	3 μsec
MICROPULSE CURRENT	60-80 A
MICROPULSE LENGTH	2-3 psec
$\gamma_{\text{FC}}$	~ 8x mm-mrad
$\gamma_{\text{FY}}$	~ 4x mm-mrad
ENERGY	38.5 MeV
ENERGY SPREAD	0.8%

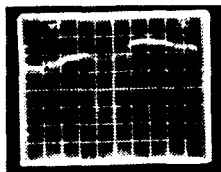
**CHARGE CONTAINED IN A MICROPULSE CAN BE ESTIMATED FROM THE AVERAGE MACROPULSE CHARGE AS MEASURED BY THE GUN AND LINAC TOROIDS**

**GUN #1 TOROID**



**MICROPULSE CHARGE**  
~ 250 pcoul

**LINAC TOROID**



**MICROPULSE CHARGE**  
~ 130 pcoul

©-MBC-010

**INDIVIDUAL MICROPULSES WERE RESOLVED USING A Au-Ge DETECTOR**

**MICROPULSES WERE SEPARATED BY 10.5 nsec**



©-MBC-010

**A PEAK INTRACAVITY POWER OF ~ 200 MW WAS MEASURED**

- OPTICAL MACROPULSE ENERGIES BETWEEN 0.3 - 0.5 mJ WERE MEASURED USING A PYROELECTRIC DETECTOR
- OPTICAL MACROPULSE DURATION WAS 2.5  $\mu$ sec
- ALPHA MAGNET CALIBRATION FROM PREVIOUS MOPA EXPERIMENTS SUGGESTS A 2 psec MICROPULSE



TYPICAL MACROPULSE ENERGY 0.35 mJ

©-MBC-010

**COMPARISON OF ELECTRON BEAM PARAMETERS (AT THE UNDULATOR) FOR THERMIONIC OPERATION AND PHOTOCATHODE OPERATION**

PARAMETER	THERMIONIC OPERATION	PHOTOCATHODE OPERATION
MICROPULSE CHARGE (pCoul) (at linac toroid)	70	170
SMALL SIGNAL GAIN (per pass)	60%	100%
MICROPULSE CURRENT (A) (as calculated from the small signal gain)	35	60
NORMALIZED EMITTANCE (mm-mrad)		
$\gamma\beta\epsilon_x$	10 $\pi$	8 $\pi$
$\gamma\beta\epsilon_y$	4 $\pi$	4 $\pi$
PEAK BRIGHTNESS ( $A/m^2$ )	$1.8 \times 10^9$	$3.9 \times 10^9$

©-MBC-010

**PHOTOCATHODE DRIVEN FEL OPTICAL MACROPULSE**

AMPLITUDE FLUCTUATIONS WITHIN THE FEL MACROPULSE RESULT FROM SMALL FLUCTUATIONS WITHIN THE DRIVE LASER MACROPULSE

"SIERRA MOUNTAIN EFFECT"



Au - Ge DETECTOR

©-MBC-010

**ROCKETDYNE/STANFORD PHOTOCATHODE ACHIEVEMENTS**

- FIRST DEMONSTRATION OF A PHOTOCATHODE DRIVEN FEL OSCILLATOR USING THE MARK III RF-LINAC AND THE ROCKETDYNE 2 METER UNDULATOR
- OBSERVED PEAK CURRENTS IN EXCESS OF 125 AMP AT 38.5 MeV
- MEASURED E-BEAM ENERGY SPREAD OF 0.8% AFTER LINAC
- EMITTANCE AFTER LINAC COMPARABLE TO THERMIONIC EMITTANCE
- OBSERVED SUSTAINABLE SMALL SIGNAL GAIN IN EXCESS OF 100% PER PASS AT 3.1  $\mu$ m
- PRELIMINARY MEASUREMENTS OF TRANSVERSE EMITTANCE AT UNDULATOR USING SPONTANEOUS EMISSION SUGGEST THE EMITTANCE IS PRESERVED THROUGH THE TRANSPORT LINE
- VERIFIED LaB<sub>6</sub> QUANTUM EFFICIENCY AT  $10^{-4}$  (@ 100 amp/cm<sup>2</sup>)
- ACCUMULATED ~ 100 HRS OF PHOTOCATHODE OPERATION WITH NO OBSERVABLE DETERIORATION OF THE LaB<sub>6</sub> CATHODE

©-MBC-010

## EX3.5

### INEX Applied to the Boeing Aerospace FEL System

R.L.Tokar, S.C.Bender, K.D.Chan, A.H.Lumpkin, B.D.McVey, L.E.Thode, L.M.Young,  
Los Alamos National Laboratory, M.S.E531, Los Alamos NM 87545

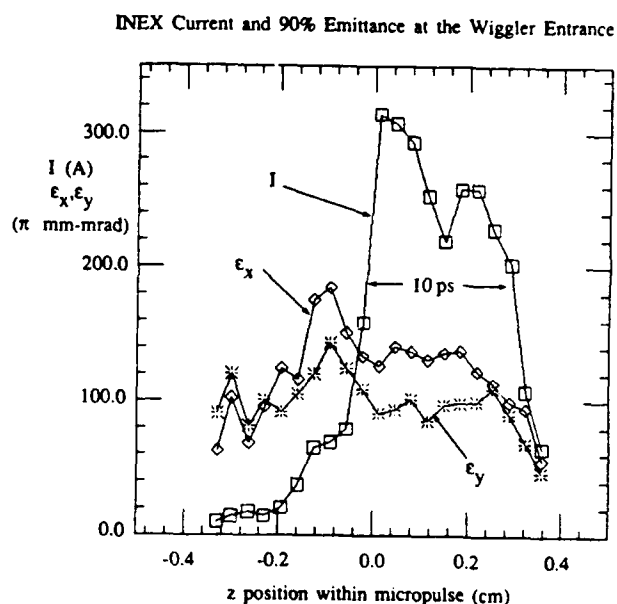
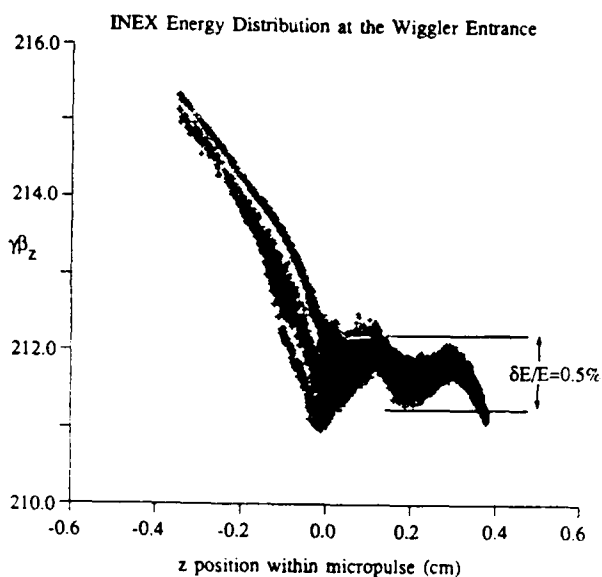
D.H.Dowell, A.R.Lowrey, A.D.Yeremian.

Boeing Aerospace Company, M.S.2R-00, Seattle, WA 98124

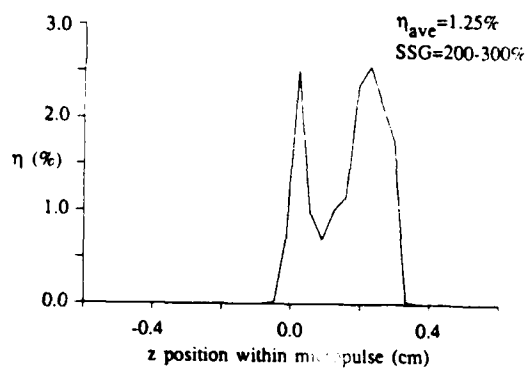
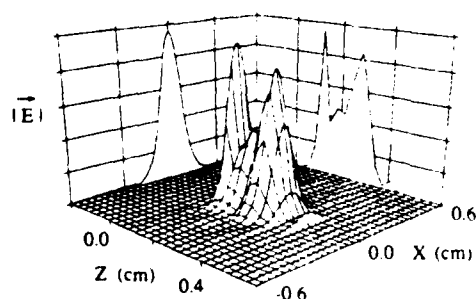
R.Justice

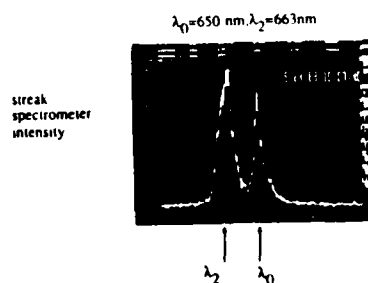
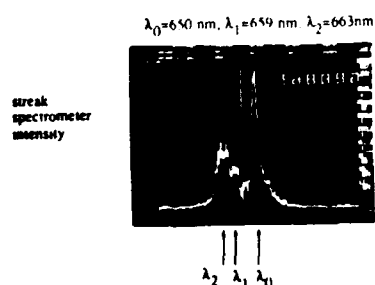
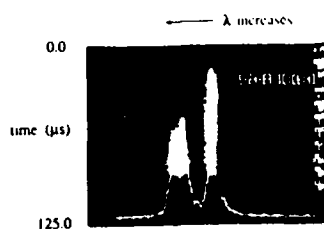
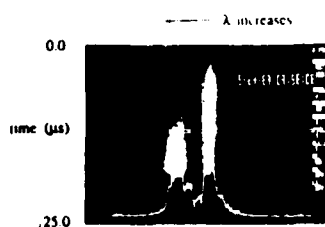
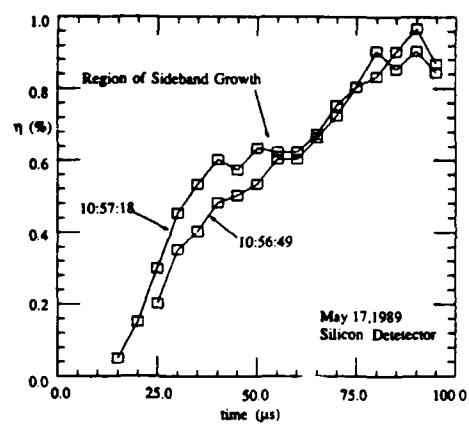
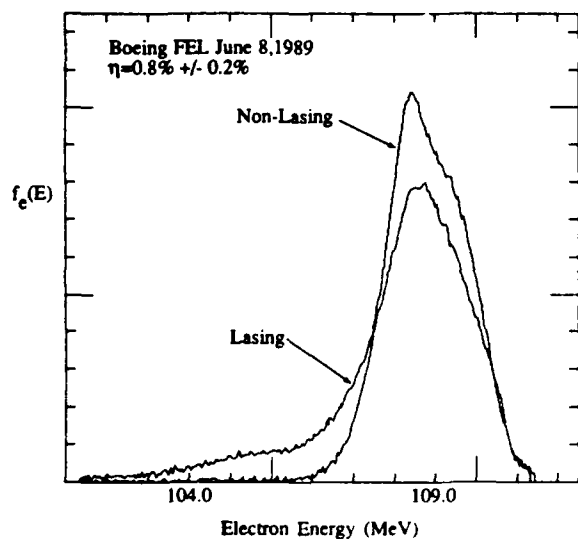
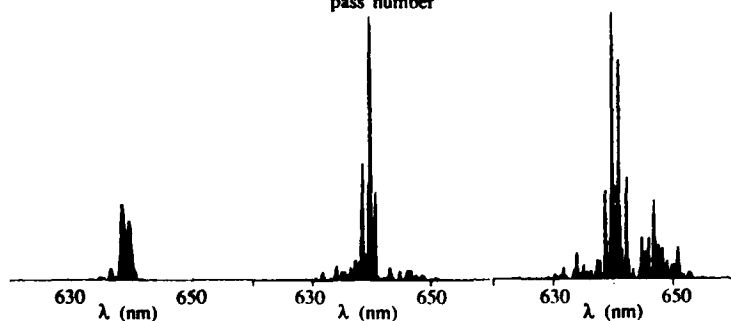
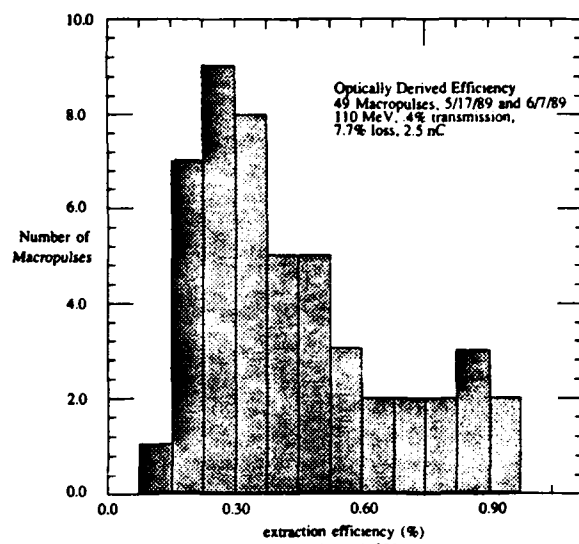
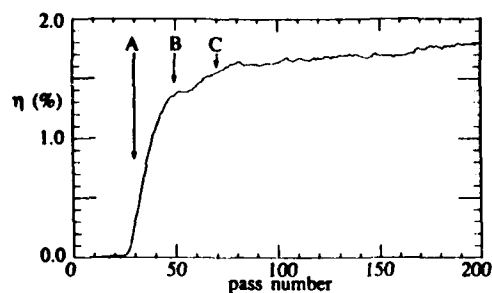
EG&G, Los Alamos, NM 87545

The INEX (integrated numerical experiment) philosophy is used to model the rf linac driven 0.6  $\mu\text{m}$  FEL oscillator at Boeing Aerospace Company (BAC). INEX links accelerator and FEL physics codes to provide an end-to-end model of the system. For a mild tapered wiggler in use in May, 1989, INEX predicts an extraction efficiency of about 1.25%, with the experiment achieving 1.0%. Sideband development in the experiment is in good agreement with 1D pulse simulations.



Pulse Shape at the Wiggler Exit and Extraction Efficiency vs.  $z$





### TH3.1

## Current Research in FEL Theory\*

E. T. Scharlemann

Lawrence Livermore National Laboratory  
University of California, Livermore, California 94550

A simple summary and explanation of several areas of current theoretical research – superradiance, harmonic emission, and wiggler field errors – is attempted. “Superradiance” refers to a modification of exponential growth and saturation at the trailing edge of an electron beam pulse, where the presence of the edge boundary condition is felt. Our understanding of harmonic emission has recently been improved with the discovery of a much stronger coupling to even harmonics, including a resonant coupling to the second harmonic. Finally, the varied effects of pole-to-pole magnetic field errors in a wiggler are summarized, along with the ways in which their effects can be reduced.

\* Work performed jointly under the auspices of the U. S. DOE by LLNL under contract W-7405-ENG-48 and for the SDIO and USASDC in support of SDIO/SDC MIPR No. W31RPD-9-D5007.

## Current research in FEL theory

**A highly prejudiced selection:**

- superradiance
- harmonic emission
- wiggler errors

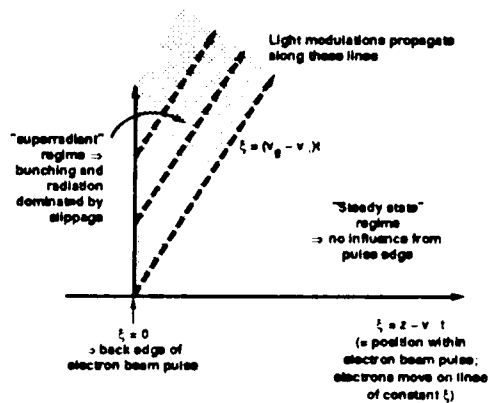
that omits

- sidebands
- optical guiding
- effects of optical guiding on sidebands
- shot noise, amplified spontaneous emission
- quantum effects
- oscillator mode evolution (e.g. with cw electron beams)
- two-stage FELs
- modeling of electron beam phase space effects
- comparisons with experiments
- analysis of unconventional FEL schemes

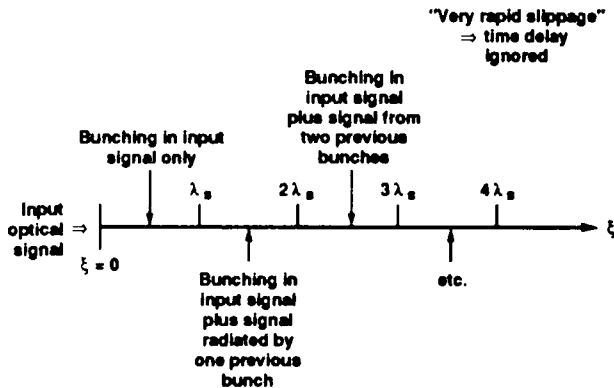
## Superradiant emission in FELS

- **Slippage of light with respect to electrons in an FEL changes exponential growth and saturation**
  - Light modulations propagate with group velocity  $v_g$
  - Electrons travel longitudinally at  $v_e$
  - Usually  $v_g > v_e$  so that light moves ahead of the electrons
- **Background**
  - Bonifacio, Casagrande JOSA B 2 (1985) 250; NIM A239 (1985) 36: Slippage represented by radiation damping term  $\rightarrow n^2$  dependence of equilibrium radiated intensity
  - Bonifacio, McNeil NIM A272 (1988) 280: very short pulse simulations with slippage exhibited spiking behavior  $\sim n^2$  at trailing edge of pulse
  - Bonifacio, Maroli, Pioella Optics Comm 68 (1988) 360: analytical treatment of exponential gain with slippage

## Superradiant effects occur at the trailing edge of an electron pulse



**Superradiance can be simply understood by considering the effect of very rapid slippage**



## "Collective variables" can be used to obtain a quantitative treatment of superradiant emission

Bunching parameter  $b = \langle e^{-i\theta} \rangle$   $\theta = (k + k_w)z - \omega t$

Field strength  $A \sim E_z$

Linearized, normalized, on resonance, and for rapid slippage:

$$\frac{\partial^2 b}{\partial \xi^2} = iA \quad \text{Bunching at fixed } \xi \text{ evolves in response to field } A$$

$$\left[ \frac{\partial A}{\partial \xi} + \right] (1 - \beta_p) \frac{\partial A}{\partial \xi} = b \quad \text{Field is amplified by bunching as the light propagates over the pulse}$$

↑  
Negligible for rapid slippage

Specific cases:

- $\beta_p \rightarrow 1$ : standard cubic dispersion relation
- $e^{i(k-k_w)z}$  dependence  $\rightarrow \omega(k)$  relation that ignores boundary condition at tail of pulse

## Specific cases (cont'd)

- Laplace transform in  $t$  to incorporate boundary conditions at  $t=0$  and  $\xi=0$   
 $\Rightarrow A, b \propto e^{(\text{coefficient}) \cdot \xi^{1/2}}$  asymptotically
  - Equations without rapid slippage assumption have an identical form with different variables  
 $u = z - v_p t \quad v = v_p t - z$   
 $\Rightarrow$  same asymptotic solution
  - If saturation is assumed to occur when "bounce frequency"  $\approx$  "growth rate" then  
 $P_{\text{saturation}} \propto n^2 \Rightarrow$  superradiance
  - Nonlinear state appears to involve very short time scale spiking with intensity  $\propto n^2$

## Connection between superradiance and sidebands

- Exponential growth is very different
  - Different equilibria:
    - Zero field, zero bunching for superradiance
    - Saturated field and bunching for sidebands
  - Different boundary conditions
  - Different growth rates
- Non-linear evolution appears identical
  - Spiking with electrons undergoing 1/2 synchrotron oscillation through each spike  
 (Warren, Goldstein, Newnam NIM A250 (1986) 19)
- Perhaps the non-linear state of all instabilities involving slippage will look the same

## Harmonic emission from a free-electron laser

Background: "standard" coupling to harmonics in  
 Colson IEEE JOE QE-17 (1981) 1417  
 Colson, Dattoli, Croci Phys Rev A31 (1985) 828

- Describes non-resonant emission in a linear wiggler (even one with a perfectly sinusoidal field)
  - Single  $e^-$  coupling arises from non-sinusoidal wiggler motion
    - $\rightarrow$  Spontaneous emission of harmonic, by itself
    - $\rightarrow$  Only odd harmonics for aligned  $e^-$
  - Non-sinusoidal bunching
    - $\rightarrow$  Coherent spontaneous emission from bunching at fundamental, or
    - $\rightarrow$  Gain at harmonics: non-resonant, so tapering cannot work  
 (Oscillation at harmonics observed by TRW, Stanford, LANL...)

## "Non-standard" harmonic emission

Schmitt, Elliott Phys Rev. A34 (1986) 4843

- Resonant coupling of 2<sup>nd</sup> harmonic to field gradient
- Can be derived from  $e^-$  energy equation:

$$\frac{dy}{dz} = -\frac{e}{mc^2} \vec{v} \cdot \vec{E}$$

Wiggle motion  $\vec{v} = \hat{x} \cos k_w z$   
 $n^{\text{th}}$  harmonic of signal field (no gradient)

$$\vec{E} = \hat{x} \sin [n(kz - \omega t) + \phi_n]$$

so

$$\vec{v} \cdot \vec{E} = \sin [(nk + k_w)z - n\omega t + \phi_n]$$

Slowly varying near resonance only for  $n=1$

$\Rightarrow$  Standard non-resonant coupling

## "Non-standard" harmonic emission (2)

- In presence of field gradient:  
 Wiggle motion  $\vec{v} = \hat{x} \cos k_w z$  (as before)  
 $n^{\text{th}}$  harmonic of signal field

$$\vec{E} = \vec{E}_0 + \frac{\partial \vec{E}_0}{\partial x} \cdot (x - x_0) \quad \text{as seen by one electron}$$

Wiggle motion  $\propto \sin k_w z$

so

$$\vec{v} \cdot \vec{E} = \cos k_w z \cdot \cos [n(kz - \omega t) + \phi_n] \cdot \sin k_w z$$

$$(\vec{v}) \quad \left( \frac{\partial \vec{E}_0}{\partial x} \right) \quad (x - x_0)$$

$$\propto \sin [(nk + 2k_w)z - n\omega t + \phi_n]$$

Slowly varying near resonance for  $n=2$

But  $x - x_0 = \frac{R_w}{\gamma}$  so coupling is reduced from fundamental



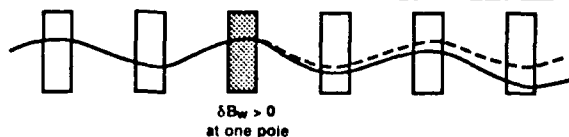
### "Non-standard" harmonic emission (3)

- Coupling to field gradient implies coherent spontaneous emission or gain in odd optical mode (e.g. rectangular TEM<sub>01</sub>)
- Resonant 2<sup>nd</sup> harmonic emission can be as strong as non-resonant 3<sup>rd</sup> harmonic emission
- Other even harmonics are emitted by an aligned e<sup>-</sup> beam through the non-resonant extension of this mechanism

#### Implications:

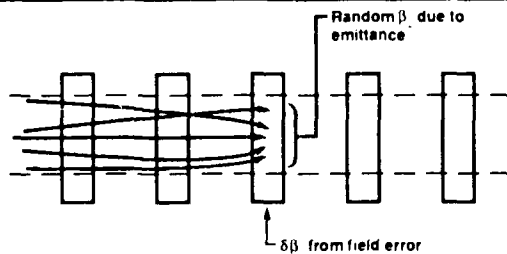
- Much stronger even harmonic emission than previously expected (Standard Mark III experiment shows yet more)
- Coherent radiation in even harmonics for perfectly aligned electron beam

### Trajectory errors arise from random transverse kicks associated with wiggler field errors



- Trajectory errors change the path length travelled by an electron and hence introduce phase errors
- Trajectory errors can walk the electron beam out of the optical beam, particularly if the optical beam is confined (by optical guiding) to about the electron beam size

### Emittance introduces an additional phase error, random among electrons



$$\delta(\psi) = -k \beta \cdot \delta \beta \text{ is a random phase error}$$

### The effect of wiggler errors on FEL performance

#### Background:

- Kincaid JOSA B 2 (1985) 1294 analyzed the effect of random (uncorrelated) pole-to-pole wiggler field errors on electron trajectories and on their phase
  - Weak fields
  - No electron beam focusing
  - Steering at wiggler entrance
- Analysis for long high-gain wigglers in *FEL Handbook* (in press)
- Nine papers in the Advance Program for this conference

### Phase errors arise from changes in path length associated with field errors

#### Ponderomotive phase

$$\psi = (k + k_w)z - \omega t + \phi = \theta + \phi$$

↑  
signal phase

#### Evolves as

$$\frac{d\psi}{dz} = k_w - \frac{k}{2\gamma^2} (1 + a_w^2 + \gamma^2 \beta_\perp^2)$$

↑                      ↑  
wobble                betatron  
motion                motion

#### For each field error

$$\delta(\psi) = -\frac{k}{\gamma^2} (a_w \delta a_w + \gamma^2 \beta_\perp \cdot \delta \beta_\perp^2)$$

### Transverse focusing reduces trajectory errors

- Without focusing, errors produce random walk in transverse velocity:

$$\langle \delta \beta_\perp^2 \rangle^{1/2} \sim \langle \delta a_w^2 \rangle^{1/2} N^{1/2}$$

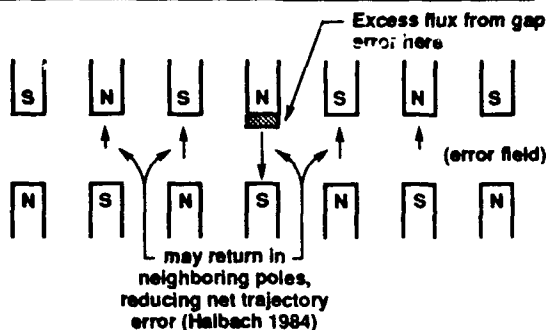
so

$$\langle \delta x^2 \rangle^{1/2} \propto \langle \delta a_w^2 \rangle^{1/2} N^{3/2}$$

- With focusing, errors produce random walk in transverse betatron amplitude:

$$\langle \delta x^2 \rangle^{1/2} \propto \langle \delta a_w^2 \rangle^{1/2} N^{1/2}$$

## Correlations of wiggler field errors can reduce their trajectory and phase effect



- 3d effects (flux leakage out sides of poles)
- Highly permeable flux path connecting many poles that prevents return of error flux in neighboring poles

→ Uncorrelated errors

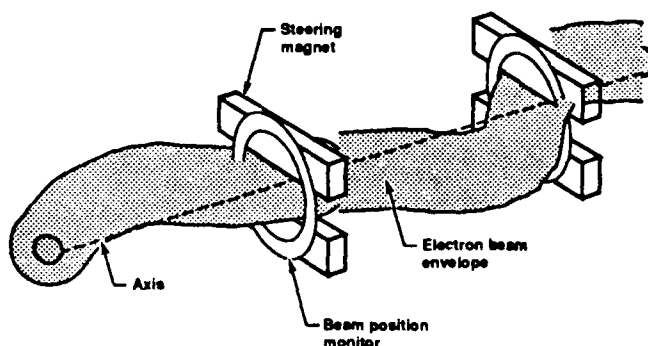
## Real-time adjustable tapering can remove the worst effect of phase errors

- $\delta(\psi) = -\frac{k}{\gamma} a_w \delta a_w$  is identical for all electrons; hence can be corrected by adjusting  $a_w$
- Simulations (with FRED) indicate that when  $\delta a_w$  is included in taper algorithm, these phase errors do not effect performance
- Experimental verification is far in the future

## High fields can reduce phase errors

- Ponderomotive potential provides longitudinal focusing analogous to transverse focusing
- In weak fields, wiggler errors produce random walk in  $\psi$   
 $\langle \delta\psi^2 \rangle^{1/2} \sim N^{1/2}$
- In strong fields, wiggler errors produce random walk in synchrotron oscillation amplitude  
 $\langle \delta\psi^2 \rangle^{1/2} \sim N^{1/2}$

## Steering can correct for trajectory errors ...



## ...but steering can make phase errors worse

- Steering is never perfect; beam position sensing can only be done to non-zero tolerances
- Because imperfect, steering cannot be done arbitrarily often
- Steering adds to emittance induced phase errors:  $\delta\psi$  from steering compounds individual  $\delta\psi$  from pole errors unless steering occurs often on a synchrotron period

## Vague generalities about errors

- Trajectory errors most important in high-gain, high-field amplifiers
  - Optical mode guided by electron beam
  - Trajectory errors weaken guiding and can walk electron beam out of optical mode
  - Phase errors controlled by deep ponderomotive wells
- Phase errors probably most important in low-gain oscillators
  - Optical mode defined by cavity and can be much bigger than electron beam
  - Trajectory errors are less likely to walk electron beam out of optical mode

# TH3.2

## TRANSVERSE AND PARALLEL BEAM QUALITY IN FREE-ELECTRON LASERS\*

C. V. Roberson

Physics Division  
Office of Naval Research  
Arlington, VA 22217  
202-696-4222

B. Hafizi

Beam Physics Branch  
Plasma Physics Division  
Naval Research Laboratory  
Washington, DC 20375  
202-767-2874

The equilibrium electron beam radius in a FEL is determined by the emittance and focusing properties of the wiggler. The spot size of the radiation beam is determined by the optical guiding effects of the FEL interaction. For filling factor equal to unity, we have obtained a simple scaling relationship connecting the beam emittance and FEL wavelength, with wiggler strength and current as parameters.

To get from where we are to  $\textcircled{1}$   
where we want to go we must  
improve the electron beam quality!

Examples

High Power (Directed energy applications)  
Short wavelength (XUV)  
microw wigglers.

Emittance, Brightness, ETC. ....  
(Transverse)

$$\epsilon_{x,y} = 4 \left[ \langle x^2 \rangle \langle (p_x/m_0 c)^2 \rangle - \langle x p_x/m_0 c \rangle^2 \right]^{1/2}$$

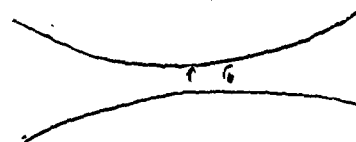
$$\frac{1}{\lambda^2} r_b^2 + \frac{\beta_0^2}{4\beta_0^2 c^2 \gamma_0^2} r_b^2 - \frac{2V}{\beta_0^2 \gamma_0^2 r_b} - \frac{\epsilon_m^2 + (\beta_0/m_0 c)^2}{\beta_0^2 \gamma_0^2 r_b^2} = 0$$

Magnetic Field      Current      Mag. Flux Cathode

Envelope Equation

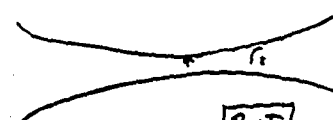
Beam Envelope

$$r_b(z) = r_b(0) \left[ 1 + \epsilon^2 z^2 / r_b^4(0) \right]^{1/2}$$



Radiation Beam

$$r_s = r_s(0) \left[ 1 + \lambda^2 z^2 / \pi^2 r_s^4(0) \right]^{1/2}$$



$$r_s = r_b$$

$$\lambda = \pi \epsilon$$

**BUT**  
wiggler focuses  
optical guiding

What about the current ?

Brightness (Transverse) phase space density

$$B_n = \frac{\epsilon_0 I_b}{\pi^2 \epsilon_n^2}$$

$$\sim \frac{I_b}{\Delta E}$$

Transverse emittance

$\epsilon = 2$   
Uniform ellipsoidal x-section

FEL Beam Quality (Parallel) <sup>③</sup>

$$B_g = \frac{I}{\Delta \gamma_z / \gamma}$$

But, Where is the FEL ? ?

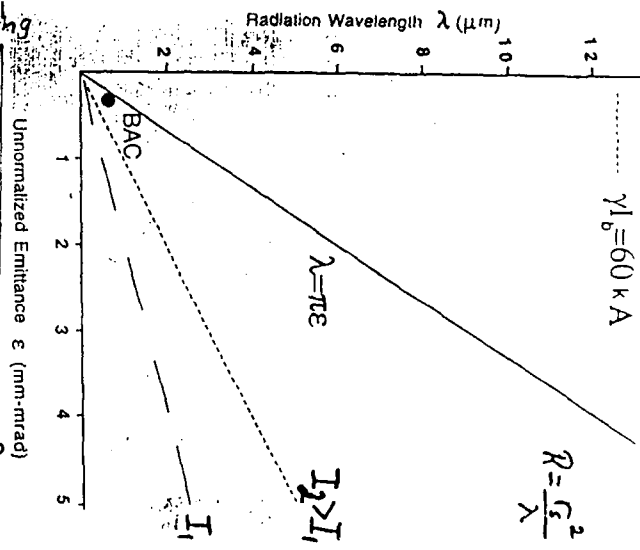
$\lambda$  vs  $E$  With wiggler focusing & optical guiding

$$\lambda = \left[ \frac{\gamma V}{1 + a_w^2/2} \right]^{1/2} E$$

$$\text{where } V = \frac{I_b (\text{KA})}{17\beta}$$

gain guiding results from

B. Hatizi, P. Sprangle and A. Ting  
Phys. Rev. A36, 1739 (1987)



# FEL DISPERSION RELATION

$$\left( \omega^2 - c^2 k^2 - \frac{\omega_p^2}{\gamma} \right) \left\{ \left[ \omega - V_0 (k + k_w) \right]^2 - \frac{\omega_p^2}{\gamma k^2} \right\}$$

E.M. mode 1 Beam mode 11

$$= \frac{\omega_p^2}{\gamma} \beta_w^2 c^2 k k_w$$

Resonant  
strong pump  
(High-Gain)

Wiggler Amplitude

## Scaled Thermal Velocity

$$\left( \omega^2 - c^2 k^2 - \frac{\omega_p^2}{\gamma} \right) \left[ \omega - V_0 (k + k_w) + i k V_{th} \right]^2$$

$$= \omega_p^2 \beta_w^2 c^2 k k_w / \gamma$$

Transform To Dimensionless Parameters.

Effective Thermal Spread is

$$S = \left( \frac{V_{th}}{V_z} \right) \left( 4 \cdot \omega^2 \gamma^3 \gamma_z^2 / \omega_p^2 a_w^2 \right)^{1/3}$$

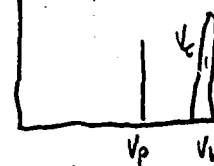
Large

Lorentzian

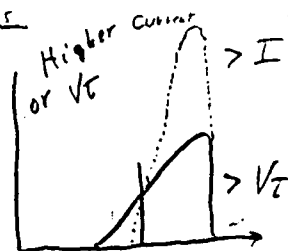
## Routes To warm beams

Cold Beam

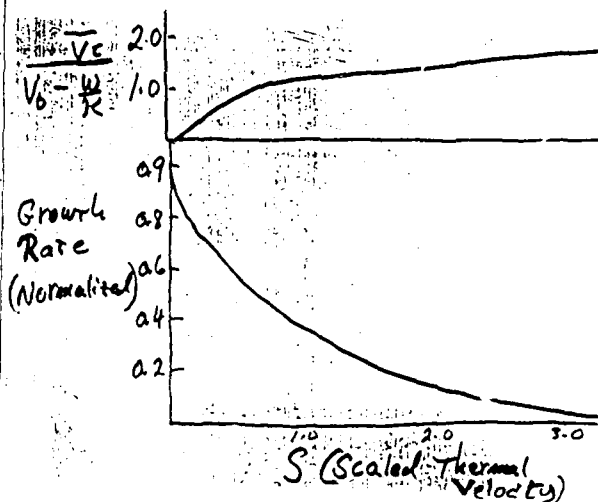
S(V)



Shorter λ



$$\frac{V_t}{V_b - V_p} \ll 1$$



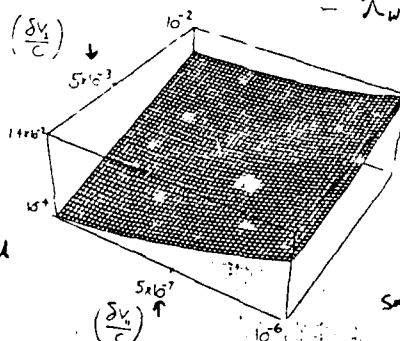
$\gamma$  vs  $\delta V_{II}$  and  $\delta V_L$

$$\left( \frac{\lambda}{\lambda_b} \right)^2 = \left[ \frac{2\pi^2}{S^3} \frac{\gamma_z^4}{\beta_w^2} \frac{1 + a_w^2/2 (\delta V_{II})^2}{\gamma V} \left( \frac{1}{c} \right) + \frac{1}{2} \frac{\gamma V}{1 + a_w^2/2} \left( \frac{\delta V_L}{c} \right)^2 \right]$$

Set  $S = 1$  to find bounding surface transition to kinetic regime of FEL operation.

$$r_b = 1 \text{ mm}$$

$$\lambda = 0.1 - 14 \mu$$



Boeing  $S = 1$   
 $V = 170 \text{ MeV}$   
 $I = 250 \text{ A}$   
 $\lambda_w = 2.18 \text{ cm}$

subharmonic bunching

2 points 1. Can be done; but require 2.  $\delta V_{II}$  4 orders smaller

Where is the light?

# TH3.4

## Equilibrium Self-Field-Induced Chaos In Electron Orbits In Free Electron Lasers

Chiping Chen and Ronald C. Davidson  
Plasma Fusion Center  
Massachusetts Institute of Technology  
Cambridge, Massachusetts 02139, U.S.A.

It is shown that the motion of an electron in the wiggler, guide and equilibrium self fields in the FEL is nonintegrable. The Group-I and Group-II orbits become chaotic when the self fields are sufficiently strong. The threshold self-field parameter for beam chaoticity is calculated for parameter regimes of experimental interest.

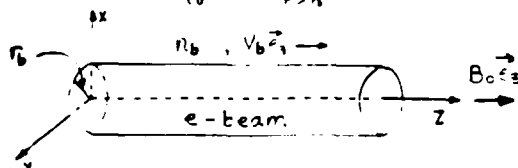
### OUTLINE

- I. INTRODUCTION
  - A. Motivation
  - B. Chaos
- II. CANONICAL FORMULATION OF THE PROBLEM
  - A. Model and Assumptions
  - B. Hamiltonian
- III. THE INTEGRABLE LIMIT ( $\epsilon = 0$ )
  - A. Fixed Points (Steady-State Orbits)
  - B. Interpretation of the Canonical Momentum
  - C. Stability of the Fixed Points
- IV. CHAOTIC MOTION ( $\epsilon \neq 0$ )
  - A. Equations of the Motion
  - B. Analysis of Self-Field-Induced Resonances
  - C. Poincare Surface-of-Section Map and Chaos
- V. CONCLUSIONS

### MODEL AND ASSUMPTIONS

- a) Helical wiggler:  $\vec{B}_w = -B_w(\vec{e}_x \cos k_w z + \vec{e}_y \sin k_w z)$
- b) Axial guide field:  $\vec{B}_0 = B_0 \vec{e}_z$
- c) Uniform-density-beam profile:

$$n_b(r) = \begin{cases} n_0 = \text{const.} & 0 \leq r < r_0 \\ 0 & r > r_0 \end{cases}$$



Equilibrium Self Fields ( $r < r_0$ ):

$$\vec{E}_0 \propto -\omega_p^2 \vec{r}, \quad \vec{B}_0 \propto -\omega_p^2 \vec{r} \times \vec{e}_z$$

Self-field parameter:

$$\epsilon = \frac{\omega_p^2}{4\Omega_e^2}$$

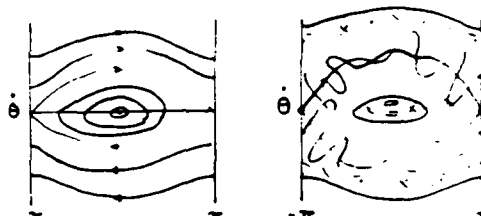
- d) Electromagnetic and electrostatic waves are not included.

### MOTIVATION

1. Most FEL analyses heretofore have ignored equilibrium self-field effects.
2. Inclusion of the self-fields results in chaotic behavior in the particle orbits.
3. It is a fast perturbation compared with the sideband and electromagnetic perturbations.

### CHAOS

1. Chaos means sensitive to the initial conditions.
2. Poincare maps, integrable and nonintegrable systems



HAMILTONIAN ( $r < r_0$ )

$$H = \frac{1}{2}(c\vec{p} + e\vec{A})^2 + m^2 c^4 \sqrt{1 + \frac{v^2}{c^2}} - e\Phi = \gamma mc^2 - e\Phi$$

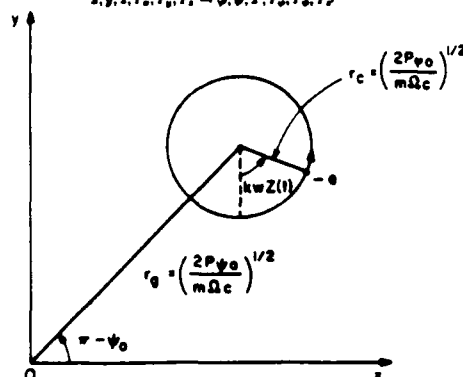
$$\Phi = \frac{m\omega_p^2}{4e}(x^2 + y^2) \propto \epsilon$$

$$\vec{A} = B_0 x \vec{e}_y + A_w(\vec{e}_x \cos k_w z + \vec{e}_y \sin k_w z) + \beta_0 \Phi_0 \vec{e}_z$$

$$A_w = \frac{B_w}{k_w} = \text{const.}$$

### New Canonical Variables

$$x, y, z, P_x, P_y, P_z = \varphi, \psi, s, P_\varphi, P_\psi, P_s$$

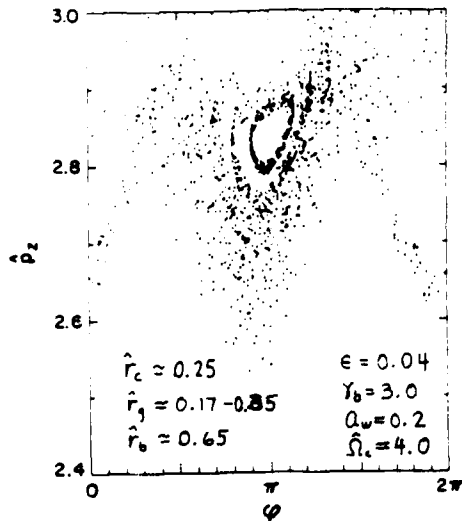
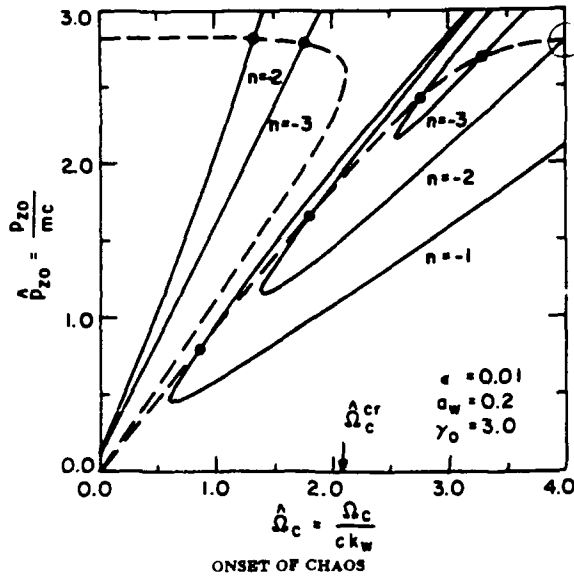


Normalized Hamiltonian: ( $m = e = c = k_w = 1$ )

$$\hat{H}_s(\varphi, \psi, \hat{P}_\varphi, \hat{P}_\psi, \hat{P}_s) = -\hat{\Phi}_s + [2\hat{\Omega}_c \hat{P}_\varphi + 2a_w(2\hat{\Omega}_c \hat{P}_\varphi)^{1/2} \cos \varphi + (\hat{P}_s - \hat{P}_\varphi + \hat{P}_\psi + \beta_b \hat{\Phi}_s)^2 + a_w^2 + 1]^{1/2}$$

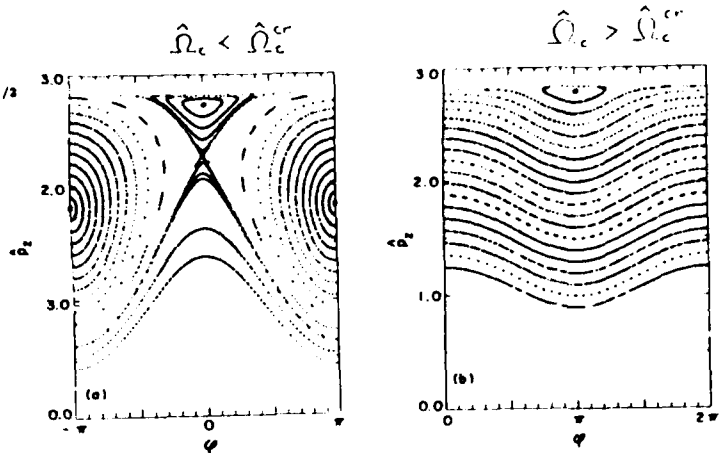
$$\hat{\Phi}_s(\varphi, \psi, \hat{P}_\varphi, \hat{P}_\psi) = 2\epsilon \hat{\Omega}_c [\hat{P}_\varphi + \hat{P}_\psi - 2(\hat{P}_\varphi \hat{P}_\psi)^{1/2} \sin(\varphi + \psi)]$$

- a)  $\hat{H}_s$  and  $\hat{P}_s$  are the constants of the motion.  
b) The motion occurs in 3d phase space and is expected to be chaotic.  
c) In the  $\epsilon = 0$  integrable limit,  $\hat{P}_s$  is an additional constant.



For  $\lambda_w = 3.0$  cm, the parameters correspond to  
 $I_b^{(th)} = 4.3$  kA  
 $B_w = 710$  G,  $B_0 = 14.2$  kG  
 $\beta_b = 0.93$ ,  $\gamma_b = 3.0$ ,  $r_b = 3.1$  mm

INTEGRABLE PHASE-SPACE STRUCTURE ( $\epsilon = 0$ )



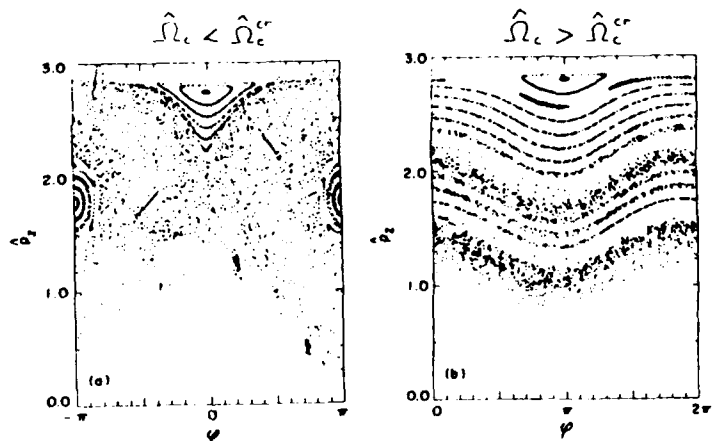
Resonance Condition:

$$n\omega + m\beta_b \approx 0$$

Resonance Width  $\omega_n$ :

$$\frac{\omega_n}{\gamma_b} \propto \left(\frac{1}{\gamma_b}\right)^{1/2} \left(\frac{r_c}{r_b}\right)^{1/2} \left(\frac{r_g}{r_b}\right)^{1/2} \left(\frac{I_b}{I_A}\right)^{1/2} \propto \epsilon^{1/2}$$

NONINTEGRABLE PHASE-SPACE STRUCTURE ( $\epsilon = 0.01$ )



## CONCLUSIONS

1. Equilibrium self fields destroy the integrability of the single particle motion in the field configuration consisting of a constant-amplitude helical wiggler field and an axial guide field and consequently the electron orbits exhibit chaotic behavior.
2. The threshold value of the self-field parameter  $\epsilon = (\omega_{pb}/2\Omega_c)^2$  for the onset of chaoticity is determined numerically in the regime of moderately beam current ( $\approx 1 - 10$  kA) and moderately relativistic beam energy.
3. The characteristic time scale for self-field-induced changes is fast and given by  $\lambda_w/V_b$ .
4. Resonance conditions and scaling relations for the resonance width were derived and found in good qualitative agreement with the numerical simulations.

# PR3.1

## OBELIX - THE OXFORD FREE ELECTRON LASER PROJECT

W W M Allison(a), C A Brau(b), C B Brooks(a), G Doucas(a), J N Elgin(c),  
W A Gillespie(d), A R Holmes(a), D A Jaroszynski(e), M F Kimmitt(e), P F Martin(d),  
J H Mulvey(a), C R Pidgeon(e), M W Poole(f).

(a)Nuclear Physics Laboratory, University of Oxford, England; (b)Vanderbilt  
University, Tennessee, USA; (c)Imperial College, London, England; (d)Dundee Institute  
of Technology, Dundee, Scotland; (e)Heriot Watt University, Edinburgh, Scotland;  
(f)SERC Daresbury Laboratory, Warrington, England.

The proposed FEL would utilise the 10 MV folded tandem accelerator at Oxford to give  
radiation output in the fundamental from 60-300  $\mu\text{m}$ ; operation at a higher harmonic  
should extend this range to at least 30  $\mu\text{m}$ . In addition to an extensive programme  
of FEL studies it is intended to set up an IR User Facility.

### Reasons for Project

- 1) Continue UK involvement, making use of  
existing experience and expertise
- 2) Preparation for future short wavelength  
facility for synchrotron radiation community
- 3) FIR source as user facility
- 4) Assist in provision of centre for accelerator  
physics studies and training at a university  
(Oxford)

### Accelerator

10 MV electrostatic device at Oxford, operated  
since 1965 and converted to folded tandem  
geometry in 1978

Utilised at ~ 4000 hours annually for nuclear  
physics, but would now be dedicated to FEL

### GAIN PREDICTIONS

$E = 9 \text{ MeV}$ ,  $I = 2 \text{ A}$ ,  $\gamma = 100 \times \text{mm-mrad}$ ,  $\Delta\gamma/\gamma = 10^{-3}$   
 $L_w = 2 \text{ m}$ ,  $\lambda_w = 34 \text{ mm}$ ,  $B_{\text{rem}} = 1 \text{ T}$

	Gap (mm)	I (A)	$\lambda$ ( $\mu\text{m}$ )	Q (%)
OKPULSE (C. A. Brau)	13.3	1	94	100
HARMONIC (A. Amir)	13.3	1	94	112
		3	31	58
		5	19	26
	12.3	1	103	125
		3	34	74
		5	21	38
	10.3	1	126	152
		3	42	114
		5	25	75
		7	18	48
		9	14	30

Saturated power 10-100 kW

Build-up time ~ 1  $\mu\text{s}$  (40 passes)

Preliminary 3D runs confirm high gain (TDA)

### PARAMETER CHOICE

Electrostatic FEL : Low emittance (gun)  
Low energy spread  
No lethargy (no rf structure)

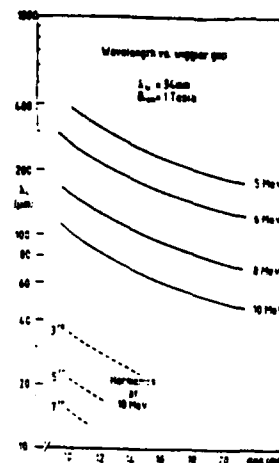
Optimum wavelength : FIR

Compact wiggler :  $L_w = 2 \text{ m}$   
 $\lambda_w = 34 \text{ mm}$

Features : Wide tuning  
Harmonic operation

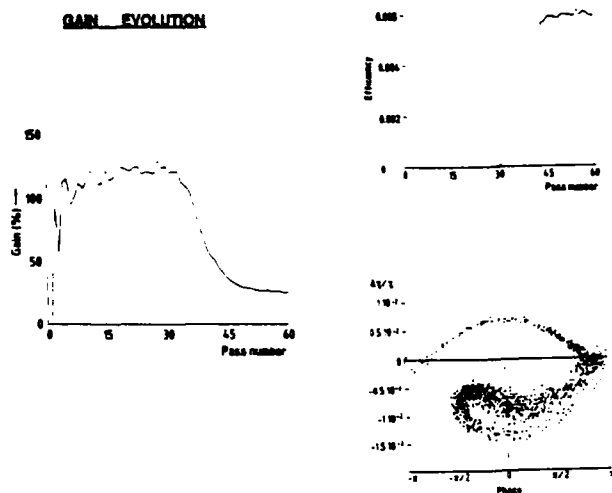
The terminal charging current is 200-300  $\mu\text{A}$   
and 90 % recovery then produces a voltage  
drop ~ 1 kV per  $\mu\text{s}$  at 2 A beam current.  
Operation for the FEL should therefore be  
possible with 10-20  $\mu\text{s}$  pulses at 10 Hz. These  
parameters are probably conservative.

### TUNING RANGE

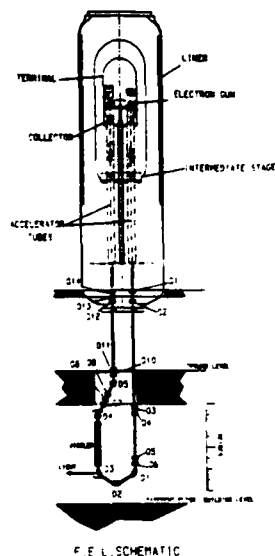




## GAIN EVOLUTION



## SATURATED LIMIT



FEL SCHEMATIC

## EXPERIMENTAL SYSTEMS

### Gun and Collector

To be designed and constructed at Daresbury  
Injection at up to 200 keV  
Collector rating is 5 kW

### Accelerator Modifications

Negative voltage tests  
Tube mods. - fields, apertures, pumping  
Off-axis injection  
Voltage stabilisation - liner, gun, wiggler  
Controls and IR link - integrate with FEL

### Beam Transport/Diagnostics

Achromatic in single plane - good recovery  
Stigmatic imaging - wiggler matching  
Screens and profile monitors  
Spectrometer - pulsed deflector?

### Wiggler

Permanent magnet system, planar geometry  
Variable gap -  $K \leq 1.6$

### Optics

Hybrid cavity - planar waveguide  
Copper mirrors, Invar stabilisation  
Dry lines essential  
Diagnostics to include transient gain  
Harmonic selection

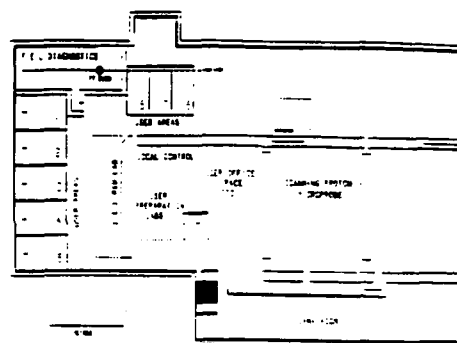
## OXFORD FEL PARAMETERS

<b>Electron beam</b>	
Energy (MeV)	5 to 10
Peak current (A)	2
Normalised emittance (r.m.s.)	$100^{(1)}$
$\Delta E/E$	$10^{-3}$ (a)
Pulse length (ps)	1 to $20^{(1)}$
Repetition frequency (Hz)	~ 10
<b>Wiggler/cavity/waveguide</b>	
Period (mm)	24
Number of periods	50
Length (m)	2
gap (mm)	10 to 20
Resonator det. (Torr)	~ 1
Cavity length (m)	3
Waveguide: min. diam. internal	5 x 70
<b>Radiation</b>	
Wavelengths (nm)	
- fundamental	60 to 300
- 3 <sup>rd</sup> harmonic	30 to 100
Peak power (fundamental, kW)	$10^{(1)}$
Average power (W)	~ 5
Line width ( $\Delta\lambda/\lambda$ )	$10^{-3}$ (a)

### Notes

- <sup>(1)</sup> These are values assumed in calculations, and are conservative. The normalised emittance for a similar electron gun at Santa Barbara has been measured to be  $< 20$  (r.m.s.) (11). Correction of voltage-droop should result in  $\Delta E/E \leq 10^{-4}$ .
- <sup>(2)</sup> Optical switching will allow optical pulses as short as a few ns. Cavity dumping, in 20ns, would yield peak power of several MW.
- <sup>(3)</sup> The line width at Santa Barbara appears dominated by pulse to pulse jitter; more selection and other measures may reduce this substantially, perhaps to  $10^{-4}$ .

## USER FACILITY



Tuning provision : Fast ( $\approx 10\%$ ) by wiggler  
Wide (1 octave) by energy  
(1-2 hours)  
Total running time : 1500 hours year  
For users : 750 hours year

## PROJECT STATUS

Design study	1988-89
Grant submission	September 1989
Approval	1990 (?)
FEL commissioning	1992

Total cost	£ 1.8 M
Includes 4 year staff costs and 1500 hr operation	
Capital cost	£ 1.1 M
Academic staff	10

### Note

Extensive consultations with FIR user community  
Accelerator mods. already in progress

SITORS SUPPORTERS AND FRIENDLY REFEREES WELCOME

## PR3.2

### A NOVEL WIGGLER DESIGN FOR USE IN A HIGH-EFFICIENCY FREE-ELECTRON LASER

A.H. Ho\*, R.H. Pantell, J. Feinstein  
Department of Electrical Engineering

\*Department of Applied Physics  
Stanford University  
Stanford, California U.S.A.

A wiggler for use in a high-efficiency FEL system utilizing microwave acceleration to maintain synchronism is proposed. The wiggler not only provides a periodic transverse magnetic field, but also acts as a loaded waveguide capable of supporting microwaves. Measurements on the wiggler confirm that it can be utilized in a high-efficiency design to attain conversion efficiencies of approximately 50% in a two-meter length at 10 microns wavelength.

This work has been supported by the United States Army, Huntsville, Alabama

#### PROBLEMS ASSOCIATED WITH TAPERED WIGGLER FELs:

- \*Reduction in gain at signal levels other than what the taper was designed for.
- \*Detrapping.
- \*Frequency shift during buildup
- \*High-efficiency requires large  $a_w$  or large  $\lambda_w$

#### ADVANTAGES OF MICROWAVE ACCELERATION:

- \*Can vary microwave field strength with time.
- \*No detrapping because wiggler parameters are constant.
- \*Large microwave field strengths can be employed, resulting in high power generation in short distances. Furthermore, the power generated can be increased simply by increasing the wiggler length (with increased microwave power, of course).

#### REQUIREMENTS ON THE WIGGLER:

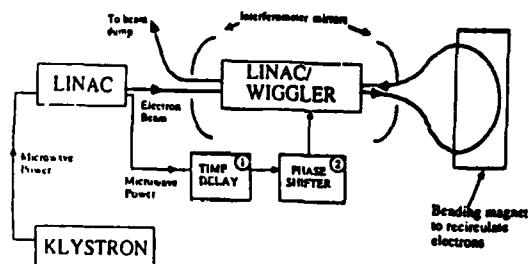
##### Magnetic Structure:

- \*Adequate wiggler field on axis.
- \*Have electron beam focussing in both transverse directions.
- \*Tunable.

##### Microwave Structure:

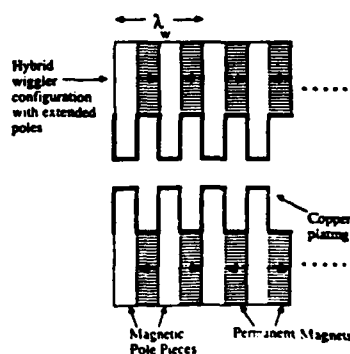
- \*Must resonate a mode at the klystron frequency and with  $v_p = c$ .
- \*Must be able to support large microwave fields; (for a given input klystron power, this means a high shunt impedance)
- \*Avoid beam break-up, and/or wakefield problems.

A block diagram of the high-efficiency FEL system



- ① There must be a time interval between the introduction of microwave power into the LINAC and into the LINAC/WIGGLER so that the FEL can have sufficient small-signal gain.
- ② A phase shifter is necessary to ensure that the electrons from the LINAC are introduced at the correct phase of the microwaves in the LINAC/WIGGLER to be accelerated.

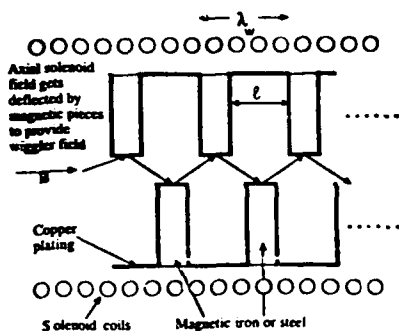
AN INITIAL DESIGN FOR THE LINAC/WIGGLER



#### PROBLEMS:

- Low wiggler field because of large leakage area ( $B_w < 1G$ )
- Low shunt impedance for microwaves. Large surface area per unit axial distance.

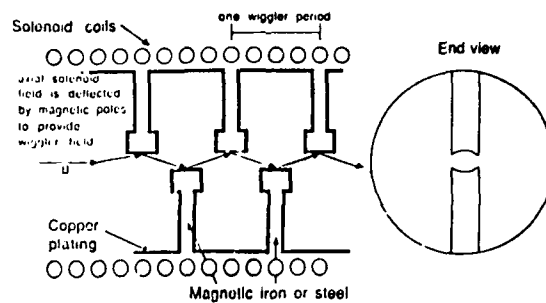
## A STAGGERED POLE CONFIGURATION WIGGLER



### ADVANTAGES:

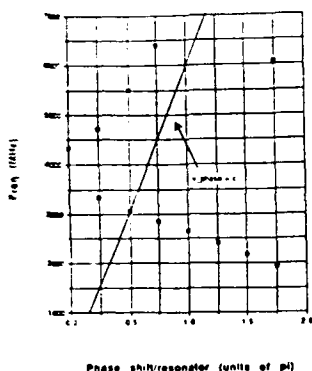
- Higher magnetic field, no equivalent problem of leakage flux.
- Bw is easily varied.
- Half the surface area per unit axial distance for the microwaves.
- Electron beam focussing is provided by the axial magnetic field.

## The linac/wiggler structure



The linac wiggler consists of a staggered array of magnetic pieces situated inside the bore of a solenoid. The poles are to deflect the longitudinal solenoid field, thus providing a transverse wiggler field. They are also copper plated to form a low-loss, accelerating structure for the microwaves. The pole pieces are curved in the transverse plane to provide focussing of the beam in both transverse directions.

Dispersion Curve for Linac/Wiggler



Phase shift/resonator (units of pi)

Note: Speed of light mode has shunt impedance of 70 M ohms/m

## WIGGLER RESULTS

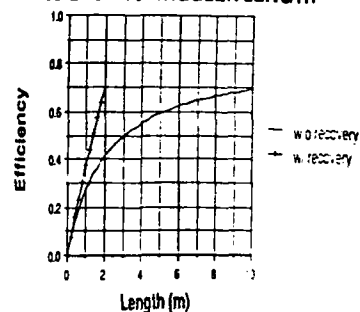
### MAGNETIC PROPERTIES:

- \*Time  $B_r > 0.5$  Sec (Mitsubishi).
- \*Curved poles give focussing in both transverse dimensions.
- \*Tunable
- \*Ability to go to short wiggler periods without loss of reserve force (in contrast to permanent magnet wigglers).

### MICROWAVE PROPERTIES:

- \*Dimensions chosen so that the structure supports a speed of light mode near the klystron frequency (2.856 GHz).
- \*Shunt impedance of 70 M ohms/m (comparable to standard linacs).
- \*Preliminary analysis indicates that neither SSU nor longitudinal wakefields are problematic (for a peak current of 20 A).

## EFFICIENCY VS. WIGGLER LENGTH



PARAMETERS

- $I_{peak}$ : peak current = 20 A
- $A_{wigg}$ : the wiggler parameter = 1.0
- $\theta_r$ : resonant phase = 50°
- $I_{tr}$ : trapping fraction = 0.84
- $\eta$ : losses = 0.05
- $L_{wigg}$ : wiggler period = 2.5 cm  $(\lambda = 2.5 \text{ cm})$   $B_{max} = 4 \text{ G}$
- $I_{avg}$ : max. dc current = 0.2 A
- $E_{mic}$ : microwave field = 12 kV/m
- $G_{ss}$ : ss gain  $(L \times 2\pi) = 70 \text{ B}$
- Drive Power required = 8.9 MW
- = 4.9 MW (using energy recovery)

## SUMMARY

### 1. MICROWAVE ACCELERATION:

- \*Acts like a time-varying taper (avoids ss-gain reduction).
- \*Large microwave field strengths mean high energy extraction in short distances.

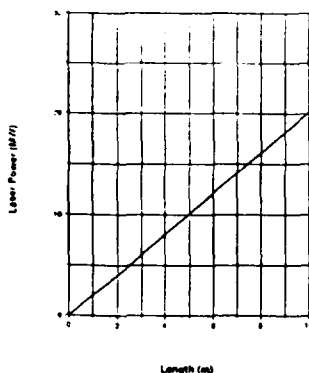
### 2. WIGGLER:

- \*Provides a strong, tunable wiggler field with focussing in both transverse dimensions.
- \*Acts as an efficient linac (70 M ohms/m).

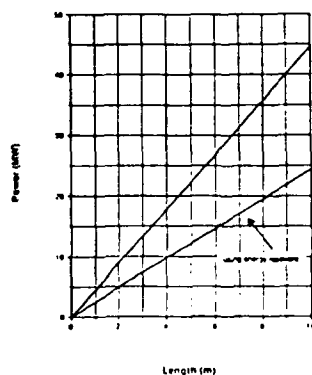
### 3. HIGH-EFFICIENCY NUMBERS:

- $\eta = 42\%$  ( $\approx 71\%$  with energy recovery), for typical parameter values.
- \*This corresponds to an output laser power of  $\approx 4 \text{ MW}$  for a 2m wiggler.
- \*Assuming a combined efficiency of the klystron and first linac to be 35%, and assuming 50% of the ohmic losses due to output coupling, we get a wall plug efficiency  $\eta_{wp} = 13\%$ .

Output Laser Power vs. Length



Microwave Power vs. Length

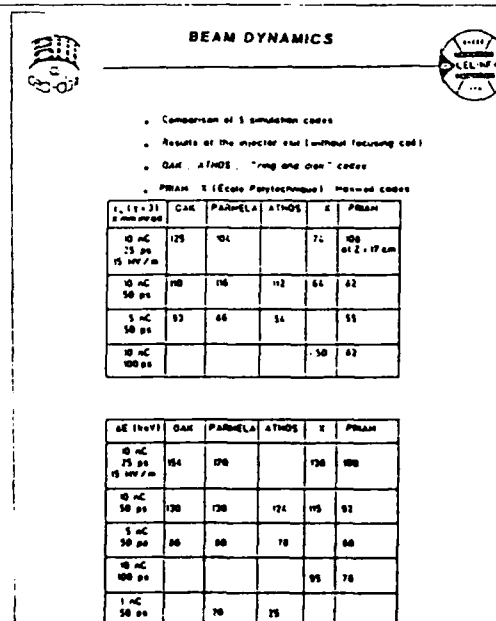
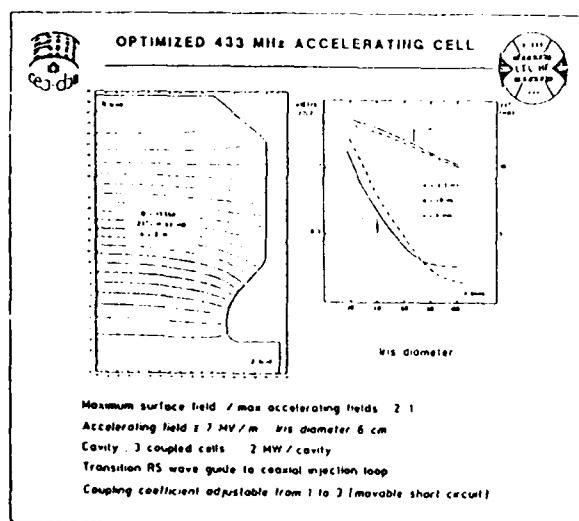
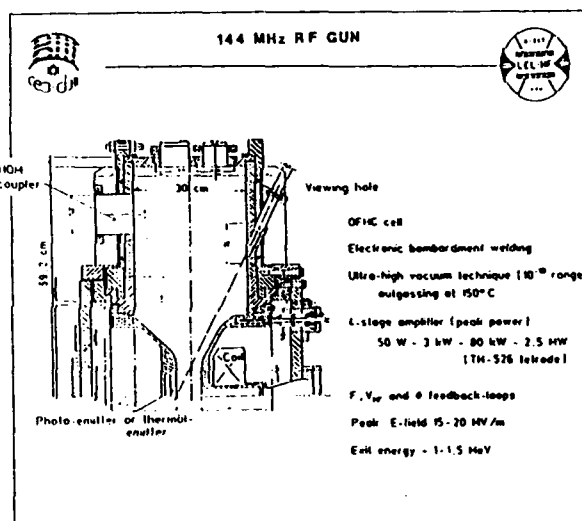
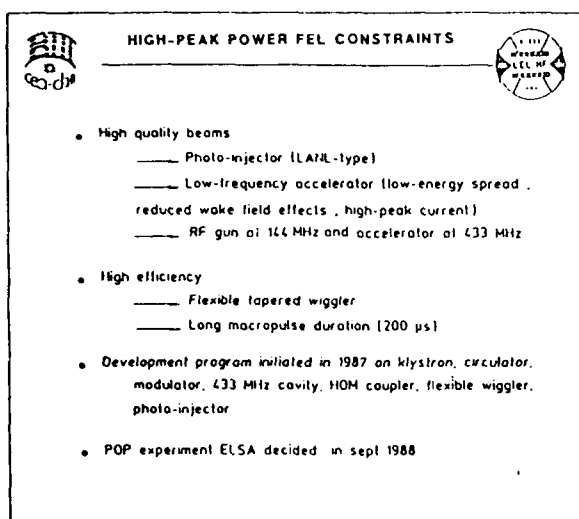


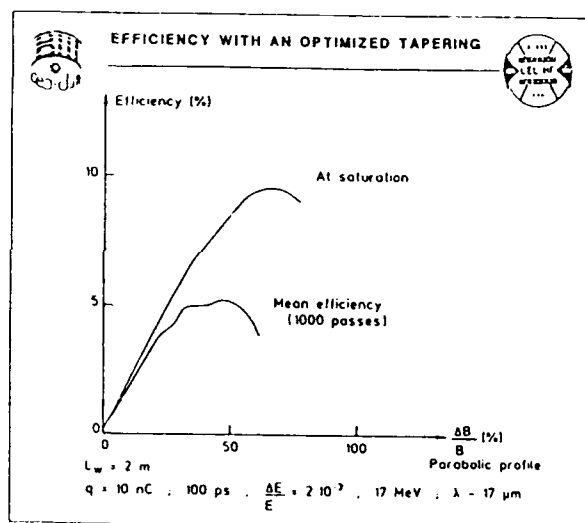
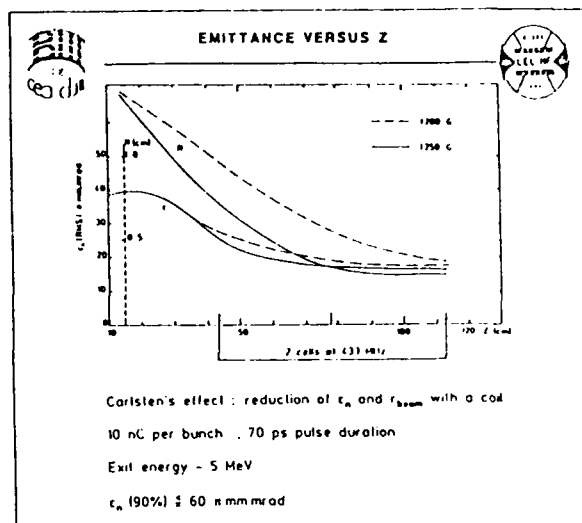
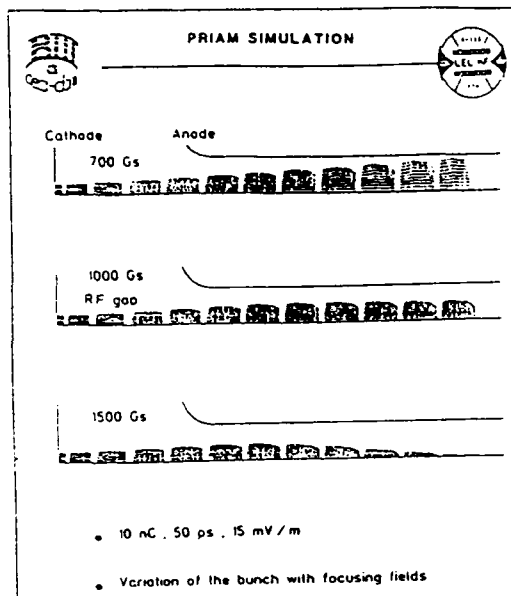
### **PR3.3 STATUS REPORT ON THE LOW-FREQUENCY PHOTO-INJECTOR AND ON THE INFRARED-FEL EXPERIMENT (ELSA)**

R. DEI-CAS and al., Commissariat à l'Energie Atomique, Service PTN, Centre d'Etudes de Bruyères-le-Châtel, B.P. n° 12, 91680 BRUYERES-LE-CHATEL, FRANCE

## Abstract

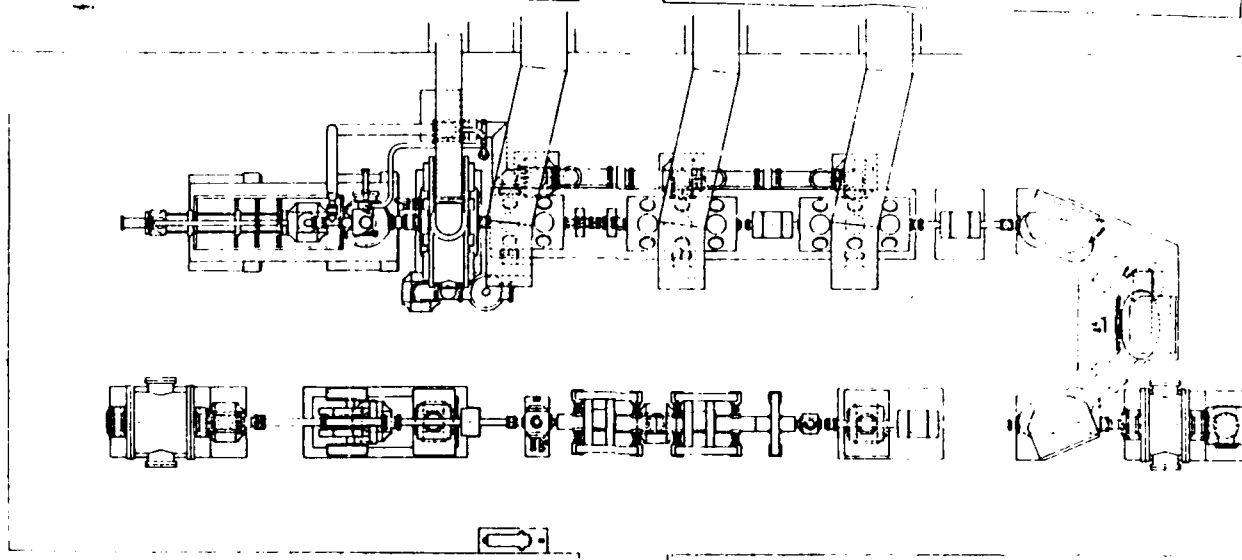
The photo-injector presented at the FEL-88 Conference is completely assembled now. Performances of the main components will be outlined. The photo-injector beam dynamics has been simulated by using different codes and the results will be compared. By integrating the main components under development : photo-injector, 433 MHz RF cavity, RF generator, wiggler and optical cavity, a FEL experiment (called ELSA), presently under construction, will be performed in the 20  $\mu\text{m}$  range. The expected performances will be presented.





### ELSA PARAMETERS

<b>Injector</b>	
Cathode Cs K <sub>2</sub> Sb	
Energy 1-15 MeV	
Charge: 10 nC	
Pulse duration 20-200 ps (with pulse compressor)	
Repetition rate 72/N MHz	
72 MHz at 2 nC or 14 MHz at 10 nC	
$\epsilon_n = 60$ mm mrad	
Peak current 50-200 A	
<b>Accelerator</b>	
Energy 17-20 MeV	
Mean current 100-200 mA	
Macropulse 200 $\mu$ s	
Repetition rate = 70 Hz	
Peak power 3 GW	
Mean power (macrol) 3 MW	
Magnetic compression 1.69 cm/% with E ramping	
<b>Wiggler</b>	
$\lambda_w = 3.2$ cm	
$L_w = 2$ m	
Gap = 16 mm	
$B_0 = 0.3$ T	
Adjustable tapering	
Fine tuning	
<b>Laser</b>	
$\lambda = 15-25$ $\mu$ m	
Optical cavity 10 3774 m	
Dynamic stabilization	
Copper mirrors	
Efficiency 3-5 %	
Peak power (macrol) = 30-50 MW	
Mean power (macrol) = 100 kW	



**FRIDAY, SEPTEMBER 1**

## EX4.1

### CONFIRMATION OF SINGLE MODE FEL OPERATION

Luis R. Elias and Isidoro Kimel  
Center for Research in Electro Optics and Lasers  
University of Central Florida, Orlando, FL 32816

Experimental results from the FEL at UCSB are reviewed. At saturation, the laser macroscopic and microscopic time structure give clear evidence of discrete time structure and single dominant longitudinal mode operation.

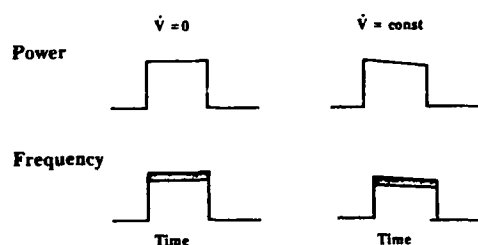
#### INTRODUCTION

Evidence of single mode FEL operation is derived from four pieces of experimental information.

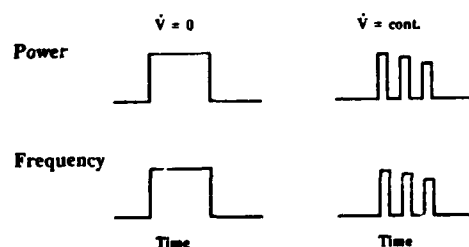
- Macroscopic power instability observed in long laser pulses
- Time resolved spectroscopic measurements of long laser pulses
- Mode beating observed with a fast detector before the onset of laser gain saturation
- Mode beating observed with a fast detector at laser gain saturation

#### LONG PULSE LASER TIME STRUCTURE

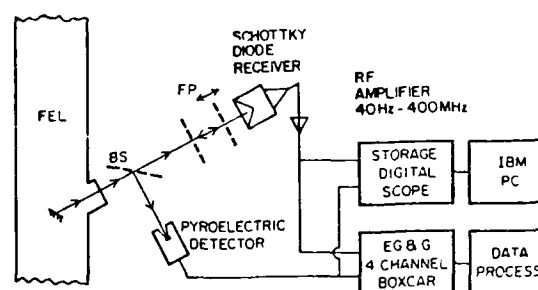
##### Multimode Operation



##### Single mode Operation



#### EXPERIMENTAL SETUP



#### FREQUENCY CHANGE DUE TO CONSTANT ENERGY DROP RATE

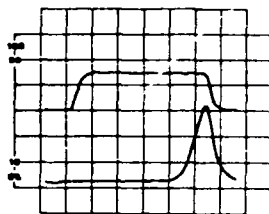
- Because of incomplete electron beam recovery, the frequency of the FEL changes linearly with time at a rate:

$$\frac{dv}{dt} = \frac{2veI_b(1-R)}{\gamma mc^2 C}$$

- For the UCSB FEL:  $v = 660 \text{ GHz}$ ,  $I_b = 1.2 \text{ A}$ ,  $R = 0.90$ ,  $C = 200 \text{ pF}$ ,  $\gamma = 7$

$$\frac{dv}{dt} = 0.25 \text{ GHz/sec}$$

# EXPERIMENTAL LASER TIME STRUCTURE



## • Short Electron Pulse

Upper trace: Beam Current

Lower trace: Laser Power

Time scale: 1 μs/div

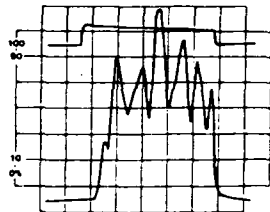
Time →

## • Long Electron Pulse

Upper trace: Beam Current

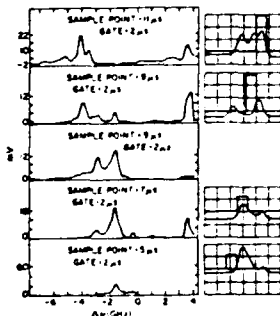
Lower trace: Laser Power

Time scale: 6.25 μs/div.



Time →

# HIGH RESOLUTION SPECTRAL MEASUREMENTS



## • High resolution Fabry-Perot scan (left). Laser power vs. time (right).

Results:

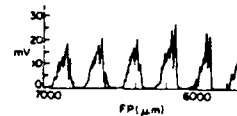
Fabry-Perot spectral resolution	220 MHz
Spectral line separation	1.5 GHz
Observed line frequency chirp	0.3 GHz/μs
Calculated frequency chirp	0.25 GHz/μs

Conclusion:

- The observed frequency spectrum is discrete
- The frequency chirp rate is well correlated to accelerator voltage drop rate.



Laser Power vs. time



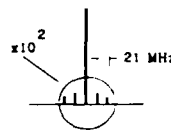
Low resolution Fabry-Perot Interferometer scan

Results:

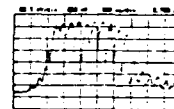
Center frequency	660 GHz
Observed spectral bandwidth	640 MHz
Fractional spectral bandwidth	$10^{-3}$
Pulse-to-pulse voltage stability	$5 \times 10^{-4}$

• A. Amir et al. Nuc. Instr. and Meth. A250 (1986)35.

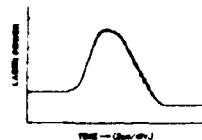
# SINGLE PULSE LASER SPECTRUM



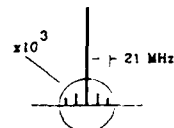
Deduced laser spectrum before onset gain of gain saturation



Laser power time structure for a short electron pulse

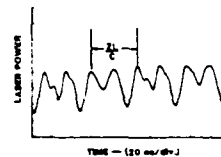


Laser power time structure after signal reaching saturation



Deduced laser spectrum at gain saturation

# SINGLE PULSE LASER BANDWIDTH



- The time structure of the above shown signal was followed for 2 ms without observing any phase change in the beat wave

Conclusion:

From :

$$\Delta\nu = \frac{1}{2\pi\Delta t}$$

$$\Delta\nu = 80 \text{ kHz}$$



## EX4.2

A Review Of Optical Guiding Experiments Done With The Columbia FEL  
 T. C. Marshall, A. Bhattacharjee, S. Y. Cai, S. P. Chang, J. W. Dodd  
 Columbia University, Department of Applied Physics  
 New York, New York 10027

A series of optical guiding experiments in an overmoded waveguide have been carried out using a 2mm wavelength FEL facility (1kA/cm<sup>2</sup>, 800kV). Two methods are used to detect guiding: analysis of the spatial "ringdown" following beam termination, and location of the sideband frequencies. Both experiments show guiding effects, and that latter indicates "refractive" guiding is important. Research supported by the NSF and ONR.

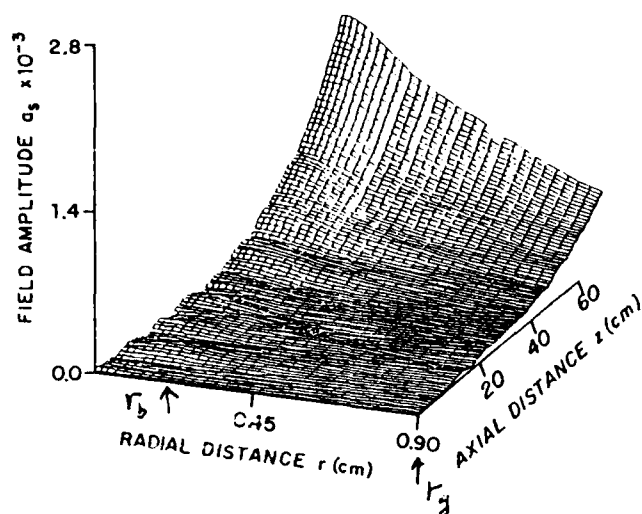


Fig. 1 Computed growing optical wave profile.

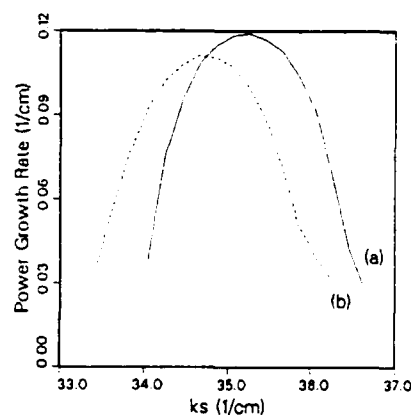


Fig. 2 Gain spectrum, guiding (a) and no guiding (b).

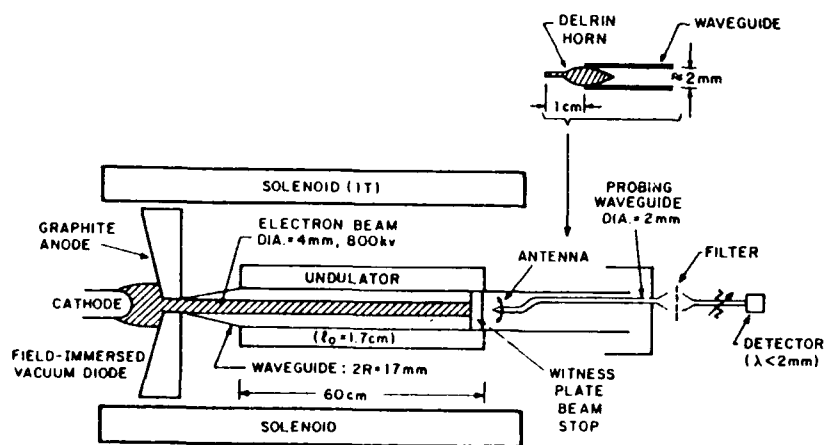


Fig. 3 Experimental apparatus.

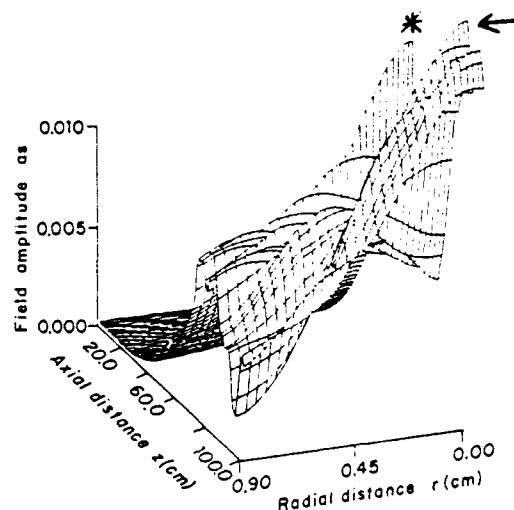


Fig. 4 Ringdown profile following beam termination. Beam terminates at \*.

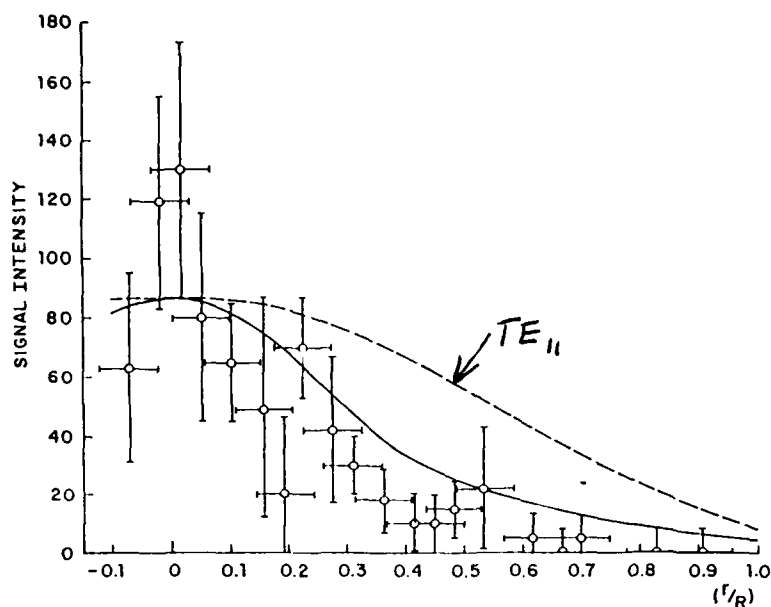


Fig. 5 Radial power profile at arrow point, Fig. 4.

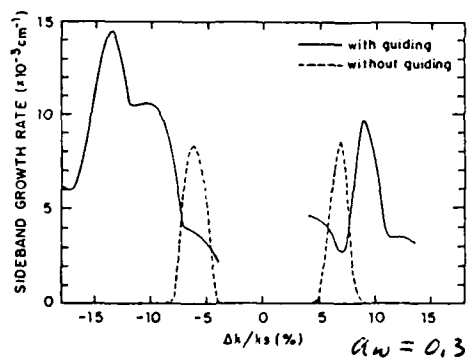
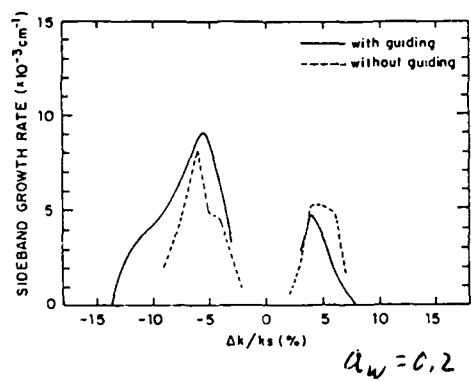


Fig. 7 Computed sideband spectrum. (Carrier not shown)

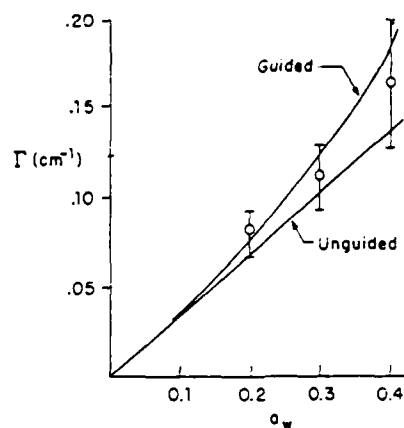


Fig. 6 Power growth rate.

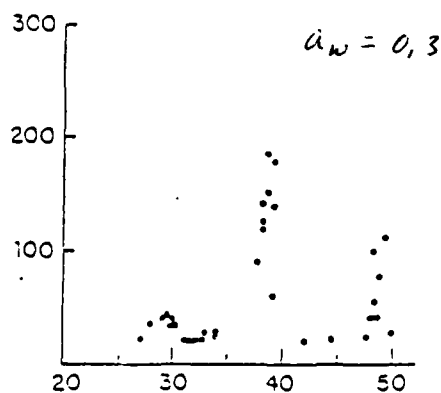
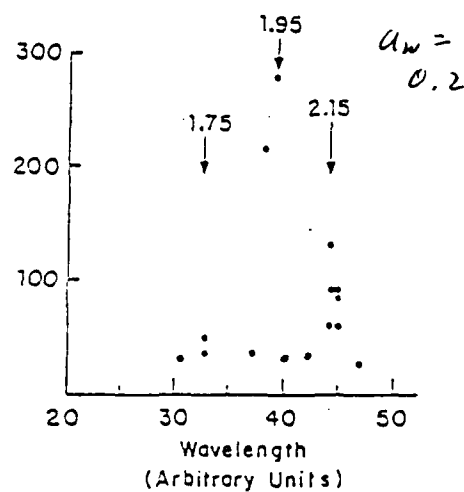


Fig. 8 Experimental FEL spectrum.

## EX4.3 HARMONIC GENERATION EXPERIMENTS ON THE MARK III FREE ELECTRON LASER

Douglas J. Bamford, David A.G. Deacon, Deacon Research, 900 Welch Road, Suite 203,  
Palo Alto, CA 94304 USA

During the past year we have made considerable progress in understanding the unusually large bandwidths of the harmonics of the Mark III FEL, which result from overbunching of the electrons at the harmonic wavelength. We have also measured the spatial profiles, small-signal risetimes, and coherent enhancement factors for the harmonics.

### HARMONIC GENERATION EXPERIMENTS ON THE MARK III FREE ELECTRON LASER

Douglas J. Bamford and David A.G. Deacon  
Deacon Research  
Palo Alto, CA

Supported by the SDIO IST office,  
managed by ONR

Table 1. Typical laser and electron beam operating parameters.

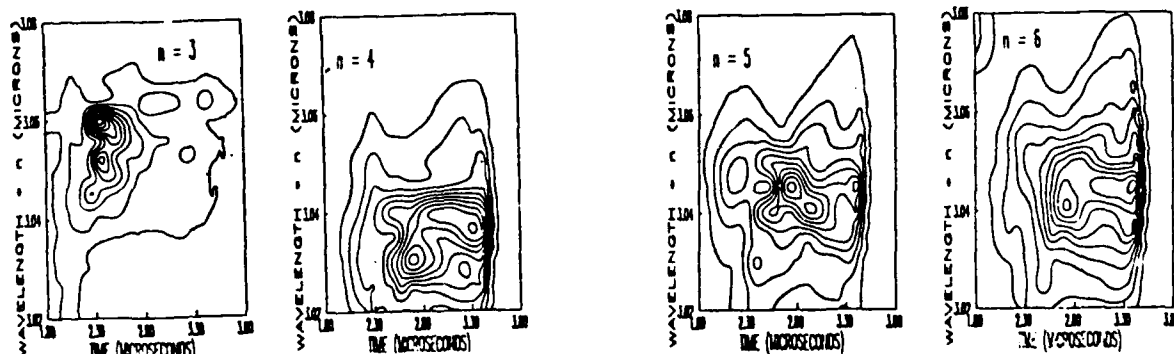
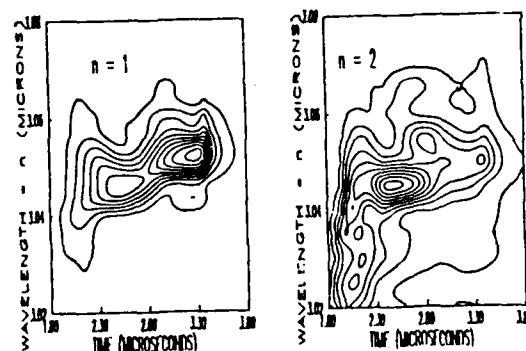
Electron beam parameters:	
Peak current	20 A
Normalized emittance (90%)	
Vertical	20 $\mu$ m-mrad
Horizontal	25 $\mu$ m-mrad
Energy	43 MeV
Energy spread (rms)	0.3 %
Macropulse Length	2.6 $\mu$ s
Microbunch Length	2.5 ps
Optical Parameters:	
Wavelength	3 $\mu$ m
Cold cavity waist	840 $\mu$ m
Resonator length	183.6 cm
Macropulse length	1 $\mu$ s
Micropulse length	2 ps
Wiggler type	linear, hybrid
N (# of wiggler periods)	4;

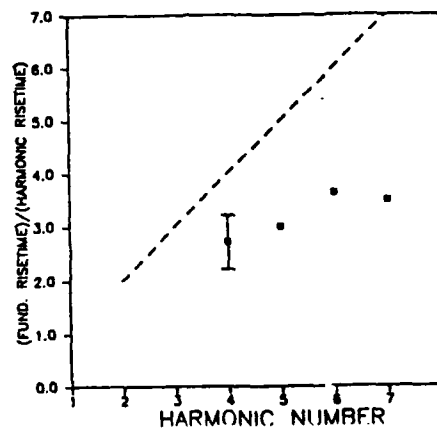
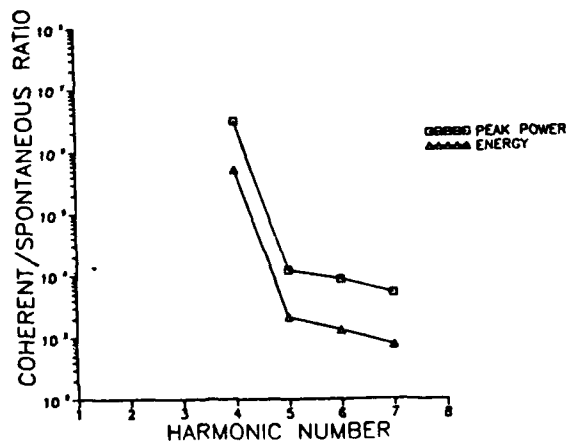
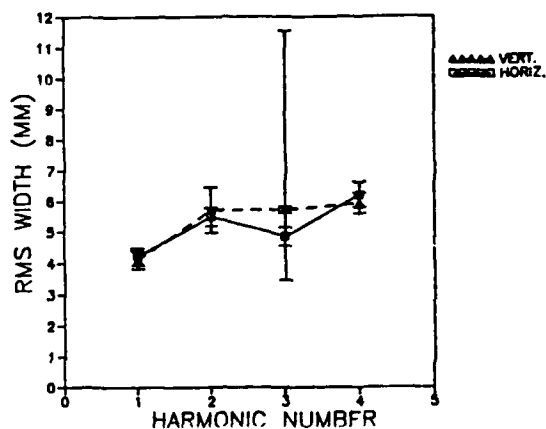
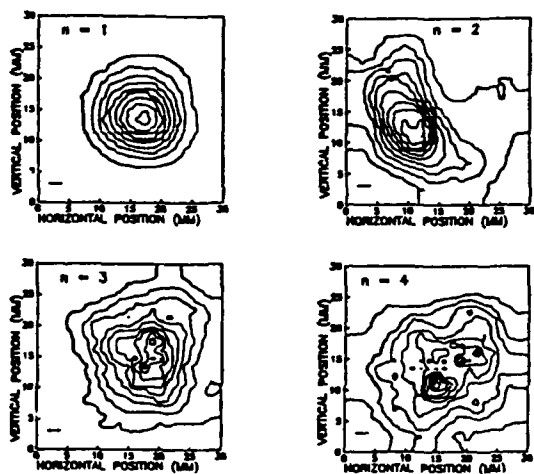
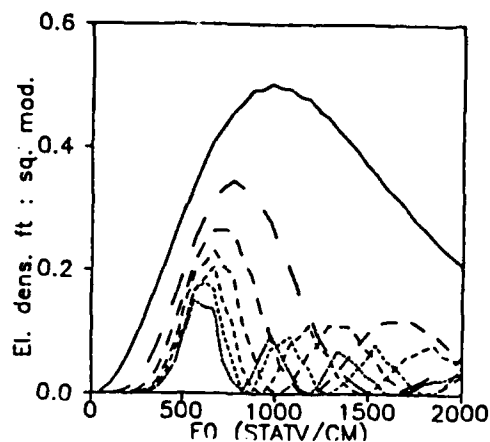
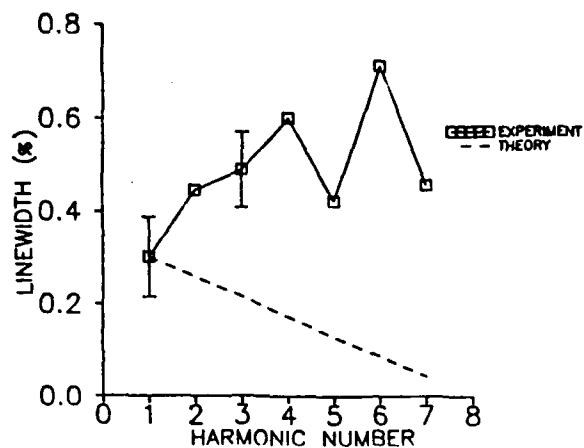
### MOTIVATION:

- Make shorter wavelengths
- Avoid optical damage
- Understand FEL physics

### RESULTS TO BE DISCUSSED:

- Bandwidths
- Spatial profiles
- Coherent/incoherent ratios
- Small-signal risetimes





#### SUMMARY AND CONCLUSIONS:

- Harmonic bandwidths are increased by saturation effects, could be reduced by tailoring micropulses.
- Spatial profiles are complicated, sensitive to electron beam properties.
- Selective enhancement/cancellation requires further research

## RECENT RESULTS OF THE ENEA-FRASCATI UNDULATOR FEL EXPERIMENT

F. Ciocci, G. Dattoli, A. De Angelis, A. Dipace, A. Doria, G.P. Gallerano,  
L. Giannessi\*, A. Renieri, E. Sabia, A. Torre and D. Jaroszynski\*\*

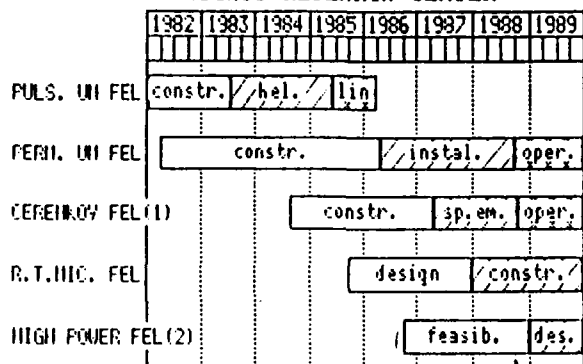
## ABSTRACT

An undulator free electron laser experiment (U-FEL) is under way at the ENEA Frascati Center. The U-FEL employs a 20 MeV microtron as electron beam source and operates in the middle infrared region around 30  $\mu\text{m}$ . Recent results of spontaneous emission measurements are discussed.

\* TIB-RIA, C.R.E. Casaccia (RM) (Italy)

\*\* Permanent address: Heriot-Watt University, Edinburg (U.K.)

## EXPERIMENTAL FEL ACTIVITY AT THE ENEA FRASCATI RESEARCH CENTER



(1) Proposed by J. Walsh (Dartmouth College)

(2) Dedicated to plasma heating (ECH)

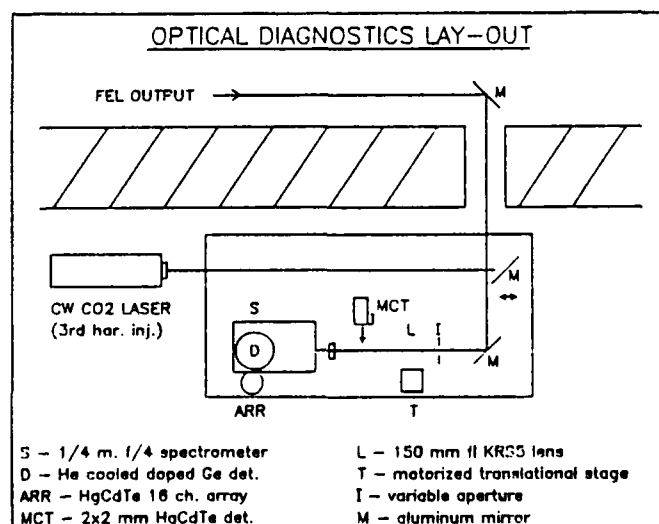
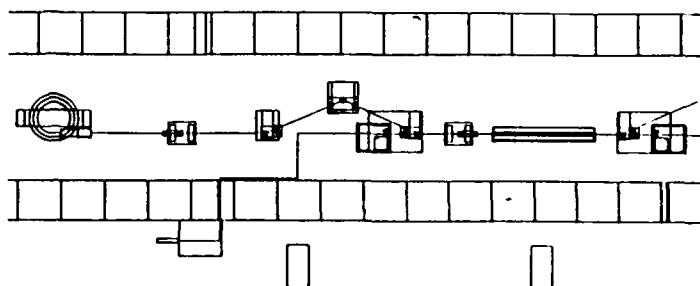
MICROTRON		
Parameter	Achieved	Design Goal
Electron beam energy (MeV)	15 ± 20	15 ± 20
Electron bunch duration (ps)	20	20
Macropulse duration (μs)	10	12
Current macropulse (mA)	160	200
Peak current (A)	3.2	4
Normalised horizontal emittance (mrad)	$7.5 \times 10^{-4}$	$7.5 \times 10^{-4}$
Normalised vertical emittance (mrad)	$2.5 \times 10^{-4}$	$2.5 \times 10^{-4}$
Energy spread	0.12%	0.12%

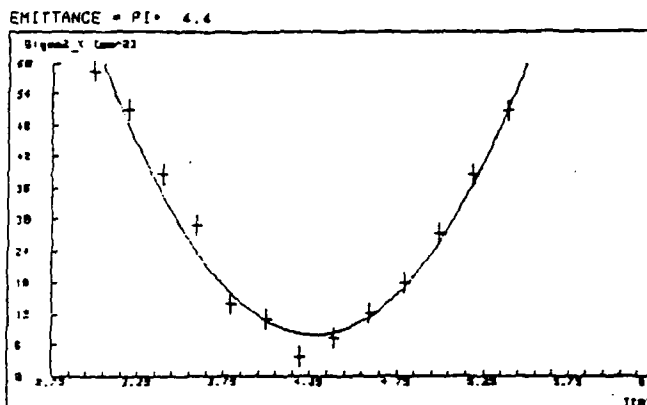
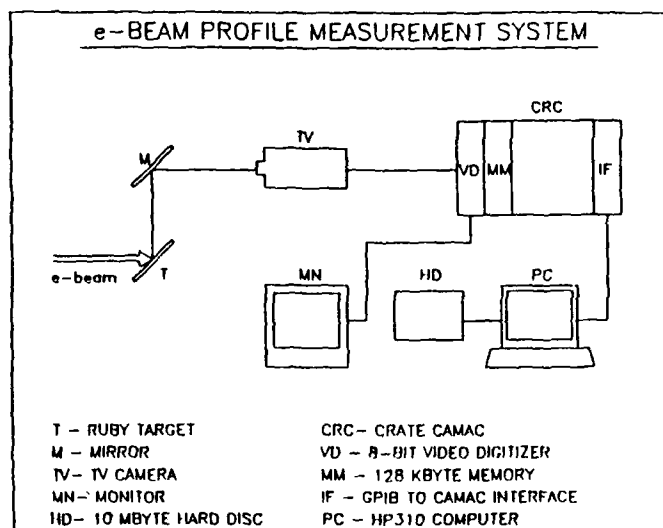
  

UNDULATOR		
Pure $\text{SmCo}_5$ constant parameters		
Period (cm)		5
Number of periods		45
Gap (cm)		0.9 ± 7
k parameter at 1.3 cm gap		2
k parameter at 2.4 cm gap		1

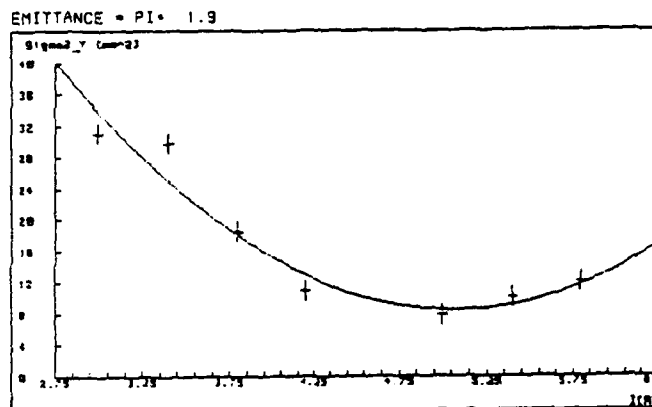
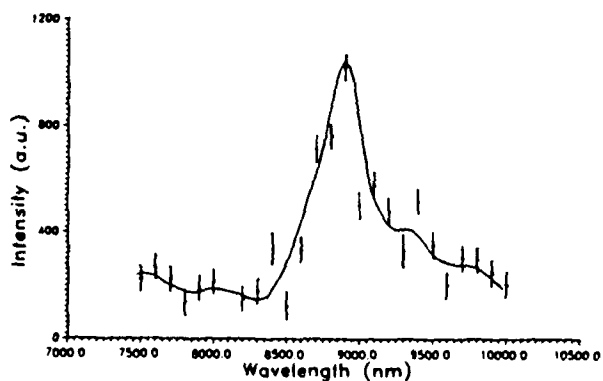
  

OPTICAL RESONATOR AND FEL CHARACTERISTICS		
Parameter	Achieved	Design Goal
Resonator length (m)	6.37	6.37
Reflectivity of the end mirror (copper)	99%	99%
Reflectivity of output coupler (coated Si)	97%	97%
Total losses	~ 4%	~ 4%
Laser wavelength (μm)		20 ± 40
Gain per pass at $\lambda = 32 \mu\text{m}$ , $I = 200 \text{ mA}$		10%
Average laser power at $\lambda = 32 \mu\text{m}$ and at 150 Hz repetition frequency (W)		5
Peak power (micropulse) (MW)		40
Peak power (macropulse) (%W)		1

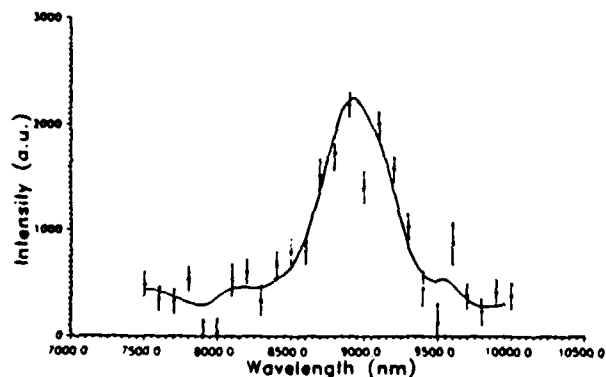




SPONTANEOUS EMISSION SPECTRUM  
third harmonic

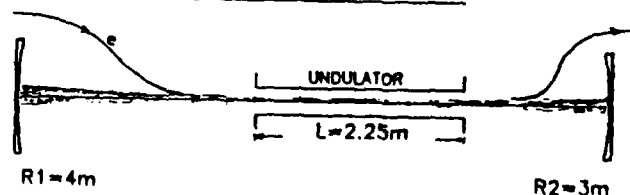


SPONTANEOUS EMISSION SPECTRUM  
third harmonic



poor cathod positioning  $\rightarrow$  large emittance

FEL OPTICAL CAVITY



MAIN CHARACTERISTICS:

- 1 - LARGE MIRROR SPACING     $d = 6.35 \text{ m}$
- 2 - STABILITY PARAMETER  $g = (1 - d/R1)(1 - d/R2)$      $= 0.6$
- 3 - SMALL UNDULATOR APERTURE     $2h = 2 \text{ cm}$
- 4 - SMALL UNDULATOR F-NUMBER  $N = h^2/\lambda L = 2$  AT  $\lambda = 30 \mu\text{m}$
- 5 - OVERLAPPING BETWEEN - UNDULATOR AXIS  
OPTICAL AXIS  
e-BEAM TRAJECTORY



# AP1.1 17.1 GHz Free-Electron Laser As A Microwave Source For TeV Colliders

R. A. Jong, R. D. Ryne, G. A. Westenskow, and S. S. Yu

Lawrence Livermore National Laboratory\*  
University of California, Livermore, California 94550

and

D. B. Hopkins and A. M. Sessler

Lawrence Berkeley Laboratory\*\*  
University of California, Berkeley, California 94720

We shall describe the development of a 17.1 GHz microwave source based on an induction-linac driven free-electron laser that is expected to produce peak power levels at the several GW level. This system is being designed to serve as the power source for a TeV linear collider or other high gradient accelerators.

\* Work performed under the auspices of the US Department of Energy by the Lawrence Livermore National Laboratory under W-7405-ENG-48.

\*\* Work performed under the auspices of the US Department of Energy by the Lawrence Berkeley Laboratory under DE-ACO3-76SF00098.

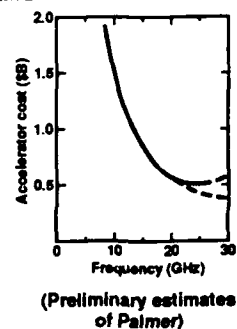
## Power source requirements for TeV colliders

- Goal for average gradient is 100-200 MeV/m
- Characteristics of RF drive source
  - High frequency, 10-20 GHz  
minimize stored energy and power  
avoid electrical breakdown
  - High peak power, .1-1 GW/m  
key to high gradient
  - Short fill time, ~50 ns  
supports high frequency structure

Short pulse length and high peak power  
are intrinsic to induction accelerators.

## TeV collider frequency choice

- Factors driving frequency up
  - accelerator cost
  - peak power  $\sim f^{-1/2}$
  - stored energy  $\sim f^{-2}$
- Factors holding frequency down
  - wakes
  - alignment and structure tolerances



## Practical limits on gradient

- 200 MeV/m upper limit based on breakdown data (primarily Loew & Wang)
  - a few carefully conditioned cavities
- Need to understand
  - breakdown in multi-cavity sections
  - effects of dark current
  - techniques for HOM damping (especially for multiple bunches)
  - effects of conditioning (~100 Hz)

## Power source requirements and status

- GW power sources at 10-20 GHz needed
- Present status
  - 11.4 GHz — 200 MW from RF
  - 17.1 GHz — no source available  
BUT 2 GW @ 35 GHz from ELF wiggler in 1986
- High quality RF power is required
  - phase and amplitude stable during pulse
- High efficiency and acceptable cost

## Quality RF power imposes requirements on induction linac

### Preliminary goals:

- Beam parameters:  
3 MeV  
1 to 3 kA
- Energy flatness  
 $\pm 1\%$  over 30 nsec
- Alignment  
 $\pm 1$  mm
- Repetition rate  
> 60 Hz

## 17.1 GHz FEL parameters

### Assumed beam and wiggler conditions

1. 3 MeV, 1 kA beam
2. 1.5 m long wiggler, with 10 cm period
3.  $\pm 1\%$  beam energy sweep (set by phase difference)
4. 1 mm beam displacement (wiggler and non-wiggler planes)
5. 0.1% rms wiggler errors
6. 2.9 by 6 cm waveguide

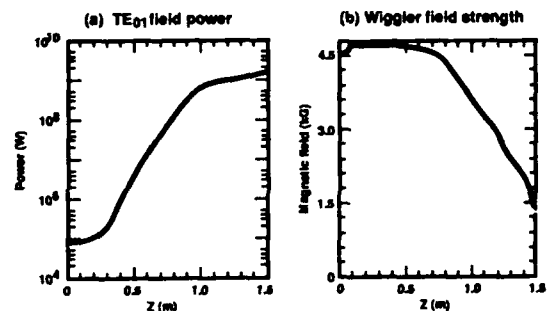
### FEL output

1. 1.4 GW peak power in TE<sub>01</sub> mode
2. 50% extraction
3. About 75% trapped
4. Fill factor about 35% in wiggler plane
5. Fill factor about 48% in non-wiggler plane

## 17.1 GHz FEL parameter constraints

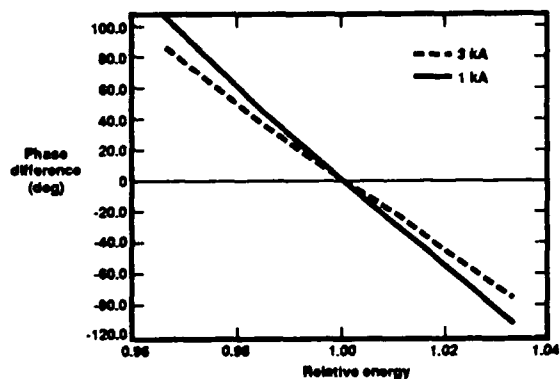
- IMP type wiggler
  1. 1 to 2 m long wiggler, with 10 cm period
  2. Maximum magnetic field of about 4.5 kG
  3. Synchronism condition limits beam energy to 3 MeV
- Accelerator
  1. Beam current of 1 to 3 kA
  2. Maximum beam energy of 3.5 MeV
- Realistic beam and wiggler tolerances
  1. 0.1% rms wiggler errors
  2. 1 mm beam displacement
  3.  $\pm 1\%$  beam energy sweep

## Axial profiles for 10 cm period wiggler

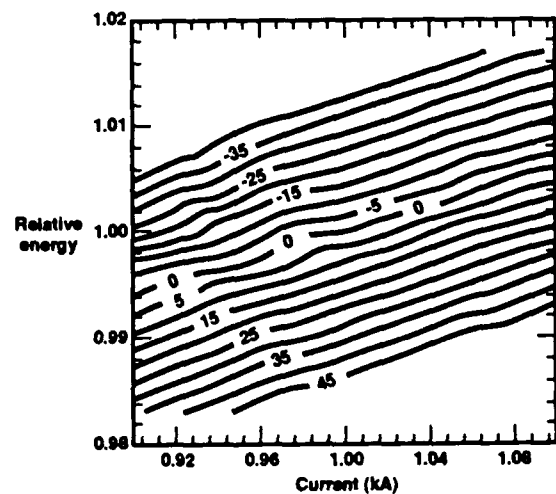


## IMP type wiggler: energy sweep

17.1 GHz, 3 MeV, 10 cm period, 2.9 cm by 6.0 cm waveguide

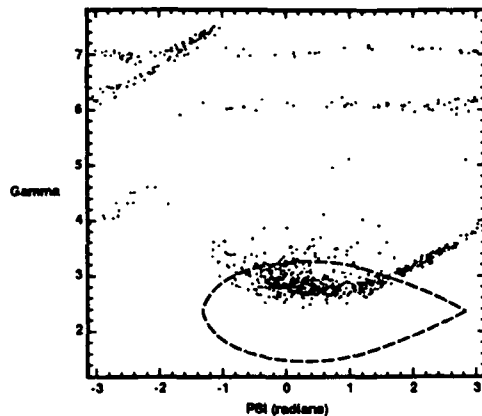


## Phase difference contours (deg)





### Phase space after 1.5 m of 10 cm period wiggler

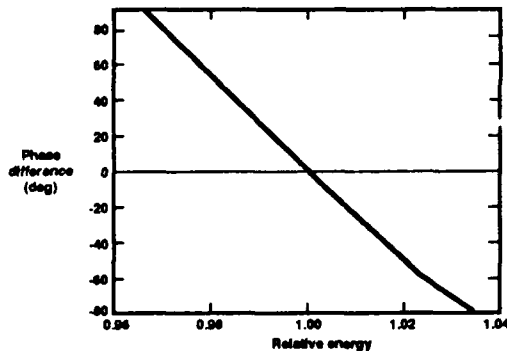


### Longer period 17.1 GHz FEL parameters

- Assumed beam and wiggler conditions
  1. 3 MeV, 1 kA beam
  2. 2 m long wiggler, with 15 cm period
  3.  $\pm 1\%$  beam energy sweep (set by phase difference)
  4. 1 mm beam displacement (wiggler and non-wiggler planes)
  5. 0.1% rms wiggler errors
  6. 2.9 by 6 cm waveguide
- FEL output (for 15 cm period wiggler)
  1. 1.0 GW peak power in  $TE_{01}$  mode
  2. 37% extraction
  3. About 75% trapped
  4. Fill factor about 40% in wiggler plane
  5. Fill factor about 47% in non-wiggler plane

### Energy sweep

17.1 GHz, 3 MeV, 1 kA, 15 cm period, 2.9 cm by 6.0 cm waveguide



### 17.1 GHz FEL summary

- IMP type wiggler (10 cm period)
  1. Peak power in excess of 1 GW can be achieved.
  2. Energy sweep limits of  $\pm 1\%$  set by phase stability requirements.
- Longer period wigglers
  1. Higher beam energy is required to best utilize longer period wigglers and increase extracted peak power levels.
  2. Simulations suggest that better phase stability can be achieved with higher beam current and longer wavelength wigglers.
  3. Peak power of about 1 GW can be achieved with 15 cm wiggler period.

### Efficiency enhancement options

- Beam re-acceleration
- Relativistic klystron "afterburner"

### Reacceleration issues

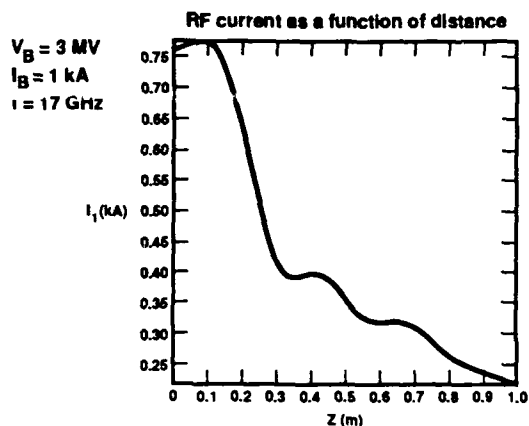
- Beam debunching due to
  - (a) energy spread
  - (b) space charge
- Beam preservation thru rf power extractors
- Power output of bunched beams through induction cells (effect minimization through special cell design)
- Phase space distortion of beam buckets due to beam loading in accelerating cells
- Matching during re-injection into wiggler/RK
- RK more relaxed than FEL since phase space requirements of RK are more tolerant

## Relativistic Klystron "afterburner"

Goal : Enhance system efficiency by extracting power from the spent FEL beam

Method : Pass the spent FEL beam through klystron transfer cavities

## The spent FEL beam debunches rapidly with distance



## RK afterburner simulations

Power output : The power extracted from a travelling wave cavity is given by

$$P = 1/2 I^2 r \cos \theta$$

Where  $I$  = RF current  
 $r$  = shunt impedance  
 $\theta$  = a phase angle

To obtain high power we need large RF currents.

Difficulty : The spent FEL beam debunches rapidly, leading to reduced RF current

## RK afterburner simulations (cont.)

Simulations indicate that we can obtain several hundred MW of power using multiple output cavities.

3 cavity afterburner :  $V_B = 3 \text{ MV}$ ,  $I_B = 1 \text{ kA}$ ,  $f = 17 \text{ GHz}$

$$L_1 = 80 \text{ cm}, L_2 = 78 \text{ cm}, L_3 = 96 \text{ cm}$$

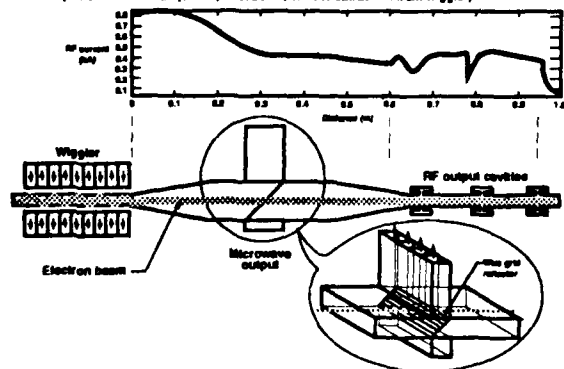
$$r_1 = r_2 = r_3 = 2000 \Omega$$

$$\theta_1 = -0.5, \theta_2 = \theta_3 = 0$$

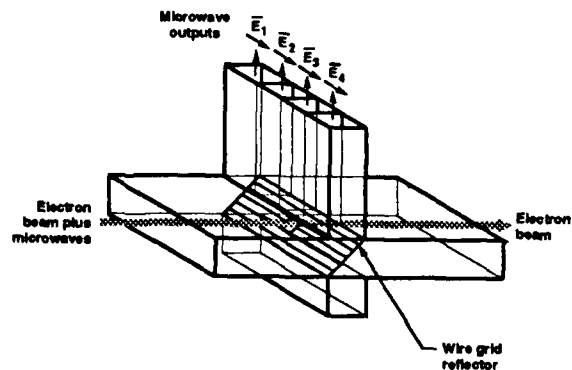
Results :  $P_1 = 100 \text{ MW}$ ,  $P_2 = 200 \text{ MW}$ ,  $P_3 = 140 \text{ MW}$

## FEL-RK Hybrid can achieve high efficiency

• 3 klystron cavities placed beyond the wiggler can produce an additional 500 MW of power at 17.1 GHz. (3 MeV, 1 kA beam, 1.4 GW extraction from wiggler)



## Microwave output coupler



## Current Applications Using the UCSB Free Electron Laser

Jann Kaminski  
*Department of Physics and Center for Free Electron Laser  
 Studies*  
*University of California*  
*Santa Barbara, CA 93106*

### Abstract

Using the far-infrared radiation produced by the UCSB FEL, various biological science and solid physics experiments have been performed. As a particular example, magneto-absorption measurements on the shallow donor system in n-GaAs are presented.

2

#### Current Applications of the UCSB FEL

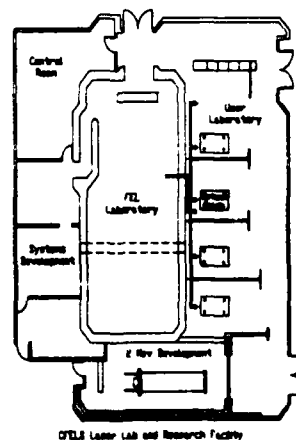
- I. Introduction
- II. Center for Free Electron Laser Studies (CFELS)
- III. FEL and Control System
- IV. Experiments
  - A. Biology
  - B. Bio-Physics
  - C. Solid State Physics
    - 1. Magnetic Systems
    - 2. Electronic Transitions
    - 2. Semiconductor
      - a. Bulk
      - b. Lower Dimensional Electron Systems

#### Collaborators:

- UCSB
  - V. Jaccarino
  - A. King
  - J. Spector
- U.K.
  - C. Pidgeon

#### Center for Free Electron Laser Studies (CFELS)

- I. CFELS contains a USER LABORATORY adjoining the FEL
  - A. 5 large aperture output ports with separate optical benches
  - B. Cryogenic equipment - optical & magnetic dewars
  - C. Optical components - detectors, detector array, off-axis mirrors.
  - D. Data reduction equipment
- II. FEL Development
  - A. 2 MeV accelerator - compact, long wavelength
  - B. Micro-undulators



FEL Laser Lab and Research Facility

## FEL

## I. FEL operating parameters

Frequency Range.....	20-75 $\text{cm}^{-1}$
.....	500-133 $\mu\text{m}$
Peak Power.....	1.5 kW
Peak Power Density.....	50 $\text{kW}/\text{cm}^2$
Pulse Width (FWHM)*.....	0.5-3 $\mu\text{sec}$
Repetition Rate.....	0.3 Hz
Frequency Linewidth (average).....	1.6 GHz
(single shot).....	10 MHz
Frequency Tunability.....	2%

(\*): Pulse lengths as short as 20 nsec have been produced by means of an external semiconductor switch.

## II. Recent Improvements

## A. Cavity dumping output

- Nd:YAG laser induced mirror in Si wafer
- 30 nsec pulse at 20 kW peak power

## B. Hybrid wiggler

- increase frequency range ( $< 130 \text{ cm}^{-1}$ )

## C. Fixed Laser Frequency Injection Locking

- reduce FEL frequency jitter from 1.6 GHz to 10 MHz

## D. Computer controlled magnet &amp; terminal electronic system

- faster & easier cold start-up
- step toward automation

## Solid State Physics

## I. Magnetic systems

- Bulk & Impurity spin modes in AFM  $\text{FeF}_2$  w/ Mn
- Thin layer AFMR in  $\text{FeF}_2$

## II. Electronic Systems

## A. Rare Earth Impurities

- samples R.E. (nominally 1%) in  $\text{LaF}_3$
- transitions of localized 4f levels in ground multiplet

## B. Bulk Semiconductor

- High purity and doped n-GaAs and n-InP
- Photoconductivity and transmission (w/ & w/o B)
- Shallow donor saturation spectroscopy at low T

## C. Lower Dimensional Electron Systems

- time structure in Si-MOSFET and GaAs/GaAlAs heterojunction of photoconductive and photovoltaic response
- saturation of 2D cyclotron resonance and 2D plasmon

## Biology/Bio-physics Applications

## I. Biology

## A. First biological effects seen with an FEL.

- samples are rat kangaroo kidney cells
- FEL frequency =  $50 \text{ cm}^{-1}$
- Cells exhibit inhibition of DNA synthesis with high intensity FIR

(Burns et al., 1989)

## II. Bio-Physics

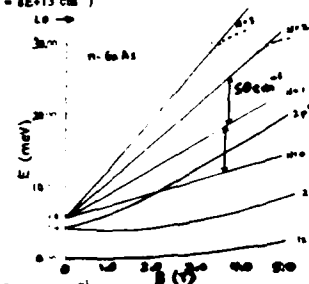
- samples are photo-dissociated sperm whale myoglobin
- FEL frequency =  $50.5 \text{ cm}^{-1}$
- blood shows enhancement of recombination rate at low temperature with intense FIR pulses

(Austin et al., 1989)

## Cyclotron Resonance in n-GaAs

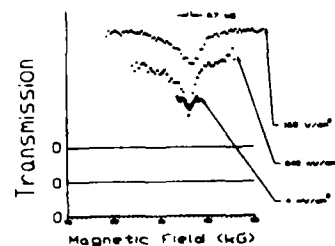
Energy level diagram of n-GaAs near conduction band

( $E = 13$ ;  $m^* = 0.067 m$ ;  $N_d - N_a = 8 \times 10^{13} \text{ cm}^{-3}$ )



Cyclotron Resonance:  $\omega_c = eB/m^*c = 13.9 \text{ cm}^{-1}/T$

- non-parabolicity from LO phonons and CB gives different m
- at low T, equilibrium population in CB is small; no absorption at low intensity
- impact ionization causes increased absorption at high intensity until saturation



## AP1.3

### APPLICATIONS OF INFRARED FEL IN PICOSECOND AND NONLINEAR OPTICAL SPECTROSCOPIES

W. S. Fann  
Stanford University  
S. Benson and J. M. J. Madey  
Duke University  
S. Etemad and G. L. Baker  
Bell Communications Research  
L. Rothberg  
AT&T Bell Laboratories  
M. Roberson and R. A. Austin  
Princeton University

In this talk we review two independent works that have used the infrared FEL, Mark III, for studies of condensed matter

1. Spectrum of  $\chi^{(3)}(-3\omega; \omega, \omega, \omega)$  in Polyacetylene: An Application of Free Electron Laser in Nonlinear Optical Spectroscopy.
2. Dynamical Test of Davydov-like Solitons in Acetanilide Using a Picosecond Free Electron Laser.


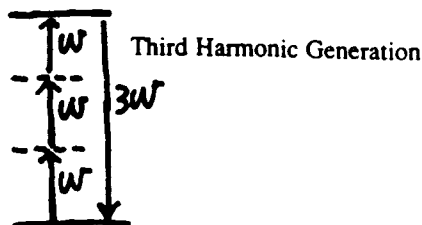
Laser Performance	
 <small>Duke Free-electron laser lab</small>	
Tuning range	1-8 $\mu\text{m}$
Demonstrated tuning range	1.4-8.1 $\mu\text{m}$
Gain	20-100%
Energy per pulse	1-200 mJ
Repetition rate	Single shot-30 Hz
Peak power	0.5-2 MW
Macropulse length	0.5-8 $\mu\text{sec}$
Micropulse length	0.5-3.0 psec.
Spectral bandwidth	0.5-1.0% FWHM
Strehl ratio	>0.7

Fig. 1- MarkIII infrared Free Electron Laser Performance.

$$\vec{P} = \chi^{(1)} \vec{E} + \chi^{(2)} \vec{E} \cdot \vec{E} + \chi^{(3)} \vec{E} \cdot \vec{E} \cdot \vec{E} + \dots$$

$$\chi^{(3)}(-3\omega; \omega, \omega, \omega) \propto \frac{1}{(\omega - 3\omega_g)(\omega - 2\omega_g)(\omega - \omega_g)}$$



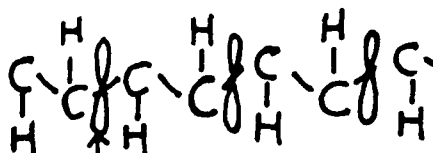
Two photon resonance could couple ground state with excited states that have same symmetry

One and three photon resonances could couple ground state with excited states that have opposed symmetry

=> Spectrum of  $\chi^{(3)}$  could provide information of all excited states

Conjugated Polymers: Long Polymers Chain with double or triple bond in the carbon backbone

Polyacetylene,  $(CH)_x$ , Simplest Conjugated Polymer



$\pi$ -electrons

=> Large Nonlinear Response => Large  $\chi^{(3)}$  due to  $\pi$ -electrons

delocalization  
=> Is its electronic structure like small molecule or one-dimensional semiconductor?

Small Molecule:  $\pi$ -electrons are highly correlated

One-dimensional Semiconductor:  $\pi$ -electrons are uncorrelated

Positions of excited states are different for two models

=> Different Prediction of relative position of two and three photon resonances

=> tunable infrared Laser to measure the spectrum of  $\chi^{(3)}(-3\omega; \omega, \omega, \omega)$

Method of measuring  $\chi^{(3)}(-3\omega; \omega, \omega, \omega)$

=> Compare the third harmonic generation signal of  $(CH)_x$  with fused silica, which  $\chi^{(3)}$  is known

=> The thickness of fused silica is larger than its coherent length, so you will observe Maker fringe as sample rotates

=> The thickness of  $(CH)_x$  is shorter than its coherent length, no fringe as sample rotates

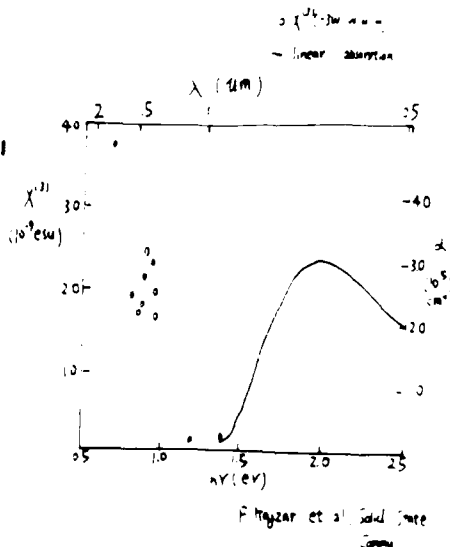
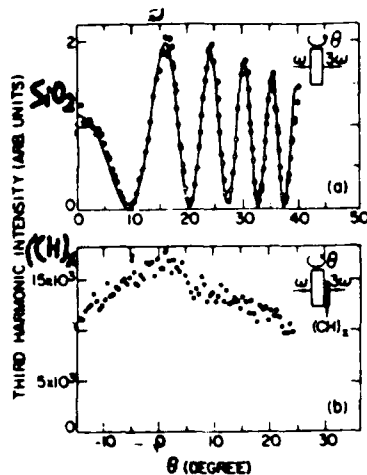


Fig 2- The open circles are  $\chi^{(3)}$  of  $(CH)_x$  measured by conventional laser. The solid line is the  $\chi^{(1)}$  of  $(CH)_x$ . (Ref.3)

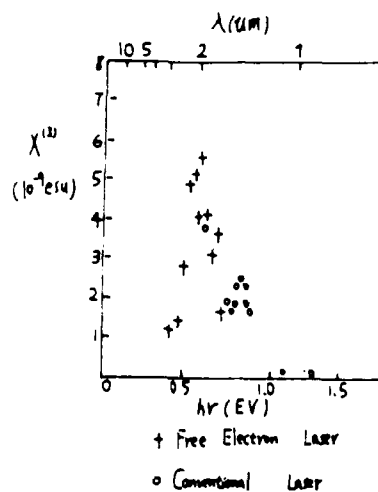


Fig 3- The full spectrum of  $\chi^{(3)}$  measured by Free Electron Laser(+), and conventional laser(o).

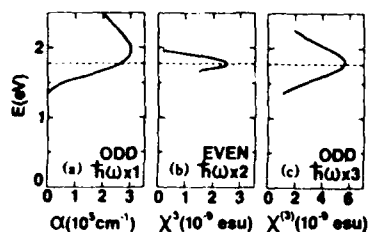


FIG. 4 (a) The spectrum of absorption coefficient  $\chi^{(1)}(\omega)$  in  $trans-(CH)_x$  as a function of  $\omega$  (Ref. 4). (b) The spectrum  $\chi^{(1)}(\omega)$  in the vicinity of the two-photon resonance as a function of  $2\omega$ . (c) The spectrum  $\chi^{(1)}(\omega)$  in the vicinity of the three-photon resonance as a function of  $3\omega$ . The dashed line is the position of the 1D energy gap (Ref. 5).

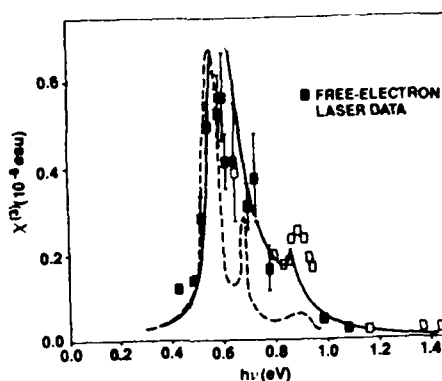


FIG. 5. The  $\chi^{(1)}(\omega)$  spectrum in  $trans-(CH)_x$ . The results obtained using the free-electron laser (filled squares) and those obtained from previous work (Ref. 3) (open squares) are shown. The solid and dashed lines are calculations of  $\chi^{(1)}$  within the free-electron (Ref. 6) and highly-correlated-electron (Ref. 7) models, respectively.

Measure spectrum from 1.1um to 3.3um

=> Three photon resonance position is determinated

=> Clearly resolved a two photon resonance and a three photon resonance

=> The  $\chi^{(3)}$  at the peak of three photon resonance is the highest among semiconductor

Conclusion:

=> Seems that free electron model, or semiconductor model, fits data better than molecular model

Dynamical Test of Davydov's-like Solitons in Acetanilide  
Using FEL to do infrared picosecond spectroscopy

Is it possible to transport vibrational energy in  $\alpha$ -Helix proteins?

Normally this is impossible because of dispersion



A.S. Davydov proposed using C=O to carry energy

=> using nonlinear interaction between C=O and low frequency phonon to balance dispersion

=> "Davydov Solitons"  
=> Propagate at the speed of sound  
=> No Conclusive Evidences in Proteins

Acetanilide: ( $CH_3CONHC_6H_5$ ), ACN

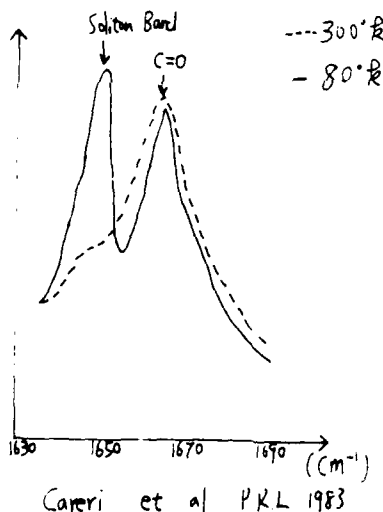
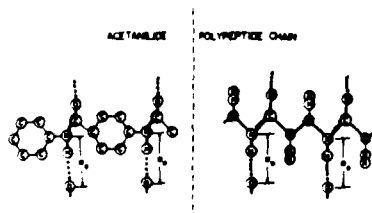
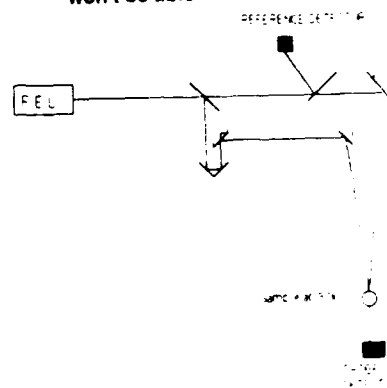


Fig. 6. The infrared absorption spectrum of ACN. The  $1665cm^{-1}$  band is the C=O, and the  $1650cm^{-1}$  band at  $80^\circ K$  is the "soliton band". (Ref. 8)

Measuring  $T_1$  (Population Life Time) of  $1650cm^{-1}$  "Soliton Band", at low temperature  
=> Need Strong IR pulse to do bleaching experiment

=> Using Micropulse structure in Markill to do picosecond spectroscopy

=> If the relaxation time  $> 350ps$ , we won't be able to measure it.



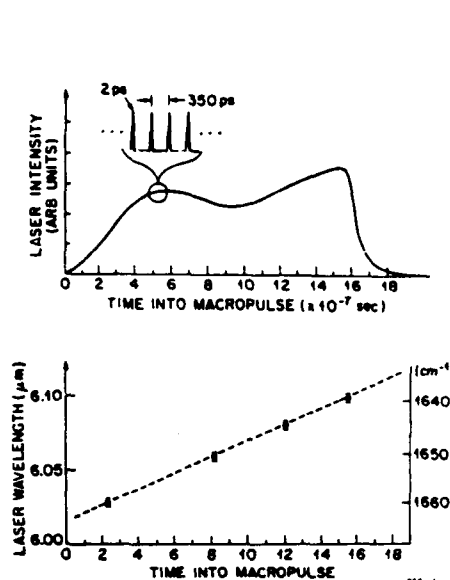
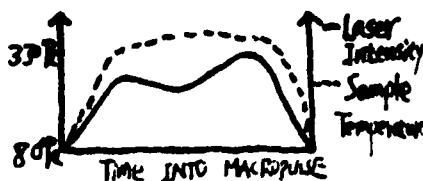


Fig. 7- Properties of the MarkIII FEL:  
(a) Temporal shape of the macropulse.  
Inset illustrates the picosecond microstructure of the pulses.  
(b) Wavelength chirp measured during the macropulse.

During the macropulse, pump beam puts in 1 millijoule of energy in sample => Sample heating due to macropulse



=> While the pump beam presents, the actual temperature of the sample is around 330K, not 80K, during the macropulse.

=> If you heat it "fast enough" the band does not disappear. The 1650cm<sup>-1</sup> band persists following rapid pulse heating.

But on the other hand, if you heat it slow, as in the F.T.I.R measurement, the band intensity decreases.

#### Conclusion:

- => There is nothing unusual about the population life time of 1650cm<sup>-1</sup> band
- => The behavior of the band depending on how fast it been heated implies the origin of the band is due to structural changes

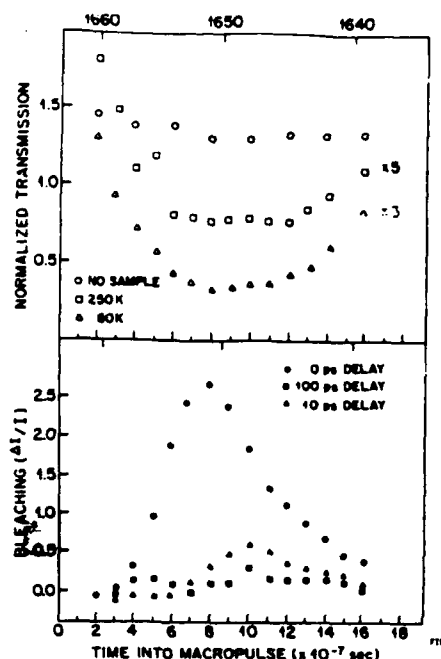


Fig. 8- (a) Top section shows absorption of ACN around 1650cm<sup>-1</sup>. Tuning occurs naturally due to chirp of the FEL. Macropulse time has been converted to wavelength on the top axis.  
(b) Bleaching versus wavelength at three different pump-probe delays.

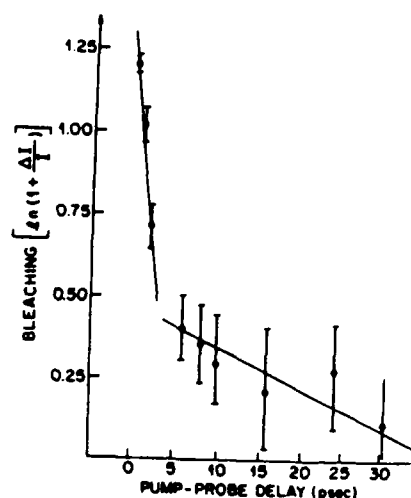


Fig. 9- Transient bleaching recovery at 1650cm<sup>-1</sup>. The fast component is due to coherent artifact. The slow component gives T<sub>1</sub> = 15 ± 5 picoseconds relaxation time.

#### Reference

- [1] W.S. Fann, S. Benson, J.M.J. Madey, S. Etemad, G.L. Baker and F. Kajzar, Phys. Rev. Lett. 62, 1492(1989).
- [2] W.S. Fann, L. Rothberg, M. Roberson, R.A. Austin, S. Benson, J.M.J. Madey and S. Etemad, submitted to Phys. Rev. Lett.
- [3] F. Kajzar, S. Etemad, G.L. Baker and J. Messier, Solid State Commun. 63, 1113(1987).
- [4] B.R. Weinberger, C.B. Roxio, S. Etemad, G.L. Baker and J. Orenstein, Phys. Rev. Lett. 53, 86(1984).
- [5] D. Moses, A. Feldblum, E. Ehrenfreund, A.J. Heeger, T.C. Chung, and A.G. MacDiarmid, Phys. Rev. B 26, 3361(1982).
- [6] Weikang Wu, Phys. Rev. Lett. 61, 1119(1988).
- [7] Z.G. Soos, and S. Ramasesha, J. Chem. Phys. 90, 1067(1989).
- [8] G. Ceren, U. Buontempo, F. Carta, E. Gratton and A.C. Scott, Phys. Rev. Lett. 51, 304(1983).

What do we learn about FEL?

Shot to shot stability is around 5%.

Better than different frequency mixing and stimulated Raman scattering => 50% fluctuation.

But sometimes there is long term, 20 mins to half hour, wavelength drifts.

Macropulse chirping could be useful for spectroscopy.

High peak power in micropulse is useful in transient experiments.

High average power in macropulse could be useful, but it could cause problems too.



# AP1.5

## HIGH AVERAGE POWER CW FREE ELECTRON LASERS FOR APPLICATION TO PLASMA HEATING: DESIGNS AND EXPERIMENTS

J.H. Booske, V.L. Granatstein, T.M. Antonsen, Jr., S. Bidwell,  
Y. Carmel, W.W. Destler, P.E. Latham, B. Levush,  
I.D. Mayergoyz, D.J. Radack, Z.X. Zhang  
University of Maryland, College Park, MD  
and H.P. Freund, SAIC, McLean, VA

A short period wiggler ( $\ell_w \sim 1$  cm), sheet beam FEL has been proposed as a low-cost source of high average power millimeter-wave radiation for plasma heating and space-based radar applications. Recent calculations and experiments — confirming the feasibility of this idea in several critical areas — will be described. Results of short-pulse FEL oscillator experiments will also be discussed.

\*Supported by DoE, ONR, and SDIO/IST through a contract managed by Harry Diamond Laboratory.

Parameter Goals:  $\sim 1$  MW, CW output rf  
 $V_b \sim 0.5 - 1.0$  MV  
 $f \sim 150 - 600$  GHz  
 $\eta_{TOTAL} \sim 30\%$

Feasibility Issues: Design flexibility  
thermal management (rf wall losses, body current)  
gun design  
spent beam energy recovery  
implications of short-period S.C. wigglers.

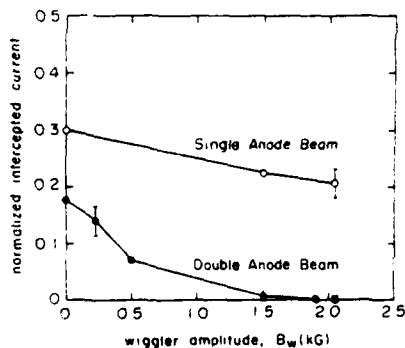
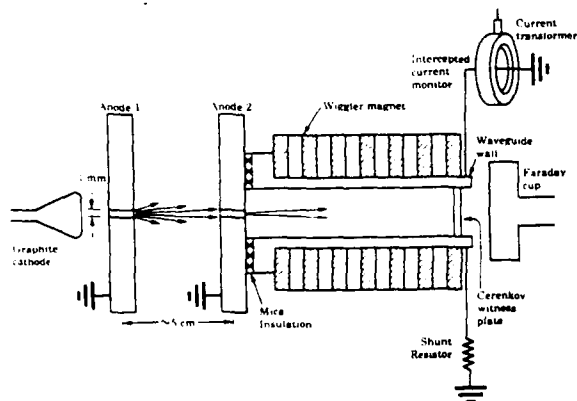


Table 1. 1 MW, 300 GHz Untapered FEL Oscillator Designs

$V_{beam}$ (kV)	650	850	1000
$I_{beam}$ (A)	48	40	34
$b_{beam}$ (cm) <sup>(1)</sup>	0.20	0.24	0.28
$a_{beam}$ (cm)	4.0	4.0	4.0
$\theta_{beam}$ (deg)	$\pm 2.0$	$\pm 2.0$	$\pm 2.0$
$b_{rf}$ (cm)	0.375	0.575	0.70
$a_{rf}$ (cm)	5.5	6.0	6.0
$T_{eff}$	0.13	0.11	0.12
$L$ (cm)	19.6	25	30
$\ell_w$ (cm)	0.85	1.25	1.50
$N_w$ (# periods)	23	20	20
$B_w$ (kG)	2.0	2.0	2.0
$\lambda_d$ (cm)	15.5	18.7	21.1
$f$ (GHz)	285	288	300
$\eta_e$	3.0%	3.1%	3.0%
$b_{7e}/(7e-1)$ (total)	$\pm 0.8\%$	$\pm 0.8\%$	$\pm 1.0\%$
beam/wall clearance (mm)	0.88	1.7	2.2
$\theta_{intercept}$ (deg)	$\pm 3.5$	$\pm 5.5$	$\pm 6.0$
$\dot{P}_{rf, wall}$ (W/cm <sup>2</sup> ) <sup>(2),(3)</sup>	72	24	< 10
$P_{cav}$ (MW)	8.9	9.3	< 8.9
$P_{out}$ (MW)	0.90	1.00	1.02
$\eta_T$ (92% beam energy recovery)	28%	28%	28%
$\phi_{LV}$ (kV)	71.5	93.5	110

### Notes:

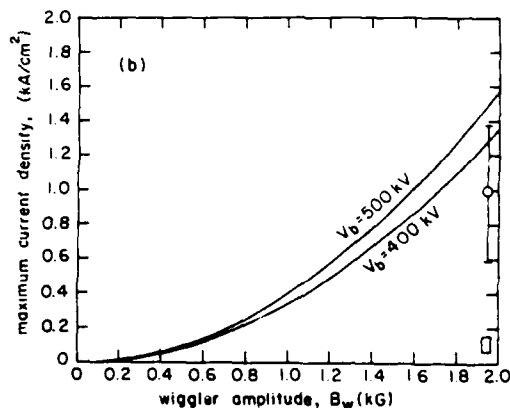
- (1) Injected beam thickness is 1 mm in all cases.
- (2) Used  $\sigma$ -values reduced  $\times 2$  from textbook values.
- (3) Maximum estimated cooling capability  $\sim 1.5$  kW/cm<sup>2</sup>.

### BODY CURRENT: SPACE CHARGE CONFINEMENT

$$\omega_p \leq (\gamma_e / \sqrt{2\epsilon_0}) \Omega_w, \quad \Omega_w \equiv eB_w / mc$$

("="  $\rightarrow$  "Brillouin" Flow Condition)

When  $\omega_p \ll (\gamma_e / \sqrt{2\epsilon_0}) \Omega_w$ , space charge is negligible.

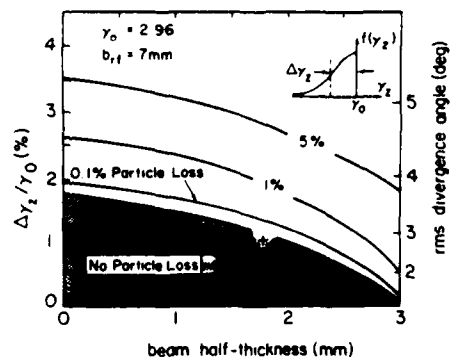
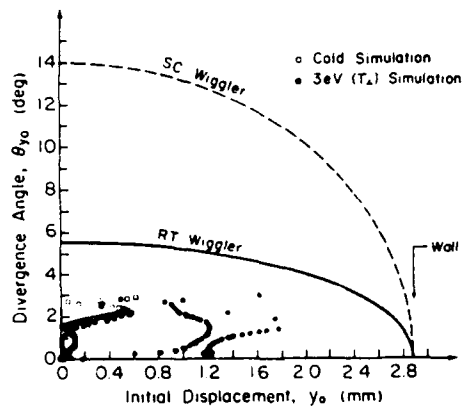
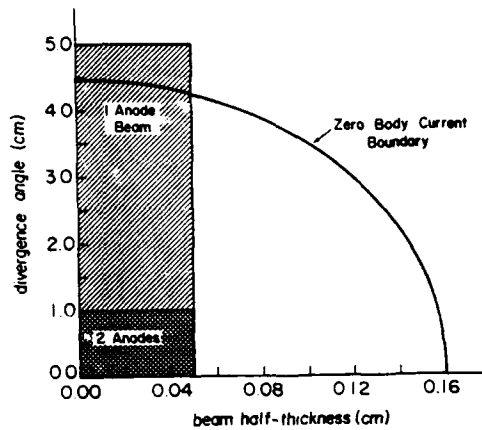


# BODY CURRENT: TRAJECTORY CONFINEMENT

$$\langle \tilde{y} \rangle_{r_w} = \langle F_p \rangle / m\gamma; \quad |\langle F_p \rangle| \lesssim [(mk_e^2 c^2 / 2) a_0^2] y$$

$$y(t) \approx y_j \sin[2\pi z / \lambda_s + t]$$

$$y_j < b_H/2, \text{ or } \theta_{y0}/2\pi < \sqrt{(b/2)^2 - (y_0)^2} / \lambda_s$$



# 1 MV SHEET BEAM GUN DESIGN

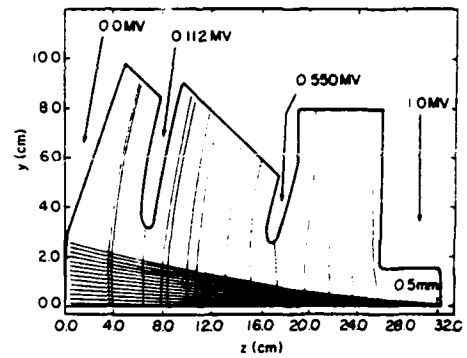
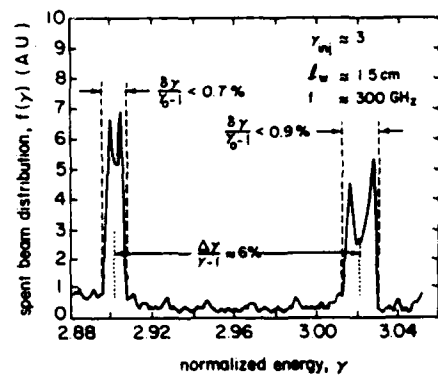
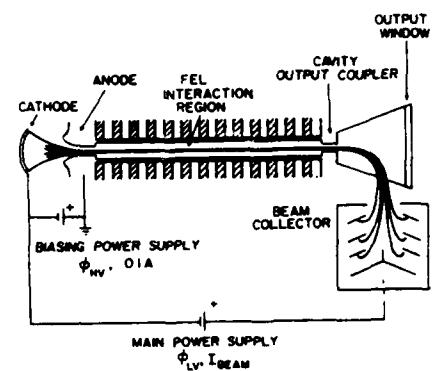


Table 2: Sheet Beam Gun Characteristics

Quantity	Desired Spec.	1st-cut Design Value
thickness	1.0 mm	1.0 mm
beam voltage	0.5 - 1.0 MV	0.7 - 1.0 MV
voltage tuning	$\geq 100$ kV	300 kV
linear current density	7.5 - 15 A/cm	5.0 A/cm
divergence angle	$\leq \pm 3^\circ$	$\leq \pm 3^\circ$
maximum electric field	$\leq 100$ kV/cm	$\leq 70$ kV/cm
beam energy spread	$\approx 0$	$< 0.06\%$
axial energy spread in FEL	$< \pm 2\%$	$\pm(1.2 - 1.0)\%$
cathode emission current density	$< 10$ A/cm <sup>2</sup>	$\sim 1$ A/cm <sup>2</sup>



## SPENT BEAM ENERGY RECOVERY

### Design Relations:

$$\eta_{TOTAL} = \eta_e / [1 - \eta_{coll}(1 - \eta_e)]$$

$$\phi_{LV}/\phi_{HV} \approx 1 - (\eta_{coll} - \eta_e)$$

### DC Power Supply Technology Status:

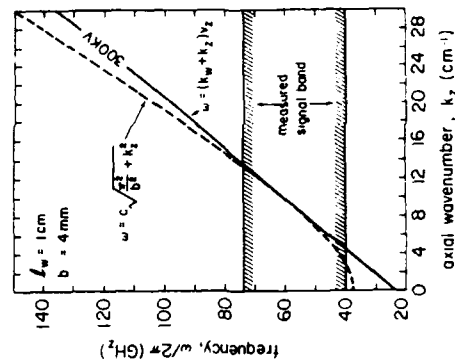
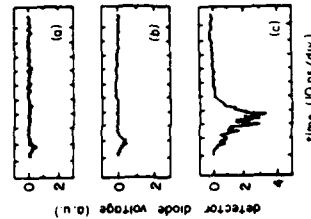
$V \approx 200$  kV,  $P \approx 1$  MW DC commercially available.

$V \approx 300$  kV,  $P \approx 1$  MW DC not currently available in practical or cost-effective form (exterior sub-stations)

### Implication:

for  $\phi_{HV} \sim 0.7 - 1.0$  MV, need

$$\eta_{coll} - \eta_e \approx 0.7, \text{ or } \eta_{coll} \approx 0.80, \eta_e \approx 0.10$$



## SHORT-PERIOD SUPERCONDUCTING WIGGLER

• Predicted parameters:  $B_w \sim 5 - 10$  kG @  $l_w \sim 1$  cm

• Implications:

- (1) Improved beam confinement
- (2) Strong pump regime +  $B_w$ -tapering  $\approx 30$ -40% efficiency?

$$-I_m(k)L \gg 1, \quad a_w/\gamma_0 \gg j_{crit}$$

$$j_{crit} \equiv 4 |\omega_p / ck_w \gamma_0^2|^{1/2}, \quad \omega_p \equiv 4\pi ne^2/m\gamma_0^2$$

Example:  $V_b \sim 1$  MV,  $I_b \sim 4$  A  
 $A_b \sim 0.2 \times 4.0$  cm  $\sim 0.8$  cm<sup>2</sup>  
 $B_w \sim 6$  kG,  $l_w \sim 1$  cm  
 $L \sim 0.7$  m

$$(*) \quad a_w/\gamma_0 \approx 0.19 \gg j_{crit} \approx 0.068 \quad \checkmark$$

$$(*) \quad -I_m(k)L \sim 3.2 \gg 1 \quad \checkmark$$

## CONCLUSIONS

1. Critical technological risk areas appear manageable with conservative safety factors.
2. Body current negligible with low emittance, low perveance beams. CW beam generation feasible with multi-anode sheet beam thermionic guns.
3.  $\eta_{coll} \sim 80\%$  necessary and advantageous with low-gain FEL oscillator
  - (a) Looks practical due to small beam energy spreads.
  - (b) Reduces beam power supply to commercially practical voltages.
4. S.C. Wiggler at  $\sim 1$  cm period provides improved focusing, possibilities for high-gain Compton regime.
5. Demonstration of lasing with 10 periods,  $\tau_p < 50$  ns,  $V_b \sim 300$  kV,  $l_w \sim 1$  cm,  $B_w \sim 1.5$  kG,  $I_b \sim 100$  A.

This work was supported by the U.S. Department of Energy.

# PLENARY PAPER

## VEPP-3 STORAGE RING OPTICAL KLYSTRON: LASING IN VISIBLE AND ULTRAVIOLET REGIONS

G.N. Kulipanov, V.N. Litvinenko, I.V. Pinayev, V.M. Popik, A.N. Skrinsky,  
A.S. Sokolov and N.A. Vinokurov.

Institute of Nuclear Physics, Siberian Branch of the USSR Academy  
of Sciences, Novosibirsk, USSR

Lasing in a wide 2400-6900 Å spectral range (from visible to ultraviolet) was reached in the optical klystron OK-4 installed on the VEPP-3 storage ring. OK-4 is the first FEL operating in UV.

### 1. Introduction

The optical klystron was proposed in 1977 by Vinokurov and Skrinsky /1/ as a modification of a free electron laser (FEL). It has a much higher gain per pass than a FEL due to using a special device - a buncher located between two undulators. Experiments with an optical klystron (OK) have been carried out at our Institute since 1979.

In late 1985, it was decided to update the VEPP-3 storage ring. One of the most important tasks of this modernization was to install an additional straight section (bypass) dedicated to OK operation. In March 1988 the bypass was successfully installed on VEPP-3, in April a circulating electron beam was captured and on June 3 lasing was attained and wavelength tunability from 5800 to 6900 Å, with a linewidth less than 0.6 Å, was achieved. In July and October 1988

### 2. A bypass on the VEPP-3

The scheme of VEPP-3 storage ring with the bypass is shown in fig. 1. The bypass consists of two bending magnets, 12 quadrupoles, a vertical wiggler and an OK mag-

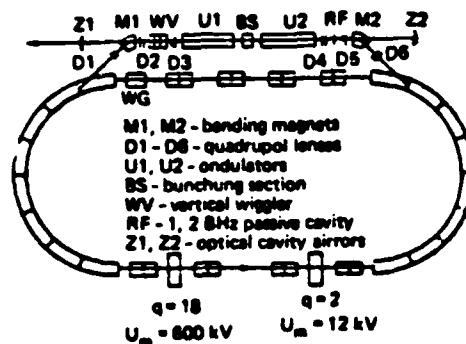


Fig. 1

netic system of 7.8 m long. The

bypass focusing system is very flexible and it gives us a possibility to optimize the electron beam parameters in the OK and to match  $\eta$ - and  $\beta$ -functions with VEPP-3 arcs under different conditions.

### 3. OK magnetic system

The OK magnetic system comprises two electromagnetic undulators with a buncher (3-pole wiggler) between them. The cross sections of the undulator are schematically shown in fig. 2 and its parameters are given in table 1.

The field in the undulator is excited by eight periodically bent copper buses with holes for water cooling. The buses are commuted on the ends of the undulator.

Each undulator has 68 poles; the ones on both ends are wound by one turn and they have half the magnetic potential. Undulators are installed on the bypass one after another and are bilaterally symmetric about the centre of the section between them. This automatically provides absence of any equilibrium orbit distortion in the storage ring.

The electromagnetic undulators allow a wavelength of fundamental harmonics tunability from 1000 up to 15000 Å by changing the

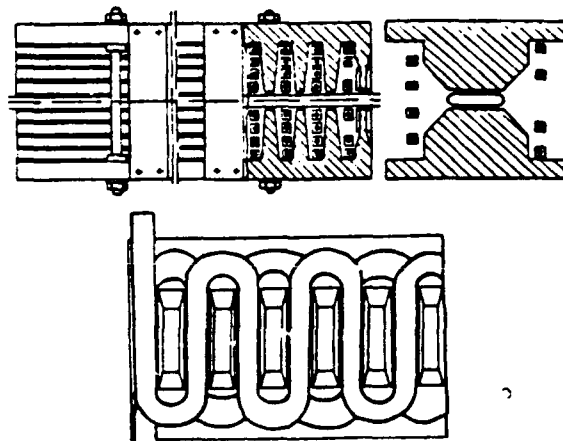


Fig. 2. Cross section of the OK-4 undulator

Table 1  
Parameters of the OK-4 undulator

Undulator length [m]	3.4
Number of periods	33.5
Period [cm]	10
Magnetic gap [cm]	2.2
Maximum magnetic field along the axis [kG]	5.3 (5.7)
Pole transverse width [cm]	9
Number of separate buses	8
Cross section of a bus [mm <sup>2</sup> ]	18 × 18
Current consumption [kA]	2.2 (3)
Power consumption [kW]	60

The gain values were measured by comparing with the optical cavity losses on the edges of the reflection bands, where lasing was stopped: 10% at 6000 Å, 5.5% at 4000 Å and 3.5% per pass at 2500 Å.

### 4. Lasing in OK

When the OK is tuned above threshold, i.e. the OK gain is more than the optical cavity losses and

the revolution frequencies of the electron and light beam are synchronized, the lasing appears on a wavelength where the OK has a maximum gain. Some of the measured spectra are shown in fig. 3.

The relative lasing line width  $\Delta\lambda/\lambda$  varies within the  $10^{-4}$ - $5 \cdot 10^{-4}$  range, depending on the detuning of the electron beam revolution frequency from the exact synchronism, on the beam current and on other parameters.

The transverse distribution of radiation intensity corresponded to the basic mode ( $TEM_{00}$ ) of the optical cavity.

Continuous tunability of the lasing wavelength was attained by changing the field in the undulators. Its boundaries (5800-6900 Å, 3750-4600 Å and 2400-2700 Å) corresponding to the reflection bands of the mirrors were used. The threshold current for lasing was 1-10 mA, depending on the optical cavity mirror conditions.

The average lasing power is limited by electron beam energy spread growth and is proportional to the full synchrotron radiation power and to the maximum admissible energy spread. In our case the maximum energy spread  $\sigma_E/E$  was limited by the gain reduction above the threshold and varies within

the  $(6-2) \times 10^{-3}$  range. The measured power (6 mW at 6300 Å and 2.5 mW at 2500 Å) at 20 mA average current corresponded to the expected values. Because only the average lasing power is limited, we realized a G-switching mode of OK operation to produce high peak power. The electron beam was shifted from the optical cavity axis using electrostatic plates and was periodically returned to the initial position.

The typical pulse duration at 10 mA current was 0.1 ms and the power was about 50 W at 6300 Å and 18 W at 2500 Å wavelength. An increase in electron energy spread during lasing was observed in both cases (continuous and G-switch mode). The energy spread was calculated from the bunch length measured by a dissector [2] with 30 ps time resolution. The maximum measured relative energy spread ( $1.5 \times 10^{-3}$ ) was twice as large as the initial one.

## 5. Lased radiation time structure

For measurement of the radiation time microstructure we used a dissector. The radiation bunch repetition frequency is  $c/2L = 8$  MHz, where  $L = 18.7$  m is the length of the optical cavity.

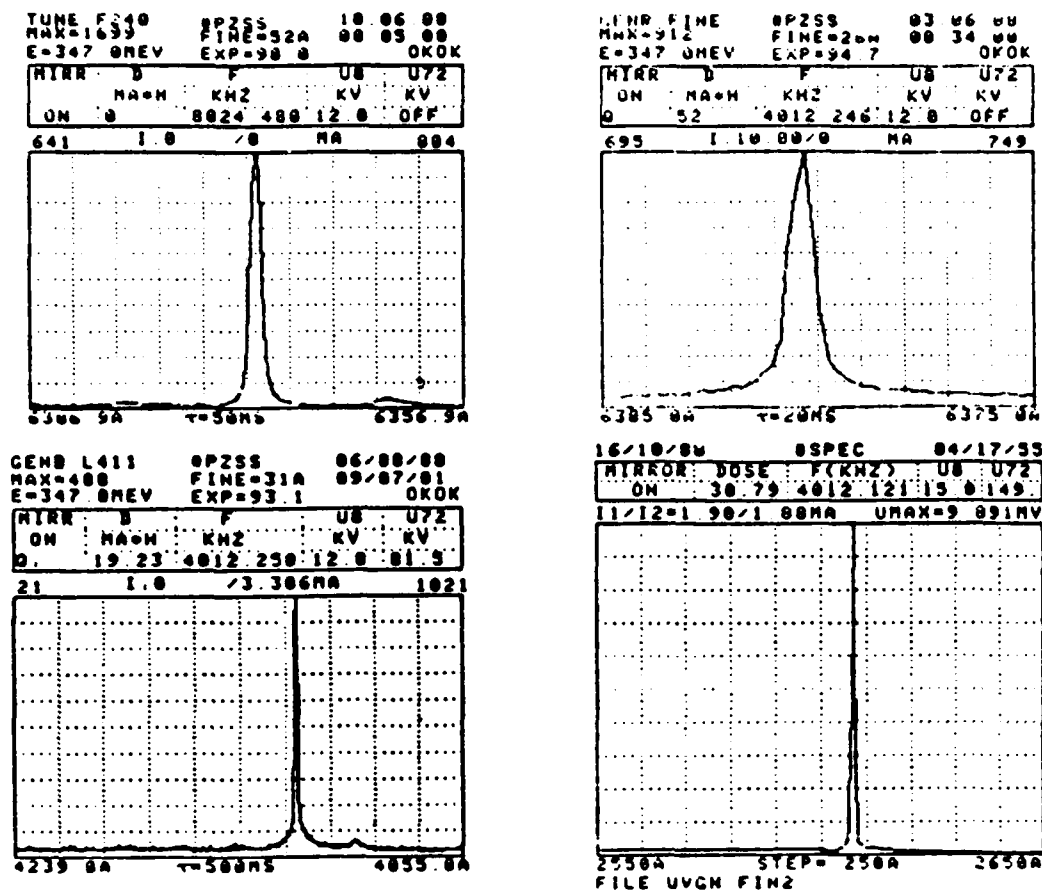


Fig. 3. Lasing lines obtained on OK-4.

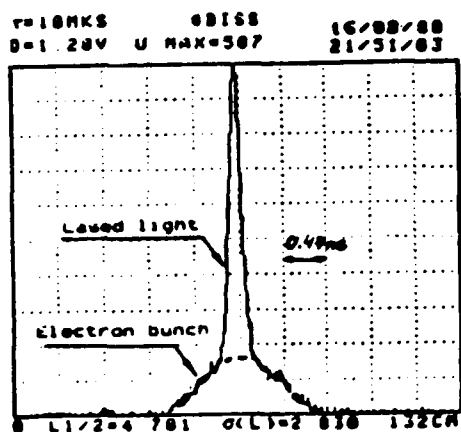


Fig. 4. The time microstructure of the electron and the lased bunches

Fig. 4 shows the time structure of the electron beam (wide peak) and the lased beam (narrow

peak on top of the electron beam. The pulse duration of the spontaneous radiation is equal to that of the electron bunch and the duration of the lased beam pulse is considerably less. This is quite natural since the gain is proportional to the instantaneous value of the electron current and, consequently, is maximum in the centre of the bunch. The lasing micropulses have a duration time of about 200 ps. According to this, the lased peak power is about 25 and 9 kW on 6300 and 2500 Å, respectively, in

G-switch mode. Within the optical cavity the peak power was 2.5 MW and 1 MW, consequently.

## 6. Plans

Preparations for further increase of the lasing power and shortening of the lasing wavelength are in progress.

## References

- 1 N.A.Vinokurov and A.N.Skrinsky, Preprint 77-59 of the Institute of Nuclear Physics, Novosibirsk, 1977.
- 2 E.I.Zinin, Nucl.Instr.Meth. 208 (1983) 439.
- 3 V.N.Litvinenko, Synchr. Radiat. News 2 (1988) 18.



# **POST DEADLINE SESSION**

## PD.3

## New Features in Weak-Field and Strong-Field FELs

W. B. Colson

Department of Physics, Naval Postgraduate School, Monterey, CA 93943

### ABSTRACT

Two new features of FELs are described: (1) an FEL using a long undulator with short periods (small  $K$ ) can have classical gain above threshold, but may not start because  $\hbar > 0$ ; (2) in high-gain, high-power amplifiers, sharp spikes may appear in the normally smooth gain spectrum.

### TWO TOPICS:

1.  $\hbar$  and FELs With Micro-Undulators
2. Gain Spectrum Spikes in FEL Amplifiers

#### 1. $\hbar$ and FELs With Micro-Undulators

- typical FEL oscillator requirements:
  - classical gain > loss, above threshold
  - no significant quantum recoil
- undulator assumptions:
  - $\lambda_0 = 1\text{mm}$ ,  $N = 1000$ ,  $L = 100\text{cm}$
  - gap = 0.06cm,  $B_r = 5000\text{G}$ ,  $\hat{B} = 1500\text{G}$
  - $I_{\text{coils}} = 140\text{A}$  in a bifilar helical winding
  - $P_{\text{undulator}} \approx 10^8\text{W}$  at 1mm wavelength

=> weak undulator  $K = 0.01$

#### Compact Visible FEL for the Future:

$I = 10\text{A}$ ,  $\gamma mc^2 = 12\text{MeV}$  (smaller accelerator)  
 $\lambda_0 = 1\text{mm}$ ,  $N = 1000$ ,  $L = 100\text{cm}$   
 gap = 6 $r_b$ ,  $K = 0.01$ ,  $F = 0.1$   
 $\lambda = 8 \times 10^{-5}\text{cm}$ ,  $w_0 = 0.03\text{cm}$ ,  $r_b = 0.01\text{cm}$   
 $Q = 100$ ,  $j = 1$  =>  $G \approx 10\%$   
 $\Delta\gamma/\gamma = 10^{-4}$ ,  $\sigma_\gamma = 2$ ,  $\varepsilon = 10^{-6}\text{cm-rad}$ ,  $\sigma_r = 0.5$   
 $r_b$  is matched,  $N_b = 0.4$ ,  $\rho = 7 \times 10^{12}\text{cm}^{-3}$

#### Design Issues:

- gain  $\propto K^2$  and  $K \propto B\lambda_0$
- as  $\lambda_0 \rightarrow 0$ ,  $K$  &  $G$  decrease
- $B$  is limited by  $B_{\text{rem}}$ ,  $I_{\text{coil}}$ , or  $P_{\text{undulator}}$   
 =>  $N = 1000$  makes gain above threshold

#### Look at Startup after one pass:

- transitions/electron into the coherent mode  
 $w_c = \alpha K^2 \approx 10^{-6}$  where  $\alpha = e^2/\hbar c$
- coherence volume is  $N^2 \lambda^2 \lambda_0$
- total transitions in one pass  
 $S_\gamma = \rho F N^2 \lambda^2 \lambda_0 w_c \approx 400$  photons
- photon fluctuations,  $N_\gamma^{-1} = 5\%$   
 => too large for gain bandwidth, 0.1%

#### Startup after many passes:

- after many passes  $\frac{dN_\gamma}{dn} = S_\gamma + N_\gamma(G - Q^{-1})$
- look for steady-state number of photons
- if  $G \approx 0$  =>  $N_\gamma = S_\gamma$ ,  $Q = 4 \times 10^4$  photons
- photon fluctuations,  $N_\gamma^{-1} = 0.5\%$   
 => still too large for gain bandwidth, 0.1% !!
- photon fluctuations <=> bad undulator  
 => FEL has sufficient gain, but won't start!

#### Conclusions

- starting requires  $N_\gamma^{-1/2} < N^{-1}$   
 =>  $\alpha Q \rho F \lambda^2 \lambda_0 K^2 > 1$
- define  $j = 8N(\theta \pi K L)^2 \rho F / \gamma^3 mc^2$   
 and  $\lambda_C = \hbar / mc$  Compton wavelength  
 =>  $j Q \gamma \lambda > (4\pi)^2 N^3 \lambda_C$
- assume FEL is just above threshold  
 >> New FEL Startup Criteria <<

$$\gamma \lambda > 4\pi N^3 \lambda_C$$

- recall the quantum recoil requirement  
 $\gamma \lambda > 4\pi N \lambda_C$

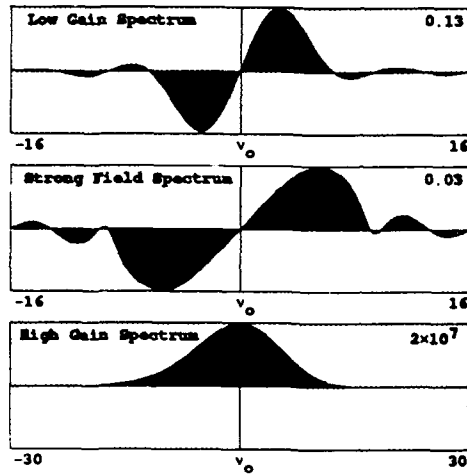
## 2. Second Topic: Gain Spectrum Spikes

- consider gain spectrum in high-gain, high-power FEL amplifiers
- nominal gain spectrum usually starts with results from a perfect beam
- a new feature on FELs similar to ELF, but with higher beam quality

### FEL Gain Spectrum Shapes

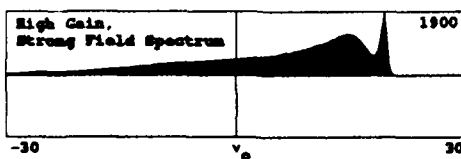
$$G(\nu_0) \Leftrightarrow G(\lambda) \Leftrightarrow G(\gamma) \Leftrightarrow G(-B)$$

Recall usual gain spectrum shapes:



=> all these examples are smooth curves of differing shape

### High-Gain and High-Power FEL Amplifier

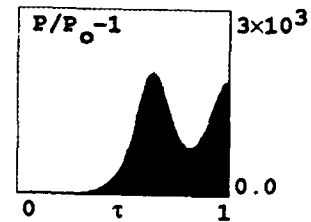


- observe spike on smooth gain spectrum
- spike is "washed out" by poor beam quality
- ELF parameters with x5 better brightness
- more spikes appear with higher power

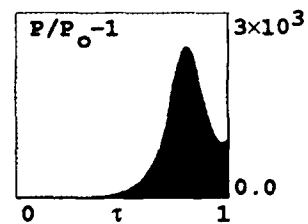
### FEL Power Growth Along Undulator

$$j = 3000 \quad a_0 = 10$$

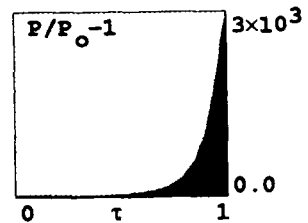
lower gain peak at  $\nu_0 = 13$



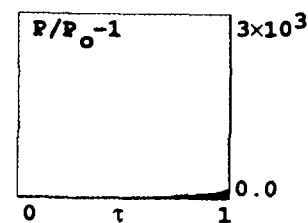
gain valley at  $\nu_0 = 18$



gain spike at  $\nu_0 = 20$



past gain spike at  $\nu_0 = 21$



### Conclusions

- existence of gain spikes essential for FEL optimization and understanding
- gain spikes may be present on ELF II with better beam quality
- spikes explain inconsistent gain behavior

# Operation of the MIT/SRL 1.2 MeV All-Solid-State Induction Linac

D. Goodman, D. Birx, D. Clarke, R. Klinkowstein, R. Shefer  
Science Research Laboratory  
Somerville, Massachusetts

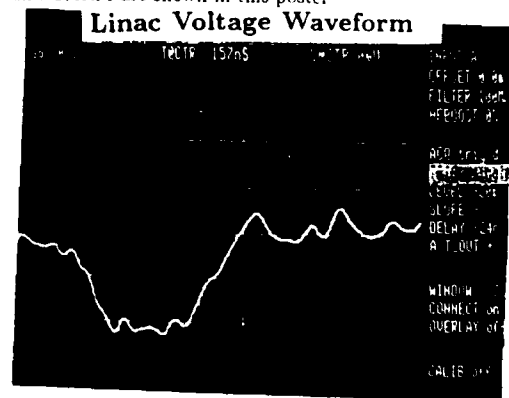
and

W. Menninger, B. Danly, R. Temkin  
Plasma Fusion Center  
Massachusetts Institute of Technology  
Cambridge, Massachusetts 02139

A compact, all-solid-state, 1.2 MeV linear induction accelerator designed and built by Science Research Laboratory has been installed and is in operation at the MIT Plasma Fusion Center. The linac is designed with a 4 cell, 600 keV injector followed by a 4 cell (+600 keV) anode block. The pulse power is provided by a SNOMAD II accelerator driver, which delivers 150J/pulse at up to 5 kHz pulse repetition rate. The SNOMAD II accelerator driver features all-solid-state magnet pulse compression technology to produce the 150 kV drive pulses from 600 VDC input. Experiments planned for this accelerator during the coming year include an x-band relativistic klystron and a 17 GHz CARM amplifier. Preliminary design parameters for the relativistic klystron and CARM will be presented.

## MIT/SRL Induction Linac Facility

An induction linear accelerator now in operation at MIT will be used to drive high power electron beam devices including a relativistic klystron and a cyclotron autoresonance maser. The new linac, designed and built by Science Research Labs of Somerville, MA, and installed in the MIT Plasma Fusion Center, features a completely solid state pulse generator as an efficient reliable pulsed power source. The SNOMAD-II injector uses SCR-commutated nonlinear magnetic pulse compression to produce 150 Joule, 50 ns duration pulses at a voltage of 150 kV. The pulses are directed to four induction accelerator cells which are placed in series to produce 600 kV on the cathode stalk. The relativistic klystron, which requires beam parameters of approximately 500 A at 500 kV, will be attached directly to the injector. Four additional accelerator cells will be added to produce the 500 A, 1.2 MeV beam required for the CARM amplifier. The relativistic klystron and CARM are expected to be operational within a year. Initial data showing the operation of the Linac, and design studies for the klystron and CARM are shown in this poster.



The cathode stalk voltage is measured by a calibrated capacitive probe. The scale is 200 kV/div vertical, 20ns/div horizontal.

## Induction Linac Parameters

### SNOMAD-II Injector

Energy per pulse	150 J
Pulse Duration	50 ns
Injection Voltage	150 kV
Repetition Rate	6 kHz
Electrical Efficiency	90 %

### Accelerator Parameters

Cathode Voltage	$4 \times 150 \text{ kV} = 600 \text{ kV}$
Beam Current	500 A
Beam Voltage	1.2 MeV
Cathode Diameter	3.5 in
Acceleration Pipe Diameter	3.75 in

### Parameters Achieved (August 1989)

Pulse Duration	50 ns
Beam Voltage	500 kV
Beam Current	2 kA

## Relativistic Klystron ‡

An X-band Relativistic Klystron will be added to the Induction Linac in the spring. A demountable tube will allow experiments with both travelling wave and standing wave (single cavity) outputs. Klystron design using a variety of computer codes is ongoing at both SRL and at Hamson Research Corp., Palo Alto, CA. Nominal klystron parameters are shown below and typical computer results are shown in the following pages.

### Klystron Parameters

Operating Frequency	11 GHz
Output Power	100 MW
Beam Voltage	500 kV
Beam Current	500 A
Beam Radius	7 mm
Beam Pipe Radius	10 mm
Magnetic Field	6 kG

### LIA-Driven TE<sub>13</sub> Mode CARM Amplifier Design

Parameter	Design Value
Beam Energy	1.2 MeV
Beam Current	500 A
Pulse Length	50 ns
$\alpha$	0.6
Frequency	17.136 GHz
Mode	TE <sub>13</sub>
Guide Radius	5 cm
$\beta_{ph}$	1.137
$P_{in}$	10 kW
$\eta$ , untapered	33.6%
$\eta$ , -0.5%/cm taper	46.4%
$z_{taper}$	0.45 m
$z_{sat}$	0.96 m
$P_{sat}$	278 MW
$B_0$	4.94 kG
Detuning ( $\Delta_0$ )	0.4

## CARM Amplifier Program

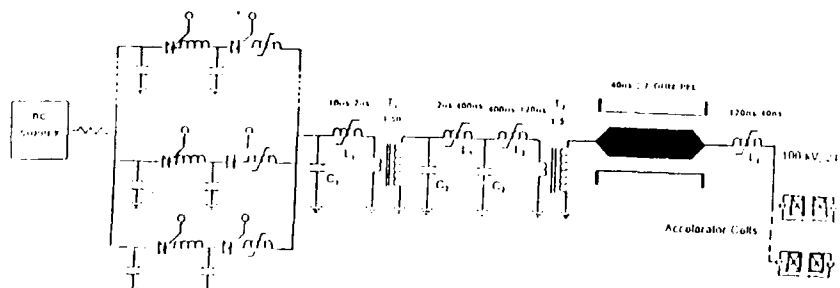
Future linear colliders will require high frequency rf sources together with high gradient accelerating structures in order to be economically feasible. The cyclotron autoresonance maser (CARM) is a promising source for application as an rf accelerator driver. This program<sup>†</sup> will investigate and evaluate the CARM amplifier as an efficient source of high peak power microwaves capable of fulfilling this future requirement.

Experiments at a frequency of 17 GHz will be performed using two different technologies for generation of the high voltage electron beam required by the CARM. A long pulse (1  $\mu$ s), 700 kV pulse modulator and a short pulse (50 ns), 1.2 MeV induction accelerator will be employed for generation of the electron beam. This will allow a comparison of two alternate methods for producing the high peak power, ~50 ns microwave pulses required by the high gradient structures. A long pulse modulator-driven CARM together with pulse compression techniques, or an induction linac driven CARM are both capable in principle of delivering the required rf pulses to the structure. In both experiments, the details of CARM amplifier operation will be investigated, including linear and nonlinear gain, stability, efficiency, and phase sensitivity.

<sup>†</sup>Funded by DoE, Basic Energy Sciences Division.

‡SUPPORTED BY NAVAL SURFACE WARFARE CENTER

### SNOMAD II Induction Linac Driver



The circuit diagram for the SNOMAD II Induction Linac driver shows an SCR commutated pulsed power supply feeding alternating sections of nonlinear inductors for pulse compression and step-up transformers for voltage multiplication.

# AUTHOR INDEX

Akiba, T. 7, 252.  
 Allison, W.W.M. 278  
 Amir, A. 177  
 Angles, J.M. 250  
 Angles, M. 250  
 Anthouard, P. 250  
 Antonsen, Jr. T.M. 194,303  
 Atkinson, D.P. 184,235  
 Austin, R.A. 299  
 Ayres, R.L. 169  
  
 Baker, G.L. 299  
 Bakshi, M.H. 25  
 Bamford, D.J. 289  
 Barbagelata, L. 86  
 Bardy, J. 239,250  
 Barletta, W.A. 158  
 Barnard, J.J. 204  
 Barrett, D.M. 235  
 Batchelor, K. 116  
 Bazin, C. 91  
 Bekefi, G. 175,245  
 Bender, S.C. 263,267  
 Bennett, G. 265  
 Benson, S.V. 5,20,36,93,96,139,  
 150,210,226,265,299  
 Ben-Zvi, I. 116,192  
 Best, R.W.B. 114  
 Bhattacharjee, A. 287  
 Bhowmik, A. 36,96,116,150,226,  
 265  
 Bidwell, S. 303  
 Billardon, M. 91,215  
 Bix, D. 313  
 Blind, B. 190  
 Bluem, H. 146,152,237  
 Bobbs, B.L. 108,135,148,206  
 Bonnafond, C. 239,250  
 Booske, J.H. 100,237,303  
 Bottollier-Curtet, H. 239,250  
 Bouquet, G. 250  
 Bourdier, A. 39,241  
 Brau, C.A. 278  
 Brinker, F. 11  
 Broberg, J.B. 169  
 Brooks, C.B. 278  
 Brown, J. 36,150  
 Bruno, C. 239,250  
 Burke, R. 135,265  
 Buzzi, J.M. 39,241

Cai, S.Y. 287  
 Carlsten, B.E. 66,122,190,254  
 Carmel, Y. 303  
 Castellano, M. 9,154  
 Cavallo, N. 9  
 Cecere, M. 25  
 Cevenini, F. 9  
 Chambers, F.W. 98  
 Chan, K.C.D. 190,208,267  
 Chang, S.P. 287  
 Chen, C. 235,276  
 Chen, S.C. 245  
 Chen, Y.C. 235  
 Choi, J. 54  
 Chong, Y.P. 98,124,166  
 Chu, T.S. 142  
 Ciocci, F.A. 9,27,86,291  
 Clark, J.C. 184,235  
 Clarke, D. 314  
 Colson, W.B. 219,312  
 Cornelius, W.D. 263  
 Couprie, M.E. 91,215  
 Cover, R.A. 108,148,206  
 Curtin, M. 36,96,150,265  
 Cutler, R.I. 160,169  
  
 Danly, B.G. 100,142,175,314  
 Dattoli, G. 9,27,291  
 Davidson, R.C. 276  
 Deacon, D.A.G. 23,25,289  
 De Angelis, A. 27,291  
 Debenham, P.H. 169  
 Dei-cas, R. 282  
 Deis, G.A. 158  
 Delmee, P.F.M. 114  
 Delvaux, J. 239,250  
 Destler, W.W. 303  
 Devin, A. 239,250  
 Dipace, A. 9,27,291  
 DiRienzo, A. 175  
 Dodd, J.W. 56,287  
 Doria, A. 27,156,291  
 Doucas, G. 278  
 Dowell, D.H. 267  
 Dulman, H.D. 243  
  
 Edighoffer, J.A. 29,98,166  
 Edighoffer, J.E. 80  
 Elgin, J.N. 278  
 Elias, L.R. 106,186,224,285

Elkonin, B.V. 112, 192  
 Elliott, C.J. 33,73,118  
 Ernst, G. J. 126  
 Esarey, E. 256  
 Etemad, S. 299  
 Evangelides, S.G. 142  
 Eyharts, P. 250  
 Eyl, P. 239,250  
  
 Faatz, B. 114  
 Fann, W.S. 93,299  
 Fauchet, A.M. 25  
 Fawley, W.M. 43  
 Feinstein, J. 18,243,280  
 Feldman, D.W. 46,104,261  
 Feldman, R.B. 66,78,200  
 Felker, B. 184  
 Ferguson, S.W. 184  
 Fernow, R. 116  
 Ferrer, J.L. 31  
 Fiorito, R.B. 66,200  
 Fisch, E. 156  
 Fillet, A.W. 130  
 Freund, H.P. 152,303  
 Frisch, J.C. 58,64,80,173  
 Fruchtmann, A. 192  
  
 Gallardo, J.C. 70,116  
 Gallerano, G.P. 9,27,156,291  
 Gardelle, J. 239,250  
 Germain, G. 239,250  
 Ghigo, A. 9,154  
 Giannessi, L. 291  
 Gilgenbach, R.M. 54  
 Gillespie, W.A. 278  
 Gitomer, S.J. 46  
 Goldstein, J.C. 122,202,254  
 Goodman, D. 313  
 Gottschalk, S.C. 110  
 Gover, A. 192  
 Granatstein, V.L. 132,237,303  
 Griffith, L.V. 235  
  
 Hafizi, B. 273  
 Halbach, K. 100  
 Hajima, R. 217  
 Hartemann, F. 188,222  
 Haselhoff, E.H. 126  
 Haynes, L.C. 46  
 Hazak, G. 192

Ho, A.H. 18,243,280  
Holmes, A.R. 278  
Hooper, B.A. 93,139  
Hopkins, D.B. 293  
Hu, J. 142

Imaski, K. 7,252  
Iracane, D. 31

Jackson, R.H. 100,146,152,237  
Jaroszynski, D.A. 114,219,278,  
291

Jerby, E. 15,162,192  
Jiang, Y. 198  
Johnson, B.C. 137,169.  
Johnson, R.G. 120,137,169  
Johnson, W.J.D. 82  
Johnston, S. 128  
Jones, M.E. 190  
Jong, R.A. 184,293  
Justice, R. 267

Kaminski, J. 297  
Kawarasaki, Y. 165  
Kennedy, P. 108,206  
Kho, T.H. 60  
Kimel, I. 106,186,285  
Kimmitt, M.F. 27,156,278  
Kirbie, H.C. 235  
Kirk, H. 116  
Kitagawa, Y. 7  
Kleinman, H. 192  
Klinkowstein, R. 314  
Knox-Seith, J.F. 177  
Kondo, S. 21  
Kulipanou, G.N. 306  
Kuruma, S. 7,50,252

Labrousche, J. 239,250  
Lachin, Y.Y. 84  
Larson, D.J. 41,144,224  
Latham, P.E. 303  
Launspach, J. 239,250  
Lee, P. 98,124,166  
Leibovitch, C. 175  
Le Taillandier, P. 239,250  
Levush, B. 132,303  
Lin, A.T. 60  
Lindstrom, E.R. 160,169  
Litvinenko, V.N. 306  
Liu, C. 76  
Livingston, P. 29  
Lowrey, A.R. 267  
Lu, Y. 76 267

Lumpkin, A.H. 66,200,267  
Madey, J.M.J. 2,5,20,23,36,  
93,96,139,150,210,226,230,  
265,299

Makowski, M.A. 184  
Mandelbaum, B. 192  
Manheimer, W.M. 130  
Manintveld, P. 114  
Mao, C. 62  
Marable, W.P. 256  
Marshall, E. 156  
Marshall, T.C. 56,287  
Martin, P.F. 278  
Mashiko, K. 165  
Mastop, W.J. 114  
Matrone, A. 86  
Matsumoto, T. 7  
Mayergoyz, I.D. 303  
McCormick, R.I. 5  
McCowan, R.B. 130  
McKee, C.B. 230  
McMullin, W.A. 96,135,150,226  
McVey, B.D. 122,196,202,267  
Meddens, B.J.H. 114  
Meier, K.L. 263  
Menninger, W. 314  
Metty, P. 36,150,265  
Miller, J.L. 98,124  
Mills, S.P. 148  
Mima, K. 7,50,252  
Minehara, E. 165  
Miyamoto, M. 7  
Mohr, D.L. 120,137,169  
Mourier, G. 188  
Mulvey, J.H. 80,250,278

Nakai, S. 7,50,252  
Negrazus, M. 11  
Neil, G.R. 29  
Newnam, B.E. 202,261  
Newton, M.A. 235  
Nexsen, W.E. 184,235  
Ng, B. 120  
Nolle, D. 11

Oepts, D. 114,219  
Ohashi, H. 217  
Ohi, K. 50,252  
Ohigashi, N. 7,50  
Ohkubo, M. 165  
Ohtani, H. 7  
Ortega, J.M. 13,91  
Orzechowski, T.J. 98,124,166

Otonello, G. 86  
Outten, C.A. 54  
Ozcan, M. 243

Pantell, R.H. 18,243,280  
Patteri, P. 9,154  
Paul, A.C. 166,235  
Paulson, K.P. 248  
Paxton, A.H. 52  
Pellegrini, C. 70,116  
Penner, S. 120,160,169  
Pershing, D.E. 152,237  
Petroff, Y. 91  
Pidgeon, C.R. 278  
Pinayev, I.V. 306  
Pitel, G. 239  
Pluygers, J. 114  
Poole, M.W. 278  
Popik, V.M. 306  
Power, J.F. 82  
Prati, P. 86  
Prazères, R. 13,91  
Prenveille, Y. 250  
Preston, D. 104  
Price, E. 156  
Price, M.S. 137  
Prosnitz, D. 98

Quimby, D.C. 73,110,118

Radack, D.J. 303  
Rakowsky, G. 108,135,148,206  
Ramian, G. 142  
Rawls, J.M. 29  
Renieri, A. 9,27,86,156,291  
Richman, B. 93,96,226  
Roberson, C.W. 273  
Roberson, M. 299  
Robinson, K.E. 110  
Rohatgi, R. 58,173  
Rosatelli, F. 86  
Rose, J.E. 169  
Rosenberg, A. 192  
Rothberg, L. 299  
Rule, D.W. 66,200  
Russell, T.J. 82  
Ryne, R.D. 293

Sabia, E. 9,27,86,291  
Sampayan, S. 235  
Sasabe, J. 165  
Sawai, K. 7  
Sawamura, M. 165  
Scharlemann, E.T. 43,98,158,  
173,269

- Schirmer, D. 11  
 Schlueter, R. 158  
 Schmitt, M.J. 33,52  
 Schwettman, H.A. 173  
 Sessler, A.M. 292  
 Shahal, O. 112,192  
 Sharp, W.M. 43,258  
 Shay, H.D. 158  
 Sheffield, R.L. 100,254  
 Shefer, R. 313  
 Shi, X. 76  
 Shiloh, J. 192  
 Skrinsky, A.N. 306  
 Slater, D. 108  
 Slater, J. 100,110  
 Smith, I. 29  
 Smith, T.E. 166  
 Smith, T.I. 64,173  
 Sokolov, A.S. 306  
 Sokolowski, J.S. 112,192  
 Sollner, T.G. 142  
 Spencer, T. 54  
 Sprangle, P. 130,169  
 Stadnikoff, W. 250  
 Stallard, B.W. 184  
 Stanford, E.R. 194  
 Stein, W.E. 46,82,261  
 Stoner, R. 245  
 Straight, R.C. 139  
 Sugimoto, M. 165  
 Sun, K.C. 196  
 Svaton, E.M. 190  
 Swent, R.L. 64,173  
 Swoyer, G. 135  
 Szarmes, E.B. 20,36,93,210  
  
 Takabe, M. 165  
 Takeda, H. 48  
 Tang, C.M. 169,256  
 Tazzioli, F. 9  
 Temkin, R.J. 142,313  
 Thevenot, M. 250  
 Thode, L.E. 48,190,263,267  
 Thomas, K.M. 120  
 Throop, A.L. 184,235  
 Tian, S. 198  
 Tokar, R.L. 196,267  
 Tommasini, D. 86  
 Toor, A. 100  
 Torre, A. 9,27,291  
 Tsunawaki, Y. 7  
 Turner, W.C. 184,235  
  
 van Amersfoort, P.W. 114,219  
 van Buuren, R. 114  
 van der Geer, C.A.J. 114  
 van der Meer, A.F.G. 114,219  
 van der Wiel, M.J. 114  
 van Steenbergen, A. 116  
 Varfolomeev, A.A. 84  
 Velghe, M.F. 91,215  
 Vetrovec, J. 68  
 Vinokurov, N.A. 306  
 Vintro, L. 93,96,226  
  
 Walsh, J.E. 27,156  
 Walstrom, P. 100  
 Wang, J.G. 54  
 Wang, M. 45  
 Wang, M.C. 132  
 Wang, Y. 62  
 Warden, M. 177  
 Warren, R.W. 46,78,100,104,254,  
 261  
 Watson, J.M. 263  
 Weir, J.T. 98,124,166  
 Weng, Z. 76  
 Westenskow, G.A. 293  
 Whittaker, J.K. 169  
 Wilkin, N.D. 169  
 Wille, K. 11  
 Wilson, M.A. 120,169  
 Wu, T. 76  
  
 Xie, J. 62  
 Xie, M. 23  
 Xu, Y. 156  
  
 Yamanaka, C. 7,252  
 Yamanaka, T. 252  
 Yang, T. 76  
 Yang, Z. 198  
 Yeremian, A.D. 267  
 Ying, R. 62  
 Yoshioka, H. 7  
 Young, L.M. 190,267  
 Younger, F.C. 120  
 Yu, S.S. 158,258,293  
  
 Zhai, X. 76  
 Zhang, Z.X. 303  
 Zhong, S. 62  
 Zhou, C. 45  
 Zhou, W. 76  
 Zhuang, J. 62



# REPORT DOCUMENTATION PAGE

1a. REPORT SECURITY CLASSIFICATION <b>UNCLASSIFIED</b>			1b. RESTRICTIVE MARKINGS		
2a. SECURITY CLASSIFICATION AUTHORITY			3. DISTRIBUTION / AVAILABILITY OF REPORT  Approved for public release; distribution is unlimited.		
2b. DECLASSIFICATION / DOWNGRADING SCHEDULE			5. MONITORING ORGANIZATION REPORT NUMBER(S) <b>AFOSR-TR. 90-0220</b>		
4. PERFORMING ORGANIZATION REPORT NUMBER(S)			7a. NAME OF MONITORING ORGANIZATION <b>AFOSR/NP</b>		
6a. NAME OF PERFORMING ORGANIZATION <b>Inst. of Electrical &amp; Electronics Engrg</b>		6b. OFFICE SYMBOL (If applicable) <b>NP</b>	7b. ADDRESS (City, State, and ZIP Code) <b>Building 410, Bolling AFB DC 20332-6448</b>		
6c. ADDRESS (City, State, and ZIP Code) <b>445 Hoes Lane Piscataway, NJ 08855</b>		9. PROCUREMENT INSTRUMENT IDENTIFICATION NUMBER <b>AFOSR-89-0409</b>			
8a. NAME OF FUNDING / SPONSORING ORGANIZATION <b>AFOSR</b>		8b. OFFICE SYMBOL (If applicable) <b>NP</b>	10. SOURCE OF FUNDING NUMBERS		
8c. ADDRESS (City, State, and ZIP Code) <b>Building 410, Bolling AFB DC 20332-6448</b>		PROGRAM ELEMENT NO. <b>61102F</b>	PROJECT NO. <b>2301</b>	TASK NO. <b>A1</b>	WORK UNIT ACCESSION NO.
11. TITLE (Include Security Classification) <b>(U) 11TH INTERNATIONAL FREE ELECTRON LASER CONFERENCE</b>					
12. PERSONAL AUTHOR(S)					
13a. TYPE OF REPORT <b>Final</b>		13b. TIME COVERED <b>FROM 1 Jun 89 TO 31 May 90</b>		14. DATE OF REPORT (Year, Month, Day) <b>Dec 1989</b>	
15. PAGE COUNT <b>340</b>					
16. SUPPLEMENTARY NOTATION					
17. COSATI CODES			18. SUBJECT TERMS (Continue on reverse if necessary and identify by block number)		
FIELD	GROUP	SUB-GROUP			
	<b>20.06</b>				
19. ABSTRACT (Continue on reverse if necessary and identify by block number) <b>The 11th International Conference on Free Electron Lasers was held on 28 Aug to 1 September, 1989.</b>					
20. DISTRIBUTION / AVAILABILITY OF ABSTRACT <input type="checkbox"/> UNCLASSIFIED/UNLIMITED <input checked="" type="checkbox"/> SAME AS RPT <input type="checkbox"/> DTIC USERS			21. ABSTRACT SECURITY CLASSIFICATION <b>UNCLASSIFIED</b>		
22a. NAME OF RESPONSIBLE INDIVIDUAL <b>H R Schlossberg</b>			22b. TELEPHONE (Include Area Code) <b>202/767 4906</b>		22c. OFFICE SYMBOL <b>AFOSR/NP</b>

A FOUR-21-0107 ✓

**Attendees List**

**11th International  
Conference  
on  
FREE ELECTRON LASERS**

Naples, Florida  
August 28 - September 1, 1989

**90 02 23 028**

Larry Altgilbers  
US Army Missile Command  
  
Redstone Arsenal, AL 35899  
USA

Robert Behringer  
Ballena Systems Corporation  
1150 Ballena Blvd.  
Alameda, CA 94501  
USA

Avner Amir  
Quantum Institute  
University of California  
Santa Barbara, CA 93106  
USA

George Bekefi  
MIT  
Room 36-213, MIT  
Cambridge, MA 02139  
USA

Dan Anderson  
Univ. of Central Florida  
12424 Research Parkway  
CREOL  
Orlando, FL 32826  
USA

Ilan Ben-Zvi  
Brookhaven National Laboratory  
NSLS Building  
725B BNL  
Upton, NY 11973  
USA

William Andre  
US Army Strategic Defense Comm  
PO Box 1500  
Huntsville, AL 35807  
USA

Stephen Benson  
Duke University  
10 Science Drive  
Dept. of Physics  
Durham, NC 27706  
USA

Douglas Bamford  
Deacon Research  
900 Welch Road  
Suite 203  
Palo Alto, CA 94304  
USA

Amitava Bhattacharjee  
Columbia University  
S. W. MUDD 210  
New York, NY 10027  
USA

Vladimir Baranov  
Inst of Atomic Energy  
Moscow, 123182, Square 46  
  
Moscow,  
USSR

Anup Bhowmik  
Rockwell Intl/Rocketdyne Div  
M/S FA40  
6633 Canoga Ave.  
Canoga Park, CA 91303  
USA

John Barnard  
Lawrence Livermore Natl Labs  
PO Box 808  
M/S L-626  
Livermore, CA 94550  
USA

Steven W. Bidwell  
University of Maryland  
Lab for Plasma Research  
Energy Research Building  
College Park, MD 20742  
USA

CEBAF  
12000 Jefferson Avenue  
Newport News, VA 23606  
USA

Daniel Boucher  
Universite Des Sciences Lille  
BAT P5  
Villeneuve  
D ASCQ 59650,  
FRANCE

Hans Bluem  
University of Maryland  
Lab for Plasma Research  
College Park, MD 20742  
USA

Alain Bourdier  
Ecole Polytech Ano Cea Limeil  
Ecole Polytechnique PMI  
Palaiseau, 92228  
FRANCE

Rodolfo Bonifacio  
INFN Univ. of Milan  
Via Celoria 16

Milan, 20133  
ITALY

Charles Brau  
Vanderbilt University  
Box 1807 B  
Nashville, TN 37122  
USA

Ulrich K. Bonse  
University of Dortmund  
Driverweg 20  
4600 Dortmund 50,  
WEST GERMANY

Brent Brenthall  
Rockwell International  
405-B Huyler Lane  
Simi Valley, CA 93065  
USA

John Booske  
University of Maryland  
7504 Edmonston Rd.  
College Park, MD 20740  
USA

Wilma Brizzi  
Naval Research Laboratory  
4555 Overlook Avenue, SW  
Washington, DC 20375  
USA

Ilario Boscolo  
Univ. of Milan  
Dept. of Physics  
Via Celoria 16  
Milan, 20133  
ITALY

Robert Burke  
Rockwell Internatl Rocketdyne  
6633 Canoga Ave. M/S FA16  
Canoga Park, CA 91303  
USA

Herve Bottollier  
CEA CESTA  
BP 2  
Le Barp, 33114  
FRANCE

Bentley Burnham  
Duke University  
Dept. of Physics  
Durham, NC 27706  
USA

Jean-Max Buzzi  
ECOLE Polytechnique  
Dept. of Physics

Palaiseau Cedex,  
FRANCE

Donald Byrd  
Los Alamos National Lab  
M/S E523  
Los Alamos, NM 87545  
USA

Shao-Yang Cai  
Columbia University  
Dept. of Applied Physics  
New York, NY 10027  
USA

Bruce Carlsten  
Los Alamos National Laboratory  
PO Box 1663  
M/S H825  
Los Alamos, NM 87545  
USA

Wayne Cassatt  
Natl Inst of Stand & Tech  
Clopper Rd. & Quince Orchard  
Gaithersburg, MD 20899  
USA

Bob Center  
Spectra Technology, Inc.  
2755 Northup Way  
Bellevue, WA 98004  
USA

Kwok-Chi Chan  
Los Alamos National Lab  
M/S - H829  
Los Alamos, NM 87544  
USA

Chiping Chen  
MIT Plasama Fusion Center  
Building NW16-264  
Cambridge, MA 02139  
USA

Shien-Chi Chen  
MIT  
NW 176  
Cambridge, MA 02139  
USA

Yee Ping Chong  
Lawrence Livermore Natl Lab  
PO Box 808 M/S L-626  
Livermore, CA 94550  
USA

Ronson Chu  
MIT  
NW 16-225  
Cambridge, MA 02139  
USA

Hans-Juergen Cirkel  
Siemens AG KWU Group  
Hammerbacherstrasse 12-14  
Erlangen D-8520,  
WEST GERMANY

Alan Cole  
TRW, Inc.  
719 Anderson St.  
Manhattan Beach, CA 90266  
USA

William B. Colson  
Department of the Navy  
Code NPS (61Cw) ns  
Naval Postgraduate School  
Monterey, CA 93943  
USA

Richard Cooper  
Los Alamos National Laboratory  
M/S H829  
Los Alamos, NM 87544  
USA

Giuseppe Dattoli  
ENEA TIB-FIS  
PO Box 65  
Frascati RM 00044,  
ITALY

Marie-Emmanuel Cooupré  
University of Paris  
Lure CNRS-CEA-MENJS  
Bat. 209D  
Orsay 91405,  
FRANCE

Lucia De Salvo  
INFN-Univ. of Milan  
Via Celoria 16  
Milan, 20133  
ITALY

Wayne Cornelius  
Los Alamos National Lab  
AT-7 M/S JS79  
Los Alamos, NM 87544  
USA

Felix C. DeGilippo  
Oak Ridge National Lab  
PO Box 2008  
Oak Ridge, TN 37831  
USA

Ralph Cover  
Rockwell Intl/Rocketdyne Div.  
M/S FA38  
6633 Canoga Ave.  
Canoga Park, CA 91303  
USA

David Deacon  
Deacon Research  
900 Welch Road  
Suite 203  
Palo Alto, CA 94304  
USA

Mark Curtin  
Rockwell Intl/Rocketdyne Div.  
M/S FA38  
6633 Canoga Ave.  
Canoga Park, CA 91303  
USA

Philippe Deck  
CEA Limeil-Valenton  
Boite Postale 27  
Villeneuve  
Saint Georges 94195,  
FRANCE

Roy Cutler  
Natl Inst. of Stands & Tech  
Building 245  
Room 119  
Gaithersburg, MD 20899  
USA

Renato Dei-Cas  
CEA SPTN  
BP 12  
Bruyeres-Le-Chatel, 91680  
FRANCE

Bruce Danly  
MIT  
M/S NW16-172  
Cambridge, MA 02139  
USA

William Dent  
Science Applications Int Corp  
416 Owens Drive  
Huntsville, AL 35801  
USA

Anthony Dirienzo  
Massachusetts Inst. of Tech  
MIT 36-213  
Cambridge, MA 02139  
USA

Luis Elias  
Univ. of Central Florida  
CREOL  
12424 Research Parkway  
Orlando, FL 32816  
USA

James W. Dodd  
Columbia University  
Dept. of Applied Physics  
New York, NY 10027  
USA

C James Elliott  
Los Alamos National Laboratory  
Group X-1  
M/S E531  
Los Alamos, NM 87545  
USA

Henri Doucet  
CEA SPTN  
BP 12  
Bruyeres Le Chatel, 91680  
FRANCE

Randall Erickson  
Los Alamos National Lab  
PO Box 1663  
M/S F607  
Los Alamos, NM 87545  
USA

David Dowell  
Boeing Aerospace Corporation  
PO Box 3999  
M/S 2R-00  
Seattle, WA 98124  
USA

Gerard Ernst  
University of Twente  
PO Box 217  
Enschede 7500 AE,  
THE NETHERLANDS

Alexandr M. Dykhne  
Inst. of Atomic Energy  
142092, Troitsk  
Moscow,  
USSR

Eric Esarey  
Naval Research Laboratory  
4555 Overlook Avenue SW  
Washington, DC 20375  
USA

Shimon Eckhouse  
Maxwell Laboratories, Inc.  
9244 Balboa Avenue  
  
San Diego, CA 92123  
USA

Claude Etievant  
CEA  
Cen Saclay  
GIF-sur-Yvette Cedex, 91191  
FRANCE

John Edighoffer  
Lawrence Livermore Natl Labs  
PO Box 808  
M/S L-626  
Livermore, CA 94550  
USA

Stephen Evangelides  
AT & T Bell Laboratories  
Room 4C318  
Crawfords Corner Rd.  
Holmdel, NJ 07733  
USA

Wunshain Fann  
Duke University  
32-Hall  
331 Newman Springs Road  
Red Bank, NJ 07701  
USA

Walter Friz  
WRDC/ELMD

Wright Patterson AFB, OH 45433  
USA

Don Feldman  
Los Alamos National Lab  
Box 1663  
Los Alamos, NM  
USA

Kohei Furukawa  
Sumitomo Elec. Ind., Ltd.  
Osaka R and D Dept  
1-12-9, Shimaya, Konohana-Ku  
Osaka 554,  
JAPAN

Renee B. Feldman  
Los Alamos National Lab  
Box 1663  
Los Alamos, NM 87545  
USA

Juan Gallardo  
Brookhaven National Laboratory  
Physics 510D  
Upton, NY 11973  
USA

Arne Fliflet  
Naval Research Laboratory  
4555 Overlook Ave., SW  
Washington, DC 20375  
USA

Gian Piero Gallerano  
ENEA TIB-FIS  
PO Box 65  
Frascati RM 00044,  
ITALY

George Frazier  
Physics International Co.  
2700 Merced St.  
San Leandro, CA 94577  
USA

Ronald Gilgenbach  
University of Michigan  
Nuclear Engineering Dept.  
Ann Arbor, MI 48109  
USA

Henry Freund  
SAIC  
1710 Goodridge Drive  
McLean, VA 22102  
USA

Ray Girouard  
Sierra Laser Systems Inc.  
754 North Pastoria Ave.  
Sunnyvale, CA 94086  
USA

Josef Frisch  
Stanford University  
HEPL Building  
Stanford, CA 94305  
USA

Steven Gitomer  
Los Alamos National Laboratory  
Group X-1  
M/S E531  
Los Alamos, NM 87545  
USA



John Goldstein  
Los Alamos National Labs  
Group X-1  
M/S E 531  
Los Alamos, NM 87545  
USA

Ryoichi Hajima  
University of Tokyo  
Shirakata-Shirane 2-22  
Tokai-Mura  
Ibaraki 319-11,  
JAPAN

Steve Gottschalk  
Spectra Technology Inc.  
2755 Northup Way  
Bellevue, WA 98004  
USA

Frederic Hartemann  
Thomson CSF/MIT  
MIT/PFC NW16-170  
Cambridge, MA 02139  
USA

Avraham Gover  
Tel Aviv University  
Dept. of Physics  
  
Tel Aviv 69355,  
ISRAEL

Eltjo Haselhoff  
Center for Laser Research  
PO Box 217  
7500 Ae Enschede,  
THE NETHERLANDS

Victor Granatstein  
University of Maryland  
Computer Engr. Dept.  
College Park, MD 20906  
USA

Giora Hazak  
Nuclear Research Cntr-NEGEL  
PO Box 9001  
Beer Sheva,  
ISRAEL

Dan Gregoire  
Hughes Research Labs  
3011 Malibu Canyon Rd.  
Malibu, CA 90265  
USA

Adrian Ho  
Stanford University  
310 McCullough Building  
Stanford, CA 94305  
USA

Juergen Gross  
Dornier GMBh  
PO Box 1420  
7990 Friedrichshafen,  
WEST GERMANY

Robert Hofland  
The Aerospace Corporation  
PO Box 92957  
Los Angeles, CA 90009  
USA

Bahman Hafizi  
Science App International Co  
1710 Goodridge Drive  
McLean, VA 22102  
USA

Ronald Holsinger  
Field Effects, Inc.  
6 Eastern Road  
Acton, MA 01741  
USA

Brett Hooper  
Duke University  
Physics Dept.  
Durham, NC 27706  
USA

Eli Jerby  
Tel-Aviv University  
co Prof. Bekefi  
(R.L.E.-MIT  
Cambridge, MA 02139  
USA

Bertram Hui  
DARPA/DSO  
1400 Wilson Blvd.  
Arlington, VA 22209  
USA

B Carol Johnson  
Natl Inst of Stands & Tech  
Building 245  
Room B-119  
Gaithersburg, MD 20899  
USA

Kazuo Imasaki  
Institute of Laser Technology  
1-8-4, Utsubo-hom-machi  
Nishiku  
Osaka 565,  
JAPAN

Ronald G. Johnson  
Natl Inst of Stands & Tech  
Building 245  
Room B-119  
Gaithersburg, MD 20899  
USA

Daniel Iracane  
CEA SPTN  
BP 12  
Bruyeres Le Chatel, 91680  
FRANCE

William Joel Johnson  
Los Alamos National Laboratory  
Box 1663  
M/S J579  
Los Alamos, NM 87544  
USA

Akira Iwata  
Kawasaki Heavy Industries Ltd  
Cryogenic Technology Research  
1-1 Kawasaki-cho  
Akashi 673,  
JAPAN

Shayne Johnston  
Jackson State University  
Physics Department  
POBox 17660  
Jackson, MS 39217  
USA

Dino Jaroszynski  
Fom-Inst for Plasma Physics  
Edisonbaan 14  
Nieuwegein 3439 MN,  
NETHERLANDS

Raynard Jong  
Lawrence Livermore Natl Lab  
PO Box 808  
M/S L-626  
Livermore, CA 94550  
USA

Judith Jensen  
Lawrence Livermore Natl Labs  
PO Box 808  
M/S L-626  
Livermore, CA 94550  
USA

Jann Kaminski  
University of California  
Santa Barbara, CA 93106  
USA

Yutaka Kawata  
Kobe Steel, LTD.  
1-5-5 Takatsukadai  
Nishi-Ku  
Kobe 678-02,  
JAPAN

Bernhard Kulke  
Lawrence Livermore Natl Lab  
PO Box 808  
M/S L-627  
Livermore, CA 94550  
USA

Hwa Kho  
University of California  
405 Hilgard Ave.  
Los Angeles, CA 90025  
USA

Gerhard Langbein  
Physicist  
Marlow 18 Oxford Road  
,  
ENGLAND

Kwang-Je Kim  
Lawrence Berkeley Laboratory  
B 2-400  
Lawrence Berkeley Lab  
Berkeley, CA 94720  
USA

Yves Lapierre  
CEA  
CEN Saclay  
GIF-sur-Yvette Cedex, 91191  
FRANCE

Isidoro Kimel  
Univ. of Central Florida  
CREOL  
12424 Research Parkway  
Orlando, FL 32816  
USA

Delbert Larson  
Univ. of Central Florida  
CREOL  
12424 Research Parkway  
Orlando, FL 32826  
USA

Masakazu Kimura  
Mitsubishi Electric Co.  
8-1-1 Tsukaguchi-Hommachi  
Amagasaki City,  
JAPAN

Jacques Launspach  
CEA CESTA  
BP 2  
Le Barp, 33114  
FRANCE

Nobuhisa Kitagawa  
New Energy & Ind Tech Dev.  
3-1-1 Higashi-ikebuhuro  
Toshima-ku  
Tokyo 170,  
JAPAN

Baruch Levush  
University of Maryland  
LPR  
College Park, MD 20742  
USA

Gerhard Konrad  
Lawrence Berkeley Labs  
1 Cyclotron Road  
Building 71-259  
Berkeley, CA 94720  
USA

Weiqliang Li  
Chinese Academy of Sciences  
Institute of Physics, Group 104  
PO Box 603  
Beijing,  
PR CHINA

Kimberly Lichy  
Am. Inst. Biological Science  
1800 N. Kent Street  
No. 930  
Arlington, VA 22209  
USA

Alfred W. Maschke  
TRW, Inc.  
PO Box 367  
White Sands Mssl Rnge, NM 88002  
USA

Anthony Lin  
University of California  
Dept. of Physics  
405 Hilgard Ave.  
Los Angeles, CA 90024  
USA

Antonio Matrone  
Ansaldo SPA Div. Ricerche  
Corso Perrone 25  
Genova 16152,  
ITALY

Vladimir Litveneko  
,

Hiroaki Matsui  
Obayashi Company  
3-37 Kyobashi, Higashi-Ku

Osaka 540,  
JAPAN

Alexander Lumpkin  
Los Alamos National Laboratory  
PO Box 1663  
M/S D406  
Los Alamos, NM 87545  
USA

Rodney McCormick  
Duke University  
Dept. of Physics  
Durham, NC 27706  
USA

John Madey  
Duke University  
Dept. of Physics  
  
Durham, NC  
USA

Chad McKee  
Duke University  
Dept. of Physics  
Durham, NC 27706  
USA

William Marable  
University of Maryland  
Astronomy Program  
College Park, MD 20742  
USA

Brian McVey  
Los Alamos National Laboratory  
M/S E 531  
Los Alamos, NM 87545  
USA

Thomas C. Marshall  
Columbia University  
213 MUDD  
Applied Physics Dept.  
New York, NY 10533  
USA

Karl Meier  
Los Alamos National Laboratory  
1183 Barranca Rd.  
M/S H825  
Los Alamos, NM 87544  
USA

ElRoy Miller  
Los Alamos National Laboratory  
926 Cheyenne  
Los Alamos, NM 87544  
USA

Masatsugu Nishi  
Hitachi, Ltd.  
Energy Research Laboratory  
1168 Moriyamacho  
Hitachi, Ibaraki,  
JAPAN

Kinioki Mima  
Institute of Laser Engineering  
Osaka University  
2-6, Yamadaoka, Suita City  
Osaka 565,  
JAPAN

Dirk Nolle  
University of Dortmund  
PO Box 500  
4600 Dortmund 50,  
WEST GERMANY

Norio Moribe  
NEC Corporation  
Laser Group  
1-10 Nisshin-cho, Fuchu City  
Tokyo 183,  
JAPAN

Shoichi Ogawa  
Sumitomo Heavy Industries, Ltd  
63-30 Yuhigaoka  
Hiratsuka City  
Kanagawa 254,  
JAPAN

Georges Mourier  
Thomson Tubes Electroniques  
2 Rue Latecoere  
Velizy, 78140  
FRANCE

Makio Ohkubo  
Japan Atomic Energy Res. Inst.  
Linac Lab, Tokai-Mura  
Naka-Gun  
Ibaraki-Ken 319-11,  
JAPAN

George Neil  
TRW, Inc.  
One Space Park  
R1/2104  
Redondo Beach, CA 90278  
USA

Koichi Okubo  
Mitsubishi Heavy Ind., Ltd.  
Dev and Engineering  
1-1-1 Wadasaki-cho  
Hyogo-ku Kobe 652,  
JAPAN

Brian Newnam  
Los Alamos National Laboratory  
M/S J564  
Los Alamos, NM 87544  
USA

Jean-Michel Ortega  
LURE-CNRS  
University of Paris  
LURE bat 209 D  
Orsay, 91500  
FRANCE

William E. Nexsen  
Lawrence Livermore Natl Lab  
PO Box 808  
Livermore, CA 94550  
USA

T J. Orzechowski  
Lawrence Livermore Natl Lab  
PO Box 808  
M/S L-626  
Livermore, CA 94550  
USA

Merik Ozcan  
Stanford University  
McCullough 308  
Stanford, CA 94305  
USA

Rafael B. Perez  
Oak Ridge National Laboratory  
PO Box Bldg 6010  
M/S 6354  
Oak Ridge, TN 37831  
USA

Richard Pantell  
Stanford University  
308 McCullough Building  
Stanford, CA 94305  
USA

Dean Pershing  
Mission Research Corporation  
8560 Cinderbed Rd., Suite 700  
Newington, VA 22122  
USA

Claude Patou  
CEA  
BP 27  
Villeneuve St Georges, 94195  
FRANCE

Paolo Pierini  
Natl Inst. of Nuclear Physics  
Via Celoria 16  
Milan,  
ITALY

Claude Patou  
CEA  
BP 27  
Villeneuve  
Saint Georges 94195,  
FRANCE

Michael Poole  
Serl Daresbury Laboratory  
Daresbury  
Warrington  
Cheshire WA4 4AD,  
ENGLAND

Piero Patteri  
INFN-Frascati  
Via E. Fermi  
Frascati,  
ITALY

Rui Prazeres  
LURE-CNRS  
University of Paris  
PO Box 209 D  
Orsay, 91405  
FRANCE

Kevin Paulson  
University of California  
  
Santa Barbara, CA 93106  
USA

Donald Prosnitz  
Lawrence Livermore Natl Labs  
PO Box 808  
M/S L-626  
Livermore, CA 94550  
USA

Alan Paxton  
Mission Research Corporation  
1720 Randolph Rd., SE  
Albuquerque, NM 87106  
USA

David Quimby  
Spectra Technology, Inc.  
2755 Northup Way  
Bellevue, WA 98004  
USA

George Rakowsky  
Rockwell Intl/Rocketdyne Div.  
M/S FA38  
6633 Canoga Ave.  
Canoga Park, CA 91303  
USA

Virgil Sanders  
Los Alamos National Laboratory  
PO Box 1663  
M/S J564  
Los Alamos, NM 87545  
USA

Gerald Ramian  
University of California  
Physics Dept.  
  
Santa Barbara, CA 93106  
USA

Ernst Scharlemann  
Lawrence Livermore Natl Lab  
PO Box 808  
Livermore, CA 94550  
USA

Alberto Renieri  
ENEA  
Dept. of Technology  
  
00044 Frascati, Rome,  
ITALY

Mark Schmitt  
Los Alamos National Labs  
M/S E-531  
Los Alamos, NM 87545  
USA

Spilios Riyopoulos  
S.A.I.C.  
1710 Goodridge Drive  
McLean, VA 22102  
USA

Alan Schwettman  
Stanford University  
Physics Department  
Stanford, CA 94305  
USA

Charles Roberson  
Office of Naval Research  
800 N. Quincy Street  
Arlington, VA 22217  
USA

Stephen Segall  
Segall Associates  
1349 King George Blvd.  
Ann Arbor, MI 48108  
USA

Rajeev Rohatgi  
Stanford University  
HEPL Building  
Stanford, CA 94305  
USA

Oded Shahal  
Nuclear Research Center  
POB 9001  
Physics Dept.  
Beer-Sheva,  
ISRAEL

Don Rule  
Naval Surface Warfare Center  
R41, Rm 4-275  
  
Silver Spring, MD 20903  
USA

William Sharp  
Lawrence Livermore Natl Labs  
PO Box 808  
M/S L-626  
Livermore, CA 94550  
USA

Earl Shaw  
AT&T Bell Labs  
600 Mountain Ave.  
Murray Hill, NJ 07924  
USA

Richart Slusher  
AT & T Bell Laboratory  
Room 10227  
600 Mountain Ave.  
Murray Hill, NJ 07974  
USA

Henry D. Shay  
Lawrence Livermore Natl Labs  
PO Box 808  
Livermore, CA 94550  
USA

Vern Smiley  
Office of Naval Research  
14134 Korrey Drive  
San Diego, CA 92129  
USA

Michael Sheaffer  
Lawrence Livermore Natl Labs  
PO Box 808  
Livermore, CA 94550  
USA

Todd Smith  
High Energy Physics Lab  
Stanford University  
Stanford, CA 94305  
USA

Ruth Shefer  
Science Research Laboratory  
15 Ward Street  
Somerville, MA 02143  
USA

Kent Sokoloff  
Sierra Laser Systems, Inc.  
754 North Pastoria Ave.  
Sunnyvale, CA 94086  
USA

Richard Sheffield  
Los Alamos National Laboratory  
M/S H825  
Los Alamos, NM 87545  
USA

Jerzy S. Sokolowski  
Weizmann Institute of Science  
PO Box 26  
Rehovot, 76100  
ISRAEL

Chun Ching Shih  
TRW, Inc.  
Mail Code 01/1251  
One Space Park  
Redondo Beach, CA 90278  
USA

Phillip Sprangle  
Naval Research Laboratory  
4555 Overlook Ave., SW  
Washington, DC 20375  
USA

Jack Slater  
Spectra Technology Inc.  
2755 Northup Way  
Bellevue, WA 98004  
USA

Edward Stanford  
University of Maryland  
Lab for Plasma Research  
College Park, MD 20742  
USA



William Stein  
Los Alamos National Lab  
AT-7 M/S J579  
Los Alamos, NM 87545  
USA

Atsumi Taniguchi  
Foundation of Osaka Sc & Tech  
1-8-4 Utsubo-hommachi  
Nishi-ku  
Osaka 550,  
JAPAN

Kenneth Sun  
Rockwell Intl/Rocketdyne Div.  
M/S FA40  
6633 Canoga Ave.  
Canoga Park, CA 91303  
USA

Lester Thode  
Los Alamos National Laboratory  
PO Box 1663  
M/S E527  
Los Alamos, NM 87545  
USA

Eric Szarmes  
Duke University  
Dept. of Physics  
Durham, NC 27706  
USA

Alan Throop  
Lawrence Livermore Natl Labs  
1832 Creek Rd.  
Livermore, CA 94550  
USA

Manabu Tada  
Daihen Company  
2-1-11 Tagawa  
Yodogawa-ku  
Osaka 532,  
JAPAN

Antonio Ting  
Naval Research Laboratory  
4555 Overlook Ave., SW  
Washington, DC 20375  
USA

Ken Takayama  
Natl Lab High Energy Physics  
Oho 1-1  
Tsukuba  
Ibaraki 305,  
JAPAN

Robert Tokar  
Los Alamos National Laboratory  
M/S E 531  
Los Alamos, NM 87545  
USA

Harunori Takeda  
Los Alamos National Laboratory  
M/S H829  
Los Alamos, NM 87545  
USA

Wim Van Amersfoort  
Fom-Inst. for Plasma Physics  
Edisonbaan 14  
Nieuwegein 3439 MN,  
NETHERLANDS

Cha-Mei Tang  
Naval Research Laboratory  
4555 Overlook Avenue, SW  
Washington, DC 20375  
USA

Marnix Van Der Wiel  
Fom-Inst. for Plasma Physics  
Edisonbaan 14  
Nieuwegein 3439 MN,  
NETHERLANDS

Peter Van der Slot  
Center for Laser Research  
PO Box 217  
7500 Ae Enschede,  
THE NETHERLANDS

Laurance Warner  
Los Alamos National Labs  
Box 1663  
M/S J579  
Los Alamos, NM 87545  
USA

Alexander Varfolomeev  
Korchatov Atomic Energy Inst  
  
Moscow,  
USSR

Roger Warren  
Los Alamos National Laboratory  
1183 Barranca Rd.  
M/S H825  
Los Alamos, NM 87545  
USA

Vincenzo Variale  
INFN-Univ. of Milan  
Via Amendola 173  
Bari,  
ITALY

Wim Witteman  
University of Twente  
PO Box 217  
Enschede 7500 AE,  
THE NETHERLANDS

Michel Velghe  
University of Paris  
Laboratoire Lure  
B209  
Orsay Cedex, 91405  
FRANCE

Ming Xie  
Lawrence Berkeley Lab  
1 Cyclotron Road 2-400  
Berkeley, CA 94720  
USA

John Vetrovec  
Rockwell Internatl/Rocketdyne  
6633 Canoga Avenue  
Canoga Park, CA  
USA

Zhenhua Yang  
IAPCM  
PO Box 8009  
Beijing 100088,  
PR CHINA

John Walsh  
Dartmouth  
Wilder Lab, Physics Dept.  
Hanover, NH 03755  
USA

L H. Yu  
Brookhaven National Laboratory  
NSLS Building 725 BNL  
Upton, NY 11973  
USA

Ming Chang Wang  
Shanghai Inst of Optics and  
Fine Mechanics, Academia Sinic  
PO Box 8211  
Shanghai,  
PR CHINA

Simon Yu  
Lawrence Livermore Natl Lab  
PO Box 808  
M/S L-626  
Livermore, CA 94550  
USA

Xinglin Zhai  
PO Box 275 17  
Beijing 102413,  
PR CHINA

PO Box 275 17  
Beijing 102413,  
PR CHINA

Chuanming Zhou  
ISEE  
PO Box 517  
Chengdu 610003,  
PR CHINA

Alexander van der Meer  
Fom-Inst. for Plasma Physics  
PO Box 1207  
Nieuwegein 3430 BE,  
NETHERLANDS